The implications of the patient microenvironment on mesenchymal stromal cell therapy in the treatment of acute respiratory distress syndrome

A thesis submitted to Maynooth University for the degree of Doctor of Philosophy

Courteney Tunstead, B.Sc.

Supervisor

Prof. Karen English,

Department of Biology,

Maynooth University,

Co. Kildare.

Head of Department

Prof. Paul Moynagh,

Department of Biology,

Maynooth University,

Co. Kildare.

TABLE OF CONTENTS

Chapter 1: General Introduction

LIST OF FIGURES AND TABLES

---

*All schematics were made using Biorender

List of figures

Chapter 1:

Chapter 2:

Chapter 3:

Chapter 4:

List of tables

Chapter 1:

Chapter 2:

Chapter 3:

Chapter 4:

CREDITS & MODULES

STATEMENT OF RESULTS - Autumn 2022

Qualification:	**PH.D. DEGREE SCIENCE**	Credits-Academic Year:	**15.0**
Period of Study:	**FIRST YEAR**	Credits-Period of Study:	**15.0**

Module Results

Subject	Module	Title	Credits Attempted	Credits Earned	Mark %	Result	Ind*
BL900	BI881	ADVANCED WRKSHP/COURSE/SUMMER SCHOOL/ M'CLASS	5.0	5.0		PASS	
BL900	BI891	ADVANCED SPECIALIST MODULE - INTERNATIONAL	5.0	5.0		PASS	
BL900	GST3	ACADEMIC WRITING MODULE	5.0	5.0		PASS	

For information on interpreting this statement of results please visit the Maynooth University Exams Office website.

*Ind= Indicator: C(apped) and/or E(xempted) and/or R(equired) and/or B(est mark)

Subject Results

Subject	Title	Credits Attempted	Credits Earned	Mark %	Result
BL900	BIOLOGY	15.0	15.0		PROGRESS ON TRACK

STATEMENT OF RESULTS - Autumn 2023

Qualification:	**PH.D. DEGREE SCIENCE**	Credits-Academic Year:	**15.0**
Period of Study:	**SECOND YEAR**	Credits-Period of Study:	**15.0**

Module Results

Subject	Module	Title	Credits Attempted	Credits Earned	Mark %	Result	Ind*
BL900	BI830	IMMUNOLOGY SEMINAR SERIES	5.0	5.0		PASS	
BL900	BI872	CONFERENCE ATTENDANCE AND POSTER PRESENTATION	5.0	5.0		PASS	
BL900	FM801	CONFERENCE ORGANISATION	5.0	5.0		PASS	

For information on interpreting this statement of results please visit the Maynooth University Exams Office website.

*Ind= Indicator: C(apped) and/or E(xempted) and/or R(equired) and/or B(est mark)

Subject Results

Subject	Title	Credits Attempted	Credits Earned	Mark %	Result
BL900	BIOLOGY	15.0	15.0		PROGRESS

DECLARATION OF AUTHORSHIP

I, Courteney Tunstead, declare that this thesis has not been previously submitted to this or any other university. This thesis is the sole work of the author, and any collaborative work has been highlighted throughout.

I agree to deposit this thesis in the University's open access institutional repository or allow the library to do so on my behalf, subject to Irish Copyright Legislation and Maynooth University Library conditions of use and acknowledgement.

Signature:  **Date:** 23/10/2025

FUNDING

The work in this thesis was funded by Science Foundation Ireland (now Research Ireland/Taighde Éireann) award to Professor Karen English, under grant number 20/FFP-A/8948. This study was supported by the National Irish COVID-19 biobank and the Irish Blood Transfusion Service.

ABSTRACT

The incidence of acute respiratory distress syndrome (ARDS) has risen exponentially in the post-SARS-CoV-2 pandemic era. Current treatments for this disease are broad-spectrum, and lack the specificity required to treat this highly-complex disease. Mesenchymal stromal cells (MSCs) are an immunomodulatory and pro-reparative cell-type, that are a prominent interest in the field of regenerative medicine. These cells can interact with other cells to dampen their inflammatory effects, while also secreting paracrine factors that can aid in immune modulation and repair. In the context of inflammatory disease, MSCs have been trialled, tested and proven to have an exquisite safety profile in the context of many diseases; including ARDS. However, they have not been therapeutically efficacious in the treatment of ARDS. Given that resident stromal cells within the lung are known to be defective within the diseased lung microenvironment, this project sought to identify the impact that elements of the ARDS patient microenvironment could have on MSC therapeutic efficacy in a pre-clinical model of acute lung inflammation. It was shown that general inflammation, by TNFα, could enhance MSC modulation of neutrophils; a key driver of ARDS. This study further highlighted the impact of differential inflammatory profiles of ARDS patients on MSC therapeutic efficacy. This first-of-its-kind patient stratification study highlighted that MSCs exposed to a highly-inflammatory ARDS microenvironment could enhance lung epithelium barrier function in a VEGF-dependent manner, but the same effect was not seen from MSCs exposed to lower levels of inflammation. It was also identified that free fatty acids within the ARDS microenvironment could enhance MSC pro-reparative capacity in an ANGPTL4-dependent manner, through activation of the PPARβ/**δ** nuclear receptor. This research largely contributes to the field of cell-therapy, by promoting a need to investigate the environment in which the cells are placed, and identifying the key mechanisms required for therapeutic effect in the inflammatory lung.

PUBLICATIONS

Publications arising from this thesis:

Tunstead, C., Volkova, E., Dunbar, H., Hawthorne, I.J., Bell, A., Crowe, L, Masterson, J.C., McNicholas, B., Dos Santos, C.C., Laffey, J.G. & English, K. (2024) 'The ARDS microenvironment enhances MSC-induced repair via VEGF in experimental acute lung inflammation', *Molecular Therapy*, 32(10).

Tunstead, C., Volkova, E., Dunlop, M., Ryan, S., Kundu, S., Johnston, E., Bitterlich, L.B., Masterson, C., Bateh, S., Dos Santos, C.C., Masterson, C., Bell, A., McNicholas, B., Laffey, J.G., & English, K (2025) 'PPARβ/δ-induced ANGPTL4^{HIGH} MSC conditioned media has cytoprotective effects in a pre-clinical model of acute lung inflammation', [under review].

Tunstead, C., Volkova, E., Dunlop, M., Ryan, S., Johnston, E., Bitterlich, L.B., Masterson, C., Dos Santos, C.C., Laffey, J.G., & English, K (2025) 'TNFα-licensed MSCs show enhanced suppression of polymorphonuclear neutrophils in a pre-clinical model of acute lung inflammation', [in preparation].

Other publications:

*Dunbar, H., *Hawthorne, I.J., **Tunstead, C**., Armstrong, M.E., Donnelly, S.C. & English, K. (2023). Blockade of MIF biological activity ameliorates house dust mite-induced allergic airway inflammation in transgenic humanised MIF mice, *FASEB Journal,* 37(8).

*Hawthorne, I.J., *Dunbar, H., **Tunstead, C**., Schorpp, T., Weiss, D., Rolandsson, E., Dos Santos, C.C., Armstrong, M.E., Donnelly, S.C. & English, K. (2023). Human macrophage migration inhibitory factor potentiates mesenchymal stromal cell efficacy in a clinically relevant model of allergic asthma, *Molecular Therapy*, 31(11).

Dunbar, H., Hawthorne, I.J., **Tunstead, C**., McNamee, E., Armstrong, M.E., Donnelly, S.C. & English, K. (2024). Mesenchymal stromal cells attenuate macrophage priming and training induced by house dust mite and enhanced by MIF in allergic airway inflammation, *Cytotherapy*, 36(10).

Bitterlich, L.M., **Tunstead, C.**, Ankrum, J.A., Hogan, A.E. & English, K (2024) 'Mesenchymal stromal cells can block palmitate training of macrophages via COX-2 and IL-1Ra', *Cytotherapy*, 27(2).

Dunbar, H., Hawthorne, I.J., **Tunstead, C.**, Dunlop, M., Volkova, E., Weiss, D.J., Dos Santos, C.C., Armstrong, M.E., Donnelly, S.C. & English, K (2024) 'The VEGF-mediated cytoprotective ability of MIF-licensed mesenchymal stromal cells in house dust mite-induced epithelial damage'*, European Journal of Immunology*, 55(1).

***Tunstead, C.,** *Bitterlich, L.M., Ankrum, J.A., Hogan, A.E. & English, K (2025) 'Palmitate enhances MSC immunomodulation of human macrophages via the ceramide/CCL2 axis *in vitro*', *Stem Cell Research & Therapy*, 16(435).

*Denotes joint authorship.

CONFERENCE PROCEEDINGS

Oral Presentations

'What are Mesenchymal Stromal Cells?', *Maynooth University Biology Summer School, 2022*.

'*(Don't)* take my breath away', *Maynooth University 3-minute Thesis Competition, 2023.*

'A *lung* way to go', *Maynooth University 3-minute Thesis Competition, 2022*.

'The Role of PPARβ/δ in Mesenchymal Stromal Cell Therapeutic Efficacy in Acute Respiratory Distress Syndrome', *Maynooth University Seminar Series, 2022*.

'Investigating the role of PPARβ/δ in Mesenchymal Stromal Cell Therapy for Acute Respiratory Distress Syndrome, Irish Thoracic Society, *2022*.

'A *lung* way to go in the treatment of ARDS', *Maynooth University Biology Summer School, 2023*.

'The Role of PPARβ/δ in Mesenchymal Stromal Cell Therapeutic Efficacy in Acute Respiratory Distress Syndrome', *Maynooth University Seminar Series, 2023*.

'Investigating the role of the Acute Respiratory Distress Syndrome disease micro-environment on human bone-marrow derived Mesenchymal Stromal Cells', Irish Thoracic Society, *2023*.

‘Life as a Medical Science PhD Student’, *Maynooth University Transition Year Student Programme, 2023* [Lecture].

‘The hyper-inflammatory ARDS microenvironment licenses MSCs and enhances their therapeutic efficacy’, *Maynooth University Research Day, 2024.*

‘The hyper-inflammatory SARS-CoV-2-induced ARDS patient micro-environment licenses MSCs and enhances their therapeutic efficacy in a model of acute lung injury’, *European Respiratory Society, 2024*.

‘Identifying Immune Cells’, *Maynooth University Transition Year Student Programme, 2024* [Lecture].

‘Shaping the mesenchymal stromal cell response in the treatment of acute respiratory distress syndrome: the not-so-micro impact of the microenvironment’, *Cell and Gene Therapy Conference, 2025*.

‘Elucidating the impact of the acute respiratory distress syndrome disease microenvironment on mesenchymal stromal cell therapeutic efficacy’, *Maynooth University Research Day, 2025.*

Posters

Tunstead, C. & English, K. (2022) Investigating the Role of the PPARβ/δ nuclear receptor in human bone-marrow derived Mesenchymal Stromal Cells in the context of Acute Respiratory Distress Syndrome, Maynooth University Biology Research Day.

Tunstead, C., Rebello, M. & English, K. (2022) The effect of PPARβ/δ on Mesenchymal Stromal Cell (MSC) gene expression in cytokine-naive and licensed MSCs, *Irish Society of Immunology.*

Tunstead, C., Rebello, M. & English, K. (2022) Investigating the role of PPARβ/δ in Mesenchymal Stromal Cell Therapy for Acute Respiratory Distress Syndrome, Irish Thoracic Society.

Tunstead, C. & English, K. (2023) Investigating the Role of the PPARβ/δ nuclear receptor in human bone-marrow derived Mesenchymal Stromal Cells in the context of Acute Respiratory Distress Syndrome, Maynooth University Biology Research Day.

Tunstead, C., Volkova, V., Dunbar, H., Hawthorne, I.J., Warren, A., McNicholas, B., Bell, A., Laffey, J.G. & English, K. (2023) Investigating the role of the Acute Respiratory Distress Syndrome disease micro-environment on human bone-marrow derived Mesenchymal Stromal Cells, Irish Thoracic Society.

Tunstead, C., Volkova, V., Dunbar, H., Hawthorne, I.J., Warren, A., McNicholas, B., Laffey, J.G. & English, K. (2023) Investigating the Role of the PPARβ/*δ* nuclear receptor in human bone-marrow derived Mesenchymal Stromal Cells in the context of Acute Respiratory Distress Syndrome, British Society of Immunology.

Tunstead, C., Volkova, E., Dunbar, H., Hawthorne, I.J., Bell, A., McNicholas, B., Dos Santos, C.C., Laffey, J.G. & English, K. (2024) PPARβ/*δ*-inhibition enhances Mesenchymal Stromal Cell-mediated immunomodulation in the context of Acute Respiratory Distress Syndrome, European Congress of Immunology.

Tunstead, C., Volkova, E., Dunbar, H., Hawthorne, I.J., Bell, A., Crowe, L, Masterson, J.C., McNicholas, B., Dos Santos, C.C., Laffey, J.G. & English, K. (2024) The hyper-inflammatory SARS-CoV-2-induced ARDS patient micro-environment licenses MSCs and enhances their therapeutic efficacy in a model of acute lung injury, European Respiratory Society.

Tunstead, C., Volkova, E., Dunbar, H., Hawthorne, I.J., Bell, A., Crowe, L, Masterson, J.C., McNicholas, B., Dos Santos, C.C., Laffey, J.G. & English, K. (2024) The importance of ARDS patient stratification prior to MSC-based therapy: and the notable impact of MSC-licensing**,** Irish Thoracic Society.

Tunstead, C., Volkova, E., Dunbar, H., Hawthorne, I.J., Bell, A., Crowe, L, Masterson, J.C., McNicholas, B., Dos Santos, C.C., Laffey, J.G. & English, K. (2025) The hyper-inflammatory ARDS microenvironment enhances MSC reparative capacity in a pre-clinical model of acute lung inflammation**,** International Society for Cell and Gene Therapy.

Tunstead, C., Volkova, E., Dunlop, M., Bitterlich, L.M., Dos Santos, C.C., Laffey, J.G. & English, K. (2025) The dual role of PPARβ/δ nuclear receptor in MSC immunomodulatory and pro-reparative capacity in a model of acute lung inflammation, International Society for Cell and Gene Therapy.

Awards Received

1st place Oral Presentation, Maynooth University Research Day, 2024

European Congress of Immunology travel grant award, 2024

Irish Thoracic Society-funded travel grant award to attend the European Respiratory Society annual meeting in Vienna, Austria, 2024

Runner up Oral Presentation, Maynooth University Research Day, 2025

ABBREVIATIONS

ACE	Angiotensin converting enzyme
AD	Activation domain
AECC	American-European Consensus Conference
AHRF	Acute hypoxemic respiratory failure
ALI	Acute lung inflammation
ALS	Amyotrophic lateral sclerosis
AMP	Adenosine monophosphate
ANGPTL	Angiopoietin-related protein
ARDS	Acute respiratory distress syndrome
ARRIVE	Animal Research: Reporting of In Vivo Experiments
AT	Adipose tissue
BALF	Broncho-alveolar lavage fluid
BM	Bone marrow
BM-MSC	Bone marrow-derived mesenchymal stromal cells
BSA	Bovine serum albumin
CBP	CREB-binding protein
CLDN	Claudin
CLP	Cecal ligation puncture
COX	Cyclooxygenase
CREB	Cyclic AMP-responsive element-binding protein
CRISPR	Clustered regularly interspaced short palindromic repeats
CS	Cecal slurry

DBD	DNA-binding domain
DEG	Differentially expressed gene
DMEM	Dulbecco's modified eagle medium
DMSO	Dimethyl sulfoxide
DNA	Deoxyribonucleic acid
DP	Dental pulp
ELISA	Enzyme-linked immunosorbent assay
FBS	Foetal bovine serum
FDA	Food and Drug Administration
FFA	Free fatty acid
FPKM	Fragments per kilobase of transcript per million reads
GVHD	Graft-versus-host disease
HCL	Hydrochloric acid
HDAC	Histone deacetylase
HGF	Human growth factor
HFNO	High-flow nasal oxygen
ICAM	Intercellular cell adhesion molecule
ICU	Intensive care unit
IFN	Interferon
IL	Interleukin
IN	Intranasal
IT	Intratracheal
IV	Intravenous
LBD	Ligand-binding domain
LPS	Lipopolysaccharide

MAPC	Multipotent adult progenitor cells
MB	Menstrual blood
MDM	Monocyte-derived macrophage
MIF	Macrophage migration inhibitory factor
MOA	Mechanisms of action
MCP	Monocyte chemoattractant protein
MPO	Myeloperoxidase
MSC	Mesenchymal stromal cell
MSC-CM	Mesenchymal stromal cell-conditioned media
MSC-EV	Mesenchymal stromal cell-extracellular vesicle
NCOA	Nuclear receptor coactivator
NCoR	Nuclear receptor corepressors
NET	Neutrophil extracellular trap
NFκB	Nuclear factor kappa B
OA	Osteoarthritis
OCLN	Occludin
OPN	Osteopontin
PBMC	Peripheral blood mononuclear cells
PBS	Phosphate buffer saline
PEEP	Positive end-expiratory pressure
PFU	Plaque-forming unit
PPAR	Peroxisome proliferator-activated receptor
PPRE	Peroxisome proliferator response element
RNA	Ribonucleic acid
RT-PCR	Real-time polymerase chain reaction

RXR	Retinoid-X-receptor
SARS-CoV-2	Severe acute respiratory syndrome coronavirus 2
SMRT	Silencing mediators of retinoid and thyroid hormone receptors
SR	Steroid-refractory
SRC	Steroid receptor co-activator
TBL	Transducin β-like protein
TEER	Transepithelial electric resistance
TF	Transcription factor
TLR	Toll-like receptor
TNF	Tumour necrosis factor
TSG	Tumour necrosis factor-inducible gene
UC	Umbilical cord
VCAM	Vascular cell adhesion molecule
VEGF	Vascular endothelial growth factor
VEGFR2	Vascular endothelial growth factor receptor 2
VILI	Ventilator-induced lung injury
WHO	World Health Organisation
ZO	Zonula occluden

ACKNOWLEDGEMENTS

Firstly, I would like to extend a huge thank you to my supervisor: Prof. Karen English. What you saw in me as a third-year undergraduate student was beyond what I ever could have imagined for myself. You guided me, mentored me, and reminded me that I am more than capable of greatness; regardless of my doubts. Thank you for being there through the highest of the highs, and the lowest of the lows; and for laughing with me through them no matter what! You always made sure I knew there was more to life, and I simply couldn't have asked for a better supervisor. I can't put into words how much you've helped me as both an academic and an individual; and I can only ever aspire to be like you as I learn and grow. Thank you for reminding me that the PhD is a marathon, not a sprint, and for ensuring I knew I was there to learn, and not to be perfect! It's all training after all. To my progress committee, Prof. Joanne Masterson, Prof. Bernard Mahon and Dr. Eoin McNamee. Thank you for being the additional mentors that I needed and for always reminding me of how far I've come. You never made me question my abilities and were always there for me both as an academic, and a human being. I would also like to extend gratitude to the BRU staff, Gillian O'Meara, Deirdre Daly and Rebecca Kerrigan. Thank you for all the hard work you do to take care of our mice, ensuring their health and happiness.

To the Cellular Immunology lab; my PhD wouldn't have been the same without you. To Dr. Hazel Dunbar, thank you for being my lab sister and my everyday source of support over your time in the lab. To Dr. Ian Hawthorne, thank you for always reminding me not to sweat the small stuff, and for having my back no matter the occasion. I hope you both know that the lab hasn't been the same without you, and I miss you both dearly. To Dr. Laura Bitterlich, thank you for providing sweet treats, and for showing us all your resilience even on the toughest days. To Molly Dunlop, Evelina Volkova and Dr. Sinead Ryan thank you for all of the BRU assistance and giggles. We had our fair share of laughs over our time shared in the lab (and we always had time for a coffee!). To Dr. Shoumo Kundu, our smiley little flow king! It's always great to walk into a room and see your smile pointing back at me; and our lab was lucky to have you! To Dr. Evangeline Johnston, where do I begin? you only started in the lab and promptly became my go-to girl. You could make anyone feel welcomed, cared for and appreciated with your everlasting kindness, generosity and positivity. I truly aspire to be more like you. They say everything happens for a reason, and I have no doubt that we met because the universe knew we needed each other. I can't wait for many more adventures together.

To the reading room; the people who witnessed most of my life over the last few years. We have been through so much in that reading room together, from tears of sadness to tears of joy. To Ellen Treacy, thank you for being a smiling face in the reading room, I can't wait to see what becomes of you in the future. To Eva Kennedy, your confidence and sureness of yourself is ever inspiring. You will go far in anything you do, and your determination will make sure of that! To Ben McLaughlin, a fellow Dub around me at long last! Thank you for bringing us pastries, and for always being there to make us smile. You made the reading room feel a little more like home for me, whether you knew it or not. To Eike Curtin, thank you for just laughing no matter what, for being you no matter what. Your giggle has made me giggle on so many occasions!

To my friends: to Dr Aaron Curtis, and (soon to be Dr) Ardena Berisha, you have both been around possibly the longest in my academic circle, and from the first day of registration to our undergraduate degree, I knew we would be life-long friends. To (soon to be Dr) Cathal Ryan, another original in my journey! Your jokes and laughter have been some of my favourite moments over the last 8 years. To (soon to be Dr) Jamie Casey, thank you for being just as much of a workaholic as I am, for always providing great ideas, fabulous sarcasm, and for letting us steal your milk on occasion (even if you didn't always know). I always knew I could turn to you anytime I needed, and no matter your headspace you would always offer support and validate what I felt. To (soon to be Dr) Conall Geoghegan Moore, you have been hanging around MU with me for 7 years now! Thank you for being someone I can go to on the hard days and know you will have my back no matter what. We will get each-other through this thing we call life for the foreseeable; you refer to yourself as my son, but you're my chosen brother forever and always. To (soon to be Dr) Sarah Harkin, thank you for being our resident designated driver, and for always having a spare fork for me. Our bookish evenings roasting marshmallows over a candle after a long day in the lab always revived me. Thank you for being one of the most genuine people I've ever met. No matter the weather, I always knew you would have my back; even on my darkest days. I've witnessed you grow into such a beautiful person over our time together (through both the ups and downs!) and I will cherish it, and you, forever more.

To Shannon Carter, thank you for being the best friend a girl could ever ask for. Thank you for being your bubbly self, for trusting me with all your craziest stories, and for welcoming me into your family. There's no doubt when I say I couldn't have gotten through the last several years of life without you here by my side, and I know we have many more years together to go! To Dr. Nicole Kavanagh (my favourite half of Nev-squared), you taught me that success deserves to be responded to with praise, not competition, and I should ignore those who suggest otherwise. You always lifted me up and reminded me of who I am. Our nightly timers have only brought us closer together, and it's hard to believe that we are both finished. Thank you for always reminding me of the Courteney you see; the Courteney who isn't an academic, just a friend. I needed those reminders (and still do!). To Beka Kinsella and Lea Bortolozzo, thank you for always being as passionate as I am; for agreeing with me on everything no matter what (supportive queens), and for being a constant source of support in the sisterhood. You always make me feel like I belong. To Cheney Li & Sri Adithyaa, thank you for never giving up on me despite my busy schedule, for staying in touch even years after leaving Takeda, and for always making me laugh with all of your hilarious jokes (you know exactly what I'm talking about, Chen), and your serious dance moves (yes, Sri – I'm talking to you). To Teigan Walsh and Daniel Olaniyi, thank you both for being just as outrageously ambitious as I am! Our similarities allow us to support each-other through everything we do (even if it might be a far-fetched idea!). We have each-others backs, whether busy or not, when it matters most. I love you all more than you will ever know, and I'm honoured to have friends like you in my life.

To my family; thank you for believing in me and supporting me through my PhD journey, and everything else that happened along the way. To Cameron Tunstead, thank you for your hugs and late-night chats about college. We got each other through our degrees for sure! You may be younger, but you've always been a big brother to me. To Travis Tunstead, thank you for always making a little extra chicken and pasta so I would get fed after a long day in the lab. It seemed small to you, but it was everything to me. To Kian Tunstead, thank you for your warm greetings, and your constant supply of snacks. No one understands my sweet tooth quite like you. You always ended each of our conversations with "if you need me, call me", and I always did. To Mason Tunstead, thank you for watching Modern Family and 'Fluffy' with me to lift my spirits, and for always providing the hot chocolate! Cosy nights in have always been our thing (even if you think you're too grown up for them now). To mam and dad, Lisa and Brian Tunstead. Thank you for believing in me, for supporting me and for encouraging me to pursue all my wildest dreams. I never thought I'd make it here, but you never doubted me. To my grandparents, Charlotte & Paddy Holmes and Pauline & Paddy Tunstead. You've all done so much for me, believed in me, reminded me it's ok not to be ok during the hard times, and always been a sincere source of support throughout my life. I hope you're looking down on me and feeling proud, grandad. To the Mahon's: Sandra, Thomas, Casey, Tammie and Farrah. I will never forget that first PhD grant rejection in your house. It killed me, but you all got me fed and motivated and back on track to write the next application. I wouldn't be here without that. To my one and only godchild, Hallie-Anna Mahon; I will always be 'Kiki' to you, no matter my title. You have provided me with so much love and laughter over the years, and I love you so much for it. It's crazy to me how much you've grown up, and I can't wait to see all the greatness that comes of you. You're the funniest person I know.

To my second family: the McGrattan's. To Lorraine and Colm McGrattan, thank you for offering me words of wisdom on both my up and down days, for supporting me through my overwhelming moments, and for always including me in your family. This made PhD life a lot easier; having not only one family for support, but two! To Adele Hanrahan, you were taken far too soon but one thing you solidified for all of us in your short time here, is how important it is to care. To truly care; about people, about animals, about anything we could care about. I hope you're at peace; and I hope the rest of us can make up for the worlds loss by helping wherever and whenever we can. To Claire McGrattan, thank you for always reminding me that having a creative self is important. Watching you craft and create always inspired me to unleash my creative side. To Cliodhna McGrattan, thank you for all our laughs. There is never a dull moment when we are together! We have shared so many funny memories over the last 10 years, and I can't wait for an abundance more. We always have each-other's backs, and we always will. I always wanted a sister and now I have two.

Last but certainly not least, to Tiernan McGrattan; my absolute rock, not only throughout my PhD, but throughout my whole life. Thank you for everything. Literally, everything; since the moment we met in 2011. Thank you for putting up with all my madness over the years; you're one strong man! Thank you for being there for me, for supporting me, for forcing me to take breaks, and for loving me through it all. You were there for me not only through my darkest moments, but also through your own; because that's just the kind of person that you are. I couldn't have gotten through any of this without you (or our Sunday brunches!). I love you with my whole heart, and I'm glad I finally have a big-girl job so we can save for many more adventures, a never-ending supply of doggies and that swanky house we always dream about (or a one-bedroom flat – as long as I have you).

These last few years have been a fever dream; and it wouldn't have been the same without each one of you. If I could write and write and continue to thank people who aided in support, I would be writing till the day I die; and that's an excellent complaint to have! Thank you so much for everything. I'm forever grateful.

Chapter 1

General Introduction

1.1 ACUTE RESPIRATORY DISTRESS SYNDROME

1.1.1 What is ARDS?

Acute respiratory distress syndrome (ARDS) was first described by Ashbaugh and Petty in 1967 [1]. ARDS is an inflammatory, degenerative, secondary condition of the lung, that occurs in response to many primary insults; including, but not exclusive to, pneumonia [2], septic shock [3] and general lung trauma [4]. ARDS is largely characterised by cellular infiltration and inflammation in the lung, leading to the destruction of the lung infrastructure, resulting in pulmonary oedema [5-7]. Ultimately, these characteristic traits of ARDS lead to shortness of breath, low blood oxygen levels and acute hypoxemic respiratory failure (AHRF) in the patient [8, 9].

1.1.2 ARDS pathogenesis

ARDS pathology differs from patient-to-patient. Typically, ARDS manifests due to a build-up of cellular infiltrate and inflammation in the lung; leading to a breakdown in the alveolar barriers [10]. This damage leads to a permeable lung epithelial layer, due to the breakdown of tight junctions; that are highly important for barrier maintenance and function [11]. This permeable, or 'leaky', barrier further allows the influx of fluid from the extracellular space [12]. As the alveolar sacs fill with fluid, pulmonary oedema comes into effect. Due to the fluid-filled alveoli, the blood oxygen level becomes decreased, and leaves the patient short of breath (figure 1) [13]. At this point of the pathogenesis, the patient may require ventilator-assistance. Importantly, ventilator-assistance has the capacity to further promote ventilator-induced lung injury (VILI); one of the leading causes of ARDS worldwide. This can cause an exacerbated disease state and significantly contribute to pathology [14-16].

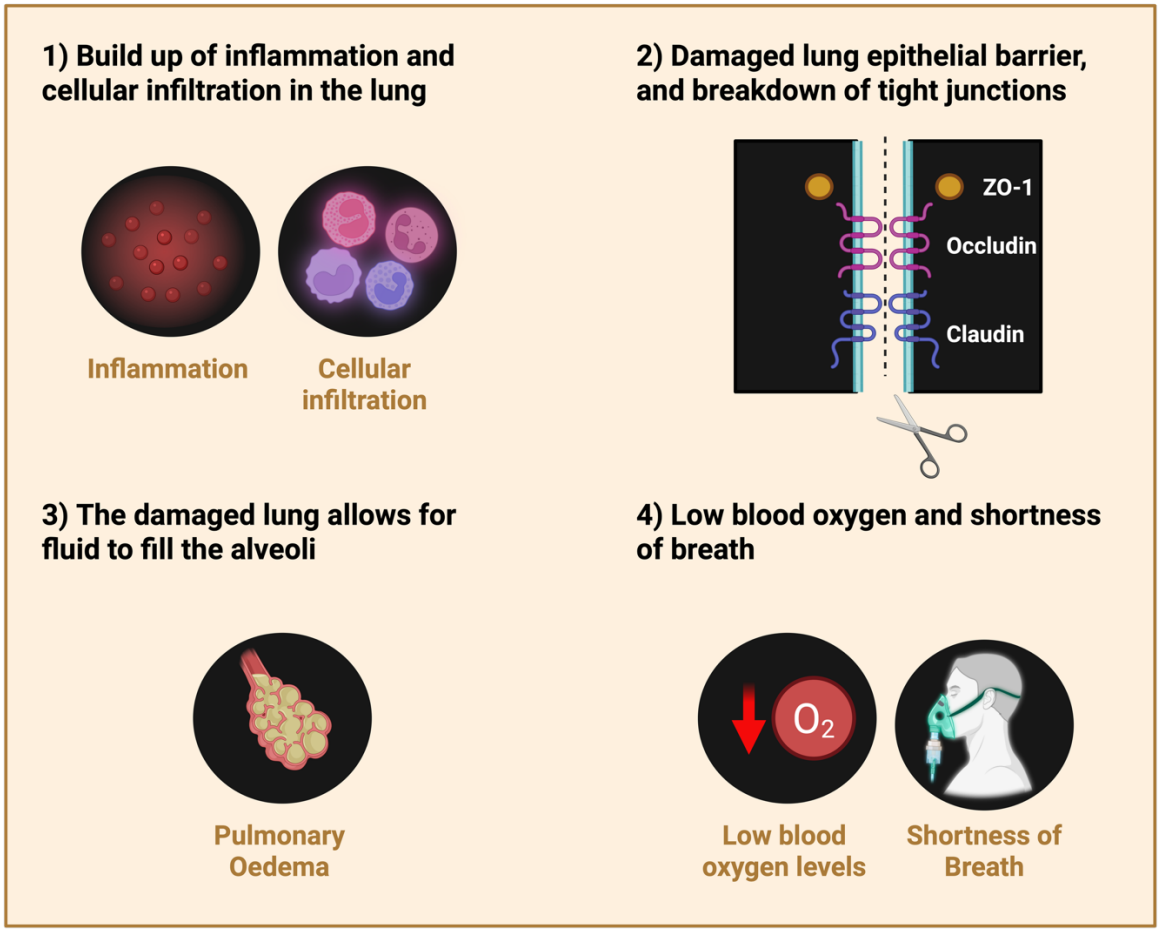

Figure 1: ARDS pathogenesis. ARDS pathogenesis is linked to a build-up of inflammation and cellular infiltration in the lung. This leads to damage in the tight junctions of the lung epithelial barrier; including zonula 1 (zo-1), occludin (ocln) and claudin (cldn). This further leads to pulmonary oedema, reduced blood oxygen levels and shortness of breath in the patient.

1.1.3 ARDS diagnostic criteria

The clinical definition and diagnostic criteria of ARDS has changed over time (table 1). The current global definition of ARDS is based on the Kigali criteria, that was defined in 2016 [17], and re-confirmed in 2024 [18]. This definition included criteria such as the requirement for high-flow nasal oxygen (HFNO) treatment at a rate of ≧ 30L/min, a PaO_2/FiO_2 of < 300mmHg and a SpO_2/FiO_2 value of ≦ 315 [17, 18]. The PaO_2/FiO_2 and SpO_2/FiO_2 values largely determine the severity of ARDS in the patients; with different ranges of values suggesting the patient has mild, moderate or severe ARDS (table 2). Prior to this updated definition, ARDS was formally defined by the Berlin definition; which included the criteria of 'required ventilation-assistance', defined by a positive end-expiratory pressure (PEEP) score of ≦ 5cm H_2O [19]. In the current definition, this measure has had reduced focus in the context of diagnostic criteria, to prevent the exclusion of patients who are being treated with less-invasive treatments, such as HFNO, but still suffer from all other components of the defining criteria [18].

Table 1: ARDS diagnostic criteria over time: 1994-2025. Highlighting the American European Consensus Conference (AECC) definition (1994), the Berlin definition (2012) and the most recent Kigali definition (2016).

Definition name	Year(s) in place	Criteria
AECC [9]	1994 - 2012	PaO_2/FiO_2 <200mmHg
Berlin definition [19]	2012 - 2016	PaO_2/FiO_2 value now indicates severity SpO_2/FiO_2 value now also indicates severity PEEP ≦ 5cm H_2O
Kigali definition [17, 18]	2016 - Now	Reduced focus on the PEEP requirement

Table 2: Current ARDS diagnostic criteria: Kigali update 2016-2025. The Kigali ARDS defining characteristics as of 2016, re-assessed and re-confirmed as of 2024 [17, 18].

Current criteria	Mild ARDS	Moderate ARDS	Severe ARDS
HFNO required	≧ 30L/min	≧ 30L/min	≧ 30L/min
PaO_2/FiO_2	200-300 mmHg	100-200 mmHg	<100 mmHg
SpO_2/FiO_2	≦ 315	≦ 235	≦ 150
Discontinued criteria			
Ventilation-assistance required	With PEEP ≦ 5cm H_2O		

1.1.4 ARDS pathophysiology

The lung is comprised of many cells. This includes alveolar epithelial cells and pulmonary endothelial cells [20, 21]. These cells are important for maintaining appropriate lung infrastructure, protecting against inhalants and must be intact for successful gas exchange in the lung [22]. The inflammatory response seen in ARDS leads to the recruitment of immune cells from the periphery. The recruitment of the immune cells leads to damage in the lung epithelial and endothelial cells, leading to the development of a permeable lung barrier [5, 23]. Once recruited, these cells can be found in the lung fluid itself or embedded in the lung tissue [24].

The two most dominant immune cells present in the ARDS lung are macrophages and neutrophils [25]. Both cell types are highly active and phagocytic in this inflammatory microenvironment. In response to the inflammation/infection present in the ARDS lung, neutrophils often release neutrophil extracellular traps (NETs) [26]. These are limb-like structures that extend from the neutrophil and protrude into the lung tissues; causing damage [27]. NETs are known to function as an antimicrobial agent, that aid in the defence against infection. NETs can do this through the production of myeloperoxidase (MPO): a microbicidal enzyme [28]. In the context of ARDS, excessive production of MPO is known to exacerbate tissue damage [29].

There is also an abundance of macrophage present in the ARDS lung. This includes alveolar macrophage and interstitial macrophage [30]. Macrophage are largely plastic and come in the form of several sub-phenotypes. In simple terms, there are several subcategories of macrophage, that are primarily defined by their inflammatory profile. The type of macrophage is largely determined by microenvironmental cues [31]. In the context of ARDS, the most prominent sub-phenotype is pro-inflammatory macrophages. These macrophages are recruited to aid in the engulfment of pathogens and limit inflammation through their anti-

inflammatory properties, that are often seen in specific macrophage sub-phenotypes [32]. However, macrophages often lean into their pro-inflammatory sub-phenotype in the context of ARDS; further exacerbating the disease state [25]. Both neutrophils and macrophages can also work together; through the binding of MPO to the mannose receptor on the macrophage [33], and through IL-1β produced from the macrophage binding to the IL-1R1 receptor on the neutrophil [34]; forming a positive feedback loop. This induces a highly reactive/pro-inflammatory macrophage and neutrophil population in the microenvironment [35]. This further influences the inflammation threshold in the lung and worsens the damaged epithelial barrier; leading to pulmonary oedema, and significant complications for the patient.

1.1.5 ARDS aetiology: the rise in SARS-CoV-2-induced ARDS

As previously mentioned, ARDS is a secondary condition of the lung that occurs in response to various primary insults. ARDS is commonly induced in response to primary conditions such as pneumonia & sepsis [2, 3]. However, due to the 2019 severe acute respiratory syndrome coronavirus 2 (SARS-CoV-2) global pandemic, whereby millions of people worldwide were exposed to this potent virus (figure 2) [36], there has been a dramatic rise in ARDS cases worldwide. Approximately 75% of SARS-CoV-2-positive patients in the intensive care unit (ICU) progressed to an ARDS diagnosis [37, 38]. In 2021, SARS-CoV-2-associated diseases, including ARDS, were the second leading cause of death worldwide; and were responsible for 8.8 million deaths globally [39]. Importantly, SARS-CoV-2-induced ARDS has a significantly higher mortality rate (~30-60%) [40] than what is seen in sepsis-induced ARDS secondary to other bacterial or viral infections (12%) [41].

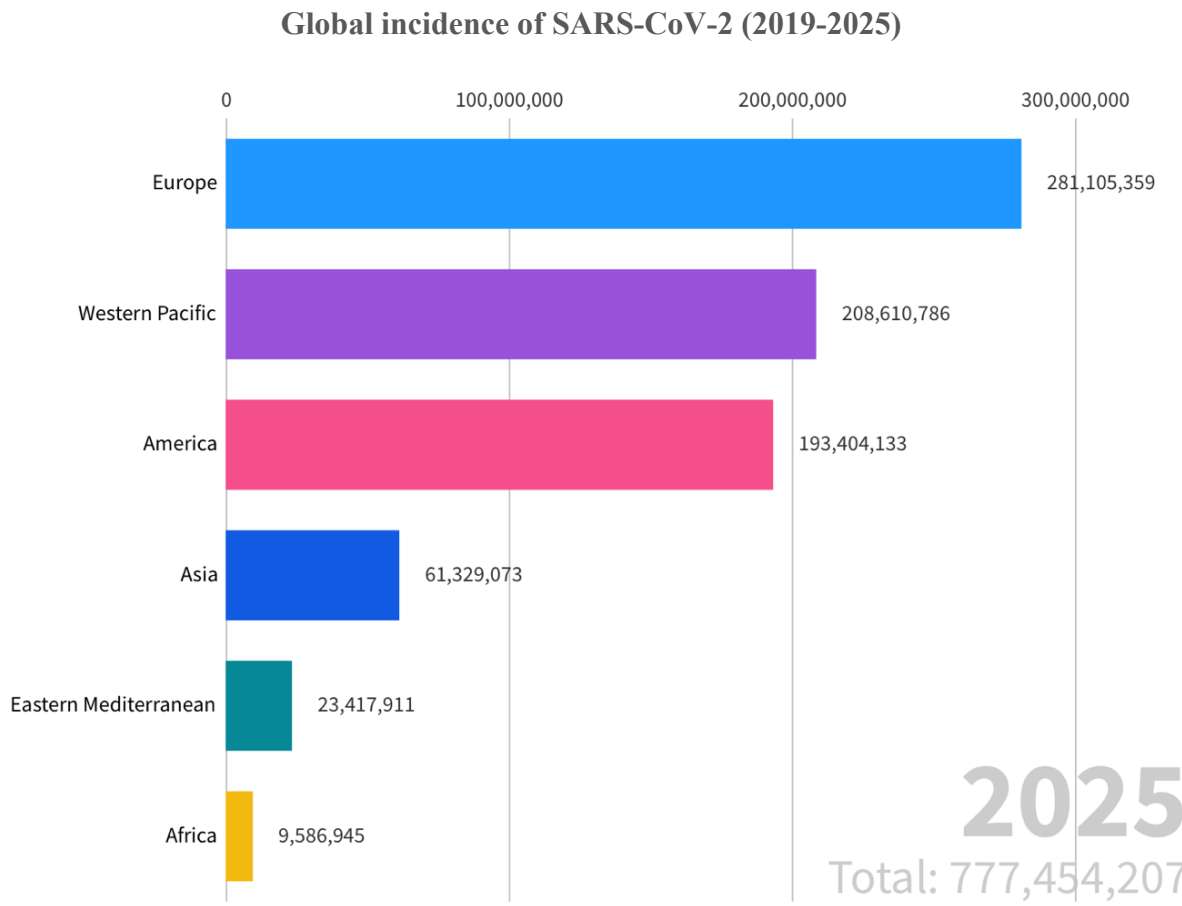

Figure 2: Global incidence of SARS-CoV-2. Highlighting the global World Health Organisation (WHO) geographical incidence of SARS-CoV-2 cases from 2019-2025 [36].

1.1.6 Classical ARDS versus SARS-CoV-2-induced ARDS

ARDS is a complex, pleiotropic condition with at least 20 aetiologies, that vary in severity and incidence [42]. Depending on the dominant target of injury, the condition will be defined as either 'primary' or 'secondary' ARDS [43]. ARDS will be defined as primary if there is damage in the type 1 and type 2 epithelial cells of the lung. This will lead to a significant reduction in gas exchange, and hypoxia in the patient. Alternatively, secondary ARDS is defined by damage to the endothelial cells; secondary to the primary damage seen in the epithelial cells. This leads to severe lung permeability, and systemic leakage of inflammatory mediators into the bloodstream [24]. In the context of classic bacterial (pneumonia) or viral (influenza)-induced ARDS, there would be an induction of primary ARDS. In the context of systemic diseases, such as sepsis, this would likely induce secondary ARDS [44, 45].

In the post-SARS-CoV-2 era, ARDS is largely divided into two sub-categories: 1) classical ARDS; including bacterial, viral and insult-induced lung injury; and 2) SARS-CoV-2-induced ARDS. Classical ARDS and SARS-CoV-2-induced ARDS share various similarities. Both subsets are characterised by inflammation, epithelial/endothelial damage, hypoxia, high mortality rates and more. Along with this, there are also several differences between the two [46, 47]. A study by Bain *et al.* (2021) highlighted that SARS-CoV-2-induced ARDS patients have generally lower levels of serum IL-6, in comparison to classical ARDS patients. This means they are often considered as 'hypo-inflammatory' ARDS patients. They also linked SARS-CoV-2-induced ARDS to an increased dependency on ventilation assistance [46]. SARS-CoV-2-induced ARDS also has a much higher mortality rate of ~30-60% [40].

The increased mortality rate seen in SARS-CoV-2-induced ARDS patients is largely due to the direct receptor-mediated impact that SARS-CoV-2-induced ARDS can have on endothelial and epithelial disruption through viral binding to the angiotensin-converting enzyme 2 (ACE2) receptor [48]. As discussed prior, there are primary and secondary forms of

ARDS; with primary being indicative of epithelial damage and secondary being indicative of secondary damage to the endothelium. In SARS-CoV-2-positive patients the membrane-bound ACE2 receptor was increased in comparison to healthy controls [49]. The ACE2 receptor is expressed in various tissues; such as in lung epithelial and endothelial cells [50]. SARS-CoV-2 has shown to bind to this receptor to enter the epithelium and endothelium of the lung (figure 3) [46, 48]. This leads to receptor-mediated damage, and high levels of lung permeability; allowing for fluid to leak into the alveoli. This direct insult on the epithelial and endothelial barriers is unique to SARS-CoV-2-induced ARDS and is not seen in classic bacterial or viral ARDS, whereby, merely inflammation and cellular infiltrates indirectly cause lung damage [51].

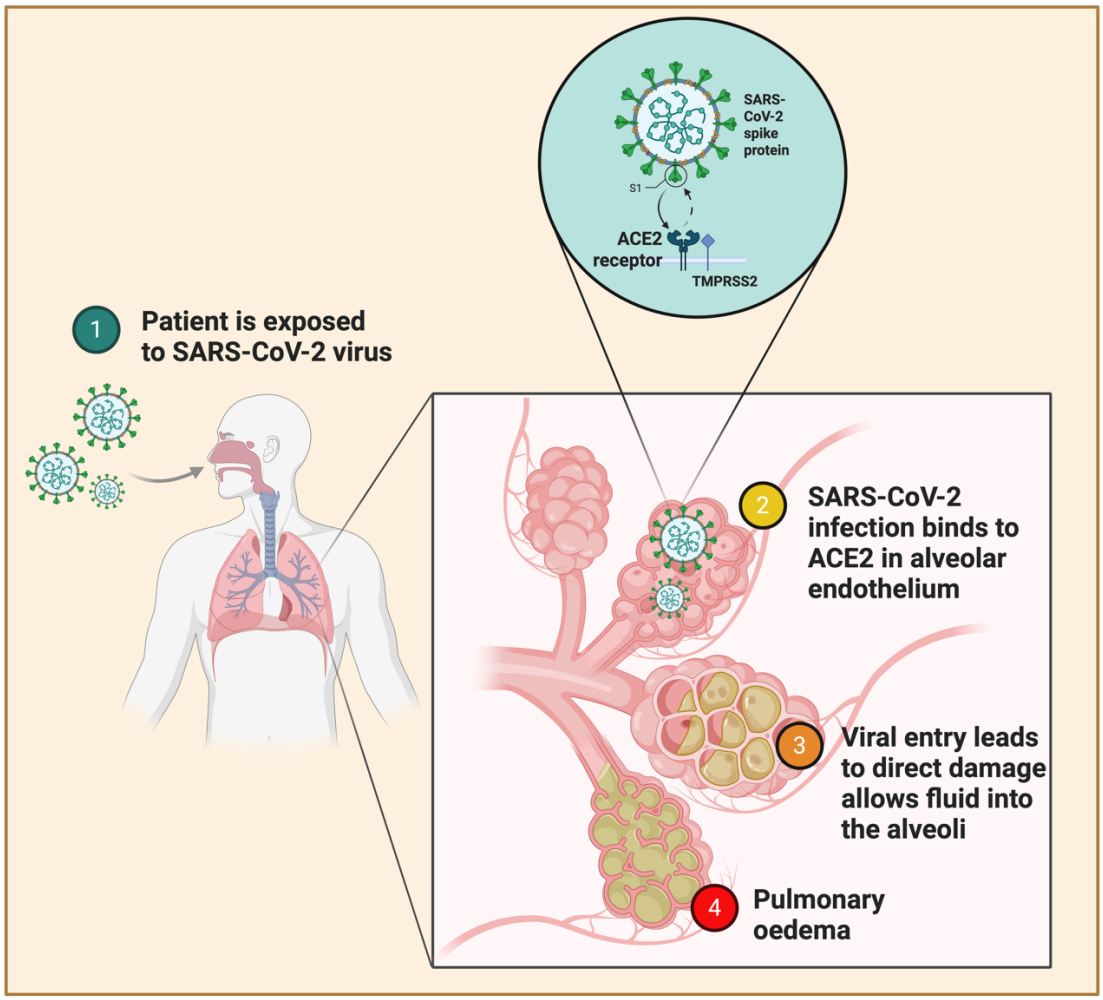

Figure 3: SARS-CoV-2-induced ARDS pathogenesis: the ACE2 receptor. Differential pathogenesis in SARS-CoV-2-induced ARDS, via ACE2 receptor binding, leading to direct endothelial and epithelial permeability and pulmonary oedema.

1.1.7 Pre-clinical models of experimental acute lung inflammation

ARDS can be, and has been, mimicked in several pre-clinical models (table 3). Many research groups focus on the induction of acute lung inflammation (ALI) through the administration of endotoxin/lipopolysaccharide (LPS) [52-55]. This model is a form of bacterial-induced ALI and is often used as a pre-clinical model of classical ARDS. Use of the LPS-induced ALI model allows researchers to mimic and observe some of the key aspects of the ARDS patient lung. This model induces high levels of inflammation, an abundance of cellular infiltration and significant tissue damage in the lung epithelium and endothelium. These are characteristics of *all* forms of ARDS; and treating these aspects of the condition are the key priority.

Along with the LPS model, there are also potent bacterial and viral models. The bacterial models include the use of *Escherichia coli* [56], *Pseudomonas aeruginosa* [57] and *Klebsiella pneumoniae* [58] in order to induce ALI. The viral models typically involve the administration of H1N1 influenza virus [59, 60], but more recently have migrated toward the use of SARS-CoV-2 viral-induction of ALI, both in standard laboratory mice [61], or in humanised ACE2-expressing mice [62]. Other models such as models of hypoxaemia [63, 64], hydrochloric acid (HCL) [65-67], smoke/vapour [68, 69] and cecal ligation and puncture (CLP) [70-72] are also frequently used to induce ALI.

In the clinic, it is likely that a patient with AHRF/ARDS will have subsequent infections that exacerbate the disease state. This led to the development of several 'two-hit models' (table 3). A study by Bilodeaux *et al.* (2023) administered a single hit of LPS, HCL or completed a lavage on mice, and followed it with ventilation assistance [73]. This allowed for the mimicking of VILI, that would be ever-present in the ICU. Other models have utilised alternative combinations of two-hit models, such as a combination of LPS and HCL [74] or a combination of a cecal slurry (CS) and hypoxaemia [75].

Table 3: Pre-clinical models of ALI.

Model	Animal(s)	Details	Source
Single-hit models			
Endotoxin/LPS	C57BL/6 or BALB/C mice	0.5mg/kg - 10ug/mouse Intratracheal (IT)/ Intranasal(IN)	[52-55]
Bacterial	Mice/Rats/ Rabbits	$2x10^9$ CFU *E. coli* $1x10^8$ CFU *K. pneumoniae* $2x10^9$ CFU *P. aeruginosa*	[57, 58, 76]
Influenza (H1N1)	C57BL/6 or BALB/C mice	LD_{40}-LD_{90} intravenously (IV)/IN	[59, 60]
SARS-CoV-2	C57BL/6 or BALB/C mice	$1x10^5$- $4x10^5$ Plaque-forming units (PFU) IN/IT	[61, 62]
Hypoxia	Mice/Rats	Hypoxia chamber	[63, 64, 77]
Smoke/vapour	C57BL/6 mice	Inhalation-exposure chamber	[68, 78]
HCL	C57BL/6 mice	0.1N HCL	[65, 66]
CLP	Mice/Rats	General CLP	[70, 72]

Two-hit models			
LPS + ventilation	C57BL/6 mice	50ug LPS IT + 25 minutes of ventilation	[73]
HCL + ventilation	C57BL/6 mice	0.1M HCL IT + 25 minutes of ventilation	[73]
Lavage injury + ventilation	C57BL/6 mice	0.15ml Saline IT + 25 minutes of ventilation	[73]
Cecal slurry (CS) + hypoxemia	C57BL/6 mice	2mg/g CS + 4-36hrs hypoxemia	[75]
HCL + LPS	BALB/C mice	0.1N HCL IT + 1mg/kg IT	[74]

1.1.8 Clinical interventions in ARDS

As of 2025, the current clinical interventions in the treatment of ARDS are limited to: ventilator-assistance [79], oxygen therapy [80], neuromuscular-blocking agents [81], use of corticosteroids [82] and immunomodulatory agents such as interleukin 1 (IL-1) and IL-6 inhibitors [83-85]. As previously mentioned, ventilation can lead to VILI, which has the capacity to exacerbate the damage in the patient [14-16]. This is also the case for oxygen therapy, whereby high concentrations of oxygen administered over time have shown to be toxic [86]. Neuromuscular-blocking agents can lead to muscle weakness and mask neurological-associated symptoms in the patient [87]. Corticosteroids appeared to be promising, with low doses of corticosteroids being somewhat effective in the treatment of ARDS, based on their immunosuppressive capacity, and their ability to reduce the overall lung injury score [82]. However, their persistent immunosuppressive capacity can cause an increased risk of infection for the patient in the ICU [88]. Steroid use can also lead to disrupted wound healing; a critical process to correct the damage associated with ARDS [89].

There are some promising trials that have investigated the use of immunomodulatory agents in the treatment of ARDS; specifically in the context of IL-1 and IL-6 inhibition [85, 90]. These studies highlighted that much of the inflammation, and therefore damage caused, in the context of ARDS is down to high levels of interleukins present in the lung. These treatments aim to combat that through the neutralisation of these molecules, ideally preventing their detrimental effects. In the sepsis-induced ARDS study [85], there was a slight increase in the prevention of multi-organ failure in the patients from this trial in response to 2mg/kg/hour of anakinra, over a period of 72 hours. Anakinra is a known and approved IL-1 receptor antagonist [91]. These studies were discontinued due to the lack of beneficial effects. The SARS-CoV-2-induced ARDS trial [90] had different results, whereby there was a significant reduction in the requirement for ventilation in the patients treated with 100mg/kg of anakinra once daily for up

to 14 days. In the context of IL-6, there have been several studies carried out that have not effectively shown beneficial effects in the treatment of ARDS [92]. This is likely due to sub-phenotypic stratification of ARDS patients; with some patients being characterised based on lower levels of IL-6, deeming this treatment ineligible. Although immunotherapy is a trending treatment approach, the studies on the relevance of this in the treatment of ARDS are not well-supported.

Importantly, it was uncovered in a 2014 study that there are two distinct phenotypes of ARDS: hypo- and hyper-inflammatory ARDS. These sub-phenotypes are largely characterised by their inflammatory profile, with hyper-inflammatory ARDS having significantly higher levels of IL-6, IL-8, IL-1 and more [93]. Considering hypo-inflammatory ARDS does not have the same level of inflammation present as hyper-inflammatory ARDS, the use of immunosuppressive agents such as corticosteroids or anakinra may not benefit those patients. With such a high mortality rate, ARDS requires more specific treatment options, not the broad options that have been explored to-date. Since ARDS is characterised by dysregulated immune cells in the lung, inflammatory responses and epithelial and endothelial damage; an approach that can both modulate the dysregulated immune system, while also aiding in repair of the damage caused, was required.

With much variation between disease presentation, sub-phenotypic stratification and general patient-to-patient heterogeneity; there have been many challenges to address in the treatment of ARDS [93]. Due to the need for a new approach that can both modulate and repair, cell therapy, specifically in the context of mesenchymal stromal cells (MSCs), has long been considered as a potential intervention for the treatment of ARDS [94, 95]. Unfortunately, this has been a challenge in itself due to the multifaceted variation to account for between both ARDS patient differences, paired with MSC-associated factors. This has made it difficult to assess appropriate clinical end-points for clinical trials; with many trials failing to reach

satisfactory outcomes within the time-frame of the primary end point [95-98]. With this in mind, a greater understanding of MSCs in the ARDS patient microenvironment is required; at both a basic research and at a clinical level.

1.2 MESENCHYMAL STROMAL CELLS

1.2.1 What are MSCs?

MSCs are a subtype of stromal cells that have the capacity to differentiate into various cell types [99]. MSCs can be derived from various tissues, such as bone-marrow (BM) [100], adipose tissue (AT) [101], umbilical cord (UC) [102], menstrual blood (MB) [103] and dental pulp (DP) (figure 4) [104]. This fascinating cell type has long been known to aid in the reduction of inflammation, and in the repair of damaged tissue, due to their immunomodulatory and regenerative capacity [105, 106], since their first recognition as a potential therapeutic agent in 1995 [107]. MSCs are often culture expanded in laboratory settings over the course of 7 days. They are plastic-adherent, spindle-shaped cells that have similar morphological properties to that of fibroblasts [108]. MSC defining-characteristics have been consistently under debate. Initially, it was thought that MSCs could be characterised based on surface markers and tri-lineage differentiation capacity [109]. However, this has since been deemed less valuable in the primary criteria for MSCs identification. The most recent published definition of MSCs, the 'Delphi-driven consensus', highlights the criteria for defining MSCs in 2025 [110]. This updated list of minimal defining criteria (table 4) focuses less on their morphological properties, and more on their functional capacity [110]. This is an ever-changing and constantly re-assessed list; but assessing the cells based on their functional capabilities, in a variety of classical functional assays, allows researchers and clinicians alike to focus on what the cells do, rather than the surface markers or differentiation capacity they possess.

MSCs have already been studied, trialled and approved in the treatment of a variety of conditions, such as; Crohn's disease [111], graft-versus-host disease (GVHD) [112], osteoarthritis (OA) [113] and amyotrophic lateral sclerosis (ALS) [114]. Administration of MSCs through various routes, such as topically [115] or intravenously [116], have proven on

several accounts to be incredibly safe and efficacious within clinical trials for the conditions listed above. There are now many MSC-based treatments on the market (table 5) [117]. Most recently, as of December 2024, we saw the approval of Ryoncil for the treatment of Steroid-refractory (SR) paediatric acute GVHD. This is the first MSC therapy on the market to acquire approval by the Food and Drug Administration (FDA) [118]. This approval allowed us to acknowledge a future for cell therapy in the context of inflammatory diseases; and drive us toward the generation of more effective therapeutics.

MSCs have long been thought of as a potential treatment for ARDS, due to their immunomodulatory [119] and reparative potential [120]. In the context of ARDS, MSCs have shown promising results in basic research; with various research groups highlighting their ability to reduce inflammation [121] and aid in repair [122, 123] in pre-clinical models of ALI. Unfortunately, this has not efficaciously translated in clinical trials to-date, but it has provided a biological rationale for the use of cell therapy in the treatment of ARDS.

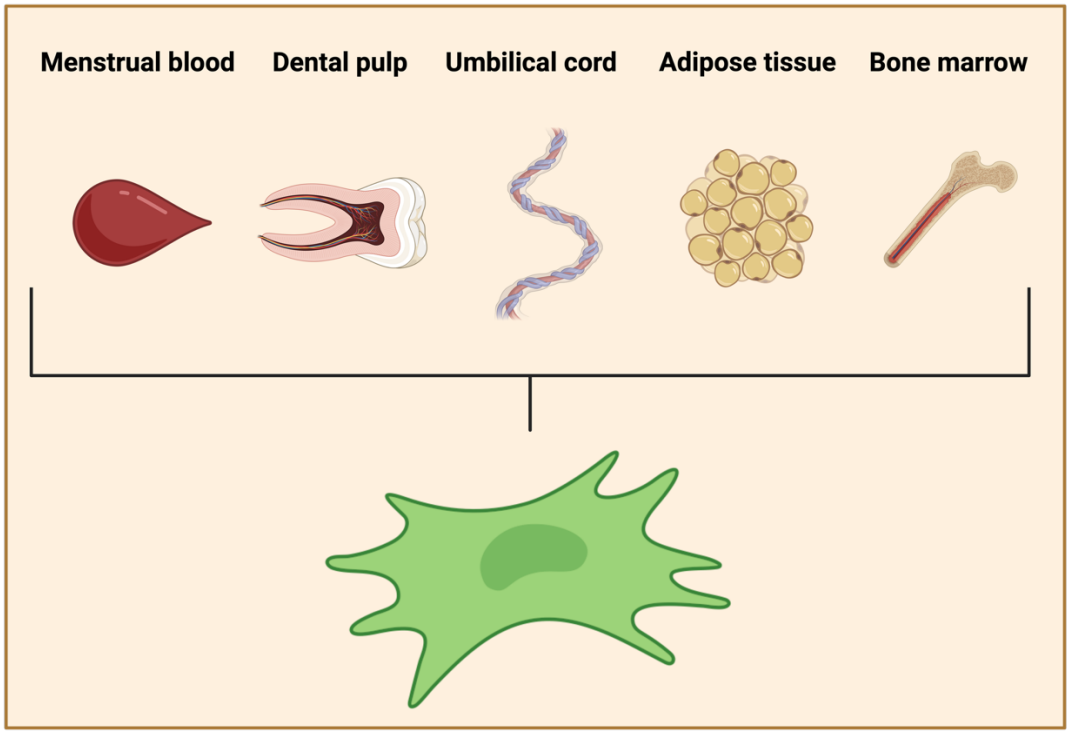

Figure 4: MSC sources. MSCs can be derived from BM, AT, UC, DP and MB. Their originating source can largely dictate their functional outcomes in clinical trials.

Table 4: The Delphi-consensus MSC-defining criteria. Adapted from Renesme *et al*. [110].

Category	Defining criteria
Terminology	'Stromal' cells, not 'stem' cells.
Surface marker expression	CD73+, CD90+, CD105+ CD45- Other markers should also be included
Tissue of origin	Source of origin should always be reported
Evidence of 'stem'-ness	If you refer to MSCs as 'stem', not 'stromal', you must provide evidence of stem-ness.
Functional assays	Functional capacity of the cells should be tested and reported prior to use in the clinic. A series of functional assays; assessing modulation, repair and other primary functions must be carried out.

Table 5: Currently approved MSC treatments to-date. MSC treatments, sources and doses of approved MSC therapies to-date (adapted from [117], including information from [118]).

Product Name	Date	Source	Dose	Treatment for:
Ryoncil	2024	BM	$2x10^6$/kg (x2 a week for 4 weeks)	SR paediatric aGVHD
Stemirac	2018	BM	Minimum of $5x10^7$	Spinal cord injuries
Mesestro-cell	2018	BM	$2x10^7$/knee	Knee OA
Alofisel	2018	AT	$5x10^6$/ml (x4)	Crohn's fistula
Stempeucel	2016	BM	$2x10^6$/kg	Critical limb ischemia (CLI)
Temcell HS	2015	BM	$2x10^6$/kg (x2 a week for 4 weeks)	GVHD
Reme-stemcel-L	2015	BM	$2x10^6$/kg to $8x10^6$/kg	SR paediatric GVHD
NeuroNataR	2014	BM	$1x10^6$/kg (x2 every 4 weeks)	ALS
Cartistem	2012	UC	$7.5x10^6$/ml	Knee OA
Cupistem	2012	AT	Based on fistula diameter	Crohn's fistula
Cellgram-AMI	2011	BM	Body weight-dependent	Acute myocardial infarction (AMI)
Queen-cell	2010	AT	$1x10^6$/ml	Connective tissue disorders

1.2.2 MSC mechanisms of action

MSCs are known for their abilities to aid in both immunomodulation and repair [124]. MSCs exert these functions in various ways. The two most common mechanisms of action (MOA) of MSCs include the secretion of paracrine factors and cell-cell contact with other cells (figure 5) [125]. MSCs constitutively secrete paracrine factors such as vascular endothelial growth factor (VEGF) [126], hepatocyte growth factor (HGF) [127] and IL-6 [128]; and to even higher levels upon pre-licensing with pro-inflammatory stimuli. These secreted factors are a mix of both immunomodulatory and reparative agents. Some studies have shown the impact of general MSC-conditioned media (MSC-CM), containing a multitude of these factors, in pre-clinical models [129-131]. Other studies have directly isolated MSC-extracellular vesicles (MSC-EVs) and observed similar results [132-134].

Cell-cell contact is a mechanism that appears to be required for certain aspects of MSC functionality [135, 136]. This occurs through basic cell-cell signalling via ligand-receptor interactions, and occasionally, through the formation of nanotubes between the MSC and the cell it has encountered, such as a macrophage [137, 138]. This mechanism involves the transfer of various organelles, primarily mitochondria, from one cell to the next [139]. This allows the MSC to donate its healthy organelles to a potentially damaged cell within a patient. This leads to a restoration of energy in the recipient cell [140, 141]. This mechanism also allows for the transfer of small molecules, such as micro ribonucleic acid (miRNAs), from one cell to the next. This can lead to altered gene expression within the recipient cell; further enhancing their functional capacity [142, 143].

In 2017, Galleu *et al.* first identified that MSCs undergo apoptosis following administration, and demonstrated the role of MSC apoptosis in mediating their therapeutic effects [144]. In 2021, this was further confirmed by Pang *et al.*, who added additional information surrounding MSC-macrophage interactions; whereby they show that the MSCs act

by releasing ‘eat me’ signals that lead to macrophage recruitment. These signals lead to the engulfment of the apoptotic MSC by the macrophage. This process is another way in which MSCs can exert their beneficial effects, through indirect measures, via macrophage-mediated anti-inflammatory effects [145]. This study further highlighted the importance of the MSC-macrophage interactions *in vivo*; a phenomenon that has been seen in many other studies to-date [146, 147]. This study showed that MSCs become apoptotic rapidly upon administration, and furthermore, showed that the administration of both viable or apoptotic MSCs had the capacity to exert the same effects *in vivo*, in a model of experimental autoimmune encephalitis (EAE) [145].

In the context of MSC immunomodulation, several studies have highlighted the capacity of MSC-derived cyclooxygenase 2 (COX-2) and indoleamine 2,3-dioxygenase (IDO) to dampen the inflammatory immune response. COX-2 is an enzyme, that when active, is known to convert arachidonic acid to prostaglandin E2 (PGE2); which MSCs are known to use to reduce inflammatory cytokines, suppress T-cell proliferation and aid in the conversion from inflammatory to anti-inflammatory macrophage [136, 148, 149]. IDO on the other hand is an enzyme that catabolizes tryptophan to kynurenine. Kynurenine functions to suppress the immune system by promoting T-cell apoptosis, aiding in the induction of regulatory T-cells and inhibiting natural killer (NK) cells [150-152].

In the context of MSC pre-reparative capacity, many studies have shown that the secretion of vascular endothelial growth factor (VEGF) and hepatocyte growth factor (HGF) can promote repair. VEGF is an angiogenic factor, known for its ability to promote proliferation and support in tissue repair. MSC-derived VEGF has shown to bind to VEGF receptor 2 (VEGFR2) on other cells to enhance tissue regeneration, repair damaged endothelial and epithelial barriers and also, in some instanced, modulate the immune system [122, 153-156]. HGF is another factor MSCs utilise to aid in their pro-reparative function. HGF has anti-

apoptotic and pro-survival effects; whereby it can promote repair by cell-death prevention. Much like VEGF, it's also known to modulate the immune response and aid in angiogenesis [127, 157, 158]. Importantly, a study by Yang *et al.*, 2015 showed that VEGF and HGF also have a synergistic effect in a pre-clinical model of ALI [159].

One interesting molecule by which MSCs signal and function is IL-6. MSC-derived IL-6 is known to function as both an immunomodulatory and pro-reparative agent [128]. In the initial stages of IL-6 secretion by the MSC, this can initiate a pro-inflammatory response; as expected in the context of IL-6. However, this pro-inflammatory induction allows for the activation of both the innate and adaptive immune cells; and allows for a full rewiring of the immune system [102]. It does this by promoting anti-inflammatory polarisation of macrophage; which can then secrete anti-inflammatory agents such as IL-10. MSC-derived IL-6 can also stimulate fibroblast activation and epithelial cell proliferation. This aids in pro-reparative capacity via both migration and proliferation of endothelial and epithelial cells [119, 128, 136, 160].

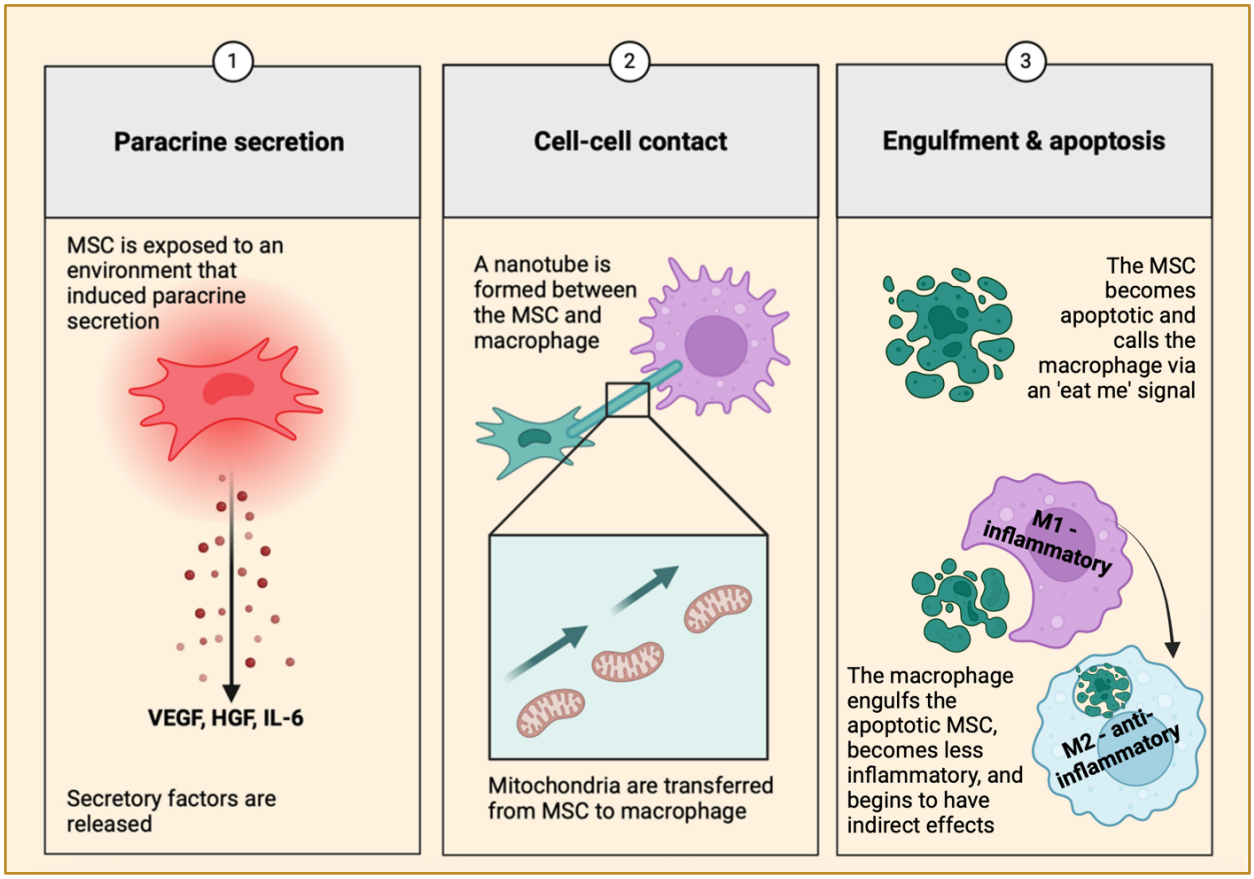

Figure 5: MSC mechanisms of action. The three primary mechanisms by which MSCs function: paracrine secretion, cell-cell contact and apoptotic-induction of macrophage engulfment.

1.2.3 MSCs in ARDS: Pre-clinical and clinical studies

MSC therapy has long been a potential therapeutic option in the treatment of ARDS [94]. Their immunomodulatory capacity allows for a treatment like that of corticosteroids, but their healing capacity also aids in repair [124]. Corticosteroids delay the healing process, and this is their primary limitation in the treatment of ARDS [89]. Cell therapy could combat this limitation. Pre-clinical studies have shown that MSCs are a useful treatment for ALI; a common model for ARDS-associated studies [54, 121, 161]. Along with this, MSCs have proven to be safe for use in the treatment of ARDS based on phase I and II clinical trials [162]. Interestingly, the pre-clinical findings of these studies have never quite translated in clinical trials; whereby only ~40% of ARDS patients respond to MSC-based treatment [97, 163, 164].

The first clinical trial of MSCs in ARDS occurred in 2014 and consisted of 12 ARDS patients, defined by the Berlin diagnostic criteria, and the administration of $1x10^6$ AT-MSCs/kg [165]. This phase I study showed that MSCs were safe but only presented weak clinical effects. There has been an abundance of MSC clinical trials in the treatment of ARDS since this initial trial (table 6); none of which have been effective enough to warrant approval for clinical use in ARDS. The most recent phase II clinical trial was carried out in 2024 and consisted of the administration of $1x10^6$ BM-MSCs/kg to SARS-CoV-2-induced ARDS patients [96]. This study reiterated that MSCs were safe for use in ARDS, however, was not therapeutically efficacious. There was a modest reduction in mortality in the MSC-treated patients, but no significant differences in inflammatory mediators as seen previously in other trials.

Table 6: MSCs in ARDS clinical trials. Adapted from [166].

Clinical Trial/Study no.	Year	Source	Dose/regime	Results
Classical ARDS clinical trials				
First reported trial/ NCT01902082 [165]	2014	AD MSC	$1x10^6$/kg	No safety hazards No efficacious difference Reduction in surfactant protein D on day 5
START/ NCT02097641 [98]	2019	BM MSC	$10x10^6$/kg	No safety hazards Significant reduction in IL-6, ANG2 and TNFR1in BAL Improved oxygenation
MUST-ARDS/ NCT02611609 [167]	2022	BM *MAPC**	$3x10^8$ - $9x10^8$ cells	No safety hazards Non-significant improvements in mortality
ONE-BRIDGE/ NCT03807804 [168]	2023	BM *MAPC**	$9x10^8$ cells	No safety hazards Non-significant improvements in mortality
REALIST/ NCT03042143 [97, 169, 170]	2019-2026	UC MSC	$1x10^8$ - $4x10^8$ cells	No safety hazards ON-GOING STUDY

SARS-CoV-2-induced ARDS clinical trials				
ChiCTR 2000031494 [171]	2020	UC MSC	$2x10^6$/kg	No safety hazards Significant reduction in clinical symptoms Significant reduction in IL-6 and CRP
NCT04392778 [172]	2021	UC MSC	$3x10^6$/kg	No safety hazards Significant reduction in mortality Significant reduction in inflammation
NCT04457609 [173]	2021	UC MSC	$1x10^6$/kg	No safety hazards Significant reduction in mortality Significant reduction in IL-6
NCT04288102 [174]	2021	UC MSC	$4x10^7$	No safety hazards Repaired lung lesions
NCT04355728 [95]	2022	UC MSC	$1x10^8$	No safety hazards Significant reduction in mortality Significant reduction in inflammation
NCT04333368 [175]	2022	UC MSC	$1x10^6$/kg	No safety hazards No difference in primary outcome
U111-1254-9819 [176]	2022	UC MSC	$5x10^5$/kg	No safety hazards Significant reduction in IL-6, MCP-1, ferritin, CRP and neutrophil number

NCT04371393 [164]	2023	BM MSC	$2x10^6$/kg	No safety hazards No difference in primary outcome
NCT03042143 [177]	2023	UC MSC	$4x10^8$	No safety hazards No difference in primary outcome
NCT04493242 [178]	2023	BM EVs	0.9-1.2 trillion EVs	No safety hazards Non-significant reduction in mortality
NCT04615429 [96]	2024	BM-MSCs	$1x10^6$/kg	No safety hazards Non-significant improvement in recovery

1.2.4 MSC-licensing

Among some of the ways researchers have attempted to improve MSC therapy includes MSC-licensing. This is the pre-conditioning of MSCs with pro-inflammatory stimuli, to enhance their therapeutic efficacy [179]. This comes from the idea that MSCs require an activation signal [180] to exert their beneficial effects; including enhanced immunomodulation of macrophage and neutrophils [181, 182], enhanced repair of damaged tissue [183] and anti-microbial activity [184] in various clinical settings. Various inflammatory stimuli have been utilised in MSC-licensing studies (table 7). One of the most common stimuli used for MSC-licensing is interferon gamma (IFNɣ) [185-187]. This has shown to be a highly effective licensing treatment and allows for MSCs to reach an enhanced level of therapeutic efficacy in many pre-clinical studies. Along with IFNɣ, other inflammatory stimuli such as tumour necrosis factor alpha (TNFα) [188], IL-1β [189] and macrophage migration inhibitory factor (MIF) [190] have been used as licensing agents; often in combination with IFNɣ. This explains why MSCs have been so effective in the treatment of inflammatory disease.

As mentioned previously, the ARDS patient microenvironment contains a variety of inflammatory mediators, including all licensing agents mentioned above [191]. With that in mind, and MSCs being highly efficacious in inflammatory environments, it was assumed that they would make a good candidate in the treatment of ARDS. Pre-clinical data has also largely agreed with this; but this has not translated in the clinic. A 2018 study carried out by Islam *et al* [192] highlighted that the microenvironment that hBM-MSCs are placed into can have detrimental effects on their therapeutic capacity. They showed that naïve MSCs in a less-than-desirable lung environment could further exacerbate disease; rather than helping to reduce inflammation and disease score. They also showed that licensing the same cells with IL-10 and/or HGF led to an efficacious cell therapy. This further supports the argument that licensing

the cells may be required for an effective cell therapy; and highlights the need to prioritise understanding the microenvironment, and the effect this can have on the cells.

Importantly, we know that ARDS can be categorised into differential sub-phenotypes: hypo- and hyper-inflammatory ARDS [93]. This is an important, but often neglected, aspect when considering MSCs in the treatment of ARDS. It's possible that MSCs, when placed in the high inflammatory hyper environment, can become licensed and functional to their full capacity. On the other hand, MSCs placed into the lower inflammatory hypo environment, may not be as efficacious. It has been shown on several occasions that MSCs placed into an environment lacking a threshold level of inflammation can exacerbate disease [152, 193]. In the ARDS patient microenvironment, there is an abundance of cytokines such as IL-6, TNFα and MIF seen in hyper-inflammatory patients. These are all stimuli that are known to license MSCs [122, 189, 190], and in theory, should enhance their therapeutic efficacy in the treatment of ARDS. Although this has been proven in pre-clinical models of ALI, this has not effectively translated in the clinic; likely due to a lack of patient stratification. An alternative solution to this would be to pre-license the cells in the lab prior to use in the clinic, or to identify the key components produced by the cell that cause the therapeutic effects across *all* patients.

Interestingly, none of the MSC-based treatments that have been used in clinical trials for ARDS involved pre-treatment or licensing, despite the abundance of literature stating the need for licensing [194, 195]. It was predicted that the ARDS patient microenvironment would have sufficient inflammation to license the cells within the body. Given that ~40% of ARDS patients respond to therapy, and only ~40% of ARDS patients are also characterised as hyper-inflammatory [196], it would be interesting to see if there's a positive correlation between hyper-inflammatory ARDS patients and MSC therapeutic efficacy. This highlights the urgent unmet need for patient stratification prior to clinical trial initiation.

Table 7: MSC-licensing studies over time.

Licensing agent	Source	Result(s)
Inflammatory stimuli		
IFNɣ [100-103]	Human BM/AT	Increased IDO, PD-L1, COX-2 Enhanced immunosuppression Enhanced glycolytic capacity
IL-1β [104, 105]	Human BM/UC	Increased COX-2, IL-8, IL-6 IL-10, IL-1RN & VEGF Enhanced immunosuppression Enhanced migration capacity
IFNβ [106]	Mouse BM	Increased CCL2, HGF, PD-L1 Enhanced immunosuppression Enhanced glycolytic capacity
TGFβ [107]	Human BM	Increased TSG-6 & CXCL6 Enhanced Immunosuppression
TNFα + TGFβ [108]	Human BM	Increased CCL2, CXCL8, COX-2
TNFα & IFNɣ [109-111]	Human BM/UC	Increased IDO, PD-L1 & TSG-6 Enhanced immunosuppression Enhanced glycolytic capacity
TNFα IL-1β & IFNɣ [93, 112]	Human UC	Increased IL-8 & IL-1RN Enhanced recruitment and pro-reparative capacity
TNFα, IL-1β & IFNɣ & IL-17 [113]	Human UC	Increased TGF, TSH-6, PD-L1, COX-2, IDO, ICAM Enhanced immunosuppression Enhanced glycolytic capacity

ARDS-microenvironmental stimuli		
ARDS bronchoalveolar lavage fluid (BALF) [97]	Human BM	Increased expression of MMP3, IL-6, IL-36, FAS & IL-8
ARDS serum [114, 115]	Human BM	Increased IL-10, IL1RN & VEGF Enhanced pro-reparative capacity Enhanced cytoprotective capacity

1.2.5 MSC: Neutrophil interactions

Although MSCs are often spoken about in the context of their interactions with T-cells [151] and macrophage [188], they play an important role in neutrophil modulation as well; which is of importance given that neutrophils are the key drivers of ARDS [26]. Neutrophils are a fascinating cell type, that are linked to the innate immune system. They are the most abundant branch of leukocyte and they are produced in the bone marrow and sent to the blood stream to fight infections. Some of the key functions of neutrophils include phagocytosis, degranulation [197], reactive oxygen species (ROS) production [198] and NETosis [199]. MSCs, especially upon administration to ARDS patients, will likely come into contact with neutrophils within the body. As mentioned previously, MSCs can prolong neutrophil survival, through their secretion of IL-6 [200]. Along with this, they can attract neutrophils by the production of chemokines such as CXCL8 and CXCL1 [189]. Other studies have shown that MSCs can reduce neutrophil-associated ROS production [161], reduce neutrophil-associated inflammation [161] and enhance phagocytosis to aid in bacterial clearance [201]. This makes MSC an excellent candidate for the treatment of neutrophil-attributed diseases such as ARDS; as they don't diminish their acute response, but they do modulate them to prevent exacerbated responses. However, in the context of ARDS, this has not been efficacious.

1.2.6 Limitations of MSCs in ARDS: the ARDS patient microenvironment

Although MSCs are an attractive potential treatment for ARDS, there are several limitations. One limitation can be seen in the mass production of MSCs for treatment. MSC treatments are costly, and unattainable for many patients [202]. Mass culture of MSCs requires large teams of professionally trained manufacturing scientists, a labour-intensive process requiring culture expansion most often in 2D-culture making the process itself costly and time-consuming. It can take several weeks to grow the cells to the level that's required for treatment preparation.

Another complication of MSC therapy can be seen in patient heterogeneity [203]. For the most part, MSCs will be taken from the patient themselves, and administered back to the patient they came from. This is an example of autologous cell therapy. However, not all MSCs are as functionally efficacious as one another. Patient A may respond well to this treatment, but if Patient B has defective cells, or a complex internal microenvironment; the cells may not be potent enough as a treatment. In the case of allogeneic MSC treatments, where one functionally efficacious MSC donor is used to treat many patients, and this should involve less variation. MSCs require specific culture conditions and become functionally defective after passaging past passage 6/7 [204]. To combat this, strenuous batch testing is performed regularly. This includes the performance of cell counts, contamination studies, cellular phenotyping, viability assessments and more [205]. Any anomalies in these tests lead to the exclusion of large batches of these costly treatments.

An additional limitation, specific to MSCs in the treatment of ARDS, can be seen in the microenvironmental impact of the ARDS patient, and the differential impact this may have on MSC-based therapy (figure 6). Microorganisms of the lung have shown to impact MSC functional capacity [206]. Inflammatory profile differences could account for insufficient MSC-licensing signals [152, 194]. Free fatty acids (FFAs) in the lung could also impact MSC functionality; through both their inflammatory nature and via their receptor-mediating effects.

FFAs are known to bind to the peroxisome proliferator-activated receptor beta/delta (PPARβ/*δ*) nuclear receptor; a receptor that is known to impact MSC-therapeutic efficacy [207-210]. A way to combat this issue would involve pre-licensing the cells *in vitro* and making use of their paracrine-secreted factors in the form of MSC-based products: such as the use of MSC-CM or MSC-EVs. Alternatively, we could place more focus on the exact agents the cells provide that have their beneficial effects, isolate them, and administer them to the patient. Although this seems like a good idea, there are several things that MSCs do, and it's unlikely isolating a selection of factors would be enough to have the same therapeutic effect as the cells/cell-based products themselves.

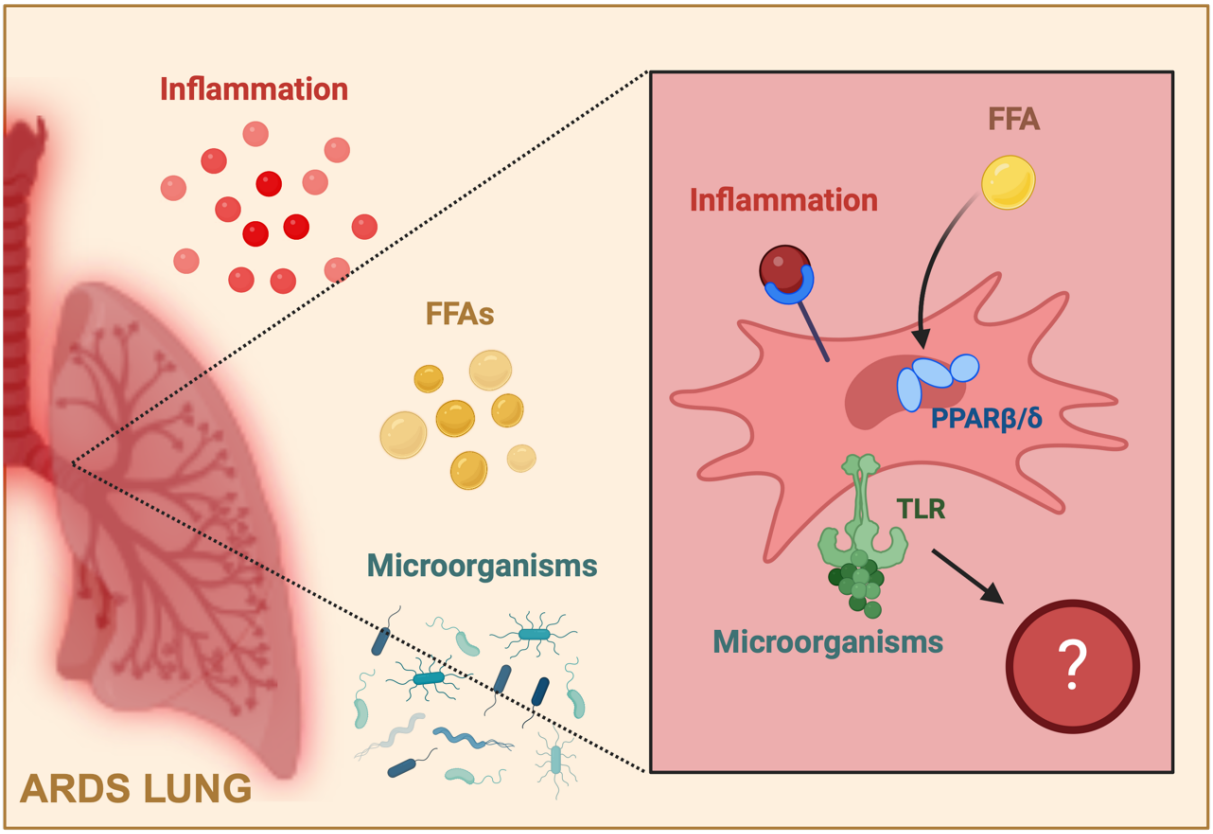

Figure 6: MSCs in the ARDS patient microenvironment. The complex ARDS microenvironment containing inflammation, FFAs and microorganisms; all of which could differentially impact MSC therapeutic efficacy. This occurs through the activation of their corresponding receptors: such as toll-like receptors (TLRs) or the PPARβ/*δ* receptor.

1.3 PEROXISOME PROLIFERATOR-ACTIVATED RECEPTOR β/δ (PPARβ/δ)

1.3.1 What are PPARs? Introduction to PPARβ/δ

Peroxisome proliferator-activated receptors (PPARs) are ligand-inducible transcription factors (TFs), that are known for the role they play in the transcriptional regulation of various genes [211]. There are three primary isoforms of PPAR: PPARα, PPARγ and PPARβ/δ. Each isoform of PPAR works in a slightly different manner, to assist in many differential functions within the cell [212]. In recent years, PPARβ/δ has shown to play an important role in human health and disease, despite being the least studied of the receptors [213]. The focus on PPARβ/δ specifically within this project stems from hBM-MSCs expressing PPARβ/δ to a much greater level than other isoforms of PPAR; making it much more relevant as a point of focus in this study.

1.3.2 Structure of PPARβ/δ

PPARβ/δ is a soluble nuclear receptor that consists of five dominant regions; two activation domain (AD) regions (AD1 (N-terminal) and AD2 (C-terminal)), a DNA-binding domain (DBD), a ligand-binding domain (LBD) containing the AD2 region, and a hinge region for elasticity (figure 7) [214]. AD1 is largely involved in ligand-dependent transactivation upon binding of a ligand to the complex [215]. The LBD itself is the location in which the ligand binds, leading to an AD2-mediated conformational change. This allows for the activation of the receptor [216]. Upon activation of the receptor, it forms a heterodimer with the retinoid-X receptor (RXR) and leads to the binding of DNA to the DBD. The DNA that binds to the DBD is referred to as the peroxisome proliferator response element (PPRE) and allows for the induction of PPARβ/δ-associated target genes [214].

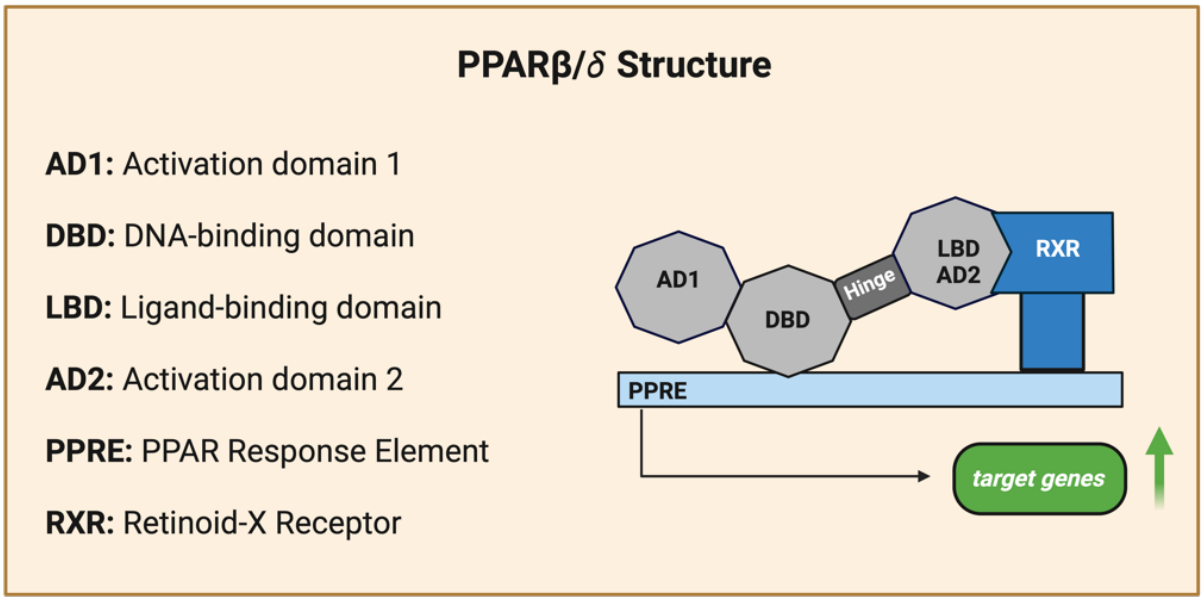

Figure 7: Biological structure of the PPARβ/δ receptor. The PPARβ/δ receptor is comprised of 5 dominant regions: AD1, DBD, a hinge, LBD and AD2.

1.3.3 The PPARβ/δ signalling pathway

Upon ligand-binding, PPARβ/*δ* undergoes a conformational change that allows for heterodimerisation with RXRα. Both PPARβ/*δ* and RXRα are orphan receptors (table 8), and upon dimerization, they form the PPAR-RXR complex [214, 217]. This is essential for PPARβ/*δ*'s biological activity (figure 8). Once the PPAR-RXR complex has been established, the DBD, is able to bind to DNA; specifically at the PPRE sequence: AGGTCANAGGTCA [217-219]. This allows for the complex to carry out its TF functions.

It is also well studied that induction of the general PPAR signalling, of any isoform, leads to the inhibition of other signalling pathways (figure 8). This includes interferences in protein complexes involved in NFκB, AP and STAT signalling [220]. A study by Zingarelli *et al.* (2010) highlighted that PPARβ/*δ* signalling, specifically, reduced NFκB signalling through displacement of the p65 sub-unit of NFκB in the promoter regions of the *tnfa* gene [221]. In the context of MSCs, the NFκB pathway is vital for the production of various immunomodulatory agents; such as tumour necrosis factor-inducible gene 6 (TSG-6) [222], cyclooxygenase 2 (COX-2) [149] and various chemokines [223].

Table 8: Orphan receptors and their corresponding ligands [224].

Receptor name	Abbreviation	Ligands
Peroxisome proliferator-activated receptors	PPARs	Eicosanoids, FFAs, Vitamin B3, carbaprostacyclin
Retinoid X receptor	RXR	Rexinoids
Constitutive androstane receptor	CAR	Androstanol
Liver X receptor	LXR	Oxysterols
Farnesoid X receptor	FXR	Chenodeoxycholic acid
Pregnane X receptor	PXR	Rifampicin

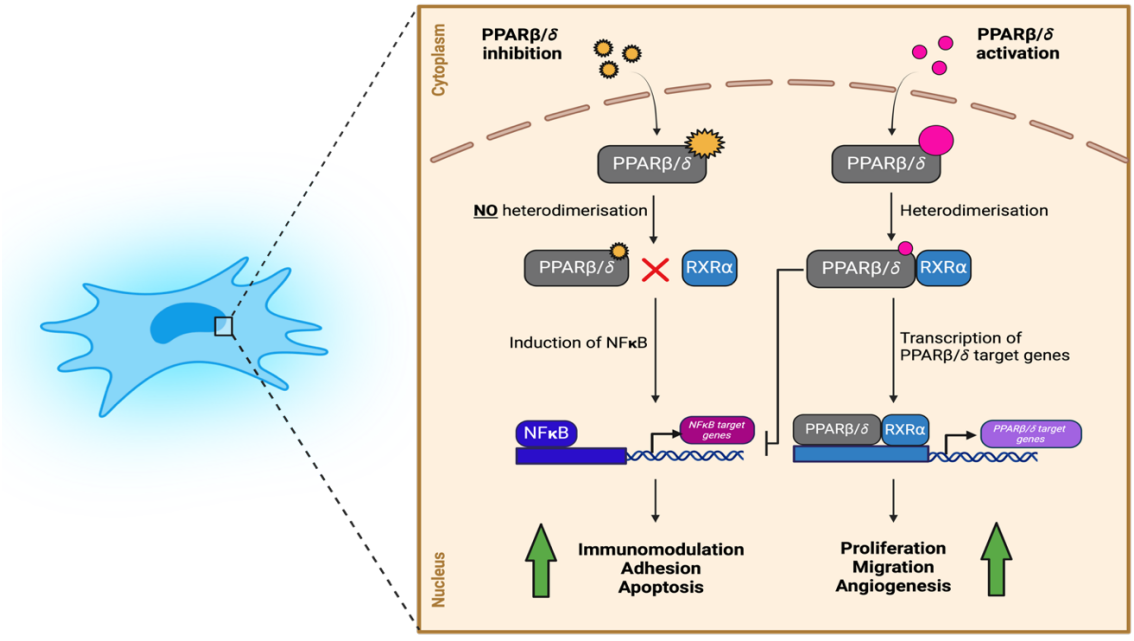

Figure 8: The PPARβ/δ receptor signalling cascade in MSCs. Upon activation of the PPARβ/δ receptor in MSCs, a confirmational change allows for the heterodimerisation with the RXR receptor and leads to the induction of various PPARβ/δ target genes.

1.3.4 PPARβ/δ ligands, co-activators and co-repressors

There are many naturally occurring ligands of PPARβ/δ. This includes metabolites such as FFAs, eicosanoids, vitamin B3 and carbaprostacyclin. Some of the most common FFAs that bind to PPARβ/δ include palmitic acid, oleic acid and palmitoleic acid [225]. Along with the naturally occurring ligands, that are all present in the human body, there are also many synthetic agonists of the PPARβ/δ receptor. Some of the most used synthetic agonists of PPARβ/δ include GW0742, GW501516 and L-165,041 [226]. Along with synthetic agonists of PPARβ/δ, there are also synthetic antagonists of PPARβ/δ. Some of the most common synthetic antagonists of PPARβ/δ include GSK3787 and GSK0660 [227].

It's important to note that PPARβ/δ function not only depends on ligand-binding, but also the presence or absence of PPARβ/δ-associated co-activators and co-repressors [215]. Upon binding of a ligand to the LBD of the receptor, there is a conformational change in the AD2 domain, leading to the recruitment of either co-activation or co-repressor complexes [228]. Co-activators are proteins that are required to fully activate the PPAR-RXR complex, and are recruited in response to PPARβ/δ-associated ligand-binding. This is known as ligand-dependant transactivation. Transcriptional co-activators of PPARβ/δ include CREB-binding protein (CBP), steroid receptor co-activator 1 (SRC1) and a group of general nuclear receptor co-activators (NCOA) [229]. In contrast, co-repressors are proteins that respond in the *absence* of ligand-binding. Co-repressors include nuclear receptor corepressors (NCoR) and silencing mediators of retinoid and thyroid hormone receptors (SMRT). They work by inducing an antagonistic response, that prevents the activation of the complex [219]. This is called ligand-independent trans-repression [215].

To activate the complex when a co-repressor is bound, agonistic ligands act to remove the co-repressors via ubiquitination. This leads to the degradation of the co-repressor and

allows for the activation of the complex. Co-activators and their associated TFs are then recruited to improve the transcriptional abilities of the complex (figure 9) [230].

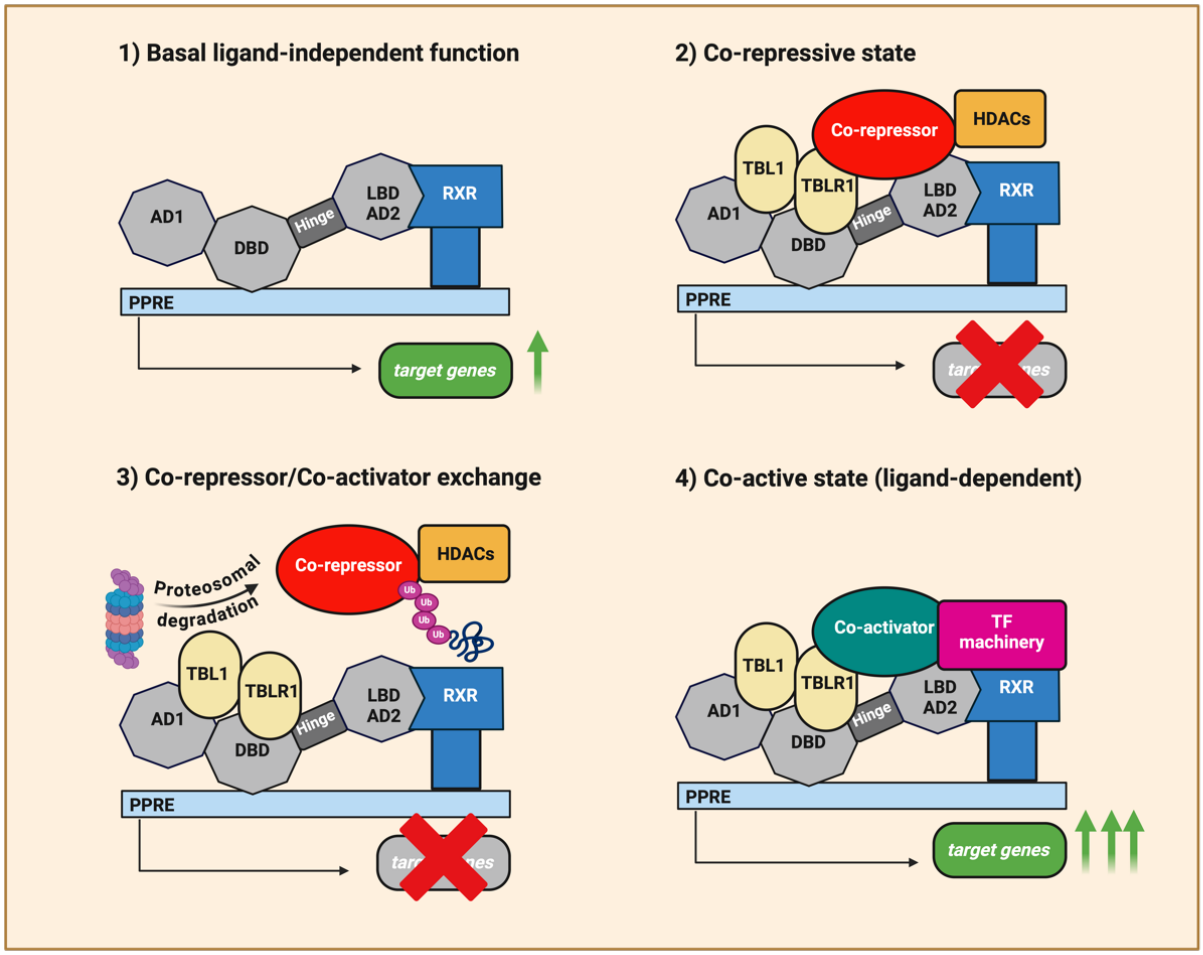

Figure 9: Co-activator and co-repressor binding to PPARβ/δ. If a co-repressor is bound, this limits PPARβ/δ receptor activator capacity. Removal of this corepressor, via ubiquitination, can allow for co-activators to bind, allowing the receptor to carry out its biological functions.

1.3.5 Functions of PPARβ/δ

PPARβ/*δ* is predominantly expressed in metabolically active tissues. It is also a well-known TF, meaning that it is involved in the control of several genes [231]. Some of its primary functions include aiding in lipid metabolism, glucose metabolism, tumorigenesis and inflammation [232]. PPARβ/*δ* has been shown to be enriched in hyperglycaemic patients. Hyperglycaemia is a high blood glucose condition characterised by insufficient insulin secretion in the body. Activation of the PPARβ/*δ* receptor enhances lipid metabolism, decreasing lipid accumulation. This in turn leads to an increase in glucose metabolism; reducing the overall sugar level in the patient [225].

The role that PPARβ/*δ* plays in lipid metabolism also crosses into its role in tumorigenesis. In cancer cells, PPARβ/*δ*'s promotion of β-oxidation enhances the proliferation qualities of the receptor, which is seen in many tumours, along with the overexpression of PPARβ/*δ* [233]. Inflammation is complex in the context of PPARβ/*δ*, as it's unclear whether the receptor shows pro- or anti-inflammatory properties. Administration of PPARβ/*δ* agonists, such as GW0742, have shown to reduce inflammation in encephalomyelitis. This is largely due to a reduction in IL-12, IL-23 and an increase in IL-4 and IL-10 [234]. This was also seen in diabetes, whereby PPARβ/*δ* agonism resulted in reduced inflammation through the suppression of monocyte chemoattractant protein 1 (MCP-1) and osteopontin (OPN) [235]. Interestingly, although PPARβ/*δ* agonism appears to reduce inflammation in some contexts, it also plays a role in promoting inflammation in psoriasis. This can be seen through PPARβ/*δ*-induced immune dysregulation, and upregulation of T-cell responses [233, 236, 237].

1.3.6 Presence of PPARβ/δ ligands in the ARDS patient microenvironment

The ARDS patient microenvironment is highly complex; with an abundance of inflammation, FFAs and microorganisms [238]. Each of these components can differentially impact cell therapy. Several studies have shown elevated levels of FFAs in the diseased lung microenvironment; which would likely activate the PPARβ/*δ* receptor in the MSCs upon administration to the patient [239, 240].

A SARS-CoV-2 study by Archambault *et al*. (2021) highlighted high levels of eicosanoids and docosanoids in the lungs of severe SARS-CoV-2 patients, in comparison to healthy controls [241]. Eicosanoids are one of the most prominent ligands of PPARβ/*δ* [225]. This was also seen in a study by Zaid *et al*. (2021), whereby severe SARS-CoV-2 patients showed elevated levels of eicosanoids in the BALF [242]. Another known ligand of PPARβ/*δ* is FFAs [225]. Lu *et al*. (2024) highlighted a correlation between elevated serum FFAs and ARDS diagnosis; attributing higher levels of FFAs to a higher likelihood of ARDS [239].

1.3.7 Implications of PPARβ/δ modulation in MSCs

Several studies have now shown that PPARβ/*δ* activation can alter MSC functionality (figure 10). The current literature shows that PPARβ/*δ* activation has anti-apoptotic properties [243] in mouse bone marrow-derived MSCs; while PPARβ/*δ* inhibition leads to enhanced levels of apoptosis [236]. This is an important observation due to the apoptotic MOA of MSCs [145]. Along with this, PPARβ/*δ* activation promoted MSC proliferation [216] and angiogenesis [208]. Activation of PPARβ/*δ* in a similar cell type, multipotent adult progenitor cells (MAPCs), led to reduced cellular retention; when in combination with IFNɣ-licensing [148]. MAPC's are similar to that of MSCs as they also promote anti-inflammatory effects; however, MAPCs are morphologically different from MSCs, and have a much broader differentiation capacity [244]. They have even been used in two ARDS clinical trials as seen in table 6 [167,

168]. Other studies have shown that MSCs derived from PPARβ/δ knock-out mice have enhanced immunosuppressive capacity on Th1 and Th17 cells [245, 246] and an enrichment in the expression of adhesion molecules, such as intercellular adhesion molecule 1 (ICAM1) and vascular cell adhesion molecule 1 (VCAM1) [245]. There was also increased glycolytic capacity in MSCs derived from PPARβ/δ knock-out mice [246].

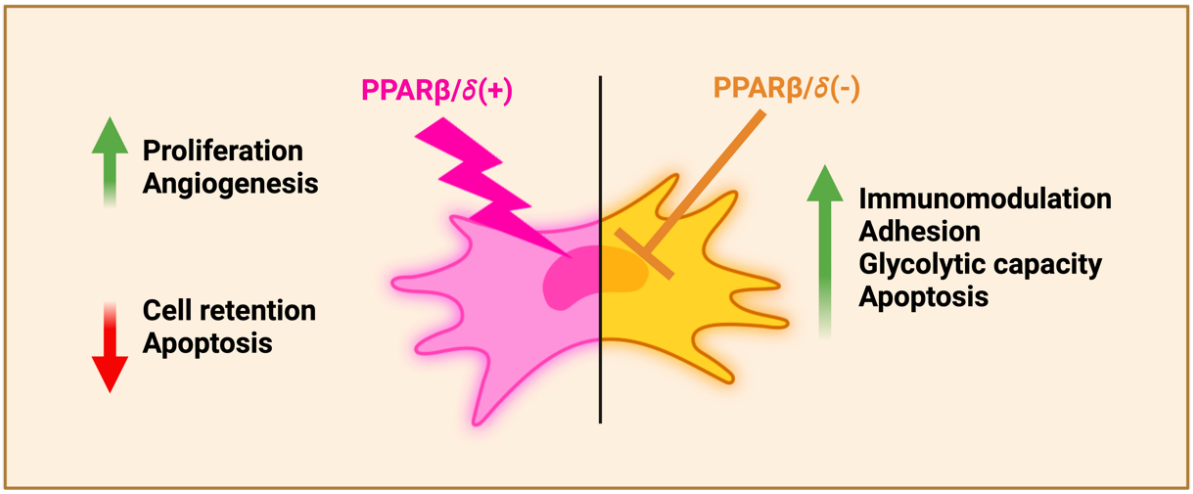

Figure 10: The functional impact of PPARβ/δ in MSCs. PPARβ/δ agonism has shown to lead to increased proliferation and angiogenesis [208], and decreased cell retention [148] and apoptosis [243]. On the other hand, PPARβ/δ antagonism has shown to increase immunomodulatory capacity [245], adhesion efficiency, glycolytic capacity and apoptosis [246] in mouse MSCs.

1.4 GAPS IN THE LITERATURE

Although MSCs have been studied in the context of ALI and ARDS for many years, there are still countless things to address. One of the primary gaps to bridge can be seen in the lack of patient stratification seen within clinical sample studies, and within clinical trials themselves. Given the 2014 publication by Calfee *et al.*, this is likely of great importance, as patients can be characterised vastly different from one another [93]. Along with this, understanding the true mechanisms by which MSCs carry out their functions are imperative to knowing the true meaning behind their therapeutic efficacy. Although many mechanisms have already been identified, there is still much we don't know; with complex interactions between various cell types simultaneously yet to be determined in a concrete manner.

1.5 THESIS HYPOTHESIS AND AIMS

We hypothesized that the ARDS patient microenvironment, and its contents, would differentially impact MSC therapeutic efficacy in a pre-clinical model of endotoxin/LPS-induced ALI.

The aims of this study included:

1) Identifying the differential role(s) of PPARβ/*δ*-modulated human MSCs *in vitro*.
2) Determining the mechanisms of action behind the discovered role(s) of PPARβ/*δ*-modulated human MSCs *in vitro*.
3) Investigating how PPARβ/*δ*-modulation effects MSC functionality *in vivo* in a pre-clinical model of acute lung inflammation.
4) Confirming the influence of the differential impact of clinically relevant hypo- and/or hyper-inflammatory ARDS patient samples on PPARβ/*δ*-modulated MSC therapeutic efficacy *in vivo*, in a pre-clinical model of acute lung inflammation.

Chapter 2

TNFα-licensed MSCs show enhanced immunomodulation of neutrophils in a model of experimental acute lung inflammation

2.1 Abstract

Mesenchymal Stromal Cell **(**MSC)-licensing has long been studied in the field; with a primary emphasis on the combination effect of various licensing stimuli. One licensing stimulus that is often observed is tumour necrosis factor alpha (TNFα). In the context of other licensing studies, TNFα is often used in combination with interferon gamma (IFNɣ). The capacity for IFNɣ-alone has been investigated in many studies to-date, however, the individual capacity for TNFα to license MSCs is often neglected. This aim of this study was to identify the role that TNFα alone plays in heightening the MSC therapeutic response, in a model of experimental acute lung inflammation (ALI). Human bone marrow-derived MSCs (hBM-MSCs) were stimulated with human recombinant TNFα and sent for bulk RNA sequencing. The sequencing dataset highlighted a prominent enrichment of chemokines, such as *CXCL8, IL-1β, ICAM1* and *CXCL1*. This would suggest a potent neutrophil-associated interaction. Through the process of mining a publicly available dataset, it became clear that naïve hBM-MSCs could play a role in dampening the production of neutrophil extracellular traps (NETs). It was hypothesised that licensed hBM-MSCs would further enhance this. *In vitro* assays highlighted that although hBM-MSCs could not alter the presence of NETs, they could reduce their activity; which was measured based on the release of myeloperoxidase (MPO); a potent microbicidal agent that exacerbates the tissue damage seen in acute respiratory distress syndrome (ARDS). Using an *in vivo* model of LPS-induced ALI it was determined that there was also a reduction of MPO and IL-1β in response to TNFα-licensed hBM-MSCs. TNFα-licensed hBM-MSCs play a role in altering the neutrophil response, by limiting NET activity in a model of ALI.

Graphical Abstract

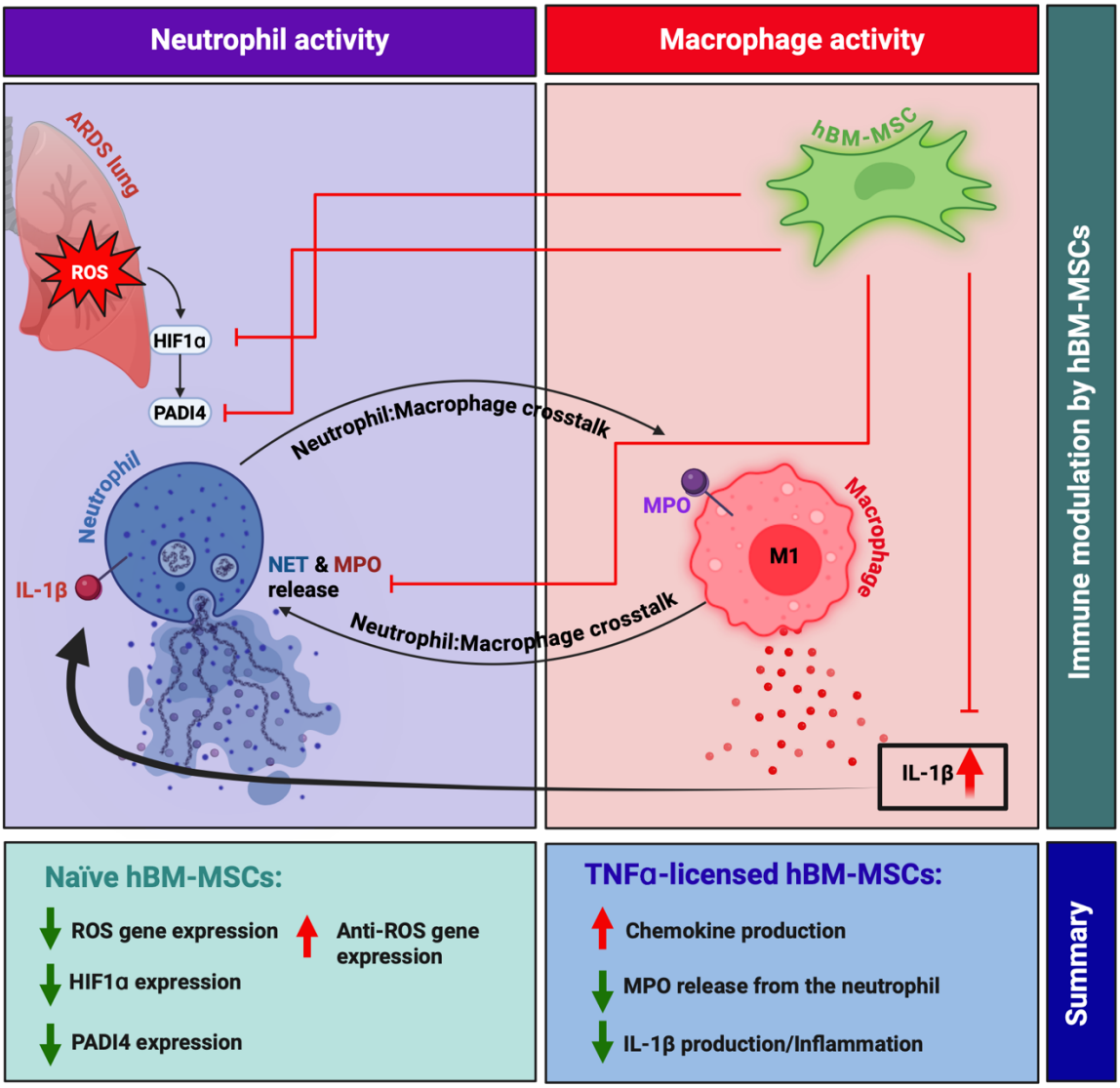

2.2 Hypothesis and aims

Hypothesis: TNFα-licensing will alter MSC immunomodulatory capacity in a model of ALI.

Aim(s):

- Identify a dose of TNFα that effectively licenses hBM-MSCs.
- Investigate the impact of TNFα-licensing on hBM-MSC gene expression.
- Understand the role of TNFα-licensed hBM-MSCs in the context of immunomodulation of other immune cells; such as neutrophils and macrophage.
- Administer TNFα-licensed hBM-MSCs into a pre-clinical model of ALI, to identify the effects *in vivo*.

2.3 Introduction

Mesenchymal stromal cells (MSCs) are immunoregulatory cells, that respond according to the environment in which they are placed in [206, 247]. In the context of inflammatory disease, MSCs are exposed to an abundance of pro-inflammatory cytokines that can further enhance their therapeutic efficacy [148, 156, 190]. This is often referred to as MSC-licensing. One cytokine that MSCs are often exposed to, directly or indirectly, within *in vitro* studies, is tumour necrosis factor alpha (TNFα) [248, 249]. This cytokine is produced by macrophage in response to stimulation with factors such as LPS [250]; and co-culture studies of MSCs and macrophage would indirectly expose MSCs to this. This pro-inflammatory cytokine is also upregulated in the context of many inflammatory diseases; such as acute respiratory distress syndrome (ARDS) [251, 252].

ARDS is an inflammatory disease of the lung that is comprised of a complex microenvironment. This microenvironment is made up of an abundance of inflammatory mediators, free fatty acids (FFAs) and microorganism [46, 238, 239]. In the context of MSCs, it has long been thought that MSCs could be used in the treatment of ARDS; but only ~40% of patients are responding to treatment in clinical trials [95, 97, 98, 170]. One cytokine that is seen in high levels in the lungs of hyper-inflammatory ARDS patients is TNFα [251]. Inflammation in the ARDS lung is highly variable. The level of inflammation differs from patient to patient, and patients can present as either hypo-inflammatory, or hyper-inflammatory [93]. In the context of MSC therapy, this is crucial information. Our recently published study observed the effects of this environment on human bone marrow-derived MSCs (hBM-MSCs), by exposing the cells to serum from either sub-group of ARDS patients [122]. This study highlighted the differential capacity of each environment to activate the cells and enhance, or hinder, their

therapeutic efficacy; with hyper-inflammatory licensing improving MSC functional capacity in a pre-clinical model of acute lung injury (ALI) [122].

Several studies have already focused on interferon gamma (IFNɣ) [151], interleukin 1 beta (IL-1β) [253], macrophage migration inhibitory factor (MIF) [156, 190] and other licensing agents, however, TNFα licensing has not yet been thoroughly investigated in solitude.

2.4. Materials and Methods

2.4.1 Ethical approval and HPRA Compliance

Ethical approval was obtained from the Maynooth University ethics committee (BRESC-2022-2453953). HPRA approval was granted under the project authorisation(s) AE19124/P031/P037.

2.4.2 hBM-MSC cell culture

hBM-MSCs (RoosterBio™; supplementary figure 1) were cultured in Dulbecco's Modified Eagle Medium (DMEM; Merck life science limited, #D6046), supplemented with 10% Foetal Bovine Serum (FBS; Thermofisher) and 1% *Penicillin streptomycin* (Merck life science limited, P4458-100ML) to create complete DMEM (cDMEM), for 5 days, at 37°C + 5% CO2.

2.4.3 RNA sequencing sample preparation

hBM-MSCs (passage 2-5) were seeded at a density of $1x10^5$ in a 6-well plate and left to adhere. The cells were then exposed to 5ng/ml TNFα (Peprotech, #300-01A-10µg). 6hrs post-stimulation, the cells were harvested in TRIzol for RNA isolation. RNA was isolated through a series of chloroform and isopropanol extractions. Concentration and purity were then assessed by a spectrophotometer (Nanodrop 200, ThermoScientific). Samples were then sent to Novogene™ for RNA sequencing (GEO accession no.: GSE281162).

2.4.4 RNA sequencing analysis

Processed RNA sequencing datasets (GEO accession no.: GSE281162) highlighting co-expression, differential expression and gene set enrichment analysis (GSEA) were all provided by Novogene™. Quality control (QC) measures were carried out by Novogene™, as per their QC manual [254]. Based on these datasets, the significantly upregulated and downregulated genes were observed. This was assessed by sorting the excel sheet for significant hits (i.e. sort from smallest to highest p-value and cut off anything with a p-value >0.05), before sorting from highest to lowest LOG2 fold change (LOG2FC). A cut off point of LOG2FC = 2 was utilised to deem what was of interest, but in most cases within this thesis, the top 10-20 hits have been observed, for ease. Heat maps were generated using both Morpheus (Broad Institute) and R Studio (pheatmap package) to highlight the most important differentially expressed genes (DEGs) between groups. The fragments per kilobase per million mapped reads (FPKM) were then plotted to assess significances and trends between the leading-edge genes from the GSEA. This data was further confirmed by gene expression studies in 3 independent hBM-MSC donors. Principle component analysis (PCA) is available in supplementary figure 2. A publicly available RNA sequencing dataset carried out on lung homogenates from mice exposed to 5mg/kg LPS intratracheally, followed by hBM-MSCs 4hr post-LPS, was also briefly consulted to assess targets of interest (GEO accession no.: GSE241186).

2.4.5 Enzyme-linked Immunosorbent Assay (ELISA)

96-well half-area ELISA plates (COSTAR™) were coated as per manufacturers guidelines (mouse TNFα, IL-1β, IL-6 (Biolegend™), mouse MPO, human CXCL8 (R&D™). Non-specific proteins were then blocked by coating the plate in reagent diluent (1% BSA in PBS, sterile filtered) for 1hr before adding samples in appropriate dilutions for 2hrs. Detection antibodies were added as per manufacturers guidelines and left for a further 1-2hrs, depending on the kit (1hr for Biolegend™, 2hrs for R&D™). Streptavidin-HRP was added for 30 minutes, before washing the plate and adding a TMB substrate solution. The reaction was stopped using a 2N stop solution made up of $H2SO_4$ and distilled H_2O. The plate was washed in an automated washer (ELx50 Biotek™) three times between each step and measured at absorbances of 450nm and 570nm/595nm using a micro-plate reader.

2.4.6 Gene expression

RNA was isolated and normalised to 100ng/µl after assessing the concentration using the Nanodrop 2000 spectrophotometer. cDNA was made using the QuantBio™ cDNA Synthesis kit (as per manufacturer's guidelines; VWR International, #733-1174). Real-time Polymerase Chain Reaction (RT-PCR) was then carried out using PerfeCta SYBR Green FastMix (QuantBio™, #95072-05K) and appropriate primers (table 1). Quantification of these results was measured by calculating the 2-ΔΔCT values, compared to the *HPRT* housekeeper gene.

Table 1: Human primer sequences.

Gene name	Brand	Species	Forward Sequence	Reverse Sequence
HPRT	Sigma ™	Human	5'ATAAGCCAGACTTTGTTGG	5'ATAGGACTCCAGATGTTTCC
CXCL8	Sigma ™	Human	5'GTTTTTGAAGAGGGCTGAG	5'TTTGCTTGAAGTTTCACTGG
IL-1β	Sigma ™	Human	5'CTAAACAGATGAAGTGCTCC	5'GGTCATTCTCCTGGAAGG
ICAM1	Sigma ™	Human	5'ACCATCTACAGCTTTCCG	5'TCACACTTCACTGTCACC
CXCL1	Sigma ™	Human	5'ATGCTGAACAGTGACAAATC	5'TCTTCTGTTCCTATAAGGGC

2.4.7 Neutrophil isolation and characterisation

Mouse bone-marrow was isolated from 3 individual mice and neutrophils were negatively selected for using the Milteny Biotech™ mouse neutrophil isolation kit (Milteny Biotech, #130-097-658) and LS columns. Neutrophils were identified and characterised by flow cytometry; whereby the percentage live cells that were CD45+ (Milteny Biotech, #130-110-805), CD11b+ (Milteny Biotech, #130-110-804) and Ly6G+ (Milteny Biotech, #130-117-500) were assessed (supplementary figure 3).

2.4.8 Neutrophil NETosis assay

NET formation, in response to both LPS and/or MSC therapy, was assessed through a co-incubation experiment. hBM-MSCs (of three individual donors) were seeded at a density of $1x10^5$ in a 6-well plate and exposed to 10ng/ml of TNFα for 6hrs, before washing thoroughly with PBS and replacing the media. Mouse neutrophils were seeded at a density of $4x10^5$ in a transwell (pore size 0.4μM), and stimulated with LPS (Sigma, serotype: 0001:B4, #L2630-100mg), or an endotoxin-free PBS control (Merck life science limited, #TMS-012-A). 4hrs post-stimulation, the neutrophils from each transwell were added to the hBM-MSCs; and left for 48hrs to mimic our *in vivo* model. The supernatants were then harvested and used for MPO detection. Alongside this, the cells were then stained with 200mM Sytox Green (Life Technologies Europe BV, #S7020), detached with 2mM EDTA solution (diluted in PBS) and stained appropriately for flow cytometry. The cells were then stained for flow cytometry with the antibodies mentioned in section 2.4.7.

2.4.9 Neutrophil chemotaxis assay

Chemotaxis, in response to both LPS and/or MSC therapy, was assessed via a similar co-incubation experiment as that described above (section 2.4.8). The following protocol also involved the use of a cell-migration chemotaxis assay kit (figure 8; Abcam, #ab235696). hBM-MSCs (of three individual donors) were seeded at a density of $2x10^4$ in a 24-well plate and exposed to 10ng/ml of TNFα for 6hrs, before washing thoroughly with PBS and replacing the media. Mouse neutrophils were seeded at a density of $8x10^4$ in a transwell (pore size 8μM, to allow for the migration of neutrophils through the pores), and stimulated with LPS (Sigma, serotype: 0001:B4, #L2630-100mg), or an endotoxin-free PBS control (Merck life science limited, #TMS-012-A). 6hrs post-stimulation, the neutrophils from each transwell were added to the hBM-MSCs; and left for 24hrs. Upon completion of the assay, the transwell inserts were

removed and placed into a fresh 24-well plate. The original 24-well plate, containing the hBM-MSCs (and any migrated neutrophils) was centrifuged at 1000xg for 5 minutes at room temperature. Post-centrifugation, the media was carefully removed from the lower chamber and replaced with wash buffer (from the kit). The plate was centrifuged again, the wash buffer was carefully removed, the transwell inserts were added back into the original plate. A 1:10 dilution of 'Cell Dye', diluted in 'Cell Dissociation Solution' (from the kit), was added to the lower well for 1hr. A standard curve of neutrophils was prepared and pipetted in duplicate in a white 96-well plate. These cells were also stained with 'Cell Dye' diluted appropriately for 1hr. The experimental cells, post-staining, were also added to the white plate. A fluorescence reading was measured using a fluorescent plate reader at Ex/Em 530/590. The experimental values were plotted against the standard curve values to assess the no. of migrated cells. This was carried out using simple linear regression on GraphPad Prism™ software (version 10). Percentage of migrating cells was calculated by diving the no. of neutrophils in the lower chamber, by the no. of neutrophils initially seeded in the upper chamber, multiplied by 100.

2.4.10 ALI mouse model

Male and female C57BL6/J mice (Charles River), aged 8+ weeks were subjected to either intranasal administration of 10mg/kg endotoxin/LPS, intratracheal administration of 2mg/kg endotoxin (Sigma, serotype: 0001:B4, #L2630-100mg), or a corresponding endotoxin-free PBS control (Merck life science limited, #TMS-012-A). Naïve hBM-MSCs, or TNFα-licensed hBM-MSCs, were administered, intravenously, 4hrs post-endotoxin administration. This was carried out using two different doses of hBM-MSCs: a low dose ($5x10^4$) and a high dose ($1x10^5$). Bronchoalveolar lavage fluid (BALF) and lungs were harvested 48hrs-post endotoxin for analysis.

2.4.11 Statistical analysis of animal studies

Power calculations were performed by Professor Karen English prior to the study, in line with HPRA recommendations, to guide sample size. All data was analysed using GraphPad Prism™ 10 software. For comparisons between two groups, a t-test with Welch's correction was carried out. For more than two groups, a one-way ANOVA followed by Tukey's post-hoc test was carried out. For multiple groups, with multiple variables, a two-way ANOVA followed by Tukey's post-hoc test was carried out. All animal data is presented as mean ± SEM; *$p<0.05$, **$p<0.01$, ***$p<0.001$, ****$p<0.0001$.

2.5 Results

2.5.1 Panther™, gene ontology (GO) and GSEA analysis; highlighting significant upregulation of several cellular pathways in hBM-MSC$_{TNFα}$

RNA sequencing carried out on TNFα-licensed hBM-MSCs (hBM-MSC$_{TNFα}$) (figure 1A) highlighted an abundance of DEGs between naïve and TNFα-licensed hBM-MSCs (figure 1B). Making use of Panther™ software, baseline pathways of interest were determined (figure 1C). This allowed for the observation of several pathways in the hBM-MSC$_{TNFα}$ group compared to control. The upregulated signalling pathways included platelet-derived growth factor (PDGF), toll-like receptor (TLR), apoptosis, cholecystokinin receptor (CCKR), gonotrophin-releasing hormone receptor (GnRH), inflammation mediated by chemokine/cytokine signalling and interleukin (IL) signalling. To investigate this further, upregulated (figure 2A) and downregulated (figure 2B) pathways in dataset were observed by gene ontology (GO). Several similar pathways were upregulated, including cytokine and chemokine signalling. To assess this at a more specific level, making use of GSEA analysis to assess the most differentially effected pathways (figure 3). GSEA analysis provided insight into several altered pathways, including but not limited to NFκB signalling (figure 3A), IL-17 signalling (figure 3B), cytokine-cytokine receptor signalling (figure 3C), NOD-like receptor signalling (figure 3D), chemokine signalling (figure 3E), TNF signalling (figure 3F), necroptosis signalling (figure 3G) and apoptosis signalling (figure 3H, I). Within these GSEA hits, the key DEGs within the altered pathways were identified. With that in mind, making use of Morpheus software, the relevant DEGs of each pathway were promptly assessed (figure 4).

Among the top hits in each of the pathways already discussed from figure 3, there was a significant enrichment in chemokines within each of the pathways observed. The top hit from the NFkB (figure 4A), IL-17 (figure 4B), cytokine (figure 4C), NOD-like (figure 4D) and chemokine signalling (figure 4E) was CXCL8. This was followed closely by hits such as CXCL1 and IL-1β, and these genes were also seen to be largely upregulated in the TNFα signalling pathway (figure 4F). In the TNFα (figure 4F), Necroptosis (figure 4G) and apoptosis (figure H, I) pathways, there was a greater increase in BIRC2 and BIRC3; two genes known for their capacity to positively regulate cell death [255].

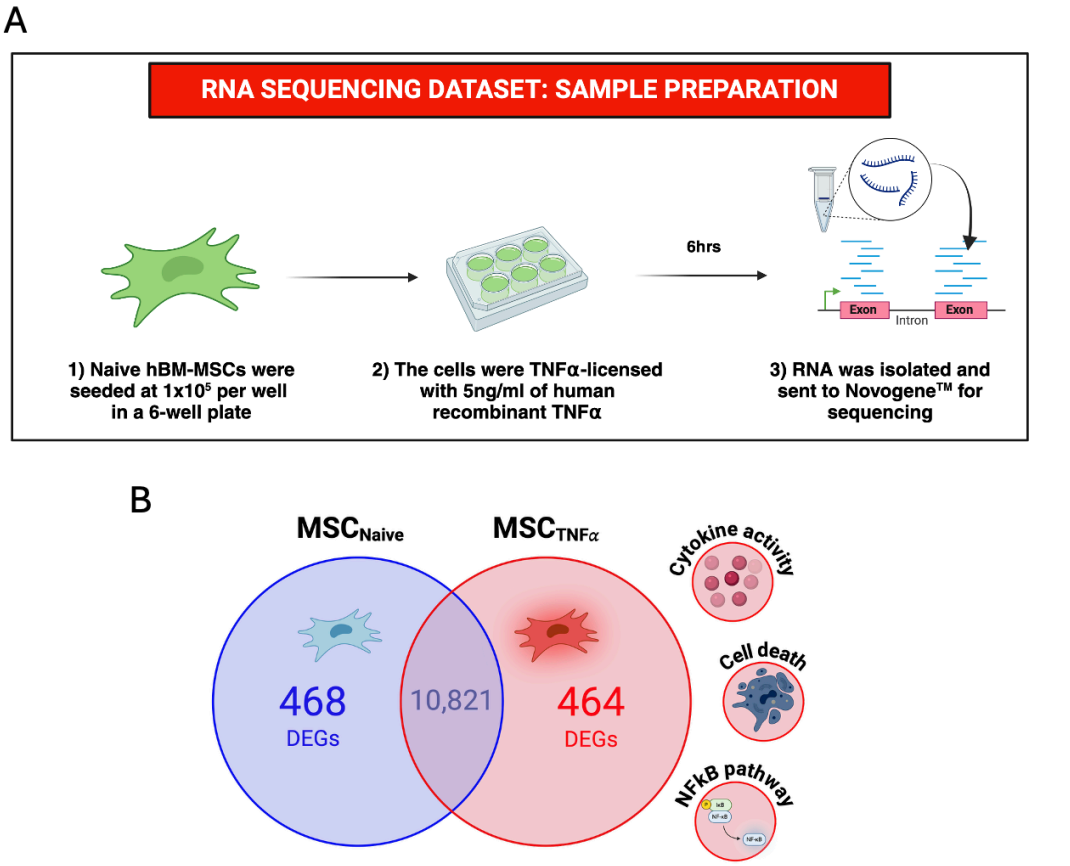

Figure legend available on next page

Figure 1: Significantly enriched genes and pathways in TNFα-licensed hBM-MSCs.

(A) hBM-MSCs were seeded at $1x10^5$ in a flat-bottom 6-well plate and exposed to 5ng/ml of human recombinant TNFα. The RNA was then isolated using a series of chloroform and isopropanol extractions before being sent to Novogene™ for bulk RNA sequencing. TNFα-licensing led to the upregulation of several (B) differentially expression genes (DEGs) and (C) various Panther™ pathways. Replicates are a representation of 3 individual hBM-MSC donors, obtained from RoosterBio™.

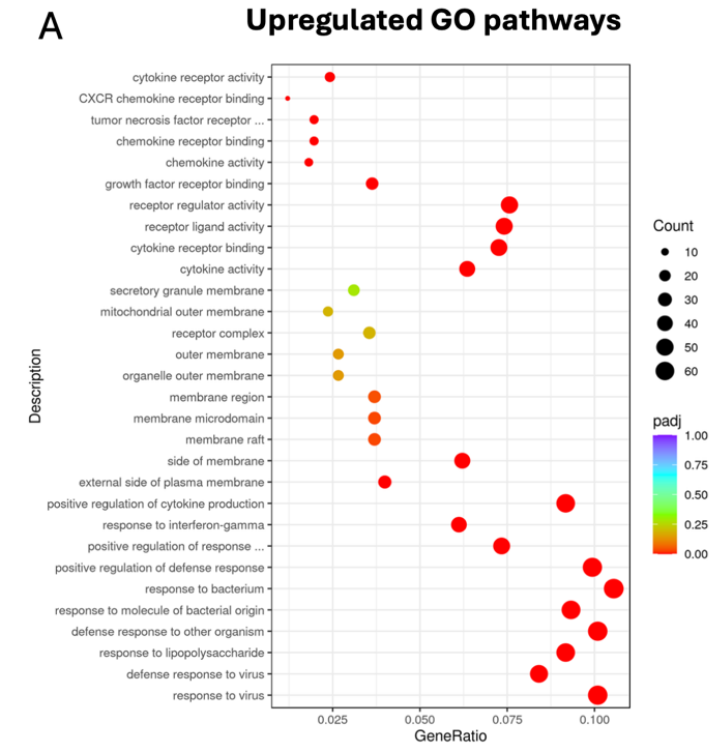

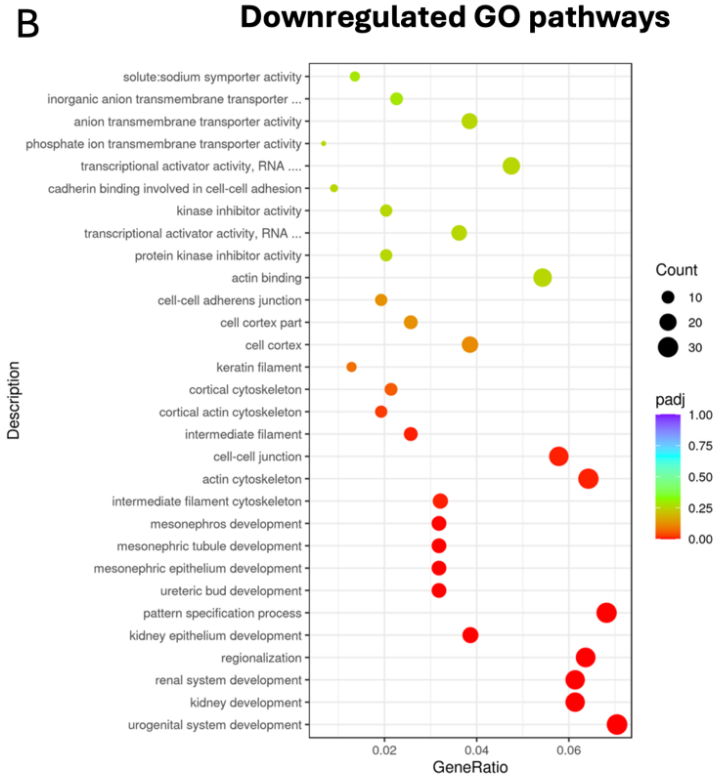

Figure legend available on next page

Figure 2: Significantly enriched gene ontology (GO) pathways in TNFα-licensed hBM-MSCs. hBM-MSCs were seeded at $1x10^5$ in a flat-bottom 6-well plate and exposed to 5ng/ml of human recombinant TNFα. The RNA was then isolated using a series of chloroform and isopropanol extractions before being sent to Novogene™ for bulk RNA sequencing. Gene ontology (GO) analysis highlighted (A) upregulation and (B) downregulation of various GO pathways. Graphs provided by Novogene™. Replicates are a representation of 3 individual hBM-MSC donors, obtained from RoosterBio™.

A

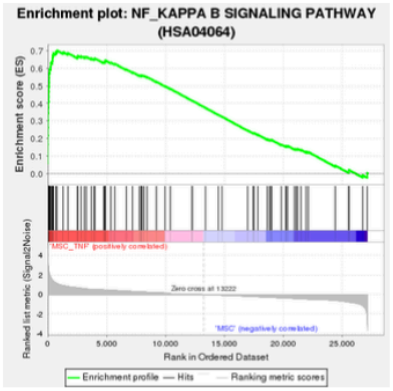

B

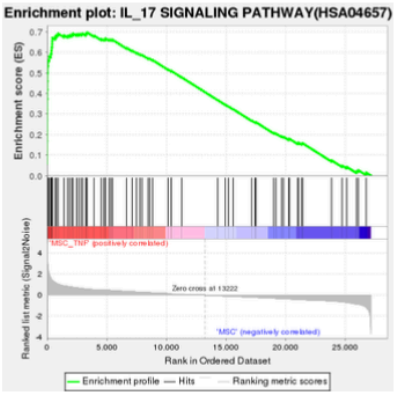

C

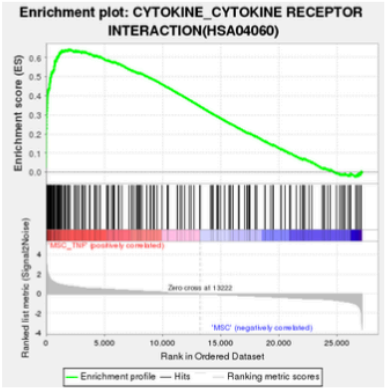

D

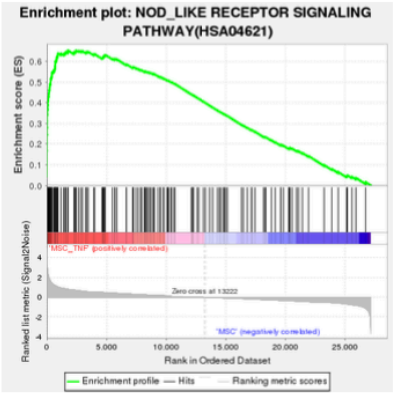

E

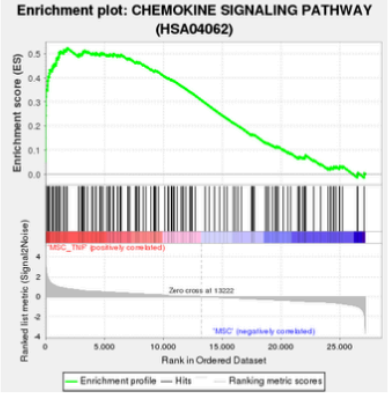

F

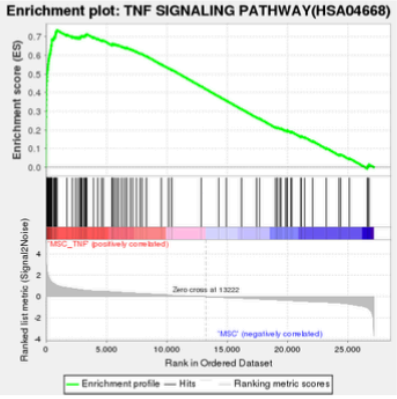

G

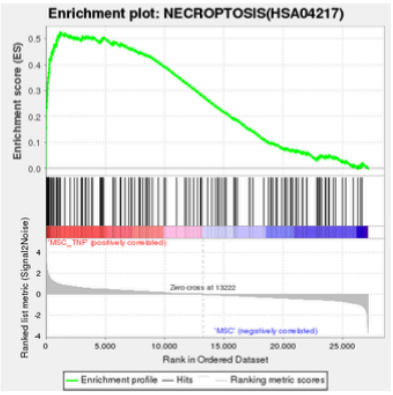

H

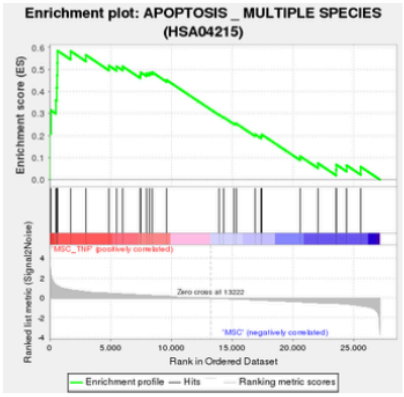

I

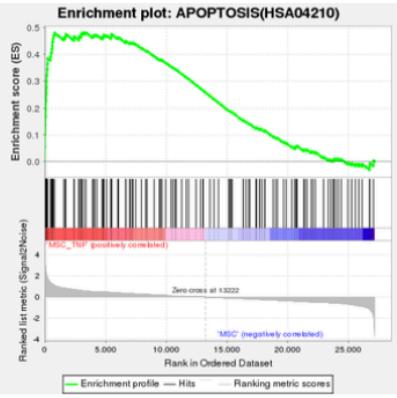

Figure legend available on next page

Figure 3: Significantly enriched gene set enrichment analysis (GSEA) pathways in TNFα-licensed hBM-MSCs. hBM-MSCs were seeded at $1x10^5$ in a flat-bottom 6-well plate and exposed to 5ng/ml of human recombinant TNFα. The RNA was then isolated using a series of chloroform and isopropanol extractions before being sent to Novogene™ for bulk RNA sequencing. Gene set enrichment analysis (GSEA) highlighted several altered pathways, including (A) NFκB signalling, (B) IL-17 signalling, (C) Cytokine signalling, (D) NOD-like receptor signalling, (E) Chemokine signalling, (F) TNF signalling and (G) Necroptosis signalling, and (H, I) Apoptosis signalling. GSEA graph plots provided by Novogene. Replicates are a representation of 3 individual hBM-MSC donors, obtained from RoosterBio™.

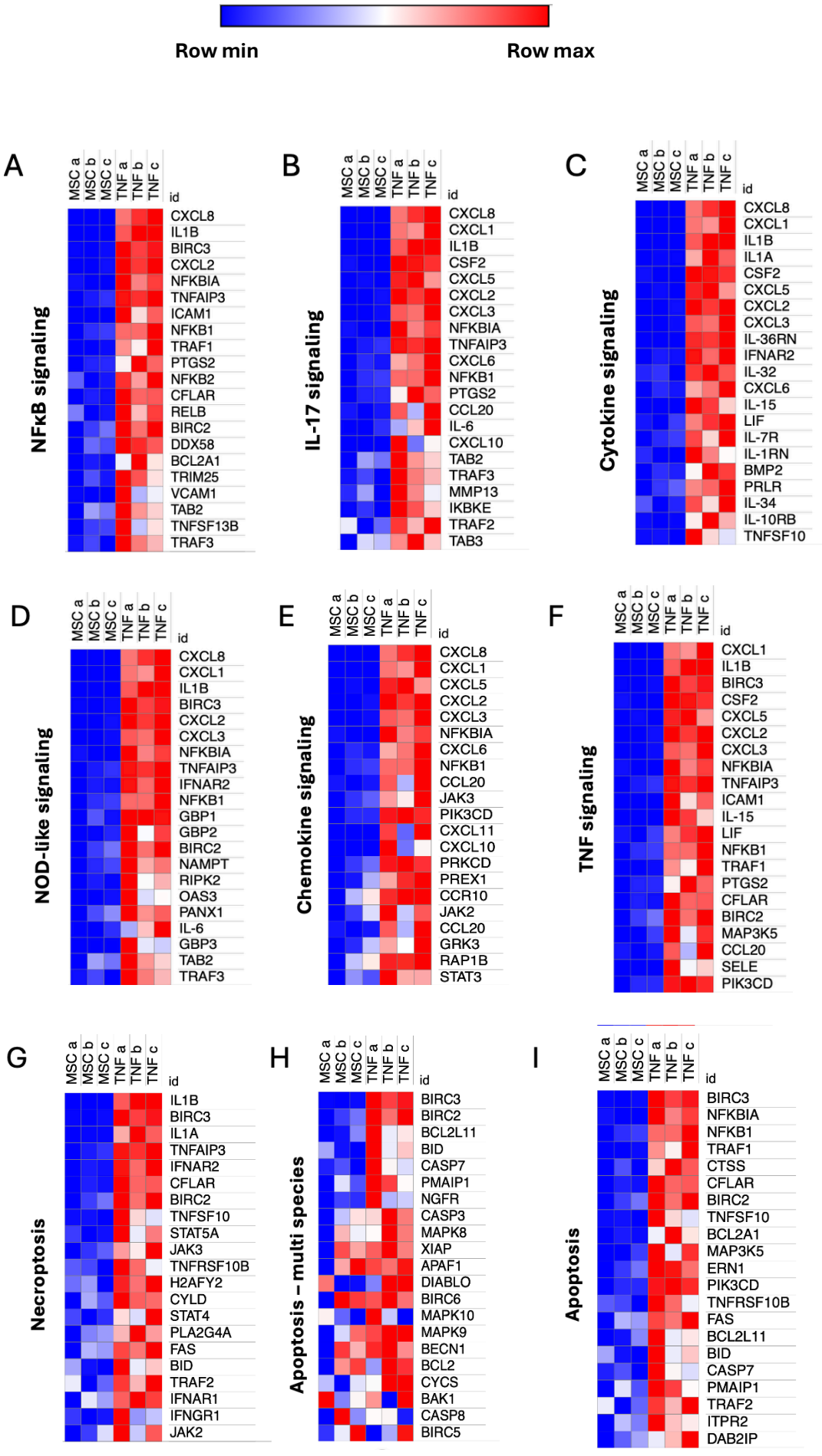

Figure legend available on next page

Figure 4: Top 20 enriched genes within each significantly altered GSEA pathway sub-group. hBM-MSCs were seeded at $1x10^5$ in a flat-bottom 6-well plate and exposed to 5ng/ml of human recombinant TNFα. The RNA was then isolated using a series of chloroform and isopropanol extractions before being sent to Novogene™ for bulk RNA sequencing. GSEA analysis highlighted significant upregulation of genes involved in several pathways, such as A) NFκB signalling, (B) IL-17 signalling, (C) Cytokine signalling, (D) NOD-like receptor signalling, (E) Chemokine signalling, (F) TNF signalling and (G) Necroptosis signalling, and (H, I) Apoptosis signalling. Heatmaps were generated using Morpheus software. Replicates are a representation of FPKM of 3 individual hBM-MSC donors, obtained from RoosterBio™.

2.5.2 hBM-MSC$_{TNFα}$ have enriched expression of chemokines

Given that there was a significant weight on cytokine and chemokine interactions seen thus far (figure 5A), we wanted to investigate this further. To account for which of the targets were most significantly altered, a volcano plot was generated using Flourish™, and *CXCL8* was noted as the most significantly increased gene (figure 5B). This was closely followed by *IL-1β, ICAM1* and *CXCL1* (figure 5B). This was confirmed by qRT-PCR for both a dose of 5ng/ml and 10ng/ml of TNFα (figure 5C-F). It was also confirmed at the protein level for CXCL8 (figure 5G). These results showed much greater expression of the chemokines of interest in response to the higher dose of 10ng/ml TNFα. This was the dose we chose to work with moving forward.

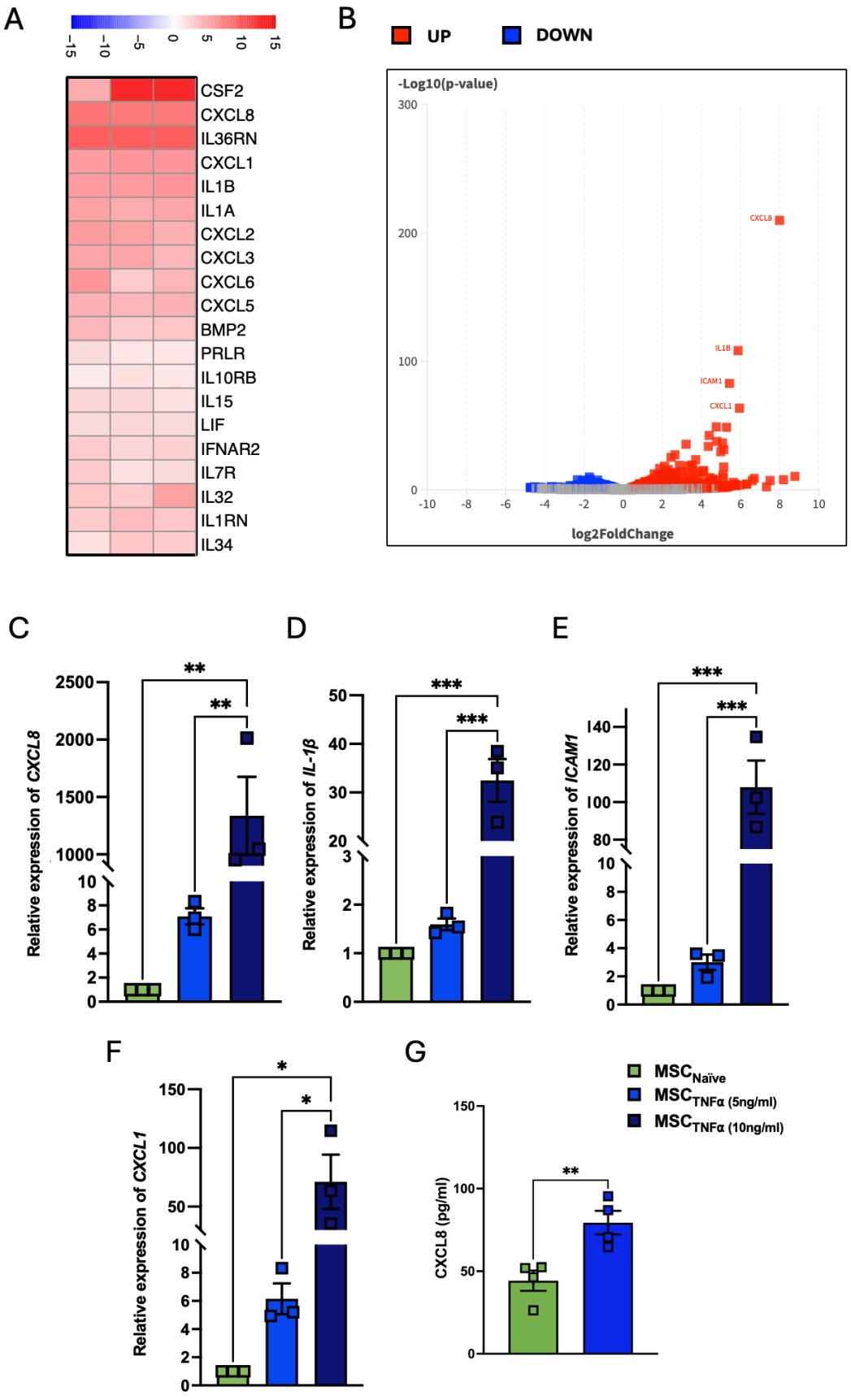

Figure legend available on next page

Figure 5: TNFα-licensing promotes chemokine expression in hBM-MSCs. hBM-MSCs were seeded at $1x10^5$ in a flat-bottom 6-well plate and exposed to 5ng/ml of human recombinant TNFα. The RNA was then isolated using a series of chloroform and isopropanol extractions before being sent to Novogene™ for bulk RNA sequencing. This led to a significant enrichment of a variety of gene sets; primarily cytokine-cytokine and chemokine interactions. (A) A heat map (generated using R studio) highlighted the dramatic increase in chemokines in response to TNFα-licensing. (B) Volcano plot analysis, using Flourish software, highlighted the most significantly enriched genes of interest. This confirmed that the most significantly enriched genes were *CXCL8, IL-1β, ICAM1* and *CXCL1*. This was confirmed by qRT-PCR for (C) *CXCL8,* (D) *IL-1β,* (E) *ICAM1* and (F) *CXCL1* (one-way ANOVA followed by Tukey's post-hoc test, n=3), and further at the (G) protein level for CXCL8 (R&D™) (t-test with Welch's correction; n=4). Replicates are a representation of 3 to 4 individual hBM-MSC donors, obtained from RoosterBio™. Sequencing data is presented as LOG2 fold change (LOG2FC) in comparison to naïve hBM-MSCs. All other data is presented as mean ± SEM; *p<0.05, **p<0.01, ***p<0.001, ****p<0.0001.

2.5.3 Naïve hBM-MSCs have the capacity to reduce factors associated with NETs

As the sequencing data suggested that TNFα-licensed hBM-MSCs showed a strong chemokine signature, it was hypothesised that TNFα-licensed hBM-MSCs would lead to enhanced chemoattraction of neutrophils; and potentially, alter their functions. Using a publicly available RNA-sequencing dataset that was carried out on lung homogenates from mice subjected to 5mg/kg of LPS intratracheally, followed by an IV injection of $1x10^6$ hBM-MSCs, we sought to investigate if there were differences in the neutrophil response (GEO accession no.: GSE241186; figure 6). Interestingly, upon observation of a variety of neutrophil-associated markers in this dataset, the data showed a significant increase in genes associated with the production of anti-NET enzymes, anti-ROS enzymes, and factors associated with protection against oxidative stress in mice who received hBM-MSCs (table 2). There was also a clear reduction seen in genes associated with NET formation and IL-1β release (table 3).

ALI mice, that had been treated with $1x10^6$ hBM-MSCs, had increased the expression of genes such as *prdx1* (figure 6B), *dnajc9* (figure 6C), *gss* (figure 6D), *cat* (figure 6E), *gpx7* (figure 6F), *mpv17* (figure 6G), *foxm1* (figure 6H), *hspe1* (figure 6I) and *nox4* (figure 6J). Both *prdx1* and *foxm1* are involved in the negative regulation of ROS production [256, 257]. As ROS production leads to the induction of NET formation [258] and neutrophil activity [198] this was of interest to us. Along with this, *gss, cat, gpx7,* and *mpv17* are all largely involved in the protection against oxidative stress and the consumption of H_2O_2; a factor that's known for its ability to induce NET formation [199]. In contrast to these genes, *hspe1* and *nox4* were also upregulated. *Hspe1* is involved in the positive regulation of NET formation, and *nox4* is largely associated with the induction of H_2O_2 [259, 260]. *DnaJc9* is a heat-shock co-chaperone, which is known to be involved in the regulation of hsp-associated genes. This is likely altered in the same manner as *hspe1*, as it is involved in the regulation of its functionality and activity [261].

ALI mice, that had been treated with $1x10^6$ hBM-MSCs also had reduced gene expression of *dnajc5* (figure 6K), *hif1a* (figure 6L), *padi4* (figure 6M), *txnrd1* (figure 6N) and *dnajb5* (figure 6O). *Padi4, hif1a, txnrd1* and *dnajb5* are all known to be involved in NET formation [262-265]. The reduction in these 4 factors could account for a large reduction in NET formation and activity; and counteract the *hspe1* induction by the hBM-MSC in the upregulated group. *Hif1a* and *txndr1* are also both largely involved in positive regulation of IL-1β production from the macrophage [266, 267]. Dnajc5 is not necessarily NET associated, but it is largely involved in the process of exocytosis; and while reduced could suggest a reduction in the exocytosis from any cell type present in the lung homogenate population [268]. It is important to note that there was no neutrophil cell count carried out in this publicly available study, and therefore, this could impede on the results found.

Table 2: Upregulated genes in LPS-induced ALI dataset, in response to hBM-MSCs.

UP_GENES	**Function in Neutrophils**
Prdx1	Anti-ROS enzyme
Dnajc9	Heat shock co-chaperone
Gss	Consumption of H_2O_2
Cat	Protection against oxidative stress and consumption of H_2O_2
Gpx7	Protection against oxidative stress
Foxm1	Anti-ROS production
Hspe1	Positive regulation of NET formation
Mpv17	Protection against oxidative stress
Nox4	Specific induction of H_2O_2, but not superoxide (O_2-)

Table 3: Downregulated genes in LPS-induced ALI dataset, in response to hBM-MSCs.

DOWN_GENES	Function in Neutrophils
Padi4	NET formation
Dnajc5	Exocytosis
Hif1α	NET formation, phagocytosis and positive regulation of IL-1β from macrophage
Txnrd1	NET formation and positive regulation of IL-1β release from macrophage
Dnajb5	NET scaffolding

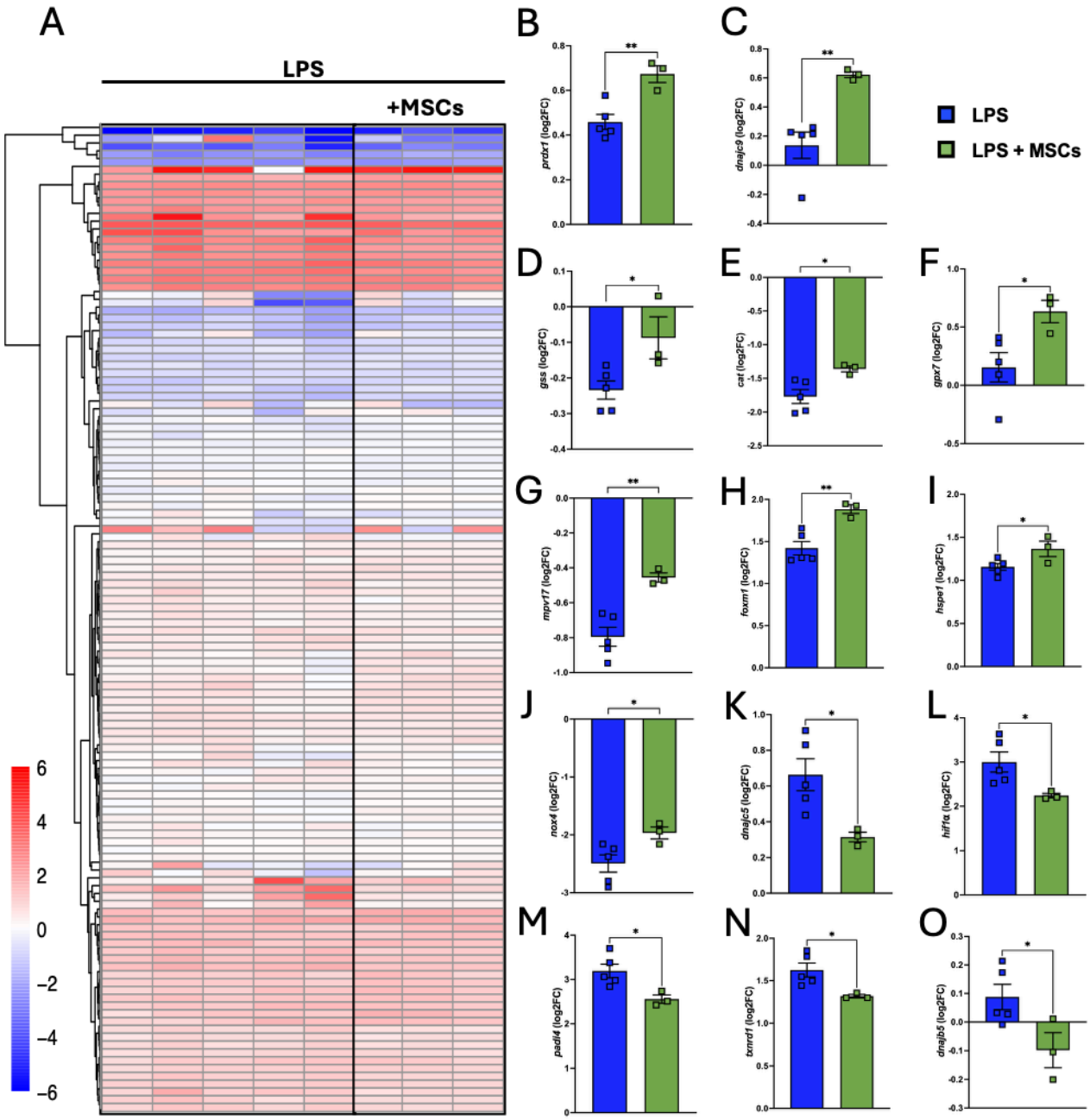

Figure 6: hBM-MSCs can reduce NET-associated markers. (A) Using a publicly available dataset (GEO: GSE241186), where mice had received 5mg/kg LPS, intratracheally, +/- 1x10^6 hBM-MSCs, intravenously, we assessed the impact of hBM-MSCs on NET-associated markers. (A) A heat map of these results was generated using R Studio (pheatmap package) and (B-O) significant results were then plotted (t-test with Welch's correction; n=3-5). Replicates are a representation of 3 to 5 mice per group. Data is presented as mean ± SEM; *p<0.05, **p<0.01, ***p<0.001, ****p<0.0001.

2.5.4 hBM-MSC$_{TNFα}$ reduce NET activity of mouse neutrophils

To confirm the effect of hBM-MSCs on the functionality of mouse bone marrow-derived neutrophils, neutrophils were isolated from whole bone-marrow (figure 7A) and seeded them in transwell inserts, co-cultured with hBM-MSCs (naive or TNFα-licensed). NET formation and activity was assessed. NET formation was measured based on the percentage of Sytox green positive cells; identified by flow cytometry. Sytox green is a DNA-binding dye that specifically binds to extracellular DNA; i.e. NETs released from neutrophils [269]. The neutrophils were characterised prior to use (figure 7B, C) and during the assay (figure 7D). Upon investigation of this by flow, it was noted that there was an increase in Sytox green positive cells upon stimulation with LPS (figure 7E). This was expected, as LPS should induce NET formation to high levels [270]. Interestingly, co-culture with hBM-MSCs, naïve or licensed, did not impact the presence of NETs in this assay (figure 7E). However, upon further investigation into NET activity, through analysing MPO release from the neutrophil; it was identified that although hBM-MSC$_{TNFα}$ could not reduce NET presence, they could reduce NET activity by significantly reducing MPO levels (figure 7F). Importantly, neither LPS-treatment, nor hBM-MSC exposure, effected cell viability (figure 7G).

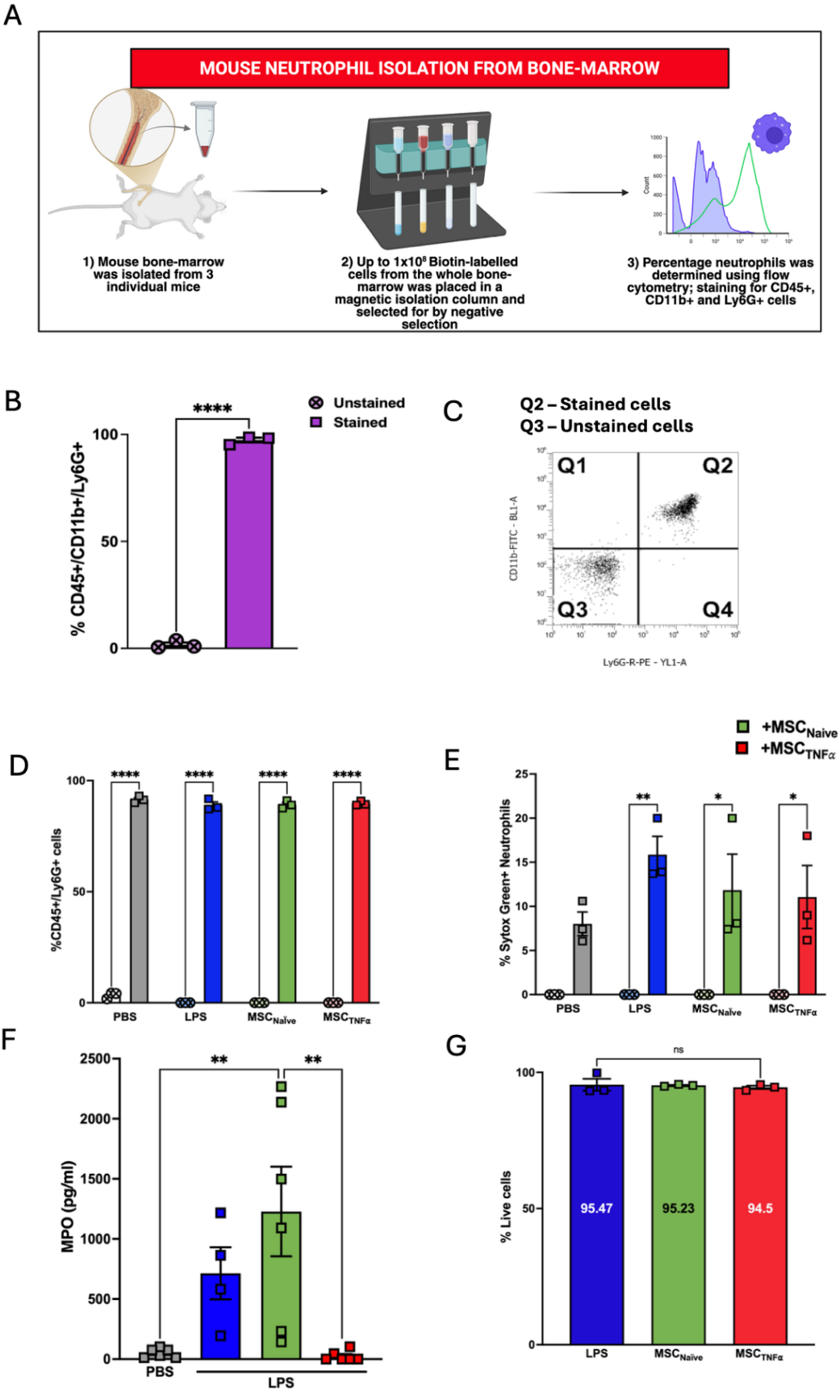

Figure legend available on next page

Figure 7: TNFα-licensed hBM-MSCs reduce NET activity. (A) Mouse bone-marrow was isolated from the femurs and tibias of 3 individual mice and neutrophils were negatively selected from using the Milteny Biotech™ mouse neutrophil isolation kit. (B, C) The neutrophils were then characterised by flow, by assessing the percentage of cells in the population were CD45+, while also CD11b+ and Ly6G+ (t-test with Welch's correction; n=3). Attune™ software was used to build overlays of both unstained and stained cells in figure (C). For the neutrophil-based assays, one mouse donor (with the highest cell count) was taken and utilised in the presence of 3 individual hBM-MSC donors. (D) Neutrophils were confirmed to remain having this signature during the assay (to account for any alterations in response to treatments) and (E) NET formation was assessed by flow cytometry (two-way ANOVA followed by Tukey's post-hoc test, n=3). (F) MPO production was further measured by ELISA, and (G) cell viability was ensured (one-way ANOVA followed by Tukey's post-hoc test, n=3). Replicates are a representation of (B, C) 3 individual mice per group or (D-G) 3 individual hBM-MSC donors, obtained from RoosterBio™. Data is presented as mean ± SEM; *p<0.05, **p<0.01, ***p<0.001, ****p<0.0001.

2.5.5 hBM-MSC$_{TNFα}$ could not enhance chemotaxis of mouse neutrophils

In addition to these studies, a neutrophil chemotaxis study was also conducted (figure 8A), but there was no significant differences between groups (figure 8B). This was likely due to a saturation of response in the naïve hBM-MSC group, due to the sheer concentration of chemokines present, with ~250pg/ml of CXCL8 alone (figure 8C).

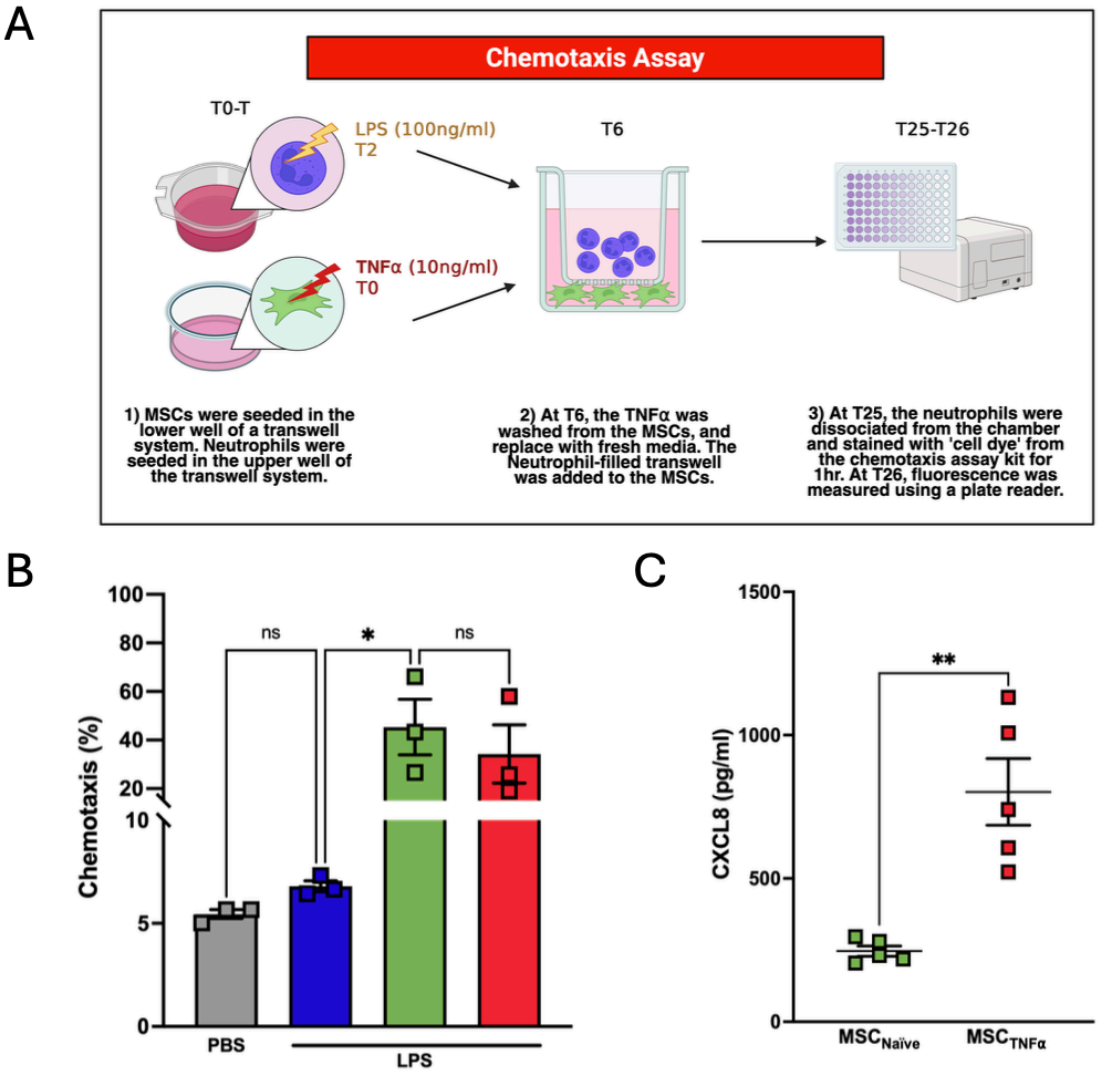

Figure 8: TNFα-licensed hBM-MSCs did not affect neutrophil chemotaxis. Mouse bone-marrow was isolated from the femurs and tibias of 3 individual mice and neutrophils were negatively selected from using the Milteny Biotech™ mouse neutrophil isolation kit. The neutrophils were then characterised by flow, by assessing the percentage of cells in the population were CD45+, while also CD11b+ and Ly6G+ before being (A) co-cultured (in a transwell) with TNFα-licensed hBM-MSCs. (B) Chemotactic capacity was observed using the Abcam chemotaxis assay kit. (C) Protein expression of MSC-secreted CXCL8 was quantified by-way-of ELISA (t-test with Welch's correction; n=5). Replicates are a representation of 3 individual hBM-MSC donors, obtained from RoosterBio™. Data is presented as mean ± SEM; *p<0.05, **p<0.01, ***p<0.001, ****p<0.0001.

2.5.6 Preparation of the ALI mouse model

Prior to *in vivo* studies, several pilot studies to determine a time-point, dose and route of administration of LPS were run. This was first attempted using intranasal (IN) administration of 10mg/kg LPS and saw variable responses; but enhanced response at 48hrs compared to 24hrs (figure 9B-D). There was not much difference upon incorporation of hBM-MSCs, intravenously (IV), largely due to the variability in response (figure 9E-G). To account for this, a more direct approach by-way-of intratracheal (IT) administration was decided upon. This showed a much less variable response, and a greater level of inflammation; even at a lower dose of 2mg/kg (figure 10A-C). This pilot was also trialled using both a low dose ($5x10^4$) or a high dose ($1x10^5$) of hBM-MSCs in the ALI model. The cells were administered IV, and the low dose was seen to not be as efficacious as the high dose (figure 10A-C). This allowed for both an effective and a less-efficacious dose that could be used for licensing moving forward.

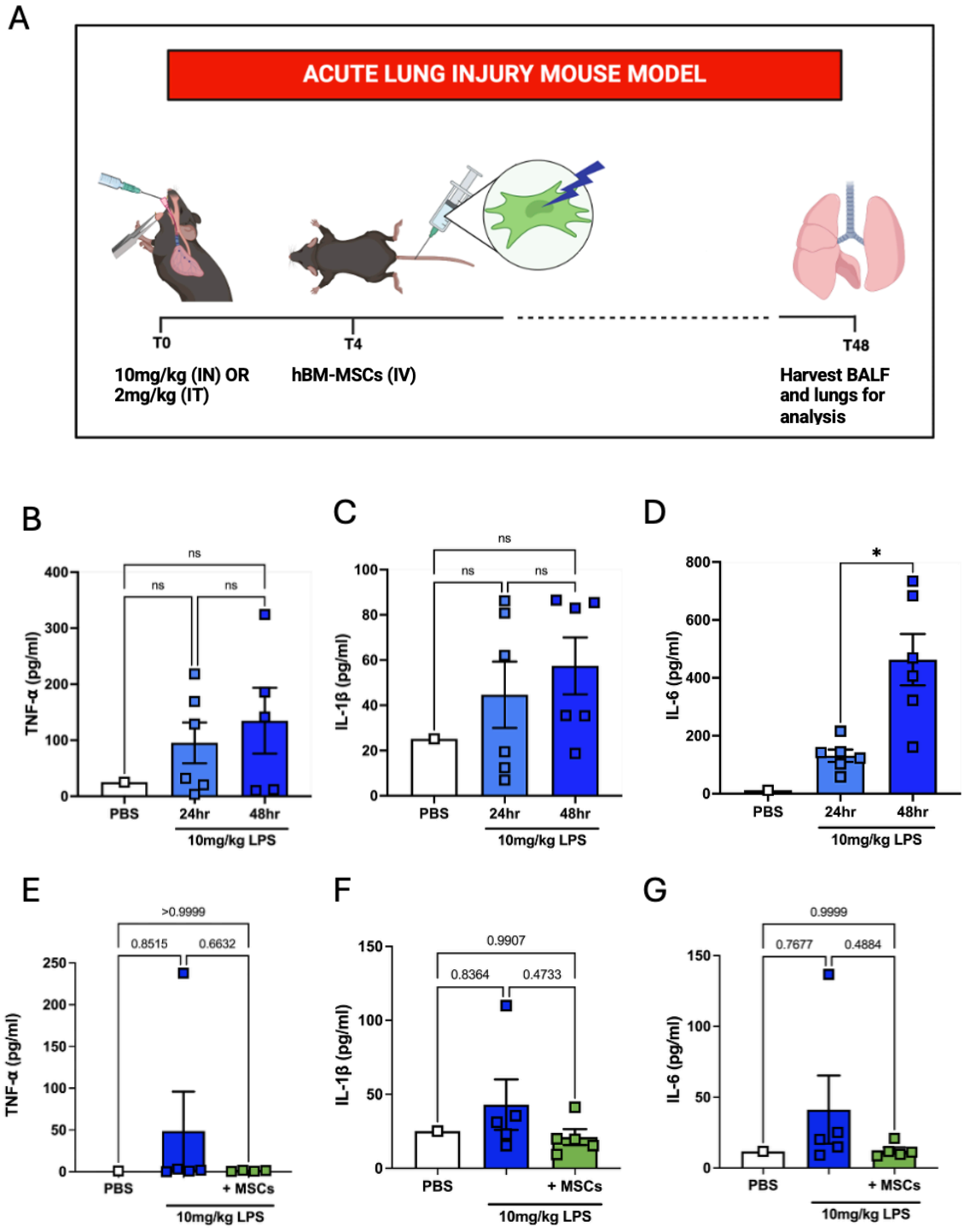

Figure legend available on next page

Figure 9: ALI mouse model pilot using intranasal administration. (A) Mice were exposed to 10mg/kg of LPS, or a PBS control, intranasally and observed over 24hr or 48hrs. The inflammatory profile of the lung was then assessed by-way-of BALF ELISA. (B) TNFα, (C) IL-1β and (D) IL-6 were measured at both time points. We re-ran this study, incorporating the administration of $1x10^6$ hBM-MSCs per moues, intravenously, and again measured (E) TNFα, (F) IL-1β and (G) IL-6 in the BALF (one-way ANOVA followed by Tukey's post-hoc test, n=1 in control group, n=5-6 in other groups). Replicates are a representation of 5 to 6 (B-D) individual mice or (E-G) individual mice in response to one hBM-MSC donor. Data is presented as mean ± SEM; *p<0.05, **p<0.01, ***p<0.001, ****p<0.0001.

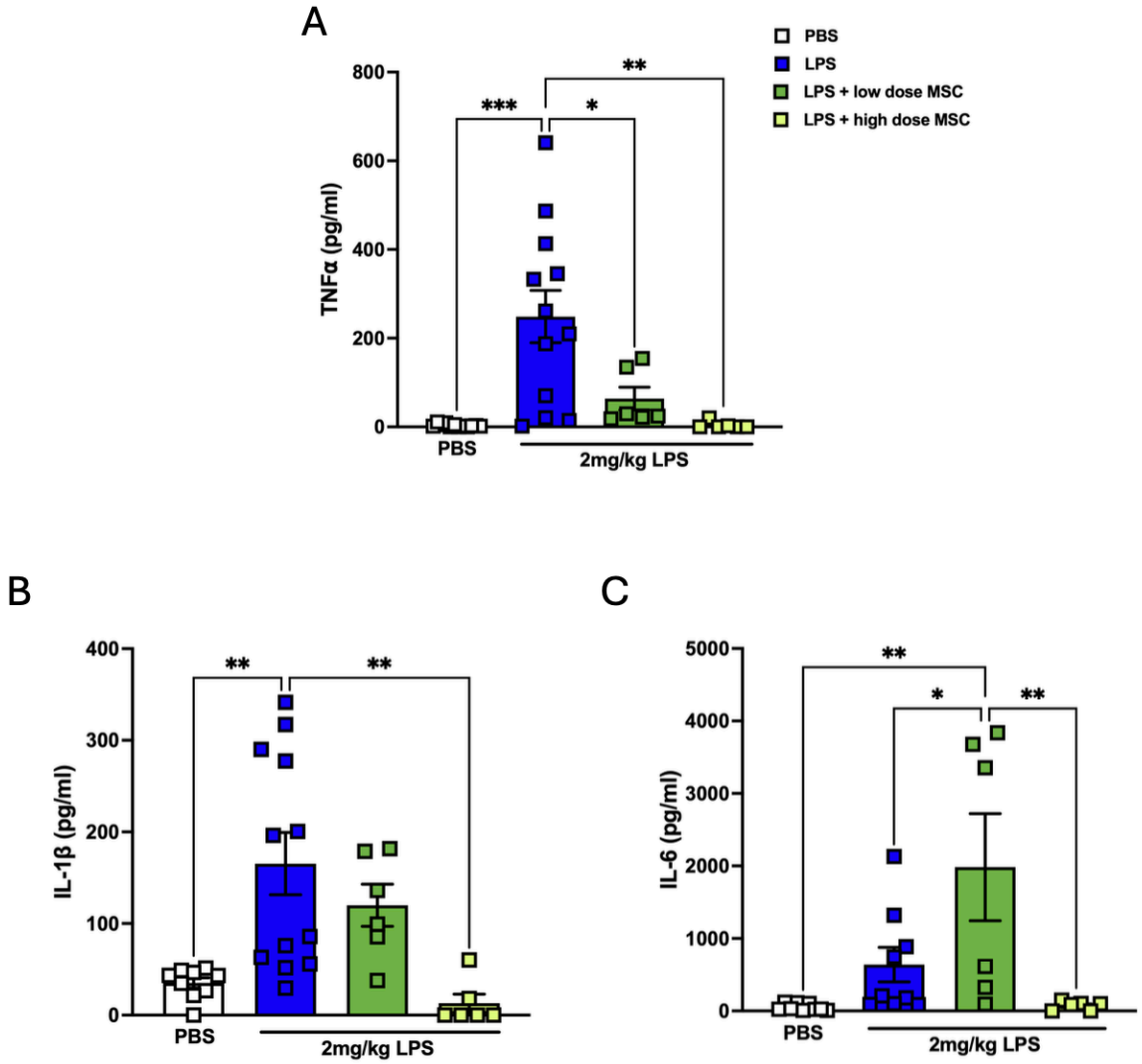

Figure 10: ALI mouse model pilot using intratracheal administration and dose range of hBM-MSCs. Mice were exposed to 2mg/kg of LPS, or a PBS control, intratracheally and observed over 48hrs. They were further subjected to the administration of a low dose ($5x10^4$) or high dose ($1x10^5$) hBM-MSCs, intravenously. The inflammatory profile of the lung BALF was assessed by ELISA. (A) TNFα, (B) IL-1β and (C) IL-6 were measured (one-way ANOVA followed by Tukey's post-hoc test, n=6-12). Replicates are a representation of 6 to 12 individual mice in response to one hBM-MSC donor. Data is presented as mean ± SEM; *p<0.05, **p<0.01, ***p<0.001, ****p<0.0001.

2.5.7 hBM-MSC$_{TNFα}$ reduce IL-1β and MPO in a pre-clinical model of ALI

Using the optimised ALI model, the impact that hBM-MSC$_{TNFα}$ would have on neutrophils *in vivo* was tested. To do this, a working dose/high dose ($1x10^5$) or a less efficacious dose/low dose ($5x10^4$) of naïve hBM-MSCs was administered to LPS-treated mice. In the context of the TNFα-licensed group, the low dose of hBM-MSCs was licensed (with 5-10ng/ml TNFα); to identify if there were any enhancements to a dose that would typically not be useful *in vivo*. Interestingly, hBM-MSC$_{TNFα}$ did not differentially effect TNFα expression in the BALF of the ALI mice, but it did however reduce IL-1β and MPO (figure 11B-D). This stood out, as it had previously been identified that hBM-MSC$_{TNFα}$ had the capacity to reduce MPO released by neutrophils *in vitro*; and this had now been confirmed *in vivo*. In addition to this, MPO is known to be promoted in response to macrophage derived IL-1β [34]. As IL-1β was also reduced in the BALF, and both neutrophils [271] and macrophage [272, 273] are key drivers of ARDS, this was a thought-provoking finding. There was no difference in total cell number between non-treated and hBM-MSC$_{TNFα}$ treated ALI mice (figure 11E), and although differential cell counts highlighted a significant increase in neutrophils in groups that received LPS; there was no reduction in neutrophil number in response to hBM-MSC$_{TNFα}$ (figure 11F).

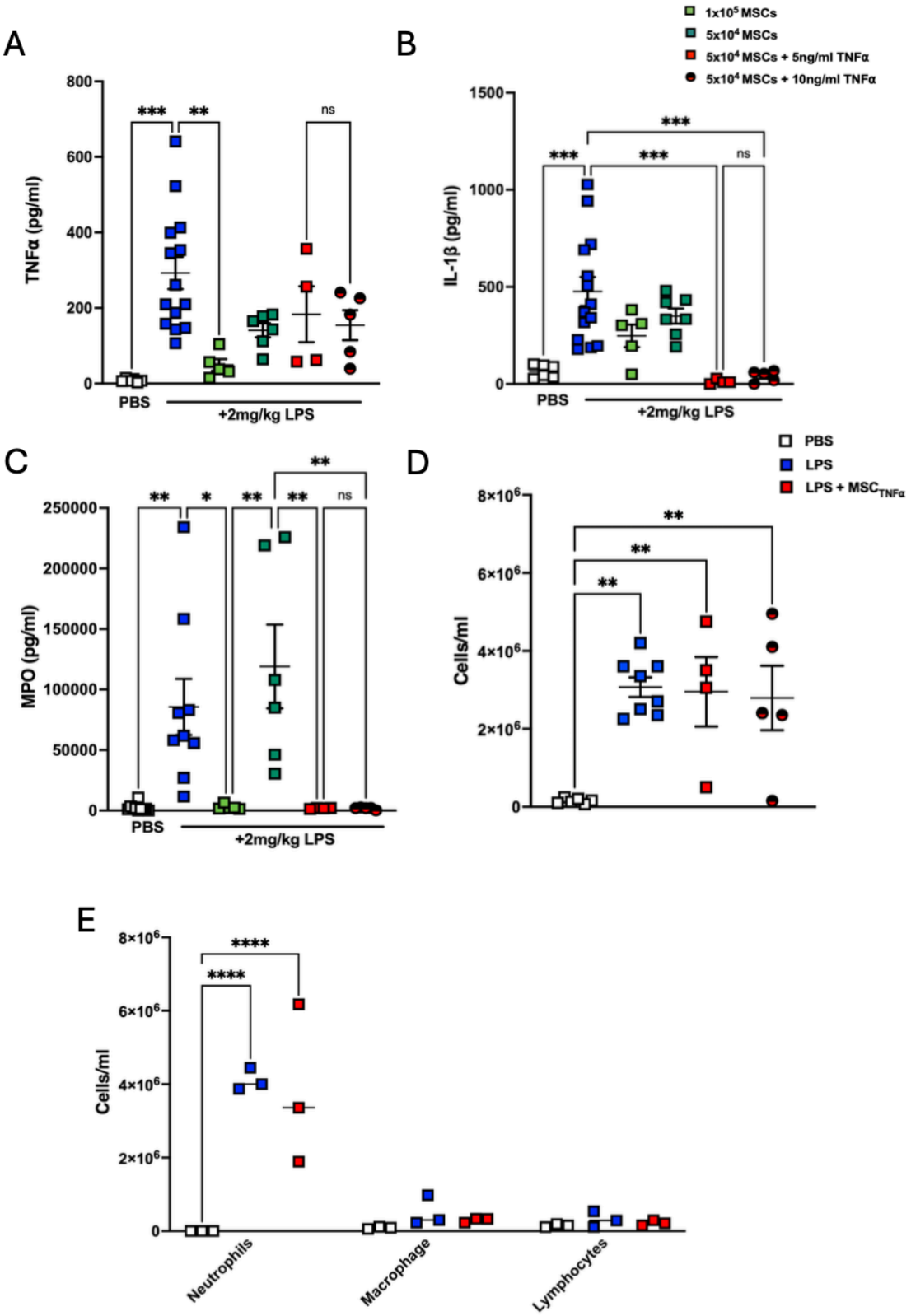

Figure legend available on next page

Figure 11: hBM-MSC$_{TNF\alpha}$ reduce IL-1β and MPO in a model of ALI. hBM-MSCs of a low dose or high dose were injected (IV) into mice exposed to LPS (IT) and BALF was harvested at a 48hr timepoint. ELISAs were carried out to assess (A) TNFα, (B) IL-1β and (C) MPO levels in the BALF of the mice. (D) Total cell counts and (E) differential cell counts were also carried out (one-way ANOVA followed by Tukey's post-hoc test, n=3-14). This figure includes replicates from the pilot study seen in figure 11. Replicates are a representation of 3 to 14 mice per group. Data is presented as mean ± SEM; *p<0.05, **p<0.01, ***p<0.001, ****p<0.0001.

2.6 Discussion

hBM-MSCs are known for their immunomodulatory and reparative capacity [124]. They are also known to react to pro-inflammatory stimuli [190, 194, 249]. In the context of the human body, specifically in the context of ARDS, there are high levels of circulating TNF in the blood [251]. This would lead to hBM-MSC exposure to this upon administration to the patient. In this report, the impact of TNFα-licensing on hBM-MSC therapeutic efficacy in a pre-clinical model of ALI was assessed. Firstly, the enriched pathways in response to TNFα-licensing, using a bulk RNA sequencing approach, were identifies (figure 1-4). This highlighted a GSEA enrichment of cytokine-cytokine receptor interactions (figure 3C; figure 4C), and a dramatic upregulation of chemokines (figure 3E; figure 4E). Upon investigation of the most significantly enriched hit in the dataset, the four dominant genes of interest: *CXCL8, IL-1β, ICAM1* and *CXCL1* were further studied (figure 5B). This is in line with a study by Hackel *et al.* (2021) that saw an enhanced chemokine signature, and enhanced neutrophil recruitment, in MSCs exposed to both TNFα and IL1β [189]. Szűcs *et al.* (2024) also saw this signature in TNFα-licensed MSCs, but their study followed on to focus on the combination of TNFα and IFNɣ as licensing agents [248]. Given that *CXCL8* was the most significantly upregulated hit, the expression of this was further confirmed this at the protein level (figure 5G). The expression of the top 4 hits were also assessed at the gene expression level, using both a 5ng/ml and a 10ng/ml dose of TNFα (figure 5C-F). Since chemokines are largely associated with neutrophil recruitment, these results allowed me to hypothesise that hBM-MSC$_{TNFα}$ may impact neutrophil functional capacity in a model of ALI; whereby neutrophils are the key drivers of disease.

With this in mind, and making use of a publicly available dataset (GEO accession no.: GSE241186) using a similar mouse model as our own, the potential impact of hBM-MSCs on lung homogenates of ALI mice was assessed. The group who published this dataset had already deduced that umbilical cord-derived MSCs (UC-MSCs) could significantly reduce *padi4* and *elane*; two genes involved in NET formation [274]. They noted that although there were also differences observed in hBM-MSCs, there was a much greater effect by UC-MSCs. To further investigate this in the case of hBM-MSCs, several neutrophil-associated factors were observed (figure 6A). In the lung homogenates from mice exposed to both LPS and hBM-MSCs, there was a decrease in NET-associated factors such as *padi4, dnajc5, hif1a, txnrd1* and *dnajb5* (table 3). Along with being NET-associated, two of these factors (*hif1a* and *txnrd1*) are also involved in positive regulation of IL-1β release from macrophage. The reduction in both factors could suggest a reduction in neutrophil: macrophage crosstalk by reduction NET associated factors, while also reducing IL-1β signalling. There was also an increase in genes involved in counteracting reactive oxygen species (ROS) and protection from oxidative stress (figure 6B-O). These genes, including *foxm1* (figure 6H) and *prdx1* (figure 6B) that are known for their involvement in promoting ROS [256, 257], would suggest limited stimulation of NET formation by ROS in the lung microenvironment. These findings suggest that naïve hBM-MSCs have the capacity to dampen the neutrophil response, macrophage production of IL-1β, and potentially neutrophil:macrophage crosstalk, in a model of ALI.

To investigate this further with hBM-MSC$_{TNFα}$ cells, co-incubation studies of hBM-MSCs and neutrophils were carried out *in vitro*. Although there was no impact of hBM-MSCs on LPS-induced NET formation (figure 7E), there was a significant reduction of MPO from the neutrophils (figure 7F). This suggested that perhaps hBM-MSCs could not reduce NET formation but could reduce NET activity. A study by Franck *et al.* (2021) showed that muscle-derived MSCs (MD-MSCs) could reduce MPO in a model of ALI, and that incubation of MSCs

with MPO itself, in a neutrophil-free environment, reduced the peroxidase activity of the compound [275]. Neutrophil Elastase (NE) was also observed in this study; both in vitro and in vivo (supplementary figure 4). These results did not show similar trends to that of MPO, further suggesting no difference in NET presence, but potentially difference in activity by-way-of MPO. Alternatively, degranulation of neutrophils should have been investigated, to determine the true cause behind MPO reduction; given that there was no difference in NE.

In vivo investigation in our own model, making use of a low (less-efficacious) dose of hBM-MSC ($5x10^4$), and licensing that dose with 10ng/ml of TNFα, we saw that although hBM-$MSC_{TNFα}$ could not enhance the suppression of TNFα in the BALF of the ALI mice (figure 12A), there was a significant reduction of IL-1β (figure 12B). Given that hBM-MSCs decreased genes involved in positive regulation of IL-1β production from the macrophage in the publicly available dataset (figure 6A-O), this was an interesting finding. Importantly, there was also a significant reduction of MPO in the BALF of these ALI mice (figure 12C), but there was no impact on the total cell of neutrophil number in the BALF (Figure 12D, E). Interestingly, IL-1β is known to bind to the IL1R1 on the neutrophil surface and lead to production of MPO [34]. This would suggest that hBM-$MSC_{TNFα}$ could be limiting both the neutrophil and macrophage functioning in ALI mice. Further studies are required to elucidate the full effect of this study.

2.7 Concluding remarks

Within this chapter, the effect of TNFα-licensing on hBM-MSC therapeutic efficacy was assessed. It was shown that TNFα-licensed hBM-MSCs had a greater enrichment of neutrophil-associated chemotactic factors, and an enhanced cytokine signature, compared to naïve hBM-MSCs. The strengths of this chapter can be seen in the use of multiple hBM-MSC donors, different doses of TNFα used to license the cells and the pre-clinical confirmation of the results in question. Although there are strengths, it's important to acknowledge the weaknesses as well. This study contains a variety of neutrophil assays; all of whom should (and will be repeated by other members of the lab) for confirmation. This is a weakness of the chapter, as these results did not agree with other published studies whereby hBM-MSCs could functionally chemoattract [189] and aid in phagocytosis [276]. This is likely due to this work being completed late in the study, with little time to optimise the assays. It would be beneficial to also observe degranulation in the context of this study, as the MPO reduction could be due to degranulation, and not NETosis. This is something that should be addressed in future work from the lab.

2.8 Supplementary figures

A

Donor ID	Tissue	Age (years)	Sex	Tri-lineage differentiation	Appropriate surface marker expression?
310305	BM	20	F	Yes	Yes
310307	BM	19	M	Yes	Yes
310310	BM	25	M	Yes	Yes

B

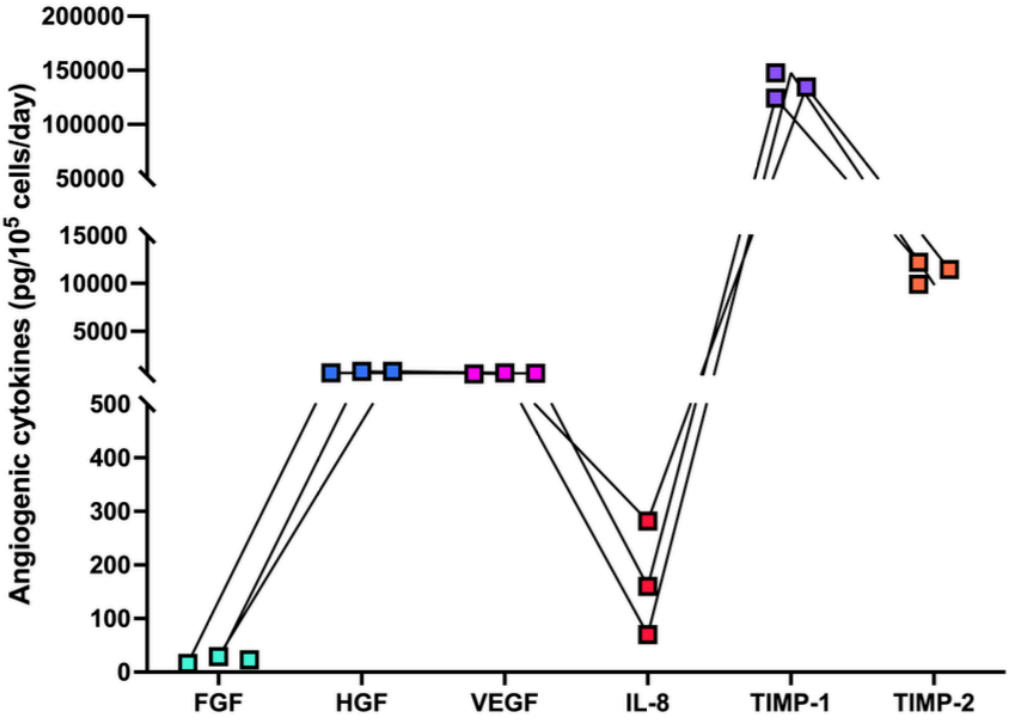

Supplementary figure 1: hBM-MSC characterisation by RoosterBio™. (A) Three individual hBM-MSC donors were selected from RoosterBio™ to use in these assays. (B) Information was provided by RoosterBio™ to allow for guidance on choosing donors for purchase. This information highlighted donor production of FGF, HGH, VEGF, IL-8, TIMP-1 and TIMP-2; all important hBM-MSC therapeutic agents, that would be expected in abundance.

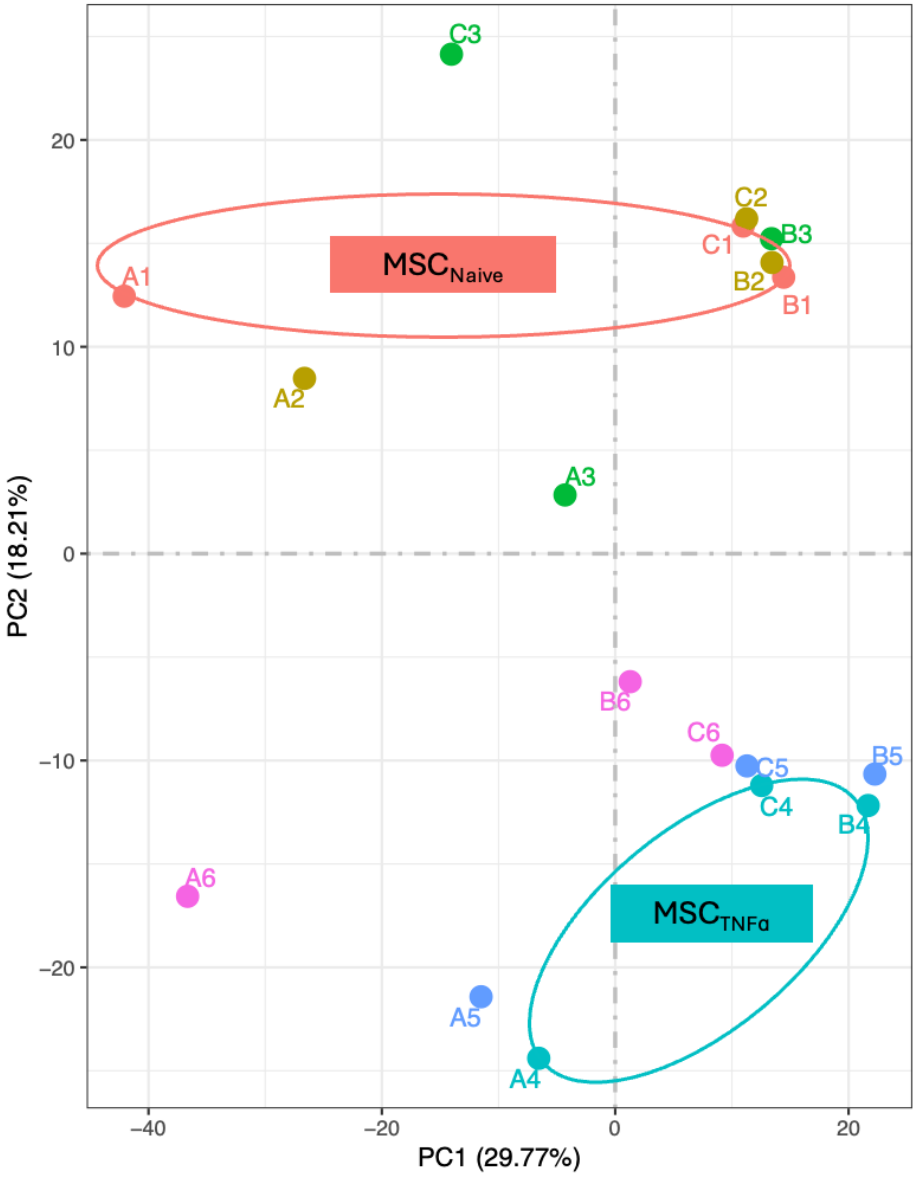

Supplementary figure 2: Naïve and TNFα-licensed hBM-MSC RNA sequencing PCA plot. 3 individual hBM-MSC donors were selected from RoosterBio™ to use in these assays. Cells were seeded at a density of $1x10^5$ per well in a 6-well plate and exposed to 5ng/ml TNFα for 6hrs, before harvesting the cells, isolating the RNA and sending for RNA sequencing. A PCA plot was created by Novogene™ to visualise the differences and similarities between groups.

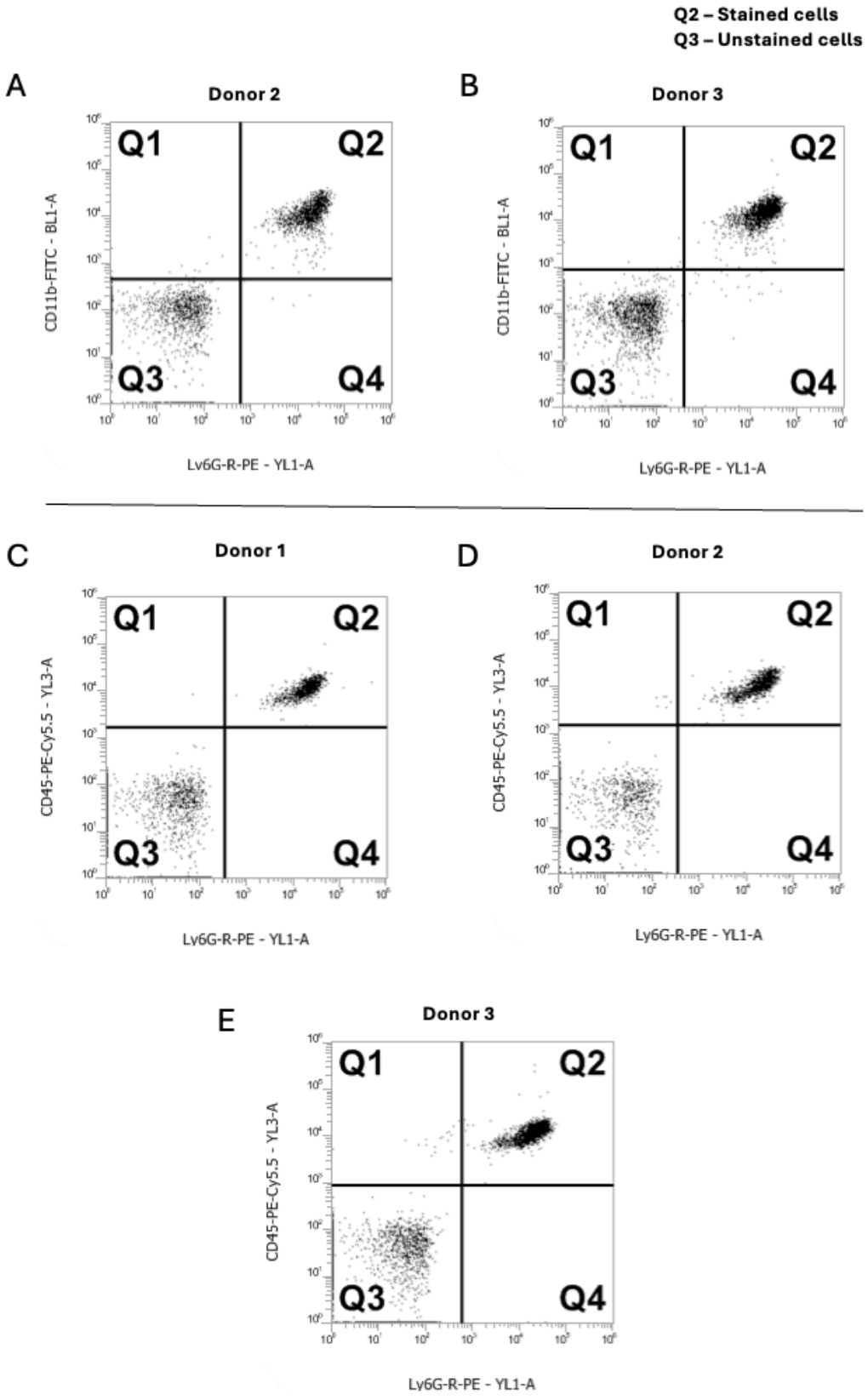

Figure legend available on next page

Supplementary figure 3: Neutrophil characterisation flow plots. Cells were selected for based on size and granularity. Live cells were then selected for, before gating on CD45+/CD11b/Ly6G+ cells. Attune™ software was used to build overlays of both unstained and stained cells for (A, B) CD11b+/Ly6G+ and (C-E) CD45+/Ly6G+ cells. Donor 1 plot for CD11b/Ly6G+ can be seen in figure 7, Donors 2 (A) and 3 (B) are represented in this figure. CD45+/Ly6G+ plots have also been included in this figure (C-E).

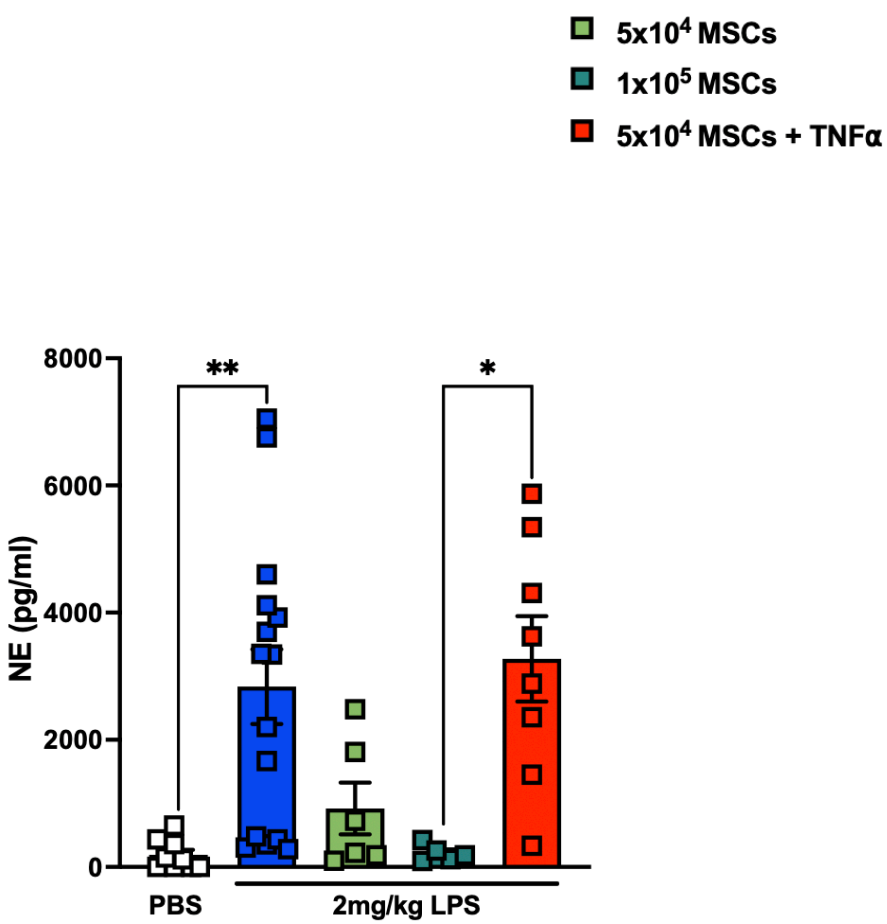

Supplementary figure 4: hBM-MSC$_{TNF\alpha}$ could not reduce neutrophil elastase (NE) in a model of ALI. hBM-MSCs of a low dose or high dose were injected (IV) into mice exposed to LPS (IT) and BALF was harvested at a 48hr timepoint. An ELISA was carried out to assess NE (one-way ANOVA followed by Tukey's post-hoc test, n=5-14). Replicates are a representation of 5 to 14 mice per group. Data is presented as mean ± SEM; *p<0.05, **p<0.01, ***p<0.001, ****p<0.0001.

Chapter 3

The ARDS microenvironment enhances MSC-induced repair via VEGF in experimental acute lung inflammation

**This chapter is from a published study that is available for view in appendix 7.1*

3.1 Abstract

Clinical trials investigating the potential of mesenchymal stromal cells (MSCs) for the treatment of inflammatory diseases, such as acute respiratory distress syndrome (ARDS), have been disappointing; with less than 50% of patients responding to treatment. Licensed MSCs show enhanced therapeutic efficacy in response to cytokine-mediated activation signals. There are two distinct sub-phenotypes of ARDS: hypo- and hyper-inflammatory. We hypothesised that pre-licensing MSCs in a hyper-inflammatory ARDS environment would enhance their therapeutic efficacy in acute lung inflammation (ALI). Serum samples from ARDS patients were segregated into hypo- and hyper-inflammatory categories based on IL-6 levels. MSCs were licensed with pooled serum from hypo- or hyper-inflammatory ARDS patients or healthy serum controls. Our findings show that hyper-inflammatory ARDS pre-licensed MSC conditioned medium (MSC-CM_{Hyper}) led to a significant enrichment in tight junction expression and enhanced barrier integrity in lung epithelial cells *in vitro* and *in vivo*; in a VEGF-dependent manner. Importantly, while both MSC-CM_{Hypo} and MSC-CM_{Hyper} significantly reduced IL-6 and TNFα levels in the bronchoalveolar lavage fluid (BALF) of LPS-induced ALI mice, only MSC-CM_{Hyper} significantly reduced lung permeability and overall clinical outcomes including weight loss and clinical score. Thus, the hypo- and hyper-inflammatory ARDS environment may differentially influence MSC cytoprotective and immunomodulatory functions.

Graphical Abstract

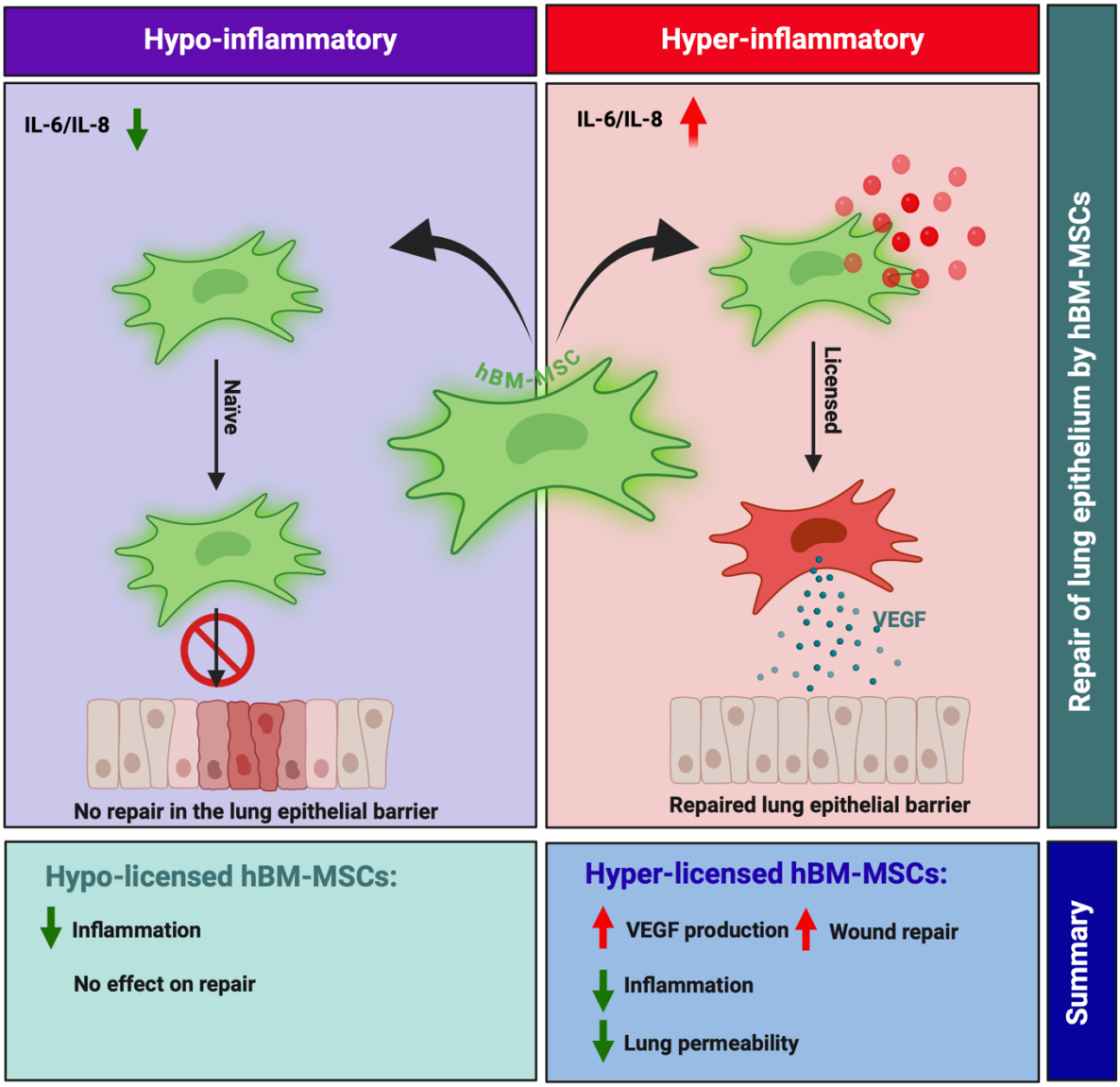

3.2 Hypothesis and aims

Hypothesis: Hyper, but not hypo-inflammatory, ARDS serum exposure will alter MSC immunomodulatory capacity in a model of ALI.

Aim(s):

- Identify sub-groups of ARDS; categorising into hypo- and hyper-inflammatory sun-phenotypes.
- Investigate the impact of ARDS-licensing on hBM-MSC gene and protein expression.
- Understand the role of ARDS-licensed hBM-MSCs in an *in vitro*, acute lung interphase lung cell culture model.
- Understand the role of ARDS-licensed hBM-MSCs in pre-clinical model of ALI.

3.3 Introduction

Acute respiratory distress syndrome (ARDS) is an inflammatory disease with a mortality rate of ~60% in SARS-CoV-2-induced ARDS patients [277, 278]. ARDS is largely characterised by low blood oxygen levels, excessive alveolar damage and acute respiratory failure [8, 9, 18]. One of the primary treatments for ARDS is mechanical ventilation; with ~70% of patients in need of ventilation. Unfortunately, ventilation can further exacerbate the disease state of the patient and contribute to disease pathology through ventilator-induced lung injury (VILI) [278, 279]. The Berlin definition of ARDS states ventilator support as a key diagnostic criterion, but the more recent global definition suggests that this is no longer a critical diagnostic component [18, 19]. Due to the lack of available treatments, cell therapies have long been investigated as a potential treatment for ARDS. Mesenchymal stromal cell (MSC) therapies have been investigated in the treatment of ARDS, due to their ability to modulate over-zealous inflammatory responses; however, clinical trials have generated disappointing results, with only ~30-50% of patients responding to treatment, as of the latest clinical trials [97, 163, 164].

MSCs are primarily known for their immunomodulatory properties and reparative capacity. This makes them an excellent candidate in the treatment of inflammatory diseases, such as ARDS. MSCs are known to show enhanced efficacy when exposed to cytokine-mediated activation signals, often referred to as *'MSC licensing'* [150, 190, 206, 238]. Although ARDS is traditionally characterised as an inflammatory disease containing the necessary levels of inflammation to effectively license the MSCs *in vivo*, sub-phenotypic stratification of patients suggests that there are two distinct sub-groups: hypo- and hyper-inflammatory ARDS [280]. Hyper-inflammatory ARDS is largely characterised by high levels of pro-inflammatory cytokines, such as IL-6 and IL-8, while hypo-inflammatory has significantly less of an inflammatory signature [281]. Since MSC licensing largely impacts

their functional capacity *in vivo*, this would suggest that MSCs would be more efficacious in the treatment of hyper-inflammatory ARDS. Unlicensed MSCs, or MSCs that are placed into an environment lacking a threshold level of inflammation are less likely to exert beneficial effects [192, 282, 283]. Therefore, understanding the MSC response to the ARDS patient microenvironment is a crucial, but often overlooked, point of interest prior to clinical trials.

The acute lung inflammation (ALI) and cellular infiltration seen in ARDS is known to lead to disruptions in the lung epithelium; leading to pulmonary oedema, and ultimately, death of the patient [5-7]. Tsikis *et al* (2024) recently highlighted that endotoxin-induced ALI in mice led to a significant reduction in vascular endothelial growth factor (VEGF), and its associated receptor: VEGF receptor 2 (VEGFR2) [284]. MSCs are already known to secrete VEGF, and many studies have already investigated the role of MSC-derived VEGF in the context of cyto-protection, wound healing, and permeability [154, 159, 285]. Other studies have highlighted the enrichment of tight junction expression, and the capacity for MSCs and MSC-derived extracellular vesicles to reduce epithelial barrier permeability [71, 286-291]. However, this study is the first to investigate the impact of the hypo- and hyper-inflammatory patient microenvironment on MSC functionality, using human bone marrow-derived MSCs (hBM-MSCs), clinically relevant ARDS patient samples and a pre-clinical model of ALI.

3.4. Materials and Methods

3.4.1 Study cohorts and ethical approval

Full ethical approval was obtained from both Galway University Medical Ethics Committee, Maynooth University Ethics Committee and St Vincent's Healthcare Group. All participants provided full consent.

3.4.2 Ethical approval and HPRA compliance

Ethical approval was granted by the ethics committee of Maynooth University (BRESC-2022-2453953) and project authorisation from the HPRA (AE19124/P031), in accordance with the Animal Research: Reporting of In Vivo Experiments (ARRIVE) criteria.

3.4.3 ARDS serum extraction

Blood samples were taken from SARS-CoV-2-induced ARDS patients, fractionated to obtain the serum, and placed in 5ml serum collection tubes. The samples were frozen at -20℃ overnight, before being transferred to -80℃. This work was carried out in Galway University Hospital, prior to delivery of the samples. Samples were derived from both male and female patients, in the age range of 40-80 years old. Healthy serum samples were sourced from St Vincent's University Hospital as a control. These samples were processed in the same manner, and age-matched accordingly.

3.4.4 ARDS patient sample pool generation

IL-6 levels were measured to stratify patient samples into either the hypo- or hyper-inflammatory ARDS sub-phenotype. Patient samples with an IL-6 level <50pg/ml were pooled and used as a representative of hypo-inflammatory ARDS (N=7). Patient samples with an IL-6 level >50pg/ml were pooled and used as a representative of hyper-inflammatory ARDS (N=7) (table 1). Once pooled, the IL-6, TNFα (Biolegend™), IL-8 & Macrophage Migration Inhibitory Factor (MIF) (R&D™) levels were analysed via Enzyme Linked Immunosorbent Assay (ELISA) to ensure that our hyper-inflammatory cohort has significantly more of both.

Table 1: ARDS patient cohort.

Biobank ID no.	Date of sampling	Il-6 (pg/ml)	Age	Sex	Date of COVID symptoms	Date of hospital admission	WHO score [292]	O_2 ratio (FiO2)	Outcome	No. days from + test to admission	No. days from + test to sample use
203-205	09/01/2021	5	59	M	01/01/2021	07/01/2021	6	0.65	Alive	6	8
203-205	07/01/2021	24	59	M	01/01/2021	07/01/2021	6	0.7	Alive	N/A	6
203-212	03/10/2020	<2.5	72	F	Pre-covid	03/10/2020	N/A	0.28	Alive	N/A	N/A
203-212	16/01/2021	8	75	F	05/01/2021	11/01/2021	8	0.4	Alive	6	11
203-213	17/01/2021	73	75	M	31/12/2020	06/01/2021	10	0.55	Deceased	6	17
203-215	25/01/2021	412	68	M	27/12/2020	12/01/2021	10	0.95	Deceased	16	29
203-217	13/01/2021	2.5	58	F	31/12/2020	11/01/2021	8	0.3	Alive	11	13
203-217	14/01/2021	4	58	F	31/12/2020	11/01/2021	8	0.45	Alive	N/A	14
203-224	30/01/2021	26	75	F	09/01/2021	18/01/2021	10	0.5	Deceased	N/A	21
203-225	22/01/2021	93	58	F	05/01/2021	18/01/2021	9	0.55	Alive	13	17
203-225	26/01/2021	316	58	F	05/01/2021	18/01/2021	9	N/A	Alive	N/A	21
203-225	25/01/2021	186	58	F	05/01/2021	18/01/2021	9	0.45	Alive	N/A	20
203-226	25/01/2021	310	45	F	15/01/2021	22/01/2021	6	0.65	Alive	7	10
203-227	26/01/2021	84	55	M	01/01/2021	20/01/2021	6	N/A	Alive	N/A	25
203-229	02/02/2021	26	60	M	10/01/2021	22/01/2021	8	0.35	Alive	12	23
203-231	26/01/2021	15	63	M	08/01/2021	19/01/2021	10	0.5	Deceased	11	18
203-231	10/02/2021	87	63	M	08/01/2021	19/01/2021	10	0.95	Deceased	N/A	33
203-240	21/02/2021	194	41	M	10/01/2021	25/01/2021	7	0.3	Alive	15	42
203-240	10/02/2021	259	41	M	10/01/2021	25/01/2021	8	0.75	Alive	N/A	31
203-260	29/01/2021	20	54	M	13/01/2021	20/01/2021	6	0.3	Alive	7	16

3.4.5 Enzyme-Linked Immunosorbent Assay (ELISA)

96-well half-area ELISA plates (COSTAR™) were coated as per manufacturers guidelines (human IL-6 (Biolegend™), IL-8, MIF, VEGF (R&D™)). The plate was then blocked with reagent diluent (1% BSA in PBS, sterile filtered) for 1hr before adding samples in appropriate dilutions for 2hrs. The detection antibody was then added as per manufacturers guidelines and left for a further 1 (Biolegend™) to 2hrs (R&D™). Streptavidin-HRP was added for 30 minutes, followed by a TMB substrate. The reaction was stopped using a 2N stop solution made up of $H2SO_4$ and distilled H_2O when colour appeared in a gradient in the standard. The plate was washed in an automated washer (ELx50 Biotek™) three times between each step and measured at absorbances of 450nm and 570nm using a CLARIOstar™ micro-plate reader.

3.4.6 Cell culture of hBM-MSCs

hBM-MSCs from three different donors were obtained from RoosterBio™ and expanded as per manufacturer's guidelines using Rooster Nourish expansion media (Rooster Basal + Rooster Booster). Cells were further cultured in Dulbecco's Modified Eagle Medium (DMEM; Merck life science limited, #D6046), supplemented with 10% Foetal Bovine Serum (FBS; Thermofisher) and 1% *Penicillin streptomycin* (Merck life science limited, P4458-100ML) to create complete DMEM (cDMEM), for 5 days, at 37°C + 5% CO2. All experiments were a representation of three independent MSC donors.

3.4.7 Generation of MSC-CM

hBM-MSCs (passage 2-4) were seeded at a density of $1x10^5$ per well in a 6-well plate in 1ml of cDMEM and left overnight to attach. Once attached, the media was removed, and 1ml of media containing 20% healthy, hypo- or hyper-inflammatory ARDS serum was added to each corresponding well and left for 24hrs. This media was then removed, the cells were washed

with PBS to remove any leftover serum, and serum-free DMEM was added for a further 24hrs to allow for the generation of MSC-CM. Supernatants were harvested, centrifuged at 300g for 5 minutes to remove debris, aliquoted and stored at -20℃ for future experiments.

3.4.8 Neutralisation of MIF using SCD-19

100µM of SCD-19 (3-(2-methylphenyl)-1H-isochromen-1-one) (Specs.net, Netherlands) was added to MSC-CM and left in a shaking incubator at 37°C for 1hr. Confirmation of MIF neutralisation was assessed by-way-of ELISA. This dosage was chosen based on a prior study from our lab [156].

3.4.9 Concentration of MSC-CM using Amicon ultra centrifugal filters

For use in *in vivo* studies, the MSC-CM was concentrated into a smaller volume of liquid for administration to the mice. MSC-CM was placed in an Amicon filter of appropriate size for VEGF purification (50kDa) and centrifuged at 14,000g for 30 minutes. The filter was then inverted, placed in a clean Eppendorf, and centrifuged at 1000g for 2 minutes to elute the concentrated MSC-CM. This concentrate was reconstituted in the appropriate amount of PBS, and 30µl was given, intranasally, per mouse.

3.4.10 Cell culture of CALU-3s

Human CALU-3 lung epithelial cells obtained from Dr. Mark Robinson (MU) were cultured in cDMEM at 37℃ + 5% CO_2. The cells were split at a 1:2 ratio every 3-4 days and monitored closely.

3.4.11 CALU-3 stimulation

CALU-3s were seeded at a density of $5x10^5$ per well in a 6-well plate and stimulated with 2ug/ml of lipopolysaccharide (LPS)/endotoxin (Sigma, serotype: 0001:B4, #L2630-100mg), or a PBS control (Merck life science limited, #TMS-012-A). 24hrs post-endotoxin stimulation, a 10μM solution of SU-5416, VEGFR2-inhibitor, or an appropriate DMSO vehicle control, were added for 4hrs. An inhibitor only control was used to address any potential inhibitor-associated effects. This was then washed away with, and the endotoxin (or PBS control) was re-added, along with 2ml of MSC-CM (containing ~1000pg/ml of VEGF) for a further 24hrs. Cells were harvested in TRIzol (Bio Sciences Ltd., #15596018) for gene expression analysis.

3.4.12 Gene expression

RNA was extracted from hBM-MSCs that had been exposed to 20% healthy, hypo- or hyper-inflammatory ARDS serum. The RNA was nano-dropped (Nanodrop 2000 spectrophotometer) to assess concentration and purity. The RNA was then normalised to 100ng/μl, and cDNA was made using the QuantBio™ cDNA Synthesis kit (as per manufacturer's instructions; VWR International, #733-1174). Real-time Polymerase Chain Reaction (RT-PCR) was then carried out using PerfeCta SYBR Green FastMix (QuantBio™, #95072-05K) and the required primers (tables 2 & 3). Expression was quantified in relation to the housekeeper gene HPRT, and the relative fold change was measured by calculating the $2^{-\Delta\Delta CT}$ values.

Table 2: Human primer sequences.

Gene name	Brand	Species	Forward Sequence	Reverse Sequence
HPRT	Sigma ™	Human	5'ATAAGCCAGACTTTGTTGG	5'ATAGGACTCCAGATGTTTCC
TJP1	Sigma ™	Human	5'TTGTCTTCAAAAACTCCCAC	5'GACTCACAGGAATAGCTTTAG
CLDN4	Sigma ™	Human	5'GAGCCATATAACTGCTCAAC	5'AGATAAAGCCAGTCCTGATG
OCLN	Sigma ™	Human	5'GGACTGGATCAGGGAATATC	5'ATTCTTTATCCAAACGGGAG

Table 3: Murine primer sequences.

Gene name	Brand	Species	Forward Sequence	Reverse Sequence
hprt	Sigma ™	Mouse	5'AGGGATTTGAATCACGTTTG	5'TTTACTGGCAACATCAACAG
tjp1	Sigma ™	Mouse	5'CTGATAGAAAGGTCTAAAGGC	5'TGAAATGTCATCTCTTTCCG
cldn4	Sigma ™	Mouse	5'GACTGTGCAAAGTTACTAGC	5'ACCAGCAATTTGGATGTAAG
ocln	Sigma ™	Mouse	5'AAAGCAAGTTAAGGGATCTG	5'TGGCATCTCTCTAAGGTTTC

3.4.13 Trans Epithelial Electric Resistance (TEER) assay

CALU-3 cells were seeded at a density of $7x10^5$ per well in a 6-well transwell insert, that had been coated with 1% fibronectin (Sigma, #F0895) for 1hr based on optimisation of the assay (supplementary figure 1). For the first week of culture, the cells were grown in submerged conditions (cDMEM in lower well and transwell). For the second week the cells were expose to air liquid interface culture conditions (cDMEM in lower well only). On day 15, the cells were stimulated with 2µg/ml of endotoxin (Serotype: 0111:B4 (Sigma™)). On day 17, the media was supplemented with 1ml of MSC-CM. Measurements were taken using the EVOM™ on days 1, 3, 5, 8, 10, 12, 15, 17 and 19. Media was changed 1hr prior to measurement. Cells were harvested in TRIzol (Bio Sciences Ltd., #15596018) for gene expression analysis. To analyse the TEER, a blank value (from a transwell containing no cells) was subtracted from each value; and the values were then multiplied by the area of the well ($4.67cm^2$). The relative TEER was then generated by dividing each replicate's final TEER value on day 19, by the corresponding PBS control well on day 19.

3.4.14 CALU-3 scratch assay

CALU-3 lung epithelial cells were seeded at a density of $5x10^5$ in a 6-well plate. Once 80% confluent, a single vertical scratch was made down the centre of the well using a p200 tip. The cells were then washed with PBS to remove debris, and MSC-CM was added for a period of 48hrs. 48hrs post-scratch, the cells were fixed with 10% formalin for 8 minutes, before leaving to dry. Once dry, the cells were stained with crystal violet for 4 minutes, dried, and imaged using a Nikon™ microscope and Optika™ software. To avoid bias in recording of results, a marker was used to pinpoint an area in the upper triad, central point and lower triad of the scratch to denote where to image post-fixing and staining (supplementary figure 2a). An image was taken from each of these areas for analysis (supplementary 2b, c).

3.4.15 Histology and staining of the CALU-3 epithelial barrier

On day 19 of the TEER, CALU-3s were fixed in 10% formalin overnight, before being processed, embedded in wax and sectioned. Sections were carefully placed on slides, immersed in xylene to remove any excess wax, and stained appropriately. Slides were stained with Haemotoxylin and Eosin (H&E) to visualise the barrier clearly. Images were taken using an Olympus BX51 light microscope.

3.4.16 ALI pre-clinical mouse model

Male and female C57BL6/J mice (Charles River), aged 12-16 weeks, were given 2mg/kg endotoxin (Sigma, serotype: 0001:B4, #L2630-100mg), or a corresponding endotoxin-free PBS control (Merck life science limited, #TMS-012-A), intratracheally and monitored closely for 48hrs. MSC-CM was concentrated using Amicon Ultra Centrifugal Filters, and incubated with either an anti-VEGF monoclonal antibody (Bevacizumab Biosimilar; *InVivo*SIM™) to inhibit VEGF functionality, or an IgG isotype control (*InVivo*MAb™). The MSC-CM was administered, intranasally, 4hrs post-endotoxin administration.

3.4.17 Evan's Blue dye

A 10% solution of Evan's Blue Tetrasodium Salt (Tocris™, #0845) was made up in PBS. The solution was filter sterilised, and 200µl was injected intravenously into the tail vein of the mice. 1hr post-injection, the mice were sacrificed using an intraperitoneal injection of pentobarbital and the blood, bronchoalveolar lavage fluid (BALF) and lungs were harvested for analysis. The BALF was used for cytokine analysis by ELISA, and all animal scoring was graphed (weight/temperature/clinical score). To analyse this, absorbance readings were taken to assess the total Evan's blue in the lung and serum (620nm and 740nm) and compared to a serial-diluted standard of Evan's Blue Dye. The total lung Evan's Blue was then divided by the serum

Evan's Blue values, to account for tail vein injection error; and this was further divided by the lung wet weight to get the absolute Evan's Blue concentration [292].

3.4.18 Statistical analysis of animal studies

One-way ANOVA, followed by the post hoc Tukey's multiple comparison test was used to assess significance; except in figure 6 (d, e), where a two-way ANOVA was used. All data is presented as mean ± SEM; n=5 per group.

3.5 Results

3.5.1 Segregation of ARDS patient serum samples

ARDS patient serum samples were stratified based on their IL-6 level on arrival to the ICU. ARDS patient demographics including age, sex, World Health Organisation (WHO) score and O_2 requirement (FiO2) are included in supplementary table 1 and figure 1A-D. For this study, patients with IL-6 levels <50pg/ml were considered hypo-inflammatory, and IL-6 levels >50pg/ml were considered hyper-inflammatory (figure 1E, F). Pooling the samples, especially in this naïve manner, is a limitation in the study. Ideally, we would have had enough sample to assess individual patient responses, or a clinical observation of which patients would be characterised as 'hypo' or 'hyper' prior to the study. For comparison, serum samples collected from healthy donors were included. Upon pooling the samples, we confirmed that the hyper-inflammatory pool contained significantly higher levels of IL-6 and IL-8; both known to be of higher levels in the hyper-inflammatory ARDS sub-phenotype (figure 1G, H). In addition, the hyper-inflammatory pool contained significantly higher levels of MIF and TNFα (figure 1I, J). All subsequent experiments were carried out using these distinct pools.

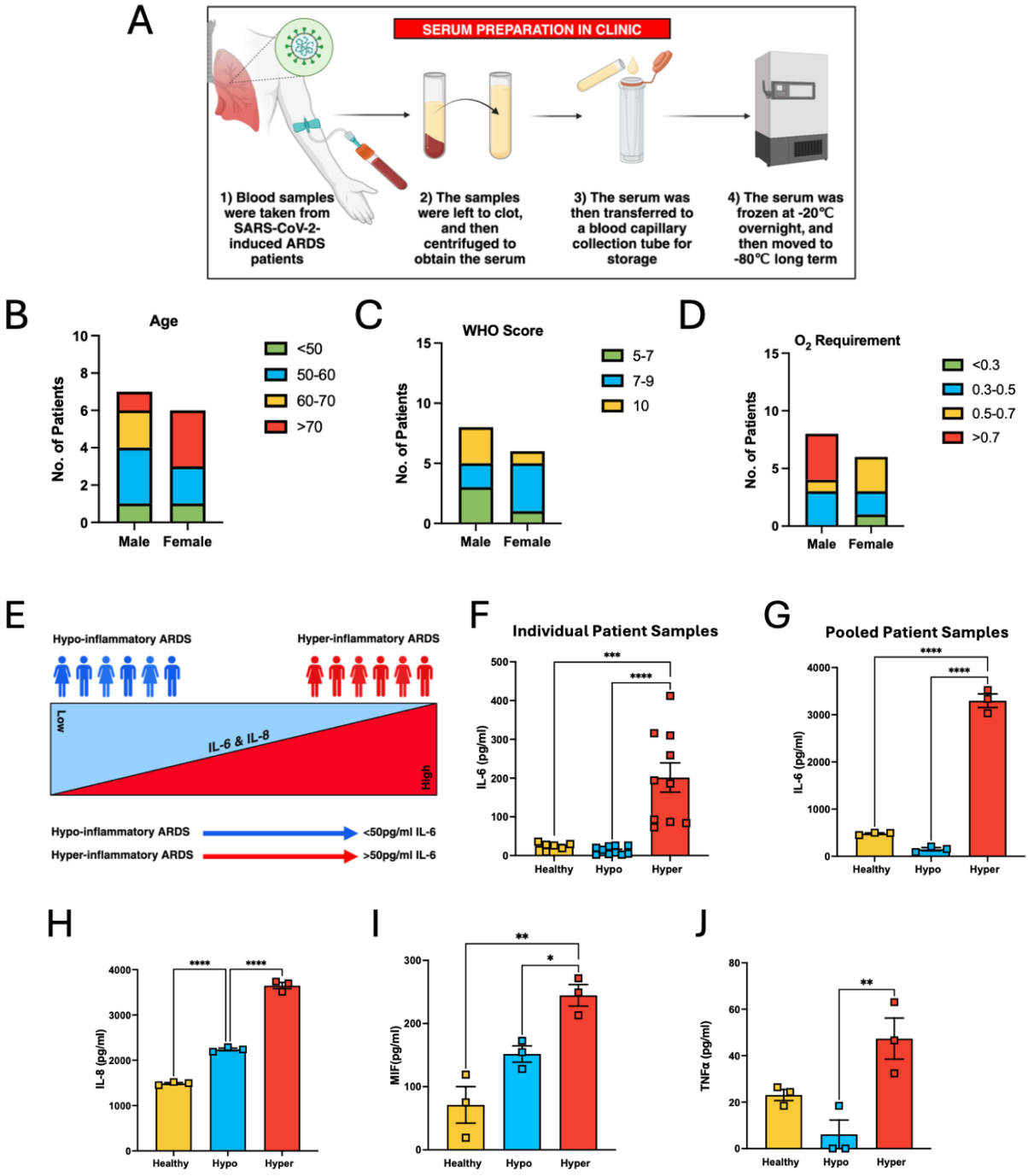

Figure legend available on next page

Figure 1: ARDS patient sub-phenotype stratification. (A) ARDS patient serum samples were obtained from patients of (B-D) differing backgrounds (age, WHO score, O2 level) and (E-F) stratified into hypo- or hyper-inflammatory sub-phenotypes based on their IL-6 levels at the time of admission (n=7). Patients with <50pg/ml IL-6 were considered hypo-inflammatory, and patients with >50pg/ml IL-6 were considered hyper-inflammatory. The samples were then pooled, and the (G) IL-6 (Biolegend™), (H) IL-8 (R&D™), (I) MIF (R&D™) and (J) TNFα (Biolegend™) levels were observed in each pool. Serum pooled from 6 healthy age-matched patients was used as a control. Data is presented as mean ± SEM; *p<0.05, **p<0.01, ***p<0.001, ****p<0.0001.

3.5.2 Hyper-, but not hypo-, inflammatory ARDS serum licenses MSCs and enhances their secretion of VEGF

MSC-CM from MSCs that had been exposed to healthy or hypo-inflammatory serum showed no significant increase in cytokines or growth factors, in comparison to naïve MSC-CM. There was no difference in IL-6 secretion between MSC-CM groups (figure 2B). Hyper-inflammatory ARDS serum, however, led to a significant increase in MSC secretion of IL-8, MIF and VEGF (figure 2C-E). Gene expression studies also highlighted that *VEGFA* and *KDR*; the genes that encode for VEGF-A and VEGFR2, respectively; were also significantly increased after exposure to hyper-inflammatory serum (figure 2F, G). There were no significant differences in expression of *IL-8*, *MIF,* or any of their corresponding receptors (*CXCR1, CXCR2, CXCR4, CD74*) (supplementary figure 3A-F. We also used a well-characterised MIF inhibitor, SCD-19, to assess if this was MIF-driven VEGF production in the MSCs; based on recent work published from our lab, but this was not MIF-driven (supplementary figure 4A, B) [156]. For this reason, we chose to further investigate the role of VEGF.

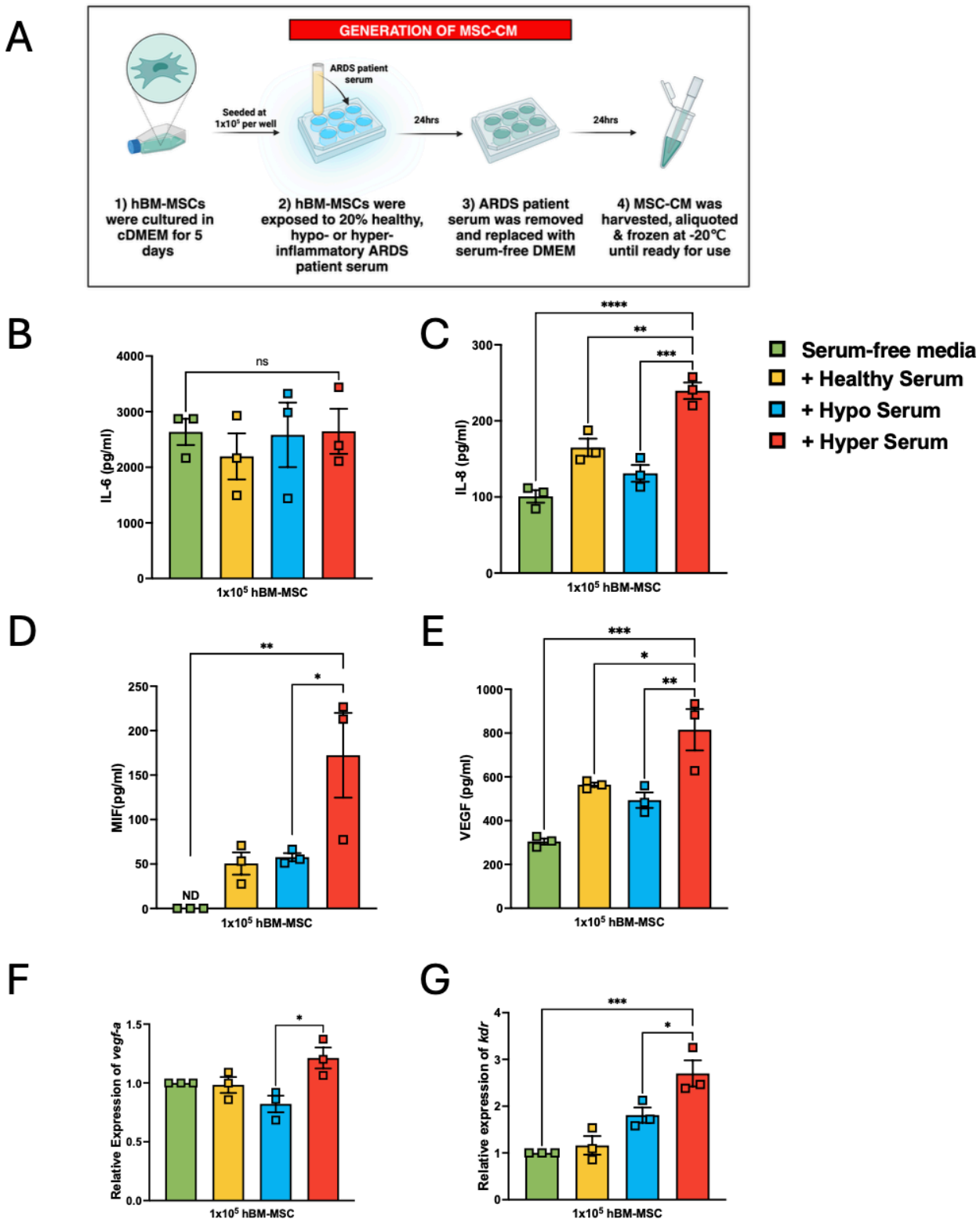

Figure legend available on next page

Figure 2: The MSC secretome in response to healthy, hypo- or hyper-inflammatory ARDS serum. (A) hBM-MSCs (n=3 donors) were seeded at a density of $1x10^5$ in a 6-well plate, left to attach and exposed to 20% ARDS patient serum, or healthy serum control. The serum was removed after 24hrs, the cells were washed with PBS, and serum-free DMEM was added for a further 24hrs to generate MSC-CM. The (B) IL-6 (Biolegend™), (C) IL-8, (D) MIF and (E) VEGF (R&D™) levels were then analysed via ELISA. Gene expression of (F) *VEGFA* and (G) *KDR* were assessed by RT-PCR. Data is presented as mean ± SEM; n=3 per group; *p<0.05, **p<0.01, ***p<0.001, ****p<0.0001.

3.5.3 MSC-CM enhances tight junction expression in CALU-3 lung epithelial cells in a VEGF-dependent manner

CALU-3s exposed to endotoxin showed a significant reduction in *TJP1,* the gene that encodes for Zonula Occludens-1 (ZO-1) (figure 3A, B). There was no significant difference in *OCLN* or *CLDN4*; the genes that encode for Occludin and Claudin-4, respectively; in response to endotoxin (figure 3C, D). However, upon exposure to 2ml of naïve MSC-CM, containing a high concentration of ~1000pg/ml of VEGF, correlating with the VEGF concentration seen in $MSC\text{-}CM_{Hyper}$ (figure 2E), there was a significant enrichment of *TJP1, OCLN* and *CLDN4* expression. Pre-treatment of CALU-3 lung epithelial cells with SU-5416, a VEGFR2 inhibitor, abrogated this effect (figure 3B-D), demonstrating that VEGF derived from MSC-CM was required for enhancement of tight junction gene expression in response to endotoxin challenge.

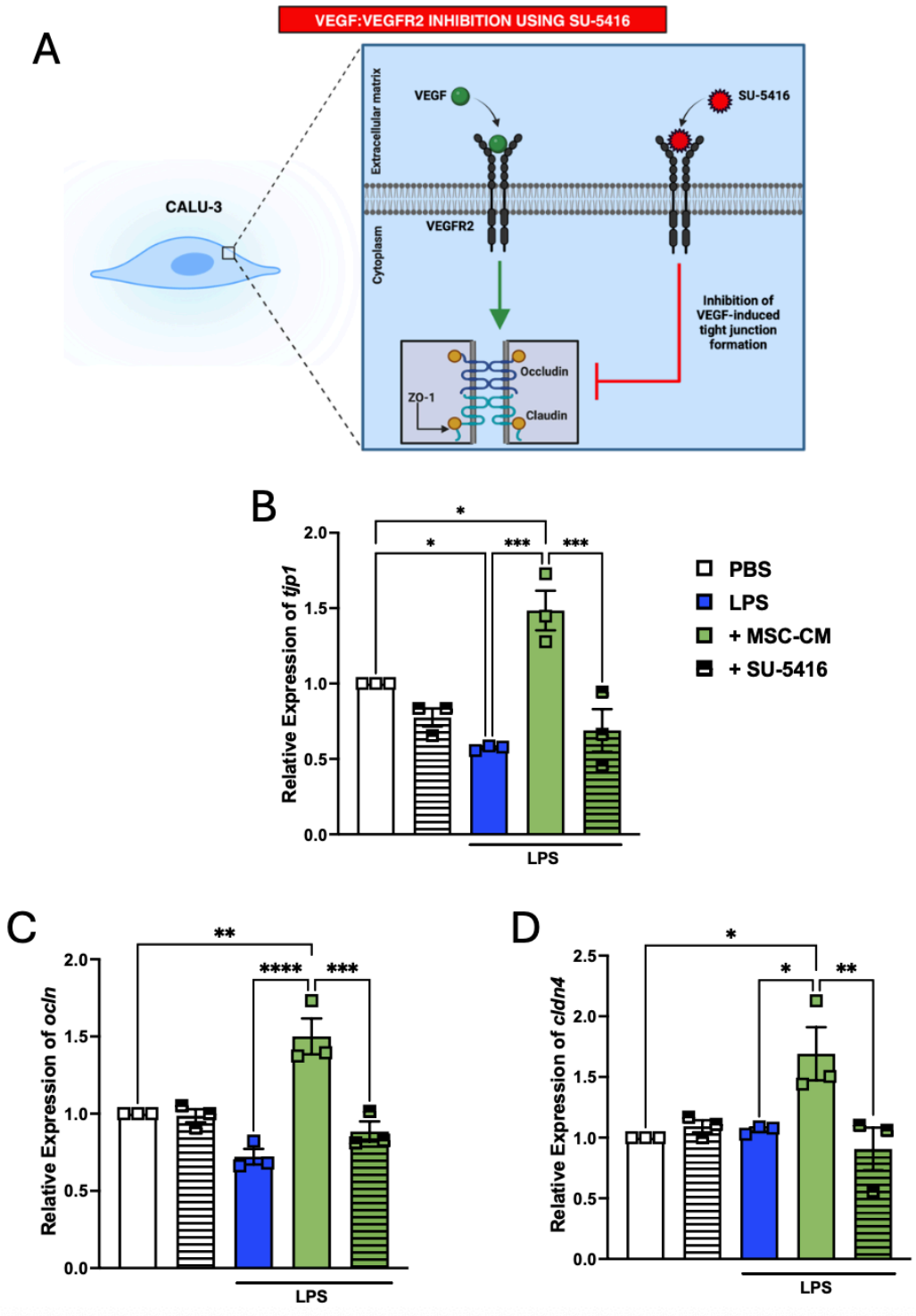

Figure legend available on next page

Figure 3: The MSC-CM enhancement of tight junction expression. (A) CALU-3 cells (passages 10-12) were seeded at a density of $5x10^5$ in a 6-well plate, left to attach and exposed to 10uM SU-5416, a VEGFR2 inhibitor for 4hrs, before stimulating with 2µg/ml endotoxin for 48hrs. Some groups were subsequently exposed to 2ml of MSC-CM containing ~1000pg/ml VEGF for 24hrs. The cells were then harvested for gene expression studies of tight junction genes: (B) *TJP1*, (C) *OCLN* and (D) *CLDN4*. Data is presented as mean ± SEM; n=3 per group; *p<0.05, **p<0.01, ***p<0.001, ****p<0.0001.

3.5.4 MSC-CM$_{Hyper}$ reduces lung permeability *in vitro*

TEER measurements were performed in CALU-3 cells in submerged cultures on days 1, 3 and 5 and in subsequent air liquid interface cultures from day 8. This was completed in wells that had been pre-coated with fibronectin due to the results seen in our pilot study, whereby the cells covered more surface area under these conditions (supplementary figure 2). This exposure to air allows for a more respiratory-like cell stratification; as lung epithelial cells are associated with exposure to both air and liquid in the body. Upon exposure to 2µg/ml of endotoxin on day 15, TEER measurements (ohm cm^2) demonstrate a significant decrease in epithelial membrane integrity by day 17 (figure 4A, B). The PBS control remained steady throughout. Subsequently, when exposed to 500µl of MSC-CM$_{Healthy}$ (containing ~500pg/ml VEGF) or MSC-CM$_{Hyper}$ (containing ~1000pg/ml VEGF) on day 17 (figure 4B, C), there was a significant improvement in barrier integrity on day 19. This was not seen in MSC-CM$_{Hypo}$ (~250pg/ml VEGF). We also observed increased epithelial wound closure in a CALU-3 scratch assay in response to MSC-CM$_{Hyper}$ (supplementary figure 5). Neutralising VEGF with a Bevacizumab biosimilar, led to the abrogation of this effect (figure 4B, C); confirming the importance of VEGF in MSC therapeutic efficacy. Gene expression studies on the cells from this assay also showed significant enrichment of *TJP1*, *OCLN* and *CLDN4* in response to MSC-CM$_{Hyper}$ (figure 4D-F). We further investigated this using histological imaging of the CALU-3 epithelial barrier; however, the effect was less clear (supplementary figure 6).

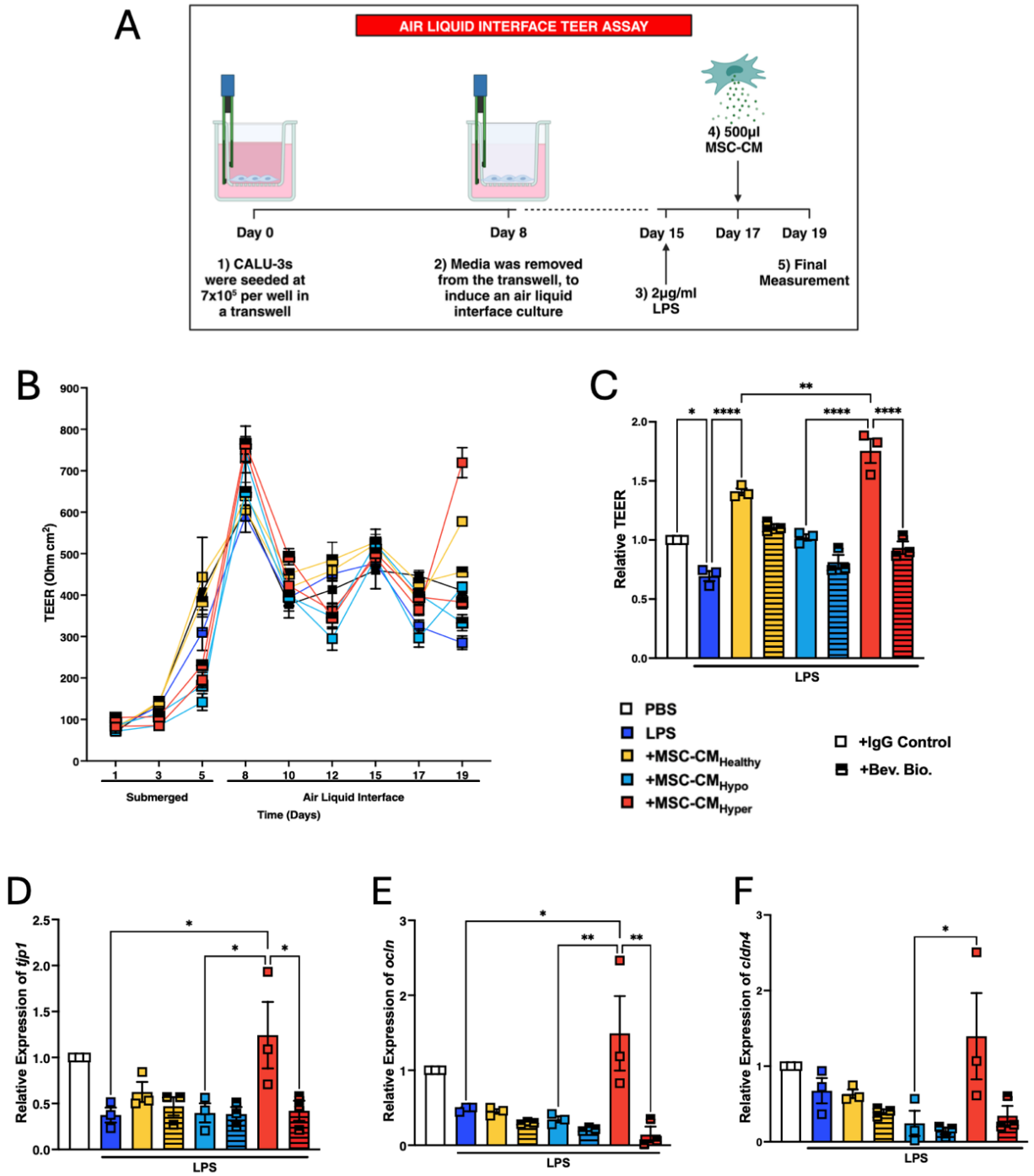

Figure legend available on next page

Figure 4: Barrier integrity of CALU-3 cells in response to MSC-CM. (A) CALU-3s were seeded at a density of $7x10^5$ in a transwell (0.4µm) and grown under air liquid interface conditions from day 8 of culture. On day 15, the cells were stimulated with 2µg/ml of endotoxin, and on day 17, they were exposed to 500µl of MSC-CM from the groups depicted in fig. 2E. (+/- Bevacizumab Biosimilar or the appropriate IgG isotype control) (B) TEER measurements were taken 3 times a week for 3 weeks, and (C) final measurements were taken on day 19. (D-F) Gene expression studies highlighted differences in tight junction expression. Data is presented as mean ± SEM; n=3 per group; *p<0.05, **p<0.01, ***p<0.001, ****p<0.0001.

3.5.5 MSC-CM_{Hyper} reduces overall disease severity in a pre-clinical model of ALI

MSC-$CM_{Healthy}$, MSC-CM_{Hypo} and MSC-CM_{Hyper} all had the ability to reduce the inflammatory profile seen in our model of ALI; primarily in the context of IL-6 and TNFα (figure 5A, B). In the context of clinical parameters in the endotoxin-induced lung inflammation model, both MSC-CM_{Hyper} (p-value = 0.0041) and MSC-$CM_{Healthy}$ (p-value = 0.0297) significantly reduced clinical score when compared to LPS-treated mice (figure 5C). In contrast, only MSC-CM_{Hyper} had the ability to significantly reduce percentage weight loss (p-value = 0.0071) when compared to LPS-treated mice (figure 5D). MSC-CM_{Hypo} did not significantly reduce the clinical score (p-value = 0.2728), or the percentage weight loss (p-value = 0.0994); however, there was no significant difference observed between MSC-CM_{Hyper} and MSC-CM_{Hypo} (p-value = 0.0690). Importantly, clinical score is a measure of percentage weight loss, temperature, appearance, clinical signs (such as 'clicking' noises from the lungs), dehydration and more. A single point of a difference can represent a huge difference in mouse health, and therefore, must not be overlooked based on what appears as a 'minor' or 'single point' difference.

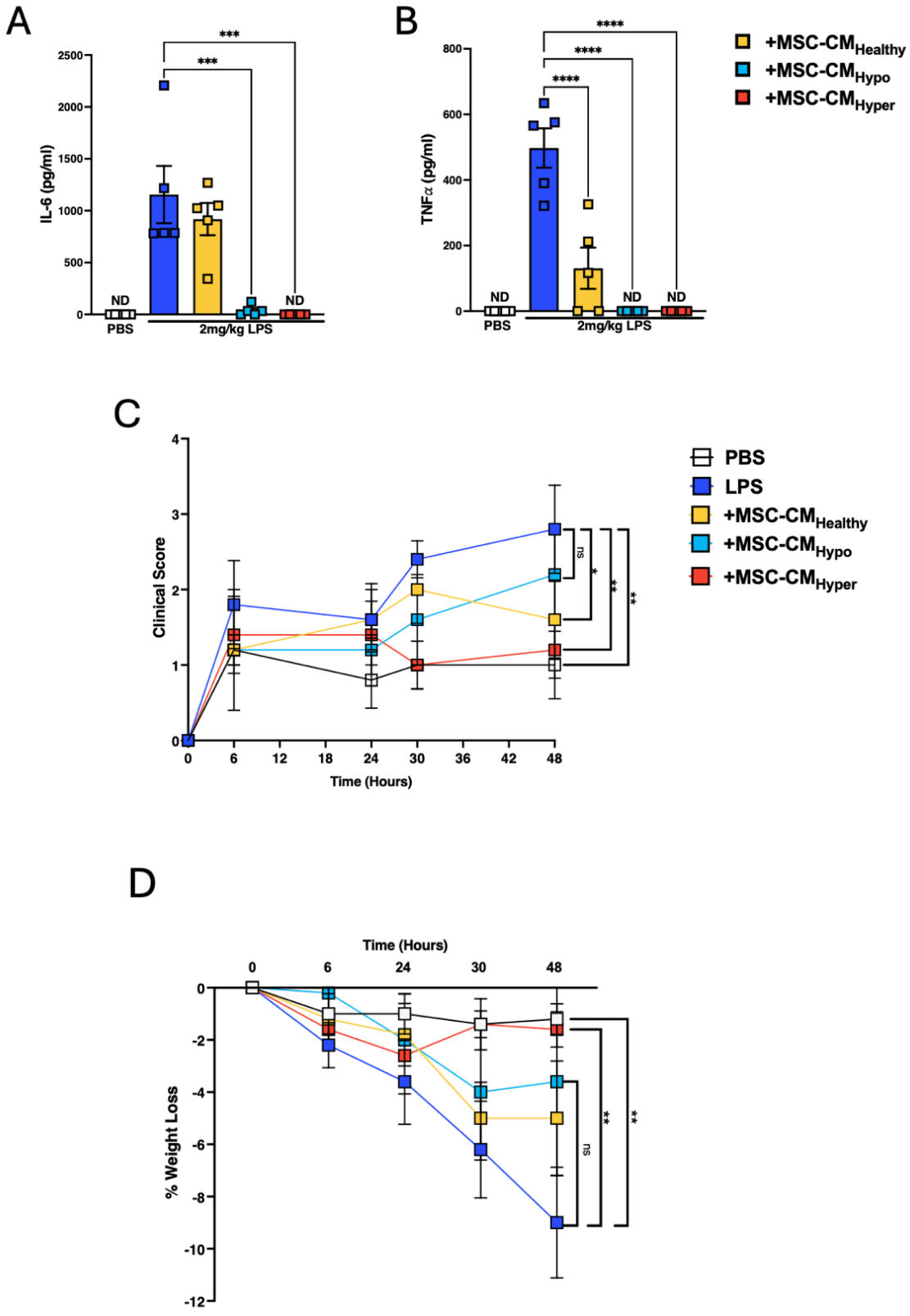

Figure legend available on next page

Figure 5: Cytokine levels in BALF and clinical scoring from ALI mouse model. BALF was harvested from C57BL6/J mice (n=5) exposed to our ALI model and (A) IL-6 and (B) TNFα were quantified by ELISA. (C) Clinical score and (D) percentage weight loss was also assessed. Data is presented as mean ± SEM; n=5 per group; *p<0.05, **p<0.01, ***p<0.001, ****p<0.0001.

3.5.6 MSC-CM$_{Hyper}$ reduces lung permeability in a pre-clinical model of ALI

Evan's blue dye was used as a measure of lung permeability *in vivo* (figure 6A). Lungs with a visible blue colouration are considered permeable, or 'leaky', as the Evan's blue dye leaks to the exterior of the lung. MSC-CM$_{Healthy}$, MSC-CM$_{Hypo}$ or MSC-CM$_{Hyper}$ was concentrated using centrifugal filters, and VEGF levels were measured following the addition of a Bevacizumab biosimilar (to neutralise VEGF) or an IgG control (figure 6B, C). The lungs from mice exposed to endotoxin, followed by MSC-CM$_{Hyper}$, showed a significant visual improvement in barrier integrity (figure 6D). This effect was abrogated when VEGF was neutralised. Mice that were treated with MSC-CM$_{Hyper}$ also showed a significant reduction in total Evan's blue in the lung extract (normalised to the serum Evan's blue and divided by the lung wet weight). This effect was abrogated when VEGF was neutralised (figure 6E). There was also a significant reduction in the wet: dry weight ratio of the lungs of mice that received MSC-CM$_{Hyper}$, which again, was lost when VEGF was neutralised (figure 6F). Further gene expression analysis on the mouse lung identified significant increases in tight junction expression in the lung in response to MSC-CM$_{Hyper}$ but not MSC-CM$_{Hypo}$ (supplementary figure 7).

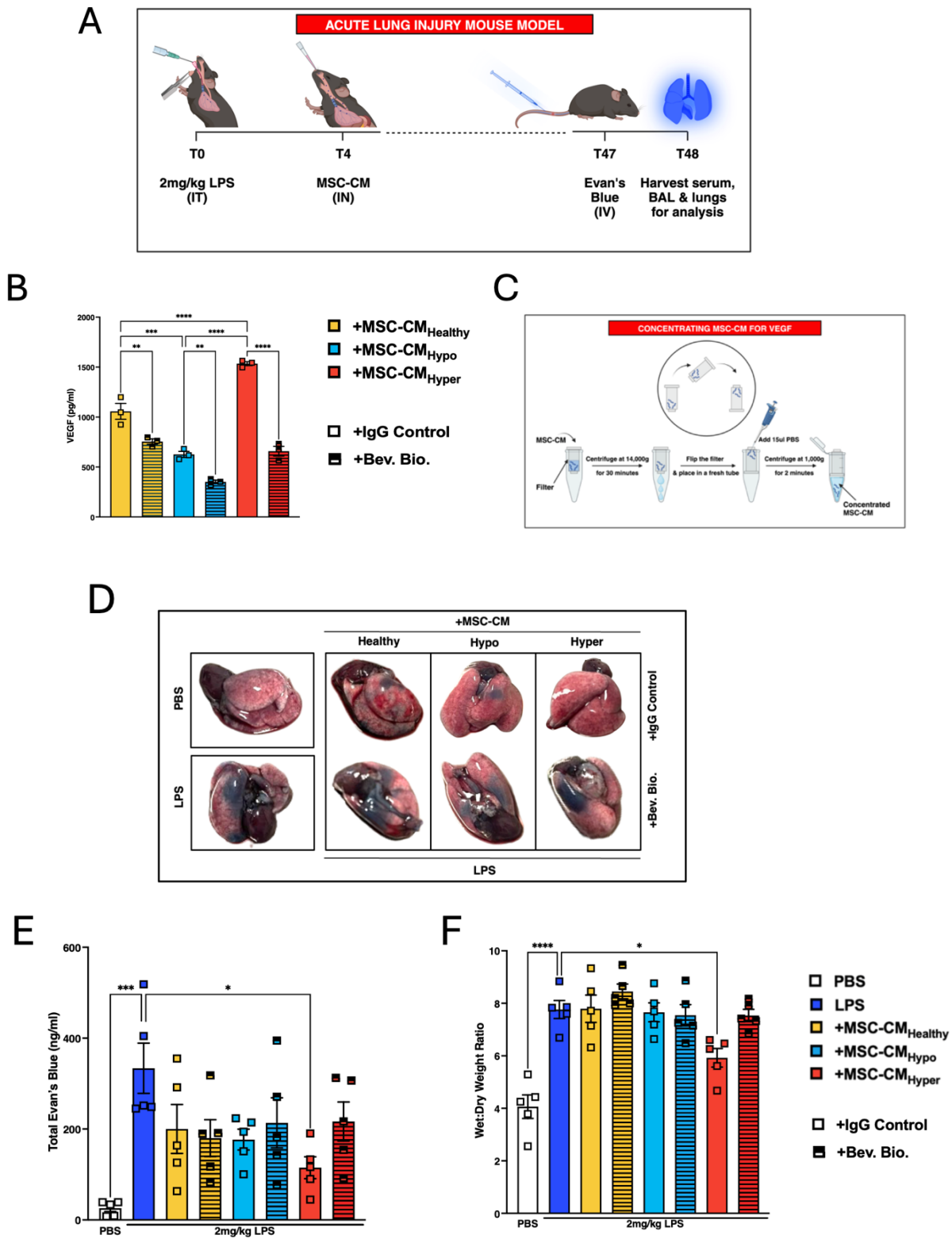

Figure legend available on next page

Figure 6: The impact of MSC-CM on lung permeability *in vivo*. (A) C57BL6/J mice (n=5) were exposed to 2mg/kg of endotoxin intratracheally at T0. (B, C) At T4, 500µl of MSC-CM that had been concentrated down to 30µl (+/- Bevacizumab Biosimilar or an appropriate IgG isotype control) was administered intranasally. 1hr before harvesting (T47), a 10% solution of Evan's Blue Dye was administered intravenously, and mice were sacrificed at T48. (D, E) Evan's Blue Dye (F) wet: dry weight ratio was used as indicators of permeability. Data is presented as mean ± SEM; n=5 per group; *p<0.05, **p<0.01, ***p<0.001, ****p<0.0001.

3.6 Discussion

The patient microenvironment is thought to have an impact on MSC therapy, with MSCs typically exerting their beneficial effects in response to an inflammatory stimulus. MSCs that have not been subjected to a threshold level of inflammation may lack therapeutic efficacy and may further contribute to disease pathology [150, 156, 190, 206, 238]. Other studies have shown that MSC-CM generated from MSCs exposed to ARDS patient bronchoalveolar lavage fluid (BALF) have had increased levels of cytokines in comparison to MSCs exposed to a healthy BALF control [293]. However, this study lacked patient stratification. This research illustrates that MSCs are more responsive to the hyper-, but not hypo-, inflammatory ARDS patient microenvironment in the context of MSC cytoprotective effects. This was outlined in figure 2, where it was shown that MSC-CM_{Hyper}, but not MSC-$CM_{Hypo,}$ had increased levels of IL-8, MIF and VEGF. MSC-CM_{Hypo} had a comparable level of protein secretion with that of MSC-$CM_{Healthy}$. Gene expression studies called further attention to VEGF; as *VEGFA* and *KDR* were significantly increased in the hyper-, but not hypo-, pre-licensed MSCs.

Based on previous literature, MSCs have already been shown to enhance epithelial tight junction gene expression in a VEGF-dependent manner [71, 159, 286-291]. Yang *et al* (2015) highlighted that MSCs could stabilise *endothelial* lung permeability in a model of ALI, through the enrichment of VEGF in the MSC-CM [159]. This work aimed to further investigate the impact of MSC-CM on tight junction enhancement as a mechanism for repairing the *epithelial* barrier. To do this, CALU-3 lung epithelial cells were exposed to endotoxin, to interrupt the epithelial barrier, and then exposed to MSC-CM (containing ~1000pg/ml of VEGF), a comparable concentration to that of hyper-licensed MSC-CM, from three independent non-treated MSC donors (figure 2E). A VEGFR2 inhibitor, SU-5416, was used to block VEGFR2 on the CALU-3 cells, to confirm VEGF-dependence (figure 3B, C). This study confirmed that

MSC-CM could enhance tight junction expression of *OCLN* while also enhancing the expression of *CLDN4* and *TJP1,* in a VEGF-dependent manner, in CALU-3 lung epithelial cells; a clinically relevant cell type for lung barrier studies due to their ability to generate tight junctions.

Furthermore, the relevance of this at a functional level was assessed, by performing a TEER assay in CALU-3 cells. Endotoxin significantly decreased the barrier integrity, and MSC-CM_{Hyper}, but not MSC-CM_{Hypo}, had the ability to significantly enhance barrier integrity in response to endotoxin (figure 4B, C). MSC-$CM_{Healthy}$ could also significantly enhance barrier integrity, but not to the same extent as MSC-CM_{Hyper}; which had the ability to fully restore the barrier. Using an anti-VEGF Bevacizumab biosimilar monoclonal antibody, or an IgG isotype control, the mechanistic impact of VEGF was investigated. This antibody functionally inhibits VEGF, and neutralising VEGF in this manner significantly abrogated the increased barrier integrity mediated by the MSC-CM_{Hyper} group. Gene expression studies further highlighted that hyper-licensed MSCs had the ability to enhance the expression of *tjp1*, *cldn4* and *ocln* in CALU-3 cells cultured at air liquid interface in a VEGF-dependent manner. There was no significant increase in these genes in the healthy-licensed MSCs. This is in line with studies in rat MSCs, whereby lentiviral VEGF knockdown rat MSCs failed to enhance epithelial barrier integrity when compared to control MSCs in a model of endotoxin-induced ALI [290].

To investigate the functional relevance *in vivo*, C57BL6/J mice were exposed to endotoxin to induce ALI, which shares some aspects of pathophysiology including the permeable, or 'leaky', human ARDS lung. The mice were then exposed to each of our treatment groups before receiving an injection of Evan's blue dye to assess lung permeability [292]. MSCs and MSC-CM have been shown to reduce pro-inflammatory cytokine levels and reduce pathology and clinical score in endotoxin-induced ALI models [294, 295]. Upon analysing the cytokine profile of the BALF of the mice subjected to each treatment, significantly less

cytokines were detected; in particular IL-6, in mice that received any form of MSC-CM. This aligns with previous studies [56, 296, 297]. The overall clinical parameters highlighted that both MSC-$CM_{Healthy}$ and MSC-CM_{Hyper} had the ability to significantly reduce clinical score; with p-values suggesting that MSC-CM_{Hyper} reduced this to a greater extent (figure 5C). MSC-CM_{Hyper} also showed a significant reduction in percentage weight loss, something we did not see in our MSC-CM_{Hypo} group (figure 5D). Importantly, only MSC-CM_{Hyper} significantly reduced lung permeability and this effect was VEGF-dependent. This data suggests that MSC cytoprotective and immunomodulatory effects may be mediated by different factors present in the secretome. This study focused on the cytoprotective effects mediated by VEGF and demonstrated that pre-licensing MSCs with high-IL-6 ARDS patient serum (denoted as hyper-inflammatory ARDS) had a significant impact in reducing lung permeability in comparison to healthy or hypo-inflammatory pre-licensed MSC-CM. However, in the same model, all MSC-CM had the ability to reduce the pro-inflammatory cytokines IL-6 and TNFα in the BALF. These findings confirm that MSCs of any form may be beneficial in the treatment of inflammatory disease, but only MSC-CM_{Hyper} appeared to be efficacious across all parameters; further highlighting the impact of the patient microenvironment on MSC functionality. Indeed, a recent study by Faircloth *et al* confirms this hypothesis showing that VEGF secretion and immunosuppression by MSCs are two distinct potency mechanisms [124].

This study provides novel insight into the impact of the patient microenvironment in dictating response to MSC therapy, offering a solution to the urgent unmet need for patient stratification prior to further MSC studies and clinical trials in the treatment of ARDS.

3.7 Concluding remarks

Within this chapter, the effect of ARDS serum-licensing on hBM-MSC therapeutic efficacy was assessed. It was shown that 'hyper' ARDS-licensed hBM-MSCs had the capacity to enhance MSC-associated cytoprotection, but 'hypo' ARDS-licensed hBM-MSCs did not have the same effect. This was shown to be VEGF-dependent, and was proven *in vivo* in a model of ALI. This study, a first of its kind, highlighted that patient stratification may be more important than once thought of in the context of MSC therapy. A strength of this study is its novelty; along with mechanistic insight. This work could be further enhanced by assessing the impact of samples from the ARDS patient lung itself on hBM-MSCs; which has been done by another group [298], but did not involve patient stratification. A weakness of this study can be seen in the limited number of patient samples. If there was access to more samples, the patients could have been stratified appropriately into their hypo- or hyper-inflammatory groupings and assessed individually. This would have provided deeper insight into whether it's as simple as 'hypo' vs 'hyper', or whether there may be more involved, as will be discussed in the next chapter.

3.8 Supplementary figures

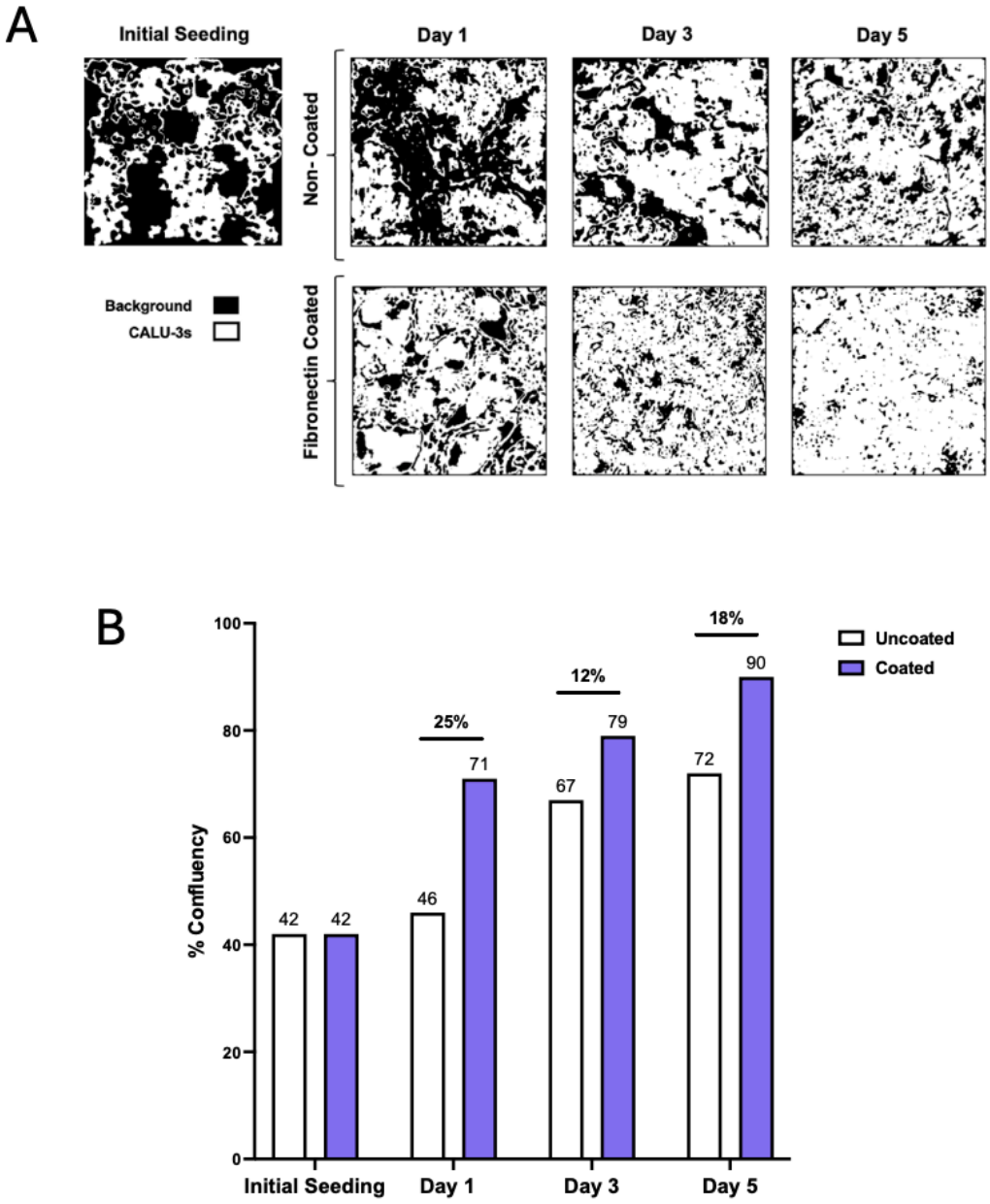

Supplementary Figure 1: Image J Analysis of CALU-3 confluency. CALU-3 lung epithelial cells were seeded at a density of $7x10^5$ per well in a fibronectin-coated, or un-coated, 6-well plate and left to attach and grow. (A) Imaging over the course of 5 days highlighted enhanced coverage in the fibronectin-coated plates. (B) Quantification of this using Image J further confirmed this. Data is presented as a mean of 3 wells per group.

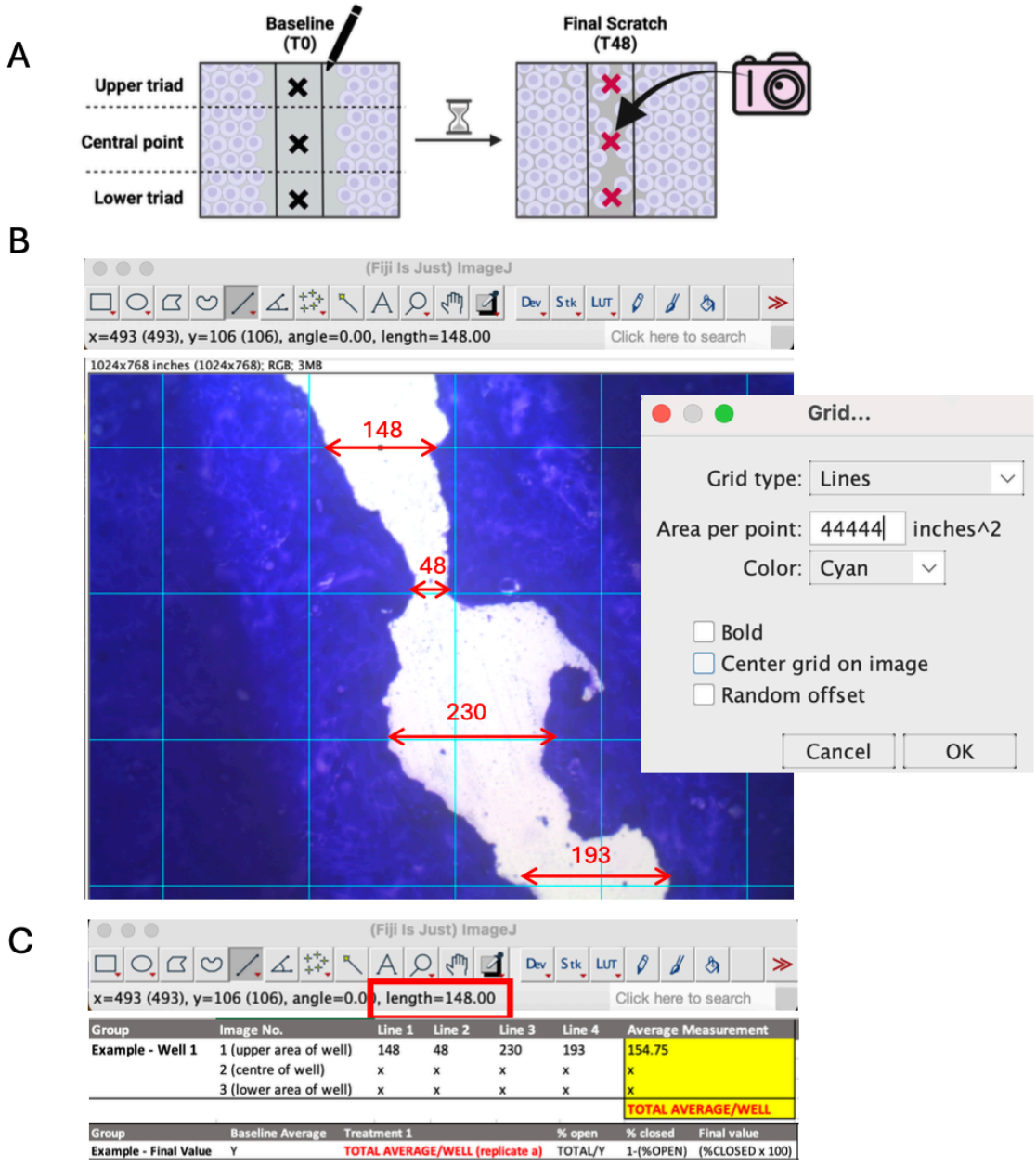

Supplementary Figure 2: Scratch Assay Analysis Protocol. Scratch assays were imaged at the sites highlighted in (A). (B) Gridlines were then placed on each image, and measurements were taken across each gridline, from one side of the wound to the next. (C) The measurement values were pasted into excel, and an average was taken per well. The average was then divided by the baseline measurement (100% open value) and the percentage wound closure was determined.

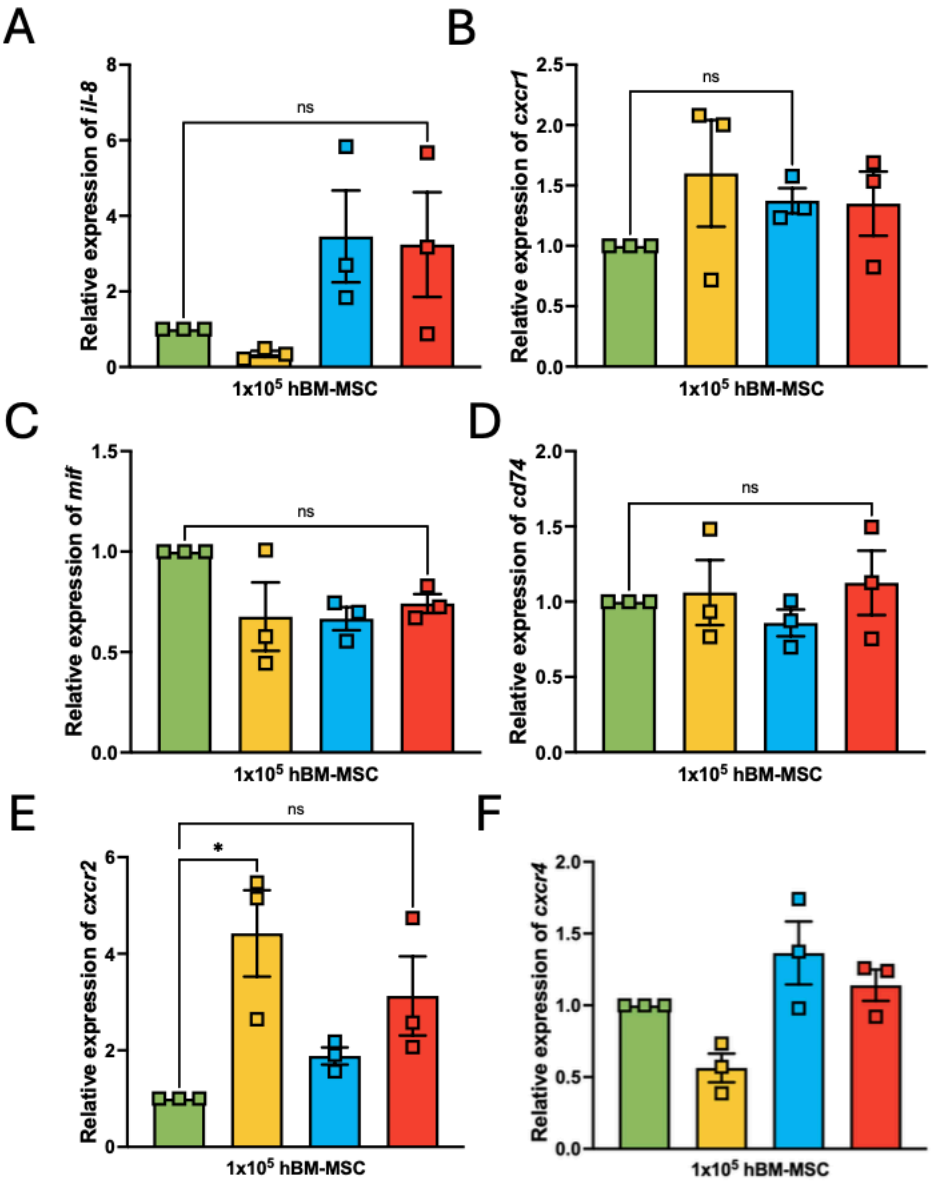

Supplementary Figure 3: Gene Expression. MSCs were exposed to 20% human patient serum from healthy, hypo- or hyper-inflammatory ARDS patients and left for 24hrs, the cells were washed with PBS, and the media was replaced with serum-free DMEM for a further 24hrs. The cells were harvested in TRIzol and RNA was eluted. Gene expression for (A) *IL-8*, (B) *CXCR1*, (C) *MIF,* (D) *CD74*, (E) *CXCR2* & (F) *CXCR4* was quantified by PCR. Data is presented as mean ± SEM; n=3 per group; *p<0.05, **p<0.01, ***p<0.001, ****p<0.0001.

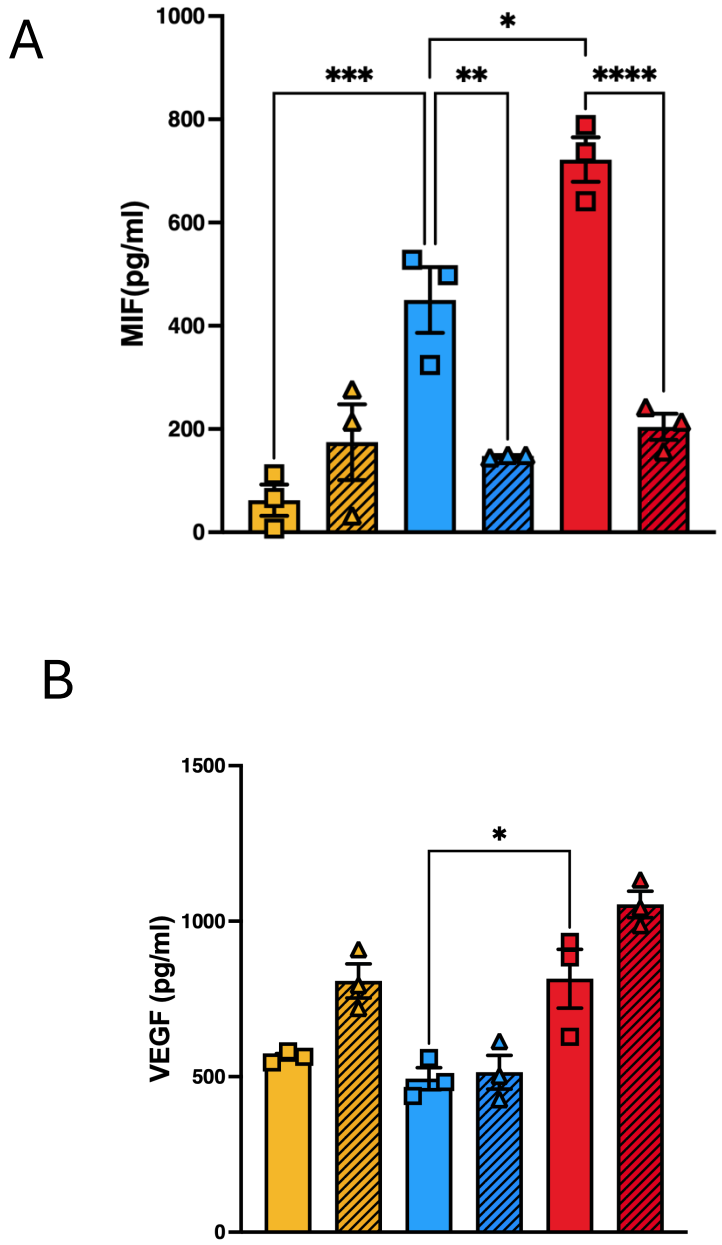

Supplementary Figure 4: SCD-19 Inhibition of MIF. MSCs were exposed to 20% human patient serum from healthy, hypo- or hyper-inflammatory (A) ARDS patients (+/- 100µM SCD-19) and left for 24hrs, the cells were washed with PBS, and the media was replaced with serum-free DMEM for a further 24hrs. (B) The MSC-CM was harvested, and a VEGF ELISA was run. Healthy controls from previous data (figure 2) used as a control in this graph. Data is presented as mean ± SEM; n=3 per group; *p<0.05, **p<0.01, ***p<0.001, ****p<0.0001.

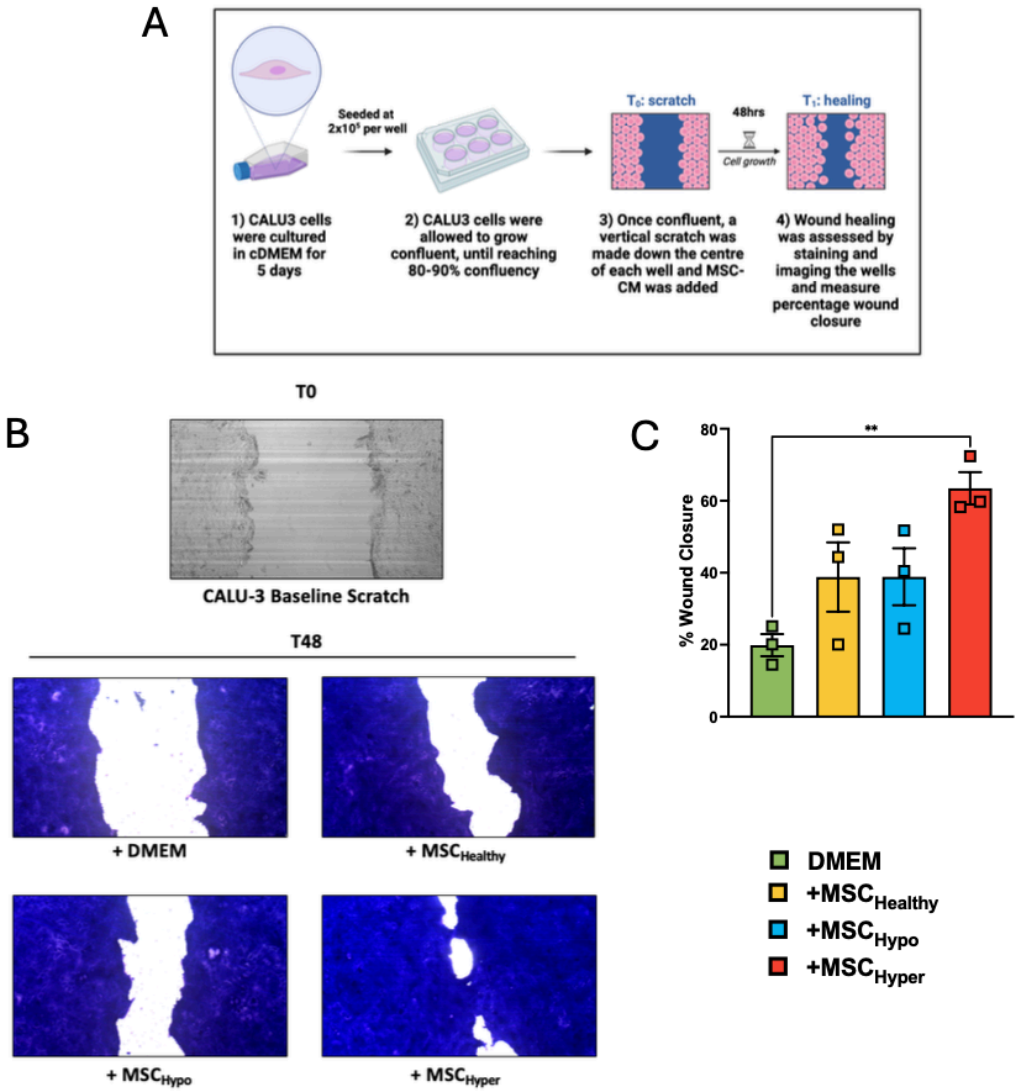

Supplementary Figure 5: CALU-3 Scratch Assay. (A,B) CALU-3s were scratched using a p200 tip and exposed to MSC-CM and left for 48hrs, before being fixed, stained and imaged. The (C) percentage wound closure was calculated as per supplementary figure 2. Data is presented as mean ± SEM; n=3 per group; *p<0.05, **p<0.01, ***p<0.001, ****p<0.0001.

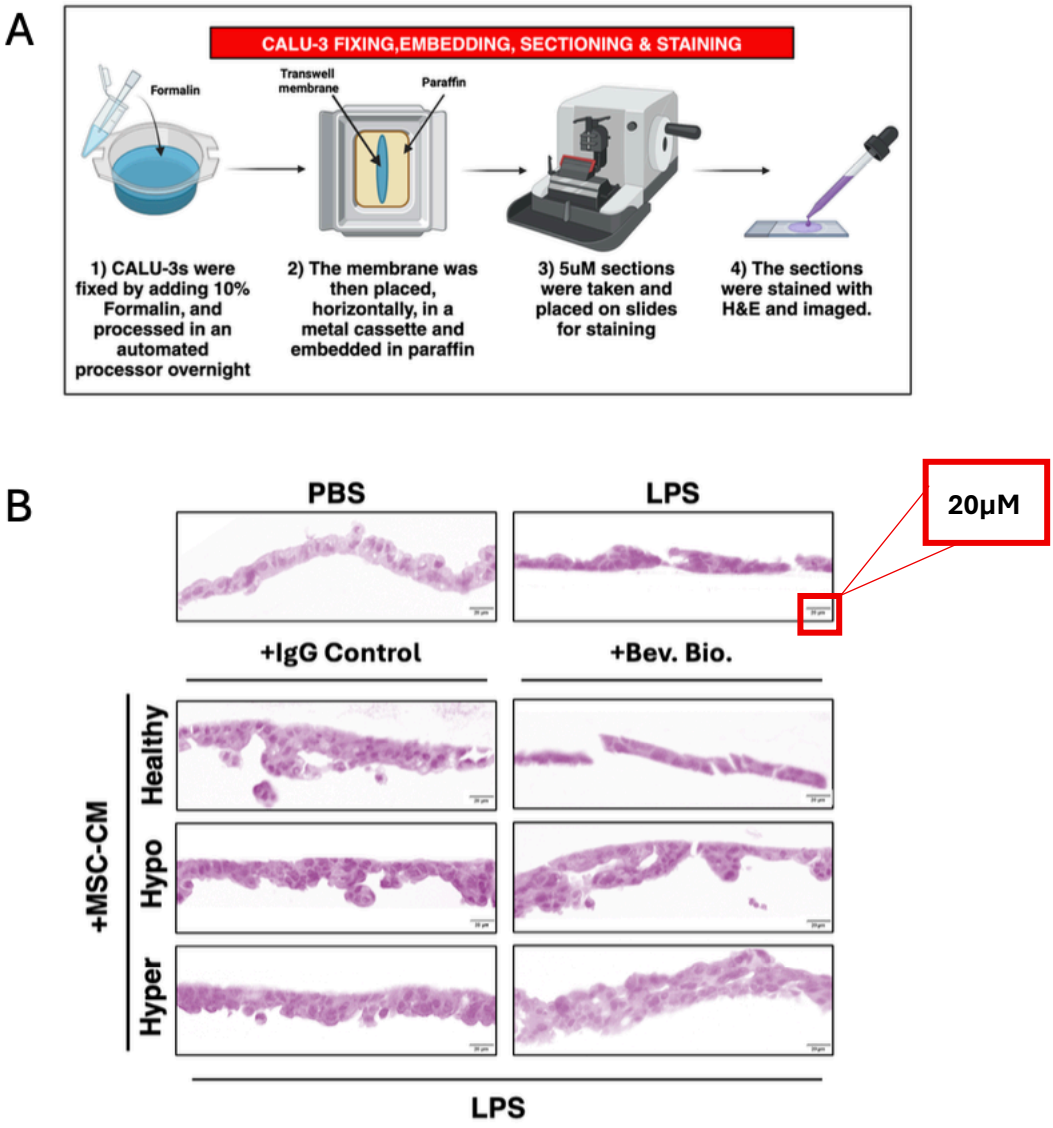

Supplementary Figure 6: CALU-3 Histology. (A, B) CALU-3s that had been cultured at the air-liquid interface were exposed to LPS and further exposed to MSC-CM from each sub-group. The barrier was then fixed, processed, embedded in wax, sectioned and stained with H&E, before imaging.

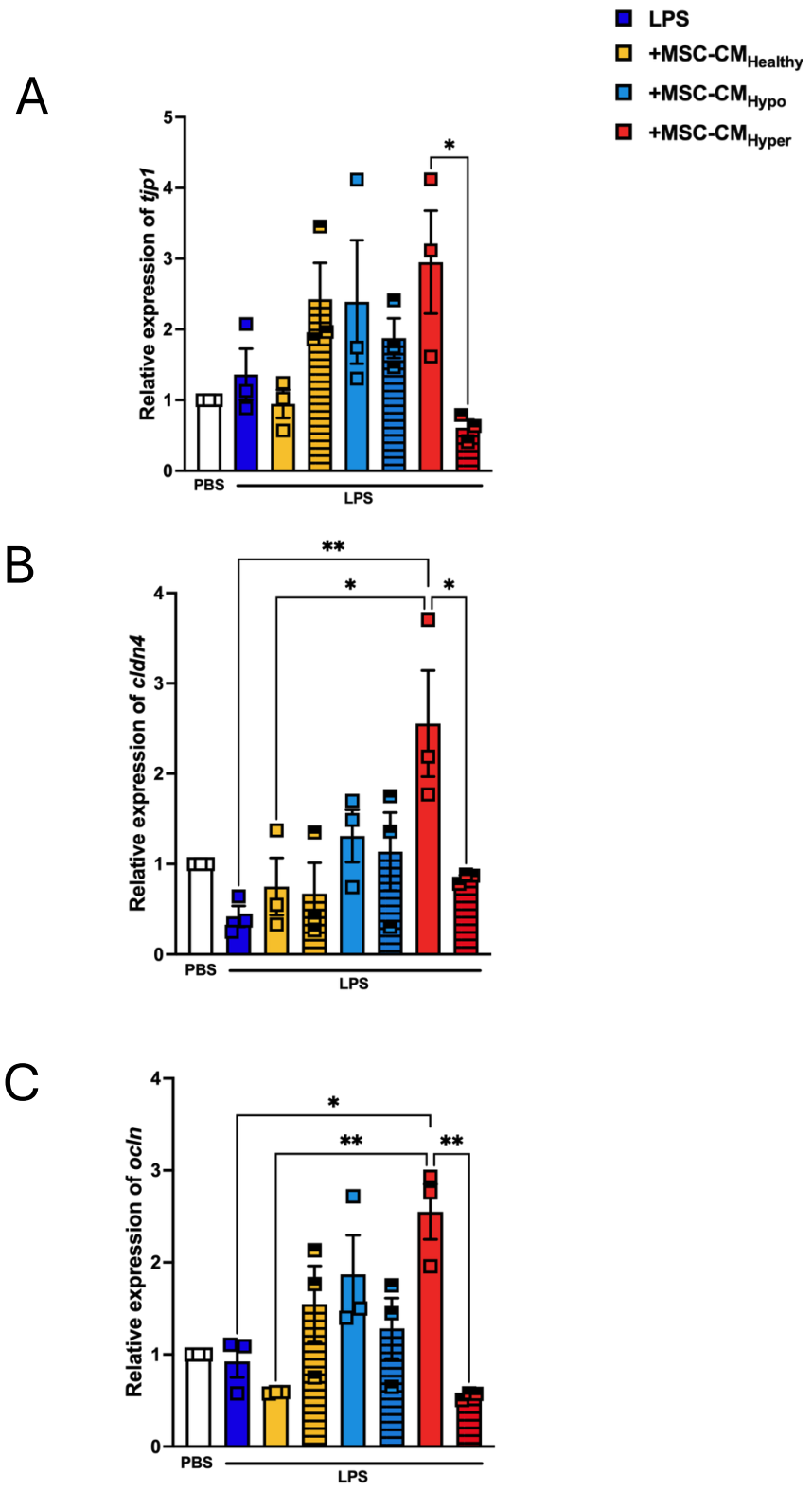

Supplementary Figure 7: Lung homogenate gene expression. Lungs from the ALI model were harvested, and a lobe from each lung was taken for gene expression analysis. The expression of (A) *tjp1,* (B) *cldn4* and (C) *ocln* was observed. Data is presented as mean ± SEM; n=3 per group; *p<0.05, **p<0.01, ***p<0.001, ****p<0.0001.

Chapter 4

The PPARβ/δ-induced MSC-secretome has cytoprotective effects via ANGPTL4 in a pre-clinical model of acute lung inflammation

**This chapter is from a study that is under review. The pre-print is available for view in appendix 7.2*

4.1 Abstract

Human bone marrow-derived mesenchymal stromal cells (hBM-MSCs) are known to exert immunomodulatory and pro-reparative effects *in vivo*. This makes them an enticing candidate therapeutic for inflammatory diseases, such as acute respiratory distress syndrome (ARDS). The ARDS microenvironment is complex and contains an abundance of free fatty-acids (FFAs); which are known to differentially impact MSC functionality. PPARβ/δ is a ubiquitously expressed nuclear receptor that is activated in response to FFA-binding. It has also been shown to impact MSC therapeutic efficacy. Due to the presence of PPARβ/δ ligands present in the ARDS microenvironment, PPARβ/δ is likely to be constitutively active upon MSC administration. This study sought to investigate the impact of this. hBM-MSCs were exposed to a PPARβ/δ agonist/antagonist and the immunomodulatory and pro-reparative capacity of the MSC secretome was then observed using both *in vitro* assays, and a pre-clinical model of LPS-induced acute lung inflammation (ALI). These results highlighted that the secretome from $MSC_{PPAR\beta/\boldsymbol{\delta}(+)}$ had enhanced pro-reparative capacity in CALU-3 lung epithelial cells by promoting the secretion of angiopoietin-like 4 (ANGPTL4). This PPARβ/δ-induced $ANGPTL4^{HIGH}$ MSC secretome showed enhanced cytoprotection, wound repair, and modulation of macrophages. This was confirmed using an anti-ANGPTL4 antibody. It was concluded that the PPARβ/δ-induced $ANGPTL4^{HIGH}$ MSC secretome has reparative and cytoprotective effects as well as some immunosuppressive effects in a pre-clinical model of ALI.

Graphical Abstract

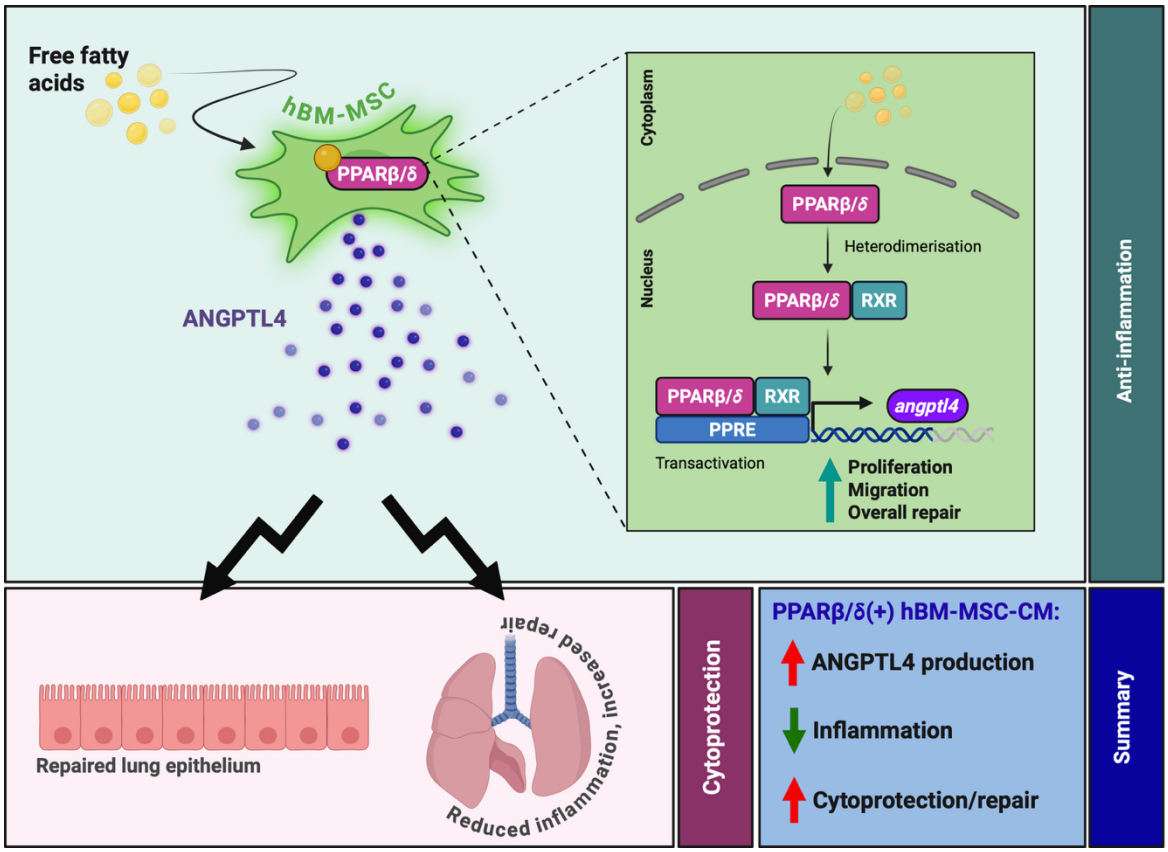

4.2 Hypothesis and aims

Hypothesis: PPARβ/δ modulation will alter MSC immunomodulatory capacity in a model of ALI.

Aim(s):

- Identify an appropriate time-point and dosage of PPARβ/δ agonist and antagonist for use in the study.
- Investigate the impact of PPARβ/δ-modulation on hBM-MSC gene and protein expression.
- Understand the mechanistic insights into any PPARβ/δ-associated alterations in hBM-MSC behaviour.
- Follow the science to identify the implications these results may have in the context of ARDS.

4.3 Introduction

Cell therapy, particularly mesenchymal stromal cell (MSC) therapy, has long been thought of as a candidate therapeutic in the treatment of many inflammatory diseases. This is largely due to their immunomodulatory and cytoprotective capacity[124]. One of the conditions that MSCs have been considered for use in is acute respiratory distress syndrome (ARDS); an inflammatory disease of the lung[277, 278]. MSCs have been investigated in ARDS over the last 20 years, but clinical trials have shown poor outcomes[163, 299, 300]. The environment in which MSCs are exposed to can impact their functional capacity[150, 190, 301]. This is severely understudied in the context of the ARDS microenvironment. The complex ARDS disease microenvironment contains inflammatory-mediators, microorganisms, and free fatty acids (FFAs). These components have all shown to impact MSC therapeutic capacity in various ways[238, 293]. The previous chapter highlighted the differential impact of the hypo-inflammatory vs hyper-inflammatory ARDS microenvironment on MSC therapeutic efficacy. This work showed a clear correlation between high levels of inflammation, and enhanced MSC-driven repair[122]. Therefore, investigating the impact of FFAs in the ARDS patient microenvironment, and the impact they have on hBM-MSCs, was a required next step.

The peroxisome proliferator-activated receptor-beta/delta (PPARβ/δ) is a ubiquitously expressed nuclear receptor, present in hBM-MSCs, that is activated in response to FFA exposure[233, 302]. In recent years, PPARβ/δ has been shown to impact MSC therapeutic efficacy[148, 207-210, 243, 245, 246, 303-305]. One study highlighted enhanced pro-reparative capacity in endothelial cells of rats in response to an intraperitoneal injection of a PPARβ/δ agonist[208]. Other studies have shown enhanced immunosuppression by PPARβ/δ-inhibited mouse MSCs; specifically in their ability to modulate T-cell proliferation[245, 246]. Due to the abundance of FFAs in the ARDS disease microenvironment, this study sought to

identify the impact of PPARβ/δ on the MSC secretome; and investigate the impact this had on immunomodulation and cytoprotection, in a model of ALI.

4.4 Materials and Methods

4.4.1 Ethical approval and HPRA compliance

Ethical approval was granted by the Maynooth University research ethics committee (BRESC-2022-2453953). HPRA approval was granted under the project authorisation(s) AE19124/P031/P037.

4.4.2 hBM-MSC cell culture

Human bone marrow-derived MSCs (hBM-MSCs; RoosterBio™) from passages 2-5 were cultured in Dulbecco's Modified Eagle Medium (DMEM; Merck life science limited, #D6046), containing 10% Foetal Bovine Serum (FBS; Thermofisher) and 1% *Penicillin streptomycin* (Merck life science limited, P4458-100ML; cDMEM). The cells were cultured for 5 days at 37℃ + 5% CO_2. All experiments are a representation of three independent MSC donors.

4.4.3 Gene & Protein expression

For gene expression, RNA was isolated and normalised to 100 ng/µl. cDNA was made using the QuantBio™ cDNA Synthesis kit (as per manufacturer's guidelines; VWR International, #733-1174). Real-time Polymerase Chain Reaction (RT-PCR) was run using PerfeCta SYBR Green FastMix (QuantBio™, #95072-05K) and pre-made Sigma™ primers. Relative expression was quantified in relation to *HPRT* by calculating the 2-ΔΔCT values. For protein expression, 96-well half-area ELISA plates (COSTAR™) were coated as per manufacturers guidelines (human ANGPTL4 , VEGF and MIF (R&D™)) and run as previously described[122].

4.4.4 Lenti-viral knock-down in hBM-MSCs

E. coli glycerol stocks containing our lenti-viral construct of interest were obtained from Sigma™. These stocks were cultured in $LBCB_{50}$ agar plates and the construct of interest was selected for by antibiotic selection using carbenicillin (50mg/ml; Merck Life Sciences Limited, #C1613-1ML). Plasmids were isolated using a plasmid purification midi-prep kit (Fischer Scientific, #12752663), and HEK293T cells were transfected with the plasmids of interest by combining the plasmids of interest with a lenti-viral packaging mix (Merck, #SHP001-0.25ML) and lipofectamine transfection inducer (Bio Sciences Ltd., #11668019). Upon expansion of the plasmids in HEK293T cells, supernatant, containing plasmids, was harvested 48hrs post-transfection and 72hrs post-transfection. The plasmids were then concentrated using a PEG-IT purification kit (Abcam™, #ab102538). Human BM-MSCs were then transduced with the isolated plasmids by incubating hBM-MSCs with concentrated particles and 4µg/ml polybrene transduction reagent (Merck, #TR-1003-G). 24hrs post-transduction, the transduced cells were selected for using puromycin antibiotic over a period of 4 days before use. A no-template control (NTC) was used to assess any impact of the knock-down process.

4.4.5 CRISPR knock-down in hBM-MSCs

The CRISPR duplex for PPARβ/δ knock-down, or an NTC, was prepared by incubating 3 individual guide RNAs (gRNA), tracrRNAs (IDT, #1072533 (20nmol))and a nuclease-free duplex buffer before heating to 95℃ for 5 minutes. The duplex was allowed to cool on the bench before being placed on ice. The ribonucleoprotein complex (RNP complex) was created by adding 0.5µl of duplex and 0.5µl of pre-prepared Cas9 enzyme (Merck Life Sciences Limited, #1081058 – 100µg) per well. hBM-MSCs were then detached, counted, washed and $1.5x10^5$ cells were resuspended in resuspension buffer R (Neon NxT kit, #N1025) and 1µl of the RNP complex was added per reaction. 2µl of electroporation enhancer (IDT, #1075915

(2nmol)) was also added per reaction. Electroporation of the constructs into the cells was carried out using the Neon NxT electroporation set-up, in collaboration with Dr. Ronan Bergin. The cells were electroporated at 1500V for 30ms, using one pulse. They were then ejected into a fresh media-containing well and left to settle over 48hrs before assessing knock-down.

4.4.6 Sequencing & metabolomic analysis

hBM-MSCs were seeded at a density of $1x10^5$ in a 6-well plate and left to adhere. Once attached, the cells were exposed to 1μM of PPARβ/δ agonist (GW0742; Tocris™, #2229) or antagonist (GSK3787; Tocris™, #3961) for 6hrs. This dose was chosen based on our dose curve (figure 1A). The cells were harvested in TRIzol (Bio Sciences Ltd., #15596018) for RNA isolation. RNA was isolated through a series of chloroform and isopropanol extractions. RNA concentration and purity was assessed using a nano-drop and samples were sent to Novogene™ for sequencing (GEO accession no.: GSE281162). Processed RNA sequencing datasets, provided by Novogene™, were then used to identify differentially expressed genes (DEGs) of interest. Volcano plots, highlighting the most significantly enriched genes, were generated using Flourish™ software. Data was also collected from publicly available RNA sequencing (GEO accession no.: GSE185263). This data was based on whole blood RNA sequencing from patients with SARS-CoV-2-induced ARDS, or classical ARDS. A metabolomic dataset (Study ID: ST000042; doi: 10.21228/M8SG64) was also used. This was a metabolomic dataset carried out on the Bronchoalveolar lavage fluid (BALF) of classical ARDS patients. Normalised values were taken from both studies and data was plotted using GraphPad Prism™ (version 10) software.

4.4.7 Scratch Assay

CALU-3 lung epithelial cells (cultured as previously described) [122]were seeded at a density of $5x10^5$ in a 6-well plate. Once 80% confluent, a single vertical scratch was made down the centre of the well using a p200 tip (Chapter 3, supplementary figure 2). The cells were then washed with PBS to remove debris, and MSC-CM was added for a period of 6-48hrs. The cells were then fixed with 10% formalin, before leaving to dry. Once dry, the cells were stained with crystal violet, left to dry, and imaged. To avoid bias, a marker was used to denote an area in the upper, central and lower regions of each scratch and images were taken from these points. Mitomycin C (Sigma™) was added to assess the impact of proliferation at a concentration of 5 µg/ml for 2hrs prior to the scratch assay. As an additional measure of proliferation inhibition, we also measured gene expression of *TOP2A*; a known proliferation-associated gene[306].

4.4.8 Scratch Assay Analysis

Three images, taken at each of the three marked points, were taken per well; for each of the three independent MSC donors (i.e. 3 images per well x 3 MSC donors = 9 images per group). Fiji/ImageJ™ software was then used to divide each picture into four distinct quadrants in an unbiased manner (Analyse -> Tools -> Grid -> set area per point to 44444 inches squared). This grid includes the addition of 4 horizontal lines imputed on the image. Using the straight-line feature in Fiji/ImageJ™ software, four measurements were then taken per picture at each of the horizontal lines. This provided 4 measurements per picture, at unbiased points, to get a clear depiction of each percentage wound closure. The average wound closure per donor was calculated, and divided by the baseline scratch value, to get the final percentage wound closure.

4.4.9 Generation and concentration of MSC-CM

hBM-MSCs (passage 2-5) from three independent donors were seeded at a density of $1x10^5$ per well in a 6-well plate in 1ml of cDMEM and left to attach. Once attached, the cells were stimulated with 1μM of PPARβ/δ agonist (GW0742, Tocris™) or antagonist (GSK3787, Tocris™), as previously done in our group. 24hr-post stimulation, the cells were washed with PBS, and the media was replaced with serum-free DMEM. This was left for a further 24hrs to allow for the generation of MSC-CM. When including ARDS serum-exposure, the agonist/antagonist were washed from the cells, and 20% ARDS serum was added for 24hrs. This was then washed away, and serum-free DMEM was added for a further 24hrs to allow for the generation of MSC-CM. All MSC-CM was harvested and stored at -20℃ for future experiments. MSC-CM was then concentrated, as required, as previously described[122], using Amicon Centrifugal filters (50kDa). The samples were centrifuged at 14,000g for 30 minutes, before removing the filter, placing upside-down in a fresh Eppendorf, and centrifuging for a further 1000g for 2 minutes. This fresh Eppendorf contains the concentrated MSC-CM.

4.4.10 ANGPTL4 Neutralisation

MSC-CM was exposed to 5 μg/ml of ANGPTL4 neutralising antibody (Cell Sciences™), or 5 μg/ml IgG2aκ isotype control (Rockland Immunochemicals™). This was incubated at room temperature for 1hr prior to use. This concentration was utilised as per manufacturer guidelines for our study.

4.4.11 ALI mouse model

Male and female C57BL6/J mice (Charles River), aged 8+ weeks, were given 2mg/kg of endotoxin (Sigma, 0001:B4 Serotype), or PBS control, intratracheally (IT) and observed twice daily for 48hrs. PPARβ/δ-modulated MSC-CM was then concentrated and administered

intranasally (IN) 4hrs post-endotoxin. An Evan's Blue permeability assay was carried out by administration of an intravenous (IV) injection of sterile-filtered Evan's Blue Dye (10%) into the tail vein of our mice 1hr prior to harvesting. The mice were sacrificed using an intraperitoneal (IP) injection of pentobarbital. BALF, blood and whole lungs were harvested for analysis. Absorbance readings were taken to assess the total Evan's blue (620nm and 740nm).

4.4.12 Statistical analysis of animal studies

Data was analysed using GraphPad Prism™ (version 10) software. Statistical tests used have been highlighted in the figure legends of each figure. For comparisons between two groups, a t-test with Welch's correction was carried out. For more than two groups, a one-way ANOVA followed by Tukey's post-hoc test was carried out. For multiple groups, with multiple variables, a two-way ANOVA followed by Tukey's post-hoc test was carried out. All animal data is presented as mean ± SEM; *p<0.05, **p<0.01, ***p<0.001, ****p<0.0001.

4.4.13 Flow cytometry *(completed in collaboration with Dr. Shoumo Kundu)*

Cell suspensions obtained from BALF were characterized using flow cytometry. Zombie-NIR (Medical Supply Company, #423106) was used to exclude dead cells. Initially Zombie NIR dye was diluted at 1:1000 in PBS and stored at room temperature in dark. A master mix of antibodies (supplementary table 1) was prepared in cold FACS buffer (PBS+ 1% BSA, 100µl per sample). Cells were collected by centrifugation (300 x g, 5 minutes) in a round-bottom 96 well plate and washed with 200µl PBS. After discarding the supernatant, cells were resuspended in 100µl of the pre-diluted Zombie NIR solution per $1x10^5$ cells and mixed by gentle pipetting. The cells were then incubated at room temperature for 15 minutes in the dark. Post incubation, the excess dye was washed off with 100µl cold FACS buffer and the plate was

centrifuged at 300 x g for 5 minutes. Cells were resuspended in 100µl of cold FACS buffer and 1.25µl Fc-block (Thermofisher) was added to each sample and incubated at 4°C for 15 minutes. The excess FACS buffer was removed and the supernatant discarded. 100µl of pre-prepared fluorophore conjugated antibody master mixes were added to the wells and incubated on ice for 30 minutes in the dark. Cells were washed in FACS buffer, collected by centrifugation and resuspended in 200µl of cold FACS buffer prior to acquisition on a Thermofisher AttuneNxT flow cytometer. Flow cytometry data was analysed using FlowJo v10 software. Immune cells such as macrophages and neutrophils were gated from an initial CD45+ live cell fraction. Neutrophils were identified as Ly6G+, while the macrophage subpopulations were identified using a CD40 vs CD206 gating from the Ly6G-CD11b+CD11c+CD64+CD24- population (supplementary figure 1). I was involved in the 1) administration and 2) harvesting of samples from the study. Shoumo Kundu processed the samples and ran the flow cytometry.

4.5 Results

4.5.1 Identifying a dose and timepoint for PPARβ/*δ* induction and inhibition in hBM-MSCs.

As an initial point of study, I confirmed PPARβ/*δ* expression in the MSC donors obtained for the study (figure 1A). An appropriate dose of the PPARβ/*δ* agonist (GW0742) and PPARβ/δ antagonist (GSK3787) was also assessed; to ensure that the chosen dose would induce or inhibit the receptor, respectively. A dose range from 0.1μM-5μM worked for both the agonist and antagonist and there were no differences seen between 0.5μM-5μM, in the context of ANGPTL4; a known PPARβ/**δ** target (figure 1B). Based on a previous study from our laboratory[148], we chose to move forward with a dose of 1μM. A time course study was also run, where it was observed that there was an effect at 6hr, 12hr and 24hrs (figure 1C). This highlighted a strong induction of the receptor at every time-point, but primarily at a 24hr timepoint. Along with this, a publication from Perez Diaz *et al.*, (2021) highlighted the dual binding properties of PPARβ/*δ*. This group highlighted, using computational chemistry, that both PPARβ/*δ* agonist and antagonists can enter the same binding pockets, suggesting dual occupancy in the ligand-binding domain of the receptor[307]. I decided to perform a co-incubation study, whereby the impact of agonism and antagonism co-incubation on PPARβ/*δ* signaling was assessed. It was seen the PPARβ/*δ* agonism always induced the expression of PPARβ/*δ* target genes, even in the presence of the antagonist (figure 1D-F). This is in line with the published findings from Perez Diaz *et al* (2021); whereby they also saw induction of PPARβ/*δ*-associated genes, even in the presence of the antagonist[307].

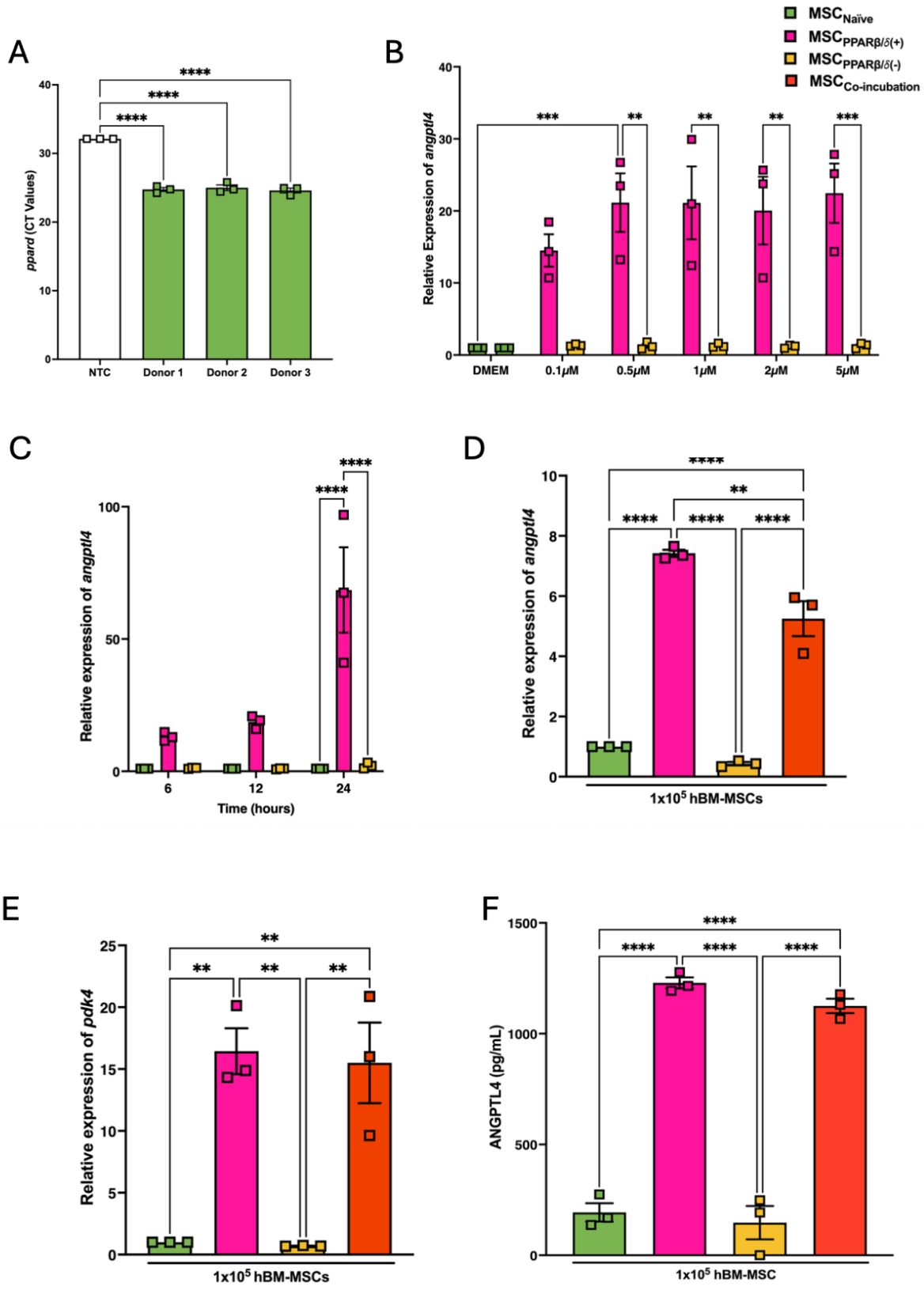

Figure legend available on next page

Figure 1: PPARβ/δ is present in hBM-MSCs and responds to a synthetic agonist. (A) RT-PCR confirming the presence of PPARβ/*δ* in hBM-MSCs (one-way ANOVA followed by Tukey's post-hoc test, n=3) allowed us to further investigate a (B) dose of PPARβ/*δ* agonist or antagonist to use in the study. (C) A time-course study confirmed high induction of the receptor at a 24hr time-point (two-way ANOVA followed by Tukey's post-hoc test, n=3). (D-F) Co-incubation studies containing both agonist and antagonist highlighted that agonism out-competes antagonism (one-way ANOVA followed by Tukey's post-hoc test, n=3). Replicates are a representation of 3 individual hBM-MSC donors. Data is presented as mean ± SEM; *p<0.05, **p<0.01, ***p<0.001, ****p<0.0001.

4.5.2 The $MSC_{PPARβ/δ(+)}$ secretome enhances pro-reparative capacity in CALU-3 lung epithelial cells via migration and proliferation *in vitro*

Preliminary results of scratched CALU-3 cells exposed to MSC-$CM_{PPARβ/δ(+)}$ or MSC-$CM_{PPARβ/δ(-)}$ highlighted a significant increase in wound closure in both MSC-CM_{Naive} and MSC-$CM_{PPARβ/δ(+)}$ groups (figure 2B, C). As ANGPTL4 is known to impact both proliferation and migration[308, 309], we repeated this experiment using Mitomycin C; a known proliferation inhibitor[310]. A time-course study confirmed that both proliferation and migration had a combination effect (figure 2D). Significantly more wound repair was seen in the MSC-$CM_{PPARβ/δ(+)}$ group compared to our MSC-CM_{Naive} group. Gene expression of *TOP2A*, a gene largely indicative of cell proliferation[306], highlighted a significant difference between the MSC-$CM_{PPARβ/δ(+)}$ and MSC-$CM_{PPARβ/δ(-)}$ groups, with the MSC-$CM_{PPARβ/δ(+)}$ group having significantly more proliferative capacity than the MSC-$CM_{PPARβ/δ(-)}$ group (figure 2E). We further confirmed this result in a second lung cell line; A549s (supplementary figure 2).

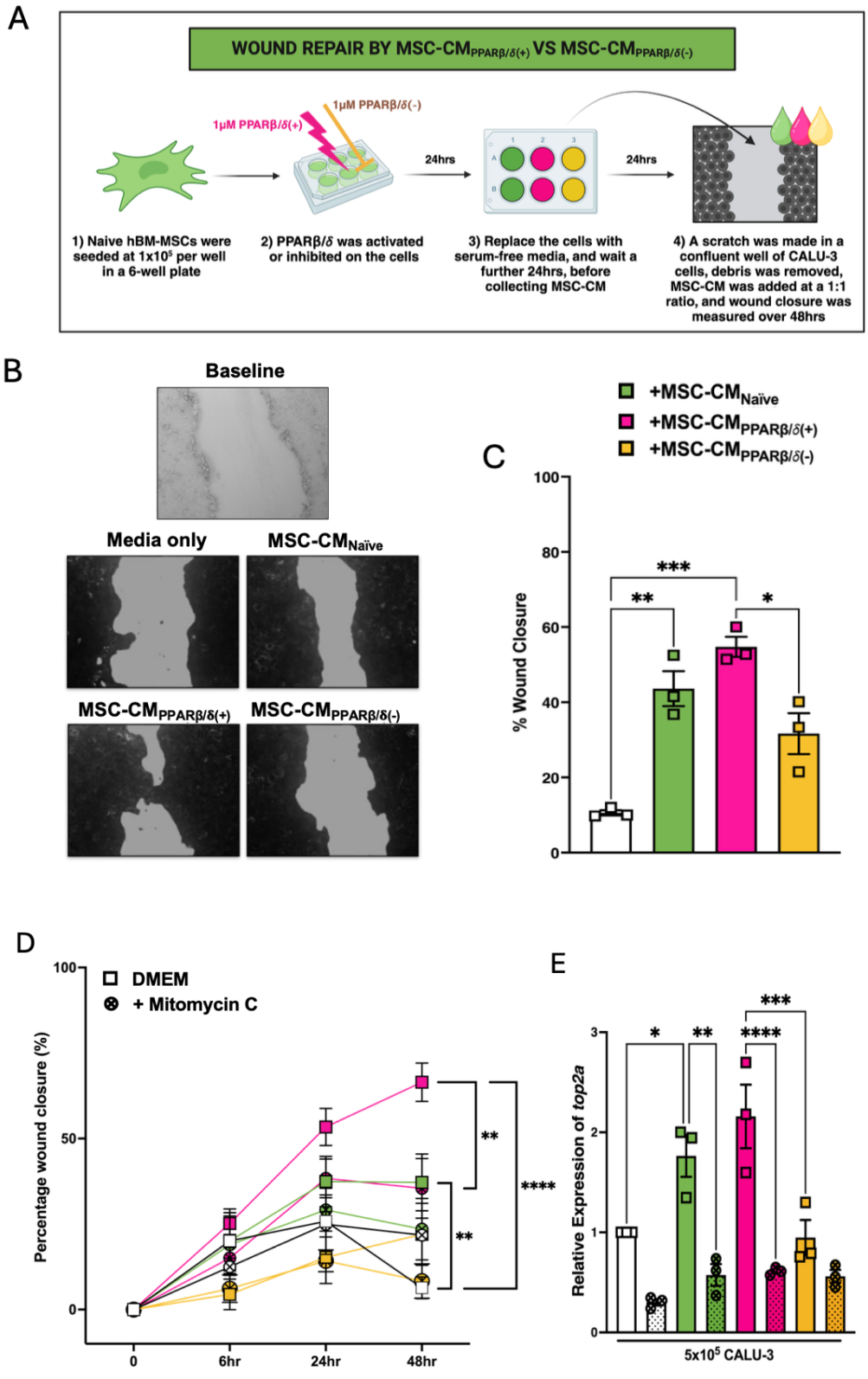

Figure legend available on next page

Figure 2: PPARβ/δ(+) hBM-MSCs show enhanced reparative capacity of CALU-3 lung epithelial cells. (A) A CALU-3 scratch assay was run, in combination with MSC-CM from PPARβ/*δ* agonized or antagonized hBM-MSCs. (B) PPARβ/*δ* (+) hBM-MSC-CM showed enhanced wound repair and this was (C) quantified using imageJ software (one-way ANOVA followed by Tukey's post-hoc test, n=3). (D) Using a mitomycin C proliferation inhibitor allowed for the investigation into the impact of this on migration or proliferation at different time-points (two-way ANOVA followed by Tukey's post-hoc test, n=3) and this was confirmed using (E) *TOP2A* gene expression by RT-PCR at a 48hr time-point (one-way ANOVA followed by Tukey's post-hoc test, n=3). Replicates are a representation of 3 individual hBM-MSC donors. Data is presented as mean ± SEM; *p<0.05, **p<0.01, ***p<0.001, ****p<0.0001.

4.5.3 The presence of PPARs in MSCs; taking a PPARβ/δ knock-down approach

As we had determined that PPARβ/*δ* would be constitutively active in the ARDS patient microenvironment, and that PPARβ/*δ* agonism would always outcompete antagonism, we wanted to try a knock-down approach. Importantly, the PPARβ/*δ* agonist used in this study (GW0742) also has the capacity to activate PPARα. Therefore, a knock-down approach would also counteract this limitation of the study. Firstly, a lenti-viral knock-down approach was taken. Upon observation of the cells throughout this process, they appeared unhealthy and unhappy. Ultimately, our team wouldn't have been confident using these cells for any of our assays, despite seeing knock-down of PPARβ/*δ* by qRT-PCR (supplementary figure 3A). We attempted to visualize this by western blotting as a second way of confirming this result, but the only available western antibody available was sub-par and only provided more questions than answers. Given these results and the impact this process had on the cells, a CRISPR

approach was trialed. This approach had much greater results; with a significant reduction of PPARβ/*δ* in the hBM-MSCs upon CRISPR-based knock-down (supplementary figure 3B). The cells also appeared to be in much healthier condition compared to the lenti-virally transduced cells (supplementary figure 3D). Interestingly, these cells had high levels of ANGPTL4; a known PPARβ/*δ* target gene (supplementary figure 3C). This appeared to be an off-target effect, as knock-down of PPARβ/*δ* should reduce target genes such as ANGPTL4. Again, this suggested that the CRISPR approach may not work moving forward. I decided to investigate the levels of PPARβ/*δ* in hBM-MSCs from the sequencing dataset, in comparison to the other PPARs. This showed that there were very low levels of PPARα and PPARɣ in the cells we had been working with, at baseline (supplementary figure 3E). There was also no induction of PPARα or PPARɣ seen in response to our agonist (supplementary figure 3E). With this in mind, we chose to move forward with our agonistic and antagonistic approach.

4.5.4 Analysis of $MSC_{PPARβ/δ(+)}$ RNA sequencing highlighted upregulation of several genes

RNA sequencing (Novogene™; GEO accession no.: GSE281162) carried out on both our $MSC_{PPARβ/δ(+)}$ and $MSC_{PPARβ/δ(-)}$ groups (figure 3A) highlighted a variety of differentially expressed genes (DEGs). The DEGs were visualised using a Venn diagram (figure 3B), showing 170 DEGs specific to the $MSC_{Naïve}$ group, 128 specific to the $MSC_{PPARβ/δ(+)}$ group, and 189 specific to the $MSC_{PPARβ/δ(-)}$ group. Volcano plot visualisation highlighted several of the most significantly altered DEGs in each group (figure 3C). The $MSC_{PPARβ/δ(+)}$ group had a significant enrichment of genes such as *PLIN2, ANGPTL4, FAM156A, CPT1A, CAT, NADK2, TMED6* and *LDHAL6B.* These genes are largely involved in lipid metabolism and protection against oxidative stress[311-313]. This group also showed significant downregulation in genes such as *MAGED4* and *FAM157B* (table 1). *MAGED4* is involved in cell cycle regulation[314],

while *FAM157b* is a non-coding gene[315]. The $MSC_{PPAR\beta/\delta(-)}$ group had a significant enrichment of genes such as *IKBKGP1, SNRPGP2, LINC01159, MIR3648-1, RARRES1, MALAT1* and *RNF217-AS1*. These genes are largely involved in cell differentiation and NFκB signalling[316, 317]. This group also showed significant downregulation in genes such as *RGPD5, PFN1P3, MIR3936HG, U2AF1* and *TSNAXIP1* (table 2). These genes are involved in various processes; including GTPase regulation, migration, proliferation and apoptosis. FPKMs of two known PPARβ/*δ* target genes were plotted to confirm the data was as expected (figure 3D, E), and this was confirmed by qRT-PCR (figure 3F, G).

Table 1: DEG functions in $MSC_{PPAR\beta/\delta(+)}$ group.

Gene name	Up/Down	Involved in
PLIN2	Up	Lipid metabolism [311]
ANGPTL4	Up	Lipid metabolism and angiogenesis [312]
FAM156A	Up	Enables protein binding [318]
CPT1A	Up	Lipid metabolism [319]
CAT	Up	Protection against oxidative stress [320]
NADK2	Up	Protection against oxidative stress [313]
TMED6	Up	Trafficking and transport [321]
LDHAL6B	Up	Lactate metabolism [322]
MAGED4	Down	Cell cycle regulation [314]
FAM157B	Down	Non-coding [315]

Table 2: DEG functions in $MSC_{PPAR\beta/\delta(-)}$ group.

Gene name	Up/Down	Involved in
IKBKGP1	Up	NFκB signalling [316]
SNRPGP2	Up	RNA processing [323]
LINC01159	Up	Cell differentiation [324]
MIR3648-1	Up	Cell differentiation [317]
RARRES1	Up	Cell differentiation & retinoid signalling [325]
MALAT1	Up	Cell differentiation [326]
RNF217-AS1	Up	Cell differentiation [327]
RGPD5	Down	GTPase regulation [328]
PFN1P3	Down	Cell motility/migration [329]
MIR3936HG	Down	Proliferation and apoptosis [330]
U2AF1	Down	ROS production/oxidative stress [331]
TSNAXIP1	Down	RNA processing and transport [332]

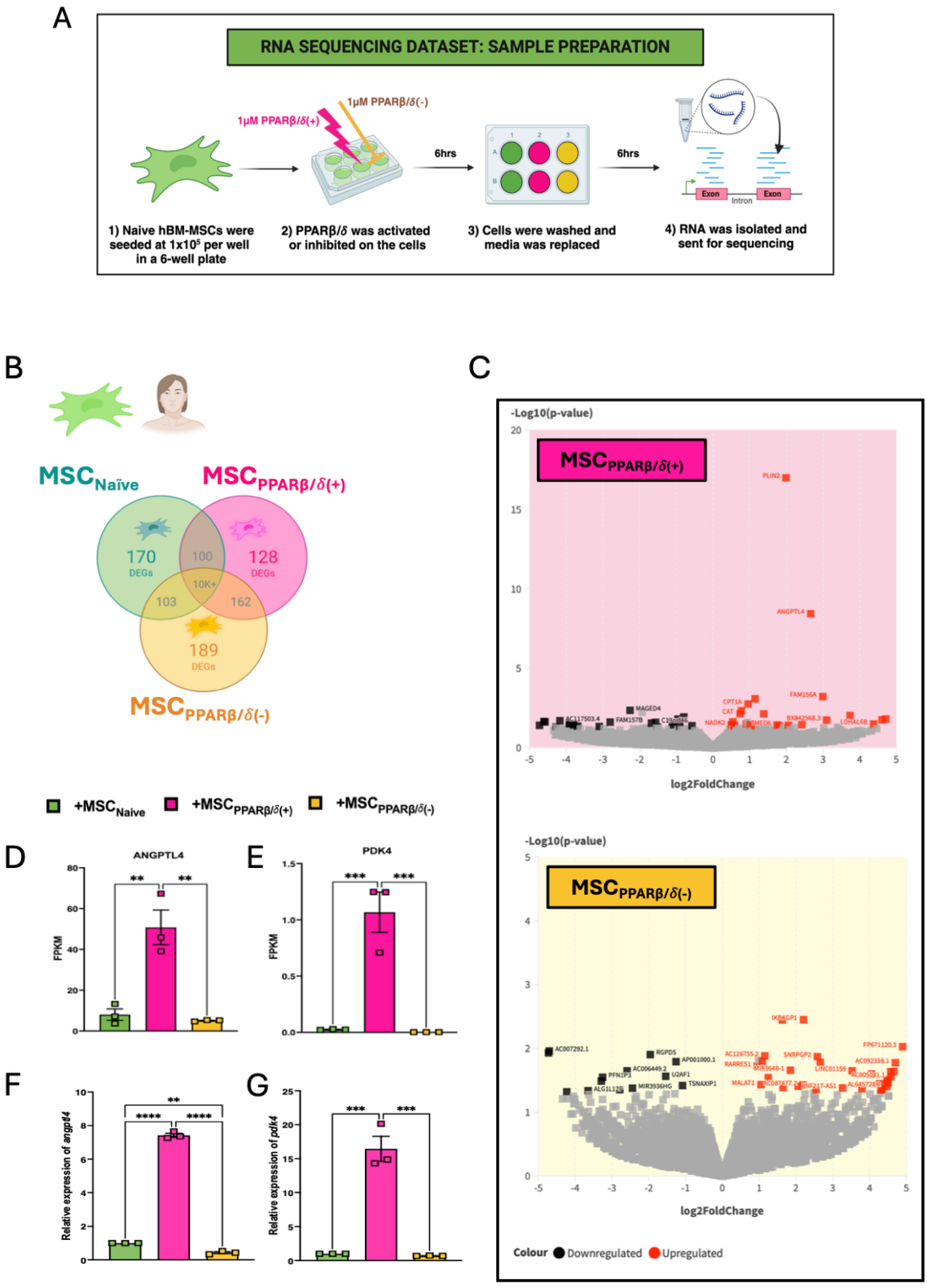

Figure legend available on next page

Figure 3: PPARβ/δ(+) hBM-MSCs show enhanced expression of ANGPTL4 by RNA sequencing. (A) hBM-MSCs exposed to 1uM of PPARβ/*δ* agonist or antagonist were sent to Novogene™ for RNA sequencing. (B) Several DEGs were highlighted and (C) the most significant hits were plotted on a volcano plot using Flourish™ software. Results were confirmed by assessing 2 known PPARβ/*δ* target genes in our sequencing dataset: (D) *ANGPTL4* and (E) *PDK4*. These results were confirmed by (F, G) RT-PCR (one-way ANOVA followed by Tukey's post-hoc test, n=3). Replicates are a representation of 3 individual hBM-MSC donors. Data is presented as mean ± SEM; *p<0.05, **p<0.01, ***p<0.001, ****p<0.0001.

4.5.5 MSC-associated genes/proteins are unaffected by PPARβ/δ agonism or antagonism; except ANGPTL4

Given the functional enhancement of MSC-$CM_{PPARβ/δ(+)}$ promotion of wound healing observed in figure 2, the production of known cytoprotective factors released by MSCs were analysed. While MSCs produced ANGPTL4, VEGF and MIF, $MSC_{PPARβ/δ(+)}$ only produced significantly higher levels of ANGPTL4 (figure 4A-C). Along with this, PPARβ/*δ* agonism/antagonism did not affect expression of typical MSC-associated immunomodulatory factors such as *PTGS2, IL-6, IDO, PTGES* or *TGFβ* (figure 4D-H).

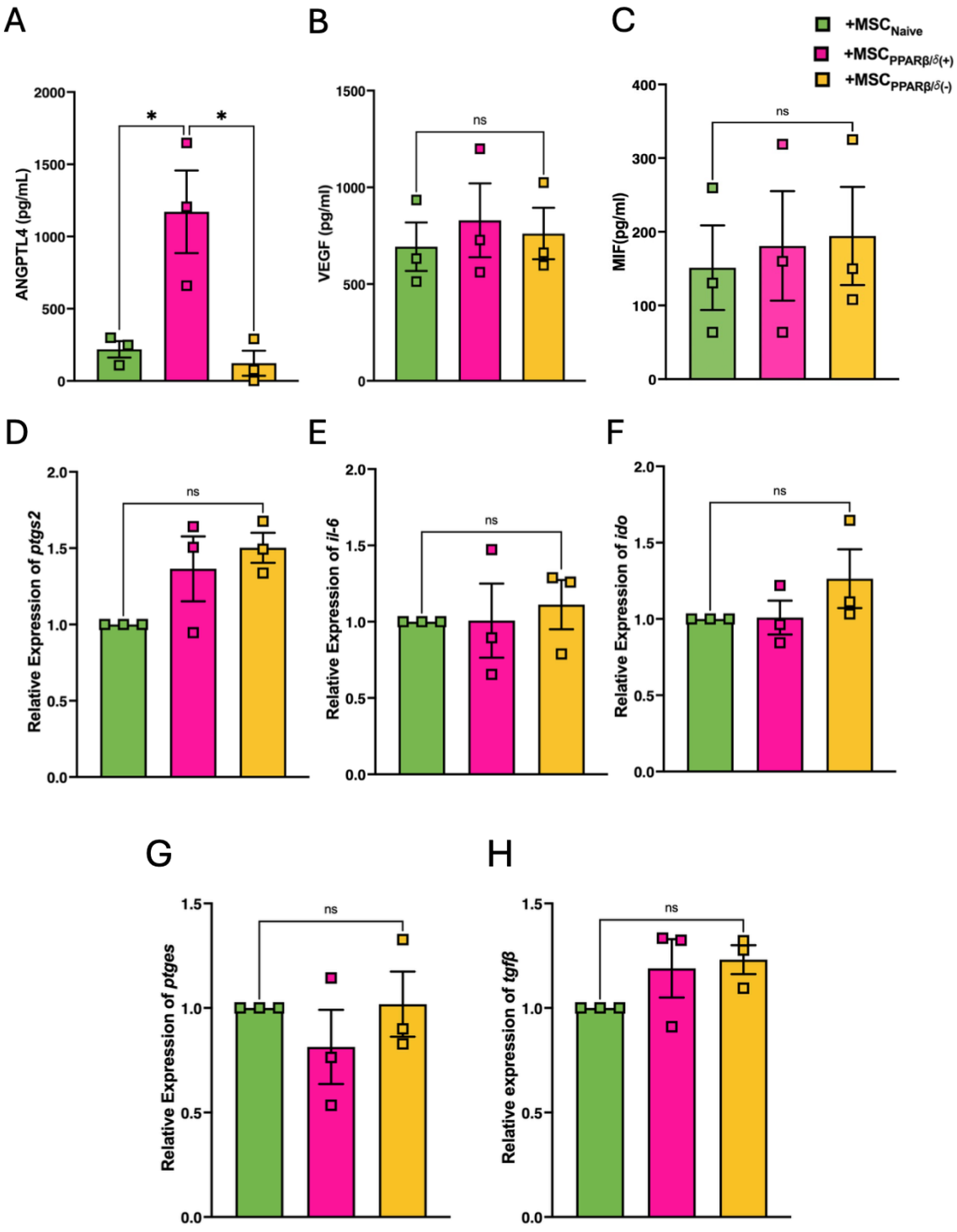

Figure legend available on next page

Figure 4: PPARβ/δ(+) hBM-MSCs show enhanced expression of ANGPTL4, but not other traditional MSC-associated genes or proteins. Supernatant from hBM-MSCs exposed to 1uM of PPARβ/*δ* agonist or antagonist were harvested before cells were collected in TRIzol for gene expression studies. Protein expression of (A) ANGPTL4, (B) VEGF and (C) MIF were assessed by ELISA and gene expression for (D) *PTGS2,* (E) *IL-6,* (F) *IDO,* (G) *PTGES* and (H) *TGFβ* were assessed (one-way ANOVA followed by Tukey's post-hoc test, n=3). Replicates are a representation of 3 individual hBM-MSC donors. Data is presented as mean ± SEM; *p<0.05, **p<0.01, ***p<0.001, ****p<0.0001.

4.5.6 The MSC-CM$_{PPARβ/δ(+)}$ enhances wound healing in CALU-3 lung epithelial cells in an ANGPTL4-dependent manner

Other studies have highlighted the role of MSC$_{PPARβ/δ(+)}$ in repair[208], and the impact ANGPTL4 can have on repair in other tissues[309, 333]. It has also already been shown that ANGPTL4 can play a significant role in proliferation and migration[308]. To see if the PPARβ/*δ*-dependent increase in ANGPTL4 was the true mechanism behind the enhanced pro-reparative capacity, I made use of an anti-ANGPTL4 neutralising-antibody (nanobody) to eliminate the functional capacity of ANGPTL4 in the MSC-CM. This would prevent it from acting on the CALU-3 lung epithelial cells (figure 5A). Scratch assay analysis from each of our groups, whereby the MSC-CM used was exposed to either the ANGPTL4 nanobody or a corresponding IgG control, highlighted that ANGPTL4-neutralisation abrogated the enhanced wound closure once seen in the MSC-CM$_{PPARβ/δ(+)}$ group (figure 5B-D).

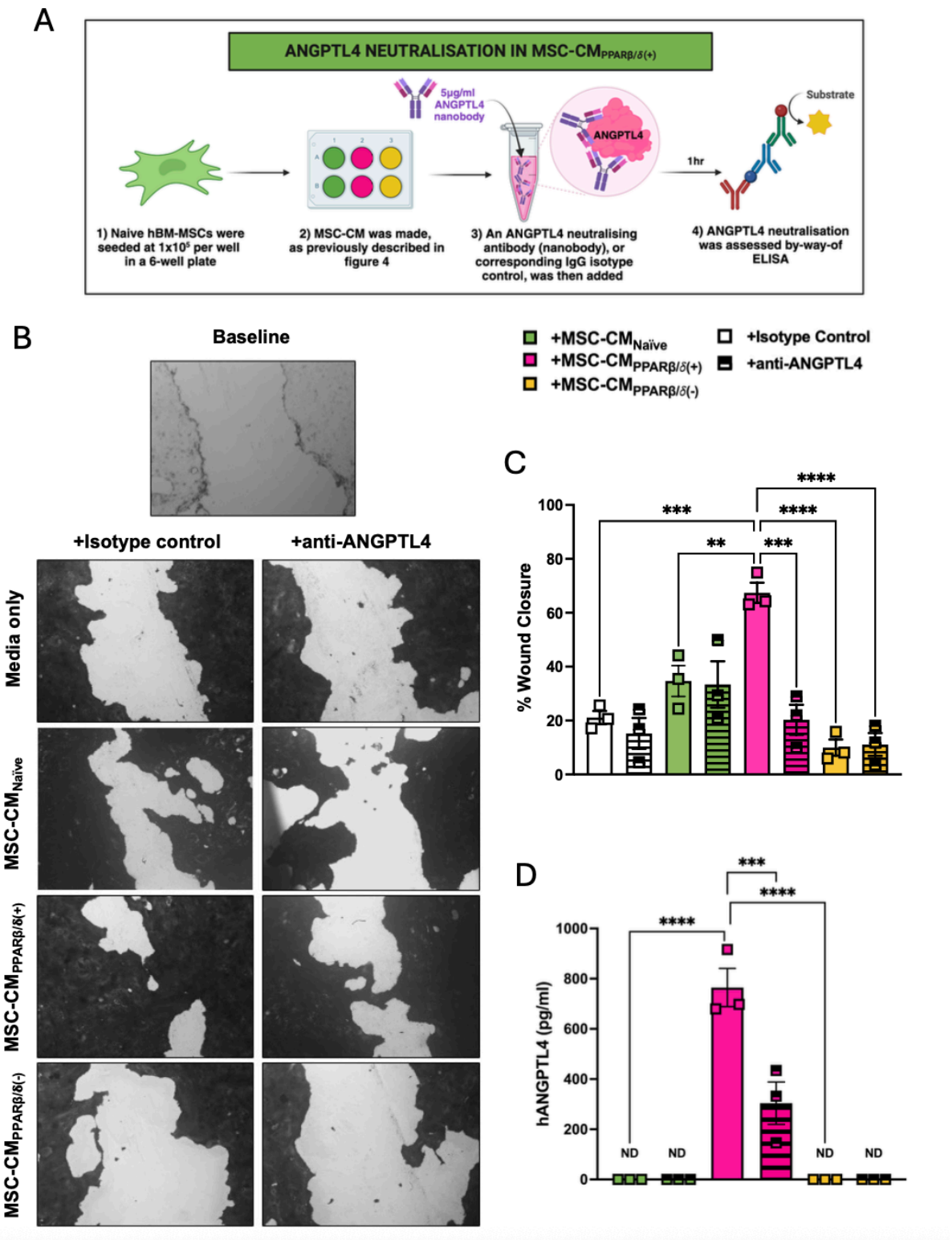

Figure legend available on next page

Figure 5: PPARβ/δ(+) hBM-MSCs show enhanced wound repair via ANGPTL4. (A) using an ANGPTL4 neutralisation approach, we assessed (B) wound closure of CALU-3 lung epithelial cells. (C) PPARβ/*δ*(+) hBM-MSCs showed enhanced wound closure, while ANGPTL4-neutralisation abrogated this effect. (D) Neutralisation of ANGPTL4 was confirmed by ELISA (one-way ANOVA followed by Tukey's post-hoc test, n=3). Replicates are a representation of 3 individual hBM-MSC donors. Data is presented as mean ± SEM; *p<0.05, **p<0.01, ***p<0.001, ****p<0.0001.

4.5.7 Ligands and co-activators of PPARβ/δ are increased, while co-repressors of PPARβ/δ are decreased, in ARDS patients

Using a publicly available metabolomics dataset (Study ID: ST000042; doi: 10.21228/M8SG64) PPARβ/*δ* ligands were identified to be more prevalent in ARDS; with higher levels of linoleate, palmitoleic acid and arachidonate (natural ligands of PPARβ/*δ*) in BALF from ARDS patients, in comparison to healthy controls (figure 6A). Using a publicly available RNA sequencing dataset (GEO accession no.: GSE185263), it was also shown that several PPARβ/*δ*-associated co-activators were increased in the blood of ARDS patients (figure 6B). This included a significant increase in *NCOA1* and *NCOA3,* a trend toward increased *PPARGC1A* and *NCOA2,* and no difference in *CREBBP* (figure 6C-G). Along with this, several PPARβ/*δ*-associated co-repressors were decreased in the blood of the same ARDS patients (figure 6B). This included a significant reduction in *SIRT1, NCOR1* and *NCOR2* (figure 6H-J). Given that *ANGPTL4* was a hit of interest in our own sequencing dataset, we wanted to investigate if *ANGPTL4* gene and protein expression in MSCs was altered upon exposure to ARDS patient serum. In comparison to the PPARβ/*δ* agonist, exposure of MSCs to ARDS patient serum significantly increased MSC secretion of ANGPTL4. Addition of both

the PPARβ/δ agonist and ARDS patient serum further enhanced MSC production of ANGPTL4 (figure 6K). Interestingly, addition of the PPARβ/δ antagonist could not block the ARDS serum induction of ANGPTL4 secretion by MSCs. This is largely down to PPARβ/δ having multiple binding-sites[334], whereby both agonists and antagonists can bind simultaneously; with agonism always out-competing antagonism (figure 1D-F). Other genes and proteins were also assessed in response to PPARβ/δ modification combined with the addition of ARDS-serum exposure (supplementary figure 4).

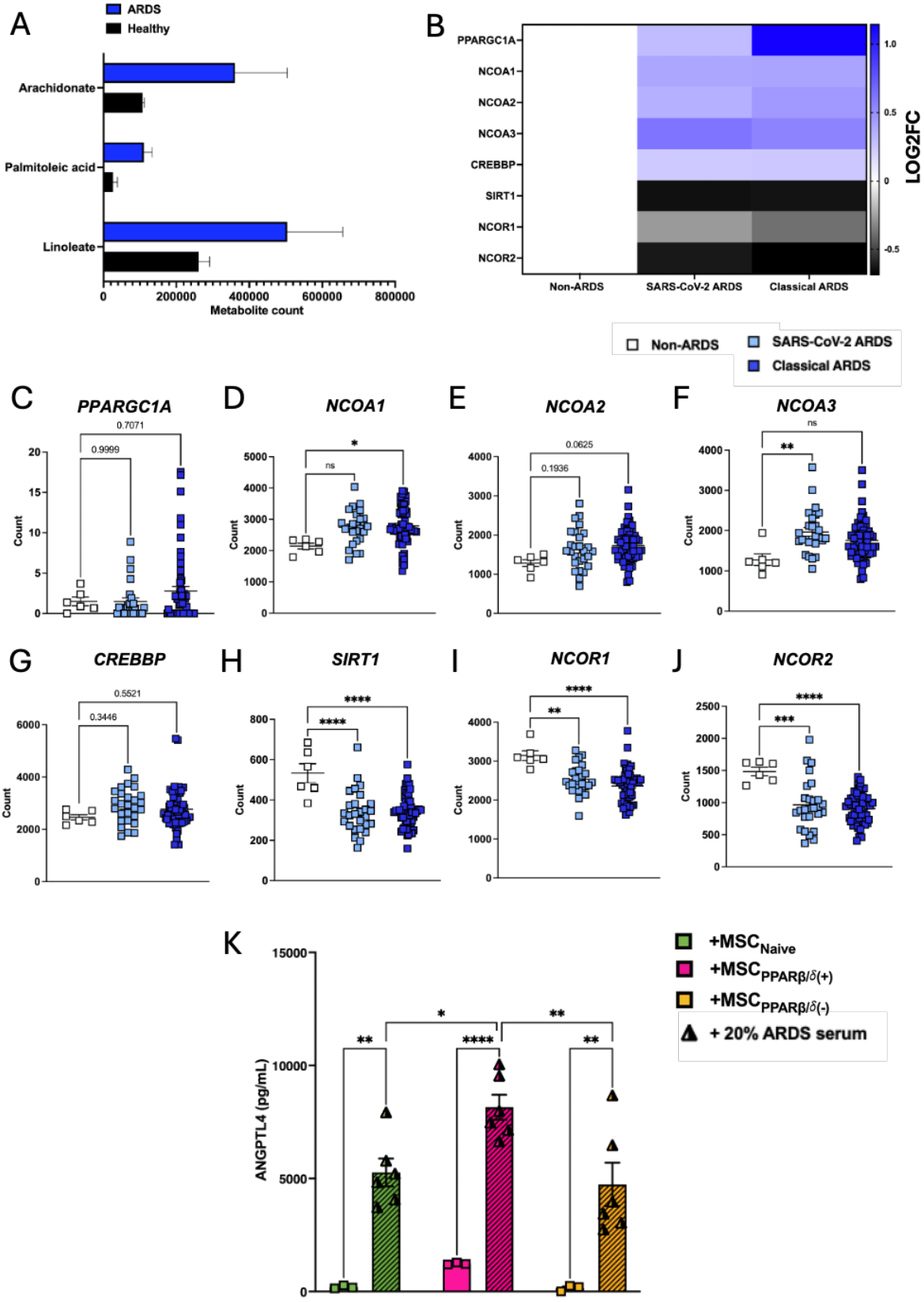

Figure legend available on next page

Figure 6: ARDS patients have higher levels of PPARβ/δ(+) ligands and co-activators. (A) a publicly available dataset (Study ID: ST000042; doi: 10.21228/M8SG64), we assessed PPARβ/*δ*(+) ligands present in the ARDS lung. (B) An additional dataset (GEO accession no.: GSE185263), based on ARDS serum, highlighted an increase in PPARβ/*δ*(+)-associated co-activators such as (C) *PPARGC1A*, (D) *NCOA1*, (E) *NCOA2*, (F) *NCOA3* and (G) *CREBBP*; and a decrease in PPARβ/*δ*(+)-associated co-repressors such as (H) *SIRT1*, (I) *NCOR1* and (J) *NCOR2* (one-way ANOVA followed by Tukey's post-hoc test, n=6+). Replicates are a representation of (A-J) individual ARDS patients, or healthy controls; or (K) 3 individual hBM-MSC donors. Data is presented as mean ± SEM; *p<0.05, **p<0.01, ***p<0.001, ****p<0.0001.

4.5.8 Pro-inflammatory licensing enhances the effects of MSC-CM$_{PPARβ/δ(+)}$ *in vivo*

Next, I sought to investigate if MSC-CM$_{PPARβ/δ(+)}$ could have a protective effect in a preclinical model of ALI. MSC-CM$_{PPARβ/δ(+)}$ significantly enhanced vascular and epithelial barrier function as measured using Evans blue dye assay (figure 7A, B). Although modest, this result was statistically powered. This effect was somewhat impacted by the anti-ANGPTL4 nanobody, but this was not significantly different from our MSC-CM$_{PPARβ/δ(+)}$ group (figure 7A, B). MSC-CM$_{PPARβ/δ(+)}$ also significantly reduced the level of TNFα in the BALF of LPS-exposed mice (figure 7C). However, the anti-ANGPTL4 nanobody was not able to reverse this effect (figure 7C). MSC-CM$_{PPARβ/δ(+)}$ had no effect on IL-6 (figure 7D) or total protein (figure 7E) in the BALF. As exposure to ARDS patient serum, along with PPARβ/*δ* agonism, allowed for a 10-fold increased induction of ANGPTL4 in MSC-CM compared to PPARβ/*δ* agonist alone (figure 6K), the efficacy of ARDS-licensed MSC-CM$_{PPARβ/δ(+)}$ was investigated in a model of ALI. In this case, the combination of ARDS serum and PPARβ/*δ* agonism led to

significantly enhanced therapeutic effects with significant reduction in TNFα and IL-6 in the BALF (figure 7C, D). Importantly, anti-ANGPTL4 reduced the anti-inflammatory effects mediated by the ARDS-licensed MSC-$CM_{PPARβ/δ(+)}$. Although there was no significant reduction in total protein, the trend toward a reduction in total protein was abrogated in the presence of the anti-ANGPTL4 nanobody (figure 7E).

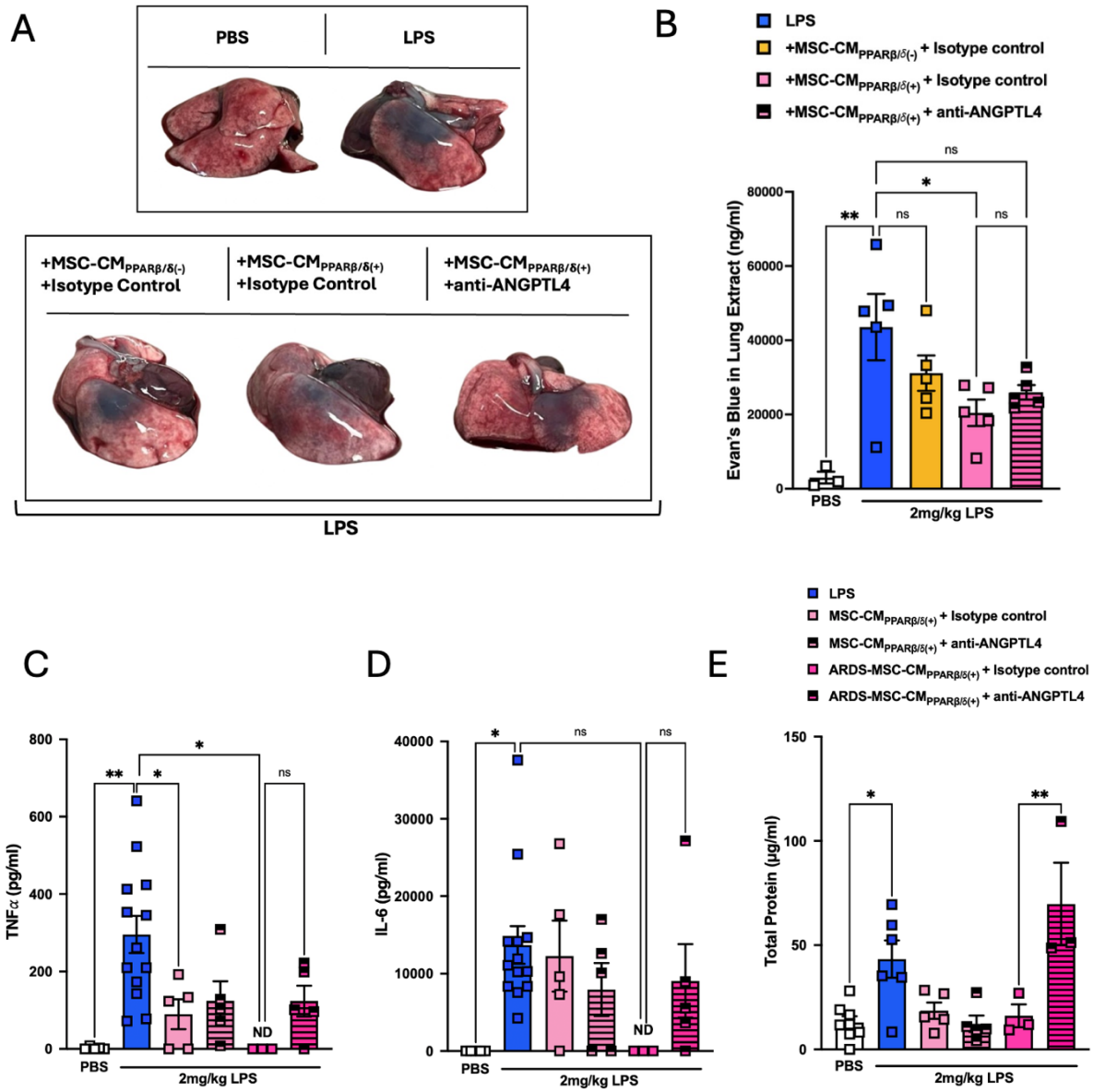

Figure 7: ARDS-licensing enhances ANGPTL4-induced cytoprotection by hBM-MSCs in a model of ALI. Mice were exposed to 2mg/kg LPS IT, or a PBS control. (A) An Evan's Blue Dye permeability assay was used to (B) deduce the amount of leakage from the lungs of mice exposed to LPS +/- our treatments of interest. Pro-inflammatory cytokines such as (C) TNFα and (D) IL-6 in the BALF were assessed by ELISA and (E) total protein was assessed using a bradford assay (one-way ANOVA followed by Tukey's post-hoc test, n=3-12). Replicates are a representation of individual mice. Data is presented as mean ± SEM; *p<0.05, **p<0.01, ***p<0.001, ****p<0.0001.

4.5.9 Pro-inflammatory licensing enhances the effects of MSC-CM$_{PPARβ/δ(+)}$ by altering the cell populations in the BALF *(completed in collaboration with Dr. Shoumo Kundu).*

Furthermore, we investigated the cell populations present in the lungs of the mice from the ARDS-licensed treatment group, compared to controls, and observed a modest shift in macrophage populations (figure 8A). The frequency of CD11b+/CD64+/CD40+/Ly6G-/CD24-/CD206- (CD40+CD206-/M1 macrophage) increased in ALI mice compared to healthy controls, and there was no difference upon administration of MSC-CM from any group (figure 7B). There was no difference noted in CD11b+/CD64+/CD206+/Ly6G-/CD24-/CD40- (CD206+CD40-/M2 macrophage) upon exposure to LPS, however, there was a trend toward an increase in M2 macrophage (figure 8C). Upon investigation of the neutrophil population, we also saw a significant increase in neutrophils (Ly6G+ cells) in response to LPS, as expected. We also noted a further increase in neutrophils in response to ARDS licensed MSC-CM$_{PPARβ/δ(-)}$ (figure 8C). Along with this, we saw a significant reduction in neutrophils in our ARDS-licensed MSC-CM$_{PPARβ/δ(+)}$ group compared to our ARDS-licensed MSC-CM$_{PPARβ/δ(-)}$ group; but not compared to LPS only (figure 8D). This effect was also abrogated in response to our anti-ANGPTL4 nanobody (figure 8D). We also made use of lung homogenates from mice exposed to LPS, followed by PPARβ/δ agonised/antagonised MSCs, to assess M1 and M2 macrophage populations by qRT-PCR (supplementary figure 5), but due to the number of different cells present in a homogenate population, these results were largely inconclusive and did not confirm our results.

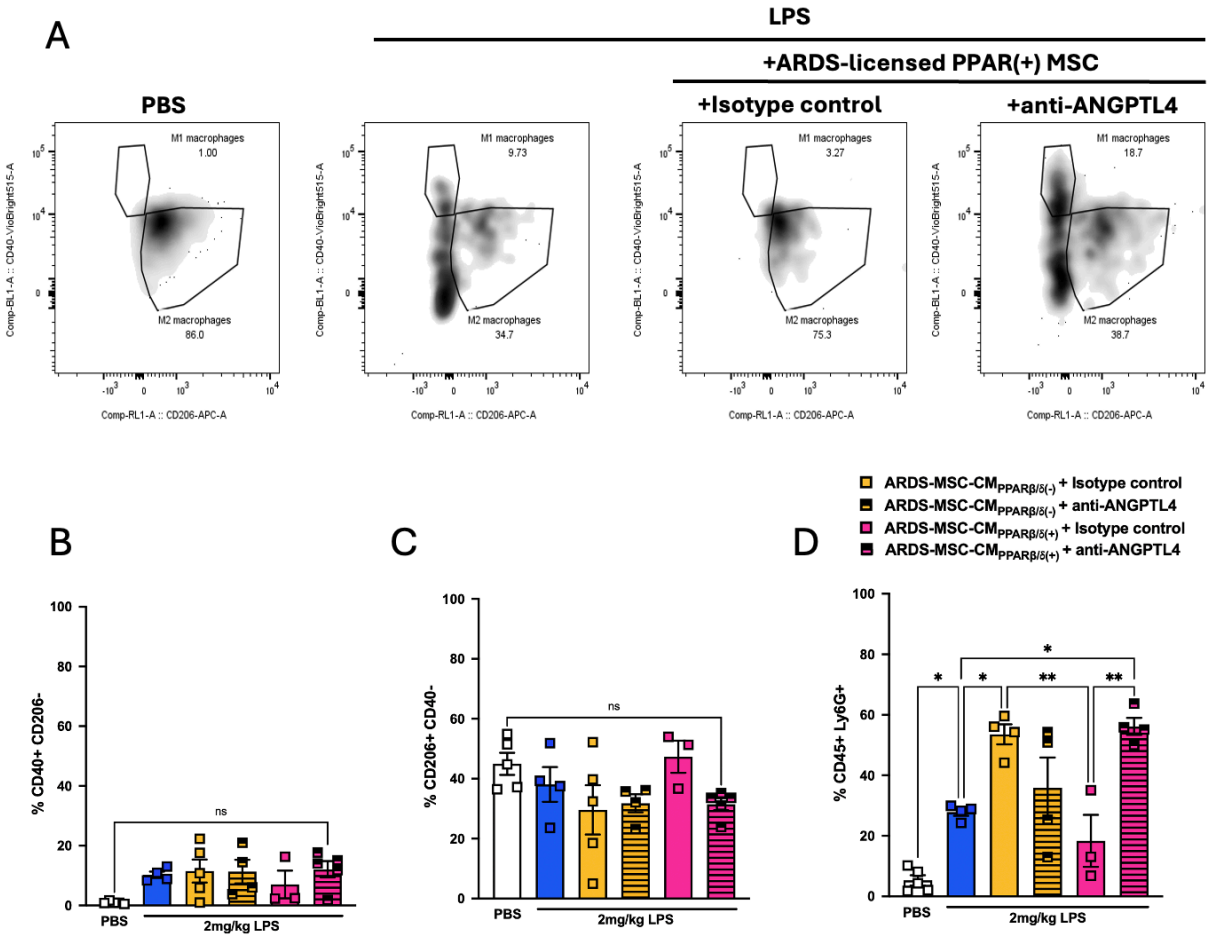

Figure 8: ARDS-licensing enhances ANGPTL4-induced cytoprotection by hBM-MSCs in a model of ALI; through the alteration of cell populations in the lung. Mice were exposed to 2mg/kg LPS IT, or a PBS control. (A) Flow cytometry was used to characterise the cell population present in the BALF of mice exposed to LPS +/- our treatments of interest. Cell populations of the lung, such as (B) M1 macrophage (CD11b+/CD64+/CD40+/Ly6G-/CD24-/CD206-), (C) M2 macrophage (CD11b+/CD64+/CD206+/Ly6G-/CD24-/CD40-) and (D) neutrophils (CD45+/Ly6G+) were assessed (one-way ANOVA followed by Tukey's post-hoc test, n=3-4). Replicates are a representation of individual mice. Data is presented as mean ± SEM; *p<0.05, **p<0.01, ***p<0.001, ****p<0.0001.

4.6 Discussion

There are two primary functions of MSCs in the context of cell therapy: immunomodulation and pro-repair[124]. It is also known that the environment can largely dictate MSC response[247, 293, 301]. In the context of ARDS, the complex lung microenvironment; containing inflammatory-agents, microorganisms and FFAs, can largely impact MSC functionality[238, 239]. I previously highlighted that higher levels of inflammation in the ARDS patient microenvironment can promote VEGF-driven repair[122]. Abreu *et al.* (2020) investigated the detrimental impact of fungal toxins present in the lung on MSC viability and showed a drastic increase in MSC cell-death in response to this microenvironmental element[301]. However, there has been little focus on how the FFAs in the ARDS patient microenvironment may impact MSCs. FFAs are known natural ligands of PPARβ/δ[213, 215, 225]. Importantly, studies have already shown that modulation of this receptor can alter MSC functionality[207, 209, 243, 245, 303]. Given this, it was important to investigate the functional impact of PPARβ/δ-modulation on the primary functions of MSCs, and their secretome, in a model of ALI.

In this study, it was highlighted that PPARβ/δ-activation could enhance wound repair in CALU-3 lung epithelial cells (figure 2B, C). CALU-3 lung epithelial cells are a clinically relevant *in vitro* cell line to use for these studies; due to their ability to generate tight junctions[335], which are traditionally impacted in the context of ARDS[336]. A time-lapse experiment, using a mitomycin C proliferation inhibitor, highlighted that this was likely a combination effect of both migration and proliferation (figure 3D, E). It has already been shown in several studies that ANGPTL4 can promote both migration and proliferation in endothelial cells[308, 309]. Ziveri *et al.* (2024) recently published a comprehensive study on the role of ANGPTL4 in endothelial cytoprotection in skin vs brain endothelial cells. They

identified that ANGPTL4 in the brain endothelium protects against *Neisseria meningitis*, and upon addition of ANGPTL4 to the skin endothelium (which naturally has lower levels of ANGPTL4), they were able to induce the same level of protection against this bacterium[305].

Importantly, ANGPTL4 is considered a biomarker in ARDS[337]. However, data mined from a publicly available dataset (GEO accession no.: GSE241186) would suggest that ANGPTL4 is downregulated in CALU-3 lung epithelial cells in response to SARS-CoV-2 infection; along with a paired reduction in tight junction expression (supplementary figure 6). Traditionally, MSCs secrete factors such as VEGF, HGF and other angiogenic factors to promote repair[155, 156, 159, 290]. With this in mind, and *ANGPTL4* being our most enriched hit from our sequencing study, we sought to investigate this angiogenic factor further. We observed ANGPTL4 production at the protein level (figure 4A), and confirmed that PPARβ/*δ* agonism enhanced the production of ANGPTL4 in hBM-MSCs. We further investigated other known MSC-associated cytoprotective factors, such as VEGF (figure 4B) and MIF (figure 4C)[156]. These were unchanged between groups. Upon investigation of other traditional MSC-associated factors, there was again no differences seen between groups (figure 4D-H). While the data was promising, further experiments were required to demonstrate the functional effect of MSC-CM derived ANGPTL4. Through the use of an anti-ANGPTL4 neutralising antibody (nanobody), ANGPTL4 could be neutralised in the MSC secretome, before addition to the CALU-3 lung epithelial cells (figure 5B-D). This abrogated the enhanced wound closure that had originally been observed in the MSC-$CM_{PPAR(+)}$ group.

To further investigate the role of the $ANGPTL4^{HIGH}$ MSC-CM, it was imperative to carry out a study in a model of ALI [122]. This study highlighted a distinct cytoprotective effect; highlighting ANGPTL4-dependent regulation of inflammation (figure 7A-E). This was seen in the significant reduction of pro-inflammatory cytokines such as TNFα and IL-6 in response to the ARDS-licensed hBM-MSC-$CM_{PPARβ/δ(+)}$ group (figure 7A, B). This was in line

with our previous study, whereby we showed ARDS-licensing could promote MSC immunomodulatory capacity in the same ALI model[122]. This effect was abrogated in response to our anti-ANGPTL4 nanobody. Huang *et al* (2025) recently highlighted the anti-inflammatory role of ANGPTL4 via M2-polarisation in the context of Kupffer cells in the liver, in a rat model of orthotopic liver transplantation[333]. Given that we had already deduced the pro-reparative effects of hBM-MSC-$CM_{PPAR\beta/\boldsymbol{\delta}(+)}$, the additional benefit of the anti-inflammatory properties highlighted a dual role for this MSC secretome in the treatment of ALI. This was further investigated by cell population analysis in the lung, in collaboration with Dr. Shoumo Kundu. This study included the observation of both macrophage and neutrophils in the lung microenvironment (figure 8). We did not see a difference in macrophage signature, but we did however see a modest reduction in neutrophils in response to our ARDS-licensed hBM-MSC-$CM_{PPAR\beta/\boldsymbol{\delta}(+)}$ group. A study by Wee *et al.* (2022) showed that ANGPTL4 can induce neutrophil clearance by increasing the activity of M2-like macrophage in a model of excisional wound healing using ANGPTL4 knock-out mice [338]. Additional replicates would be required to determine the full effects of this in our model.

Interestingly, other studies investigating the role of PPARβ/*δ*-modulation in MSCs have not seen enhanced immunomodulation in response to PPARβ/*δ* agonism, like has been seen here. A study by Contreras-Lopex *et al.* (2020) highlighted that inhibition of the PPARβ/*δ* receptor on mouse MSCs led to enhanced modulation of T-cells, via increased glycolytic capacity[246]. Another study by Luz-Crawford *et al.* (2016) further highlighted a positive correlation between PPARβ/*δ*-inhibition in mouse MSCs, and immunomodulation in an arthritic mouse model[245]. Importantly, both of these studies made use of 1) mouse MSCs and 2) whole cells. It is already known from the literature that PPARβ/*δ* agonism can induce ANGPTL4[230], and that this is both an angiogenic and immunomodulatory factor[308, 333]. It is also known that whole cell treatments are more complex than use of secreted factors[339];

due to the potential cell-cell interactions *in vivo*. With this in mind, it's likely that by moving toward a secretome approach, we have eliminated potential negative effects of the receptor on the therapy in question.

It was concluded that the hBM-MSC-CM$_{PPAR\beta/\delta(+)}$ had the capacity to 1) aid in repair 2) enhance immunomodulation and 3) alter the neutrophil population in the lung microenvironment in an ANGPTL4-dependent manner in a pre-clinical model of ALI. Further studies are required to fully elucidate the impact of this study.

4.7 Concluding remarks

Within this chapter, the effect of PPARβ/δ-modulation on hBM-MSC therapeutic efficacy was assessed. It was shown that PPARβ/δ-activation of hBM-MSCs led to an enhance pro-reparative MSC phenotype. The was carried out through the promotion of ANGPTL4; a pro-angiogenic factor produced in response to PPARβ/δ-activation. This study provided novel mechanistic insight into non-growth factor associated form of MSC-induced repair, and highlighted powerful results. Unfortunately, there was not enough time to produce a robust enough flow cytometry dataset, to fully profile the mouse lung environment. This is something the laboratory plans to elaborate on in my absence, and I look forward to seeing the result.

4.8 Supplementary

Supplementary table 1: Flow cytometry antibodies.

Marker	Fluorochrome	Laser/ filter	Clone	Volume (µl/sample)	Supplier	Cat No
CD24	Vio Green	VL2 (512/25)	REA743 | M1/69	0.5	Milteny Biotec	130-110-832
CD64	BV711	VL4 (710/50)	X54-5/7.1	0.5	Biolegend	139311
CD40	Vio Bright 515	BL1 (530/30)	REA965 | FGK45.5	0.5	Milteny Biotec	130-116-115
Ly-6G	Per-CP Vio700	BL3 (695/40)	REA526 | 1A8	0.5	Milteny Biotec	130-117-500
CD11c	PE	YL1 (585/16)	REA754 | N418	0.5	Milteny Biotec	130-110-701
CD45	PE-Vio615	YL2 (620/15)	REA737 | 30F11	0.5	Milteny Biotec	130-110-804
CD11b	PE-Vio770	YL4 (780/60)	REA592 | M1/70.15.11.5	0.5	Milteny Biotec	130-113-808
CD206	APC	RL1 (670/14)	C068C2	0.5	Biolegend	141708
MHC-II A/E	Vio Bright R720	RL2 (720/30)	REA813 | M5/114.15.2	0.5	Milteny Biotec	130-128-972
Viability	Z-NIR	RL3 (780/60)	-		Biolegend	423106
Fc block	-	-	93		Thermo-fisher	14-0161-85

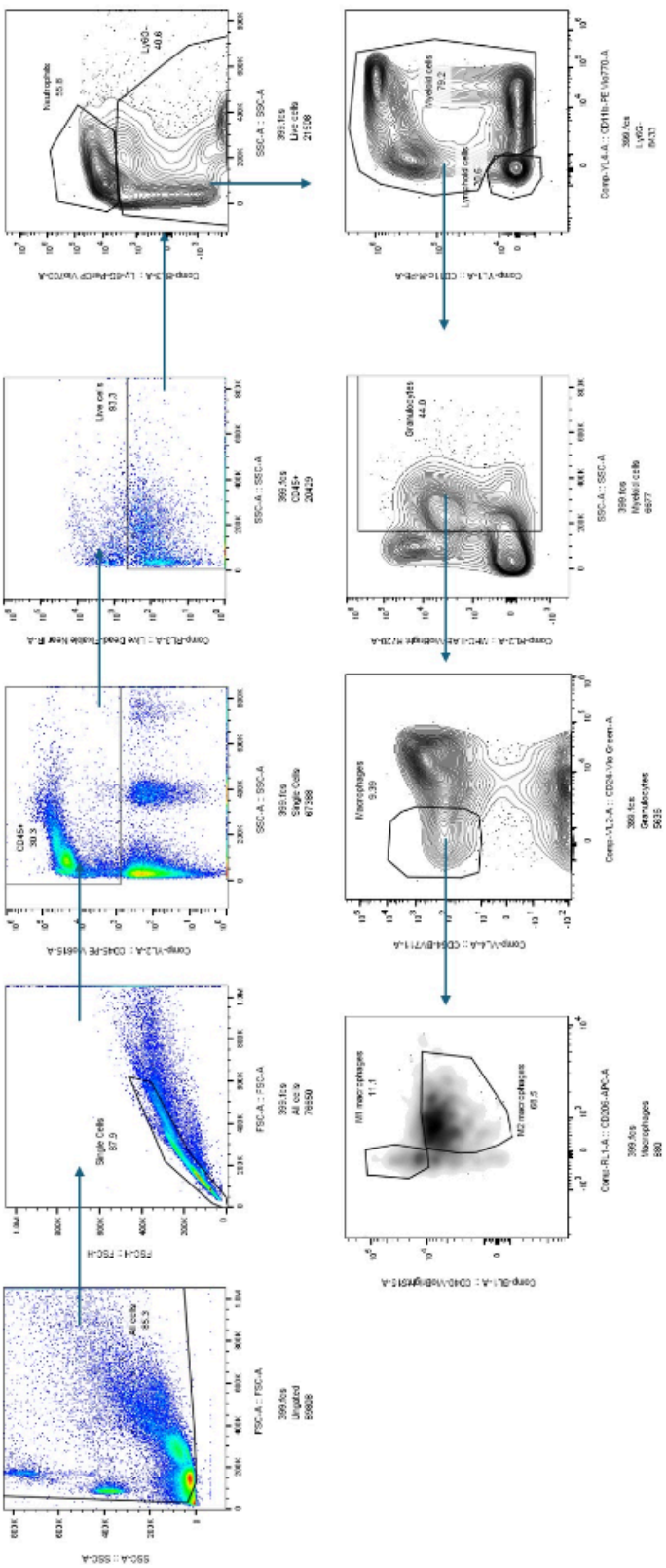

Supplementary figure 1: Flow gating strategy for lung cell population identification. This study was completed in collaboration with Dr. Shoumo Kundu.

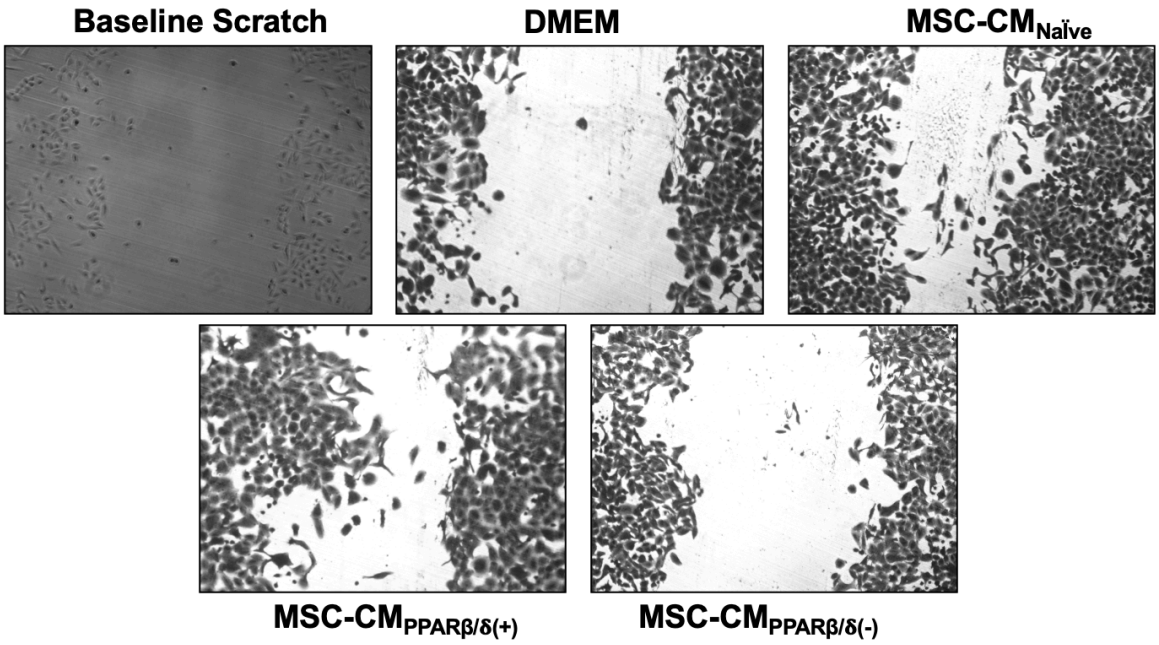

Supplementary figure 2: Wound repair in A549 lung epithelial cells in response to PPARβ/δ(+/-) hBM-MSC. Highlighting an increased wound closure in response to PPARβ/*δ*(+) hBM-MSC.

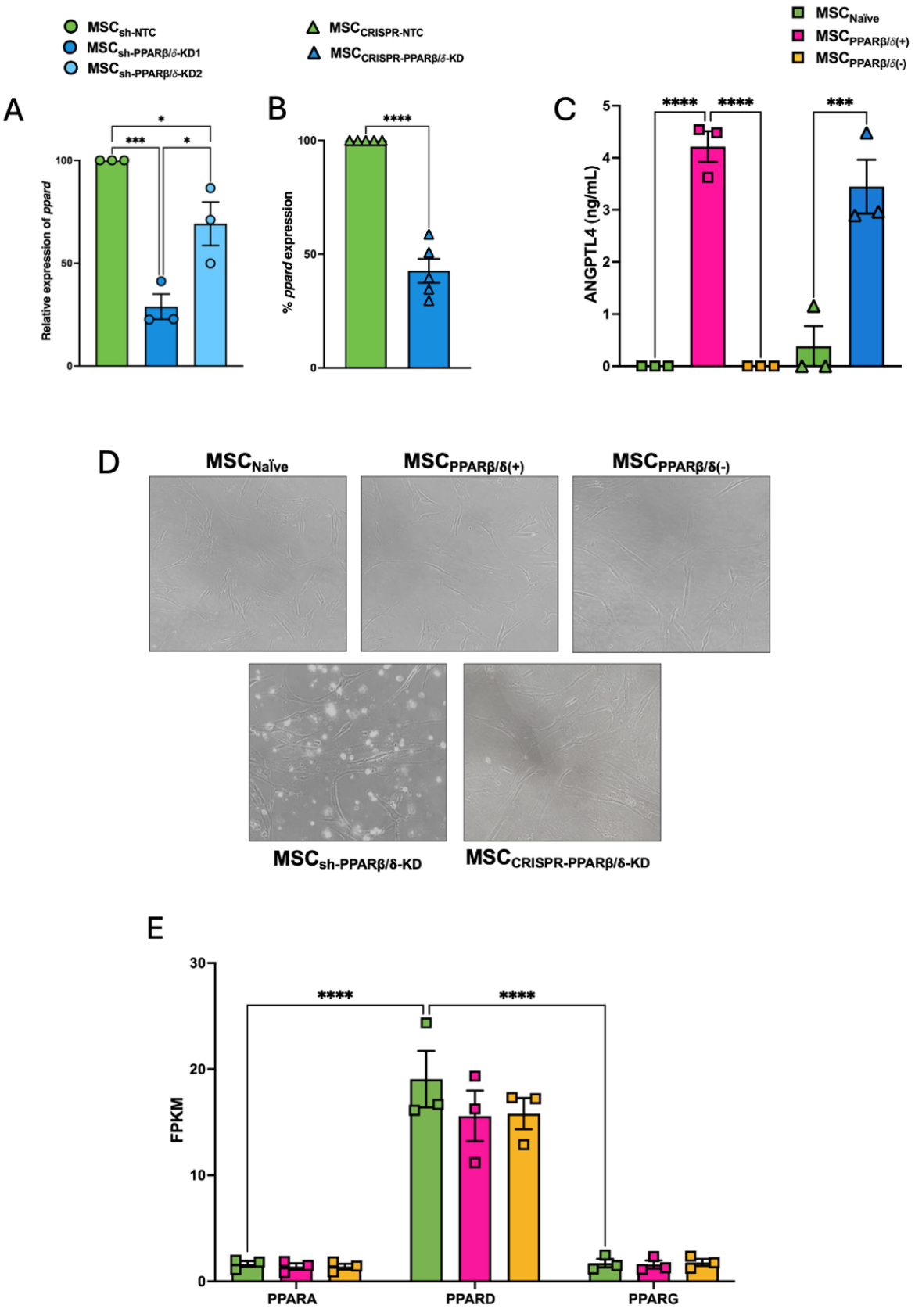

Figure legend available on next page

Supplementary figure 3: PPARβ/δ knock-down in hBM-MSCs. hBM-MSCs were lenti-virally transduced and knock-down was assessed by (A) RT-PCR for PPARβ/**δ** (one-way ANOVA followed by Tukey's post-hoc test, n=3). CRISPR was then used to knock-down PPARβ/*δ*, and (B) RT-PCR was also used to assess percentage knock-down. (C) ANGPTL4 levels were assessed in the CRISPR knock-downs to address off-target effects, and (D) images were taken of each cell during the process to visualise the effects of the processes. (E) Our sequencing dataset was further utilised to assess the levels of each PPAR family member in our cells (one-way ANOVA followed by Tukey's post-hoc test, n=3). Replicates are a representation of individual hBM-MSC donors. Data is presented as mean ± SEM; *p<0.05, **p<0.01, ***p<0.001, ****p<0.0001.

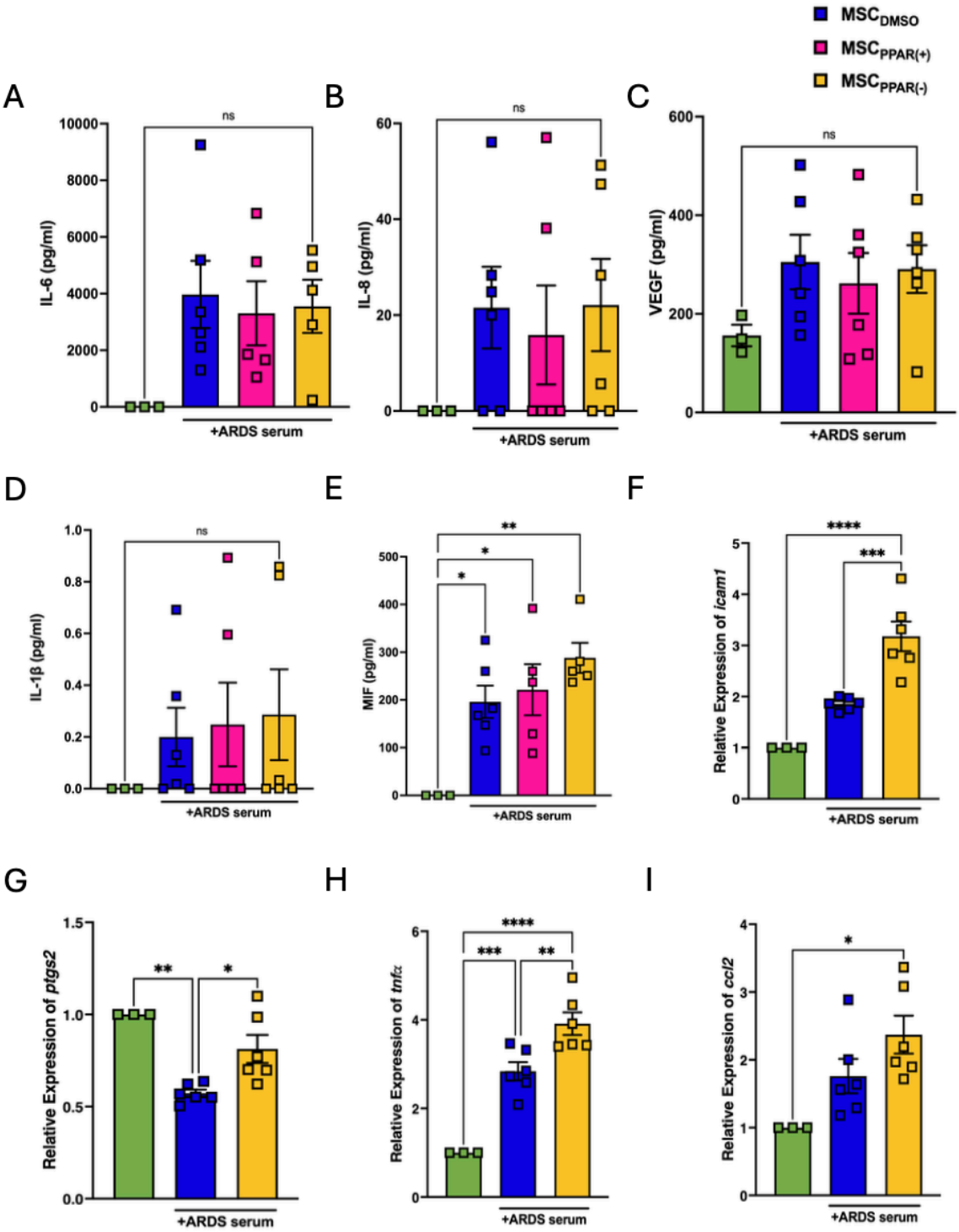

Figure legend available on next page

Supplementary figure 4: PPARβ/δ(+/-) hBM-MSCs in response to ARDS patient serum. hBM-MSCs were exposed to 1uM of a PPARβ/*δ* agonist or antagonist, and further exposed to ARDS patient serum. Gene/protein expression was assessed for (A) IL-6, (B) IL-8, (C) VEGF, (D) IL-1β, (E) MIF, (F) *ICAM1*, (G) *PTGS2,* (H) *TNFA* and (I) *CCL2* (one-way ANOVA followed by Tukey's post-hoc test, n=3+). Replicates are a representation of individual hBM-MSC donors. Data is presented as mean ± SEM; *p<0.05, **p<0.01, ***p<0.001, ****p<0.0001.

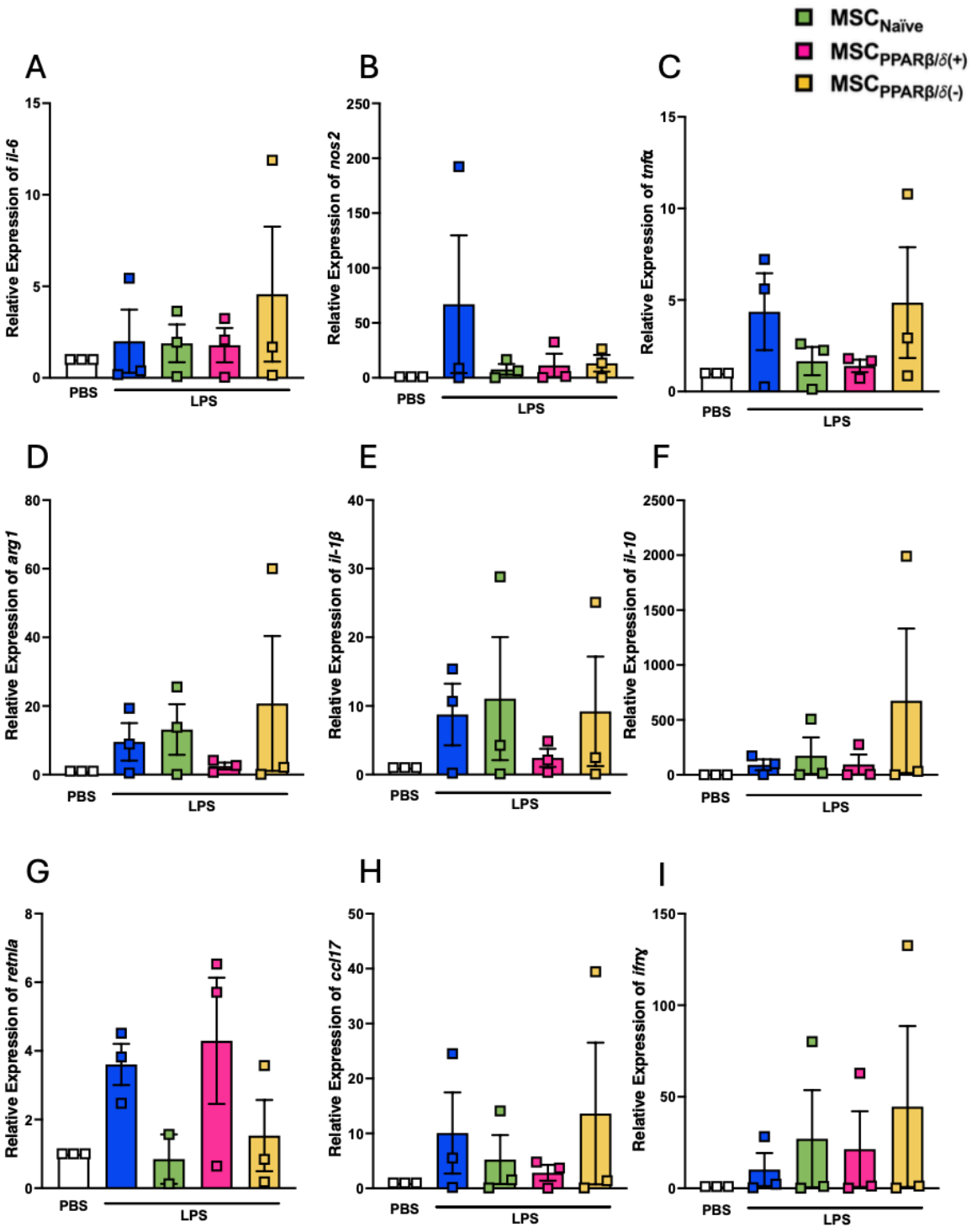

Figure legend available on next page

Supplementary figure 5: Lung homogenates from mice exposed to LPS +/- PPARβ/δ-modulated hBM-MSCs. Lungs were collected from mice in our ALI model and homogenised for RNA isolation. RT-PCR was used to assess several M1-like or M2-like macrophage markers. This included (A) *il-6,* (B) *nos2,* (C) *tnfa,* (D) *arg1,* (E) *Il-1β,* (F) *il-10,* (G) *retnla,* (H) *ccl17* and (I) *ifnɣ* (one-way ANOVA followed by Tukey's post-hoc test, n=2+). Replicates are a representation of individual mice. Data is presented as mean ± SEM; *p<0.05, **p<0.01, ***p<0.001, ****p<0.0001.

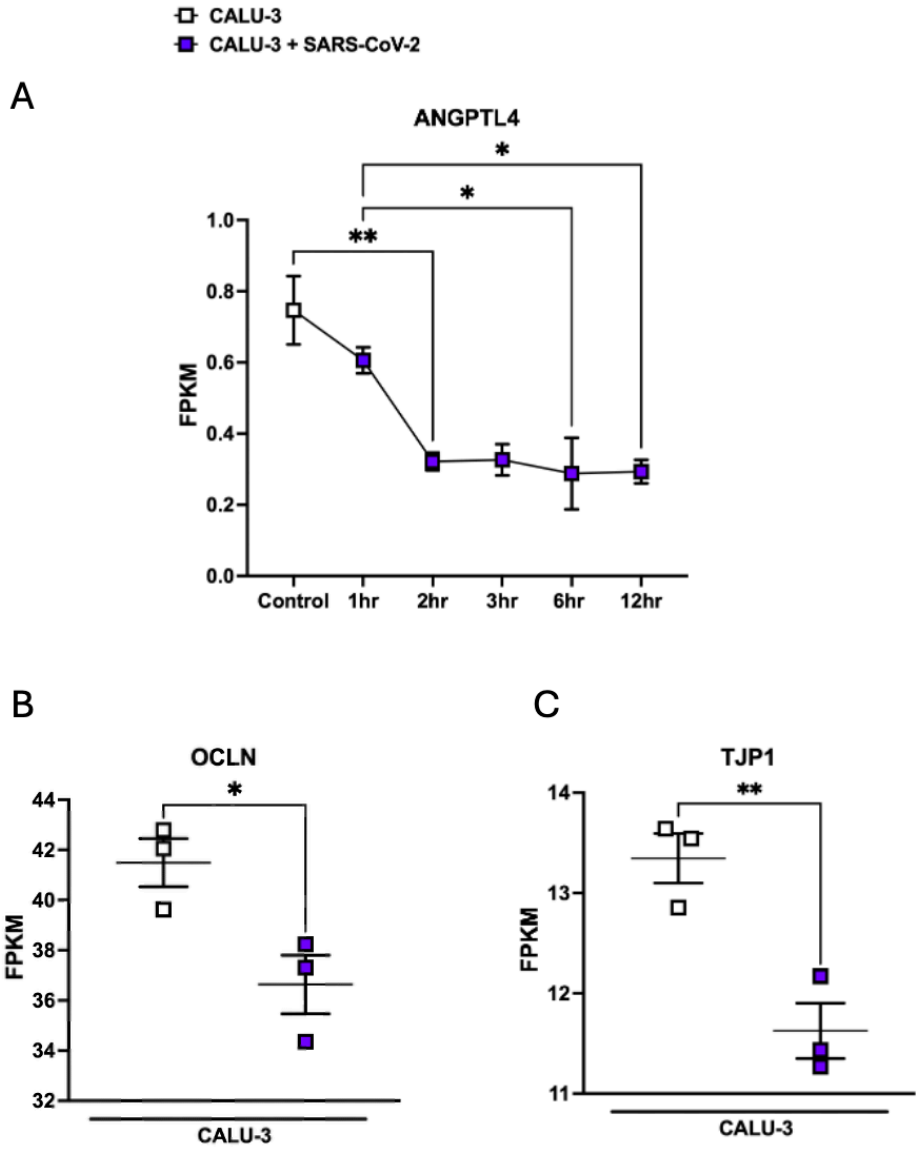

Supplementary figure 6: ANGPTL4, and tight junction expression, is reduced in SARS-CoV-2 treated CALU-3 cells. A publicly available dataset of CALU-3 lung epithelial cells in response to SARS-CoV-2 infection (GEO accession no.: GSE241186) was mined and (A) *angtpl4* and (B, C) tight junction expression were accessed. Replicates are a representation of CALU-3 cells in response to SARS-CoV-2. Data is presented as mean ± SEM; *p<0.05, **p<0.01, ***p<0.001, ****p<0.0001.

Chapter 5

General Discussion

5.1 Discussion

MSCs that are present in diseased lung microenvironments have shown to have impaired functionality [340-342]. For cell therapy to be effective, healthy/non-diseased MSCs are utilised, and introduced into the diseased system. However, the impact the disease microenvironment has on these healthy MSCs has largely been neglected. With this in mind, we sought to investigate the impact the ARDS disease microenvironment had on healthy/non-diseased MSCs. There are various components of the ARDS lung that could potentially impact MSC therapeutic efficacy. Predominantly, 1) inflammatory stimuli, 2) FFAs and 3) microorganisms; two of which have been covered in this thesis [46, 192, 238]. Inflammation has long been studied in the context of MSC research; with numerous publications highlighting the ability for inflammatory cytokines to activate or 'license' MSCs, leading to enhanced therapeutic efficacy [190, 194, 249]. Inflammatory cytokines such as IL-6, IL-8, TNFα, IL-1β, MIF and IFNɣ are all found in abundance in the ARDS patient microenvironment; with higher levels of the cytokines being indicative of the hyper-inflammatory sub-phenotype of ARDS [93, 122]. The impact that many of these cytokines have on MSCs has already been investigated, both individually and in combination [148, 190, 248, 249]. One cytokine that has not yet been looked at individually was TNFα; a cytokine that we were already indirectly exposing our MSCs to upon co-incubation with LPS-stimulated macrophages throughout our studies. To assess the impact that TNFα-licensing would have on MSCs, we exposed MSCs to human recombinant TNFα and carried out an RNA sequencing study (chapter 2, figures 1-4). Much like other MSC-licensing studies, we saw a dramatic increase in chemoattractant expression (chapter 2, figure 5) [248].

Given the upregulation in chemoattractant expression in our TNFα-licensed group, we sought to investigate the impact $MSC_{TNF\alpha}$ would have on neutrophil recruitment *in vitro*. Our

results showed that CXCL8 was the most significantly altered chemokine in response to $MSC_{TNFα}$ (chapter 2, figure 5B). This is in line with a published study by Ren *et al* (2008) that showed upregulation of chemokines in response to several pro-inflammatory stimuli [193]. There was also a significant upregulation of the expression of other chemokines/cytokines, such as *il-1β, icam1* and *cxcl1* (chapter 2, figure 5B). While investigating chemoattraction towards MSC_{TNFa}, we did not find a significant increase in neutrophil chemotaxis over MSC control (chapter 2, figure 8B). Importantly, our MSC_{Naive} group alone had ~250pg/ml of CXCL8 alone, without quantification of any other chemokines present in the well (chapter 2, figure 8C). Although doses of 1-10ng/ml of chemokines has been used in the field without reaching maximum capacity [343], it's important to note that there were several other chemokines enriched in our sequencing study, that we have not quantified here. This was paired with an upregulation in IL-17 signalling (chapter 2, figure 3); which can also enhance chemotaxis [344]. The synergistic response of all chemokine's and cytokines present acting together could have led to a saturated response; preventing us from detecting increase chemotaxis in our $MSC_{TNFα}$ group. To investigate this further, we would need to further optimise this assay, potentially reduce the co-incubation timing or make use of diluted MSC-CM from either group.

Along with our chemoattraction study, we also sought to investigate functional differences in both macrophage and neutrophils; two key drivers of ARDS. Upon co-incubation of $MSC_{TNFα}$ with human MDMs, we saw heightened immunomodulatory capacity (chapter 2, figure 13D). This was carried out by observing the ability for the cells to reduce TNFα-production from MDMs in response to LPS stimulation. Interestingly, when we used MSC-CM from the $MSC_{TNFα}$ group, we saw no difference in immunomodulatory capacity between $MSC_{TNFα}$ and $MSC_{Naïve}$ (chapter 2, figure 13E). This would suggest that cell-cell contact was required for this functional difference to occur. In the context of neutrophil modulation, we

investigated phagocytic capacity and NET formation/activity. We began by making use of a publicly available dataset (GEO accession no.: GSE241186) to identify the role of MSCs in neutrophil-modulation (chapter 2, figure 6). This showed that mice exposed to 5mg/kg of LPS, intratracheally, responded to human MSC therapy by reducing ROS and NET-associated markers, and increasing anti-NET/anti-ROS markers in lung tissue (chapter 2, figure 6A-O). When we investigated this ourselves in our pre-clinical model, we saw that although there was no significant reduction in NET formation in our MSC groups *in vitro*, there was a significant reduction in MPO production by the neutrophils in response to the $MSC_{TNFα}$ group (chapter 2, figure 7E, F). This would suggest that although $MSC_{TNFα}$ cannot reduce NET presence, they can reduce NET activity.

We wanted to further investigate these results in our pre-clinical model of ALI. Upon investigation of the inflammatory profile of the lung, we noted a significant reduction in IL-1β in response to $MSC_{TNFα}$ (chapter 2, figure 11C). It's important to note that this was carried out using a non-functional dose of MSCs, that we pre-licensed with TNFα. This was to allow us to measure notable pre-clinical differences between groups; and is perhaps an approach we should have taken for our chemotaxis assay. We did not note any significant differences in TNFα production (figure 11B). Due to the reduced MPO we saw in our *in vitro* assays, we sought to investigate this in the lungs of these mice. We saw a significant reduction in MPO is response to $MSC_{TNFα}$ (chapter 2, figure 11D). This was interesting, as IL-1β produced by the macrophage is known to enhance MPO release from the neutrophil [34]; and MPO released from the neutrophil is known to enhance IL-1β production from the macrophage [35]. Through the use of basic cell counts and cytospin studies, we deduced that the number of cells in the lungs were not altered in response to MSC-therapy, but there was a significant influx of neutrophils to the lung in response to LPS treatment in each group; as expected (chapter 2, figure 11F). This would suggest that $MSC_{TNFα}$ does not impact cell number, but does impact their functionality.

We concluded that, through the upregulation of a variety of chemokines, $MSC_{TNF\alpha}$ could suppress the macrophage pro-inflammatory profile, aid in neutrophil recruitment and alter neutrophil functional capacity in a pre-clinical model of ALI.

TNFα-licensing was a simplistic approach to investigate the impact of the inflammatory microenvironment on MSC therapeutic efficacy. We sought to further enhance our research by exposing MSCs to ARDS patient serum; containing an abundance of inflammatory mediators, lipids and more that could have a great impact on MSC functionality *in vivo*. We specifically wanted to investigate if there were any differences seen in MSC therapeutic efficacy in response to hypo-, or hyper-, inflammatory ARDS serum; characterised by the levels of inflammatory cytokines present in the serum of these patients [93]. Given the literature of previous MSC-licensing studies [190, 194, 249], we hypothesised that hyper-, but not hypo-, inflammatory ARDS serum would license MSCs and enhance their therapeutic efficacy.

To investigate this, we first profiled the ARDS serum itself based on data provided from the samples themselves (chapter 3, figure 1A-D). We determined that there were several patients with high levels of IL-6 (>50pg/ml), and we categorised those patients into our hyper-inflammatory sub-group. There were also several patients with lower levels of IL-6 (<50pg/ml), and we categorised them into our hypo-inflammatory sub-group (chapter 3, figure 1E-G). This is a very simplistic approach to ARDS patient stratification, and moving forward, if there was access to larger quantities of ARDS patient samples, it would be more accurate to stratify the patients based on the numerous factors that define hypo- vs hyper-inflammatory ARDS patients; as defined by Calfee *et al.* (2014) [93]. It's also important to note that although the majority of SARS-CoV-2-induced ARDS patients fall under the hypo-inflammatory profile, and would have lower levels of IL-6; there are still many patient who are characterised at hyper-inflammatory. A study by Singha *et* al. (2020) showed this, by suggesting 4-8% of SARS-CoV-2-induced ARDS patients fall under the hyper-inflammatory sub-phenotype [345].

Upon pooling donors into categories of either the low-IL-6 (hypo) or the high-IL-6 (hyper) sub-groups, we further characterised the serum profile by investigating the presence of other inflammatory mediators such as IL-8, MIF and TNFα (chapter 3, figure 1H-J). This solidified that our hypo-inflammatory sub-group indeed had significantly less of all inflammatory mediators present, while our hyper-inflammatory sub-group had significantly enriched levels of the same factors. Secondary to our serum profiling, we wanted to expose MSCs, from various donors, to either hypo-, or the hyper-, inflammatory ARDS serum; or a healthy serum control (chapter 3, figure 2A). Upon exposure of MSCs to each sub-group, we identified that there was significantly higher levels of VEGF produced in the secretome of hyper-inflammatory licensed hBM-MSCs (chapter 3, figure 2E). There was also significant increase in *vegfa* and *kdr*; the gene that encodes for VEGFR2; in our hyper-exposed MSC group (chapter 3, figure 2F, G). This is in line with a study from Dunbar *et al.* (2025), that highlighted a significant enhancement of MSC-associated cytoprotection in a VEGF-dependent manner, in response to pro-inflammatory licensing with MIF [156]. Due to the permeable lung epithelial and endothelial barriers seen in ARDS, and with VEGF being a known reparative factor utilised by MSCs [124, 156, 290], we wanted to further investigate VEGF.

We identified that $VEGF^{HIGH}$ MSC-CM had the capacity to enhance tight junction expression in CALU-3 lung epithelial cells that had been exposed to a high dose of LPS (chapter 3, figure 3A). This increased gene expression was seen in the case of *tjp1*, *cldn4* and *ocln* (chapter 3, figure 3B-D). We also highlighted that this effect was abrogated in the presence of a VEGFR2 inhibitor; SU-5416. This is in line with work carried out by Zacharek *et al* (2007), who showed that MSC-derived VEGF had the capacity to repair through the upregulation of ocln in a model of ischemic stroke [153]. We further confirmed this at a functional level

through the use of both a scratch assay (chapter 3, supplementary figure 5) and a TEER assay (chapter 3, figure 4A). Our scratch assay study highlighted a significant enhancement in the wound closure of CALU-3 lung epithelial cells in our MSC-CM_{Hyper} group compared to control (chapter 3, supplementary figure 5B, C). We also saw this in our TEER assay, whereby MSC-CM_{Hyper} showed a significant enhancement of barrier integrity of CALU-3 lung epithelial cells (chapter 3, figure 4B, C). We also highlighted that this affect was abrogated in the presence of a biosimilar of a known VEGF-neutralising antibody, Bevacizumab. We further confirmed that there was again a significant increase in tjp1, ocln and cld4 in LPS-exposed CALU-3 lung epithelial cells in response to the MSC-CM_{Hyper} treatment; whereby this affect was also lost in the presence of a VEGF-neutralising antibody (chapter 3, figure 4D-F).

To confirm our results at a pre-clinical level, we sought to expose mice from our ALI model to the MSC-CM from each group. Interestingly, MSCs exposed to both hypo- and hyper-inflammatory ARDS serum had the capacity to reduce the inflammatory profile of the lungs of the ALI mice (chapter 3, figure 5A, B). This is in line with various other studies that have shown even low levels of inflammation may be enough to license MSCs to exert their immunomodulatory effects [346]. Interestingly, only the MSC-CM_{Hyper} group had the capacity to reduce the clinical score and percentage weight loss in these same mice (chapter 3, figure 5C, D). Upon further investigation into the lungs of these mice, we identified that there was also a significant reduction in Evans Blue leakage and wet: dry lung weight ratio; both common measures of lung permeability in models of ALI (chapter 3, figure 6D-F) [292]. We also saw a significant upregulation of *tjp1, ocln* and *cld4* expression in the lungs if the MSC-CM_{Hyper} treated mice (chapter 3, supplementary figure 7A-C). This would suggest that although there was a reduction in the inflammatory profile of both MSC-CM_{Hypo} and MSC-CM_{Hyper} groups, but only MSC-CM_{Hyper} had enhanced barrier integrity; only the scores of these mice were reduced. We concluded that the hyper-, but not hypo-, inflammatory ARDS microenvironment

had the capacity to license MSCs into the beneficial exertion of their cytoprotective capacity in a VEGF-dependent manner in a model of experimental ALI. This is a critical addition to what's currently known on MSCs in the treatment of ARDS, as there are no other studies that have stratified patients for MSC-based pre-clinical or clinical trials. Given the differential results we have seen in response to both sub-phenotypes; this is likely something of importance to keep in mind upon administration of MSCs to patients.

Along with inflammation, there are many other factors that could affect MSC therapeutic efficacy upon administration. Another component to take into account in the presence of FFAs in the microenvironment. Several studies had previously focused on the impact of FFAs on MSC therapeutic efficacy; including studies focusing on the binding of FFAs to the PPARβ/**δ** receptor on the cells [208, 209, 245, 303]. Given the increased prevalence of FFAs observed in ARDS patients [239], we sought to investigate further the impact of this receptor on the cells. Due to the nature of ARDS, and the lung epithelial damage present, we first carried out a wound closure assay. Using a synthetic PPARβ/**δ** agonist or antagonist, we generated PPARβ/**δ** (+) or PPARβ/**δ** (-) MSC-CM to use in our assay (chapter 4, figure 1A). Upon exposure of scratched CALU-3 lung epithelial cells to our MSC-CM, we saw increased wound closure in our MSC-$CM_{PPARβ/δ(+)}$ sub-group (chapter 4, figure 1B, C). We further identified that this effect was due to a combination of both proliferation and migration, based on a study whereby we blocked proliferation using mitomycin c; a known proliferation inhibitor (chapter 4, figure 1D, E) [310].

In order to investigate this further, we sent $MSC_{PPARβ/δ(+)}$ and $MSC_{PPARβ/δ(-)}$ for RNA sequencing (chapter 4, figure 2A). This allowed us to investigate any primary targets of interest. Volcano plot visualisation highlighted significant upregulation of two stand-out genes: *plin2* and *angptl4* (chapter 4, figure 2C). Further characterisation of these cells in the lab confirmed a significant upregulation of ANGPTL4 at the protein level (chapter 4, figure 3A).

Interestingly, there were no differences observed in traditional MSC-associated cytoprotective factors such as VEGF, MIF (chapter 4, figure 3B, C). It also highlighted that there were no differences in traditionally MSC-associated genes, such as *ptgs2, il-6, ido, ptges* and *tgfβ* (chapter 4, figure 3D-H). Given the known role of ANGPTL4 in proliferation and migration, we sought to investigate this further [308, 309]. We made use of an ANGPTL4-neutralising antibody (nanobody) to further assess this (chapter 4, figure 4A). Repetition of the initial scratch assay, including the use of this nanobody, allowed us to identify that the PPARβ/**δ**-induced repair was ANGPTL4-dependent (chapter 4, figure 4B-D).

Upon further investigation into the ARDS microenvironment, using a publicly available metabolomic dataset, we identified that there were increased levels of arachidonate, palmitoleic acid and linoleate in the ARDS lung in comparison to health controls (chapter 4, figure 5A). All three of these metabolites are known natural ligands of PPARβ/**δ** [225]. We also noted significant upregulation of PPARβ/**δ** co-activators in the serum of ARDS patients compared to healthy controls; specifically in the case of *ncoa1* and *ncoa3* (chapter 4, figure 5C-G). We further noted a significant downregulation of PPARβ/**δ** co-repressors in the serum of ARDS patients compared to healthy controls; specifically in the case of *sirt1, ncor1* and *ncor2* (chapter 4, figure 5H-J). These findings would suggest that PPARβ/**δ** on MSCs would be constitutively active when administered to an ARDS patient. With this in mind, we sought to investigate the impact of this receptor on the MSCs.

We highlighted enhanced pro-reparative capacity of hBM-MSC$_{PPARβ/δ(+)}$, specifically in the repair of CALU-3 lung epithelial cells (chapter 4, figure 1A-C). We further identified that this was through both the processes of proliferation and migration (chapter 4, figure 1D, E). Through a series of RNA sequencing analysis (chapter 4, figure 2) and gene/protein expression studies (chapter 4, figure 3), we isolated a target of interest: ANGPTL4. Neutralisation of this protein in our MSC-CM abrogated the enhanced wound closure (chapter

4, figure 4) and allowed us to deduce the mechanism by which hBM-MSC$_{PPAR\beta/\boldsymbol{\delta}(+)}$ enhanced wound repair. Several studies have already investigated the impact of ANGPTL4 on repair; due to its angiogenic nature. Many of these studies have highlighted that ANGPTL4 can enhance wound closure through migration and proliferation; as we have seen in our own study as well [308, 309]. Another study by Ziveri *et al* (2024) showed that ANGPTL4-low tissues, such as the dermal endothelium, are partial to damage; but supplementing ANGPTL4 in that tissue can reverse this effect and offer cytoprotective capacity. This group also showed that ANGPTL4-rich tissues, such as the brain endothelium, have natural cytoprotection against infection [305]. Importantly, although ANGPTL4 is known to be high, and even considered a biomarker, in ARDS patient serum [337], we have data to support that it is in fact reduced in lung cells in response to SARS-CoV-2 infection (chapter 4, supplementary figure 6A). This was also paired with a significant reduction of tight junction expression in the same study (chapter 4, supplementary figure 6B, C).

To investigate this effect in vivo, we again made use of our pre-established LPS-induced ALI mouse model [122]. We concentrated ANGPTL4-rich MSC-CM, and administered it to the mice intranasally in the presence of absence of an anti-ANGPTL4 neutralising antibody. This study highlighted enhanced pro-reparative capacity *in vivo*, but to a very modest level (chapter 4, figure 6A, B). We knew, from our previous analysis, that ARDS-licensed hBM-MSCs had enriched levels of ANGPTL4, 10-fold higher than that of synthetic agonism alone; due to the high levels of PPARβ/**δ** ligands (chapter 4, figure 5K). With this in mind, we concentrated ARDS-licensed PPARβ/**δ**(+) MSC-CM, and administered this instead. We saw enhanced cytoprotective capacity in mice that received ARDS-licensed hBM-MSC-CM$_{PPAR\beta/\boldsymbol{\delta}(+)}$ compared to other groups; specifically, through the significant reduction seen in pro-inflammatory cytokines (chapter 4, supplementary figure 4C-E).

We further analysed the lung profile from the mice who had received ARDS-licensed hBM-MSC-CM$_{PPAR\beta/\boldsymbol{\delta}(+)}$ by characterising the BALF cell populations by flow cytometry (chapter 4, figure 7). There was a modest trend toward increased M2, anti-inflammatory, macrophage in response to ANGPTL4^{HIGH} MSC-CM; but a larger sample size is needed to confirm these results (chapter 4, figure 7C). This was not seen when ANGPTL4 was neutralised. This was in line with a study from Huang *et al* (2025) who highlighted that ANGPTL4 can promote M2 macrophage polarisation in a model of acute liver transplantation [333]. Interestingly, we saw an altered neutrophil response; whereby ANGPTL4^{HIGH} MSC-CM could modestly reduce the percentage of CD45+/Ly6G+ cells in our ALI model (chapter 4, figure 7D). This was interesting, as a 2022 study by Wee *et al* highlighted that ANGPTL4 is responsible for the clearance of neutrophils through the promotion of macrophage to aid in the clearance. This study was carried out in ANGPTL4 knock-out mice [338]. It's important to note that there were no differences in neutrophil number response to MSCs in earlier work from this study. The initial approach involved differential cell counts based on stained Cytospin images. The approach taken in this study was flow cytometry-based, and is a much more sensitive approach.

MSCs are largely defined by their functional attributes as of recent years [110]. We have elucidated that, in response pro-inflammatory stimuli hBM-MSCs can have an enhanced immunomodulatory profile, while also aiding in repair in a VEGF-dependent manner. We also deduced that FFAs in the environment can lead to an enrichment of ANGPTL4 via the induction of the PPARβ/**δ** receptor; allowing for both anti-inflammatory and pro-reparative effects in the lung epithelium. Importantly, to induce ANGPTL4 secretion, the PPARβ/**δ** receptor was activated. This is a receptor-mediated effect, and thus, we cannot draw conclusions simply based on the effect of ANGPTL4. These findings have provided novel insight into the relationship between MSCs and the environment in which they have been

placed in. Here we show the importance of elucidating the impact of the disease microenvironment, prior to the administration of a cell-based therapy. Although we cover several key aspects of the patient microenvironment and have identified key mechanisms and pathways that have been altered throughout the process; there are many other factors within the environment, that could affect MSC-therapy, that are yet to be determined.

5.2 Future directions

Over the course of this study, many lessons were learned and many new ideas were established. To continue this research, it would be crucial to put time into optimisation of the neutrophil assays. These assays were carried out late in the study and were not optimised to the highest level; and would benefit from the inclusion of an appropriate positive control such as phorbol myristate acetate (PMA) for NET induction. This is something that the lab intends to continue to focus on over the coming years. It is also imperative that more patient sample studies are completed. Limited volumes of patient sample meant that pooling patient samples was the only option for our study. Ideally, this would be repeated using a larger sample size and including much more stratified patient exclusion criteria (i.e. characterisation of hypo- and hyper-patients based on more than simply IL-6 levels). Importantly, this study was the first of its kind; given that the ARDS patient serum was stratified based on the inflammatory profile of the patients, before exposing the cells to the patient serum. I hope this guides the formation of future studies of MSC-based therapies, based on the differential responses seen between groups. Above all, it's crucial that we, as a collective, continue to elucidate the true mechanisms by which these fascinating cells, MSCs, function in response to various microenvironmental stimuli.

If there was more time, it would have been exciting to investigate healthy-derived human MSCs, in comparison to that of a person with ARDS. This would allow for a side-by-side comparison of the physiological and functional differences between the two; and potentially provide better insight into the true ARDS patient microenvironmental impact. It would also be nice to have a side-by-side comparison of the impact of SARS-CoV-2 ARDS patient serum compared to classical ARDS serum on hBM-MSCs; as I would hypothesise that these would show different responses due to a variety of factors. I would also like to administer

VEGF, without the cells, to see if the same effect was maintained; or whether there is a cumulative effect of other MSC-associated agents; such as ANGPTL4. With this in mind, it also would have been interesting to investigate obese-derived hBM-MSCs; to identify their functional differences in comparison to healthy or ARDS patient-derived hBM-MSCs. Given PPARβ/δ activation in response to FFAs, this may have shown interesting results; both morphologically and functionally.

Chapter 6

Bibliography

1. Ashbaugh, D.G., et al., *Acute respiratory distress in adults.* Lancet, 1967. **2**(7511): p. 319-23.
2. Frenzel, J., et al., *Outcome prediction in pneumonia induced ALI/ARDS by clinical features and peptide patterns of BALF determined by mass spectrometry.* PLoS One, 2011. **6**(10): p. e25544.
3. Li, W., et al., *Classic Signaling Pathways in Alveolar Injury and Repair Involved in Sepsis-Induced ALI/ARDS: New Research Progress and Prospect.* Dis Markers, 2022. **2022**: p. 6362344.
4. Nam, J.J., et al., *Experience With Trauma-Induced ARDS: A Retrospective Study of US Wartime Casualties 2003-2015.* J Spec Oper Med, 2022. **22**(4): p. 111-116.
5. Smith, P., L.A. Jeffers, and M. Koval, *Effects of different routes of endotoxin injury on barrier function in alcoholic lung syndrome.* Alcohol, 2019. **80**: p. 81-89.
6. Fein, A., et al., *The value of edema fluid protein measurement in patients with pulmonary edema.* Am J Med, 1979. **67**(1): p. 32-8.
7. Ware, L.B. and M.A. Matthay, *Alveolar fluid clearance is impaired in the majority of patients with acute lung injury and the acute respiratory distress syndrome.* Am J Respir Crit Care Med, 2001. **163**(6): p. 1376-83.
8. Richardson, S., et al., *Presenting Characteristics, Comorbidities, and Outcomes Among 5700 Patients Hospitalized With COVID-19 in the New York City Area.* JAMA, 2020. **323**(20): p. 2052-2059.
9. Bernard, G.R., et al., *Report of the American-European consensus conference on ARDS: definitions, mechanisms, relevant outcomes and clinical trial coordination. The Consensus Committee.* Intensive Care Med, 1994. **20**(3): p. 225-32.
10. Huppert, L.A., M.A. Matthay, and L.B. Ware, *Pathogenesis of Acute Respiratory Distress Syndrome.* Semin Respir Crit Care Med, 2019. **40**(1): p. 31-39.

11. Butt, Y., A. Kurdowska, and T.C. Allen, *Acute Lung Injury: A Clinical and Molecular Review.* Arch Pathol Lab Med, 2016. **140**(4): p. 345-50.

12. Xia, L., et al., *AdMSC-derived exosomes alleviate acute lung injury via transferring mitochondrial component to improve homeostasis of alveolar macrophages.* Theranostics, 2022. **12**(6): p. 2928-2947.

13. Mowery, N.T., W.T.H. Terzian, and A.C. Nelson, *Acute lung injury.* Curr Probl Surg, 2020. **57**(5): p. 100777.

14. Smith, B.J., et al., *Three Alveolar Phenotypes Govern Lung Function in Murine Ventilator-Induced Lung Injury.* Front Physiol, 2020. **11**: p. 660.

15. Ju, Y.N., et al., *Endothelial Progenitor Cells Attenuate Ventilator-Induced Lung Injury with Large-Volume Ventilation.* Cell Transplant, 2019. **28**(12): p. 1674-1685.

16. Sammani, S., et al., *eNAMPT Neutralization Preserves Lung Fluid Balance and Reduces Acute Renal Injury in Porcine Sepsis/VILI-Induced Inflammatory Lung Injury.* Front Physiol, 2022. **13**: p. 916159.

17. Riviello, E.D., et al., *Hospital Incidence and Outcomes of the Acute Respiratory Distress Syndrome Using the Kigali Modification of the Berlin Definition.* Am J Respir Crit Care Med, 2016. **193**(1): p. 52-9.

18. Matthay, M.A., et al., *A New Global Definition of Acute Respiratory Distress Syndrome.* Am J Respir Crit Care Med, 2024. **209**(1): p. 37-47.

19. Ranieri, V.M., et al., *Acute respiratory distress syndrome: the Berlin Definition.* JAMA, 2012. **307**(23): p. 2526-33.

20. Kadota, T., et al., *Extracellular vesicle-mediated cellular crosstalk in lung repair, remodelling and regeneration.* Eur Respir Rev, 2022. **31**(163).

21. Peng, M., et al., *Correlation between circulating endothelial cell level and acute respiratory distress syndrome in postoperative patients.* World J Clin Cases, 2021. **9**(32): p. 9731-9740.

22. Waters, C.M., E. Roan, and D. Navajas, *Mechanobiology in lung epithelial cells: measurements, perturbations, and responses.* Compr Physiol, 2012. **2**(1): p. 1-29.

23. Wang, Y., et al., *YuPingFengSan ameliorates LPS-induced acute lung injury and gut barrier dysfunction in mice.* J Ethnopharmacol, 2023. **312**: p. 116452.

24. Pelosi, P., et al., *Pulmonary and extrapulmonary acute respiratory distress syndrome are different.* Eur Respir J Suppl, 2003. **42**: p. 48s-56s.

25. Li, H., et al., *Neutrophil Extracellular Traps Augmented Alveolar Macrophage Pyroptosis via AIM2 Inflammasome Activation in LPS-Induced ALI/ARDS.* J Inflamm Res, 2021. **14**: p. 4839-4858.

26. Chen, Y., et al., *A causal effects of neutrophil extracellular traps and its biomarkers on acute respiratory distress syndrome: a two-sample Mendelian randomization study.* Sci Rep, 2025. **15**(1): p. 11995.

27. Brinkmann, V., et al., *Neutrophil extracellular traps kill bacteria.* Science, 2004. **303**(5663): p. 1532-5.

28. Allen, R.C. and J.T. Stephens, *Myeloperoxidase selectively binds and selectively kills microbes.* Infect Immun, 2011. **79**(1): p. 474-85.

29. Meyer, N.J., et al., *Myeloperoxidase-derived 2-chlorofatty acids contribute to human sepsis mortality via acute respiratory distress syndrome.* JCI Insight, 2017. **2**(23).

30. Hou, F., et al., *Diversity of Macrophages in Lung Homeostasis and Diseases.* Front Immunol, 2021. **12**: p. 753940.

31. Wang, N., H. Liang, and K. Zen, *Molecular mechanisms that influence the macrophage m1-m2 polarization balance.* Front Immunol, 2014. **5**: p. 614.

32. Chen, Y., C. Qiu, and W. Cai, *Identification of key immune genes for sepsis-induced ARDS based on bioinformatics analysis.* Bioengineered, 2022. **13**(1): p. 697-708.

33. Lefkowitz, D.L. and S.S. Lefkowitz, *Macrophage-neutrophil interaction: a paradigm for chronic inflammation revisited.* Immunol Cell Biol, 2001. **79**(5): p. 502-6.

34. Sil, P., et al., *Macrophage-derived IL-1β enhances monosodium urate crystal-triggered NET formation.* Inflamm Res, 2017. **66**(3): p. 227-237.

35. Popat, R.J., et al., *Anti-myeloperoxidase antibodies attenuate the monocyte response to LPS and shape macrophage development.* JCI Insight, 2017. **2**(2): p. e87379.

36. World Health Organisation, *COVID-19 epidemiological update*. 2025; 177:[Available from: https://www.who.int/publications/m/item/covid-19-epidemiological-update-edition-177.

37. Azagew, A.W., et al., *Global prevalence of COVID-19-induced acute respiratory distress syndrome: systematic review and meta-analysis.* Syst Rev, 2023. **12**(1): p. 212.

38. Tzotzos, S.J., et al., *Incidence of ARDS and outcomes in hospitalized patients with COVID-19: a global literature survey.* Crit Care, 2020. **24**(1): p. 516.

39. World Health Organisation, *The top 10 causes of death*. 2024; Available from: https://www.who.int/news-room/fact-sheets/detail/the-top-10-causes-of-death.

40. Tolossa, T., et al., *Acute respiratory distress syndrome among patients with severe COVID-19 admitted to treatment center of Wollega University Referral Hospital, Western Ethiopia.* PLoS One, 2022. **17**(6): p. e0267835.

41. Wang, D.H., et al., *Attributable mortality of ARDS among critically ill patients with sepsis: a multicenter, retrospective cohort study.* BMC Pulm Med, 2024. **24**(1): p. 110.

42. Bos, L.D.J. and L.B. Ware, *Acute respiratory distress syndrome: causes, pathophysiology, and phenotypes.* Lancet, 2022. **400**(10358): p. 1145-1156.

43. Shaver, C.M. and J.A. Bastarache, *Clinical and biological heterogeneity in acute respiratory distress syndrome: direct versus indirect lung injury.* Clin Chest Med, 2014. **35**(4): p. 639-53.

44. An, A.Y., et al., *Persistence is key: unresolved immune dysfunction is lethal in both COVID-19 and non-COVID-19 sepsis.* Front Immunol, 2023. **14**: p. 1254873.

45. An, A.Y., et al., *Severe COVID-19 and non-COVID-19 severe sepsis converge transcriptionally after a week in the intensive care unit, indicating common disease mechanisms.* Front Immunol, 2023. **14**: p. 1167917.

46. Bain, W., et al., *COVID-19 versus Non-COVID-19 Acute Respiratory Distress Syndrome: Comparison of Demographics, Physiologic Parameters, Inflammatory Biomarkers, and Clinical Outcomes.* Ann Am Thorac Soc, 2021. **18**(7): p. 1202-1210.

47. Fan, E., et al., *COVID-19-associated acute respiratory distress syndrome: is a different approach to management warranted?* Lancet Respir Med, 2020. **8**(8): p. 816-821.

48. Tang, N., et al., *Abnormal coagulation parameters are associated with poor prognosis in patients with novel coronavirus pneumonia.* J Thromb Haemost, 2020. **18**(4): p. 844-847.

49. Gheware, A., et al., *ACE2 protein expression in lung tissues of severe COVID-19 infection.* Sci Rep, 2022. **12**(1): p. 4058.

50. Katsura, H., et al., *Human Lung Stem Cell-Based Alveolospheres Provide Insights into SARS-CoV-2-Mediated Interferon Responses and Pneumocyte Dysfunction.* Cell Stem Cell, 2020. **27**(6): p. 890-904.e8.

51. Zinserling, V.A., et al., *SARS-CoV-2-Induced Pathology-Relevance to COVID-19 Pathophysiology.* Pathophysiology, 2022. **29**(2): p. 281-297.

52. Xiao, K., et al., *Mesenchymal stem cells reverse EMT process through blocking the activation of NF-κB and Hedgehog pathways in LPS-induced acute lung injury.* Cell Death Dis, 2020. **11**(10): p. 863.

53. Li, J., et al., *Panaxydol attenuates ferroptosis against LPS-induced acute lung injury in mice by Keap1-Nrf2/HO-1 pathway.* J Transl Med, 2021. **19**(1): p. 96.

54. Liu, P., et al., *Mesenchymal Stem Cells-Derived Exosomes Alleviate Acute Lung Injury by Inhibiting Alveolar Macrophage Pyroptosis.* Stem Cells Transl Med, 2024. **13**(4): p. 371-386.

55. Lu, Y., et al., *Fuzhengjiedu formula exerts protective effect against LPS-induced acute lung injury via gut-lung axis.* Phytomedicine, 2024. **123**: p. 155190.

56. Zhu, Y.G., et al., *Human mesenchymal stem cell microvesicles for treatment of Escherichia coli endotoxin-induced acute lung injury in mice.* Stem Cells, 2014. **32**(1): p. 116-25.

57. Miyazaki, H., et al., *The effects of two antiinflammatory pretreatments on bacterial-induced lung injury.* Anesthesiology, 1999. **90**(6): p. 1650-62.

58. Jing, X.H., et al., *Naringin alleviates pneumonia caused by Klebsiella pneumoniae infection by suppressing NLRP3 inflammasome.* Biomed Pharmacother, 2024. **170**: p. 116028.

59. Li, Y., et al., *Aromatic Molecular Compatibility Attenuates Influenza Virus-Induced Acute Lung Injury via the Lung-Gut Axis and Lipid Droplet Modulation.* Pharmaceuticals (Basel), 2025. **18**(4).

60. Gopalakrishnan, A., et al., *Protection against influenza-induced Acute Lung Injury (ALI) by enhanced induction of M2a macrophages: possible role of PPARγ/RXR ligands in IL-4-induced M2a macrophage differentiation.* Front Immunol, 2022. **13**: p. 968336.

61. Leist, S.R., et al., *A Mouse-Adapted SARS-CoV-2 Induces Acute Lung Injury and Mortality in Standard Laboratory Mice.* Cell, 2020. **183**(4): p. 1070-1085.e12.

62. Bi, Z., et al., *Inactivated SARS-CoV-2 induces acute respiratory distress syndrome in human ACE2-transgenic mice.* Signal Transduct Target Ther, 2021. **6**(1): p. 439.

63. Chen, J., et al., *The role of ferroptosis in chronic intermittent hypoxia-induced lung injury.* BMC Pulm Med, 2022. **22**(1): p. 488.

64. Wang, R., et al., *Sodium Hydrosulfide Protects Rats from Hypobaric-Hypoxia-Induced Acute Lung Injury.* Int J Mol Sci, 2024. **25**(19).

65. Colunga Biancatelli, R.M.L., et al., *The Heat Shock Protein 90 Inhibitor, AT13387, Protects the Alveolo-Capillary Barrier and Prevents HCl-Induced Chronic Lung Injury and Pulmonary Fibrosis.* Cells, 2022. **11**(6).

66. Colunga Biancatelli, R.M.L., et al., *HSP70 Is a Critical Regulator of HSP90 Inhibitor's Effectiveness in Preventing HCl-Induced Chronic Lung Injury and Pulmonary Fibrosis.* Int J Mol Sci, 2024. **25**(3).

67. Shah, A.R. and R. Banerjee, *Mitigation of Hydrochloric Acid (HCl)-Induced Lung Injury in Mice by Aerosol Therapy of Surface-Active Nanovesicles Containing Antioxidant and Anti-inflammatory Drugs.* ACS Appl Bio Mater, 2019. **2**(12): p. 5379-5389.

68. Ko, H.K., et al., *The role of transforming growth factor-β2 in cigarette smoke-induced lung inflammation and injury.* Life Sci, 2023. **320**: p. 121539.

69. Wang, M., et al., *Roles of TRPA1 and TRPV1 in cigarette smoke -induced airway epithelial cell injury model.* Free Radic Biol Med, 2019. **134**: p. 229-238.

70. Liang, W., et al., *MEF2C alleviates acute lung injury in cecal ligation and puncture (CLP)-induced sepsis rats by up-regulating AQP1.* Allergol Immunopathol (Madr), 2021. **49**(5): p. 117-124.

71. Ranjbaran, M., et al., *Mesenchymal stem cells and their conditioned medium as potential therapeutic strategies in managing comorbid anxiety in rat sepsis induced by cecal ligation and puncture.* Iran J Basic Med Sci, 2022. **25**(6): p. 690-697.

72. Luo, J., et al., *Nrf2 Deficiency Exacerbated CLP-Induced Pulmonary Injury and Inflammation through Autophagy- and NF-κB/PPARγ-Mediated Macrophage Polarization.* Cells, 2022. **11**(23).

73. Bilodeaux, J., et al., *Differential effects of two-hit models of acute and ventilator-induced lung injury on lung structure, function, and inflammation.* Front Physiol, 2023. **14**: p. 1217183.

74. Sahu, B., R. Sandhir, and A.S. Naura, *Two hit induced acute lung injury impairs cognitive function in mice: A potential model to study cross talk between lung and brain.* Brain Behav Immun, 2018. **73**: p. 633-642.

75. Bastarache, J.A., et al., *A two-hit model of sepsis plus hyperoxia causes lung permeability and inflammation.* Am J Physiol Lung Cell Mol Physiol, 2022. **322**(2): p. L273-L282.

76. Masterson, C., et al., *Syndecan-2-positive, Bone Marrow-derived Human Mesenchymal Stromal Cells Attenuate Bacterial-induced Acute Lung Injury and Enhance Resolution of Ventilator-induced Lung Injury in Rats.* Anesthesiology, 2018. **129**(3): p. 502-516.

77. Ai, L., et al., *Tempol attenuates chronic intermittent hypoxia-induced lung injury through the miR-145-5p/Nrf2 signaling pathway.* Cell Mol Biol (Noisy-le-grand), 2023. **69**(13): p. 225-234.

78. Roxlau, E.T., et al., *Nicotine promotes e-cigarette vapour-induced lung inflammation and structural alterations.* Eur Respir J, 2023. **61**(6).

79. Sasidharan, S., et al., *COVID-19 ARDS: A Multispecialty Assessment of Challenges in Care, Review of Research, and Recommendations.* J Anaesthesiol Clin Pharmacol, 2021. **37**(2): p. 179-195.

80. Ricard, J.D., et al., *Use of nasal high flow oxygen during acute respiratory failure.* Intensive Care Med, 2020. **46**(12): p. 2238-2247.

81. Papazian, L., et al., *Neuromuscular blockers in early acute respiratory distress syndrome.* N Engl J Med, 2010. **363**(12): p. 1107-16.

82. Chang, X., et al., *Safety and efficacy of corticosteroids in ARDS patients: a systematic review and meta-analysis of RCT data.* Respir Res, 2022. **23**(1): p. 301.

83. van de Veerdonk, F.L. and M.G. Netea, *Blocking IL-1 to prevent respiratory failure in COVID-19.* Crit Care, 2020. **24**(1): p. 445.

84. Khan, F.A., et al., *Systematic review and meta-analysis of anakinra, sarilumab, siltuximab and tocilizumab for COVID-19.* Thorax, 2021. **76**(9): p. 907-919.

85. Shakoory, B., et al., *Interleukin-1 Receptor Blockade Is Associated With Reduced Mortality in Sepsis Patients With Features of Macrophage Activation Syndrome: Reanalysis of a Prior Phase III Trial.* Crit Care Med, 2016. **44**(2): p. 275-81.

86. Vakaet, V., et al., *Minimizing preparation time for repeated prolonged deep-inspiration breath holds during breast cancer irradiation using pre-oxygenation with high-flow nasal oxygen and voluntary hyperventilation.* Br J Radiol, 2025. **98**(1165): p. 45-49.

87. Price, D.R., et al., *Neuromuscular Blocking Agents and Neuromuscular Dysfunction Acquired in Critical Illness: A Systematic Review and Meta-Analysis.* Crit Care Med, 2016. **44**(11): p. 2070-2078.

88. Yang, M., et al., *Inhaled corticosteroids and risk of upper respiratory tract infection in patients with asthma: a meta-analysis.* Infection, 2019. **47**(3): p. 377-385.

89. Weinberg, E., et al., *The Impact of Corticosteroid Administration at Different Time Points on Mucosal Wound Healing in Rats: An Experimental Pilot In Vivo Study.* Biology (Basel), 2022. **11**(9).

90. Kharazmi, A.B., et al., *A randomized controlled clinical trial on efficacy and safety of anakinra in patients with severe COVID-19.* Immun Inflamm Dis, 2022. **10**(2): p. 201-208.

91. Ramírez, J. and J.D. Cañete, *Anakinra for the treatment of rheumatoid arthritis: a safety evaluation.* Expert Opin Drug Saf, 2018. **17**(7): p. 727-732.

92. Gandini, L., et al., *Interleukin-6 inhibitors in non-COVID-19 ARDS: analyzing the past to step into the post-COVID-19 era.* Crit Care, 2023. **27**(1): p. 124.

93. Calfee, C.S., et al., *Subphenotypes in acute respiratory distress syndrome: latent class analysis of data from two randomised controlled trials.* Lancet Respir Med, 2014. **2**(8): p. 611-20.

94. Wilson, J.G., et al., *Mesenchymal stem (stromal) cells for treatment of ARDS: a phase 1 clinical trial.* Lancet Respir Med, 2015. **3**(1): p. 24-32.

95. Lanzoni, G., et al., *Umbilical cord mesenchymal stem cells for COVID-19 acute respiratory distress syndrome: A double-blind, phase 1/2a, randomized controlled trial.* Stem Cells Transl Med, 2021. **10**(5): p. 660-673.

96. Martínez-Muñoz, M.E., et al., *Mesenchymal stromal cell therapy for COVID-19 acute respiratory distress syndrome: a double-blind randomised controlled trial.* Bone Marrow Transplant, 2024. **59**(6): p. 777-784.

97. Gorman, E., et al., *Repair of acute respiratory distress syndrome by stromal cell administration (REALIST) trial: A phase 1 trial.* EClinicalMedicine, 2021. **41**: p. 101167.

98. Matthay, M.A., et al., *Treatment with allogeneic mesenchymal stromal cells for moderate to severe acute respiratory distress syndrome (START study): a randomised phase 2a safety trial.* Lancet Respir Med, 2019. **7**(2): p. 154-162.

99. Ding, D.C., W.C. Shyu, and S.Z. Lin, *Mesenchymal stem cells.* Cell Transplant, 2011. **20**(1): p. 5-14.

100. Shimizu, Y., et al., *Characterization of patient-derived bone marrow human mesenchymal stem cells as oncolytic virus carriers for the treatment of glioblastoma.* J Neurosurg, 2022. **136**(3): p. 757-767.

101. Krawczenko, A. and A. Klimczak, *Adipose Tissue-Derived Mesenchymal Stem/Stromal Cells and Their Contribution to Angiogenic Processes in Tissue Regeneration.* Int J Mol Sci, 2022. **23**(5).

102. Nakao, M. and K. Nagase, *Harvesting methods of umbilical cord-derived mesenchymal stem cells from culture modulate cell properties and functions.* Regen Ther, 2024. **26**: p. 80-88.

103. Sanchez-Mata, A. and E. Gonzalez-Muñoz, *Understanding menstrual blood-derived stromal/stem cells: Definition and properties. Are we rushing into their therapeutic applications?* iScience, 2021. **24**(12): p. 103501.

104. Ledesma-Martínez, E., V.M. Mendoza-Núñez, and E. Santiago-Osorio, *Mesenchymal Stem Cells Derived from Dental Pulp: A Review.* Stem Cells Int, 2016. **2016**: p. 4709572.

105. Li, P., et al., *Immunomodulatory properties of mesenchymal stem cells/dental stem cells and their therapeutic applications.* Cell Mol Immunol, 2023. **20**(6): p. 558-569.

106. Jo, H., et al., *Applications of Mesenchymal Stem Cells in Skin Regeneration and Rejuvenation.* Int J Mol Sci, 2021. **22**(5).

107. Lazarus, H.M., et al., *Ex vivo expansion and subsequent infusion of human bone marrow-derived stromal progenitor cells (mesenchymal progenitor cells): implications for therapeutic use.* Bone Marrow Transplant, 1995. **16**(4): p. 557-64.

108. Long, E.G., et al., *Human mesenchymal stem cell morphology, migration, and differentiation on micro and nano-textured titanium.* Bioact Mater, 2019. **4**: p. 249-255.

109. Dominici, M., et al., *Minimal criteria for defining multipotent mesenchymal stromal cells. The International Society for Cellular Therapy position statement.* Cytotherapy, 2006. **8**(4): p. 315-7.

110. Renesme, L., et al., *Delphi-driven consensus definition for mesenchymal stromal cells and clinical reporting guidelines for mesenchymal stromal cell-based therapeutics.* Cytotherapy, 2025. **27**(2): p. 146-168.

111. Colombo, F., et al., *Stem Cell Injection for Complex Refractory Perianal Fistulas in Crohn's Disease: A Single Center Initial Experience.* Front Surg, 2022. **9**: p. 834870.

112. Kurtzberg, J., et al., *A Phase 3, Single-Arm, Prospective Study of Remestemcel-L, Ex Vivo Culture-Expanded Adult Human Mesenchymal Stromal Cells for the Treatment of Pediatric Patients Who Failed to Respond to Steroid Treatment for Acute Graft-versus-Host Disease.* Biol Blood Marrow Transplant, 2020. **26**(5): p. 845-854.

113. Matas, J., et al., *Umbilical Cord-Derived Mesenchymal Stromal Cells (MSCs) for Knee Osteoarthritis: Repeated MSC Dosing Is Superior to a Single MSC Dose and to Hyaluronic Acid in a Controlled Randomized Phase I/II Trial.* Stem Cells Transl Med, 2019. **8**(3): p. 215-224.

114. Reis, A.L.G., et al., *Proteomic analysis of cerebrospinal fluid of amyotrophic lateral sclerosis patients in the presence of autologous bone marrow derived mesenchymal stem cells.* Stem Cell Res Ther, 2024. **15**(1): p. 301.

115. Chandran, N.S., et al., *A phase 1, open-label study to determine safety and tolerability of the topical application of mesenchymal stem/stromal cell (MSC) exosome ointment to treat psoriasis in healthy volunteers.* Cytotherapy, 2025. **27**(5): p. 633-641.

116. Li, Z., Z. Han, and Z.C. Han, *Mesenchymal Stem Cells in Clinical Trials for Immune Disorders.* Glob Med Genet, 2024. **11**(3): p. 196-199.

117. Fernández-Garza, L.E., S.A. Barrera-Barrera, and H.A. Barrera-Saldaña, *Mesenchymal Stem Cell Therapies Approved by Regulatory Agencies around the World.* Pharmaceuticals (Basel), 2023. **16**(9).

118. Blanc, K.L., et al., *ISCT MSC committee statement on the US FDA approval of allogenic bone-marrow mesenchymal stromal cells.* Cytotherapy, 2025. **27**(4): p. 413-416.

119. Aggarwal, S. and M.F. Pittenger, *Human mesenchymal stem cells modulate allogeneic immune cell responses.* Blood, 2005. **105**(4): p. 1815-22.

120. Chen, P., et al., *Single-Cell and Spatial Transcriptomics Decodes Wharton's Jelly-Derived Mesenchymal Stem Cells Heterogeneity and a Subpopulation with Wound Repair Signatures.* Adv Sci (Weinh), 2023. **10**(4): p. e2204786.

121. Zhu, J., et al., *MSCs alleviate LPS-induced acute lung injury by inhibiting the proinflammatory function of macrophages in mouse lung organoid-macrophage model.* Cell Mol Life Sci, 2024. **81**(1): p. 124.

122. Tunstead, C., et al., *The ARDS microenvironment enhances MSC-induced repair via VEGF in experimental acute lung inflammation.* Mol Ther, 2024. **32**(10): p. 3422-3432.

123. Jerkic, M., et al., *Key Role of Mesenchymal Stromal Cell Interaction with Macrophages in Promoting Repair of Lung Injury.* Int J Mol Sci, 2023. **24**(4).

124. Faircloth, T.U., et al., *Vascular endothelial growth factor secretion and immunosuppression are distinct potency mechanisms of human bone marrow mesenchymal stromal cells.* Stem Cells, 2024. **42**(8): p. 736-751.

125. Bagno, L.L., et al., *Mechanism of Action of Mesenchymal Stem Cells (MSCs): impact of delivery method.* Expert Opin Biol Ther, 2022. **22**(4): p. 449-463.

126. Dai, W., et al., *Human umbilical cord-derived mesenchymal stem cells (hUC-MSCs) alleviate excessive autophagy of ovarian granular cells through VEGFA/PI3K/AKT/mTOR pathway in premature ovarian failure rat model.* J Ovarian Res, 2023. **16**(1): p. 198.

127. Zhuang, K., et al., *MSCs-derived HGF alleviates senescence by inhibiting unopposed mitochondrial fusion-based elongation in post-acute kidney injury.* Stem Cell Res Ther, 2024. **15**(1): p. 438.

128. Xu, H., et al., *Tumor-derived mesenchymal-stem-cell-secreted IL-6 enhances resistance to cisplatin via the STAT3 pathway in breast cancer.* Oncol Lett, 2018. **15**(6): p. 9142-9150.

129. Montero-Vilchez, T., et al., *Mesenchymal Stromal Cell-Conditioned Medium for Skin Diseases: A Systematic Review.* Front Cell Dev Biol, 2021. **9**: p. 654210.

130. Behzadifard, M., et al., *Neuroprotective Effects of Conditioned Medium of Mesenchymal Stem Cells (MSC-CM) as a Therapy for Ischemic Stroke Recovery: A Systematic Review.* Neurochem Res, 2023. **48**(5): p. 1280-1292.

131. Lin, H., et al., *Advances in mesenchymal stem cell conditioned medium-mediated periodontal tissue regeneration.* J Transl Med, 2021. **19**(1): p. 456.

132. Zheng, L., et al., *Strategies to improve the therapeutic efficacy of mesenchymal stem cell-derived extracellular vesicle (MSC-EV): a promising cell-free therapy for liver disease.* Front Bioeng Biotechnol, 2023. **11**: p. 1322514.

133. Harrell, C.R., et al., *Mesenchymal Stem Cell-Derived Exosomes and Other Extracellular Vesicles as New Remedies in the Therapy of Inflammatory Diseases.* Cells, 2019. **8**(12).

134. Mathew, B., et al., *Mesenchymal stem cell-derived extracellular vesicles and retinal ischemia-reperfusion.* Biomaterials, 2019. **197**: p. 146-160.

135. Li, Y., et al., *Cell-cell contact with proinflammatory macrophages enhances the immunotherapeutic effect of mesenchymal stem cells in two abortion models.* Cell Mol Immunol, 2019. **16**(12): p. 908-920.

136. Duffy, M.M., et al., *Mesenchymal stem cell inhibition of T-helper 17 cell-differentiation is triggered by cell-cell contact and mediated by prostaglandin E2 via the EP4 receptor.* Eur J Immunol, 2011. **41**(10): p. 2840-51.

137. Pajarinen, J., et al., *Mesenchymal stem cell-macrophage crosstalk and bone healing.* Biomaterials, 2019. **196**: p. 80-89.

138. Court, A.C., et al., *Mitochondrial transfer from MSCs to T cells induces Treg differentiation and restricts inflammatory response.* EMBO Rep, 2020. **21**(2): p. e48052.

139. Irwin, R.M., et al., *Connexin 43 Regulates Intercellular Mitochondrial Transfer from Human Mesenchymal Stromal Cells to Chondrocytes.* bioRxiv, 2024.

140. Wang, R., et al., *MSC-mediated mitochondrial transfer restores mitochondrial DNA and function in neural progenitor cells of Leber's hereditary optic neuropathy.* Sci China Life Sci, 2024. **67**(11): p. 2511-2519.

141. Wang, J., et al., *MSC-mediated mitochondrial transfer promotes metabolic reprograming in endothelial cells and vascular regeneration in ARDS.* Redox Rep, 2025. **30**(1): p. 2474897.

142. Zheng, H., et al., *Exosomal miR-9-5p derived from iPSC-MSCs ameliorates doxorubicin-induced cardiomyopathy by inhibiting cardiomyocyte senescence.* J Nanobiotechnology, 2024. **22**(1): p. 195.

143. Xiao, X., et al., *Mesenchymal stem cell-derived small extracellular vesicles mitigate oxidative stress-induced senescence in endothelial cells via regulation of miR-146a/Src.* Signal Transduct Target Ther, 2021. **6**(1): p. 354.

144. Galleu, A., et al., *Apoptosis in mesenchymal stromal cells induces in vivo recipient-mediated immunomodulation.* Sci Transl Med, 2017. **9**(416).

145. Pang, S.H.M., et al., *Mesenchymal stromal cell apoptosis is required for their therapeutic function.* Nat Commun, 2021. **12**(1): p. 6495.

146. Bessa-Gonçalves, M., et al., *Fibrinogen and magnesium combination biomaterials modulate macrophage phenotype, NF-kB signaling and crosstalk with mesenchymal stem/stromal cells.* Acta Biomater, 2020. **114**: p. 471-484.

147. Sridharan, R., D.J. Kelly, and F.J. O'Brien, *Substrate Stiffness Modulates the Crosstalk Between Mesenchymal Stem Cells and Macrophages.* J Biomech Eng, 2021. **143**(3).

148. Carty, F., et al., *IFN-γ and PPARδ influence the efficacy and retention of multipotent adult progenitor cells in graft vs host disease.* Stem Cells Transl Med, 2021. **10**(11): p. 1561-1574.

149. Medina, J.P., et al., *MSC therapy ameliorates experimental gouty arthritis hinting an early COX-2 induction.* Front Immunol, 2023. **14**: p. 1193179.

150. Corbett, J.M., et al., *Cyclosporine A and IFNγ licencing enhances human mesenchymal stromal cell potency in a humanised mouse model of acute graft versus host disease.* Stem Cell Res Ther, 2021. **12**(1): p. 238.

151. Chinnadurai, R., et al., *IDO-independent suppression of T cell effector function by IFN-γ-licensed human mesenchymal stromal cells.* J Immunol, 2014. **192**(4): p. 1491-501.

152. Li, W., et al., *Mesenchymal stem cells: a double-edged sword in regulating immune responses.* Cell Death Differ, 2012. **19**(9): p. 1505-13.

153. Zacharek, A., et al., *Angiopoietin1/Tie2 and VEGF/Flk1 induced by MSC treatment amplifies angiogenesis and vascular stabilization after stroke.* J Cereb Blood Flow Metab, 2007. **27**(10): p. 1684-91.

154. Yu, M., et al., *Exosomes derived from atorvastatin-pretreated MSC accelerate diabetic wound repair by enhancing angiogenesis via AKT/eNOS pathway.* Stem Cell Res Ther, 2020. **11**(1): p. 350.

155. Zisa, D., et al., *Vascular endothelial growth factor (VEGF) as a key therapeutic trophic factor in bone marrow mesenchymal stem cell-mediated cardiac repair.* Biochem Biophys Res Commun, 2009. **390**(3): p. 834-8.

156. Dunbar, H., et al., *The VEGF-Mediated Cytoprotective Ability of MIF-Licensed Mesenchymal Stromal Cells in House Dust Mite-Induced Epithelial Damage.* Eur J Immunol, 2025. **55**(1): p. e202451205.

157. Cahill, E.F., et al., *Hepatocyte Growth Factor Is Required for Mesenchymal Stromal Cell Protection Against Bleomycin-Induced Pulmonary Fibrosis.* Stem Cells Transl Med, 2016. **5**(10): p. 1307-1318.

158. Kennelly, H., B.P. Mahon, and K. English, *Human mesenchymal stromal cells exert HGF dependent cytoprotective effects in a human relevant pre-clinical model of COPD.* Sci Rep, 2016. **6**: p. 38207.

159. Yang, Y., et al., *Synergism of MSC-secreted HGF and VEGF in stabilising endothelial barrier function upon lipopolysaccharide stimulation via the Rac1 pathway.* Stem Cell Res Ther, 2015. **6**: p. 250.

160. Hong, S.Y., et al., *Allogeneic human umbilical cord-derived mesenchymal stem cells reduce lipopolysaccharide-induced inflammation and acute lung injury.* Am J Transl Res, 2020. **12**(10): p. 6740-6750.

161. Feng, B., et al., *Mesenchymal stem cells shift the pro-inflammatory phenotype of neutrophils to ameliorate acute lung injury.* Stem Cell Res Ther, 2023. **14**(1): p. 197.

162. Wang, J., et al., *Safety, efficacy and biomarkers analysis of mesenchymal stromal cells therapy in ARDS: a systematic review and meta-analysis based on phase I and II RCTs.* Stem Cell Res Ther, 2022. **13**(1): p. 275.

163. Kaffash Farkhad, N., et al., *Mesenchymal stromal cell therapy for COVID-19-induced ARDS patients: a successful phase 1, control-placebo group, clinical trial.* Stem Cell Res Ther, 2022. **13**(1): p. 283.

164. Bowdish, M.E., et al., *A Randomized Trial of Mesenchymal Stromal Cells for Moderate to Severe Acute Respiratory Distress Syndrome from COVID-19.* Am J Respir Crit Care Med, 2023. **207**(3): p. 261-270.

165. Zheng, G., et al., *Treatment of acute respiratory distress syndrome with allogeneic adipose-derived mesenchymal stem cells: a randomized, placebo-controlled pilot study.* Respir Res, 2014. **15**(1): p. 39.

166. Curley, G.F., et al., *Cell-based Therapies for Acute Respiratory Distress Syndrome: Where Are We Now?* Am J Respir Crit Care Med, 2024. **209**(7): p. 789-797.

167. Bellingan, G., et al., *Safety and efficacy of multipotent adult progenitor cells in acute respiratory distress syndrome (MUST-ARDS): a multicentre, randomised, double-blind, placebo-controlled phase 1/2 trial.* Intensive Care Med, 2022. **48**(1): p. 36-44.

168. Ichikado, K., et al., *Clinical efficacy and safety of multipotent adult progenitor cells (invimestrocel) for acute respiratory distress syndrome (ARDS) caused by pneumonia:*

a randomized, open-label, standard therapy-controlled, phase 2 multicenter study (ONE-BRIDGE). Stem Cell Res Ther, 2023. **14**(1): p. 217.

169. Gorman, E., et al., *Repair of Acute Respiratory Distress Syndrome by Stromal Cell Administration in COVID-19 (REALIST-COVID-19): A structured summary of a study protocol for a randomised, controlled trial.* Trials, 2020. **21**(1): p. 462.

170. Gorman, E., et al., *Repair of acute respiratory distress syndrome by stromal cell administration (REALIST): a structured study protocol for an open-label dose-escalation phase 1 trial followed by a randomised, triple-blind, allocation concealed, placebo-controlled phase 2 trial.* Trials, 2022. **23**(1): p. 401.

171. Shu, L., et al., *Treatment of severe COVID-19 with human umbilical cord mesenchymal stem cells.* Stem Cell Res Ther, 2020. **11**(1): p. 361.

172. Adas, G., et al., *The Systematic Effect of Mesenchymal Stem Cell Therapy in Critical COVID-19 Patients: A Prospective Double Controlled Trial.* Cell Transplant, 2021. **30**: p. 9636897211024942.

173. Dilogo, I.H., et al., *Umbilical cord mesenchymal stromal cells as critical COVID-19 adjuvant therapy: A randomized controlled trial.* Stem Cells Transl Med, 2021. **10**(9): p. 1279-1287.

174. Shi, L., et al., *Effect of human umbilical cord-derived mesenchymal stem cells on lung damage in severe COVID-19 patients: a randomized, double-blind, placebo-controlled phase 2 trial.* Signal Transduct Target Ther, 2021. **6**(1): p. 58.

175. Monsel, A., et al., *Treatment of COVID-19-associated ARDS with mesenchymal stromal cells: a multicenter randomized double-blind trial.* Crit Care, 2022. **26**(1): p. 48.

176. Rebelatto, C.L.K., et al., *Safety and long-term improvement of mesenchymal stromal cell infusion in critically COVID-19 patients: a randomized clinical trial.* Stem Cell Res Ther, 2022. **13**(1): p. 122.

177. Gorman, E.A., et al., *Repair of Acute Respiratory Distress Syndrome in COVID-19 by Stromal Cells (REALIST-COVID Trial): A Multicenter, Randomized, Controlled Clinical Trial.* Am J Respir Crit Care Med, 2023. **208**(3): p. 256-269.

178. Lightner, A.L., et al., *Bone Marrow Mesenchymal Stem Cell-Derived Extracellular Vesicle Infusion for the Treatment of Respiratory Failure From COVID-19: A Randomized, Placebo-Controlled Dosing Clinical Trial.* Chest, 2023. **164**(6): p. 1444-1453.

179. Koch, D.W. and L.V. Schnabel, *Mesenchymal stem cell licensing: enhancing MSC function as a translational approach for the treatment of tendon injury.* Am J Vet Res, 2023. **84**(10): p. 1-8.

180. Kavanagh, D.P., et al., *Pretreatment of Mesenchymal Stem Cells Manipulates Their Vasculoprotective Potential While Not Altering Their Homing Within the Injured Gut.* Stem Cells, 2015. **33**(9): p. 2785-97.

181. Lu, D., et al., *Mesenchymal Stem Cell-Macrophage Crosstalk and Maintenance of Inflammatory Microenvironment Homeostasis.* Front Cell Dev Biol, 2021. **9**: p. 681171.

182. Liang, Y., et al., *Protection of neutrophils by bone marrow mesenchymal stromal cells is enhanced by tumor-associated inflammatory cytokines.* Front Immunol, 2024. **15**: p. 1361596.

183. Horie, S., et al., *Cytokine pre-activation of cryopreserved xenogeneic-free human mesenchymal stromal cells enhances resolution and repair following ventilator-*

induced lung injury potentially via a KGF-dependent mechanism. Intensive Care Med Exp, 2020. **8**(1): p. 8.

184. Sutton, M.T., et al., *Antimicrobial Properties of Mesenchymal Stem Cells: Therapeutic Potential for Cystic Fibrosis Infection, and Treatment.* Stem Cells Int, 2016. **2016**: p. 5303048.

185. Wang, S., et al., *Pre-Conditioning with IFN-γ and Hypoxia Enhances the Angiogenic Potential of iPSC-Derived MSC Secretome.* Cells, 2022. **11**(6).

186. Calligaris, M., et al., *Proteomic analysis and functional validation reveal distinct therapeutic capabilities related to priming of mesenchymal stromal/stem cells with IFN-γ and hypoxia: potential implications for their clinical use.* Front Cell Dev Biol, 2024. **12**: p. 1385712.

187. Yao, M., et al., *Cross talk between glucose metabolism and immunosuppression in IFN-γ-primed mesenchymal stem cells.* Life Sci Alliance, 2022. **5**(12).

188. Nakao, Y., et al., *Exosomes from TNF-α-treated human gingiva-derived MSCs enhance M2 macrophage polarization and inhibit periodontal bone loss.* Acta Biomater, 2021. **122**: p. 306-324.

189. Hackel, A., et al., *TNF-α and IL-1β sensitize human MSC for IFN-γ signaling and enhance neutrophil recruitment.* Eur J Immunol, 2021. **51**(2): p. 319-330.

190. Hawthorne, I.J., et al., *Human macrophage migration inhibitory factor potentiates mesenchymal stromal cell efficacy in a clinically relevant model of allergic asthma.* Mol Ther, 2023. **31**(11): p. 3243-3258.

191. Jonassen, T.B., et al., *Alveolar cytokines and interferon autoantibodies in COVID-19 ARDS.* Front Immunol, 2024. **15**: p. 1353012.

192. Islam, D., et al., *Identification and Modulation of Microenvironment Is Crucial for Effective Mesenchymal Stromal Cell Therapy in Acute Lung Injury.* Am J Respir Crit Care Med, 2019. **199**(10): p. 1214-1224.

193. Ren, G., et al., *Mesenchymal stem cell-mediated immunosuppression occurs via concerted action of chemokines and nitric oxide.* Cell Stem Cell, 2008. **2**(2): p. 141-50.

194. Kolliopoulos, V., et al., *Inflammatory Licensed hMSCs Exhibit Enhanced Immunomodulatory Capacity in a Biomaterial Mediated Manner.* ACS Biomater Sci Eng, 2023. **9**(8): p. 4916-4928.

195. Bulati, M., et al., *The Immunomodulatory Properties of the Human Amnion-Derived Mesenchymal Stromal/Stem Cells Are Induced by INF-γ Produced by Activated Lymphomonocytes and Are Mediated by Cell-To-Cell Contact and Soluble Factors.* Front Immunol, 2020. **11**: p. 54.

196. Valda Toro, P.L., et al., *Rapidly improving ARDS differs clinically and biologically from persistent ARDS.* Crit Care, 2024. **28**(1): p. 132.

197. Hellberg, L., et al., *Proinflammatory stimuli enhance phagocytosis of apoptotic cells by neutrophil granulocytes.* ScientificWorldJournal, 2011. **11**: p. 2230-6.

198. Winterbourn, C.C., A.J. Kettle, and M.B. Hampton, *Reactive Oxygen Species and Neutrophil Function.* Annu Rev Biochem, 2016. **85**: p. 765-92.

199. Parker, H. and C.C. Winterbourn, *Reactive oxidants and myeloperoxidase and their involvement in neutrophil extracellular traps.* Front Immunol, 2012. **3**: p. 424.

200. Raffaghello, L., et al., *Human mesenchymal stem cells inhibit neutrophil apoptosis: a model for neutrophil preservation in the bone marrow niche.* Stem Cells, 2008. **26**(1): p. 151-62.

201. Hwang, N., et al., *Carbon monoxide-induced autophagy enhances human mesenchymal stromal cell function via paracrine actions in murine polymicrobial sepsis.* Mol Ther, 2024. **32**(7): p. 2232-2247.

202. Zhou, T., et al., *Challenges and advances in clinical applications of mesenchymal stromal cells.* J Hematol Oncol, 2021. **14**(1): p. 24.

203. Li, J., et al., *The heterogeneity of mesenchymal stem cells: an important issue to be addressed in cell therapy.* Stem Cell Res Ther, 2023. **14**(1): p. 381.

204. Sareen, N., et al., *Early passaging of mesenchymal stem cells does not instigate significant modifications in their immunological behavior.* Stem Cell Res Ther, 2018. **9**(1): p. 121.

205. Montemurro, T., et al., *Off-the-Shelf Cord-Blood Mesenchymal Stromal Cells: Production, Quality Control, and Clinical Use.* Cells, 2024. **13**(12).

206. Abreu, S.C., et al., *Differential effects of the cystic fibrosis lung inflammatory environment on mesenchymal stromal cells.* Am J Physiol Lung Cell Mol Physiol, 2020. **319**(6): p. L908-l925.

207. Lim, J. and E.K. Park, *Effect of fibroblast growth factor-2 and retinoic acid on lineage commitment of bone marrow mesenchymal stem cells.* Tissue Eng Regen Med, 2016. **13**(1): p. 47-56.

208. Park, J.R., et al., *Effects of Peroxisome Proliferator-Activated Receptor-δ Agonist on Cardiac Healing after Myocardial Infarction.* PLoS One, 2016. **11**(2): p. e0148510.

209. Kim, D.H., et al., *PPAR-δ agonist affects adipo-chondrogenic differentiation of human mesenchymal stem cells through the expression of PPAR-γ.* Regen Ther, 2020. **15**: p. 103-111.

210. Nernpermpisooth, N., et al., *PPARβ/δ Is Required for Mesenchymal Stem Cell Cardioprotective Effects Independently of Their Anti-inflammatory Properties in Myocardial Ischemia-Reperfusion Injury.* Front Cardiovasc Med, 2021. **8**: p. 681002.

211. Christofides, A., et al., *The role of peroxisome proliferator-activated receptors (PPAR) in immune responses.* Metabolism, 2021. **114**: p. 154338.

212. Korbecki, J., R. Bobiński, and M. Dutka, *Self-regulation of the inflammatory response by peroxisome proliferator-activated receptors.* Inflamm Res, 2019. **68**(6): p. 443-458.

213. Mirza, A.Z., I.I. Althagafi, and H. Shamshad, *Role of PPAR receptor in different diseases and their ligands: Physiological importance and clinical implications.* Eur J Med Chem, 2019. **166**: p. 502-513.

214. Amber-Vitos, O., et al., *The effect of regulating molecules on the structure of the PPAR-RXR complex.* Biochim Biophys Acta, 2016. **1861**(11): p. 1852-1863.

215. Capelli, D., et al., *Structural basis for PPAR partial or full activation revealed by a novel ligand binding mode.* Sci Rep, 2016. **6**: p. 34792.

216. Boitier, E., J.C. Gautier, and R. Roberts, *Advances in understanding the regulation of apoptosis and mitosis by peroxisome-proliferator activated receptors in pre-clinical models: relevance for human health and disease.* Comp Hepatol, 2003. **2**(1): p. 3.

217. Ziouzenkova, O. and J. Plutzky, *Retinoid metabolism and nuclear receptor responses: New insights into coordinated regulation of the PPAR-RXR complex.* FEBS Lett, 2008. **582**(1): p. 32-8.

218. Wójtowicz, S., et al., *The Novel Role of PPAR Alpha in the Brain: Promising Target in Therapy of Alzheimer's Disease and Other Neurodegenerative Disorders.* Neurochem Res, 2020. **45**(5): p. 972-988.

219. Brunmeir, R. and F. Xu, *Functional Regulation of PPARs through Post-Translational Modifications.* Int J Mol Sci, 2018. **19**(6).

220. Chinetti, G., J.C. Fruchart, and B. Staels, *Peroxisome proliferator-activated receptors (PPARs): nuclear receptors at the crossroads between lipid metabolism and inflammation.* Inflamm Res, 2000. **49**(10): p. 497-505.

221. Zingarelli, B., et al., *Peroxisome proliferator-activated receptor {delta} regulates inflammation via NF-{kappa}B signaling in polymicrobial sepsis.* Am J Pathol, 2010. **177**(4): p. 1834-47.

222. Huang, P., et al., *HSD11B1 is upregulated synergistically by IFNγ and TNFα and mediates TSG-6 expression in human UC-MSCs.* Cell Death Discov, 2020. **6**: p. 24.

223. Escobar, P., et al., *IL-1β produced by aggressive breast cancer cells is one of the factors that dictate their interactions with mesenchymal stem cells through chemokine production.* Oncotarget, 2015. **6**(30): p. 29034-47.

224. Sladek, F.M., *What are nuclear receptor ligands?* Mol Cell Endocrinol, 2011. **334**(1-2): p. 3-13.

225. Grygiel-Górniak, B., *Peroxisome proliferator-activated receptors and their ligands: nutritional and clinical implications--a review.* Nutr J, 2014. **13**: p. 17.

226. Da'adoosh, B., et al., *Discovering highly selective and diverse PPAR-delta agonists by ligand based machine learning and structural modeling.* Sci Rep, 2019. **9**(1): p. 1106.

227. Shearer, B.G., et al., *Identification and characterization of a selective peroxisome proliferator-activated receptor beta/delta (NR1C2) antagonist.* Mol Endocrinol, 2008. **22**(2): p. 523-9.

228. Krogsdam, A.M., et al., *Nuclear receptor corepressor-dependent repression of peroxisome-proliferator-activated receptor delta-mediated transactivation.* Biochem J, 2002. **363**(Pt 1): p. 157-65.

229. Sheppard, H.M., et al., *Analysis of the steroid receptor coactivator 1 (SRC1)-CREB binding protein interaction interface and its importance for the function of SRC1.* Mol Cell Biol, 2001. **21**(1): p. 39-50.

230. Legrand, N., et al., *PPARβ/δ recruits NCOR and regulates transcription reinitiation of ANGPTL4.* Nucleic Acids Res, 2019. **47**(18): p. 9573-9591.

231. Quintela, A.M., et al., *PPARβ activation restores the high glucose-induced impairment of insulin signalling in endothelial cells.* Br J Pharmacol, 2014. **171**(12): p. 3089-102.

232. Li, Y., et al., *Peroxisome proliferator-activated receptors: A key link between lipid metabolism and cancer progression.* Clin Nutr, 2024. **43**(2): p. 332-345.

233. Liu, Y., et al., *The Role of PPAR-δ in Metabolism, Inflammation, and Cancer: Many Characters of a Critical Transcription Factor.* Int J Mol Sci, 2018. **19**(11).

234. Kanakasabai, S., et al., *Peroxisome proliferator-activated receptor delta agonists inhibit T helper type 1 (Th1) and Th17 responses in experimental allergic encephalomyelitis.* Immunology, 2010. **130**(4): p. 572-88.

235. Matsushita, Y., et al., *Activation of peroxisome proliferator-activated receptor delta inhibits streptozotocin-induced diabetic nephropathy through anti-inflammatory mechanisms in mice.* Diabetes, 2011. **60**(3): p. 960-8.

236. Wei, Z., et al., *Daturataturin A Ameliorates Psoriasis by Regulating PPAR Pathway.* Biochem Genet, 2024. **62**(6): p. 4952-4966.

237. Romanowska, M., et al., *Activation of PPARbeta/delta causes a psoriasis-like skin disease in vivo.* PLoS One, 2010. **5**(3): p. e9701.

238. Dunbar, H., et al., *The Inflammatory Lung Microenvironment; a Key Mediator in MSC Licensing.* Cells, 2021. **10**(11).

239. Lu, P., et al., *Serum Free Fatty Acid Concentration Predicts ARDS after Off-Pump CABG: A Prospective Observational Study.* Lung, 2024. **202**(5): p. 523-532.

240. Yazdani, R., et al., *Effect of plasma free fatty acids on lung function in male COPD patients.* Sci Rep, 2025. **15**(1): p. 3377.

241. Archambault, A.S., et al., *High levels of eicosanoids and docosanoids in the lungs of intubated COVID-19 patients.* FASEB J, 2021. **35**(6): p. e21666.

242. Zaid, Y., et al., *Chemokines and eicosanoids fuel the hyperinflammation within the lungs of patients with severe COVID-19.* J Allergy Clin Immunol, 2021. **148**(2): p. 368-380.e3.

243. Sarre, C., et al., *PPARβ/δ priming enhances the anti-apoptotic and therapeutic properties of mesenchymal stromal cells in myocardial ischemia-reperfusion injury.* Stem Cell Res Ther, 2022. **13**(1): p. 167.

244. Khan, R.S. and P.N. Newsome, *A Comparison of Phenotypic and Functional Properties of Mesenchymal Stromal Cells and Multipotent Adult Progenitor Cells.* Front Immunol, 2019. **10**: p. 1952.

245. Luz-Crawford, P., et al., *PPARβ/δ directs the therapeutic potential of mesenchymal stem cells in arthritis.* Ann Rheum Dis, 2016. **75**(12): p. 2166-2174.

246. Contreras-Lopez, R.A., Elizondo-Vega, R., Torres, M.J. *et al*, *PPARβ/δ-dependent MSC metabolism determines their immunoregulatory properties.* 2020: p. 11423

247. Kornicka, K., J. Houston, and K. Marycz, *Dysfunction of Mesenchymal Stem Cells Isolated from Metabolic Syndrome and Type 2 Diabetic Patients as Result of Oxidative Stress and Autophagy may Limit Their Potential Therapeutic Use.* Stem Cell Rev Rep, 2018. **14**(3): p. 337-345.

248. Szűcs, D., et al., *Licensing effects of inflammatory factors and TLR ligands on the regenerative capacity of adipose-derived mesenchymal stem cells.* Front Cell Dev Biol, 2024. **12**: p. 1367242.

249. Boland, L., et al., *IFN-γ and TNF-α Pre-licensing Protects Mesenchymal Stromal Cells from the Pro-inflammatory Effects of Palmitate.* Mol Ther, 2018. **26**(3): p. 860-873.

250. Babcock, T.A., et al., *Omega-3 fatty acid lipid emulsion reduces LPS-stimulated macrophage TNF-alpha production.* Surg Infect (Larchmt), 2002. **3**(2): p. 145-9.

251. Roten, R., et al., *Plasma levels of tumor necrosis factor in the adult respiratory distress syndrome.* Am Rev Respir Dis, 1991. **143**(3): p. 590-2.

252. Park, W.Y., et al., *Cytokine balance in the lungs of patients with acute respiratory distress syndrome.* Am J Respir Crit Care Med, 2001. **164**(10 Pt 1): p. 1896-903.

253. Liu, K., et al., *Interleukin-1β-Treated Mesenchymal Stem Cells Inhibit Inflammation in Hippocampal Astrocytes Through Exosome-Activated Nrf-2 Signaling.* Int J Nanomedicine, 2021. **16**: p. 1423-1434.

254. Novogene, *C analysis report*. Available from: https://www.novogene.com/eu-en/wp-content/uploads/sites/4/2020/07/mRNA-demo-report.pdf.

255. Roohollahi, K., et al., *BIRC2-BIRC3 amplification: a potentially druggable feature of a subset of head and neck cancers in patients with Fanconi anemia.* Sci Rep, 2022. **12**(1): p. 45.

256. Moriwaki, T., et al., *PRDX1 is essential for the viability and maintenance of reactive oxygen species in chicken DT40.* Genes Environ, 2021. **43**(1): p. 35.

257. Park, H.J., et al., *FoxM1, a critical regulator of oxidative stress during oncogenesis.* EMBO J, 2009. **28**(19): p. 2908-18.

258. Stoiber, W., et al., *The Role of Reactive Oxygen Species (ROS) in the Formation of Extracellular Traps (ETs) in Humans.* Biomolecules, 2015. **5**(2): p. 702-23.

259. Wang, Y., et al., *Composition and Function of Neutrophil Extracellular Traps.* Biomolecules, 2024. **14**(4).

260. Freitas, D.F., et al., *Neutrophil extracellular traps (NETs) modulate inflammatory profile in obese humans and mice: adipose tissue role on NETs levels.* Mol Biol Rep, 2022. **49**(4): p. 3225-3236.

261. Hammond, C.M., et al., *DNAJC9 integrates heat shock molecular chaperones into the histone chaperone network.* Mol Cell, 2021. **81**(12): p. 2533-2548.e9.

262. Burczyk, G., I. Cichon, and E. Kolaczkowska, *Itaconate Suppresses Formation of Neutrophil Extracellular Traps (NETs): Involvement of Hypoxia-Inducible Factor 1α (Hif-1α) and Heme Oxygenase (HO-1).* Front Immunol, 2022. **13**: p. 864638.

263. Liu, X., et al., *PAD4 takes charge during neutrophil activation: Impact of PAD4 mediated NET formation on immune-mediated disease.* J Thromb Haemost, 2021. **19**(7): p. 1607-1617.

264. Lee, D., et al., *Induction of Oxidative Stress Through Inhibition of Thioredoxin Reductase 1 Is an Effective Therapeutic Approach for Hepatocellular Carcinoma.* Hepatology, 2019. **69**(4): p. 1768-1786.

265. Ago, T., et al., *A redox-dependent pathway for regulating class II HDACs and cardiac hypertrophy.* Cell, 2008. **133**(6): p. 978-93.

266. Zhang, J., et al., *Hypoxia-inducible factor-1α/interleukin-1β signaling enhances hepatoma epithelial-mesenchymal transition through macrophages in a hypoxic-inflammatory microenvironment.* Hepatology, 2018. **67**(5): p. 1872-1889.

267. Staples, S., et al., *Selenium-independent antioxidant and anti-inflammatory effects of thioredoxin reductase inhibition in alveolar macrophages.* Life Sci, 2020. **259**: p. 118285.

268. Logan, M.R., S.O. Odemuyiwa, and R. Moqbel, *Understanding exocytosis in immune and inflammatory cells: the molecular basis of mediator secretion.* J Allergy Clin Immunol, 2003. **111**(5): p. 923-32; quiz 933.

269. Matta, B., J. Battaglia, and B.J. Barnes, *Detection of neutrophil extracellular traps in patient plasma: method development and validation in systemic lupus erythematosus and healthy donors that carry.* Front Immunol, 2022. **13**: p. 951254.

270. Tong, Y., et al., *Excessive neutrophil extracellular trap formation induced by.* Front Cell Infect Microbiol, 2023. **13**: p. 1108228.

271. Yang, S.C., et al., *Understanding the role of neutrophils in acute respiratory distress syndrome.* Biomed J, 2021. **44**(4): p. 439-446.

272. Mahida, R.Y., et al., *Acute respiratory distress syndrome is associated with impaired alveolar macrophage efferocytosis.* Eur Respir J, 2021. **58**(3).

273. Dang, W., et al., *The role of lung macrophages in acute respiratory distress syndrome.* Inflamm Res, 2022. **71**(12): p. 1417-1432.

274. Regmi, S., et al., *Evaluating the therapeutic potential of different sources of mesenchymal stem cells in acute respiratory distress syndrome.* Stem Cell Res Ther, 2024. **15**(1): p. 385.

275. Franck, T., et al., *Muscle Derived Mesenchymal Stem Cells Inhibit the Activity of the Free and the Neutrophil Extracellular Trap (NET)-Bond Myeloperoxidase.* Cells, 2021. **10**(12).

276. Ng, J., et al., *Augmenting emergency granulopoiesis with CpG conditioned mesenchymal stromal cells in murine neutropenic sepsis.* Blood Adv, 2020. **4**(19): p. 4965-4979.

277. Matthay, M.A. and G.A. Zimmerman, *Acute lung injury and the acute respiratory distress syndrome: four decades of inquiry into pathogenesis and rational management.* Am J Respir Cell Mol Biol, 2005. **33**(4): p. 319-27.

278. Yang, X., et al., *Clinical course and outcomes of critically ill patients with SARS-CoV-2 pneumonia in Wuhan, China: a single-centered, retrospective, observational study.* Lancet Respir Med, 2020. **8**(5): p. 475-481.

279. Whitehead, T. and A.S. Slutsky, *The pulmonary physician in critical care * 7: ventilator induced lung injury.* Thorax, 2002. **57**(7): p. 635-42.

280. Shankar-Hari, M., E. Fan, and N.D. Ferguson, *Acute respiratory distress syndrome (ARDS) phenotyping.* Intensive Care Med, 2019. **45**(4): p. 516-519.

281. Kitsios, G.D., et al., *Host-Response Subphenotypes Offer Prognostic Enrichment in Patients With or at Risk for Acute Respiratory Distress Syndrome.* Crit Care Med, 2019. **47**(12): p. 1724-1734.

282. Weiss, D.J., et al., *The Necrobiology of Mesenchymal Stromal Cells Affects Therapeutic Efficacy.* Front Immunol, 2019. **10**: p. 1228.

283. Ankrum, J.A., J.F. Ong, and J.M. Karp, *Mesenchymal stem cells: immune evasive, not immune privileged.* Nat Biotechnol, 2014. **32**(3): p. 252-60.

284. Tsikis, S.T., et al., *Lipopolysaccharide-induced murine lung injury results in long-term pulmonary changes and downregulation of angiogenic pathways.* Sci Rep, 2022. **12**(1): p. 10245.

285. Yang, J., et al., *Umbilical Cord-Derived Mesenchymal Stem Cell-Derived Exosomes Combined Pluronic F127 Hydrogel Promote Chronic Diabetic Wound Healing and Complete Skin Regeneration.* Int J Nanomedicine, 2020. **15**: p. 5911-5926.

286. Carbone, A., et al., *Correction of defective CFTR/ENaC function and tightness of cystic fibrosis airway epithelium by amniotic mesenchymal stromal (stem) cells.* J Cell Mol Med, 2014. **18**(8): p. 1631-43.

287. Dutra Silva, J., et al., *Mesenchymal stromal cell extracellular vesicles rescue mitochondrial dysfunction and improve barrier integrity in clinically relevant models of ARDS.* Eur Respir J, 2021. **58**(1).

288. Park, H.J., et al., *Mesenchymal stem cells stabilize the blood-brain barrier through regulation of astrocytes.* Stem Cell Res Ther, 2015. **6**: p. 187.

289. Tak, L.J., et al., *Superoxide Dismutase 3-Transduced Mesenchymal Stem Cells Preserve Epithelial Tight Junction Barrier in Murine Colitis and Attenuate Inflammatory Damage in Epithelial Organoids.* Int J Mol Sci, 2021. **22**(12).

290. Yang, Y., et al., *The Vascular Endothelial Growth Factors-Expressing Character of Mesenchymal Stem Cells Plays a Positive Role in Treatment of Acute Lung Injury In Vivo.* Mediators Inflamm, 2016. **2016**: p. 2347938.

291. Zhang, W., et al., *Protective effect of bone marrow mesenchymal stem cells in intestinal barrier permeability after heterotopic intestinal transplantation.* World J Gastroenterol, 2014. **20**(23): p. 7442-51.

292. Smith, P., L.A. Jeffers, and M. Koval, *Measurement of Lung Vessel and Epithelial Permeability In Vivo with Evans Blue.* Methods Mol Biol, 2021. **2367**: p. 137-148.

293. Rolandsson Enes, S., et al., *Healthy versus inflamed lung environments differentially effect mesenchymal stromal cells.* Eur Respir J, 2021. **58**(4).

294. Su, Y., H. Guo, and Q. Liu, *Effects of mesenchymal stromal cell-derived extracellular vesicles in acute respiratory distress syndrome (ARDS): Current understanding and future perspectives.* J Leukoc Biol, 2021. **110**(1): p. 27-38.

295. Matthay, M.A., et al., *Mesenchymal stem cells for acute lung injury: preclinical evidence.* Crit Care Med, 2010. **38**(10 Suppl): p. S569-73.

296. Shah, T.G., D. Predescu, and S. Predescu, *Mesenchymal stem cells-derived extracellular vesicles in acute respiratory distress syndrome: a review of current literature and potential future treatment options.* Clin Transl Med, 2019. **8**(1): p. 25.

297. Lee, J.W., et al., *Therapeutic effects of human mesenchymal stem cells in ex vivo human lungs injured with live bacteria.* Am J Respir Crit Care Med, 2013. **187**(7): p. 751-60.

298. Morrison, T.J., et al., *Mesenchymal Stromal Cells Modulate Macrophages in Clinically Relevant Lung Injury Models by Extracellular Vesicle Mitochondrial Transfer.* Am J Respir Crit Care Med, 2017. **196**(10): p. 1275-1286.

299. Bowdish, M.E., et al., *A Randomized Trial of Mesenchymal Stromal Cells for Moderate to Severe Acute Respiratory Distress Syndrome from COVID-19.* Am J Respir Crit Care Med, 2023. **207**(3): p. 261-270.

300. Gorman, E., et al., *Repair of acute respiratory distress syndrome by stromal cell administration (REALIST) trial: A phase 1 trial.* EClinicalMedicine, 2021. **41**: p. 101167.

301. Abreu, S.C., et al., *Differential effects of the cystic fibrosis lung inflammatory environment on mesenchymal stromal cells.* Am J Physiol Lung Cell Mol Physiol, 2020. **319**(6): p. L908-L925.

302. Kota, B.P., T.H. Huang, and B.D. Roufogalis, *An overview on biological mechanisms of PPARs.* Pharmacol Res, 2005. **51**(2): p. 85-94.

303. Heck, B.E., et al., *PPAR-δ Agonist With Mesenchymal Stem Cells Induces Type II Collagen-Producing Chondrocytes in Human Arthritic Synovial Fluid.* Cell Transplant, 2017. **26**(8): p. 1405-1417.

304. Djouad, F., et al., *PPARβ/δ: A master regulator of mesenchymal stem cell functions.* Biochimie, 2017. **136**: p. 55-58.

305. Ziveri, J., et al., *Angiopoietin-like 4 protects against endothelial dysfunction during bacterial sepsis.* Nat Microbiol, 2024. **9**(9): p. 2434-2447.

306. Neubauer, E., et al., *Comparative evaluation of three proliferation markers, Ki-67, TOP2A, and RacGAP1, in bronchopulmonary neuroendocrine neoplasms: Issues and prospects.* Oncotarget, 2016. **7**(27): p. 41959-41973.

307. Perez Diaz, N., et al., *Co-Incubation with PPARβ/δ Agonists and Antagonists Modeled Using Computational Chemistry: Effect on LPS Induced Inflammatory Markers in Pulmonary Artery.* Int J Mol Sci, 2021. **22**(6).

308. Goh, Y.Y., et al., *Angiopoietin-like 4 interacts with integrins beta1 and beta5 to modulate keratinocyte migration.* Am J Pathol, 2010. **177**(6): p. 2791-803.

309. Zhan, W., et al., *ANGPTL4 attenuates palmitic acid-induced endothelial cell injury by increasing autophagy.* Cell Signal, 2022. **98**: p. 110410.

310. An, Q., et al., *In vitro effects of mitomycin C on the proliferation of the non-small-cell lung cancer line A549.* Int J Clin Exp Med, 2015. **8**(11): p. 20516-23.

311. Mardani, I., et al., *Plin2-deficiency reduces lipophagy and results in increased lipid accumulation in the heart.* Sci Rep, 2019. **9**(1): p. 6909.

312. Sylvers-Davie, K.L. and B.S.J. Davies, *Regulation of lipoprotein metabolism by ANGPTL3, ANGPTL4, and ANGPTL8.* Am J Physiol Endocrinol Metab, 2021. **321**(4): p. E493-E508.

313. Kim, D., et al., *Mitochondrial NADPH fuels mitochondrial fatty acid synthesis and lipoylation to power oxidative metabolism.* Nat Cell Biol, 2025. **27**(5): p. 790-800.

314. Šutić, M., et al., *Transcriptomic Profiling for Prognostic Biomarkers in Early-Stage Squamous Cell Lung Cancer (SqCLC).* Cancers (Basel), 2024. **16**(4).

315. Li, R., H. Zhu, and Y. Luo, *Understanding the Functions of Long Non-Coding RNAs through Their Higher-Order Structures.* Int J Mol Sci, 2016. **17**(5).

316. Frans, G., et al., *Conventional and Single-Molecule Targeted Sequencing Method for Specific Variant Detection in IKBKG while Bypassing the IKBKGP1 Pseudogene.* J Mol Diagn, 2018. **20**(2): p. 195-202.

317. Rashid, F., et al., *Induction of miR-3648 Upon ER Stress and Its Regulatory Role in Cell Proliferation.* Int J Mol Sci, 2017. **18**(7).

318. Galvan, A., et al., *Gene expression signature of non-involved lung tissue associated with survival in lung adenocarcinoma patients.* Carcinogenesis, 2013. **34**(12): p. 2767-73.

319. Dong, J., et al., *ACACA reduces lipid accumulation through dual regulation of lipid metabolism and mitochondrial function via AMPK- PPARα- CPT1A axis.* J Transl Med, 2024. **22**(1): p. 196.

320. Loprasert, S., et al., *Regulation of the oxidative stress protective enzymes, catalase and superoxide dismutase in Xanthomonas--a review.* Gene, 1996. **179**(1): p. 33-7.

321. Wang, X., et al., *Transmembrane emp24 protein transport domain 6 is selectively expressed in pancreatic islets and implicated in insulin secretion and diabetes.* Pancreas, 2012. **41**(1): p. 10-4.

322. Huang, X., et al., *Lactate dehydrogenase a-like 6B is not essential for spermatogenesis and male fertility in mice.* Gene, 2025. **936**: p. 149100.

323. Moursy, A., et al., *RNA recognition by Npl3p reveals U2 snRNA-binding compatible with a chaperone role during splicing.* Nat Commun, 2023. **14**(1): p. 7166.

324. Singh, N., *Role of mammalian long non-coding RNAs in normal and neuro oncological disorders.* Genomics, 2021. **113**(5): p. 3250-3273.

325. Patel, J., et al., *Loss of RARRES1 function Promotes Follicular Lymphomagenesis and Inhibits B cell Differentiation in Mice.* Int J Biol Sci, 2022. **18**(7): p. 2670-2682.

326. Kanbar, J.N., et al., *The long noncoding RNA Malat1 regulates CD8+ T cell differentiation by mediating epigenetic repression.* J Exp Med, 2022. **219**(6).

327. Ma, Q., et al., *The short peptide encoded by long non-coding RNA RNF217-AS1 inhibits stomach cancer tumorigenesis, macrophage recruitment, and pro-inflammatory responses.* Amino Acids, 2024. **56**(1): p. 45.

328. Erben, E.D., et al., *A genome-wide tethering screen reveals novel potential post-transcriptional regulators in Trypanosoma brucei.* PLoS Pathog, 2014. **10**(6): p. e1004178.

329. Ding, Z., Y.H. Bae, and P. Roy, *Molecular insights on context-specific role of profilin-1 in cell migration.* Cell Adh Migr, 2012. **6**(5): p. 442-9.

330. Wang, S., F.X. Claret, and W. Wu, *MicroRNAs as Therapeutic Targets in Nasopharyngeal Carcinoma.* Front Oncol, 2019. **9**: p. 756.

331. Li, Y., et al., *U2AF1 mutation causes an oxidative stress and DNA repair defect in hematopoietic and leukemic cells.* Free Radic Biol Med, 2025. **228**: p. 379-391.

332. Sultana, T., T. Iwamori, and N. Iwamori, *TSNAXIP1 is required for sperm head formation and male fertility.* Reprod Med Biol, 2023. **22**(1): p. e12520.

333. Huang, W., et al., *ANGPTL4 induces Kupffer cell M2 polarization to mitigate acute rejection in liver transplantation.* Sci Rep, 2025. **15**(1): p. 986.

334. Batista, F.A., et al., *Structural insights into human peroxisome proliferator activated receptor delta (PPAR-delta) selective ligand binding.* PLoS One, 2012. **7**(5): p. e33643.

335. Wan, H., et al., *Tight junction properties of the immortalized human bronchial epithelial cell lines Calu-3 and 16HBE14o-.* Eur Respir J, 2000. **15**(6): p. 1058-68.

336. Godbole, N.M., et al., *Tight Junctions, the Epithelial Barrier, and Toll-like Receptor-4 During Lung Injury.* Inflammation, 2022. **45**(6): p. 2142-2162.

337. Hu, J., et al., *Prognostic Value of Angiopoietin-like 4 in Patients with Acute Respiratory Distress Syndrome.* Shock, 2021. **56**(3): p. 403-411.

338. Wee, W.K.J., et al., *Single-cell analysis of skin immune cells reveals an Angptl4-ifi20b axis that regulates monocyte differentiation during wound healing.* Cell Death Dis, 2022. **13**(2): p. 180.

339. Shan, Y., et al., *Pharmacokinetic characteristics of mesenchymal stem cells in translational challenges.* Signal Transduct Target Ther, 2024. **9**(1): p. 242.

340. Foronjy, R.F. and S.M. Majka, *The potential for resident lung mesenchymal stem cells to promote functional tissue regeneration: understanding microenvironmental cues.* Cells, 2012. **1**(4): p. 874.

341. Lau, A.N., et al., *Stem cells and regenerative medicine in lung biology and diseases.* Mol Ther, 2012. **20**(6): p. 1116-30.

342. Doherty, D.F., L. Roets, and A.D. Krasnodembskaya, *The Role of Lung Resident Mesenchymal Stromal Cells in the Pathogenesis and Repair of Chronic Lung Disease.* Stem Cells, 2023. **41**(5): p. 431-443.

343. Teijeira, A., et al., *Differential Interleukin-8 thresholds for chemotaxis and netosis in human neutrophils.* Eur J Immunol, 2021. **51**(9): p. 2274-2280.

344. Lin, I.C., et al., *Involvement of IL-17 A/IL-17 Receptor A with Neutrophil Recruitment and the Severity of Coronary Arteritis in Kawasaki Disease.* J Clin Immunol, 2024. **44**(3): p. 77.

345. Sinha, P., et al., *Prevalence of phenotypes of acute respiratory distress syndrome in critically ill patients with COVID-19: a prospective observational study.* Lancet Respir Med, 2020. **8**(12): p. 1209-1218.

346. Rossello-Gelabert, M., et al., *Fine-tuning licensing strategies to boost MSC-based immunomodulatory secretome.* Stem Cell Res Ther, 2025. **16**(1): p. 183.

Please cite this article in press as: Tunstead et al., The ARDS microenvironment enhances MSC-induced repair via VEGF in experimental acute lung inflammation, Molecular Therapy (2024), https://doi.org/10.1016/j.ymthe.2024.08.003

7.1

Molecular Therapy
Original Article

The ARDS microenvironment enhances MSC-induced repair via VEGF in experimental acute lung inflammation

Courteney Tunstead,[1,2] Evelina Volkova,[1,2] Hazel Dunbar,[1,2] Ian J. Hawthorne,[1,2] Alison Bell,[3,4] Louise Crowe,[2,5] Joanne C. Masterson,[2,5] Claudia C. Dos Santos,[6] Bairbre McNicholas,[3,4] John G. Laffey,[3,4] and Karen English[1,2]

[1]Cellular Immunology Lab, Department of Biology, Maynooth University, Maynooth, Co. Kildare, Ireland; [2]Kathleen Lonsdale Institute for Human Health Research, Maynooth University, Maynooth, Co. Kildare, Ireland; [3]Anesthesia and Intensive Care Medicine, School of Medicine, College of Medicine Nursing and Health Sciences, University of Galway, Galway, Ireland; [4]Anesthesia and Intensive Care Medicine, Galway University Hospitals, Saolta University Hospitals Groups, Galway, Ireland; [5]Allergy, Inflammation & Remodelling Research Lab, Department of Biology, Maynooth University, Maynooth, Co. Kildare, Ireland; [6]Keenan Research Centre for Biomedical Research, St. Michael's Hospital, Toronto, ON, Canada

Clinical trials investigating the potential of mesenchymal stromal cells (MSCs) for the treatment of inflammatory diseases, such as acute respiratory distress syndrome (ARDS), have been disappointing, with less than 50% of patients responding to treatment. Licensed MSCs show enhanced therapeutic efficacy in response to cytokine-mediated activation signals. There are two distinct sub-phenotypes of ARDS: hypo- and hyper-inflammatory. We hypothesized that pre-licensing MSCs in a hyper-inflammatory ARDS environment would enhance their therapeutic efficacy in acute lung inflammation (ALI). Serum samples from patients with ARDS were segregated into hypo- and hyper-inflammatory categories based on interleukin (IL)-6 levels. MSCs were licensed with pooled serum from patients with hypo- or hyper-inflammatory ARDS or healthy serum controls. Our findings show that hyper-inflammatory ARDS pre-licensed MSC conditioned medium (MSC-CM_{Hyper}) led to a significant enrichment in tight junction expression and enhanced barrier integrity in lung epithelial cells *in vitro* and *in vivo* in a vascular endothelial growth factor (VEGF)-dependent manner. Importantly, while both MSC-CM_{Hypo} and MSC-CM_{Hyper} significantly reduced IL-6 and tumor necrosis factor alpha (TNF-α) levels in the bronchoalveolar lavage fluid (BALF) of lipopolysaccharide (LPS)-induced ALI mice, only MSC-CM_{Hyper} significantly reduced lung permeability and overall clinical outcomes including weight loss and clinical score. Thus, the hypo- and hyper-inflammatory ARDS environments may differentially influence MSC cytoprotective and immunomodulatory functions.

INTRODUCTION

Acute respiratory distress syndrome (ARDS) is an inflammatory disease with a mortality rate of ∼60% in patients with severe acute respiratory syndrome coronavirus 2 (SARS-CoV-2)-induced ARDS.[1,2] ARDS is largely characterized by low blood oxygen levels, excessive alveolar damage, and acute respiratory failure.[3–5] One of the primary treatments for ARDS is mechanical ventilation, with ∼70% of patients in need of ventilation. Unfortunately, ventilation can further exacerbate the disease state of the patient and contribute to disease pathology through ventilator-induced lung injury.[2,6] The Berlin definition of ARDS states ventilator support as a key diagnostic criterion, but the more recent global definition suggests that this is no longer a critical diagnostic component.[3,7] Due to the lack of available treatments, cell therapies have long been investigated as a potential treatment for ARDS. Mesenchymal stromal cell (MSC) therapies have been investigated in the treatment of ARDS due to their ability to modulate over-zealous inflammatory responses; however, clinical trials have generated disappointing results, with only ∼30%–50% of patients responding to treatment as of the latest clinical trials.[8–10]

MSCs are primarily known for their immunomodulatory properties and reparative capacity. This makes them an excellent candidate in the treatment of inflammatory diseases, such as ARDS. MSCs are known to show enhanced efficacy when exposed to cytokine-mediated activation signals, often referred to as "MSC licensing."[11–14] Although ARDS is traditionally characterized as an inflammatory disease containing the necessary levels of inflammation to effectively license the MSCs *in vivo*, sub-phenotypic stratification of patients suggests that there are two distinct sub-groups: hypo- and hyper-inflammatory ARDS.[15] Hyper-inflammatory ARDS is largely characterized by high levels of pro-inflammatory cytokines, such as interleukin (IL)-6 and IL-8, while hypo-inflammatory has significantly less of an inflammatory signature.[16] Since MSC licensing largely impacts their functional capacity *in vivo*, this would suggest that MSCs would be

Received 23 April 2024; accepted 2 August 2024;
https://doi.org/10.1016/j.ymthe.2024.08.003.

Correspondence: Karen English, Cellular Immunology Lab, Department of Biology, Maynooth University, Maynooth, Co. Kildare, Ireland.
E-mail: karen.english@mu.ie

Please cite this article in press as: Tunstead et al., The ARDS microenvironment enhances MSC-induced repair via VEGF in experimental acute lung inflammation, Molecular Therapy (2024), https://doi.org/10.1016/j.ymthe.2024.08.003

more efficacious in the treatment of hyper-inflammatory ARDS. Unlicensed MSCs, or MSCs that are placed into an environment lacking a threshold level of inflammation, are less likely to exert beneficial effects.[17–19] Therefore, understanding the MSC response to the ARDS patient microenvironment is a crucial, but often overlooked, point of interest prior to clinical trials.

The acute lung inflammation (ALI) and cellular infiltration seen in ARDS is known to lead to disruptions in the lung epithelium, thus leading to pulmonary edema and, ultimately, death of the patient.[20–22] Tsikis et al. recently highlighted that endotoxin-induced ALI in mice led to a significant reduction in vascular endothelial growth factor (VEGF) and its associated receptor, VEGF receptor 2 (VEGFR2).[23] MSCs are already known to secrete VEGF, and many studies have already investigated the role of MSC-derived VEGF in the context of cytoprotection, wound healing, and permeability.[24–26] Other studies have highlighted the enrichment of tight junction expression and the capacity for MSCs and MSC-derived extracellular vesicles to reduce epithelial barrier permeability.[27–33] However, this study is the first to investigate the impact of the hypo- and hyper-inflammatory patient microenvironments on MSC functionality, using human bone marrow-derived MSCs (hBM-MSCs), clinically relevant ARDS patient samples, and a pre-clinical model of ALI.

RESULTS

Segregation of ARDS patient serum samples

ARDS patient serum samples were stratified based on their IL-6 level upon arrival to the intensive care unit. ARDS patient demographics, including age, sex, World Health Organization score[34], and O_2 requirement, are included in Table S1 and Figures 1A–1D. For this study, patients with IL-6 levels <50 pg/mL were considered hypo-inflammatory, and IL-6 levels >50 pg/mL were considered hyper-inflammatory (Figures 1E and 1F). For comparison, serum samples collected from healthy donors were included. Upon pooling the samples, we confirmed that the hyper-inflammatory pool contained significantly higher levels of IL-6 and IL-8, both known to be of higher levels in the hyper-inflammatory ARDS sub-phenotype (Figures 1G and 1H). In addition, the hyper-inflammatory pool contained significantly higher levels of migration inhibitory factor (MIF) and tumor necrosis factor alpha (TNF-α) (Figures 1I and 1J). All subsequent experiments were carried out using these distinct pools.

Hyper-, but not hypo-, inflammatory ARDS serum licenses MSCs and enhances their secretion of VEGF

MSC conditioned medium (MSC-CM) from MSCs that had been exposed to healthy or hypo-inflammatory serum showed no significant increase in cytokines or growth factors in comparison to naive MSC-CM. There was no difference in IL-6 secretion between MSC-CM groups (Figure 2B). Hyper-inflammatory ARDS serum, however, led to a significant increase in MSC secretion of IL-8, MIF, and VEGF (Figures 2C–2E). Gene expression studies also highlighted that *vegf-a* and *kdr*, the genes that encode for VEGF-A and VEGFR2, respectively, were also significantly increased after exposure to hyper-inflammatory serum (Figures 2F and 2G). There were no significant differences in expression of *il-8*, *mif*, or any of their corresponding receptors (*cxcr1*, *cxcr2*, *cxcr4*, *cd74*) (Figures S1A–S1F). For this reason, we chose to further investigate the role of VEGF.

MSC-CM enhances tight junction expression in CALU-3 lung epithelial cells in a VEGF-dependent manner

CALU-3 lung epithelial cells exposed to endotoxin showed a significant reduction in *tjp1*, the gene that encodes for zonula occludens-1 (Figures 3A and 3B). There was no significant difference in *ocln* or *cld4*, the genes that encode for occludin and claudin-4, respectively, in response to endotoxin (Figures 3C and 3D). However, upon exposure to 2 mL of naive MSC-CM, containing a high concentration of ∼1,000 pg/mL VEGF, correlating with the VEGF concentration seen in MSC-CM_{Hyper} (Figure 2E), there was a significant enrichment of *tjp1*, *ocln*, and *cldn4* expression. Pre-treatment of CALU-3 lung epithelial cells with SU-5416, a VEGFR2 inhibitor, abrogated this effect (Figures 3B–3D), demonstrating that VEGF derived from MSC-CM was required for the enhancement of tight junction gene expression in response to endotoxin challenge.

MSC-CM_{Hyper} reduces lung permeability *in vitro*

Transepithelial electric resistance (TEER) measurements were performed in CALU-3 cells in submerged cultures on days 1, 3, and 5 and in subsequent air-liquid interface cultures from day 8. This exposure to air allows for a more respiratory-like cell stratification, as lung epithelial cells are associated with exposure to both air and liquid in the body. Upon exposure to 2 μg/mL of endotoxin on day 15, TEER measurements (ohm cm^2) demonstrate a significant decrease in epithelial membrane integrity by day 17 (Figures 4A and 4B). The PBS control remained steady throughout. Subsequently, when exposed to 500 μL of MSC-$CM_{Healthy}$ (containing ∼500 pg/mL VEGF) or MSC-CM_{Hyper} (containing ∼1,000 pg/mL VEGF) on day 17 (Figures 4B and 4C), there was a significant improvement in barrier integrity on day 19. This was not seen in MSC-CM_{Hypo} (∼250 pg/mL VEGF). Neutralizing VEGF with a bevacizumab biosimilar led to the abrogation of this effect (Figures 4B and 4C), confirming the importance of VEGF in MSC therapeutic efficacy. Gene expression studies on the cells from this assay also showed significant enrichment of *tjp1*, *ocln*, and *cldn-4* in response to MSC-CM_{Hyper} (Figures 4D–4F).

MSC-CM_{Hyper} reduces overall disease severity in a pre-clinical model of ALI

MSC-$CM_{Healthy}$, MSC-CM_{Hypo}, and MSC-CM_{Hyper} all had the ability to reduce the inflammatory profile seen in our model of ALI, primarily in the context of IL-6 and TNF-α (Figures 5A and 5B). In the context of clinical parameters in the endotoxin-induced lung inflammation model, both MSC-CM_{Hyper} ($p = 0.0041$) and MSC-$CM_{Healthy}$ ($p = 0.0297$) significantly reduced the clinical score when compared to lipopolysaccharide (LPS)-treated mice (Figure 5C). In contrast, only MSC-CM_{Hyper} had the ability to significantly reduce the percentage of weight loss ($p = 0.0071$) when compared to LPS-treated mice (Figure 5D). MSC-CM_{Hypo} did not significantly reduce the clinical score ($p = 0.2728$) or the percentage of weight loss ($p = 0.0994$); however,

Please cite this article in press as: Tunstead et al., The ARDS microenvironment enhances MSC-induced repair via VEGF in experimental acute lung inflammation, Molecular Therapy (2024), https://doi.org/10.1016/j.ymthe.2024.08.003

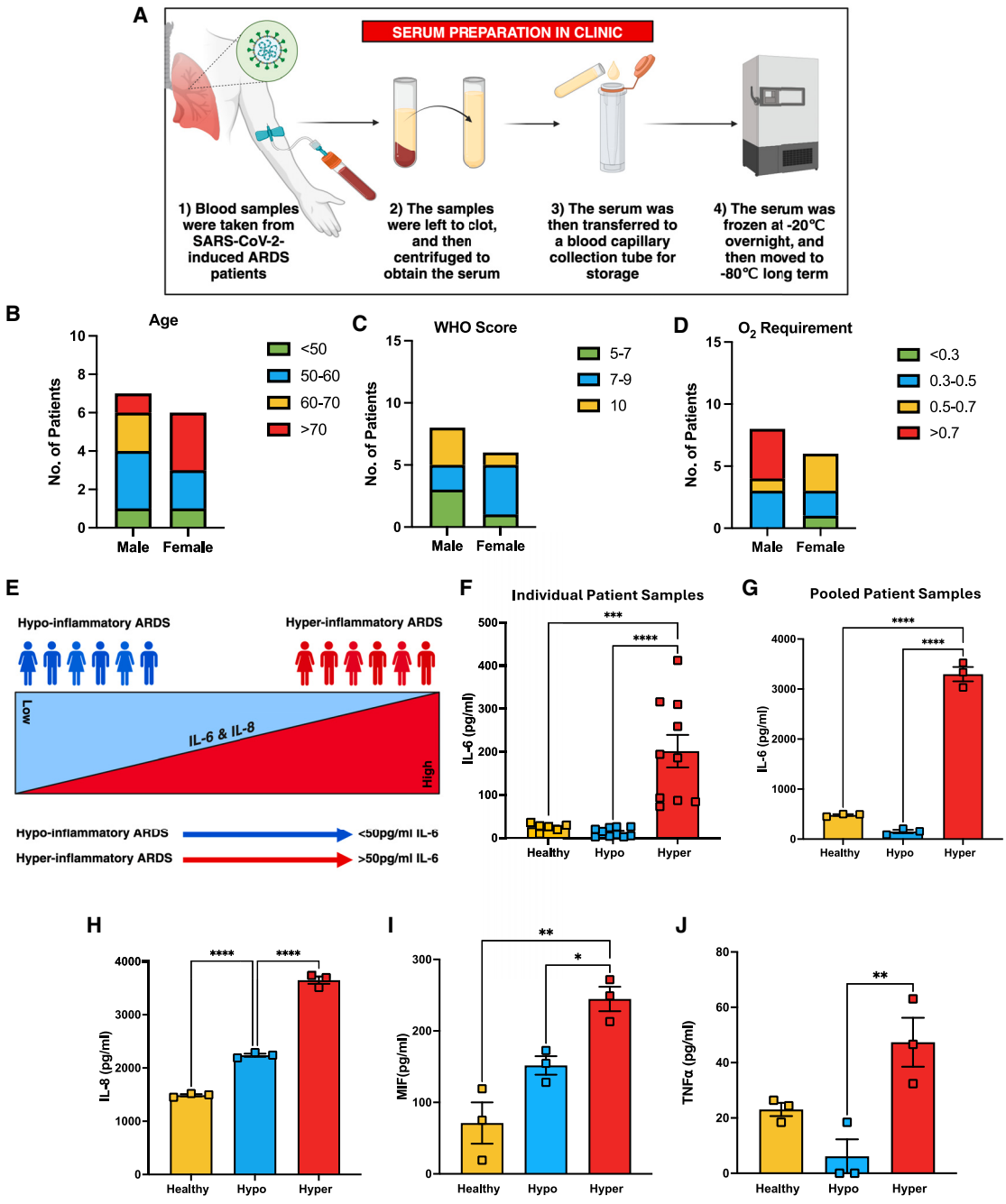

Figure 1. ARDS patient sub-phenotype stratification

(A) Schematic created using Biorender.com. ARDS patient serum samples were obtained from patients of (B–D) differing backgrounds (age, World Health Organization [WHO] score, O_2 level) and (E and F) stratified into a hypo- or hyper-inflammatory sub-phenotype based on their IL-6 levels at the time of admission ($n = 7$). Patients with <50 pg/mL IL-6 were considered hypo-inflammatory, and patients with >50 pg/mL IL-6 were considered hyper-inflammatory. The samples were then pooled, and the (G) IL-6 (BioLegend), (H) IL-8 (R&D), (I) MIF (R&D), and (J) TNF-α (BioLegend) levels were observed in each pool. Serum pooled from 6 healthy age-matched patients was used as a control. Data are presented as mean ± SEM; $^{*}p < 0.05$, $^{**}p < 0.01$, $^{***}p < 0.001$, and $^{****}p < 0.0001$.

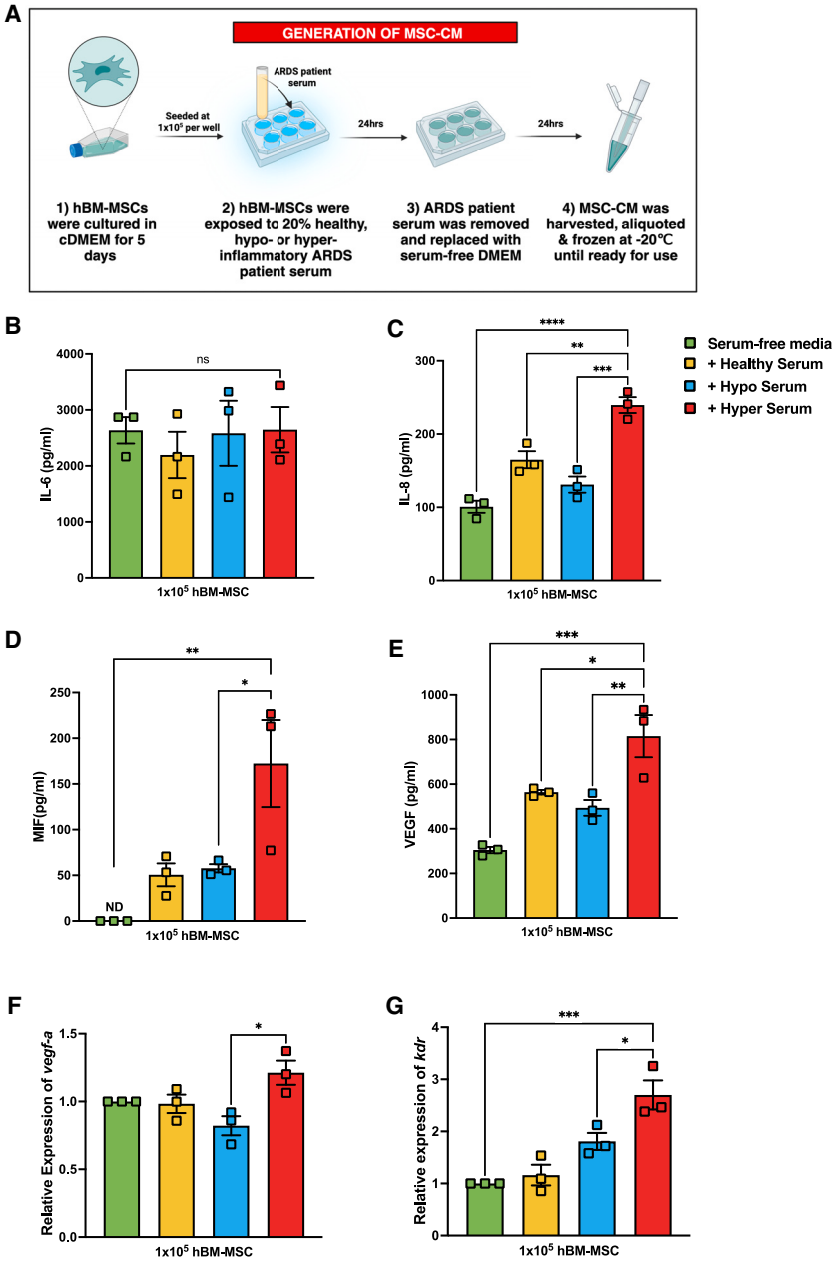

Figure 2. The MSC secretome in response to healthy or hypo- or hyper-inflammatory ARDS serum

(A) Schematic created using Biorender.com. hBM-MSCs ($n = 3$ donors) were seeded at a density of 1×10^5 in a 6-well plate, left to attach, and exposed to 20% ARDS patient serum or healthy serum control. The serum was removed after 24 h, the cells were washed with PBS, and serum-free DMEM was added for a further 24 h to generate MSC-CM. The (B) IL-6 (BioLegend), (C) IL-8, (D) MIF, and (E) VEGF (R&D) levels were then analyzed via ELISA. RT-PCR was also carried out on (F) *vegf-a* and (G) *kdr*. Data are presented as mean ± SEM; $n = 3$ per group; $^*p < 0.05$, $^{**}p < 0.01$, $^{***}p < 0.001$, and $^{****}p < 0.0001$.

there was no significant difference observed between MSC-CM_{Hyper} and MSC-CM_{Hypo} ($p = 0.0690$).

MSC-CM_{Hyper} reduces lung permeability in a pre-clinical model of ALI

Evans Blue dye was used as a measure of lung permeability *in vivo* (Figure 6A). Lungs with a visible blue coloration are considered permeable, or "leaky," as the Evans Blue dye leaks to the exterior of the lung. MSC-$CM_{Healthy}$, MSC-CM_{Hypo}, or MSC-CM_{Hyper} was concentrated using centrifugal filters, and VEGF levels were measured following the addition of a bevacizumab biosimilar (to neutralize VEGF) or an immunoglobulin G (IgG) control (Figures 6B and 6C). The lungs from mice exposed to endotoxin followed by MSC-CM_{Hyper} showed a significant visual improvement in barrier integrity (Figure 6D). This effect was abrogated when VEGF was neutralized. Mice that were treated with MSC-CM_{Hyper} also showed a significant reduction in total Evans Blue in the lung extract (normalized to the serum Evans Blue and divided by the lung wet weight). This effect was abrogated when VEGF was neutralized (Figure 6E). There was also a significant reduction in the wet:dry weight ratio of the lungs of mice that received MSC-CM_{Hyper}, which, again, was lost when VEGF was neutralized (Figure 6F).

DISCUSSION

The patient microenvironment is thought to have an impact on MSC therapy, with MSCs typically exerting their beneficial effects in response to an inflammatory stimulus. MSCs that have not been subjected to a threshold level of inflammation may lack therapeutic efficacy and may further contribute to disease pathology.[11–14] Other studies have shown that MSC-CMs generated from MSCs exposed to ARDS patient bronchoalveolar lavage fluid (BALF) have had increased levels of cytokines in comparison to MSCs exposed to a healthy BALF control.[35] However, this study lacked patient stratification. Our research illustrates that MSCs are more responsive to the hyper-, but not hypo-, inflammatory ARDS patient microenvironment in the context of MSC cytoprotective effects. This is outlined in Figure 2, where we show that MSC-CM_{Hyper}, but not MSC-CM_{Hypo}, had increased levels of IL-8, MIF, and VEGF. MSC-CM_{Hypo} had a comparable level of protein secretion to that of MSC-$CM_{Healthy}$. Gene expression studies called further attention to VEGF, as *vegf-a* and *kdr* were significantly increased in the hyper-, but not hypo-, pre-licensed MSCs.

Based on previous literature, MSCs have already been shown to enhance epithelial tight junction gene expression in a VEGF-dependent

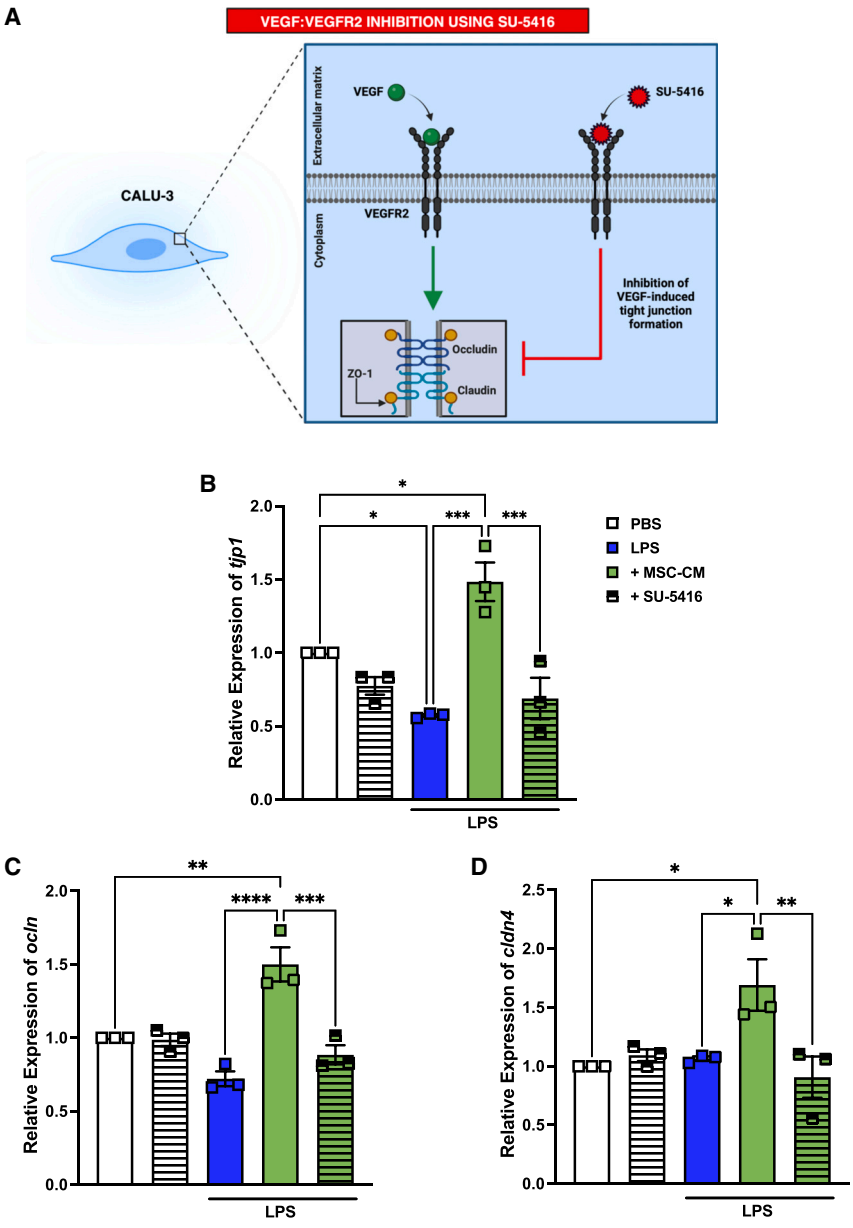

Figure 3. The MSC-CM enhancement of tight junction expression

(A) Schematic created using Biorender.com. CALU-3 cells (passages 10–12) were seeded at a density of 5×10^5 in a 6-well plate, left to attach, and exposed to 10 μM SU-5416, a VEGFR2 inhibitor, for 4 h before being stimulating with 2 μg/mL endotoxin for 48 h. Some groups were subsequently exposed to 2 mL of MSC-CM containing ~1,000 pg/mL VEGF for 24 h. The cells were then harvested for gene expression studies of tight junction genes: (B) *tjp1*, (C) *ocln*, and (D) *cldn4*. Data are presented as mean ± SEM; $n = 3$ per group; $^*p < 0.05$, $^{**}p < 0.01$, $^{***}p < 0.001$, and $^{****}p < 0.0001$.

manner.[26–33] Yang et al. highlighted that MSCs could stabilize endothelial lung permeability in a model of ALI through the enrichment of VEGF in the MSC-CM.[26] We wanted to further investigate the impact of MSC-CM on tight junction enhancement as a mechanism for repairing the epithelial barrier. To do this, we exposed CALU-3 lung epithelial cells to endotoxin to interrupt the epithelial barrier and then exposed them to MSC-CM (containing ~1,000 pg/mL of VEGF), a comparable concentration to that of hyper-licensed MSC-CM, from three independent, non-treated MSC donors (Figure 2E). We also used a VEGFR2 inhibitor, SU-5416, to block VEGFR2 on the CALU-3 cells to confirm VEGF dependence (Figures 3B and 3C). Our study confirmed that MSC-CM could enhance tight junction expression of *ocln*, *cldn4* and *tjp1* in a VEGF-dependent manner in CALU-3 lung epithelial cells, a clinically relevant cell type for lung barrier studies due to their ability to generate tight junctions.

Furthermore, we investigated the relevance of this at a functional level, *in vitro*, by performing a TEER assay in CALU-3 cells. Endotoxin significantly decreased the barrier integrity, and MSC-CM_{Hyper}, but not MSC-CM_{Hypo}, had the ability to significantly enhance barrier integrity in response to endotoxin (Figures 4B and 4C). MSC-$CM_{Healthy}$ could also significantly enhance barrier integrity but not to the same extent as MSC-CM_{Hyper}, which had the ability to fully restore the barrier. Using an anti-VEGF bevacizumab biosimilar monoclonal antibody or an IgG isotype control, we investigated the mechanistic impact of VEGF. This antibody functionally inhibits VEGF, and neutralizing VEGF in this manner significantly abrogated the increased barrier integrity mediated by the MSC-CM_{Hyper} group. Gene expression studies further highlighted that hyper-licensed MSCs had the ability to enhance the expression of *tjp1*, *cldn4*, and *ocln* in CALU-3 cells cultured at the air-liquid interface in a VEGF-dependent manner. There was no significant increase in these genes in the healthy-licensed MSCs. This is in line with studies in rat MSCs, whereby lentiviral VEGF knockdown rat MSCs failed to enhance epithelial barrier integrity when compared to control MSCs in a model of endotoxin-induced ALI.[32]

To investigate the functional relevance *in vivo*, we exposed C57BL6/J mice to endotoxin-induced ALI, which shares some aspects of human ARDS pathology, including the permeable, or leaky, lung. We then exposed the mice to each of our treatment groups before injecting Evans Blue dye to assess the lung permeability.[36] MSCs and MSC-CM have been shown to reduce pro-inflammatory cytokine levels and reduce pathology and clinical score in endotoxin-induced ALI models.[37,38] Upon analyzing the cytokine profile of the BALF of the

Please cite this article in press as: Tunstead et al., The ARDS microenvironment enhances MSC-induced repair via VEGF in experimental acute lung inflammation, Molecular Therapy (2024), https://doi.org/10.1016/j.ymthe.2024.08.003

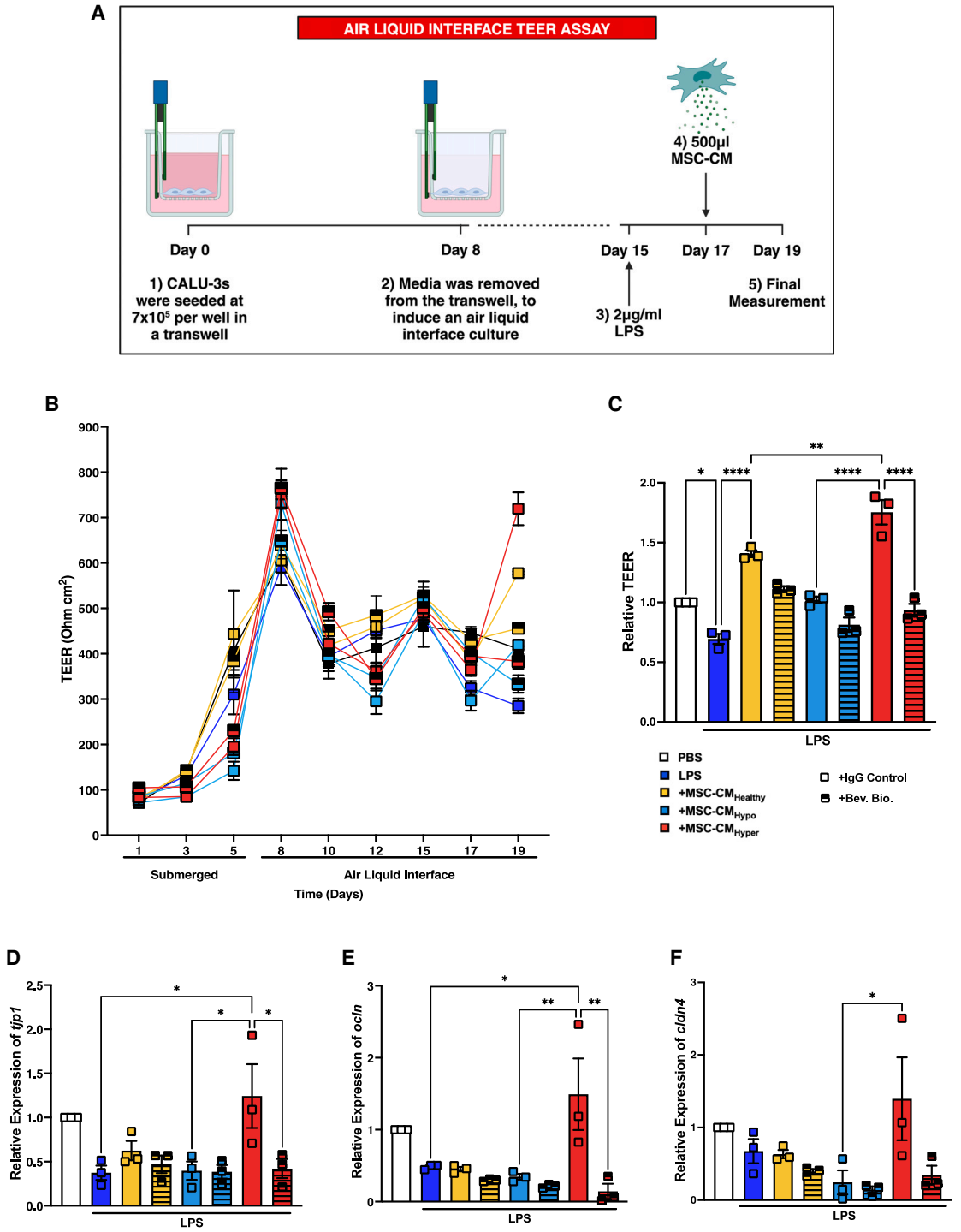

Figure 4. Barrier integrity of CALU-3 cells in response to MSC-CM

(A) Schematic created using Biorender.com. CALU-3s were seeded at a density of 7 × 10^5 in a Transwell (0.4 µm) and grown under air-liquid interface conditions from day 8 of culture. On day 15, the cells were stimulated with 2 µg/mL of endotoxin, and on day 17, they were exposed to 500 µL of MSC-CM from the groups depicted in Figure 2E (± bevacizumab biosimilar or the appropriate IgG isotype control). (B) TEER measurements were taken 3 times a week for 3 weeks, and (C) final measurements were taken on day 19. (D–F) Gene expression studies highlighted differences in tight junction expression. Data are presented as mean ± SEM; $n = 3$ per group; $^*p < 0.05$, $^{**}p < 0.01$, $^{***}p < 0.001$, and $^{****}p < 0.0001$.

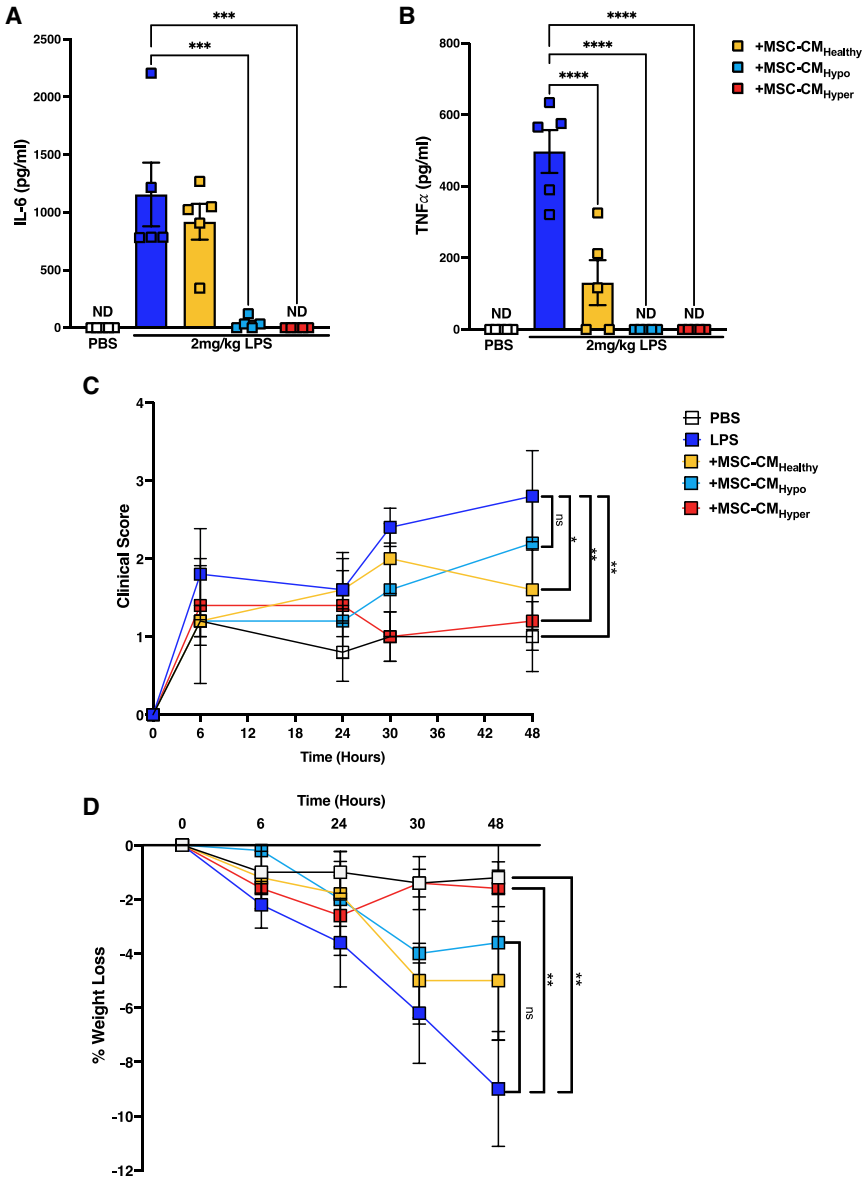

Figure 5. Cytokine levels in BALF and clinical scoring from ALI mouse model

BALF was harvested from C57BL6/J mice (n = 5) exposed to our ALI model and (A) IL-6 and (B) TNF-α were quantified by ELISA. (C) Clinical score and (D) percentage of weight loss were also assessed. Data are presented as mean ± SEM; n = 5 per group; $^{*}p < 0.05$, $^{**}p < 0.01$, $^{***}p < 0.001$, and $^{****}p < 0.0001$.

mice subjected to each treatment, we detected significantly less cytokines, in particular IL-6, in mice that received any form of MSC-CM, and this aligns with previous studies.[39–41] The overall clinical parameters highlighted that both MSC-$CM_{Healthy}$ and MSC-CM_{Hyper} had the ability to significantly reduce clinical score, with p values suggesting that MSC-CM_{Hyper} reduced this to a greater extent (Figure 5C). MSC-CM_{Hyper} also showed a significant reduction in the percentage of weight loss, something we did not see in our MSC-CM_{Hypo} group (Figure 5D). Importantly, only MSC-CM_{Hyper} significantly reduced lung permeability, and this effect was VEGF dependent. This data suggests that MSC cytoprotective and immunomodulatory effects may be mediated by different factors present in the secretome. Our study focused on the cytoprotective effects mediated by VEGF and demonstrated that pre-licensing MSCs with high-IL-6 ARDS patient serum (denoted as hyper-inflammatory ARDS) had a significant impact in reducing lung permeability in comparison to healthy or hypo-inflammatory pre-licensed MSC-CM. However, in the same model, all MSC-CMs had the ability to reduce the pro-inflammatory cytokines IL-6 and TNF-α in the BALF. These findings confirm that MSCs of any form may be beneficial in the treatment of inflammatory disease, but only MSC-CM_{Hyper} appeared to be efficacious across all parameters, further highlighting the impact of the patient microenvironment on MSC functionality. Indeed, a recent study by Faircloth et al. confirms this hypothesis, showing that VEGF secretion and immunosuppression by MSCs are two distinct potency mechanisms.[42]

This study provides novel insight into the impact of the patient microenvironment in dictating response to MSC therapy, offering a solution to the urgent unmet need for patient stratification prior to further MSC studies and clinical trials in the treatment of ARDS.

MATERIALS AND METHODS

Study cohorts and ethical approval

Full ethical approval was obtained from both the Galway University Medical Ethics Committee and the Maynooth University Ethics Committee. A cohort of healthy adult donors was recruited from St Vincent's Healthcare Group. All participants provided full consent.

Ethical approval and HPRA compliance

Ethical approval was granted by the ethics committee of Maynooth University (BRESC-2022-2453953) and project authorization from the HPRA (AE19124/P031), in accordance with the Animal Research: Reporting of In Vivo Experiments criteria.

ARDS serum extraction

Blood samples were taken from patients with SARS-CoV-2-induced ARDS, fractionated to obtain the serum, and placed in 5 mL serum collection tubes. The samples were frozen at −20°C overnight before

Please cite this article in press as: Tunstead et al., The ARDS microenvironment enhances MSC-induced repair via VEGF in experimental acute lung inflammation, Molecular Therapy (2024), https://doi.org/10.1016/j.ymthe.2024.08.003

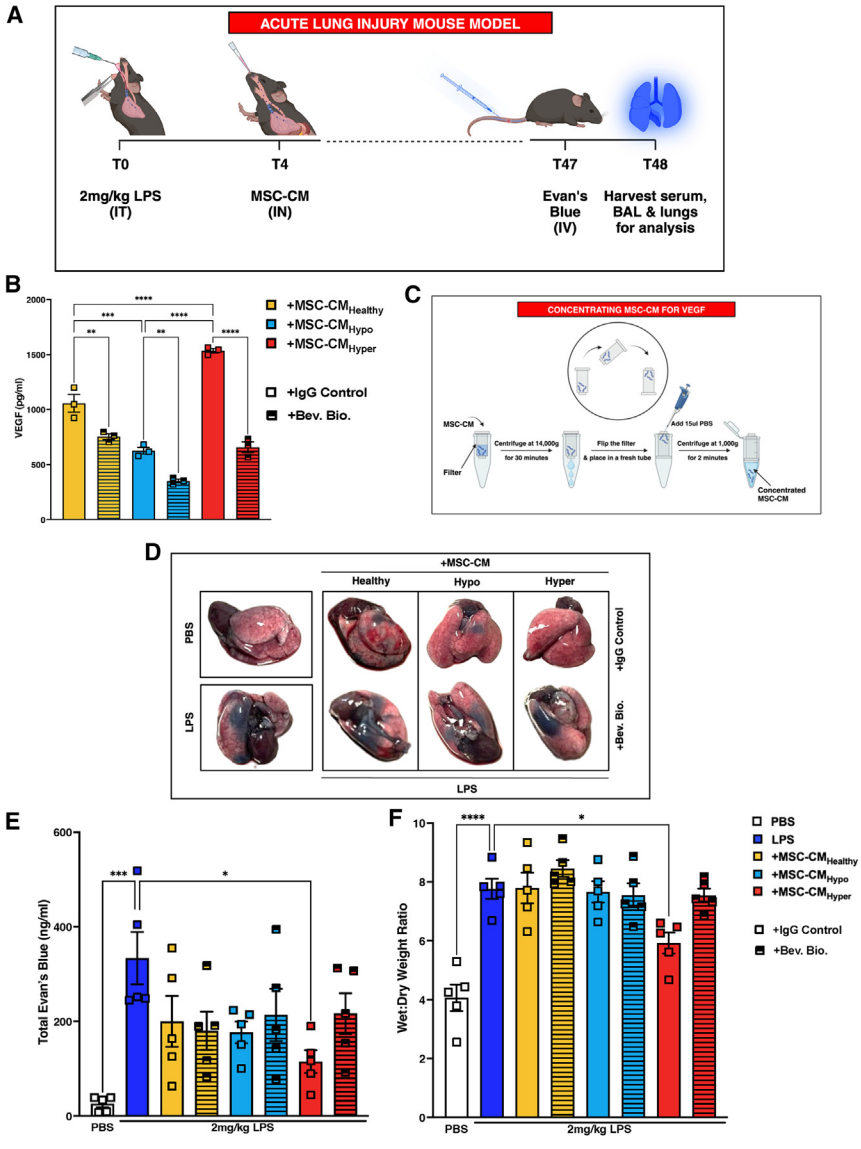

Figure 6. The impact of MSC-CM on lung permeability *in vivo*

(A) Schematic created using Biorender.com. C57BL6/J mice (n = 5) were exposed to 2 mg/kg of endotoxin intratracheally at T0. (B and C) At T4, 500 μL of MSC-CM that had been concentrated down to 30 μL (± bevacizumab biosimilar or an appropriate IgG isotype control) was administered intranasally. 1 h before harvesting (T47), a 10% solution of Evans Blue dye was administered intravenously, and mice were sacrificed at T48. (D and E) Evans Blue dye and (F) wet:dry weight ratio were used as indicators of permeability. Data are presented as mean ± SEM; n = 5 per group; $^{*}p < 0.05$, $^{**}p < 0.01$, $^{***}p < 0.001$, and $^{****}p < 0.0001$.

being transferred to −80°C. Samples were derived from both male and female patients in the age range of 40–80 years old. Healthy serum samples were sourced from St Vincent's University Hospital as a control. These samples were processed in the same manner and age matched accordingly.

ARDS patient sample pool generation

IL-6 levels were measured to stratify patient samples into either the hypo- or hyper-inflammatory ARDS sub-phenotype. Patient samples with an IL-6 level <50 pg/mL were pooled and used as a representative of hypo-inflammatory ARDS (n = 7). Patient samples with an IL-6 level > 50 pg/mL were pooled and used as a representative of hyper-inflammatory ARDS (n = 7). Once pooled, the IL-6, TNF-α (BioLegend), IL-8, and macrophage MIF (R&D) levels were analyzed via enzyme-linked immunosorbent assay (ELISA) to ensure that our hyper-inflammatory cohort has significantly more of both.

ELISA

96-well half-area ELISA plates (COSTAR) were coated as per manufacturer guidelines (human IL-6 [BioLegend], IL-8, MIF, VEGF [R&D]). The plate was then blocked with reagent diluent (1% BSA in PBS, sterile filtered) for 1 h before adding samples in appropriate dilutions for 2 h. The detection antibody was then added as per manufacturer guidelines and left for a further 1 (BioLegend) to 2 h (R&D). Streptavidin-HRP was added for 30 min, followed by a TMB substrate. The reaction was stopped using a 2N stop solution made up of $H2SO_4$ and distilled H_2O when color appeared in a gradient in the standard. The plate was washed in an automated washer (ELx50 Biotek) three times between each step and measured at absorbances of 450 and 570 nm using a CLARIOstar microplate reader.

Cell culture of hBM-MSCs

hBM-MSCs from three different donors were obtained from RoosterBio and expanded as per the manufacturer's guidelines using Rooster Nourish expansion media (Rooster Basal + Rooster Booster). Cells were further cultured in Dulbecco's modified Eagle medium (DMEM), supplemented with 10% fetal bovine serum and 1% *Penicillin streptomycin* (cDMEM), for 5 days at 37°C + 5% CO_2. All experiments were a representation of three independent MSC donors.

Generation of MSC-CM

hBM-MSCs (passage 2–4) were seeded at a density of 1×10^5 per well in a 6-well plate in 1 mL of cDMEM and left overnight to attach. Once attached, the medium was removed, and 1 mL of medium containing 20% healthy or hypo- or hyper-inflammatory ARDS serum was added to each corresponding well and left for 24 h. This medium was then removed, the cells were washed with PBS to remove any leftover serum, and serum-free DMEM was added for a further 24 h to allow

for the generation of MSC-CM. Supernatants were harvested, centrifuged at 300*g* for 5 min to remove debris, aliquoted, and stored at −20°C for future experiments.

Concentration of MSC-CM using Amicon Ultra Centrifugal Filters

For use in *in vivo* studies, the MSC-CM was concentrated into a smaller volume of liquid for administration to the mice. MSC-CM was placed in an Amicon filter of appropriate size for VEGF purification (50 kDa) and centrifuged at 14,000*g* for 30 min. The filter was then inverted, placed in a clean Eppendorf, and centrifuged at 1,000*g* for 2 min to elute the concentrated MSC-CM. This concentrate was reconstituted in the appropriate amount of PBS, and 30 μL was given, intranasally, per mouse.

Cell culture of CALU-3s

Human CALU-3 lung epithelial cells obtained from Dr. Mark Robinson (MU) were cultured in cDMEM at 37°C + 5% CO_2. The cells were split at a 1:2 ratio every 3–4 days and monitored closely.

CALU-3 stimulation

CALU-3s were seeded at a density of 5×10^5 per well in a 6-well plate and stimulated with 2 μg/mL of LPS/endotoxin or a PBS control. 24 h post-endotoxin stimulation, a 10 μM solution of SU-5416, a VEGFR2-inhibitor, or an appropriate DMSO vehicle control was added for 4 h. The cells were then washed with PBS, and the endotoxin (or PBS control) was re-added, along with 2 mL of MSC-CM (containing ∼1,000 pg/mL of VEGF) for a further 24 h. Cells were harvested in TRIzol for gene expression analysis.

Gene expression

RNA was extracted from hBM-MSCs that had been exposed to 20% healthy or hypo- or hyper-inflammatory ARDS serum. The RNA was nano-dropped to assess concentration and purity. The RNA was then normalized to 100 ng/μL, and cDNA was made using the QuantBio cDNA Synthesis kit (as per the manufacturer's instructions). Real-time PCR (RT-PCR) was then carried out using PerfeCta SYBR Green FastMix (QuantBio) and the required primers (Table S1). Expression was quantified in relation to the housekeeper gene HPRT, and the relative fold change was measured by calculating the $2^{-\Delta\Delta CT}$ values.

TEER assay

CALU-3 cells were seeded at a density of 7×10^5 per well in a 6-well Transwell insert that had been coated with 1% fibronectin for 1 h. For the first week of culture, the cells were grown in submerged conditions (cDMEM in the lower well and Transwell). For the second week, the cells were exposed to air-liquid interface culture conditions (cDMEM in the lower well only). On day 15, the cells were stimulated with 2 μg/mL of endotoxin (Serotype: 0111:B4 [Sigma]). On day 17, the medium was supplemented with 1 mL of MSC-CM. Measurements were taken using the EVOM on days 1, 3, 5, 8, 10, 12, 15, 17, and 19. The medium was changed 1 h prior to measurement. Cells were harvested in TRIzol for gene expression analysis. To analyze the TEER, a blank value (from a Transwell containing no cells) was subtracted from each value, and the values were then multiplied by the area of the well (4.67 cm^2). The relative TEER was then generated by dividing each replicate's final TEER value on day 19 by the corresponding PBS control well on day 19.

ALI mouse model

Male and female C57BL6/J mice (Charles River), aged 12–16 weeks, were given 2 mg/kg of endotoxin, or a PBS control, intratracheally and monitored closely for 48 h. MSC-CM was concentrated using Amicon Ultra Centrifugal Filters and incubated with either an anti-VEGF monoclonal antibody (bevacizumab biosimilar [InVivoSIM]) to inhibit VEGF functionality or an IgG isotype control (InVivoMAb). The MSC-CM was administered, intranasally, 4 h post-endotoxin administration.

Evans Blue dye

A 10% solution of Evans Blue tetrasodium salt (Tocris) was made up in PBS. The solution was filter sterilized, and 200 μL was injected intravenously into the tail vein of the mice. 1 h post-injection, the mice were sacrificed using an intraperitoneal injection of pentobarbital, and the blood, BALF, and lungs were harvested for analysis. The BALF was used for cytokine analysis by ELISA, and all animal scoring was graphed (weight/temperature/clinical score). To analyze this, absorbance readings were taken to assess the total Evans Blue in the lung and serum (620 and 740 nm) and compared to a serial-diluted standard of Evans Blue dye. The total lung Evans Blue was then divided by the serum Evans Blue values to account for tail vein injection error, and this was further divided by the lung wet weight to get the absolute Evans Blue concentration.[36]

Statistical analysis of animal studies

Power calculations were performed to guide sample size, and data were analyzed using GraphPad Prism 10 software. One-way ANOVA, followed by the post hoc Tukey's multiple comparison test, was used to assess significance except in Figures 6D and 6E, where a two-way ANOVA was used. All data are presented as mean ± SEM, with $n = 5$ per group.

DATA AND CODE AVAILABILITY

The data supporting the findings of this study are available upon request from the corresponding author.

SUPPLEMENTAL INFORMATION

Supplemental information can be found online at https://doi.org/10.1016/j.ymthe.2024.08.003.

ACKNOWLEDGMENTS

This research was supported by a Science Foundation Ireland Award to K.E. and J.G.L. (20/FFP-A/8948). This publication has emanated from research supported in part by the National Irish Covid Biobank, through which our patient samples were collected and stored. We would like to thank Deirdre Daly and Gillian O'Meara for the outstanding care of the animals used in this study. We would also

like to extend gratitude to Ritu Negi, who assisted in sample collection.

AUTHOR CONTRIBUTIONS

C.T. performed research, data analysis, and study design and wrote the manuscript. E.V., H.D., and I.J.H. performed research and data analysis. A.B. and B.McN. provided patient samples and data for the study. L.C. and J.C.M. provided reagents and contributed to study design and data analysis. C.C.D.S. and J.G.L. contributed to study design. K.E. designed and supervised the study and wrote the manuscript. All authors approved the final manuscript.

DECLARATION OF INTERESTS

The authors declare no competing interests.

REFERENCES

1. Matthay, M.A., and Zimmerman, G.A. (2005). Acute Lung Injury and the Acute Respiratory Distress Syndrome: Four Decades of Inquiry into Pathogenesis and Rational Management. Am. J. Respir. Cell Mol. Biol. *33*, 319–327.
2. Yang, X., Yu, Y., Xu, J., Shu, H., Xia, J., Liu, H., Wu, Y., Zhang, L., Yu, Z., Fang, M., et al. (2020). Clinical course and outcomes of critically ill patients with SARS-CoV-2 pneumonia in Wuhan, China: a single-centred, retrospective, observational study. Lancet Respir. Med. *8*, 475–481.
3. Matthay, M.A., Arabi, Y., Arroliga, A.C., Bernard, G., Bersten, A.D., Brochard, L.J., Calfee, C.S., Combes, A., Daniel, B.M., Ferguson, N.D., et al. (2024). A New Global Definition of Acute Respiratory Distress Syndrome. Am. J. Respir. Crit. Care Med. *209*, 37–47.
4. Bernard, G.R., Artigas, A., Brigham, K.L., Carlet, J., Falke, K., Hudson, L., Lamy, M., LeGall, J.R., Morris, A., and Spragg, R. (1994). Report of the American-European consensus conference on ARDS: Definitions, mechanisms, relevant outcomes and clinical trial coordination. Intensive Care Med. *20*, 225–232.
5. Richardson, S., Hirsch, J.S., Narasimhan, M., Crawford, J.M., McGinn, T., Davidson, K.W., the Northwell COVID-19 Research Consortium, Barnaby, D.P., Becker, L.B., Chelico, J.D., et al. (2020). Presenting Characteristics, Comorbidities, and Outcomes Among 5700 Patients Hospitalized With COVID-19 in the New York City Area. JAMA *323*, 2052–2059.
6. Whitehead, T., and Slutsky, A.S. (2002). The pulmonary physician in critical care * 7: Ventilator induced lung injury. Thorax *57*, 635–642.
7. ARDS Definition Task Force, Ranieri, V.M., Rubenfeld, G.D., Thompson, B.T., Ferguson, N.D., Caldwell, E., Fan, E., Camporota, L., and Slutsky, A.S. (2012). Acute respiratory distress syndrome: The Berlin Definition. JAMA *307*, 2526–2533.
8. Kaffash Farkhad, N., Sedaghat, A., Reihani, H., Adhami Moghadam, A., Bagheri Moghadam, A., Khadem Ghaebi, N., Khodadoust, M.A., Ganjali, R., Tafreshian, A.R., and Tavakol-Afshari, J. (2022). Mesenchymal stromal cell therapy for COVID-19-induced ARDS patients: a successful phase 1, control-placebo group, clinical trial. Stem Cell Res. Ther. *13*, 283.
9. Gorman, E., Shankar-Hari, M., Hopkins, P., Tunnicliffe, W.S., Perkins, G.D., Silversides, J., McGuigan, P., Krasnodembskaya, A., Jackson, C., Boyle, R., et al. (2021). Repair of acute respiratory distress syndrome by stromal cell administration (REALIST) trial: A phase 1 trial. eClinicalMedicine *41*, 101167.
10. Bowdish, M.E., Barkauskas, C.E., Overbey, J.R., Gottlieb, R.L., Osman, K., Duggal, A., Marks, M.E., Hupf, J., Fernandes, E., Leshnower, B.G., et al. (2023). A Randomized Trial of Mesenchymal Stromal Cells for Moderate to Severe Acute Respiratory Distress Syndrome from COVID-19. Am. J. Respir. Crit. Care Med. *207*, 261–270.
11. Abreu, S.C., Hampton, T.H., Hoffman, E., Dearborn, J., Ashare, A., Singh Sidhu, K., Matthews, D.E., McKenna, D.H., Amiel, E., Barua, J., et al. (2020). Differential effects of the cystic fibrosis lung inflammatory environment on mesenchymal stromal cells. Am. J. Physiol. Lung Cell. Mol. Physiol. *319*, L908–L925.
12. Hawthorne, I.J., Dunbar, H., Tunstead, C., Schorpp, T., Weiss, D.J., Enes, S.R., Dos Santos, C.C., Armstrong, M.E., Donnelly, S.C., and English, K. (2023). Human macrophage migration inhibitory factor potentiates mesenchymal stromal cell efficacy in a clinically relevant model of allergic asthma. Mol. Ther. *31*, 3243–3258.
13. Corbett, J.M., Hawthorne, I., Dunbar, H., Coulter, I., Chonghaile, M.N., Flynn, C.M., and English, K. (2021). Cyclosporine A and IFNγ licencing enhances human mesenchymal stromal cell potency in a humanised mouse model of acute graft versus host disease. Stem Cell Res. Ther. *12*, 238.
14. Dunbar, H., Weiss, D.J., Rolandsson Enes, S., Laffey, J.G., and English, K. (2021). The Inflammatory Lung Microenvironment; a Key Mediator in MSC Licensing. Cells *10*, 2982.
15. Shankar-Hari, M., Fan, E., and Ferguson, N.D. (2019). acute respiratory distress syndrome (ARDS) phenotyping. Intensive Care Med. *45*, 516–519.
16. Kitsios, G.D., Yang, L., Manatakis, D.V., Nouraie, M., Evankovich, J., Bain, W., Dunlap, D.G., Shah, F., Barbash, I.J., Rapport, S.F., et al. (2019). Host-Response Sub phenotypes Offer Prognostic Enrichment in Patients With or at Risk for Acute Respiratory Distress Syndrome. Crit. Care Med. *47*, 1724–1734.
17. Weiss, D.J., English, K., Krasnodembskaya, A., Isaza-Correa, J.M., Hawthorne, I.J., and Mahon, B.P. (2019). The Necro biology of Mesenchymal Stromal Cells Affects Therapeutic Efficacy. Front. Immunol. *10*, 1228.
18. Islam, D., Huang, Y., Fanelli, V., Delsedime, L., Wu, S., Khang, J., Han, B., Grassi, A., Li, M., Xu, Y., et al. (2019). Identification and Modulation of Microenvironment Is Crucial for Effective Mesenchymal Stromal Cell Therapy in Acute Lung Injury. Am. J. Respir. Crit. Care Med. *199*, 1214–1224.
19. Ankrum, J.A., Ong, J.F., and Karp, J.M. (2014). Mesenchymal stem cells: immune evasive, not immune privileged. Nat. Biotechnol. *32*, 252–260.
20. Smith, P., Jeffers, L.A., and Koval, M. (2019). Effects of different routes of endotoxin injury on barrier function in alcoholic lung syndrome. Alcohol *80*, 81–89.
21. Fein, A., Grossman, R.F., Jones, J.G., Overland, E., Pitts, L., Murray, J.F., and Staub, N.C. (1979). The value of edema fluid protein measurement in patients with pulmonary edema. Am. J. Med. *67*, 32–38.
22. Ware, L.B., and Matthay, M.A. (2001). Alveolar Fluid Clearance Is Impaired in the Majority of Patients with Acute Lung Injury and the Acute Respiratory Distress Syndrome. Am. J. Respir. Crit. Care Med. *163*, 1376–1383.
23. Tsikis, S.T., Fligor, S.C., Hirsch, T.I., Pan, A., Yu, L.J., Kishikawa, H., Joiner, M.M., Mitchell, P.D., and Puder, M. (2022). Lipopolysaccharide-induced murine lung injury results in long-term pulmonary changes and downregulation of angiogenic pathways. Sci. Rep. *12*, 10245.
24. Yang, J., Chen, Z., Pan, D., Li, H., and Shen, J. (2020). Umbilical Cord-Derived Mesenchymal Stem Cell-Derived Exosomes Combined Pluronic F127 Hydrogel Promote Chronic Diabetic Wound Healing and Complete Skin Regeneration. Int. J. Nanomedicine *15*, 5911–5926.
25. Yu, M., Liu, W., Li, J., Lu, J., Lu, H., Jia, W., and Liu, F. (2020). Exosomes derived from atorvastatin- pretreated MSC accelerate diabetic wound repair by enhancing angiogenesis via AKT/eNOS pathway. Stem Cell Res. Ther. *11*, 350.
26. Yang, Y., Chen, Q.H., Liu, A.R., Xu, X.P., Han, J.B., and Qiu, H.B. (2015). Synergism of MSC-secreted HGF and VEGF in stabilising endothelial barrier function upon lipopolysaccharide stimulation via the Rac1 pathway. Stem Cell Res. Ther. *6*, 250.
27. Carbone, A., Castellani, S., Favia, M., Diana, A., Paracchini, V., Di Gioia, S., Seia, M., Casavola, V., Colombo, C., and Conese, M. (2014). Correction of defective CFTR/ENaC function and tightness of cystic fibrosis airway epithelium by amniotic mesenchymal stromal (stem) cells. J. Cell. Mol. Med. *18*, 1631–1643.
28. Dutra Silva, J., Su, Y., Calfee, C.S., Delucchi, K.L., Weiss, D., McAuley, D.F., O'Kane, C., and Krasnodembskaya, A.D. (2021). Mesenchymal stromal cell extracellular vesicles rescue mitochondrial dysfunction and improve barrier integrity in clinically relevant models of ARDS. Eur. Respir. J. *58*, 2002978.
29. Park, H.J., Shin, J.Y., Kim, H.N., Oh, S.H., Song, S.K., and Lee, P.H. (2015). Mesenchymal stem cells stabilize the blood–brain barrier through regulation of astrocytes. Stem Cell Res. Ther. *6*, 187.
30. Ranjbaran, M., Kianian, F., Kadkhodaee, M., Seifi, B., Ashabi, G., Akhondzadeh, D., Adelipour, M., Izad, M., and Abdolmohammadi, K. (2022). Mesenchymal stem cells and their conditioned medium as potential therapeutic strategies in managing comorbid anxiety in rat sepsis induced by caecal ligation and puncture. Iran J. Basic Med. Sci. *25*, 690–697.

31. Tak, L.J., Kim, H.Y., Ham, W.K., Agrahari, G., Seo, Y., Yang, J.W., An, E.J., Bang, C.H., Lee, M.J., Kim, H.S., and Kim, T.Y. (2021). Superoxide Dismutase 3-Transduced Mesenchymal Stem Cells Preserve Epithelial Tight Junction Barrier in Murine Colitis and Attenuate Inflammatory Damage in Epithelial Organoids. Int. J. Mol. Sci. *22*, 6431.

32. Yang, Y., Hu, S., Xu, X., Li, J., Liu, A., Han, J., Liu, S., Liu, L., and Qiu, H. (2016). The Vascular Endothelial Growth Factors-Expressing Character of Mesenchymal Stem Cells Plays a Positive Role in Treatment of Acute Lung Injury *In Vivo*. Mediators Inflamm. *2016*, 1–12.

33. Zhang, W., Shen, Z.Y., Song, H.L., Yang, Y., Wu, B.J., Fu, N.N., and Liu, T. (2014). Protective effect of bone marrow mesenchymal stem cells in intestinal barrier permeability after heterotopic intestinal transplantation. World J. Gastroenterol. *20*, 7442–7451.

34. WHO Working Group on the Clinical Characterisation and Management of COVID-19 infection (2020). A minimal common outcome measure set for COVID-19 clinical research. Lancet Infect. Dis. *20*, e192–e197.

35. Rolandsson Enes, S., Hampton, T.H., Barua, J., McKenna, D.H., Dos Santos, C.C., Amiel, E., Ashare, A., Liu, K.D., Krasnodemskaya, A.D., English, K., et al. (2021). Healthy versus Inflamed Lung Environments Differentially effect MSCs. Eur. Respir. J. *58*, 2004149.

36. Smith, P., Jeffers, L.A., and Koval, M. (2021). Measurement of lung vessel and epithelial permeability *in vivo* with Evan's Blue. Methods Mol. Biol. *2367*, 137–148.

37. Su, Y., Guo, H., and Liu, Q. (2021). Effects of mesenchymal stromal cell-derived extracellular vesicles in acute respiratory distress syndrome (ARDS): current understanding and future perspectives. J. Leukoc. Biol. *110*, 27–38.

38. Matthay, M.A., Goolaerts, A., Howard, J.P., and Lee, J.W. (2010). Mesenchymal stem cells for acute lung injury: preclinical evidence. Crit. Care Med. *38*, 569–573.

39. Zhu, Y.G., Feng, X.M., Abbott, J., Fang, X.H., Hao, Q., Monsel, A., Qu, J.M., Matthay, M.A., and Lee, J.W. (2014). Human mesenchymal stem cell microvesicles for treatment of Escherichia coli endotoxin-induced acute lung injury in mice. Stem Cells *32*, 116–125.

40. Shah, T.G., Predescu, D., and Predescu, S. (2019). Mesenchymal stem cells-derived extracellular vesicles in acute respiratory distress syndrome: a review of current literature and potential future treatment options. Clin. Transl. Med. *8*, 25.

41. Lee, J.W., Krasnodembskaya, A., McKenna, D.H., Song, Y., Abbott, J., and Matthay, M.A. (2013). Therapeutic effects of human mesenchymal stem cells in ex vivo human lungs injured with live bacteria. Am. J. Respir. Crit. Care Med. *187*, 751–760.

42. Faircloth, T.U., Temple, S., Parr, R.N., Tucker, A.B., Rajan, D., Hematti, P., Kugathasan, S., and Chinnadurai, R. (2024). Vascular endothelial growth factor secretion and immunosuppression are distinct potency mechanisms of human bone marrow mesenchymal stromal cells. Stem Cells *42*, sxae040.

The PPARβ/δ-induced mesenchymal stromal cell secretome has cytoprotective effects via ANGPTL4 in a pre-clinical model of acute lung inflammation

Courteney Tunstead[1], Molly Dunlop[1], Sinéad Ryan[1], Evelina Volkova[1], Evangeline Johnston[1], Sabrina Batah[2], Claudia C. Dos Santos[2], Bairbre McNicholas [3,4], Claire Masterson[3,4], John G. Laffey[3,4] & Karen English[1,5]

[1]*Cellular Immunology Lab, Department of Biology, Maynooth University, Maynooth, Co. Kildare, Ireland.*

[2] *Keenan Research Centre for Biomedical Research, St. Michael's Hospital, Toronto, Canada.*

[3]*Anesthesia and Intensive Care Medicine, School of Medicine, College of Medicine Nursing and Health Sciences, University of Galway, Galway, Ireland.*

[4]*Anesthesia and Intensive Care Medicine, Galway University Hospitals, Saolta University Hospitals Groups, Galway, Ireland.*

[5]*Kathleen Lonsdale Institute for Human Health Research, Maynooth University, Maynooth, Co. Kildare, Ireland.*

ABSTRACT

Rationale: Human bone marrow-derived mesenchymal stromal cells (hBM-MSCs) are known to exert immunomodulatory and pro-reparative effects *in vivo*. This makes hBM-MSCs an enticing therapeutic candidate for inflammatory diseases, such as acute respiratory distress syndrome (ARDS). The ARDS microenvironment is complex and contains an abundance of free fatty-acids (FFAs); which are known to differentially impact MSC functionality. PPARβ/**δ** is a ubiquitously expressed nuclear receptor that is activated in response to FFA-binding. It has shown to impact the therapeutic efficacy of mouse MSCs. **Objective:** This study sought to investigate the impact of PPARβ/**δ**-modulation on MSC functionality *in vitro* and *in vivo*. **Methods:** hBM-MSCs were exposed to a synthetic PPARβ/**δ** agonist/antagonist in the presence or absence of ARDS patient serum and the immunomodulatory and pro-reparative capacity of the MSC secretome was investigated using *in vitro* assays, and a pre-clinical model of LPS-induced acute lung inflammation (ALI). **Results:** Our results highlighted that the secretome from PPARβ/**δ**-agonised hBM-MSCs had enhanced pro-reparative capacity in CALU-3 lung epithelial cells by promoting the secretion of angiopoietin-like 4 (ANGPTL4). This PPARβ/**δ**-induced ANGPTL4-high MSC secretome also showed enhanced cytoprotection, wound repair, and reduced pro-inflammatory cytokines in the bronchoalveolar lavage fluid (BALF) of mice in a pre-clinical model of ALI. Importantly LPS-ALI mice that received PPARβ/**δ**-induced ANGPTL4-high MSC secretome had reduced clinical score and weight loss. This was confirmed using an anti-ANGPTL4 antibody. **Conclusion:** These findings conclude that the PPARβ/**δ**-induced ANGPTL4-high MSC secretome has anti-inflammatory, reparative and cytoprotective effects in a pre-clinical model of ALI.

INTRODUCTION

Cell therapy, particularly mesenchymal stromal cell (MSC) therapy, has long been thought of as a therapeutic candidate in the treatment of many inflammatory diseases. This is largely due to their immunomodulatory and cytoprotective capacity [1]. One of the conditions that MSCs have been considered for is acute respiratory distress syndrome (ARDS); an inflammatory, degenerative condition of the lung [2, 3]. MSCs have been trialled and tested for ARDS over the last 20 years, but clinical trials have shown poor outcomes; with ~60% non-responders [4-6]. The environment into which MSCs are administered can alter their functional capacity [7-9]. There is limited understanding of how the ARDS microenvironment may impact MSCs. The complex ARDS microenvironment contains inflammatory-mediators, microorganisms, and free fatty acids (FFAs). These components have all been shown to impact MSC therapeutic capacity in various ways [10, 11]. Our previous work highlighted the differential effect of the hypo-inflammatory vs hyper-inflammatory ARDS microenvironment on MSC therapeutic efficacy. This work showed a clear correlation between high levels of inflammation, and enhanced MSC-driven repair [12]. We, and others, have also demonstrated that FFAs can influence MSC-induced immunosuppressive effects [13, 14]. In this study, we wanted to investigate the influence of FFAs present in the ARDS patient microenvironment, and the impact they have on hBM-MSCs in a pre-clinical model of acute lung inflammation (ALI).

The peroxisome proliferator-activated receptor-beta/delta (PPARβ/**δ**) is a ubiquitously-expressed nuclear receptor, present on all nucleated cells including hBM-MSCs, that is activated in response to FFA exposure [15, 16]. In recent years, PPARβ/**δ** has been shown to impact MSC therapeutic efficacy [17-27]. Interestingly, there are differential findings with some studies showing that deficiency of PPARβ/**δ** enhances MSC immunosuppressive effects [21, 22], while other studies demonstrate similar immunosuppressive effects mediated by both

naive and PPARβ/**δ**-deficient mouse MSCs [24]. Studies have shown enhanced immunomodulatory capacity of T-cells by PPARβ/**δ**-inhibited mouse MSCs [21, 22]. Differentialy, PPARβ/**δ** antagonism of MSCs impaired MSC therapeutic effects while priming of mouse MSCs with a PPARβ/**δ** agonist enhanced MSC cardioprotective effects *in vivo* [25]. Moreover, cardioprotective effects of MSCs were shown to be PPARβ/**δ**-dependent as the therapeutic effect was lost when PPARβ/**δ**-deficient mouse MSCs were administered [24]. These findings suggest that natural ligands of PPARβ/**δ** may have positive or detrimental effects on MSC efficacy *in vivo*. Due to the abundance of FFAs in the ARDS microenvironment, we sought to investigate the impact of PPARβ/**δ** (via synthetic agonism or antagonism) on the human BM-MSC secretome; and report the impact this had on immunomodulation and cytoprotection, in a model of ALI.

MATERIALS AND METHODS

hBM-MSC cell culture

Human bone marrow-derived MSCs (hBM-MSCs; RoosterBio™) were cultured in Dulbecco's Modified Eagle Medium (DMEM) containing 10% Foetal Bovine Serum (FBS) and 1% *Penicillin streptomycin* (cDMEM). The cells were cultured for 5 days at 37°C + 5% CO_2. All experiments are a representation of three independent MSC donors.

Generation and concentration of MSC-CM

hBM-MSCs (passage 2-5) from three independent donors were seeded at a density of $1x10^5$ per well in a 6-well plate in 1ml of cDMEM and left to attach. Once attached, the cells were stimulated with 1µM of PPARβ/**δ** agonist (GW0742, Tocris™) or antagonist (GSK3787, Tocris™), as previously done in our group [12]. 24hr-post stimulation, the cells were washed with PBS, and the media was replaced with serum-free DMEM. This was left for a further 24hrs to allow for the generation of MSC-CM. When including ARDS serum-exposure, the agonist/antagonist were washed from the cells, and 20% ARDS serum was added for 24hrs. This was then washed away, and serum-free DMEM was added for a further 24hrs to allow for the generation of MSC-CM. All MSC-CM was harvested and stored at -20°C for future experiments. MSC-CM was then concentrated, as required, as previously described [12].

Gene & Protein expression

For gene expression, RNA was isolated and normalised to 100 ng/µl. cDNA was made using the QuantBio™ cDNA Synthesis kit (as per manufacturer's instructions). Real-time Polymerase Chain Reaction (RT-PCR) was run using PerfeCta SYBR Green FastMix (QuantBio™) and pre-made Sigma™ primers (supplementary table 1). Relative expression

was quantified in relation to *hprt* by calculating the 2-ΔΔCT values. For protein expression, 96-well half-area ELISA plates (COSTAR™) were coated as per manufacturers guidelines (human ANGPTL4 and VEGF (R&D™)) and run as previously described [12].

Sequencing & metabolomic analysis

hBM-MSCs were seeded at a density of $1x10^5$ in a 6-well plate and left to adhere. Once attached, the cells were exposed to 1μM of PPARβ/**δ** agonist (GW0742, Tocris™) or antagonist (GSK3787, Tocris™) and left for 6hrs. This dose was chosen based on previous research from our group [19]. The cells were harvested in TRIzol for RNA isolation. RNA was isolated through a series of chloroform and isopropanol extractions. RNA concentration and purity was assessed using Nanodrop 2000 (Thermofisher) and samples were sent to Novogene™ for sequencing (GEO accession no.: GSE281162). Processed RNA sequencing datasets, provided by Novogene™, were then used to identify differentially expressed genes (DEGs) of interest. Volcano plots, highlighting the most significantly enriched genes, were generated using Flourish™ software. Data was also collected from publicly available RNA sequencing (GEO accession no.: GSE185263) and metabolomic datasets (Study ID: ST000042; doi: 10.21228/M8SG64). Normalised values were taken from both studies and data was plotted using GraphPad Prism™ (version 10) software.

Scratch Assay

CALU-3 lung epithelial cells (cultured as previously described) [12] were seeded at a density of $5x10^5$ in a 6-well plate. Once 80% confluent, a single vertical scratch was made down the centre of the well using a p200 tip. The cells were then washed with PBS to remove debris, and MSC-CM was added for a period of 6-48hrs. The cells were then fixed with 10% formalin, before leaving to dry. Once dry, the cells were stained with crystal violet, left to dry, and

imaged. To avoid bias, a marker was used to denote an area in the upper, central and lower regions of each scratch and images were taken from these points (supplementary figure 1). Mitomycin C (Sigma™) was added to assess the impact of proliferation at a concentration of 5 µg/ml for 2hrs prior to the scratch assay.

Scratch Assay Analysis

Three images, taken at each of the three marked points, were taken per well; for each of the three independent MSC donors (i.e. 3 images per well x 3 MSC donors = 9 images per group). Fiji/ImageJ™ software was then used to divide each picture into four distinct quadrants in an unbiased manner (Analyse -> Tools -> Grid -> set area per point to 44444 inches squared). This grid includes the addition of 4 horizontal lines imputed on the image. Using the straight-line feature in Fiji/ImageJ™ software, four measurements were then taken per picture at each of the horizontal lines. This provided 4 measurements per picture, at unbiased points, to get a clear depiction of each percentage wound closure. The average wound closure per donor was calculated, and divided by the baseline scratch value, to get the final percentage wound closure (supplementary figure 1).

Study cohorts and ethical approval for patient samples

Ethical approval was obtained from Galway University Medical Ethics Committee and Maynooth University Ethics Committee. All participants provided full consent.

ARDS serum extraction

Serum samples from both male and female patients, aged 40-80 years old, were taken from patients with SARS-CoV-2-induced ARDS, from the patient pools we previously characterised and described [12].

ANGPTL4 Neutralisation

MSC-CM was exposed to 5 µg/ml of ANGPTL4 neutralising antibody (Cell Sciences™), or 5 µg/ml IgG2aκ isotype control (Rockland Immunochemicals™). This was incubated at room temperature for 1hr prior to use. This concentration was utilised as per manufacturer guidelines for our study.

ALI mouse model

Male and female C57BL6/J mice (Charles River), aged 8+ weeks, 2mg/kg of endotoxin (Sigma, 0001:B4 Serotype), or PBS control, was administered intratracheally (IT) and observed twice daily for 48hrs. MSC-CM was prepared as described above. 500µl of PPARβ/**δ**-modulated MSC-CM, i.e. the equivalent of what would be produced from $5x10^4$ (low dose) of hBM-MSCs, was then concentrated to a volume of 30µl and administered intranasally (IN) 4hrs post-endotoxin challenge per mouse. An Evan's Blue permeability assay was carried out by administration of an intravenous (IV) tail vein injection of sterile-filtered Evan's Blue Dye (10%) 1hr prior to harvesting. The mice were sacrificed using an intraperitoneal (IP) injection of pentobarbital. Absorbance readings were taken to assess the total Evan's blue (620nm and 740nm) in BALF, blood and whole lungs.

Statistical analysis of animal studies

Power calculations were performed to guide sample size and data was analysed using GraphPad Prism™ (version 10) software. Statistical tests used have been highlighted in the figure legends of each figure.

RESULTS

The MSC$_{PPAR\beta/\delta(+)}$ secretome enhances pro-reparative capacity in CALU-3 lung epithelial cells via migration and proliferation *in vitro*

A scratch assay in CALU-3 cells was used to investigate the impact of PPARβ/**δ** agonism (+) or antagonism (-) on MSC conditioned medium (MSC-CM) capacity to promote wound healing *in vitro* (figure 1A). Our data highlighted a significant increase in wound closure in both MSC-CM$_{Naive}$ and MSC-CM$_{PPAR\beta/\delta(+)}$ groups (figure 1B, C). It is known that wound closure can involve proliferation and or migration [28, 29], thus this experiment was repeated using Mitomycin C; a known proliferation inhibitor [30]. While the addition of Mitomycin C significantly reduced wound closure in the MSC-CM$_{Naive}$ and MSC-CM$_{PPAR\beta/\delta(+)}$ groups at the 48hr time point, the percentage wound healing in these groups with Mitomycin C remained higher than the DMEM only group suggesting that both proliferation and migration had a combination effect (figure 1D). Interestingly, significantly more wound repair was observed in our MSC-CM$_{PPAR\beta/\delta(+)}$ group compared to our MSC-CM$_{Naive}$ group, while the MSC-CM$_{PPAR\beta/\delta(-)}$ group did not inhibit or enhance would healing (figure 1D). *TOP2A is* a gene largely indicative of cell proliferation [31] and has previously been used as an indicator for cell proliferation in wound healing. Gene expression analysis of *TOP2A* in CALU-3 cells highlighted a significant difference between the MSC-CM$_{PPAR\beta/\delta(+)}$ and MSC-CM$_{PPAR\beta/\delta(-)}$ groups, with the MSC-CM$_{PPAR\beta/\delta(+)}$ group having significantly more proliferative capacity than the MSC-CM$_{PPAR\beta/\delta(+)}$ group (figure 1E).

Analysis of MSC$_{PPAR\beta/\delta(+)}$ RNA sequencing highlighted upregulation of several genes

To try to identify the potential mechanisms associated with enhanced wound healing capacity in MSC$_{PPAR\beta/\delta(+)}$, RNA sequencing (Novogene™; GEO accession no.: GSE281162) was

performed on $MSC_{PPARβ/δ(+)}$, $MSC_{PPARβ/δ(-)}$ and MSC_{Naive} (figure 2A). The data highlighted a variety of differentially expressed genes (DEGs) between the three groups. The DEGs were visualised using a Venn diagram (figure 2B), showing 170 DEGs specific to the MSC_{Naive} group, 128 specific to the $MSC_{PPARβ/δ(+)}$ group, and 189 specific to the $MSC_{PPARβ/δ(-)}$ group. Volcano plot visualisation highlighted several of the most significantly altered DEGs in each group (figure 2C). The $MSC_{PPARβ/δ(+)}$ group had a significant enrichment of genes such as *PLIN2, ANGPTL4, FAM156A, CPT1A, CAT, NADK2, TMED6,* and *LDHAL6B*. This group also showed significant downregulation in genes such as *MAGED4* and *FAM157B* (table 1). The $MSC_{PPARβ/δ(-)}$ group had a significant enrichment of genes such as *IKBKGP1, SNRPGP2, LINC01159, MIR3648-1, RARRES1, MALAT1* and *RNF217-AS1*. This group also showed significant downregulation in genes such as *RGPD5, PFN1P3, MIR3936HG, U2AF1* and *TSNAXIP1*(table 2). Fragments per kilobase of exon per million mapped fragments (FPKMs) of two known PPARβ/**δ** target genes were plotted to confirm the data was as expected (figure 2D, E), and this was confirmed by qRT-PCR (figure 2F, G).

MSC-associated genes/proteins are unaffected by PPARβ/δ agonism or antagonism; except ANGPTL4

Given the functional enhancement of MSC-$CM_{PPARβ/δ(+)}$ promotion of wound healing observed in figure 1, the production of known cytoprotective factors released by MSCs were assessed. While MSC_{Naive} produced ANGPTL4, VEGF and MIF, $MSC_{PPARβ/δ(+)}$ only produced significantly higher levels of ANGPTL4 (figure 3A-C). This aligns with the RNA-sequencing data as *ANGPTL4* was the only cytoprotective factor differentially expressed in $MSC_{PPARβ/δ(+)}$. Along with this, PPARβ/**δ** agonism/antagonism did not affect expression of typical MSC-associated immunomodulatory factors such as *PTGS2, IL-6, IDO, PTGES* or *TGFβ (figure 3D-H)*.

The MSC-CM$_{PPARβ/δ(+)}$ enhances wound healing in CALU-3 lung epithelial cells in an ANGPTL4-dependent manner

Other studies have highlighted the role of a PPARβ/**δ** agonist in repair [18], and the impact ANGPTL4 can have on repair in other tissues [29, 32]. It has also already been shown that ANGPTL4 can play a significant role in proliferation and migration [28]. To determine if the increased levels of ANGPTL4 present in MSC-CM$_{PPARβ/δ(+)}$ was the true mechanism behind the enhanced pro-reparative capacity, we made use of an anti-ANGPTL4 neutralising-antibody to eliminate the functional capacity of ANGPTL4 in the MSC-CM (figure 4A). This would prevent it from acting on the CALU-3 lung epithelial cells. Scratch assay analysis from each of our groups, whereby the MSC-CM used was exposed to either the ANGPTL4 neutralising antibody or a corresponding IgG control, highlighted that ANGPTL4-neutralisation abrogated the enhanced wound closure once seen in the MSC-CM$_{PPARβ/δ(+)}$ group (figure 4B-C). The ability of the ANGPTL4 neutralising antibody to interfere with ANGPTL4 was quantified by ELISA (figure 4D).

Ligands and co-activators of PPARβ/δ are increased, while co-repressors of PPARβ/δ are decreased, in ARDS patients

Thus far, PPARβ/**δ** agonism has shown to enhance the cytoprotective effects of MSC-CM. Previously, it was deduced that MSC-CM derived from ARDS-serum licensed MSCs has superior therapeutic effects in a pre-clinical model of ALI [12]. To ensure translational relevance of our findings from this study in human conditions such as ARDS, a publicly available metabolomics dataset (Study ID: ST000042; doi: 10.21228/M8SG64) was mined and it was identified that PPARβ/**δ** ligands are more prevalent in ARDS. Higher levels of linoleate, palmitoleic acid and arachidonate were present in the bronchoalveolar lavage fluid (BALF)

from ARDS patients, in comparison to healthy controls (figure 5A). Using a publicly available RNA sequencing dataset (GEO accession no.: GSE185263), it was shown that several PPARβ/**δ**-associated co-activators that were increased in the blood of ARDS patients (figure 5B). This included a significant increase in *NCOA1* and *NCOA3,* a trend toward increased *PPARGC1A* and *NCOA2,* and no difference in *CREBBP* (figure 5C-G). Along with this, several PPARβ/**δ**-associated co-repressors were decreased in the blood of the same ARDS patients (figure 5B). This included a significant reduction in *SIRT1, NCOR1* and *NCOR2* (figure 5H-J). Given that *ANGPTL4* was significantly upregulated in the sequencing dataset, this was further assessed upon MSC-exposure to ARDS patient serum. In comparison to the PPARβ/**δ** agonist, exposure of MSCs to ARDS patient serum significantly increased MSC secretion of ANGPTL4. Addition of both the PPARβ/**δ** agonist and ARDS patient serum further enhanced MSC production of ANGPTL4 (figure 5K). Interestingly, addition of the PPARβ/**δ** antagonist could not block the ARDS serum induction of ANGPTL4 secretion by MSCs. This is largely down to PPARβ/**δ** having multiple binding-sites [33], whereby both agonists and antagonists can bind simultaneously; with agonism always out-competing antagonism (supplementary figure 2).

ARDS-licensed MSC-CM$_{PPARβ/δ(+)}$ provides enhanced therapeutic effects in ALI in an ANGPTL4 dependent manner

Next, investigation into the protective effects of MSC-CM$_{PPARβ/δ(+)}$ were assessed in a preclinical model of LPS induced-ALI. In a pilot study, a low dose of MSCs (5 x 10^4) with reduced therapeutic efficacy was determined in ALI, alongside a higher dose of MSCs (1x10^5) demonstrating efficacy (supplementary figure 3). Following this, MSC-CM that was generated from the equivalent of the low dose was used; with the idea that we would detect enhanced therapeutic efficacy following PPARβ/**δ** agonism or antagonism. This showed that MSC-

CM$_{PPARβ/δ(+)}$ but not MSC-CM$_{PPARβ/δ(-)}$ significantly improved the therapeutic efficacy of the non-efficacious dose of MSC-CM; by enhancing vascular and epithelial barrier function as measured using Evans blue dye assay (figure 6A, B). Although modest, this result was statistically powered. This effect was somewhat impacted by pre-exposing the MSC-CM to anti-ANGPTL4 neutralising antibody, but this was not significantly different from the MSC-CM$_{PPARβ/δ(+)}$ group (figure 6A, B). MSC-CM$_{PPARβ/δ(+)}$ also significantly reduced the level of TNFα in the BALF of LPS-exposed mice (figure 6C). However, ANGPTL4-neutralisation could not reverse this effect (figure 6C). MSC-CM$_{PPARβ/δ(+)}$ had no effect on IL-6 (figure 6D) or total protein (figure 6E) in the BALF. Interestingly exposure to ARDS patient serum, along with PPARβ/**δ** agonism, allowed for a 10-fold increased induction of ANGPTL4 in MSC-CM compared to PPARβ/**δ** agonist alone (figure 5K). Other proteins examined including IL-6, IL-8, VEGF, IL-1β and MIF (supplementary figure 4) were not increased in MSCs that had been exposed to ARDS patient serum, along with PPARβ/**δ** agonism. Next, investigation into the efficacy of ARDS-licensed MSC-CM$_{PPARβ/δ(+)}$ in the ALI model. In this case, the combination of ARDS serum and PPARβ/**δ** agonism led to significantly enhanced therapeutic effects with significant reduction in TNFα and IL-6 in the BALF (figure 6C, D). Importantly, anti-ANGPTL4 reduced the anti-inflammatory effects mediated by the ARDS-licensed MSC-CM$_{PPARβ/δ(+)}$. Although there was no significant reduction in total protein, the trend toward a reduction in total protein was abrogated in the presence of the anti-ANGPTL4 neutralising antibody (figure 6E).

ARDS-licensed MSC-CM$_{PPARβ/δ(+)}$ reduced the severity of the clinical score and percentage weight-loss in ALI in an ANGPTL4 dependent manner

Following on from our pre-clinical study, the clinical scores and percentage weight-loss were plotted (figure 6F, G). Interestingly, we saw a non-significant trend toward a reduced clinical

score in mice exposed to ARDS-licensed MSC-CM$_{PPAR\beta/\boldsymbol{\delta}(+)}$ (figure 6F) and this was not seen in the non-licensed group. ANGPTL4-neutralisation abrogated this effect (figure 6F). Along with this, percentage weight-loss was also observed. There was a significant reduction in percentage weight-loss in mice exposed to ARDS-licensed MSC-CM$_{PPAR\beta/\boldsymbol{\delta}(+)}$ (figure 6G), and again, this effect was abrogated in the presence of the anti-ANGPTL4-neutralising antibody (figure 6G).

DISCUSSION

There are two primary functions of MSCs in the context of cell therapy: immunomodulation and pro-repair [1]. It is known that the environment can largely dictate MSC response [7, 11, 34]. In the context of ARDS, the complex patient microenvironment; containing inflammatory-agents, microorganisms and FFAs, can notably impact MSC functionality [10, 35]. We previously highlighted that higher levels of inflammation in the ARDS patient microenvironment can promote VEGF-driven repair [12]. Abreu *et al.* (2020) investigated the detrimental impact of fungal toxins present in the lung on MSC viability and showed a drastic increase in MSC cell-death in response to this microenvironmental element [7]. However, there has been little focus on how the FFAs in the ARDS patient microenvironment may impact MSCs [36]. FFAs are known natural ligands of PPARβ/**δ** [37-39]. Importantly, studies have already shown that modulation of this receptor can alter MSC functionality [17, 20, 21, 23, 25]. Given this, we wanted to investigate the functional impact of PPARβ/**δ**-modulation on both primary functions of MSCs; immunomodulation and/or pro-reparative capacity.

In the case of pro-reparative capacity, PPARβ/**δ**-activation enhanced MSC-CM mediated wound repair in CALU-3 lung epithelial cells (figure 1B, C). A time-lapse

experiment, using a mitomycin C proliferation inhibitor, highlighted that this was likely a combination effect of both migration and proliferation (figure 1D, E). In the context of promoting tissue repair, MSC secretion of VEGF [40-43], and HGF [44, 45] among other factors have been shown to play key roles. However, PPARβ/**δ**-activation did not lead to differential expression of VEGF or HGF. Interestingly, ANGPTL4 was significantly increased in PPARβ/**δ** agonised MSCs. It has already been shown in several studies that ANGPTL4 can promote both migration and proliferation in endothelial cells [28, 29]. Ziveri *et al.* (2024) recently published a comprehensive study on the role of ANGPTL4 in endothelial cytoprotection in skin vs brain endothelial cells. They identified that ANGPTL4 in the brain endothelium protects against bacterial sepsis, and upon addition of ANGPTL4 to the skin endothelium (which naturally has lower levels of ANGPTL4), they demonstrated protection against bacterial sepsis [27]. Moreover, ANGPTL4 has been shown to improve cardiac function in a mouse model of myocardial infarction [46]. Human MSCs produced increased levels of ANGPTL4 following co-culture with THP-1 macrophages *in vitro* [46]. Based on the identification of increased expression of ANGPTL4 in PPARβ/**δ** agonised MSCs in our RNA-seq data set, we used an anti-ANGPTL4 antibody to neutralise the ANGPTL4 in the MSC secretome, before addition to the CALU-3 lung epithelial cells (figure 4B-D). This abrogated the enhanced wound closure we had originally observed in our MSC-CM$_{PPAR\beta/\delta(+)}$ group.

We identified increased levels of PPARβ/**δ** ligands and co-activators in ARDS patient samples using publicly available datasets. Exposure of MSCs to ARDS patient serum samples significantly increased ANGPTL4 levels. A combination of MSC exposure to ARDS patient serum and a PPARβ/**δ** agonist further increased ANGPTL4 levels. This proves that MSCs are receptive to FFAs/other PPARβ/**δ** ligands presents in the ARDS microenvironment. This aligns to our previous study where we identified that human BM-MSCs produce significantly increased levels of ANGPTL4 in response to the FFA palmitate [14].

To enhance the clinical relevance of our findings, we showed that MSC-CM$_{PPARβ/δ(+)}$ mediated protective effects in ALI significantly enhancing vascular and epithelial barrier integrity *in vivo*. Indeed, other studies have demonstrated that MSC-CM can mediate therapeutic effects *in vivo* in ALI models [47] including our own study [12]. Using MSC-CM generated from the equivalent of half the dose of MSC-CM used in our previous study [12]. This allowed us to observe whether MSC-CM$_{PPARβ/δ(+)}$ provided enhanced efficacy over and above MSC-CM$_{PPARβ/δ(-)}$ in a pre-clinical model of ALI. While there was a significant difference in the capacity for MSC-CM$_{PPARβ/δ(+)}$ in enhancing barrier function, addition of the ANGPTL4-neutralising antibody failed to significantly impair this effect. Our study demonstrated that ARDS patient serum induced significantly higher levels of ANGPTL4 in MSC-CM and that combination with a PPARβ/**δ** agonist further increased it. While MSC-CM$_{PPARβ/δ(+)}$ did not significantly reduce proinflammatory cytokines in the BALF, ARDS licensed MSC-CM$_{PPARβ/δ(+)}$ significantly reduced TNFα in the BALF of ALI mice. By combining the PPARβ/**δ** agonist and licensing with ARDS patient serum, we created MSC-CM with greater immunosuppressive capacity when compared to MSC-CM$_{PPARβ/δ(+)}$ alone. This is likely associated with the ~10-fold increase in ANGPTL4 levels when using the combined licensing approach as addition of the ANGPTL4 neutralising antibody reversed the trend.

Here we provide novel findings to demonstrate that human BM-MSCs are responsive to FFAs present in the ARDS patient environment, leading to significantly increased levels of ANGPTL4 production. For the first time, we show that MSC-derived ANGPTL4 plays an important role in promoting epithelial repair and enhancing vascular barrier integrity. As most published studies have focused on mouse MSCs, we have also addressed the gap in the knowledge of how PPARβ/**δ** influences human BM-MSC cytoprotective and immunosuppressive functions. In this study, focusing on ALI, we did not detect any positive

or negative effects associated with PPARβ/**δ** antagonism in hBM-MSCs. However, PPARβ/**δ** agonism enhanced MSC-CM promotion of wound healing *in vitro* and vascular and barrier integrity *in vivo*. Furthermore, the combined approach of PPARβ/**δ** agonism and licensing with ARDS patient serum produced an MSC-CM that could suppress pro-inflammatory cytokines in the BALF of ALI mice.

Author Contributions

C.T. performed research, data analysis, and study design and wrote the manuscript. M.D., S.R., E.V., E.J., S.B. and C.M. provided expertise and or performed research and data analysis. B.McN and J.G.L. provided patient samples and data for the study. C.C.D.S and J.G.L. contributed to study design. K.E. designed and supervised the study and wrote the manuscript. All authors approved the final manuscript.

Funding

This research was supported by a Science Foundation Ireland Award to K.E. and J.G.L (20/FFP-A/8948). This publication has emanated from research supported in part by the National Irish Covid Biobank, through which our patient samples were collected and stored.

Competing interests

The authors declare no conflicts of interest.

Ethical Approval and HPRA Compliance

Ethical approval was granted by the Maynooth University research ethics committee (BRESC-2022-2453953) under the title: Cell based therapeutics for acute respiratory distress syndrome for the animal studies and by Galway University Hospitals Research Ethics Committee and by

the Maynooth University research ethics committee (BSRESC-2022-2482563) under the title: Human serum Sepsis/ARDS MSC. HPRA approval was granted under the project authorisation(s) AE19124/P031/P037.

Data availability statement

The RNA-sequencing dataset generated in our lab is available through GEO accession no.: GSE281162. The other publicly available data sets are available online as outlined in the Methods section. The remaining data supporting the findings of this study are available upon request from the corresponding author.

Acknowledgements

The authors are grateful to the ARDS patients who donated the samples used in this study. We would like to thank Deirdre Daly and Gillian O'Meara for the outstanding care of the animals used in this study. Schematic figures contained in this manuscript have been created using biorender.com.

Table 1: DEG functions in MSC$_{PPAR\beta/\delta(+)}$ group.

Gene name	Up/Down	Involved in
plin2	Up	Lipid metabolism
angptl4	Up	Lipid metabolism and angiogenesis
fam156A	Up	Enables protein binding
cpt1A	Up	Lipid metabolism
cat	Up	Protection against oxidative stress

nadk2	Up	Protection against oxidative stress
tmed6	Up	Trafficking and transport
ldhal6B	Up	Lactate metabolism
maged4	Down	Cell cycle regulation
fam157B	Down	Non-coding

Table 2: DEG functions in MSC$_{PPAR\beta/\delta(-)}$ group.

Gene name	**Up/Down**	**Involved in**
ikbkgp1	Up	NFκB signalling
snrpgp2	Up	RNA processing
linc01159	Up	Cell differentiation
mir3648-1	Up	Cell differentiation
rarres1	Up	Cell differentiation & retinoid signalling
malat1	Up	Cell differentiation
rnf217-as1	Up	Cell differentiation
rgpd5	Down	GTPase regulation
pfn1p3	Down	Cell motility/migration
mir3936hg	Down	Proliferation and apoptosis
u2af1	Down	ROS production/oxidative stress
tsnaxip1	Down	RNA processing and transport

REFERENCES

1. Faircloth, T.U., et al., *Vascular endothelial growth factor secretion and immunosuppression are distinct potency mechanisms of human bone marrow mesenchymal stromal cells.* Stem Cells, 2024. **42**(8): p. 736-751.
2. Matthay, M.A. and G.A. Zimmerman, *Acute lung injury and the acute respiratory distress syndrome: four decades of inquiry into pathogenesis and rational management.* Am J Respir Cell Mol Biol, 2005. **33**(4): p. 319-27.
3. Yang, X., et al., *Clinical course and outcomes of critically ill patients with SARS-CoV-2 pneumonia in Wuhan, China: a single-centered, retrospective, observational study.* Lancet Respir Med, 2020. **8**(5): p. 475-481.
4. Kaffash Farkhad, N., et al., *Mesenchymal stromal cell therapy for COVID-19-induced ARDS patients: a successful phase 1, control-placebo group, clinical trial.* Stem Cell Res Ther, 2022. **13**(1): p. 283.
5. Bowdish, M.E., et al., *A Randomized Trial of Mesenchymal Stromal Cells for Moderate to Severe Acute Respiratory Distress Syndrome from COVID-19.* Am J Respir Crit Care Med, 2023. **207**(3): p. 261-270.
6. Gorman, E., et al., *Repair of acute respiratory distress syndrome by stromal cell administration (REALIST) trial: A phase 1 trial.* EClinicalMedicine, 2021. **41**: p. 101167.
7. Abreu, S.C., et al., *Differential effects of the cystic fibrosis lung inflammatory environment on mesenchymal stromal cells.* Am J Physiol Lung Cell Mol Physiol, 2020. **319**(6): p. L908-L925.
8. Hawthorne, I.J., et al., *Human macrophage migration inhibitory factor potentiates mesenchymal stromal cell efficacy in a clinically relevant model of allergic asthma.* Mol Ther, 2023. **31**(11): p. 3243-3258.

9. Corbett, J.M., et al., *Cyclosporine A and IFNγ licencing enhances human mesenchymal stromal cell potency in a humanised mouse model of acute graft versus host disease.* Stem Cell Res Ther, 2021. **12**(1): p. 238.

10. Dunbar, H., et al., *The Inflammatory Lung Microenvironment; a Key Mediator in MSC Licensing.* Cells, 2021. **10**(11).

11. Rolandsson Enes, S., et al., *Healthy versus inflamed lung environments differentially affect mesenchymal stromal cells,* Eur Respir J, 2021. **58**(4).

12. Tunstead, C., et al., *The ARDS microenvironment enhances MSC-induced repair via VEGF in experimental acute lung inflammation.* Mol Ther, 2024. **32**(10): p. 3422-3432.

13. Boland, L., et al., *IFN-γ and TNF-α Pre-licensing Protects Mesenchymal Stromal Cells from the Pro-inflammatory Effects of Palmitate.* Mol Ther, 2018. **26**(3): p. 860-873.

14. Tunstead, C., Bitterlich, L.B.*, Ankrum, J.A., Hogand, A.E. and English, K., *Palmitate enhances MSC immunomodulation of human macrophages via the ceramide/CCL2 axis in vitro.* Stem Cell Research and Therapy, 2025.

15. Liu, Y., et al., *The Role of PPAR-δ in Metabolism, Inflammation, and Cancer: Many Characters of a Critical Transcription Factor.* Int J Mol Sci, 2018. **19**(11).

16. Kota, B.P., T.H. Huang, and B.D. Roufogalis, *An overview on biological mechanisms of PPARs.* Pharmacol Res, 2005. **51**(2): p. 85-94.

17. Lim, J. and E.K. Park, *Effect of fibroblast growth factor-2 and retinoic acid on lineage commitment of bone marrow mesenchymal stem cells.* Tissue Eng Regen Med, 2016. **13**(1): p. 47-56.

18. Park, J.R., et al., *Effects of Peroxisome Proliferator-Activated Receptor-δ Agonist on Cardiac Healing after Myocardial Infarction.* PLoS One, 2016. **11**(2): p. e0148510.

19. Carty, F., et al., *IFN-γ and PPARδ influence the efficacy and retention of multipotent adult progenitor cells in graft vs host disease.* Stem Cells Transl Med, 2021. **10**(11): p. 1561-1574.

20. Heck, B.E., et al., *PPAR-δ Agonist With Mesenchymal Stem Cells Induces Type II Collagen-Producing Chondrocytes in Human Arthritic Synovial Fluid.* Cell Transplant, 2017. **26**(8): p. 1405-1417.

21. Luz-Crawford, P., et al., *PPARβ/δ directs the therapeutic potential of mesenchymal stem cells in arthritis.* Ann Rheum Dis, 2016. **75**(12): p. 2166-2174.

22. Contreras-Lopez, R.A., Elizondo-Vega, R., Torres, M.J. *et al*, *PPARβ/δ-dependent MSC metabolism determines their immunoregulatory properties.* 2020: p. 11423

23. Kim, D.H., et al., *PPAR-δ agonist affects adipo-chondrogenic differentiation of human mesenchymal stem cells through the expression of PPAR-γ.* Regen Ther, 2020. **15**: p. 103-111.

24. Nernpermpisooth, N., et al., *PPARβ/δ Is Required for Mesenchymal Stem Cell Cardioprotective Effects Independently of Their Anti-inflammatory Properties in Myocardial Ischemia-Reperfusion Injury.* Front Cardiovasc Med, 2021. **8**: p. 681002.

25. Sarre, C., et al., *PPARβ/δ priming enhances the anti-apoptotic and therapeutic properties of mesenchymal stromal cells in myocardial ischemia-reperfusion injury.* Stem Cell Res Ther, 2022. **13**(1): p. 167.

26. Djouad, F., et al., *PPARβ/δ: A master regulator of mesenchymal stem cell functions.* Biochimie, 2017. **136**: p. 55-58.

27. Ziveri, J., et al., *Angiopoietin-like 4 protects against endothelial dysfunction during bacterial sepsis.* Nat Microbiol, 2024. **9**(9): p. 2434-2447.

28. Goh, Y.Y., et al., *Angiopoietin-like 4 interacts with integrins beta1 and beta5 to modulate keratinocyte migration.* Am J Pathol, 2010. **177**(6): p. 2791-803.

29. Zhan, W., et al., *ANGPTL4 attenuates palmitic acid-induced endothelial cell injury by increasing autophagy.* Cell Signal, 2022. **98**: p. 110410.

30. An, Q., et al., *In vitro effects of mitomycin C on the proliferation of the non-small-cell lung cancer line A549.* Int J Clin Exp Med, 2015. **8**(11): p. 20516-23.

31. Neubauer, E., et al., *Comparative evaluation of three proliferation markers, Ki-67, TOP2A, and RacGAP1, in bronchopulmonary neuroendocrine neoplasms: Issues and prospects.* Oncotarget, 2016. **7**(27): p. 41959-41973.

32. Huang, W., et al., *ANGPTL4 induces Kupffer cell M2 polarization to mitigate acute rejection in liver transplantation.* Sci Rep, 2025. **15**(1): p. 986.

33. Batista, F.A., et al., *Structural insights into human peroxisome proliferator activated receptor delta (PPAR-delta) selective ligand binding.* PLoS One, 2012. **7**(5): p. e33643.

34. Kornicka, K., J. Houston, and K. Marycz, *Dysfunction of Mesenchymal Stem Cells Isolated from Metabolic Syndrome and Type 2 Diabetic Patients as Result of Oxidative Stress and Autophagy may Limit Their Potential Therapeutic Use.* Stem Cell Rev Rep, 2018. **14**(3): p. 337-345.

35. Lu, P., et al., *Serum Free Fatty Acid Concentration Predicts ARDS after Off-Pump CABG: A Prospective Observational Study.* Lung, 2024. **202**(5): p. 523-532.

36. Boland, L., et al., *Translating MSC Therapy in the Age of Obesity.* Front Immunol, 2022. **13**: p. 943333.

37. Grygiel-Górniak, B., *Peroxisome proliferator-activated receptors and their ligands: nutritional and clinical implications--a review.* Nutr J, 2014. **13**: p. 17.

38. Mirza, A.Z., I.I. Althagafi, and H. Shamshad, *Role of PPAR receptor in different diseases and their ligands: Physiological importance and clinical implications.* Eur J Med Chem, 2019. **166**: p. 502-513.

39. Capelli, D., et al., *Structural basis for PPAR partial or full activation revealed by a novel ligand binding mode.* Sci Rep, 2016. **6**: p. 34792.

40. Yang, Y., et al., *Synergism of MSC-secreted HGF and VEGF in stabilising endothelial barrier function upon lipopolysaccharide stimulation via the Rac1 pathway.* Stem Cell Res Ther, 2015. **6**: p. 250.

41. Zisa, D., et al., *Vascular endothelial growth factor (VEGF) as a key therapeutic trophic factor in bone marrow mesenchymal stem cell-mediated cardiac repair.* Biochem Biophys Res Commun, 2009. **390**(3): p. 834-8.

42. Yang, Y., et al., *The Vascular Endothelial Growth Factors-Expressing Character of Mesenchymal Stem Cells Plays a Positive Role in Treatment of Acute Lung Injury In Vivo.* Mediators Inflamm, 2016. **2016**: p. 2347938.

43. Dunbar, H., et al., *The VEGF-Mediated Cytoprotective Ability of MIF-Licensed Mesenchymal Stromal Cells in House Dust Mite-Induced Epithelial Damage.* Eur J Immunol, 2025. **55**(1): p. e202451205.

44. Cahill, E.F., et al., *Hepatocyte Growth Factor Is Required for Mesenchymal Stromal Cell Protection Against Bleomycin-Induced Pulmonary Fibrosis.* Stem Cells Transl Med, 2016. **5**(10): p. 1307-1318.

45. Kennelly, H., B.P. Mahon, and K. English, *Human mesenchymal stromal cells exert HGF dependent cytoprotective effects in a human relevant pre-clinical model of COPD.* Sci Rep, 2016. **6**: p. 38207.

46. Cho, D.I., et al., *Antiinflammatory activity of ANGPTL4 facilitates macrophage polarization to induce cardiac repair.* JCI Insight, 2019. **4**(16).

47. Curley, G.F., et al., *Effects of intratracheal mesenchymal stromal cell therapy during recovery and resolution after ventilator-induced lung injury.* Anesthesiology, 2013. **118**(4): p. 924-32.

Figure Legends

Figure 1: PPARβ/δ(+) hBM-MSCs show enhanced reparative capacity of CALU-3 lung epithelial cells. (A) Experimental Design. A CALU-3 scratch assay was run, in combination with MSC-CM from PPARβ/**δ** agonized (+) or antagonized (-) hBM-MSCs. (B) Images of the wound healing assay at baseline or following 48hr were fixed and stained with crystal violet dye and (C) quantified using imageJ software (one-way ANOVA followed by Tukey's post-hoc test, n=3). (D) Using a mitomycin C proliferation inhibitor allowed for the investigation into the impact of this on migration or proliferation at different time-points (two-way ANOVA followed by Tukey's post-hoc test, n=3) and this was confirmed using (E) *TOP2A* gene expression by RT-PCR at a 48hr time-point (one-way ANOVA followed by Tukey's post-hoc test, n=3). Replicates are a representation of 3 individual hBM-MSC donors. Data is presented as mean ± SEM; *p<0.05, **p<0.01, ***p<0.001, ****p<0.0001.

Figure 2: PPARβ/δ(+) hBM-MSCs show enhanced expression of ANGPTL4 by RNA sequencing. (A) hBM-MSCs exposed to 1uM of PPARβ/**δ** agonist or antagonist were sent to Novogene™ for RNA sequencing. (B) Several DEGs were highlighted, and (C) the most significant hits were plotted on a volcano plot using Flourish™ software. Results were confirmed by assessing 2 known PPARβ/**δ** target genes in our sequencing dataset: (D) *ANGPTL4* and (E) *PDK4*. These results were confirmed by (F, G) RT-PCR (one-way ANOVA followed by Tukey's post-hoc test, n=3). Replicates are a representation of 3 individual hBM-MSC donors. Data is presented as mean ± SEM; *p<0.05, **p<0.01, ***p<0.001, ****p<0.0001.

Figure 3: PPARβ/δ(+) hBM-MSCs show enhanced expression of ANGPTL4, but not other traditional MSC-associated genes or proteins. Supernatant from hBM-MSCs exposed

to 1uM of PPARβ/**δ** agonist or antagonist were harvested before cells were collected in TRIzol for gene expression studies. Protein expression of (A) ANGPTL4, (B) VEGF and (C) MIF were assessed by ELISA and gene expression for (D) *PTGS2,* (E) *IL-6,* (F) *IDO,* (G) *PTGES* and (H) *TGFβ* were assessed (one-way ANOVA followed by Tukey's post-hoc test, n=3). Replicates are a representation of 3 individual hBM-MSC donors. Data is presented as mean ± SEM; *p<0.05, **p<0.01, ***p<0.001, ****p<0.0001.

Figure 4: PPARβ/δ(+) hBM-MSCs show enhanced wound repair via ANGPTL4. (A) Using an ANGPTL4 neutralisation approach, we assessed (B) wound closure of CALU-3 lung epithelial cells. (C) PPARβ/**δ**(+) hBM-MSCs showed enhanced wound closure, while ANGPTL4-neutralisation abrogated this effect. (D) Neutralisation of ANGPTL4 was confirmed by ELISA (one-way ANOVA followed by Tukey's post-hoc test, n=3). Replicates are a representation of 3 individual hBM-MSC donors. ND represents not-detected protein levels. Data is presented as mean ± SEM; *p<0.05, **p<0.01, ***p<0.001, ****p<0.0001.

Figure 5: ARDS patients have higher levels of PPARβ/δ(+) ligands and co-activators. (A) A publicly available dataset (Study ID: ST000042; doi: 10.21228/M8SG64) was mined for PPARβ/**δ** ligands present in the ARDS lung. (B) An additional dataset (GEO accession no.: GSE185263), based on ARDS serum, highlighted an increase in PPARβ/**δ**(+)-associated co-activators such as (C) *PPARGC1A*, (D) *NCOA1*, (E) *NCOA2*, (F) *NCOA3* and (G) *CREBBP;* and a decrease in PPARβ/**δ** (+)-associated co-repressors such as (H) *SIRT1*, (I) *NCOR1* and (J) *NCOR2* (one-way ANOVA followed by Tukey's post-hoc test, n=6+). Replicates are a representation of (A-J) individual ARDS patients, or healthy controls. (K) ANGPTL4 production from 3 individual hBM-MSC donors exposed to PPARβ/**δ** agonist (+) or antagonist

(-) in the presence or absence of 20% ARDS patient serum. Data is presented as mean ± SEM; *p<0.05, **p<0.01, ***p<0.001, ****p<0.0001.

Figure 6: ARDS-licensed MSC-CM$_{PPAR\beta/\delta(+)}$ provides enhanced therapeutic effects in ALI in an ANGPTL4 dependent manner. Mice were exposed to 2mg/kg LPS IT, or PBS control. (A) An Evan's Blue Dye permeability assay was used to (B) quantify the amount of leakage from the lungs of mice exposed to LPS +/- our treatments of interest. Pro-inflammatory cytokines (C) TNFα and (D) IL-6 were assessed by ELISA and (E) total protein was assessed using a bradford assay (one-way ANOVA followed by Tukey's post-hoc test, n=3+). (F) Clinical scores and (G) % weigh loss were recorded over the course of the model. Replicates are a representation of individual mice. Data is presented as mean ± SEM; *p<0.05, **p<0.01, ***p<0.001, ****p<0.0001.

Graphical Abstract

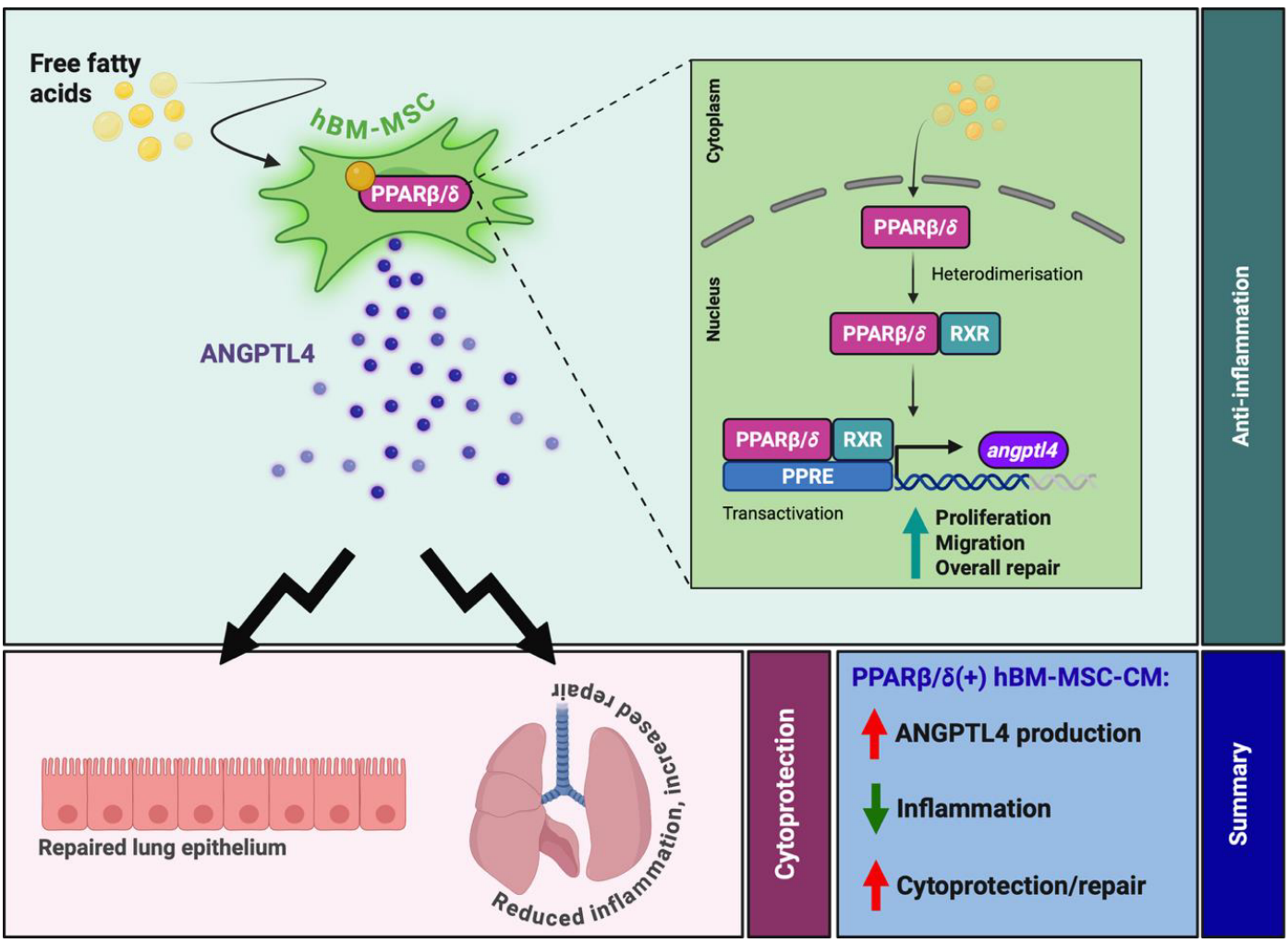

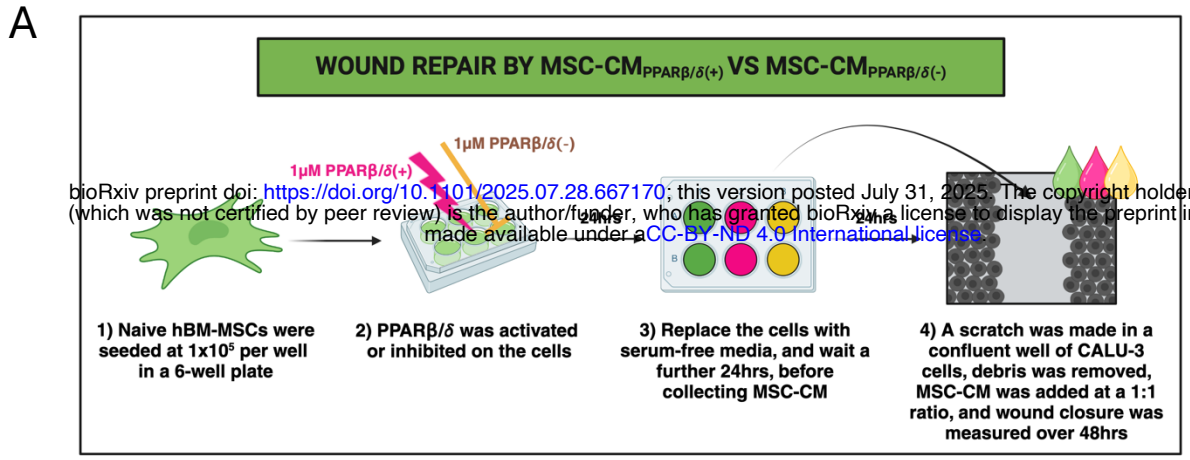

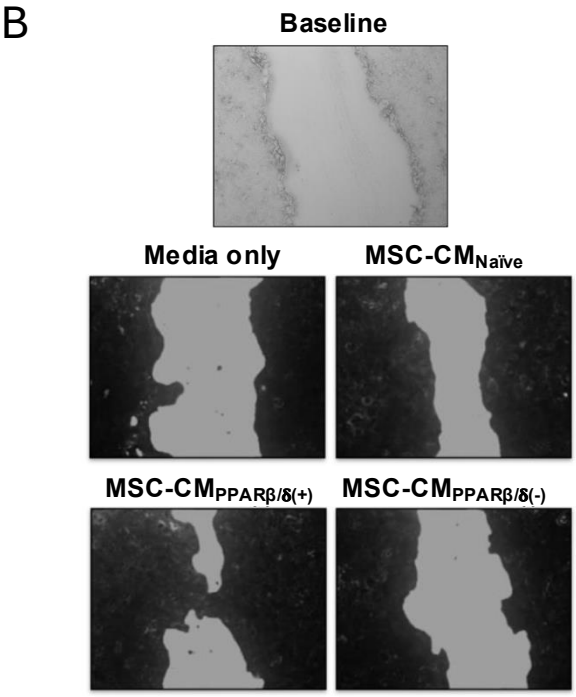

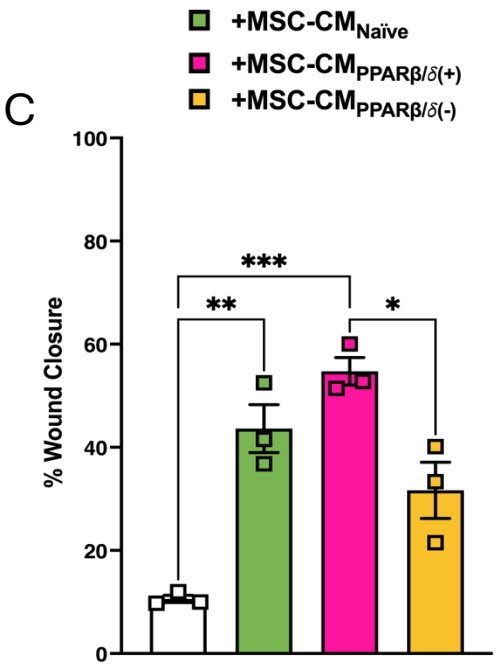

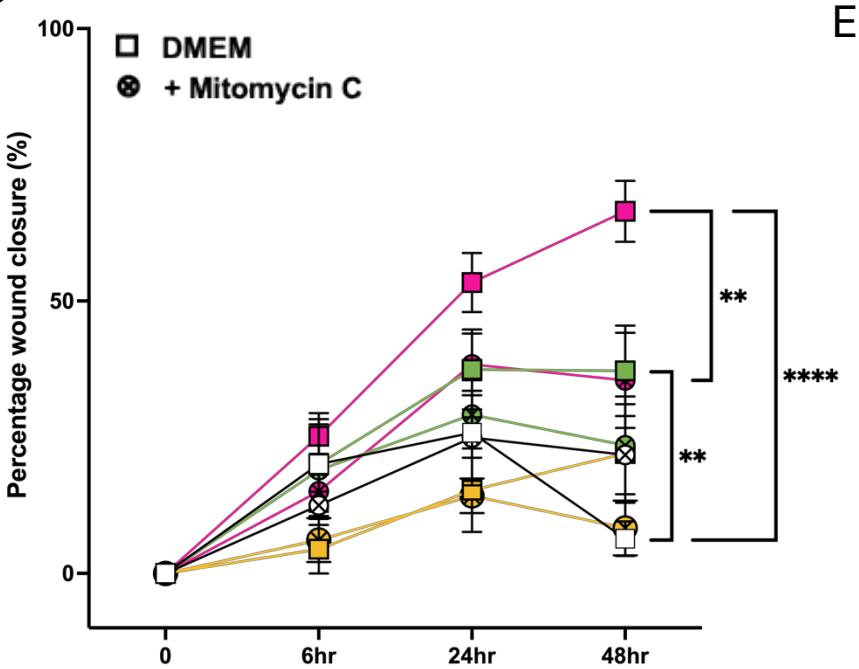

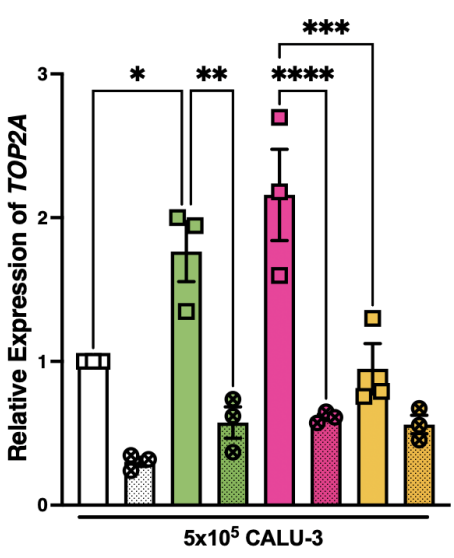

Figure 1

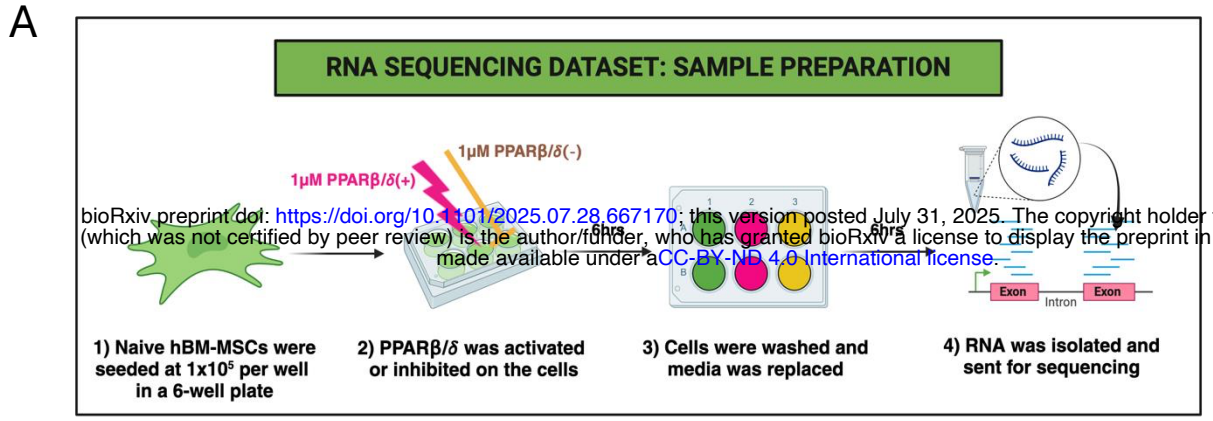

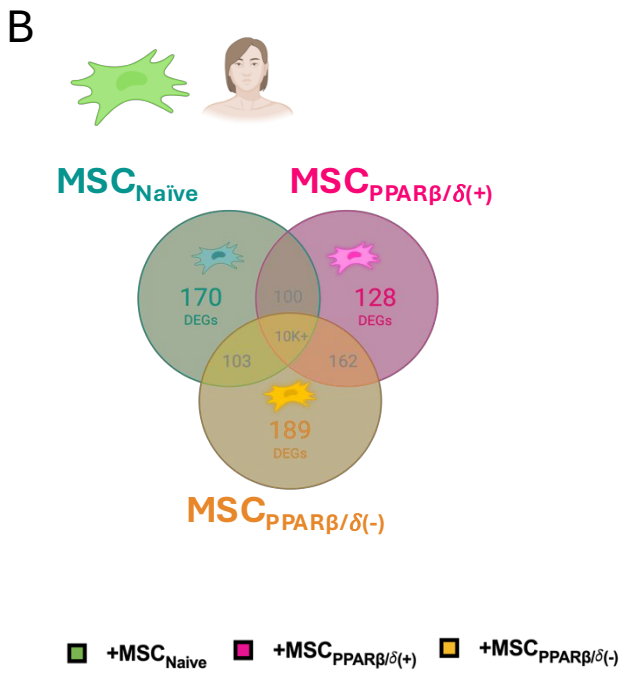

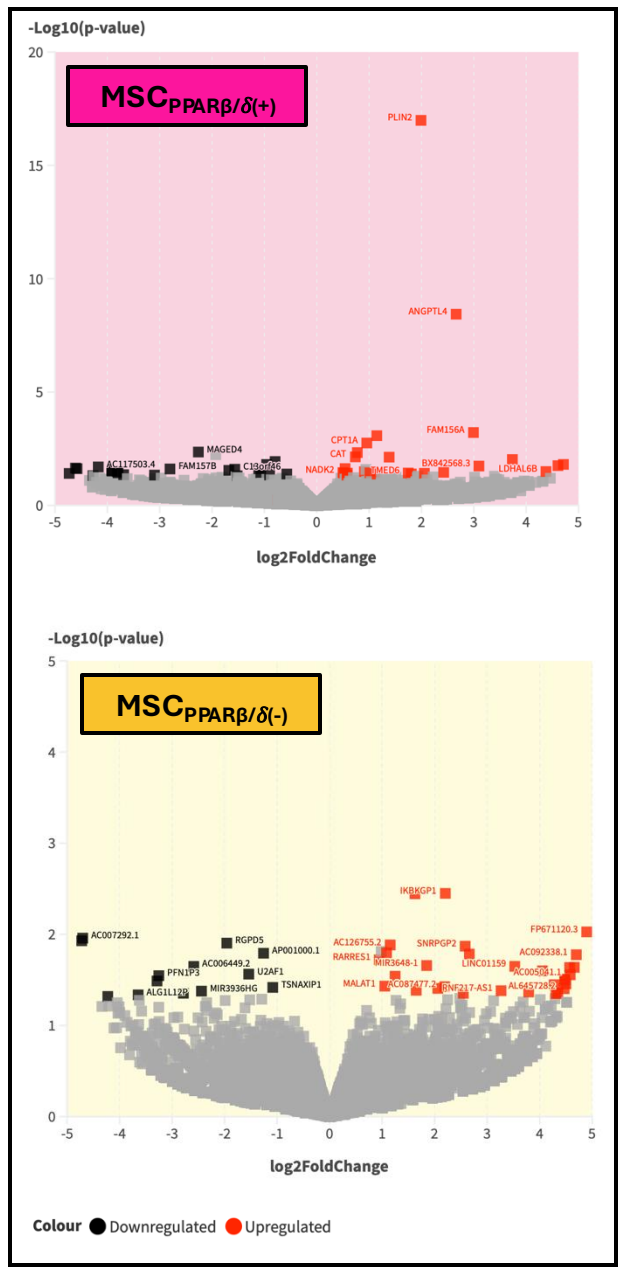

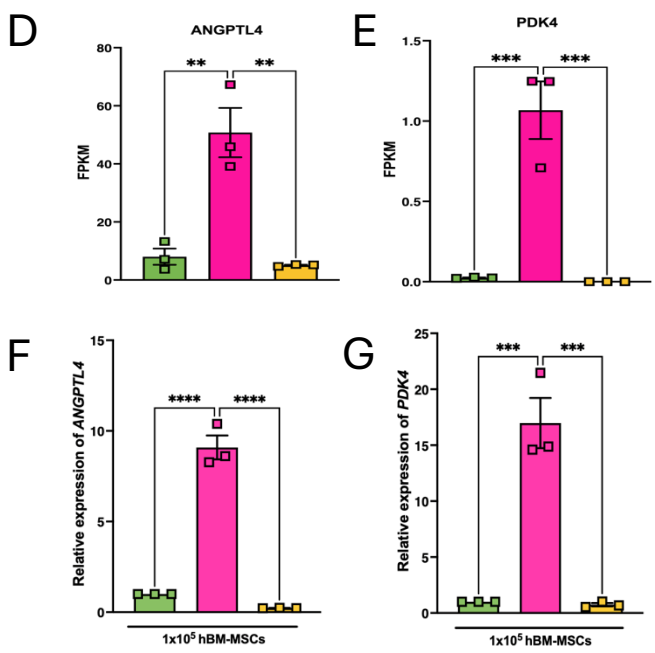

Figure 2

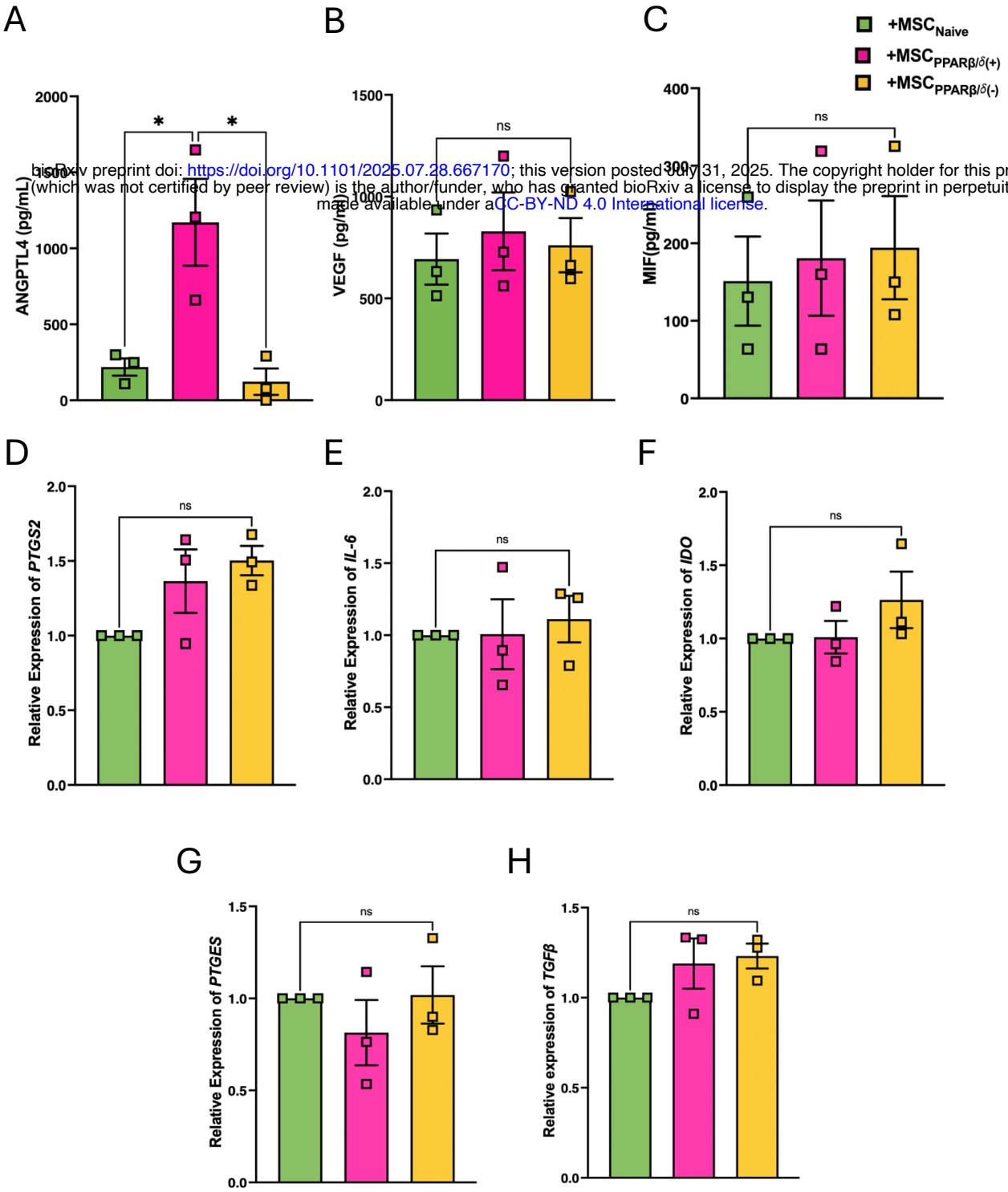

Figure 3

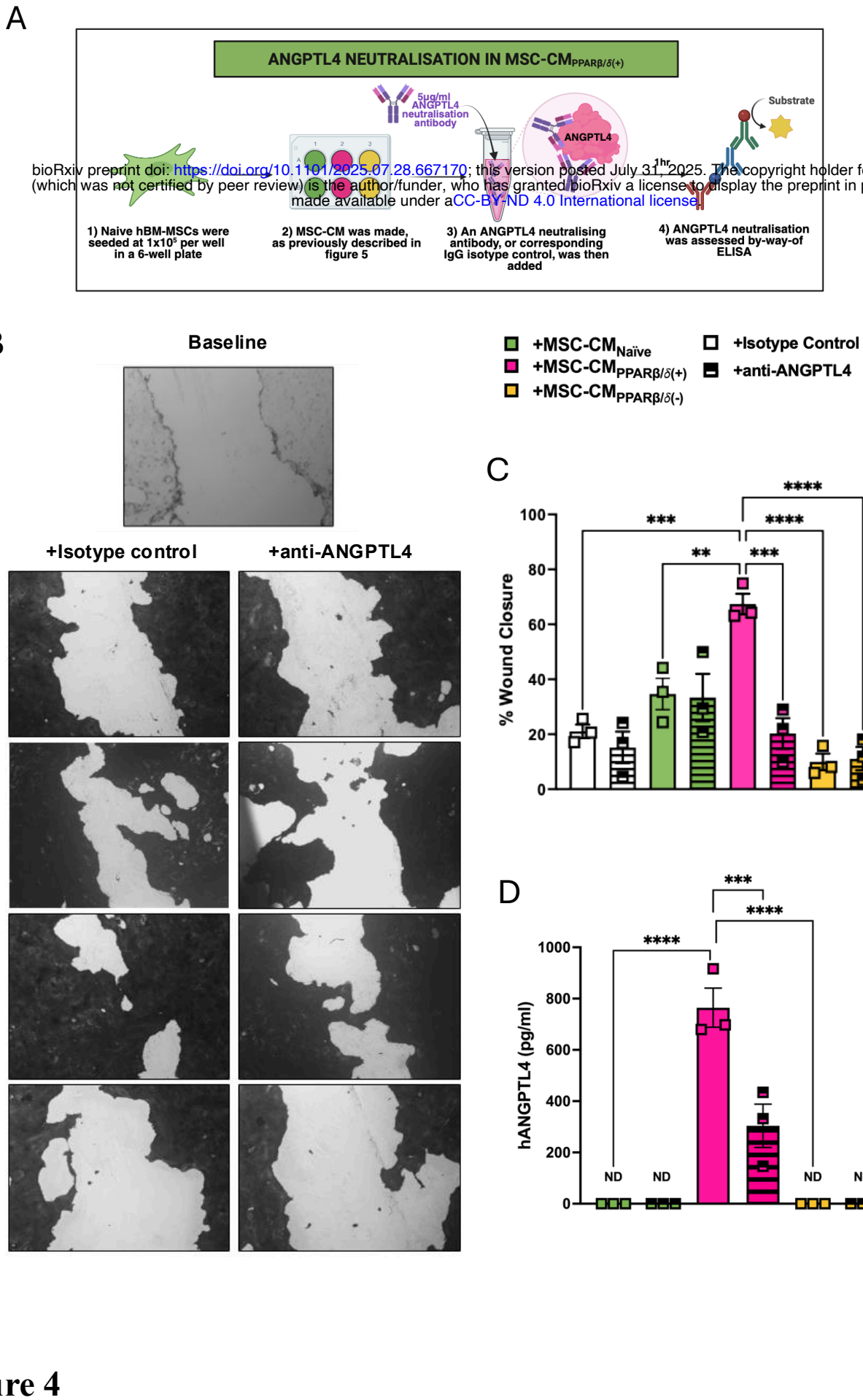

Figure 4

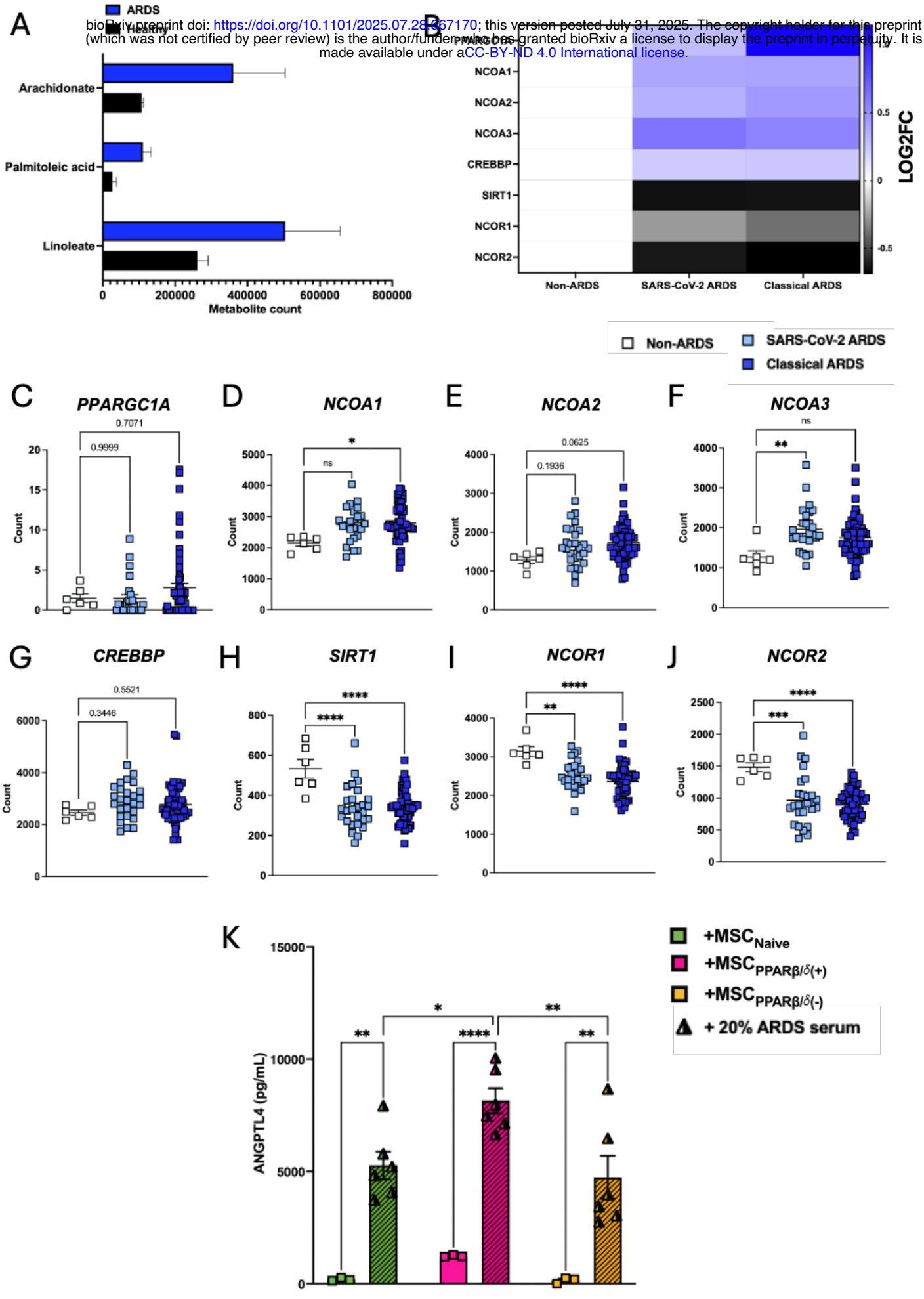

Figure 5

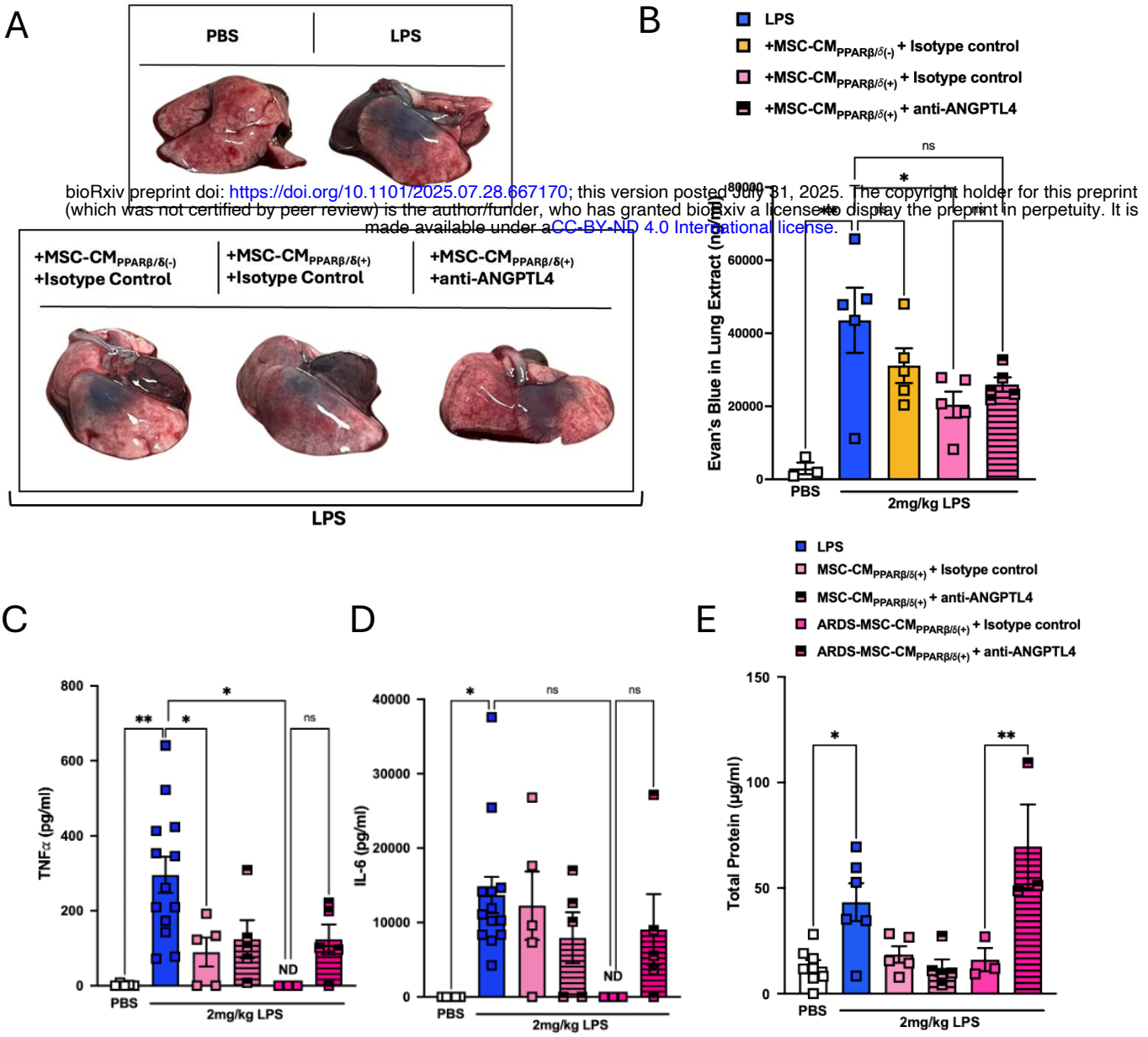

Figure 6

Stem Cell Research & Therapy

RESEARCH Open Access

Palmitate enhances MSC immunomodulation of human macrophages via the ceramide/CCL2 axis in vitro

Courteney Tunstead[1,2†], Laura M. Bitterlich[1,2†], James A. Ankrum[3,4], Andrew E. Hogan[1,2] and Karen English[1,2*]

Abstract

Background The immunomodulatory function of human mesenchymal stromal cells (MSCs) strongly depends on external factors; such as cytokines and other signalling molecules encountered in the disease microenvironment. An insufficiently inflammatory environment can fail to activate MSCs, and certain signals can impair their function. Obesity is on the rise worldwide, making it an additional factor to be considered prior to MSC therapy, as the microenvironment presents its own challenges. Elevated levels of serum free fatty acids, specifically palmitate, have the potential to affect MSC therapy. Palmitate-exposure has been shown to impair MSC immunomodulation of T cells in vitro. However, this is yet to be studied in the context of macrophages.

Methods MSCs from three independent donors were exposed to 0.4mM of palmitate for 6–24 h. Gene expression, protein production and functional capacity were then assessed in response to palmitate. A ceramide synthesis inhibitor (Fumonisin B1) and a CC-chemokine ligand 2 (CCL2)-neutralising antibody were further used to assess the impact of these components on palmitate-associated immunomodulation.

Results We demonstrated that palmitate-exposed MSCs have enhanced suppression of human monocyte-derived macrophage (MDM) production of tumour necrosis factor α (TNFα), in a CCL2-dependent manner. We further elucidated parts of the pathway, such as ceramide synthesis, through which palmitate promotes this enhanced immunomodulation of macrophages.

Conclusion Palmitate-exposed MSCs show enhanced immunomodulation of human MDMs, through the ceramide/CCL2 axis in vitro.

†Courteney Tunstead and Laura M. Bitterlich contributed equally to this work.

*Correspondence:
Karen English
karen.english@mu.ie

Full list of author information is available at the end of the article

Graphical Abstract

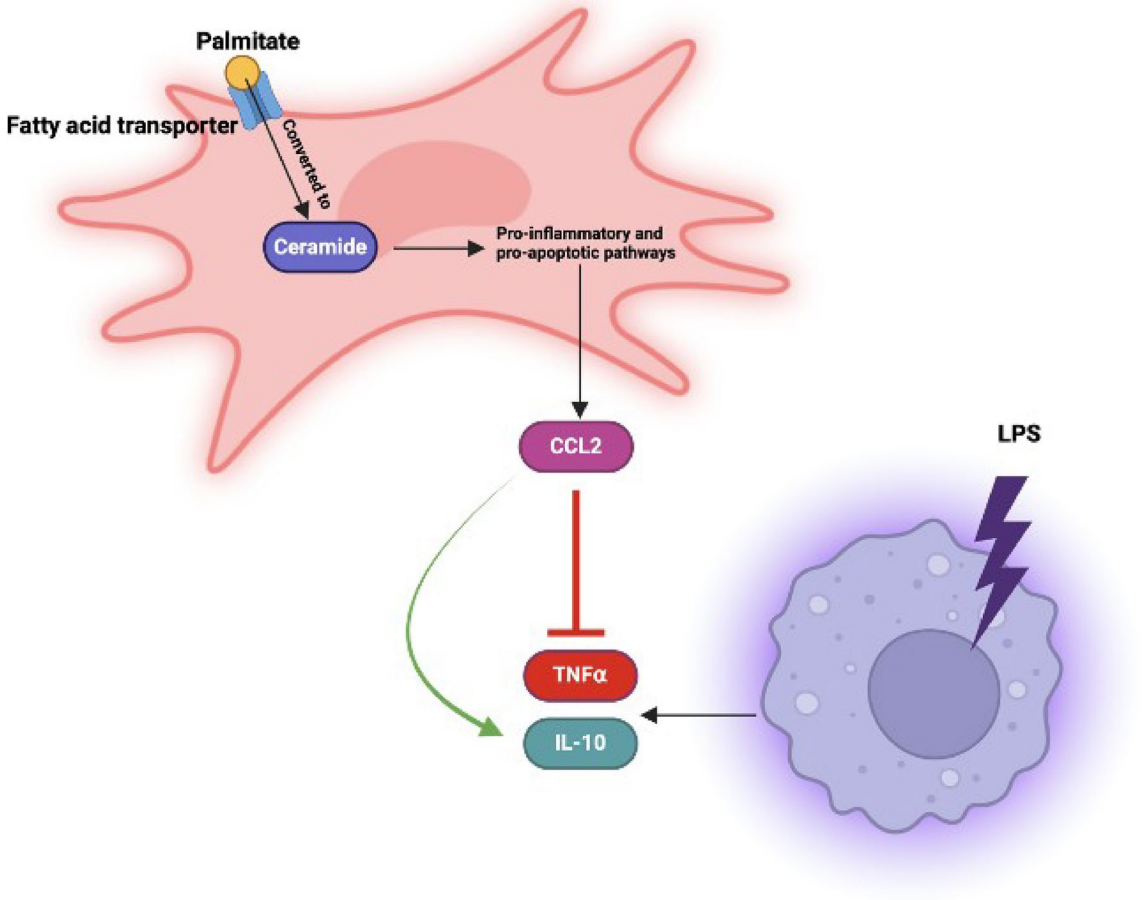

Keywords Mesenchymal stromal cells, Immunomodulation, Macrophages, Palmitate, Obesity, Ceramide, CCL2

Background

The immune calming properties of mesenchymal stromal cells (MSCs) makes them a promising therapeutic for a range of inflammatory conditions [1–5]. MSCs can suppress T cell proliferation [6] and reduce pro-inflammatory macrophage activation and function [7, 8]. Moreover, MSCs can polarise macrophages towards a more pro-resolving, non-classical, M2 phenotype [9]. In fact, the communication between MSCs and macrophages in vivo is now thought to play an essential role in MSC therapeutic efficacy; as depleting macrophages prevents MSCs from mediating their therapeutic effects [10, 11].

The microenvironment MSCs encounter upon administration to patients has an important impact of the efficacy of MSCs. MSCs require a minimal threshold of pro-inflammatory activation to carry out their immunomodulatory functions and in some cases the disease microenvironment may not provide adequate signals for this activation [14–18]. In the context of MSC administration in acute graft versus host disease (aGvHD) and in Crohn's Fistula there is evidence that differences in patients are associated with response or non-response to MSC therapy [19, 20]. Thus, the microenvironment within patients who are to receive MSC therapy requires further investigation.

Worldwide, the number of individuals living with obesity is on the rise, with over half of the adults in the EU being overweight [21–23]. This would suggest an increase in the number of patients receiving cell-based therapies, including MSC therapy, that will also be living with the complication of obesity. Patients who are living with obesity, alongside additional inflammatory conditions, have an increased level of complexity within their disease microenvironment. In addition to increased levels of pro-inflammatory cytokines [22–24] and adipokines [25, 26], obesity is associated with elevated levels of

serum free fatty acids (FFAs). Palmitate, the most abundant inflammatory FFA in the body, has been shown to exacerbate obesity-related insulin resistance through increased ceramide synthesis and inhibition of Akt phosphorylation [27, 28]. The anti-tumour response is also impacted by palmitate via de-sensitisation of monocytes and macrophages to stimulator of interferon genes (STING)-induced type-I interferon signalling, and induction of programmed cell death protein 1 (PD-1) [29, 30]. Moreover, palmitate has shown to induce endoplasmic reticulum (ER) stress in lung epithelial cells leading to apoptosis [31]. Palmitate-induced ER stress has also been described in MSCs [32], and exposure to palmitate for 48 h or more is associated with significant cell lipotoxicity [33]. Additionally, the ability of MSCs to suppress T cell proliferation in vitro is drastically impaired by the presence of palmitate, owing at least in part to decreased indoleamine 2,3-dioxygenase (IDO) activity, resulting in a lower conversion of tryptophan into kynurenine [6, 10, 34–41]. Although suppression of T cell proliferation is considered an important mechanism of action for MSCs [42, 43], recent evidence increasingly points towards an important role for MSC-macrophage interactions [19, 20, 44–46].

The aim of this study was to investigate how MSC immunomodulation of human monocyte-derived macrophages (MDMs) would be affected by exposure to palmitate in vitro. We demonstrated that palmitate significantly enhanced MSC suppression of pro-inflammatory macrophages. We identified enhanced MSC expression of *PTGS2*, *IL-6*, *CCL2* and *ANGPTL4* following exposure to palmitate. We also identified CC-chemokine ligand 2 (CCL2) as the protein responsible for mediating this improvement in MSC immunomodulation. We further elucidated the pathway through which palmitate promoted increased production of CCL2 by MSCs, by-way-of investigating ceramide de novo synthesis. We showed that palmitate led to the induction of ceramide de novo synthesis, and blockade of this pathway prevented both CCL2 production by MSCs and the associated MDM suppression.

Methods

Ethical approval

Ethical approval was granted by the Medical Research Ethics Committees at St Vincent's University Hospital and by Maynooth University Ethics Committee entitled: Metabolic and Immunological Links Between Obesity, Systemic Inflammation, Type 2 Diabetes Mellitus and Non-Alcoholic Fatty Liver Disease granted on 28th June 2024 (BSRESC-2024-38575) and Investigating the role of macrophage education by MSCs in mediating MSC therapeutic efficacy granted on 11th February 2022 (BSRESC-2022-2460651). All patients gave written informed consent prior to partaking in the study.

Human MSC culture

Human bone marrow-derived MSCs (three independent donors) were purchased from RoosterBio (Frederick, MD, USA). Initially, MSCs were expanded in RoosterBio expansion medium (RoosterBasal and RoosterBooster) for passages 1 and 2 according to the manufacturer's instructions. After, MSCs were cultured and maintained up to passage 6 in low glucose Dulbecco's modified Eagle medium (DMEM; Sigma-Aldrich, Wicklow, Ireland) supplemented with 10% (v/v) fetal bovine serum (FBS; ThermoFisher Scientific, Dublin, Ireland) and 1% (v/v/) penicillin/streptomycin (Sigma-Aldrich, Wicklow, Ireland). MSCs were seeded at 1×10^6 cells per T175 flask and cultured at 37 °C in 5% CO_2. Medium was replenished every 2–3 days and cells were passaged at 80% confluency. All experiments were carried out between passages 3–6. For palmitate and C2 ceramide experiments, MSCs were exposed to 0.4 mM palmitate-BSA (palmitate; Cayman Chemicals, MI, USA) or BSA as a control (6 to 24 h), 40 µM fumonisin B1 (ThermoFisher Scientific, Dublin, Ireland), or 10 µM C2 ceramide (Sigma-Aldrich, Wicklow, Ireland) or vehicle control (ethanol) (3 to 6hrs). For serum studies, MSCs (3 independent donors) were exposed to 20% of lean or obese patient serum for 24 h. This was then removed, the cells were washed with PBS, and serum-free media was added for a further 24 h. This was then harvested and CCL2 secretion was quantified by ELISA.

Culture of human monocyte derived macrophages (MDMs)

Human peripheral blood mononuclear cells (PBMCs) were isolated from buffy coats received from the Irish Blood Transfusion Service (Saint James' hospital, Dublin, Ireland) by lymphoprep (StemCell, Vancouver, Canada) density gradient centrifugation. PBMCs were seeded at a density of 2×10^6 cells per well in tissue culture 24-well plates and allowed to adhere for 60 min. Cells were washed with Dulbecco's Phosphate-Buffered Saline (DPBS; Merck, Cork, Ireland) to remove any non-adherent cells and medium was replaced with 300 µL cRPMI, supplemented with 5% human male AB plasma (Merck, Cork, Ireland) and topped up to 600 µL after 24 h. Monocytes were differentiated into monocyte-derived macrophages for 6 days. After 5 days, cells were washed with DPBS and medium replenished. On day 6, cells were detached by first washing them with DPBS, then adding 300 µL per well of lidocaine detachment buffer (0.5% bovine serum albumin (BSA; Merck) and 5 mg/mL lidocaine HCL (Fluorochem, Cork, Ireland)) for 20 min at 37 °C. Cells were gently pipetted up and down and transferred to a centrifugation tube. 400 µL DPBS was added

to wells, remaining cells were gently dislodged using the tip of a Pasteur pipette, collected, and centrifuged at 300 g for 5 min. MDMs were then seeded into 96 well flat bottom plates at a density of 2×10^4 cells per well for macrophage suppression assays.

Flow cytometry for MDM characterisation

MDMs were detached using a lidocaine detachment buffer (0.5% BSA, 5 mg/mL lidocaine in DPBS). 2% rat serum was used to block non-specific binding of antibodies. Cells were incubated for 15 min at 4 °C with fluorescent antibodies. Cells were then first washed, then resuspended in cold flow cytometry staining (FACS) buffer (2% FBS in Dulbecco's Phosphate Buffered Saline (DPBS/PBS)) and then acquired using the Attune Nxt flow cytometer (ThermoFisher Scientific, Dublin, Ireland). Gating was performed on live (live/dead stain, near-IR fluorescent reactive dye, Invitrogen), CD14+ (PE) cells (Supplementary Fig. 1) using antibodies against CD206 (Pacific Blue), HLA-DR (FITC), CD11b (PE-Cy7), CD86 (APC), and CD163 (PerCP). Data were analysed using floreada.io.

Intracellular staining of COX-2

MSCs were seeded at a density of 1×10^5 cells per well in tissue culture 6-well plates and allowed to adhere overnight. MSCs were then exposed to 0.4 mM palmitate-BSA (palmitate; Cayman Chemicals, MI, USA) for 24 h. After 20 h, a protein transport inhibitor cocktail containing Brefeldin A and Monensin (Invitrogen, Massachusetts, US) was added to block protein transport. Cell viability was determined using the Zombie Aqua™ Fixable Viability Kit (Biolegend, CA, USA). Cells were then washed and prepared for intracellular staining using the Foxp3/Transcription Factor Staining Buffer Set (Biosciences, Dublin, Ireland) following the manufacturer's instructions. Samples were stained for COX-2 (PE) for 45 min. Cells were then washed in flow cytometry staining buffer (2% FBS in DPBS) and acquired using the Attune Nxt flow cytometer (ThermoFisher Scientific, Dublin, Ireland). Gating for COX-2 was performed on live single cells. Data were analysed using floreada.io.

Table 1 Sequences for primers used in real-time PCR

Primer	Forward primer sequence (5′-3′)	Reverse primer sequence (3′-5′)
HPRT	ATAAGCCAGACTTTGTTGG	ATAGGACTCCAGATGTTTCC
CERS4	ATCCTCTACACCACATACTAC	TACGAATGTCCTTCTCCATC
CERS5	CTGGCATAACTATCCATTTCAG	GACCAATAGAAGGCCAATTC
CERS6	CTTTACATGTGTCCAAGGATG	TTGGGACTTGTAGTTTTGAG
PTGS2	AAGCAGGCTAATACTGATAGG	TGTTGAAAAGTAGTTCTGGG
IL-6	GCAGAAAAAGGCAAAGAATC	CTACATTTGCCGAAGAGC
IDO	TTGTTCTCATTTCGTGATGG	TACTTTGATTGCAGAAGCAG
CCL2	AGACTAACCCAGAAACATCC	ATTGATTGCATCTGGCTG
ANGPTL4	AGGCAGAGTGGACTATTTG	CCTCCATCTGAGGTCATC
VEGFA	AATGTGAATGCAGACCAAAG	GACTTATACCGGGATTTCTTG

Enzyme-linked immunosorbent assay (ELISA)

Levels of human ANGPTL4, IL-10, TNFα, and CCL2 (R&D and BioLegend, CA, USA) in cell culture supernatant were determined using ELISA kits following the manufacturer's instructions. Samples were diluted as necessary to stay within the range of the kits. Analysis was carried out in Corning 96-well half-area plates and volumes adjusted accordingly (ThermoFisher Scientific, Dublin, Ireland).

Analysis of gene expression

Total ribonucleic acid (RNA) was extracted from MSCs using TRIzol (Ambion Life Sciences, Cambridgeshire, UK) following the manufacturer's instructions. RNA concentrations were measured via spectrophotometry (Nanodrop 2000, ThermoFisher Scientific, DE, USA). For coding deoxyribonucleic acid (cDNA) synthesis, 500 ng RNA were used following the manufacturer's instructions (Quantabio, MA, USA). Real-time polymerase chain reaction (PCR) was carried out using PerfeCta SYBR Green FastMix (Quantabio, MA, USA). Expression of genes of interest (for primer sequence information see Table 1) was qualified in relation to the housekeeping gene hypoxanthine-guanine phosphoribosyl transferase (hprt), using the ΔCT method. The fold change in gene expression relative to the control was determined via calculating the $2^{-\Delta\Delta CT}$ values.

Macrophage suppression assay

MDMs were cultured as described and co-cultured with MSCs at a MSC to macrophage ratio of 1:20. MSCs were incubated with 0.4 mM palmitate-BSA (palmitate; Cayman Chemicals, MI, USA), 5 μg/mL neutralising CCL2/MCP-1 neutralising antibody (R&D Systems, Abingdon, UK), 40 μM fumonisin B1 (ThermoFisher Scientific, Dublin, Ireland), or 10 μM C2 ceramide (Sigma-Aldrich, Wicklow, Ireland) for 24 h prior to co-culture. MSCs were washed with DPBS before addition of MDMs. Co-culture was stimulated with 100 ng/mL lipopolysaccharide for 24 h (LPS; *E. coli* O111:B4, Sigma-Aldrich, Wicklow, Ireland). Supernatants were collected, and TNFα and IL-10 concentration was quantified using ELISA.

Statistical analysis

An ordinary One-Way ANOVA with Tukey's multiple comparisons test was performed to test for statistical significance between multiple experimental groups, and an unpaired t test with Welch's correction was performed to test for statistical significance between two experimental groups. GraphPad Prism version 10.2.3 was used for statistical computations and graphing.

Results

Palmitate-enhanced Immunomodulation of MDMs by MSCs is linked to CCL2

MSCs reduce LPS-stimulated MDM production of TNFα in a dose-dependent manner (Supplementary Fig. 2). To investigate if palmitate enhanced or reduced TNFα production by MDMs, low dose MSC (1 MSC: 20 MDMs) were exposed to palmitate for 24 h and used in a macrophage suppression assay (Fig. 1A). Pre-exposure to palmitate significantly improved MSC ability to decrease the production of TNFα by MDMs compared to naive or BSA control MSCs (Fig. 1B). Others have shown a small induction of apoptosis following exposure of MSCs to palmitate for 96 h [36], we did not observe a significant induction of apoptosis following 24 h exposure to 0.4. mM palmitate (Supplementary Fig. 3). MSCs produce a multitude of immunomodulatory factors in response to pro-inflammatory stimulation [12, 47]. In response to palmitate, the expression of *PTGS2* (Fig. 1C), *IL-6* (Fig. 1D), *CCL2* (Fig. 1E), and *ANGPTL4* (Fig. 1F) were increased. While *CCL2* was significantly increased at 6 h and 24 h, *PTGS2*, *IL-6* and *ANGPTL4* were only significantly upregulated at 24 h post-palmitate exposure (Fig. 1). In contrast, MSC expression of *VEGF* and *IDO* were unaffected by palmitate exposure (data not shown).

Given that *PTGS2*, *CCL2* and ANGPTL4 have been associated with macrophage suppression, the gene expression results were confirmed at the protein level. While both COX-2 (Fig. 1G) CCL2 (Fig. 1H) and ANGPTL4 (Fig. 1I) protein production were increased following palmitate exposure, only CCL2 and ANGPTL4 reached significance. In our assay, naive or palmitate exposed MSCs were co-cultured with MDMs and LPS. Therefore, it was possible that changes in gene expression observed could also be mediated by LPS or the combination of palmitate and LPS. LPS and palmitate-exposed MSCs showed further enhanced expression of *CCL2*, *PTGS2* and *IL-6* but not *ANGPTL4* (Fig. 2A-D). Given the increase in both the gene and the protein expression of CCL2 (Figs. 1 and 2), we decided to pursue a CCL2-neutralisation approach. This experiment highlighted that neutralisation of CCL2 abrogated the enhanced immunosuppressive capacity of palmitate-treated MSCs (Fig. 2E).

MSCs and palmitate stimulated MSCs promote an increase in CD206 expression by MDMs

MSCs have been shown to promote an M2 switch in LPS stimulated macrophages [48, 49]. LPS stimulated macrophages expressed significantly increased levels of the M1 activation marker CD86 and reduced levels of CD11b. Naive MSCs at a MSC: MDM ratio of 1:20 significantly increased the frequency of MDMs expressing the M2 marker CD206 but had limited effects on M1 markers CD86 or HLA-DR. Palmitate stimulated MSCs had similar effects to naive MSCs increasing the frequency of CD206 expressing cells although not significantly (Supplementary Fig. 4).

Blocking ceramide de novo synthesis negates the effects of palmitate on MSC Immunomodulation of MDMs

Ceramide synthases (CERS) are essential enzymes required for the de novo synthesis of ceramides [50]. Palmitate exposure significantly increased expression of the ceramide synthase (CERS) genes *CERS4* (Fig. 3A) and *CERS5* (Fig. 3B), but not *CERS6* (Fig. 3C), suggesting increased ceramide de novo synthesis in response to palmitate. Inhibition of CERS activity using fumonisin B1 [51, 52], did not affect *CCL2* gene expression at 6 h (Fig. 3D), but significantly reduced CCL2 production by MSCs in response to palmitate at 24 h (Fig. 3E). This confirmed the hypothesis that palmitate-induced production of CCL2 by MSCs was linked to the de novo synthesis of ceramide. We further confirmed CCL2 production from MSCs in response to clinically relevant samples from patients with obesity, or healthy controls (Fig. 3F). MDMs in co-culture with MSCs exposed to both palmitate and fumonisin B1 produced the same levels of TNFα as those in co-culture with BSA control MSCs (Fig. 3G, including BSA and palmitate groups seen in Fig. 1B for comparison). Interestingly, palmitate exposed MSCs enhanced IL-10 production by MDMs following LPS stimulation and addition of fumonisin B1 abrogated this effect (Fig. 3H).

C2 ceramide can enhance MDM Immunomodulation by MSCs

Aside from being used for energy generation through fatty acid oxidation, palmitate is an important substrate for the de novo synthesis of sphingolipids, specifically ceramide [53–56]. To confirm that ceramide is the crucial link between palmitate uptake and CCL2 secretion, MSCs were exposed to the cell membrane-permeable ceramide analogue: C2 ceramide [57]. Gene expression of key genes was measured after 3 and 6 h. *PTGS2* was significantly elevated at the 3 h time point, reducing at the 6 h timepoint (Fig. 4A). *ANGPTL4* was elevated at both 3 and 6 h (Fig. 4B). *IL-6* expression only increased at the 6 h time point (Fig. 4C). Neither expression of *VEGF* (Fig. 4D) nor *IDO* (Fig. 4E) were affected by exposure to C2 ceramide. Overall, these patterns in gene expression mimicked those observed in response to palmitate (Fig. 1).

MSCs were also exposed to 10 μM ceramide or vehicle control for 24 h, and CCL2 production was measured (Fig. 4F). Ceramide promoted the production of CCL2 in all three MSC donors. Ceramide-exposed MSCs also showed improved suppression of TNFα production by

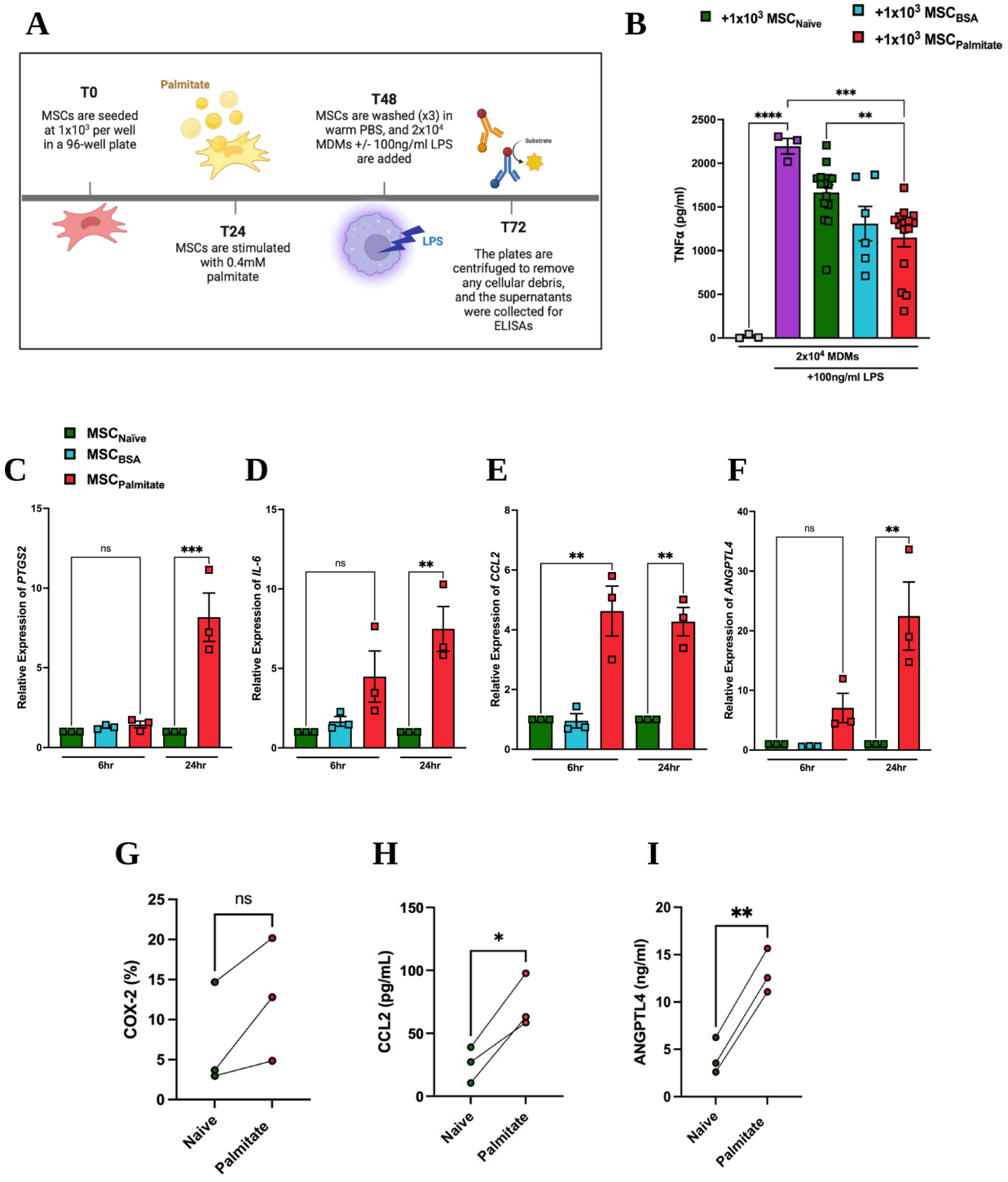

Fig. 1 Palmitate enhances MSC immunomodulation of MDMs. (**A**) Experimental design graphic: Human bone marrow MSCs were exposed to 0.4 mM palmitate for 24 h, washed with PBS and co-cultured with human MDMs at 1:20 ratio of MSC: MDMs. The co-culture was stimulated with 100 ng/mL of LPS for 24 h, and MDM production of TNFα was measured by (**B**) ELISA ($n = 3$ MSC donors + 3–4 MDM donors). Relative gene expression of MSCs in response to 0.4 mM palmitate after 6–24 h was measured for (**C**) *PTGS2*, (**D**) *IL-6*, (**E**) *CCL2*, and (**F**) *ANGPTL4* ($n = 3$). The protein production of (**G**) COX-2, (**H**) CCL2 and (**I**) ANGPTL4 were also measured using flow cytometry (COX-2) or ELISA (CCL2 and ANGPTL4). Data is presented as mean ± SEM. *$p < 0.05$, **$p < 0.01$, ***$p < 0.001$, ****$p < 0.0001$, ns: not significant. Statistical test: Ordinary one-way ANOVA with Tukey's multiple comparisons test (**B**-**F**) and unpaired t test with Welch's correction (**G**-**I**)

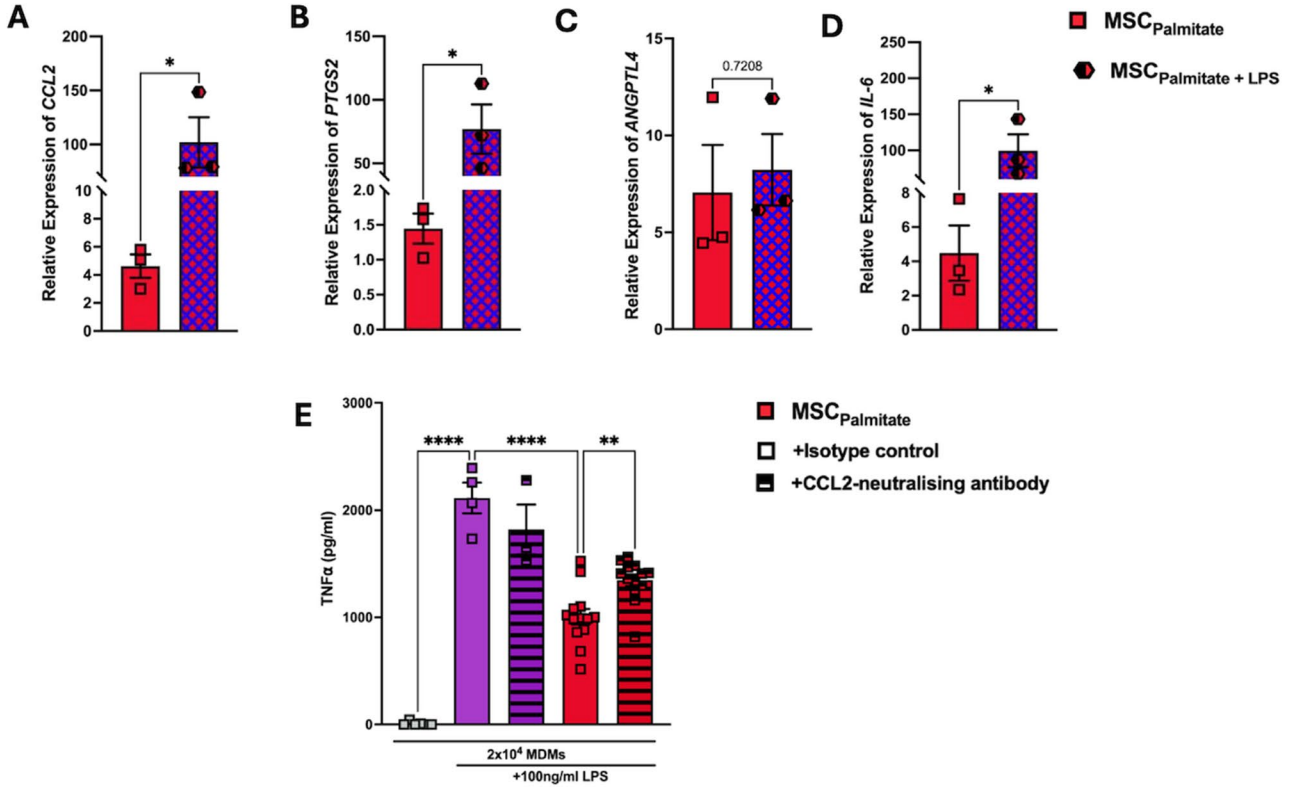

Fig. 2 Palmitate enhances MSC immunomodulation of MDMs via increased CCL2 production. Human bone marrow MSCs that were exposed to both 0.4 mM palmitate, and 100ng/ml LPS, for 6 h and analysed for gene expression of (**A**) *CCL2*, (**B**) *PTGS2*, (**C**) *ANGPTL4* and (**D**) *IL-6* ($n = 3$). Using the same approach as seen in Fig. 1A, palmitate exposed MSCs were cocultured with MDMs (1:20 MSC: MDM ratio) and LPS (100ng/ml). A CCL2-neutralising antibody or isotype control (5 ug/mL) were added to the culture and LPS stimulated MDM production of TNFa was measured by ELISA after 24 h (**E**) ($n = 3$ MSC donors + 3–4 MDM donors). Data is presented as mean ± SEM. $^{*}p < 0.05$, $^{**}p < 0.01$, $^{****}p < 0.0001$. Statistical test: unpaired t test with Welch's correction (**A**-**D**) and ordinary one-way ANOVA with Tukey's multiple comparisons test (**E**)

MDMs (Fig. 4G), and while naïve MSCs had no effect on IL-10 production, C2 ceramide pre-treated MSCs significantly increased the IL-10 production (Fig. 4H).

Discussion

Tissue source [12, 13], donor [58–60], and recipient disease microenvironment [14, 15, 17] all influence the therapeutic efficacy of MSCs. Increasing glycolytic metabolism in MSCs by culturing them under hypoxia [42, 61, 62] or suppressing mitochondrial respiration with oligomycin [63] can drastically improve their ability to suppress the proliferation of T cells. In many cases, stimulation with pro-inflammatory cytokines like IFNγ [42, 64, 65], TNFα, and IL-1β [66–68] enhances MSC immunomodulation. Importantly there are also external factors that can impair MSC immunomodulation. Exposure to dexamethasone [69] or an activation of the proliferator-activated receptor (PPAR)-δ [70] negatively impact the ability of MSCs to suppress T cell proliferation. The same is true for MSC exposure to palmitate, with palmitate at certain concentrations even promoting a pro-inflammatory response in MSCs, leading to increased T cell proliferation [36]. Importantly, high levels of palmitate are found in the serum of patients with obesity and type 2 diabetes mellitus (T2DM) and may have a negative impact on MSC efficacy in palmitate rich environments. The interaction between MSCs and macrophages have been identified as essential in the mode of action used by MSCs to reduce or control inflammation in various inflammatory conditions [44, 71, 72]. Thus, we sought to better understand the impact that a palmitate rich environment may have on MSCs immunomodulation of MDMs in vitro.

Interestingly, palmitate did not negatively impact macrophage suppression by MSCs. Pre-exposure of MSCs to palmitate enhanced MSC suppression of macrophage-produced TNFα and led to increased IL-10 secretion in response to LPS stimulation, compared to the naive MSCs. A range of MSC secreted factors have been implicated in immunosuppression of macrophages or promotion of a more anti-inflammatory pro-resolving macrophage phenotype. Prostaglandin-endoperoxide synthase 2 (*PTGS2*), the gene encoding for COX-2, is strongly associated with MSC suppression of

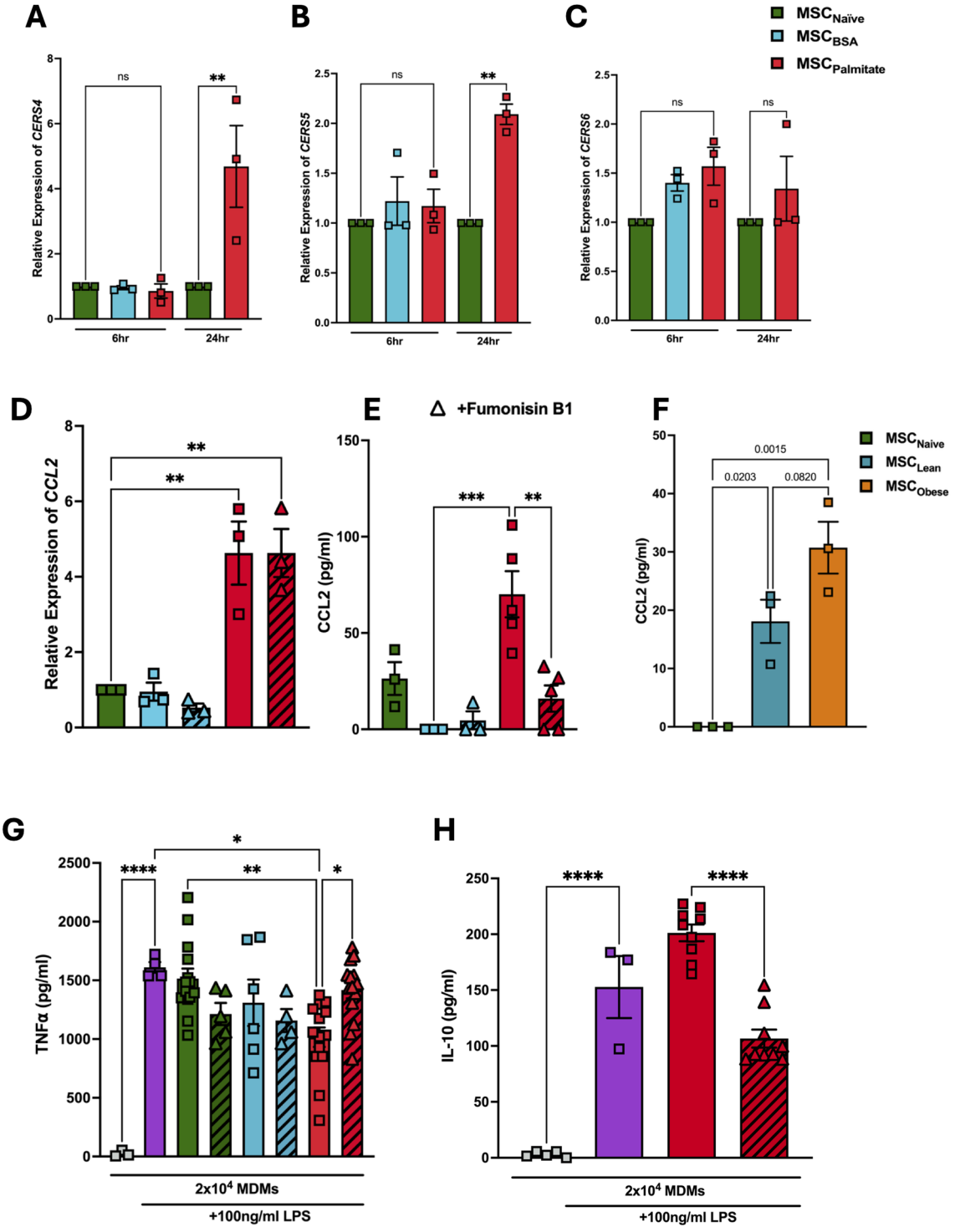

Fig. 3 Palmitate enhances MSC immunomodulation of MDMs via ceramide de novo synthesis. Human bone marrow mesenchymal stromal cells (MSCs) were exposed to 0.4 mM palmitate for 24 h, and relative gene expression of the ceramide synthase genes (**A**) *CERS4*, (**B**) *CERS5*, and (**C**) *CERS6* was measured via qPCR ($n = 3$). MSCs were further exposed to 0.4 mM palmitate and 40 µM fumonisin B1 for 6 h (for gene expression) or 24 h (for protein production). (**D**) *CCL2* gene expression was measured by qPCR and (**E**) CCL2 production was measured by ELISA. We further confirmed CCL2 production by MSCs in response to 20% obese serum (**F**). MSCs were thoroughly washed with PBS and used in a human monocyte-derived macrophage (MDM) suppression assay at a MSCs to MDM ratio of 1:20. After 24 h of stimulation with 100 ng/mL LPS, concentration of (**G**) TNFα and (**H**) IL-10 production was measured by ELISA ($n = 3$ MSC donors + 3–4 MDM donors). It is important to note that the BSA and palmitate-treated control groups have been taken from Fig. 1B, which we added to allow for accurate comparison. Data is presented as mean ± SEM. *$p < 0.05$, **$p < 0.01$, ***$p < 0.001$, ****$p < 0.0001$. Statistical test: Ordinary one-way ANOVA with Tukey's multiple comparisons test (**A**-**H**)

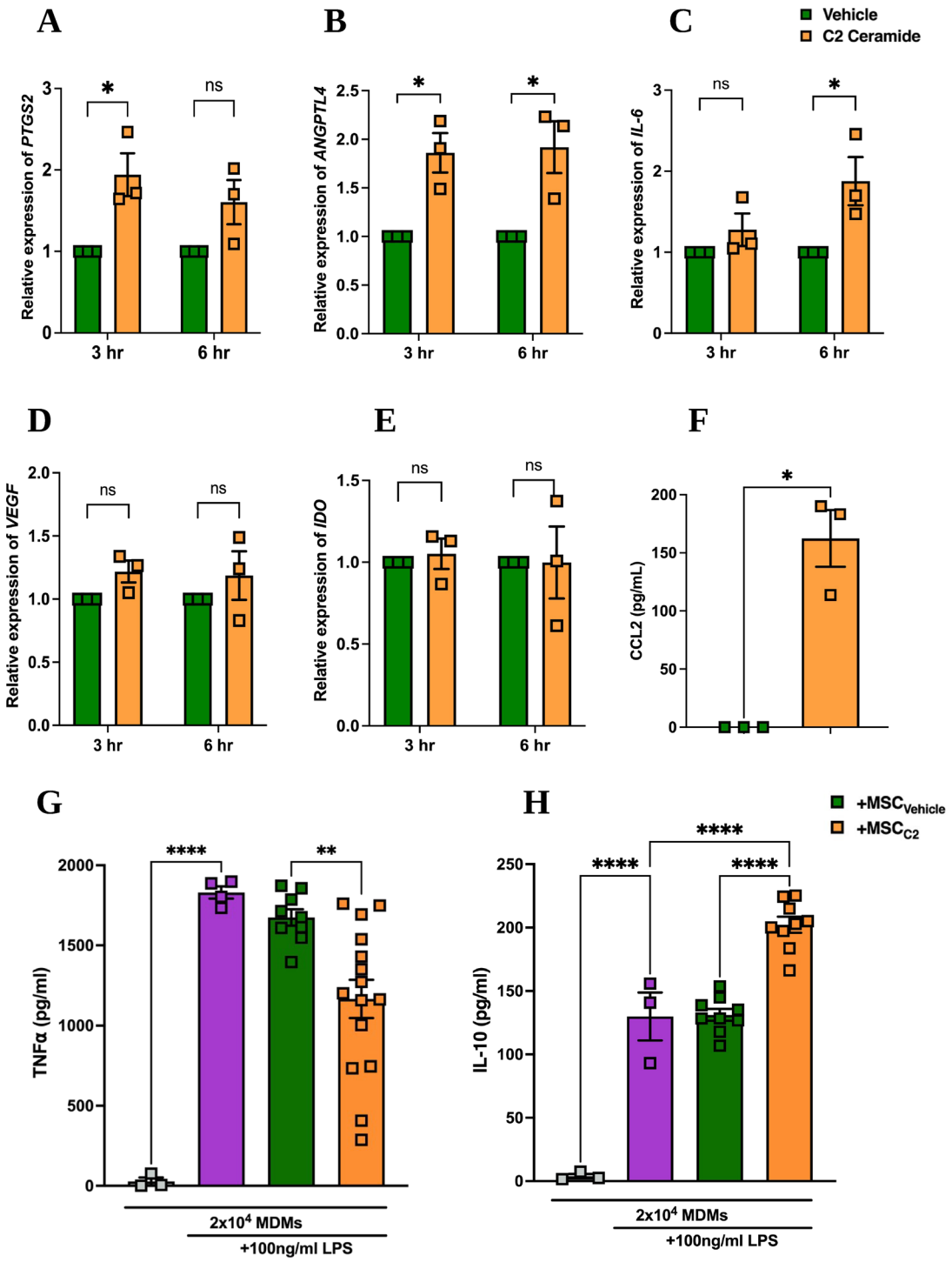

Fig. 4 C2 ceramide exposure shows similar effects to that of palmitate in the context of MDM immunomodulation. Human bone marrow MSCs were exposed to 10 μM C2 ceramide and gene expression was measured via qPCR after 3 and 6 h for (**A**) *PTGS2*, (**B**) *ANGPTL4*, (**C**) *IL-6*, (**D**) *VEGF*, and (**E**) *IDO*. (**F**) After 24 h of exposure, CCL2 protein production was measured by ELISA ($n = 3$). MSCs were also exposed to 10 μM C2 ceramide for 24 h, thoroughly washed, and co-cultured with human MDMs at a MSCs to MDM ratio of 1:20. The co-culture was stimulated with 100 ng/mL LPS for 24 h and concentration of (**G**) TNFα and (**H**) IL-10 in the supernatant was measured by ELISA ($n = 3$ MSC donors + 3–4 MDM donors). Data is presented as mean ± SEM. *$p < 0.05$, **$p < 0.01$, ***$p < 0.001$, ****$p < 0.0001$. Statistical test: Unpaired t test with Welch's correction (**A**-**F**) and ordinary one-way ANOVA with Tukey's multiple comparisons test (**G**, **H**)

macrophages [8, 9, 20, 41]. MSC-derived *IL-6* plays a role in MSC homeostasis, suppression of T cell proliferation [73], and inhibition of dendritic cell differentiation [74]. *CCL2* derived from MSCs has been associated with MSC promotion of IL-10 production by macrophages [10, 44]. The enzyme IDO plays a major role in MSC suppression of T cell proliferation and MSCs have been shown to promote macrophage production of IDO [1, 6, 75, 76]. In addition to calming immune cells, MSCs can also promote angiogenesis and tissue repair via release of *ANGPTL4* [77, 78] and vascular endothelial growth factor (*VEGF*) [15].

While MSCs increased the frequency of CD206 expressing macrophages, palmitate pre-exposed MSCs did not have a greater effect on macrophage polarisation. Interestingly, palmitate pre-exposure of MSCs led to increased gene expression of *PTGS2*, *IL-6*, *CCL2*, and *ANGPTL4*, but not *VEGF* or *IDO*. Protein production of COX-2, ANGPTL4 and CCL2 was also enhanced. Boland et al. [36] have previously showed that palmitate impaired MSC suppression of T cell suppression is associated with a defect in kynurenine activity. In line with our data, Boland et al. also show enhanced expression of PTGS2 and IL-6 alongside defective kynurenine activity and loss of T cell suppression in palmitate exposed MSCs. The palmitate-induced altered signalling associated with defective T cell suppression by MSCs remains unclear. Palmitate has been shown to induce endoplasmic reticulum (ER) stress and apoptosis in MSCs [34]. For successful suppression of T cell proliferation, MSCs need to be activated by proinflammatory cytokines such as IFN-γ leading to induction of IDO production by MSCs, which then turns tryptophan into kynurenine, depriving T cells of this essential amino acid [6, 42, 75, 79, 80]. Interestingly upregulation of genes associated with lipid and sterol biosynthesis in MSCs may alter the capacity for MSCs to be activated by pro-inflammatory cytokines [81]. While COX-2 and PGE2 activity have been shown to play a partial role in MSC suppression of T cell proliferation, IDO induced kynurenine activity is thought to be the dominant mechanism. In the context of MSC suppression of macrophages COX-2, CCL2, and the phagocytosis of apoptotic MSCs have been named repeatedly as important factors [10, 38, 39, 44, 48]. Thus, our data suggest that palmitate exposure leads to enhanced production of immunomodulatory factors associated with MSC suppression of macrophages.

As neutralisation of CCL2 abrogated the effects of palmitate on MSCs in an MDM suppression assay, we concluded that CCL2 is likely the primary mechanism of action through which palmitate enhances MSC immunomodulation of MDMs. While CCL2 is primarily considered a chemoattractant, MSC-derived CCL2 has recently been associated with increased IL-10 production in macrophages and monocytes and a promotion of an M2 macrophage phenotype [10, 44, 82]. CCL2 also enhances LPS-induced IL-10 production in macrophages [83] and has been shown to promote adipose tissue macrophage infiltration [84]. Evidence from the literature shows that following i.v. administration, MSCs undergo apoptosis and release high levels of CCL2 which attract monocytes [20, 85]. Furthermore, a link between ceramide de novo synthesis from palmitate and a resulting production of CCL2 prompted by ceramide activation of the NFκB pathway has been reported in adipocytes [86, 87]. Ceramide de novo synthesis from palmitate and direct administration of ceramide have been associated with activation of nuclear factor kappa-light-chain-enhancer of activated B cells (NFκB) and p38 signalling, and subsequent production of COX-2 [88, 89]. In adipocytes, which are closely related to MSCs, palmitate exposure and de novo ceramide synthesis led to the secretion of CCL2 [86, 87, 90].

We were able to show that palmitate promotes the expression of genes associated with ceramide de novo synthesis in MSCs, and that the suppression of ceramide de novo synthesis using fumonisin B1 blocks palmitate-enhanced production of MSC derived CCL2. Fumonisin B1 also blocked the palmitate-enhanced MSC immunomodulation of MDMs, both regarding decreased TNFα and increased IL-10 production.

Finally, we were able to show that exposing MSCs directly to ceramide had similar effects to palmitate exposure, both in relation to gene expression, CCL2 production, and immunomodulation of MDMs. While palmitate likely has multiple other effects in the cell, the data suggests a role for the palmitate/ceramide/CCL2 axis in the improved MDM immunomodulation of palmitate-exposed MSCs. Although we have not identified the signalling pathways through which ceramide C2 induces CCL2 in MSCs, there is evidence from the literature showing that ceramide-enriched LDL induces CCL2 in human monocytes via activation of CD14 and TLR4 [91]. Other studies have demonstrated that palmitate enhances TLR4 signal transduction [92, 93]), and that palmitate upregulates CCL2 in pancreatic beta cells in a TLR4/MyD88/NFkB dependent manner [97]. Palmitate can also induce ER stress leading to activation of ER stress sensors IRE1a and PERK with subsequent activation of NFkB and NLRP3 signalling. Several studies have linked palmitate enhanced activation of TLR4 or TRIF/IRF3 inflammatory signalling cascades in macrophages [94–96].

While our data shows that palmitate has a beneficial effect on macrophage immunomodulation by MSCs in vitro, this finding needs to be confirmed in a more complex in vivo setting.

There are limitations of our study. The question of how palmitate induced MSC-derived CCL2 interacts with MDMs to enhance MSC immunosuppressive effects remains unanswered. We have not determined if CCL2 binds to CCR2 or another receptor on MDMs and the sequence of signalling events involved remain to be uncovered. In addition, we have not measured the effect of CCL2 neutralisation on LPS stimulated MDM production of IL-10 induced by palmitate exposed MSCs or in ceramide C2 mediated enhanced MSC suppression of MDMs.

Although an interesting finding that exposure to palmitate enhances MSC capacity to suppress cytokine production by macrophages in vitro it is unsuitable as a potential licensing strategy to enhance MSC therapeutic efficacy given the additional negative effects. However, the knowledge that a palmitate rich environment likely does not negatively affect MSC therapy in conditions where macrophages play a key role such as ARDS [97], atherosclerosis [98], and Crohn's disease [99] may be valuable when treating patients with obesity. In fact, MSCs have been administered to T2DM patients for the treatment of diabetic nephropathy. These trials included patients with obesity (average patient BMI was defined as obese) and initial findings showed trends of stabilizing or improving eGFR and mGFR at week twelve post infusion [100, 101]. Administration of MSCs for treatment of Osteoarthritis in patients with obesity have also been shown to be efficacious [102]. A major consequence of elevated levels of palmitate in the blood is insulin resistance. Macrophages can promote insulin resistance via production of pro-inflammatory cytokines such as TNFa [103]. In preclinical models of high fat diet induced obesity there are several studies that show MSC administration improved insulin sensitivity, decreased triglyceride levels and lipotoxicity [104–107]. Indeed, MSCs have been shown to inhibit macrophage related inflammation in adipose tissue [108]. Thus, despite the negative effects of a palmitate rich environment on MSC suppression of T cell proliferation in vitro, there is a significant body of evidence to suggest that a palmitate rich environment such as that found in T2DM or obesity may not negatively impact MSC therapeutic efficacy where the mode of action involves immunomodulation of macrophages or other MSC cytoprotective functions. Combined with these published findings, our data suggests that MSCs may reduce insulin resistance via suppression of TNFa by macrophages. Moreover, our study elucidates further the role that MSC-derived CCL2 has on macrophage immunomodulation, which can be used for further research into MSC-macrophage interactions.

Conclusion

The environment in which MSCs are exposed to will be indicative of their functional capacity in vivo. With obesity levels rising worldwide, there is an unmet need for understanding the complexities of this environment, and the impact it may have on MSC-based cell therapy. Our study, where we exposed MSCs to the highly inflammatory FFA palmitate, highlights an enhanced immunomodulatory capacity in the context of human MDMs. We further elucidated that this occurs due to the promotion of the ceramide/CCL2 axis. This study, although limited, provides novel insight into the mechanism by which palmitate-exposed MSCs aid in the immunomodulation of macrophage in vitro.

Abbreviations

ANGPTL4	Angiopoietin-like 4
APC	Allophycocyanin
BSA	Bovine serum albumin
CCL	CC-chemokine ligand
cDNA	Coding deoxyribonucleic acid
CERS	Ceramide synthase
COX-2	Cyclooxygenase-2
DMEM	Dulbecco's modified Eagle medium
DPBS/PBS	Dulbecco's Phosphate Buffered Saline
ELISA	Enzyme linked immunosorbent assay
FACS	Flow cytometry staining
FBS	Fetal bovine serum
FFA	Free fatty acid
FPKM	Fragments per kilobase million
HPRT	Hypoxanthine-guanine phosphoribosyl transferase
IDO	Indoleamine 2,3-dioxygenase
IFN	Interferon
IL	Interleukin
LCFA	Long-chain fatty acid
LPS	Lipopolysaccharide
NFκB	Nuclear factor kappa-light-chain-enhancer of activated B cells
Palmitate	Palmitate-BSA
PBMCs	Peripheral blood mononuclear cells
PCR	Polymerase chain reaction
PE	R-Phycoerythrin
PGE2	Prostaglandin E_2
PTGS2	Prostaglandin-endoperoxide synthase 2
RBC	Red blood cell
SCFA	Short-chain fatty acid
SLC27	Solute carrier family 27
TNF	Tumour necrosis factor
VEGF	Vascular endothelial growth factor

Supplementary Information

The online version contains supplementary material available at https://doi.org/10.1186/s13287-025-04536-7.

Supplementary Material 1: Supplementary Figure 1: Characterisation of MDM surface factors via flow cytometry. Human peripheral blood mononuclear cells (PBMCs) were isolated from buffy coats, monocytes were selected via plastic adherence and differentiated into monocyte-derived macrophages (MDMs) over 6 days. MDMs were then detached using a lidocaine detachment buffer, stained for CD14, CD86, and CD206, and analysed by flow cytometry. Some MDMs were stimulated with 100 ng/mL LPS to observe changes in CD86 expression. ***n*** = 3 (3 different PBMC donors)

Supplementary Material 2: Supplementary Figure 2: MSC dose dependently suppress LPS induced MDM production of TNFα. Human bone-marrow derived mesenchymal stromal cells (MSCs) and human monocyte-derived

macrophages (MDMs) were co-cultured at ratios of 1:5, 1:10, and 1:20 and stimulated with 100 ng/mL LPS for 24 hr. MDM production of TNFα was measured by ELISA. ***n*** = 3 (3 different PBMC donors, 1 MSC donor). Data are presented as mean ± SEM. *****p***<0.01, *******p***<0.0001. Statistical test: Ordinary one-way ANOVA with Tukey's multiple comparisons test

Supplementary Material 3: Supplementary Figure 3: Analysis of palmitate induction of apoptosis in MSCs. MSCs were exposed to 0.4 mM or 1 mM palmitate or 0.5 uM Staurosporine as a positive control for 24 hr. MSC viability and induction of apoptosis was examined using an Annexin V/PI assay. ***N***=3, 3 independent MSC donors. Data are presented as mean ± SEM.

Supplementary Material 4: Supplementary Figure 4: MSCs promote an M2 switch in MDMs, and this is not further enhanced by palmitate pre-exposed MSC. MSCs from 3 donors were seeded at $2.5x10^3$ cells/well in a 24 well plate and treated with 0.4 mM palmitate for 24 hr. MSCs were then washed thoroughly twice with warm PBS and $5x10^3$ MDMs were added in abRPMI for an MSC to MDM ratio of 1:20. The co-culture was stimulated with 100 ng/mL LPS for 24 hr and cells were harvested using a lidocaine detachment buffer. Cells were incubated with fluorochrome labelled antibodies and surface phenotype was analysed using the Attune Nxt flow cytometer. Gating was performed on live (live/dead stain, near-IR fluorescent reactive dye, Invitrogen), CD14+ (PE) cells using antibodies for CD206 (Pacific Blue), HLA-DR (FITC), CD11b (PE-Cy7), CD86 (APC), and CD163 (PerCP). Data were analysed using floreada.io. Statistical test: Ordinary one-way ANOVA with Tukey's multiple comparisons test ****p***<0.05, ns; not significant. ***n*** = 3 human MDM donors.

Acknowledgements
We would like to acknowledge the Irish Blood Transfusion Service for providing access to anonymized blood components for our research. Any non-data illustrations were created with BioRender.

Author contributions
CT & LMB: Conception and design, generation of data, data analysis and interpretation, manuscript writing. AEH: Conception and design, manuscript writing. JAA: Manuscript writing. KE: Conception and design, manuscript writing, final approval of manuscript. All authors read and approved the final manuscript.

Funding
This publication has emanated from research supported by the John & Pat Hume doctoral awards of Maynooth University, and in part by a research grant from Science Foundation Ireland (SFI) under Grant Number 16/RI/3399, and Science Foundation Ireland Frontiers for the Future Award to K.E. (20/FFP-A/8948).

Data availability
The datasets used and/or analysed during the current study are available from the corresponding author on reasonable request.

Declarations

Ethics approval and consent to participate statement
Ethical approval was granted by the Medical Research Ethics Committees at St Vincent's University Hospital and by Maynooth University Ethics Committee entitled: Metabolic and Immunological Links Between Obesity, Systemic Inflammation, Type 2 Diabetes Mellitus and Non-Alcoholic Fatty Liver Disease granted on 28th June 2024 (BSRESC-2024-38575) and Investigating the role of macrophage education by MSCs in mediating MSC therapeutic efficacy granted on 11th February 2022 (BSRESC-2022-2460651). All patients gave written informed consent prior to partaking in the study. RoosterBio (company where the human BM-MSCs were purchased) has confirmed that there was initial ethical approval for collection of human cells, and that the donors had signed informed consent. RoosterBio state "RoosterBio sources commercially available in vitro research only human bone marrow aspirate from qualified donors. All human bone marrow aspirate collections are from healthy adult consented donors. Collection protocols and the donor-informed consent document are approved by an Institutional Review Board (IRB)".

Use of AI
The authors declare that they have not used AI-generated work in this manuscript.

Competing interests
The authors declare that they have no competing interests.

Author details
[1]Kathleen Lonsdale Institute for Human Health Research, Maynooth University, Maynooth, Co. Kildare, Ireland
[2]Department of Biology, Maynooth University, Maynooth, Co. Kildare, Ireland
[3]University of Iowa Fraternal Order of Eagles Diabetes Research Center, University of Iowa, Iowa City, IA 52242, USA
[4]Roy J. Carver Department of Biomedical Engineering, University of Iowa, Iowa City, IA 52242, USA

Received: 23 October 2024 / Accepted: 18 July 2025
Published online: 06 August 2025

References

1. Galleu A, Riffo-Vasquez Y, Trento C, Lomas C, Dolcetti L, Cheung TS, et al. Apoptosis in mesenchymal stromal cells induces in vivo recipient-mediated Immunomodulation. Sci Transl Med. 2017;9. https://doi.org/10.1126/scitranslmed.aam7828.
2. Naji A, Eitoku M, Favier B, Deschaseaux F, Rouas-Freiss N, Suganuma N. Biological functions of mesenchymal stem cells and clinical implications. Cell Mol Life Sci. 2019;76:3323–48. https://doi.org/10.1007/s00018-019-03125-1.
3. Dos Santos CC, Amatullah H, Vaswani CM, Maron-Gutierrez T, Kim M, Mei SHJ, et al. Mesenchymal stromal (stem) cell therapy modulates miR-193b-5p expression to attenuate sepsis-induced acute lung injury. Eur Respir J. 2022;59:2004216. https://doi.org/10.1183/13993003.04216-2020.
4. Li T-T, Zhang B, Fang H, Shi M, Yao W-Q, Li Y, et al. Human mesenchymal stem cell therapy in severe COVID-19 patients: 2-year follow-up results of a randomized, double-blind, placebo-controlled trial. EBioMedicine. 2023;92:104600. https://doi.org/10.1016/j.ebiom.2023.104600.
5. Ringdén O, Uzunel M, Rasmusson I, Remberger M, Sundberg B, Lönnies H, et al. Mesenchymal stem cells for treatment of therapy-resistant graft-versus-host disease. Transplantation. 2006;81:1390–7. https://doi.org/10.1097/01.tp.0000214462.63943.14.
6. English K, Barry FP, Field-Corbett CP, Mahon BP. IFN-γ and TNF-α differentially regulate Immunomodulation by murine mesenchymal stem cells. Immunol Lett. 2007;110:91–100. https://doi.org/10.1016/j.imlet.2007.04.001.
7. Dave M, Dev A, Somoza RA, Zhao N, Viswanath S, Mina PR, et al. MSCs mediate long-term efficacy in a crohn's disease model by sustained anti-inflammatory macrophage programming via efferocytosis. Npj Regen Med. 2024;9:1–16. https://doi.org/10.1038/s41536-024-00347-1.
8. Vasandan AB, Jahnavi S, Shashank C, Prasad P, Kumar A, Prasanna SJ. Human mesenchymal stem cells program macrophage plasticity by altering their metabolic status via a PGE2-dependent mechanism. Sci Rep. 2016;6:38308. https://doi.org/10.1038/srep38308.
9. Braza F, Dirou S, Forest V, Sauzeau V, Hassoun D, Chesné J, et al. Mesenchymal stem cells induce suppressive macrophages through phagocytosis in a mouse model of asthma. Stem Cells. 2016;34:1836–45. https://doi.org/10.1002/stem.2344.
10. Takeda K, Webb TL, Ning F, Shiraishi Y, Regan DP, Chow L, et al. Mesenchymal stem cells recruit CCR2 + Monocytes to suppress allergic airway inflammation. J Immunol. 2018;200:1261–9. https://doi.org/10.4049/jimmunol.1700562.
11. Zhao J, Li X, Hu J, Chen F, Qiao S, Sun X, et al. Mesenchymal stromal cell-derived exosomes attenuate myocardial ischaemia-reperfusion injury through miR-182-regulated macrophage polarization. Cardiovascular Res. 2019;115:1205–16. https://doi.org/10.1093/cvr/cvz040.
12. Burja B, Barlič A, Erman A, Mrak-Poljšak K, Tomšič M, Sodin-Semrl S, et al. Human mesenchymal stromal cells from different tissues exhibit unique responses to different inflammatory stimuli. Curr Res Translational Med. 2020;68:217–24. https://doi.org/10.1016/j.retram.2020.05.006.
13. Wegmeyer H, Bröske A-M, Leddin M, Kuentzer K, Nisslbeck AK, Hupfeld J, et al. Mesenchymal stromal cell characteristics vary depending on their origin. Stem Cells Dev. 2013;22:2606–18. https://doi.org/10.1089/scd.2013.0016.

14. Dunbar H, Hawthorne IJ, Tunstead C, McNamee EN, Weiss DJ, Armstrong ME, et al. Mesenchymal stromal cells dampen trained immunity in house dust mite-primed macrophages expressing human macrophage migration inhibitory factor polymorphism. Cytotherapy. 2024;S1465–32492400717–5. https://doi.org/10.1016/j.jcyt.2024.05.010.
15. Tunstead C, Volkova E, Dunbar H, Hawthorne IJ, Bell A, Crowe L, et al. The ARDS microenvironment enhances MSC-induced repair via VEGF in experimental acute lung inflammation. Mol Ther. 2024. https://doi.org/10.1016/j.ymthe.2024.08.003. S1525-0016(24)00525-2.
16. Carty F, Dunbar H, Hawthorne IJ, Ting AE, Stubblefield SR, Van't Hof W, et al. IFN-γ and PPARδ influence the efficacy and retention of multipotent adult progenitor cells in graft vs host disease. Stem Cells Transl Med. 2021;10:1561–74. https://doi.org/10.1002/sctm.21-0008.
17. Saldaña L, Bensiamar F, Vallés G, Mancebo FJ, García-Rey E, Vilaboa N. Immunoregulatory potential of mesenchymal stem cells following activation by macrophage-derived soluble factors. Stem Cell Res Ther. 2019;10:58. https://doi.org/10.1186/s13287-019-1156-6.
18. Islam D, Huang Y, Fanelli V, Delsedime L, Wu S, Khang J, et al. Identification and modulation of microenvironment is crucial for effective mesenchymal stromal cell therapy in acute lung injury. Am J Respir Crit Care Med. 2019;199:1214–24. https://doi.org/10.1164/rccm.201802-0356OC.
19. Cheung TS, Giacomini C, Cereda M, Avivar-Valderas A, Capece D, Bertolino GM, delaRosa O, Hicks R, Ciccocioppo R, Franzoso G, Galleu A, Ciccarelli FD, Dazzi F. Apoptosis in mesenchymal stromal cells activates an immunosuppressive secretome predicting clinical response in crohn's disease. Mol Ther. 2023;31(12):3531–44. Epub 2023 Oct 7. PMID: 37805713; PMCID: PMC10727969.
20. Cheung TS, Galleu A, von Bonin M, Bornhäuser M, Dazzi F. Apoptotic mesenchymal stromal cells induce prostaglandin E2 in monocytes: implications for the monitoring of mesenchymal stromal cell activity. Haematologica. 2019;104(10):e438–41. https://doi.org/10.3324/haematol.2018.214767. Epub 2019 Mar 7. PMID: 30846505; PMCID: PMC6886441.
21. European Commission. Over half of adults in the EU are overweight. Eurostat 2019. https://ec.europa.eu/eurostat/web/products-eurostat-news/-/ddn-20210721-2 (accessed March 21, 2022).
22. Flegal KM, Kruszon-Moran D, Carroll MD, Fryar CD, Ogden CL. Trends in obesity among adults in the United States, 2005 to 2014. JAMA. 2016;315:2284–91. https://doi.org/10.1001/jama.2016.6458.
23. Worldwide trends in underweight and obesity. From 1990 to 2022: a pooled analysis of 3663 population-representative studies with 222 million children, adolescents, and adults. Lancet. 2024;403:1027–50. https://doi.org/10.1016/S0140-6736(23)02750-2.
24. Gruchała-Niedoszytko M, Małgorzewicz S, Niedoszytko M, Gnacińska M, Jassem E. The influence of obesity on inflammation and clinical symptoms in asthma. Adv Med Sci. 2013;58:15–21. https://doi.org/10.2478/v10039-012-0082-y.
25. Cildir G, Akincilar SC, Tergaonkar V. Chronic adipose tissue inflammation: all immune cells on the stage. Trends Mol Med. 2013;19:487–500. https://doi.org/10.1016/j.molmed.2013.05.001.
26. Schmidt FM, Weschenfelder J, Sander C, Minkwitz J, Thormann J, Chittka T, et al. Inflammatory cytokines in general and central obesity and modulating effects of physical activity. PLoS ONE. 2015;10:e0121971. https://doi.org/10.1371/journal.pone.0121971.
27. Vendrell J, Broch M, Vilarrasa N, Molina A, Gómez JM, Gutiérrez C, et al. Resistin, adiponectin, ghrelin, leptin, and proinflammatory cytokines: relationships in obesity. Obes Res. 2004;12:962–71. https://doi.org/10.1038/oby.2004.118.
28. Leal V, de O, Mafra D. Adipokines in obesity. Clin Chim Acta. 2013;419:87–94. https://doi.org/10.1016/j.cca.2013.02.003.
29. Sarabhai T, Koliaki C, Mastrototaro L, Kahl S, Pesta D, Apostolopoulou M, et al. Dietary palmitate and oleate differently modulate insulin sensitivity in human skeletal muscle. Diabetologia. 2022;65:301–14. https://doi.org/10.1007/s00125-021-05596-z.
30. Hammerschmidt P, Steculorum SM, Bandet CL, Del Río-Martín A, Steuernagel L, Kohlhaas V, et al. CerS6-dependent ceramide synthesis in hypothalamic neurons promotes er/mitochondrial stress and impairs glucose homeostasis in obese mice. Nat Commun. 2023;14:7824. https://doi.org/10.1038/s41467-023-42595-7.
31. Heath BR, Gong W, Taner HF, Broses L, Okuyama K, Cheng W et al. Saturated fatty acids dampen the immunogenicity of cancer by suppressing STING. Cell Rep 2023;42. https://doi.org/10.1016/j.celrep.2023.112303
32. Bader JE, Wolf MM, Lupica-Tondo GL, Madden MZ, Reinfeld BI, Arner EN, et al. Obesity induces PD-1 on macrophages to suppress anti-tumour immunity. Nature. 2024;630:968–75. https://doi.org/10.1038/s41586-024-07529-3.
33. Chu SG, Villalba JA, Liang X, Xiong K, Tsoyi K, Ith B, et al. Palmitic Acid–Rich High-Fat diet exacerbates experimental pulmonary fibrosis by modulating Endoplasmic reticulum stress. Am J Respir Cell Mol Biol. 2019;61:737–46. https://doi.org/10.1165/rcmb.2018-0324OC.
34. Lu J, Wang Q, Huang L, Dong H, Lin L, Lin N, et al. Palmitate causes endoplasmic reticulum stress and apoptosis in human mesenchymal stem cells: prevention by AMPK activator. Endocrinology. 2012;153:5275–84. https://doi.org/10.1210/en.2012-1418.
35. Gillet C, Spruyt D, Rigutto S, Dalla Valle A, Berlier J, Louis C, et al. Oleate abrogates Palmitate-Induced lipotoxicity and proinflammatory response in human bone marrow-derived mesenchymal stem cells and osteoblastic cells. Endocrinology. 2015;156:4081–93. https://doi.org/10.1210/en.2015-1303.
36. Boland L, Burand AJ, Brown AJ, Boyt D, Lira VA, Ankrum JA. IFN-γ and TNF-α pre-licensing protects mesenchymal stromal cells from the pro-inflammatory effects of palmitate. Mol Ther. 2018;26:860–73. https://doi.org/10.1016/j.ymthe.2017.12.013.
37. Weiss DJ, English K, Krasnodembskaya A, Isaza-Correa JM, Hawthorne IJ, Mahon BP. The necrobiology of mesenchymal stromal cells affects therapeutic efficacy. Front Immunol. 2019;10:1228. https://doi.org/10.3389/fimmu.2019.01228.
38. Schrodt MV, Behan-Bush RM, Liszewski JN, Humpal-Pash ME, Boland LK, Scroggins SM, et al. Efferocytosis of viable versus heat-inactivated MSC induces human monocytes to distinct immunosuppressive phenotypes. Stem Cell Res Ther. 2023;14:206. https://doi.org/10.1186/s13287-023-03443-z.
39. Pang SHM, D'Rozario J, Mendonca S, Bhuvan T, Payne NL, Zheng D, et al. Mesenchymal stromal cell apoptosis is required for their therapeutic function. Nat Commun. 2021;12:6495. https://doi.org/10.1038/s41467-021-26834-3.
40. Maggini J, Mirkin G, Bognanni I, Holmberg J, Piazzón IM, Nepomnaschy I, et al. Mouse bone marrow-derived mesenchymal stromal cells turn activated macrophages into a regulatory-like profile. PLoS ONE. 2010;5:e9252. https://doi.org/10.1371/journal.pone.0009252.
41. Kota DJ, Prabhakara KS, Toledano-Furman N, Bhattarai D, Chen Q, DiCarlo B, et al. Prostaglandin E2 indicates therapeutic efficacy of mesenchymal stem cells in experimental traumatic brain injury. Stem Cells. 2017;35:1416–30. https://doi.org/10.1002/stem.2603.
42. Wobma HM, Kanai M, Ma SP, Shih Y, Li HW, Duran-Struuck R, et al. Dual IFN-γ/hypoxia priming enhances immunosuppression of mesenchymal stromal cells through regulatory proteins and metabolic mechanisms. J Immunol Regen Med. 2018;1:45–56. https://doi.org/10.1016/j.regen.2018.01.001.
43. Luz-Crawford P, Kurte M, Bravo-Alegría J, Contreras R, Nova-Lamperti E, Tejedor G, et al. Mesenchymal stem cells generate a CD4 + CD25 + Foxp3 + regulatory T cell population during the differentiation process of Th1 and Th17 cells. Stem Cell Res Ther. 2013;4:65. https://doi.org/10.1186/scrt216.
44. Giri J, Das R, Nylen E, Chinnadurai R, Galipeau J. CCL2 and CXCL12 derived from mesenchymal stromal cells cooperatively polarize IL-10 + Tissue macrophages to mitigate gut injury. Cell Rep. 2020;30:1923–34. https://doi.org/10.1016/j.celrep.2020.01.047.e4.
45. Dunbar H, Hawthorne IJ, McNamee EN, Armstrong ME, Donnelly SC, English K. The human MIF polymorphism CATT7 enhances pro-inflammatory macrophage polarization in a clinically relevant model of allergic airway inflammation. FASEB J. 2024;38(6):e23576. doi: 10.1096/fj.202400207R. PMID: 38530238.https://doi.org/10.1186/s13287-023-03443-z. PMID: 37592321; PMCID: PMC10433682.
46. Dunbar H, Hawthorne IJ, English K. MAC attack: MSCs and macrophages join forces against chronic lung infection. Thorax. 2024;79(8):698–699. https://doi.org/10.1136/thorax-2024-221637. PMID: 38575316.
47. Massaro F, Corrillon F, Stamatopoulos B, Dubois N, Ruer A, Meuleman N, et al. Age-related changes in human bone marrow mesenchymal stromal cells: morphology, gene expression profile, Immunomodulatory activity and MiRNA expression. Front Immunol. 2023;14:1267550. https://doi.org/10.3389/fimmu.2023.1267550.
48. Luque-Campos N, Bustamante-Barrientos FA, Pradenas C, García C, Araya MJ, Bohaud C, et al. The macrophage response is driven by mesenchymal stem Cell-Mediated metabolic reprogramming. Front Immunol. 2021;12:624746. https://doi.org/10.3389/fimmu.2021.624746.
49. Cho D-I, Kim MR, Jeong H, Jeong HC, Jeong MH, Yoon SH, et al. Mesenchymal stem cells reciprocally regulate the M1/M2 balance in mouse bone marrow-derived macrophages. Exp Mol Med. 2014;46:e70–70. https://doi.org/10.1038/emm.2013.135.

50. Levy M, Futerman AH, Mammalian Ceramide Synthases. IUBMB Life. 2010;62:347–56. https://doi.org/10.1002/iub.319.
51. Riley RT, Merrill AH. Ceramide synthase Inhibition by fumonisins: a perfect storm of perturbed sphingolipid metabolism, signaling, and disease [S]. J Lipid Res. 2019;60:1183–9. https://doi.org/10.1194/jlr.S093815.
52. Zitomer NC, Mitchell T, Voss KA, Bondy GS, Pruett ST, Garnier-Amblard EC, et al. Ceramide synthase Inhibition by Fumonisin B1 causes accumulation of 1-Deoxysphinganine: A novel category of bioactive 1-deoxysphingoid bases and 1-deoxydihydroceramides biosynthesized by mammalian cell lines and animals *. J Biol Chem. 2009;284:4786–95. https://doi.org/10.1074/jbc.M808798200.
53. Tran TTT, Postal BG, Demignot S, Ribeiro A, Osinski C, Pais de Barros J-P, et al. Short term palmitate supply impairs intestinal insulin signaling via ceramide production. J Biol Chem. 2016;291:16328–38. https://doi.org/10.1074/jbc.M115.709626.
54. McNally BD, Ashley DF, Hänschke L, Daou HN, Watt NT, Murfitt SA, et al. Long-chain ceramides are cell non-autonomous signals linking lipotoxicity to endoplasmic reticulum stress in skeletal muscle. Nat Commun. 2022;13:1748. https://doi.org/10.1038/s41467-022-29363-9.
55. Watt MJ, Barnett AC, Bruce CR, Schenk S, Horowitz JF, Hoy AJ. Regulation of plasma ceramide levels with fatty acid oversupply: evidence that the liver detects and secretes de novo synthesised ceramide. Diabetologia. 2012;55:2741–6. https://doi.org/10.1007/s00125-012-2649-3.
56. Yoshida K, Morishima Y, Ishii Y, Mastuzaka T, Shimano H, Hizawa N. Abnormal saturated fatty acids and sphingolipids metabolism in asthma. Respir Investig. 2024;62:526–30. https://doi.org/10.1016/j.resinv.2024.04.006.
57. Sot J, Goñi FM, Alonso A. Molecular associations and surface-active properties of short- and long-N-acyl chain ceramides. Biochimica et biophysica acta (BBA). - Biomembr. 2005;1711:12–9. https://doi.org/10.1016/j.bbamem.2005.02.014.
58. Zhukareva V, Obrocka M, Houle JD, Fischer I, Neuhuber B. Secretion profile of human bone marrow stromal cells: donor variability and response to inflammatory stimuli. Cytokine. 2010;50:317–21. https://doi.org/10.1016/j.cyto.2010.01.004.
59. Russell AL, Lefavor R, Durand N, Glover L, Zubair AC. Modifiers of mesenchymal stem cell quantity and quality. Transfusion. 2018;58:1434–40. https://doi.org/10.1111/trf.14597.
60. Kang I, Lee B-C, Choi SW, Lee JY, Kim J-J, Kim B-E, et al. Donor-dependent variation of human umbilical cord blood mesenchymal stem cells in response to hypoxic preconditioning and amelioration of limb ischemia. Exp Mol Med. 2018;50:1–15. https://doi.org/10.1038/s12276-017-0014-9.
61. Alekseeva OYu, Bobyleva PI, Andreeva ER. Effect of multipotent mesenchymal stromal cells on functional activity of monocyte-derived macrophages under Short-Term hypoxic stress in vitro. Hum Physiol. 2022;48:899–905. https://doi.org/10.1134/S0362119722070155.
62. Byrnes D, Masterson CH, Brady J, Alagesan S, Gonzalez HE, McCarthy SD, et al. Differential effects of cytokine versus hypoxic preconditioning of human mesenchymal stromal cells in pulmonary sepsis induced by antimicrobial-resistant klebsiella pneumoniae. Pharmaceuticals. 2023;16:149. https://doi.org/10.3390/ph16020149.
63. Contreras-Lopez R, Elizondo-Vega R, Paredes MJ, Luque-Campos N, Torres MJ, Tejedor G, et al. HIF1α-dependent metabolic reprogramming governs mesenchymal stem/stromal cell immunoregulatory functions. FASEB J. 2020;34:8250–64. https://doi.org/10.1096/fj.201902232R.
64. Corbett JM, Hawthorne I, Dunbar H, Coulter I, Chonghaile MN, Flynn CM, et al. Cyclosporine A and IFNγ licencing enhances human mesenchymal stromal cell potency in a humanised mouse model of acute graft versus host disease. Stem Cell Res Ther. 2021;12:238. https://doi.org/10.1186/s13287-021-02309-6.
65. Vigo T, La Rocca C, Faicchia D, Procaccini C, Ruggieri M, Salvetti M, et al. IFNβ enhances mesenchymal stromal (Stem) cells Immunomodulatory function through STAT1-3 activation and mTOR-associated promotion of glucose metabolism. Cell Death Dis. 2019;10:85. https://doi.org/10.1038/s41419-019-1336-4.
66. Hackel A, Aksamit A, Bruderek K, Lang S, Brandau S. TNF-α and IL-1β sensitize human MSC for IFN-γ signaling and enhance neutrophil recruitment. Eur J Immunol. 2021;51:319–30. https://doi.org/10.1002/eji.201948336.
67. Murphy N, Treacy O, Lynch K, Morcos M, Lohan P, Howard L, et al. TNF-α/IL-1β—licensed mesenchymal stromal cells promote corneal allograft survival via myeloid cell-mediated induction of Foxp3 + regulatory T cells in the lung. FASEB J. 2019;33:9404–21. https://doi.org/10.1096/fj.201900047R.
68. Fan H, Zhao G, Liu L, Liu F, Gong W, Liu X, et al. Pre-treatment with IL-1β enhances the efficacy of MSC transplantation in DSS-induced colitis. Cell Mol Immunol. 2012;9:473–81. https://doi.org/10.1038/cmi.2012.40.
69. Wang H, Pang B, Li Y, Zhu D, Pang T, Liu Y. Dexamethasone has variable effects on mesenchymal stromal cells. Cytotherapy. 2012;14:423–30. https://doi.org/10.3109/14653249.2011.652735.
70. Luz-Crawford P, Ipseiz N, Espinosa-Carrasco G, Caicedo A, Tejedor G, Toupet K, et al. PPARβ/δ directs the therapeutic potential of mesenchymal stem cells in arthritis. Ann Rheum Dis. 2016;75:2166–74. https://doi.org/10.1136/annrheumdis-2015-208696.
71. Ghanem LY, Mansour IM, Abulata N, Akl MM, Demerdash ZA, El Baz HG, Mahmoud SS, Mohamed SH, Mahmoud FS, Hassan ASM. Liver macrophage depletion ameliorates the effect of mesenchymal stem cell transplantation in a murine model of injured liver. Sci Rep. 2019;9:35.
72. Carty F, Mahon BP, English K. The influence of macrophages on mesenchymal stromal cell therapy: passive or aggressive agents? Clinical and experimental immunology, 188, issue 1, April 2017, Pages 1–11, https://doi.org/10.1111/cei.12929
73. Dorronsoro A, Lang V, Ferrin I, Fernández-Rueda J, Zabaleta L, Pérez-Ruiz E, et al. Intracellular role of IL-6 in mesenchymal stromal cell immunosuppression and proliferation. Sci Rep. 2020;10:21853. https://doi.org/10.1038/s41598-020-78864-4.
74. Djouad F, Charbonnier L-M, Bouffi C, Louis-Plence P, Bony C, Apparailly F, et al. Mesenchymal stem cells inhibit the differentiation of dendritic cells through an Interleukin-6-Dependent mechanism. Stem Cells. 2007;25:2025–32. https://doi.org/10.1634/stemcells.2006-0548.
75. Jitschin R, Böttcher M, Saul D, Lukassen S, Bruns H, Loschinski R, et al. Inflammation-induced glycolytic switch controls suppressivity of mesenchymal stem cells via STAT1 glycosylation. Leukemia. 2019;33:1783–96. https://doi.org/10.1038/s41375-018-0376-6.
76. Boyt DT, Boland LK, Burand AJ, Brown AJ, Ankrum JA. Dose and duration of interferon γ pre-licensing interact with donor characteristics to influence the expression and function of indoleamine-2,3-dioxygenase in mesenchymal stromal cells. J R Soc Interface. 2020;17:20190815. https://doi.org/10.1098/rsif.2019.0815.
77. Li J, Xu X, Fei S, Wang R, Wang H, Zhu W, et al. Small extracellular vesicles derived from human umbilical cord mesenchymal stem cells enhanced proangiogenic potential of cardiac fibroblasts via Angiopoietin-Like 4. Stem Cells Int. 2022;2022:3229289. https://doi.org/10.1155/2022/3229289.
78. Cho DI, Kang H-J, Jeon JH, Eom GH, Cho HH, Kim MR, et al. Antiinflammatory activity of ANGPTL4 facilitates macrophage polarization to induce cardiac repair. JCI Insight. 2019;4. https://doi.org/10.1172/jci.insight.125437.
79. Munn DH, Shafizadeh E, Attwood JT, Bondarev I, Pashine A, Mellor AL. Inhibition of T cell proliferation by macrophage Tryptophan catabolism. J Exp Med. 1999;189:1363–72. https://doi.org/10.1084/jem.189.9.1363.
80. Bender DA. Biochemistry of Tryptophan in health and disease. Mol Aspects Med. 1983;6:101–97. https://doi.org/10.1016/0098-2997(83)90005-5.
81. Campos AM, Maciel E, Moreira AS, Sousa B, Melo T, Domingues P, Curado L, Antunes B, Domingues MR, Santos F. Lipidomics of mesenchymal stromal cells: Understanding the adaptation of phospholipid profile in response to Pro-Inflammatory cytokines. J Cell Physiol. 2016;231(5):1024–32. https://doi.org/10.1002/jcp.25191. Epub 2015 Oct 8. PMID: 26363509.
82. Shinohara I, Tsubosaka M, Toya M, Lee ML, Kushioka J, Murayama M, et al. C-C motif chemokine ligand 2 enhances macrophage chemotaxis, osteogenesis, and angiogenesis during the inflammatory phase of bone regeneration. Biomolecules. 2023;13:1665. https://doi.org/10.3390/biom13111665.
83. Sierra-Filardi E, Nieto C, Domínguez-Soto A, Barroso R, Sánchez-Mateos P, Puig-Kroger A, López-Bravo M, Joven J, Ardavín C, Rodríguez-Fernández JL, Sánchez-Torres C, Mellado M, Corbí AL. CCL2 shapes macrophage polarization by GM-CSF and M-CSF: identification of CCL2/CCR2-dependent gene expression profile. J Immunol. 2014;192(8):3858–67. https://doi.org/10.4049/jimmunol.1302821. Epub 2014 Mar 17. PMID: 24639350.
84. Lee SJ, Kang JS, Kim HM, Lee ES, Lee JH, Chung CH, Lee EY. CCR2 knockout ameliorates obesity-induced kidney injury through inhibiting oxidative stress and ER stress. PLoS ONE. 2019;14(9):e0222352. https://doi.org/10.1371/journal.pone.0222352. PMID: 31498850; PMCID: PMC6733486.
85. English K, Apoptotic, MSCs. COX2/PGE2 and clinical efficacy in Crohn fistula. Mol Ther. 2023;31(12):3364–6. https://doi.org/10.1016/j.ymthe.2023.11.006. Epub 2023 Nov 18. PMID: 37980902; PMCID: PMC10727974.
86. Hamada Y, Nagasaki H, Fujiya A, Seino Y, Shang Q-L, Suzuki T, et al. Involvement of de novo ceramide synthesis in pro-inflammatory adipokine

secretion and adipocyte-macrophage interaction. J Nutr Biochem. 2014;25:1309–16. https://doi.org/10.1016/j.jnutbio.2014.07.008.
87. Morita N, Hosaka T, Kitahara A, Murashima T, Onuma H, Sumitani Y, et al. Novel mechanisms modulating palmitate-induced inflammatory factors in hypertrophied 3T3-L1 adipocytes by AMPK. J Diabetes Res. 2018;2018:9256482. https://doi.org/10.1155/2018/9256482.
88. Doyle T, Chen Z, Muscoli C, Obeid LM, Salvemini D. Intraplantar-injected ceramide in rats induces hyperalgesia through an NF-κB- and p38 kinase-dependent cyclooxygenase 2/prostaglandin E2 pathway. FASEB J. 2011;25:2782–91. https://doi.org/10.1096/fj.10-178095.
89. Oh E, Yun M, Kim SK, Seo G, Bae JS, Joo K, et al. Palmitate induces COX-2 expression via the sphingolipid pathway-mediated activation of NF-κB, p38, and ERK in human dermal fibroblasts. Arch Dermatol Res. 2014;306:339–45. https://doi.org/10.1007/s00403-013-1434-6.
90. Wang J, Liu J, Yuan C, Yang B, Pang H, Chen K, et al. Palmitic acid-activated GPRs/KLF7/CCL2 pathway is involved in the crosstalk between bone marrow adipocytes and prostate cancer. BMC Cancer. 2024;24:75. https://doi.org/10.1186/s12885-024-11826-5.
91. Estruch M, Sánchez-Quesada JL, Ordóñez-Llanos J, Benítez S. Ceramide-enriched LDL induces cytokine release through TLR4 and CD14 in monocytes. Similarities with electronegative LDL. Clin Investig Arterioscler. 2014 May-Jun;26(3):131-7. https://doi.org/10.1016/j.arteri.2013.12.003. Epub 2014 Mar 12. PMID: 24630524.
92. Eguchi K, Manabe I, Oishi-Tanaka Y, Ohsugi M, Kono N, Ogata F, Yagi N, Ohto U, Kimoto M, Miyake K, Tobe K, Arai H, Kadowaki T, Nagai R. Saturated fatty acid and TLR signaling link β cell dysfunction and islet inflammation. Cell Metab. 2012;15(4):518– 33. doi: 10.1016/j.cmet.2012.01.023. Epub 2012 Mar 29. PMID: 22465073.
93. Lancaster GI, Langley KG, Berglund NA, Kammoun HL, Reibe S, Estevez E, Weir J, Mellett NA, Pernes G, Conway JRW, Lee MKS, Timpson P, Murphy AJ, Masters SL, Gerondakis S, Bartonicek N, Kaczorowski DC, Dinger ME, Meikle PJ, Bond PJ, Febbraio MA. Evidence that TLR4 is not a receptor for saturated fatty acids but mediates Lipid-Induced inflammation by reprogramming macrophage metabolism. Cell Metab. 2018;27(5):1096–e11105. https://doi.org/10.1016/j.cmet.2018.03.014. Epub 2018 Apr 19. PMID: 29681442.
94. Cullberg K, Larsen J, Pedersen S et al. Effects of LPS and dietary free fatty acids on MCP-1 in 3T3-L1 adipocytes and macrophages in vitro. Nutr & Diabetes 4, e113 (2014). https://doi.org/10.1038/nutd.2014.10
95. Tashiro H, Takahashi K, Sadamatsu H, et al. Saturated fatty acid increases lung macrophages and augments house dust Mite-Induced airway inflammation in mice fed with High-Fat diet. Inflammation. 2017;40:1072–86. https://doi.org/10.1007/s10753-017-0550-4.
96. Ahmad R, Al-Roub A, Kochumon S, Akther N, Thomas R, Kumari M, Koshy MS, Tiss A, Hannun YA, Tuomilehto J, Sindhu S, Rosen ED. The synergy between palmitate and TNF-αfor CCL2 production is dependent on the TRIF/IRF3 pathway: implications for metabolic inflammation. J Immunol. 2018;52. https://doi.org/10.4049/jimmu.
97. Morrell ED, Bhatraju PK, Mikacenic CR, Radella F, Manicone AM, Stapleton RD, et al. Alveolar macrophage transcriptional programs are associated with outcomes in acute respiratory distress syndrome. Am J Respir Crit Care Med. 2019;200:732–41. https://doi.org/10.1164/rccm.201807-1381OC.
98. Susser LI, Rayner KJ. Through the layers: how macrophages drive atherosclerosis across the vessel wall. J Clin Invest. 2022;132. https://doi.org/10.1172/JCI157011.
99. Gorreja F. Macrophages in Crohn's Disease: Innate immune cellular and molecular mechanisms driving intestinal inflammation and fibrosis. 2023.
100. Packham DK, Fraser IR, Kerr PG, Segal KR. Allogeneic mesenchymal precursor cells (MPC) in diabetic nephropathy: A randomized, placebo-controlled, dose escalation study. EBioMedicine. 2016;12:263–9. https://doi.org/10.1016/j.ebiom.2016.09.011. Epub 2016 Sep 17. PMID: 27743903; PMCID: PMC5078602.
101. Skyler JS, Fonseca VA, Segal KR, Rosenstock J. MSB-DM003 investigators. Allogeneic mesenchymal precursor cells in type 2 diabetes: A randomized, placebo-controlled, dose-escalation safety and tolerability pilot study. Diabetes Care. 2015;38(9):1742–9. https://doi.org/10.2337/dc14-2830. Epub 2015 Jul 7. PMID: 26153271; PMCID: PMC4542273.
102. Song JS, Hong KT, Kim NM, Park HS, Choi NH. Human umbilical cord blood-derived mesenchymal stem cell implantation for osteoarthritis of the knee. Arch Orthop Trauma Surg. 2020;140(4):503–9. https://doi.org/10.1007/s00402-020-03349-y. Epub 2020 Jan 24. PMID: 31980879.
103. Khodabandehloo H, Gorgani-Firuzjaee S, Panahi G, Meshkani R. Molecular and cellular mechanisms linking inflammation to insulin resistance and β-cell dysfunction. Transl Res. 2016;167(1):228–56. Epub 2015 Sep 5. PMID: 26408801.
104. Jaber H, Issa K, Eid A, Saleh FA. The therapeutic effects of Adipose-Derived-Mesenchymal stem cells on obesity and its associated diseases in Diet-InducedObese mice. Sci Rep. 2021;11:6291. https://doi.org/10.1038/s41598-021-85917-9.
105. Lee C-W, Hsiao W-T, Lee OK-S. Mesenchymal stromal cell-basedtherapies reduce obesity and metabolic syndromes induced by a high-fat diet. Trans Res. 2017;182:61–e748. https://doi.org/10.1016/j.trsl.2016.11.003.
106. Shree N, Venkategowda S, Venkatranganna MV, Datta I, Bhonde RR. Human adipose tissue mesenchymal stem cells as a novel treatmentmodality for correcting obesity induced metabolic dysregulation. Int JObes. 2019;43:2107–18. https://doi.org/10.1038/s41366-019-0438-5.
107. Boland L, Bitterlich LM, Hogan AE, Ankrum JA, English K. Translating MSC therapy in the age of obesity. Front Immunol. 2022;13:943333. https://doi.org/10.3389/fimmu.2022.943333. PMID: 35860241; PMCID: PMC9289617.
108. Wang Y, Fu J, He W, Gao Y, Du J, Xu J, Guo L, Liu Y. Bone marrow mesenchymal stem cells ameliorate diet-induced obesity by activating thermogenesis and alleviating inflammation in adipose tissue. Biochem Biophys Res Commun. 2025;747:151172. Epub 2024 Dec 20. PMID: 39793396.

Publisher's note

Received: 20 April 2023 | Revised: 26 May 2023 | Accepted: 21 June 2023

DOI: 10.1096/fj.202300787R

RESEARCH ARTICLE

The FASEB Journal

Blockade of MIF biological activity ameliorates house dust mite-induced allergic airway inflammation in humanized MIF mice

Hazel Dunbar[1,2] | **Ian J. Hawthorne**[1,2] | **Courteney Tunstead**[1,2] | **Michelle E. Armstrong**[3] | **Seamas C. Donnelly**[3] | **Karen English**[1,2]

[1]Kathleen Lonsdale Institute for Human Health Research, Maynooth University, Maynooth, Ireland

[2]Department of Biology, Maynooth University, Maynooth, Ireland

[3]Department of Medicine, Trinity College Dublin, Tallaght University Hospital, Co., Dublin, Ireland

Correspondence
Karen English, Department of Biology, Kathleen Lonsdale Institute for Human Health Research, Maynooth University, Maynooth, Co. Kildare, Ireland.
Email: karen.english@mu.ie

Funding information
Irish Research Council (An Chomhairle um Thaighde in Éirinn), Grant/Award Number: IRCLA/2017/288

Abstract

Macrophage migration inhibitory factor (MIF) expression is controlled by a functional promoter polymorphism, where the number of tetranucleotide repeats ($CATT_n$) corresponds to the level of MIF expression. To examine the role of this polymorphism in a pre-clinical model of allergic asthma, novel humanized MIF mice with increasing CATT repeats ($CATT_5$ and $CATT_7$) were used to generate a physiologically relevant scale of airway inflammation following house dust mite (HDM) challenge. $CATT_7$ mice expressing high levels of human MIF developed an aggressive asthma phenotype following HDM challenge with significantly elevated levels of immune cell infiltration, production of inflammatory mediators, goblet cell hyperplasia, subepithelial collagen deposition, and airway resistance compared to wild-type controls. Importantly the potent MIF inhibitor SCD-19 significantly mitigated the pathophysiology observed in $CATT_7$ mice after HDM challenge, demonstrating the fundamental role of endogenous human MIF expression in the severity of airway inflammation in vivo. Up to now, there are limited reproducible in vivo models of asthma airway remodeling. Current asthma medications are focused on reducing the acute inflammatory response but have limited effects on airway remodeling. Here, we present a reproducible pre-clinical model that capitulates asthma airway remodeling and suggests that in addition to having pro-inflammatory effects MIF may play a role in driving airway remodeling.

Abbreviations: AHR, airway hyperresponsiveness; ANOVA, analysis of variance; BALF, bronchoalveolar lavage fluid; BMDM, bone marrow derived macrophage; CATT, tetranucleotide repeat sequence; CD74, cluster of differentiation 74; G, tissue damping; H, tissue elasticity; H&E, haematoxylin & eosin; HDM, house dust mite; hMIF, human macrophage migration inhibitory factor; IgE, Immunoglobulin E; IL, interleukin; I.N., intranasal; I.P., intraperitoneal; ISO-1, (S,R)-3-(4-hydroxyphenyl)-4,5-dihydro-5-isoxazole acetic acid methyl ester; Mch, methacholine; MIF, macrophage migration inhibitory factor; OVA, ovalbumin; PAS, periodic acid-schiff; PBS, phosphate buffered saline; R_N, airway resistance; RNA, ribonucleic acid; SCD-19, 3-(2-methylphenyl)-1H-isochromen-1-one; SEM, standard error mean; Th2, T helper type 2; WT, wildtype.

Hazel Dunbar and Ian J. Hawthorne joint first authors.

KEYWORDS
airway inflammation, airway remodeling, allergic asthma, house dust mite, macrophage migration inhibitory factor, MIF, MIF inhibitors, severe asthma

1 | INTRODUCTION

Asthma is a complex multifactorial disease affecting over 300 million people worldwide.[1] Allergic asthma is characterized by sensitization to specific and/or non-specific stimuli resulting in airway hyperresponsiveness (AHR), airway inflammation, and goblet cell hyperplasia.[2,3] Common environmental stimuli include house dust mite (HDM), mold, cigarette smoke, and pet dander.[4,5] HDM, a trigger in up to 85% of asthmatic patients,[6] has proteolytic activity to cleave epithelial tight junctions after inhalation to permit uptake by submucosal antigen-presenting cells surrounding the upper airways.[7] Lung inflammation is orchestrated by the release of prototypical Th2 cytokines, IL-4, IL-5, and IL-13 which drive the release of inflammatory mediators into the surrounding microenvironment.[8] Preclinical models of allergic asthma have provided significant contributions for the understanding of allergic airway inflammation; however, we have limited access to reproducible models of asthma airway remodeling.[9]

Macrophage migration inhibitory factor (MIF) is detected at high levels in the bronchoalveolar lavage fluid (BALF) and serum of asthmatic patients.[10] The level of MIF expression can vary in humans due to a functional repeat polymorphism implicating a tetranucleotide sequence 'CATT', found at position -794 in the promoter region of the MIF gene.[11] Four types of allelic variations were found, classified as 5-CATT, 6-CATT, 7-CATT, and 8-CATT, with the 5-CATT repeat allele presenting the lowest promoter activity.[12] Interestingly low MIF 5-CATT allele correlates with lower levels of inflammation and thus milder forms of asthma. Studies have established a role for MIF in asthma, with the use of MIF deficient mice ($MIF^{-/-}$), anti-MIF antibodies, and small molecular weight inhibitors. In a mouse model of ovalbumin (OVA)-induced allergic airway inflammation, $MIF^{-/-}$ mice had lower levels of pulmonary inflammation, Th2 cytokines, and airway hyperresponsiveness (AHR) compared to wild-type controls.[10] Administration of a MIF neutralizing antibody mitigated the MIF-related induction of AHR in an OVA model, but notably had no effect on the production of Th2 cytokines or IgE.[13] The prototypical MIF antagonist ISO-1 could abrogate AHR and airway inflammation in mice challenged with HDM, along with illustrating MIF's role in epithelial barrier dysfunction in vitro.[14] A polyclonal anti-MIF antibody decreased cellular infiltration in BALF from OVA-induced allergic mice but failed to decrease Th2 cytokines or IgE.[15] The link between MIF and airway remodeling has also been investigated in OVA-challenged mice. ISO-1 decreased autophagy in smooth muscle cells, thus reducing the incidence of airway remodeling after OVA sensitization.[16]

Current treatments for asthma focus on the management of symptoms and consist of utilization of bronchodilators and glucocorticoid steroids to control the intensity and number of allergic exacerbations. The more recently developed biologics target Th2-driven inflammation; however, these medications have limited effects on airway remodeling.[9] MIF is known to suppress the action of glucocorticoids[17,18] and therefore the levels of MIF expressed by asthma patients may have a major impact on their responsiveness to therapeutic strategies.

To better understand the potential impact of high allele human MIF expression on the severity of allergic airway inflammation and remodeling, we have generated novel humanized mice expressing high (CATT7) or low (CATT5) levels of human MIF. Using a specific MIF inhibitor, we have examined the specificity of human MIF expression in driving HDM-induced allergic airway inflammation.

2 | MATERIALS AND METHODS

2.1 | Ethics statement

All procedures involving the use of animals were carried out by licensed personnel. Ethical approval for all work was granted by the ethics committee of Maynooth University (BRESC-2018-13). Project Authorization was received from the HPRA (AE19124/P022), whereby the terms of the animal experiments within this project were outlined and adhered to.

2.2 | Humanized MIF mice

Two mouse strains expressing the human high- or low-expression *MIF* alleles (e.g., MIF^{CATT7} [C57BL/6NTac-Miftm3884.1(MIF)Tac-Tg(CAG-Flpe)2Arte] and MIF^{CATT5} [C57BL/6NTac-Miftm3883.1(MIF)Tac-Tg(CAG-Flpe)2Arte] mice) were created using vector-based recombinant replacement of murine *Mif* by Taconic Biosciences (Rensselaer, NY, US). Validation of the expression of human and not murine *MIF* mRNA was verified by qPCR, and -794 CATT-length dependent stimulated MIF production was confirmed in vivo.[19]

2.3 | Mouse model of house dust mite-induced acute allergic airway inflammation

WT, CATT5 and CATT7 mice (6–18 weeks old) were challenged with 25 μg of house dust mite (HDM) allergen, *Dermatophagoides pteronyssinus* (Greer Labs, Lenoir, NC, US) or PBS control intranasally (I.N.) 3 days weekly for 3 weeks under light isoflurane anesthesia.

2.4 | MIF inhibitors

SCD-19 (3-(2-methylphenyl)-1H-isochromen-1-one) (Specs.net), or ISO-1 ((S,R)-3-(4-hydroxyphenyl)-4,5-dihydro-5-isoxazole acetic acid methyl ester) (Tocris) small molecular weight inhibitors of macrophage migration inhibitory factor (MIF) enzymatic activity was used in a house dust mite model of acute allergic airway inflammation. 35 mg/kg of SCD-19 was administered intraperitoneally (I.P.) twice weekly for three weeks; day 0, 4, 7, 11, 14, and 18.

2.5 | Histology

On day 21 of the model, lungs were harvested. Tissue was fixed in 10% (v/v) neutral buffered formalin (Sigma-Aldrich) for 24 h. Tissue was then processed using an automated processor (Shandon Pathcentre, Runcorn, UK) and embedded in paraffin wax using a Shannon Histocentre 2 (Shandon). Once sectioned with a Shandon Finesse 325 microtome (Thermo-Shandon, Waltham, MA, USA), tissue sections (5 μm) were stained for Masson's Trichrome (Sigma-Aldrich), Periodic Acid Schiff (Abcam) and Haemotoxylin and Eosin-Y (Richard Allan Scientific). Samples were air dried and a coverslip was mounted with DPX mounting media (BDH). 4× and 20× images were taken using an Olympus BX51 light microscope.

2.6 | Histological scoring

Following staining, slides were coded without reference to prior treatment and examined in a blind manner. For H&E, images were scored using a composite scale from 1 to 9; comprising of infiltration or aggregation of inflammatory cells in air space or vessel wall [1 = only wall, 2 = few cells (1–5 cells) in air space, 3 = intermediate, 4 = severe (air space congested)]; interstitial congestion and hyaline membrane [formation: 1 = normal lung, 2 = moderate (<25% of lung section), 3 = intermediate (25%–50% of lung section), 4 = severe (>50% of lung section)]; hemorrhage: (0 = absent, 1 = present).[20] For periodic acid-schiff (PAS), images were scored by counting the number of PAS-positive (magenta) mucin-producing goblet cells present within the airway, relative to the diameter to the airway. Collagen deposition was calculated by analyzing the % of positive staining following Masson's Trichrome staining using the trainable Weka segmentation plugin on Fiji open-source software.

2.7 | Bronchoalveolar lavage fluid (BALF) Retrieval

Mice were sacrificed by lethal overdose of sodium pentobarbital via I.P. injection on day 18 of the model, 4 hr after last challenge. A tracheostomy and cannulation was performed, where a 27 gauge cannula was secured in place with sutures. 1 mL of cold endotoxin-free PBS was infused into the lungs through the cannula using a 1 mL syringe for 3 gentle instillations. BALF was placed into an eppendorf and kept on ice before being centrifuged at 300*g* for 5 min at 4°C. The supernatant was collected, aliquoted and 10× protease inhibitor solution (Roche) was added to prevent protein degradation.

2.8 | BALF cell analysis

Cells were isolated and resuspended in 100 μL of endotoxin-free PBS for counting. Cyto-spin funnels were pre-wet by spinning with 300 μL of PBS onto glass slides at 600 rpm for 5 min. 1×10^5 cells in a volume of 300 μL of PBS were spun onto fresh labeled glass slides at 600 rpm for 10 min using a RotoFix 32 cytocentrifuge (Hettich Zentrifugen). Slides were airdried before being stained with Kwik-Diff™ Stain (Shandon, ThermoScientific); 25 s in fixative, 15 s in solution I and 15 s in solution II. Slides were imaged on an Olympus BX51 light microscope until 300 cells could be counted. Cells were identified as being neutrophils, eosinophils, macrophages, or lymphocytes.

2.9 | Cytokine analysis

BALF supernatants were analyzed for Th2 cytokines IL-4 (Biolegend), IL-5 (Biolegend), IL-13 (eBioscience), and human MIF (R&D Systems) by ELISA following the manufacturer's instructions.

2.10 | FlexiVent® lung function

Mice were anesthetized with 150 mg/kg ketamine and 2 mg/kg medetomidine via subcutaneous injection and

the surgical plane of anesthesia was reached. A tail vein catheter was inserted. Tracheostomy and cannulation was carried out. The mouse was placed close to the FlexiVent FX system (SCIREQ, Emka Technologies, Paris, France) and mechanical ventilation was initiated by selecting a predefined ventilation. Every 6 min, alfaxan and 0.5 mg/kg Tracium, a neuromuscular blocking agent (NMBA), was administered through the tail vail catheter. The measurement of lung function was initiated and approximately 100 µL of PBS or increasing concentrations of the bronchoconstrictor methacholine (MCh) (3.125, 12.5, and 25 mg/mL) was loaded into the nebulizer. Upon completion of lung function measurements at baseline and following increasing aerosolized methacholine challenges, the ventilator was stopped and the mouse was euthanized using either I.P. injection of sodium pentobarbital or via cervical dislocation.

2.11 | Statistical methods

All data are presented as mean ± SEM. Results of two or more groups were compared by analysis of variance (ANOVA) followed by the post-hoc Tukey's multiple comparison test. were analyzed using a statistical software package (GraphPad Prism, San Diego, CA). Response to different concentrations of methacholine was analyzed by 2-way ANOVA followed by the *post-hoc* Tukey's multiple comparison test. GraphPad Prism (GraphPad Software Inc, San Diego, CA, USA) was used for all statistical analyses.

3 | RESULTS

3.1 | Functional –794CATT polymorphic mouse tissues express different levels of hMIF under basal and disease conditions

Novel humanized MIF mice were generated to capitulate the varying levels of MIF expression under the functional promoter polymorphism within the human population. C57BL/6 mice were humanized by replacing the murine MIF gene with the human counterpart. Within this human MIF gene, 794 downstream of the promoter region, where the number of tetranucleotide repeats correlates with MIF allele expression,[11] 5 repeats of this tetranucleotide sequence 'CATT' generated $CATT_5$ mice, containing the low expressing MIF allele. 7 repeats of this tetranucleotide sequence 'CATT' generated $CATT_7$ mice, containing the high expressing MIF allele (Figure 1A). To characterize the effect of the CATT microsatellite repeat we analyzed hMIF production under basal and disease conditions. Bronchoalveolar lavage fluid (BALF) (Figure 1B), bone marrow-derived macrophages (BMDMs) (Figure 1C), and splenocytes (Figure 1D) isolated from $CATT_7$ mice secrete significantly higher levels of hMIF than $CATT_5$ or wildtype (WT) mice (Figure 1B–D).

To investigate the role of the human MIF polymorphism in a disease setting, a model of acute allergic airway inflammation was generated. The clinically relevant house dust mite (HDM) allergen was administered intranasally three times a week for three weeks to induce airway inflammation (Figure 1E). BALF was obtained, and lungs were snap frozen for RNA isolation and qPCR analysis on day 21. Significantly higher levels of hMIF were detected in $CATT_7$ BALF compared to BALF from $CATT_5$ or WT mice (Figure 1F). Similarly, the relative expression of human *Mif* was significantly increased in the $CATT_7$ compared to the $CATT_5$ mouse lung tissue (Figure 1G).

These data comprehensively show that the CATT polymorphism is responsible for differential production of hMIF under basal and disease conditions. This model allows us to investigate the role of high versus low hMIF in the pathophysiology of acute airway inflammation in a relevant pre-clinical model.

3.2 | Human $CATT_7$ allele significantly increases the Th2 signature in an HDM model of allergic airway inflammation

Absence of MIF in models of allergic inflammation has been shown to reduce the levels of Th2 cytokines in the BALF.[10,21] To study the effect of different levels of endogenous MIF on asthma severity, $CATT_7$, $CATT_5$, and WT C57BL/6 mice were challenged with HDM intranasally 3 times a week for 3 consecutive weeks. 4 hr post final challenge the mice were sacrificed, and the BALF was obtained. The BALF total leukocyte counts show that $CATT_7$ mice challenged with HDM have significantly higher numbers of immune cells in the bronchoalveolar space compared to WT mice (Figure 2A). $CATT_7$ mice also exhibit a marked increase in cell number compared to $CATT_5$ although not significant (Figure 2A). Differential cell counts demonstrated that the predominant cell type in the BALF are eosinophils (Figure 2B,C).

To further characterize the influence of hMIF on asthma pathophysiology we explored its effects on the prototypical Th2 signature. IL-4, IL-5, and IL-13 have been shown to be critical in the development of airway hyperresponsiveness, eosinophilic responses, and goblet cell hyperplasia, and responsible for the overall asthma phenotype. Th2 cytokines were detected in the BALF of $CATT_5$ and WT HDM mice (Figure 2D–F). However, we observed significantly elevated levels of IL-4, IL-5,

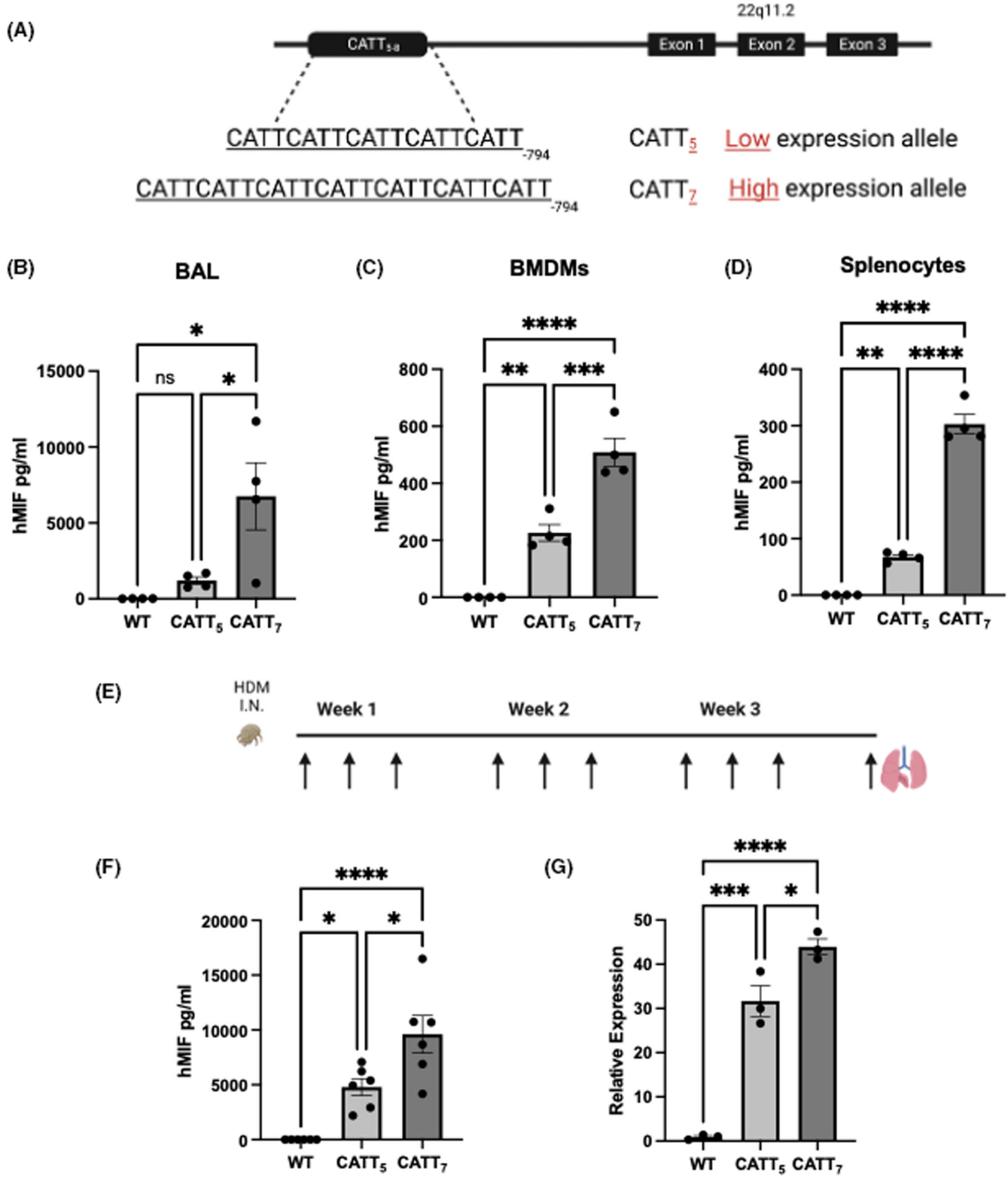

FIGURE 1 Functional –794CATT polymorphisms lead to different expression levels of hMIF under basal and disease conditions. (A) Human MIF gene containing a functional polymorphism in position 794 downstream of the promoter region, where the number of tetranucleotide repeats correlates with promoter activity and MIF allele expression; 5 repeats = $CATT_5$ mice, 7 repeats = $CATT_7$ mice. (B) hMIF levels in BAL fluid of naïve WT, $CATT_5$ and $CATT_7$ mice. (C) hMIF production from BMDMs of WT, $CATT_5$, and $CATT_7$ mice. (D) hMIF production from splenocytes of WT, $CATT_5$, and $CATT_7$ mice. (E) Timeline for HDM exposure. Mice were intranasally challenged with HDM 3 times a week for 3 consecutive weeks. (F) Levels of hMIF detected in the BAL fluid of WT, $CATT_5$, and $CATT_7$ mice challenged with HDM. (G) Relative expression of hMIF detected in lung homogenates of WT, $CATT_5$, and $CATT_7$ mice challenged with HDM detected by real-time PCR. Data are presented as mean ± SEM; $N = 3–6$ per group. *$p < .05$; **$p < .01$; ****$p < .0001$.

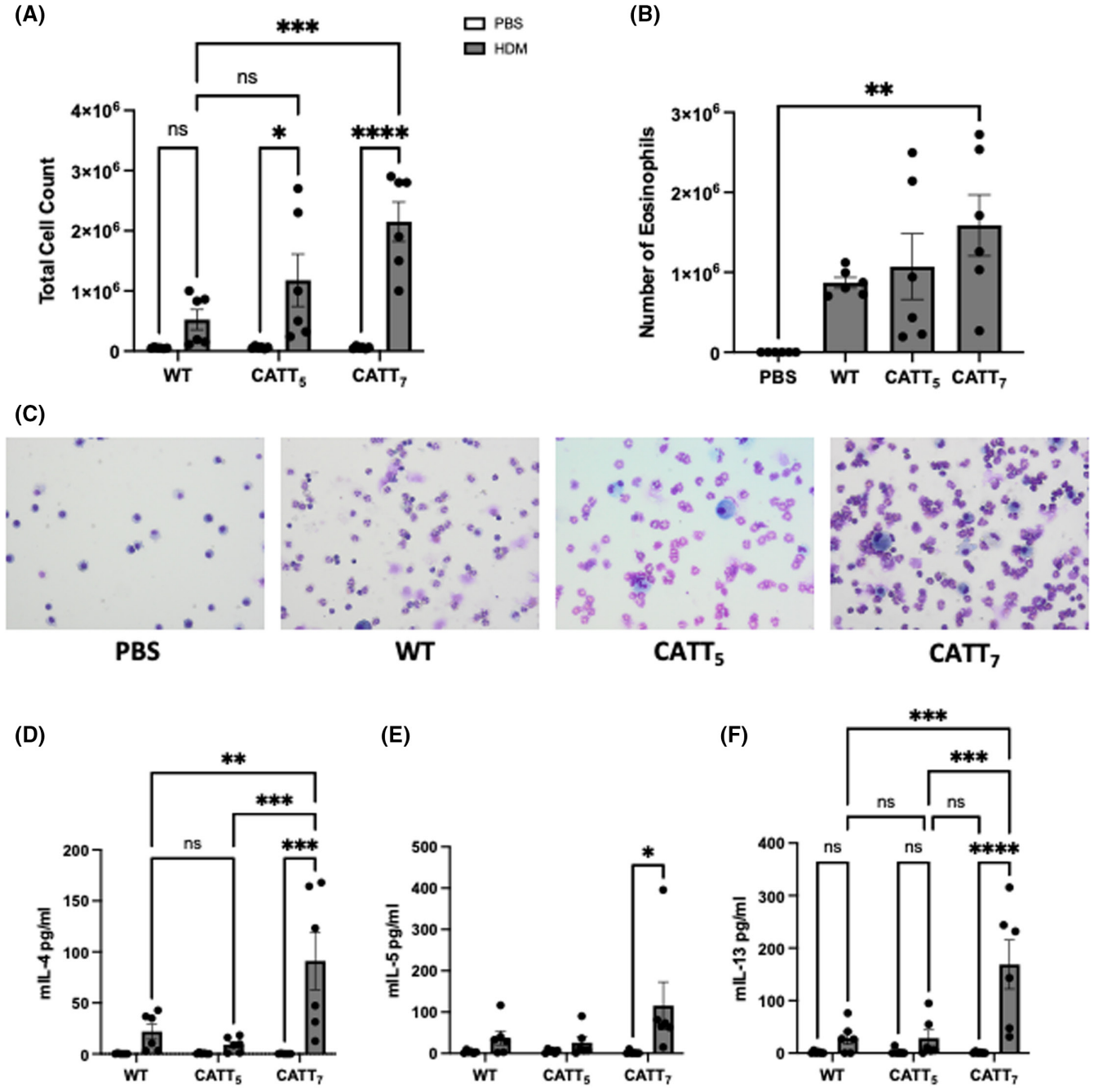

FIGURE 2 Human $CATT_7$ allele significantly increases the Th2 cytokine signature in a HDM model of allergic airway inflammation. (A) Total cell count recovered from the BAL. (B) BAL fluid eosinophil count determined by differential staining of cytospins. (C) Representative imgaes of cytosins. Cytokine levels of (D) IL-4, (E) IL-5, and (F) IL-13 in the BAL fluid determined by ELISA. Data are presented as mean ± SEM; $N = 6$ per group. *$p < .05$; **$p < .01$; ***$p < .001$; ****$p < .0001$.

ad IL-13 in $CATT_7$ HDM compared to $CATT_7$ PBS group (Figure 2D–F). Furthermore, significantly higher levels of IL-4 and IL-13 were detected in $CATT_7$ HDM compared to $CATT_5$ and WT HDM (Figure 2D,F). A marked increase in IL-5 was also detected although not significant (Figure 2E). These data show that the $CATT_7$ polymorphism generates a prominent Th2 cytokine profile which may contribute to a more severe asthma phenotype.

3.3 | The human $CATT_7$ allele exacerbates hallmarks of asthma pathophysiology

Excessive production of mucus and the associated pathophysiological changes are hallmarks in a range of respiratory diseases including asthma.[22] We investigated the effect of the CATT polymorphism on goblet cell hyperplasia by staining lung tissue with PAS (Figure 3A). PBS control groups exhibited very low levels of PAS-positive

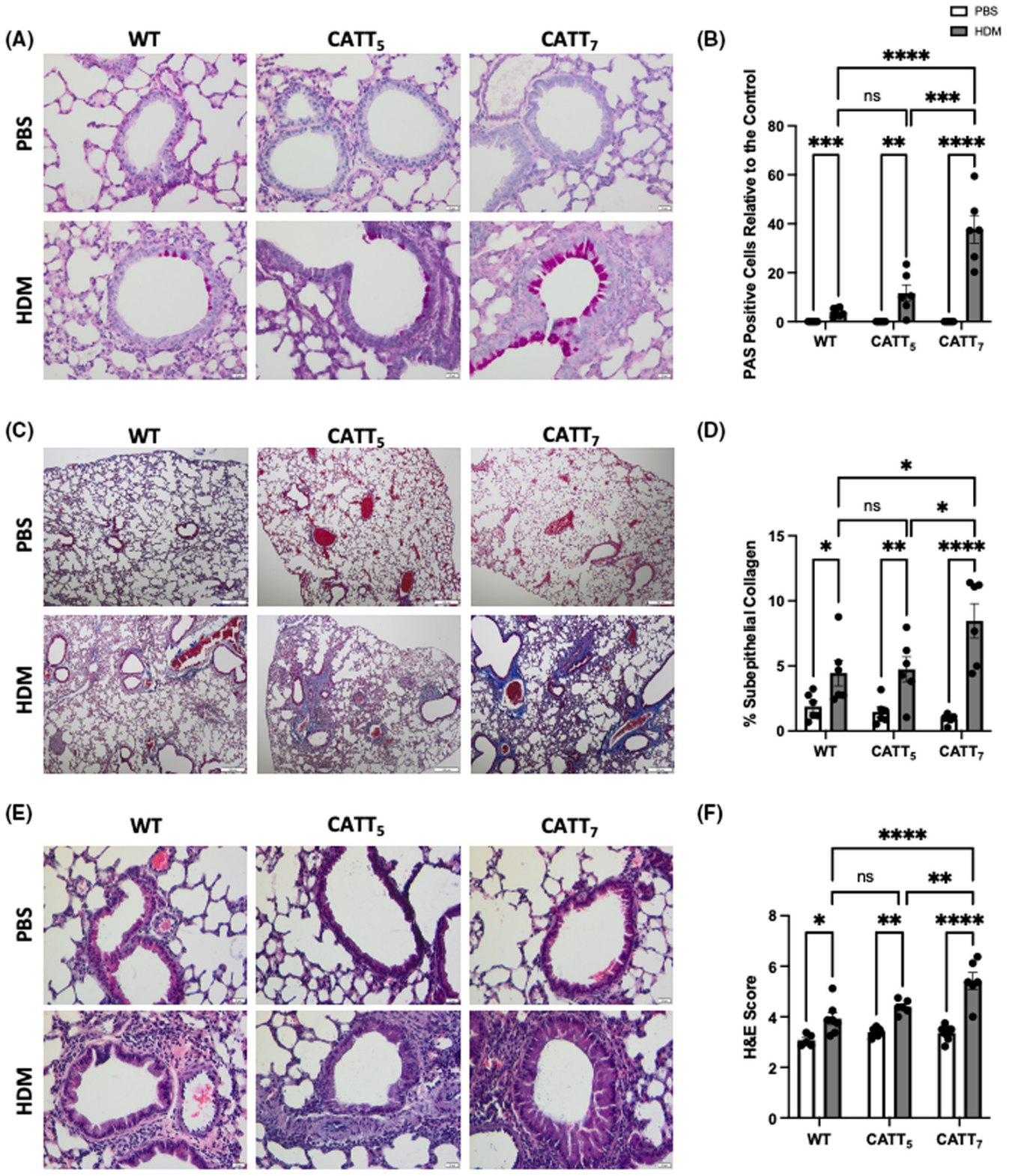

FIGURE 3 Human $CATT_7$ allele exacerbates airway inflammation in a house dust mite model of allergic asthma. (A) Representative images of lung tissue stained with periodic acid Schiff at 20× magnification, scale bar = 20 μm. (B) Goblet cell hyperplasia was investigated through the quantitation of PAS-positive cells. (C) Representative images of lung tissue stained with Masson's trichrome at 4× magnification, scale bar = 200 μm. (D) Quantitation of % subepithelial collagen. (E) Representative images of lung tissue stained with H&E from WT, 5CATT, and 7CATT mice challenged with HDM or PBS control at 20× magnification, scale bar = 20 μm. (F) Quantitation of airway inflammation in H&E-stained lung tissue. Data are presented as mean ± SEM; $N = 6$ per group. *$p < .05$; **$p < .01$; ***$p < .001$; ****$p < .0001$.

staining, whilst $CATT_5$ HDM exhibit slightly higher numbers of PAS-positive cells relative to the control compared to the WT (Figure 3A,B). Strikingly, $CATT_7$ mice have significantly higher levels of goblet cell hyperplasia compared to $CATT_5$ and WT mice following the HDM challenge (Figure 3B).

In addition to investigating goblet cell hyperplasia, we examined the effect of the −794CATT polymorphism on airway remodeling. To determine the extent of remodeling, we stained lung tissue with Masson's trichrome to highlight subepithelial collagen. The trends in the Masson's trichrome staining mirrored that of the PAS, with $CATT_5$, and WT mice displaying similar levels of disease pathology. Both groups exhibit a significant yet small increase in collagen deposition compared to the PBS controls (Figure 3C,D). $CATT_7$ mice challenged with HDM display significantly higher levels of subepithelial fibrosis compared to the lower MIF expressing $CATT_5$ allele and WT groups (Figure 3D); suggesting that high levels of hMIF contribute to airway remodeling in a HDM model of allergic airway inflammation.

H&E staining revealed that HDM significantly induces cellular infiltration surrounding the airways in all groups compared to the PBS control (Figure 3E,F). However, $CATT_7$ HDM exhibited significantly higher airway immune cell infiltration compared to both $CATT_5$ and WT HDM (Figure 3E,F). There was no significant difference in immune cell infiltration between the $CATT_5$ and WT HDM groups according to the H&E score (Figure 3F).

These data suggest that high levels of human MIF exacerbate allergic airway pathophysiology by increasing mucin production through the induction of goblet cell hyperplasia, increasing deposition of subepithelial collagen thereby contributing to airway remodeling, and increasing the infiltration of immune cells surrounding the airways.

3.4 | High levels of human MIF alter HDM-induced lung mechanics in response to increasing concentrations of methacholine

Airway hyperresponsiveness (AHR) and remodeling are a major hallmark of asthma and allergic airway inflammation, and as such it is important for models to represent this. We examined HDM-induced AHR in response to aerosolized methacholine challenge using the FlexiVent system. $CATT_7$ HDM mice exhibited a marked increase in airway resistance (R_N) at 12.5 mg/mL and 25 mg/mL doses compared to the rest of the groups (Figure 4A). A trend of increased tissue damping (G) (Figure 4B) and tissue elastance (H) (Figure 4C) was demonstrated in the $CATT_7$ mice at the 25 mg/mL dose. It has been well documented

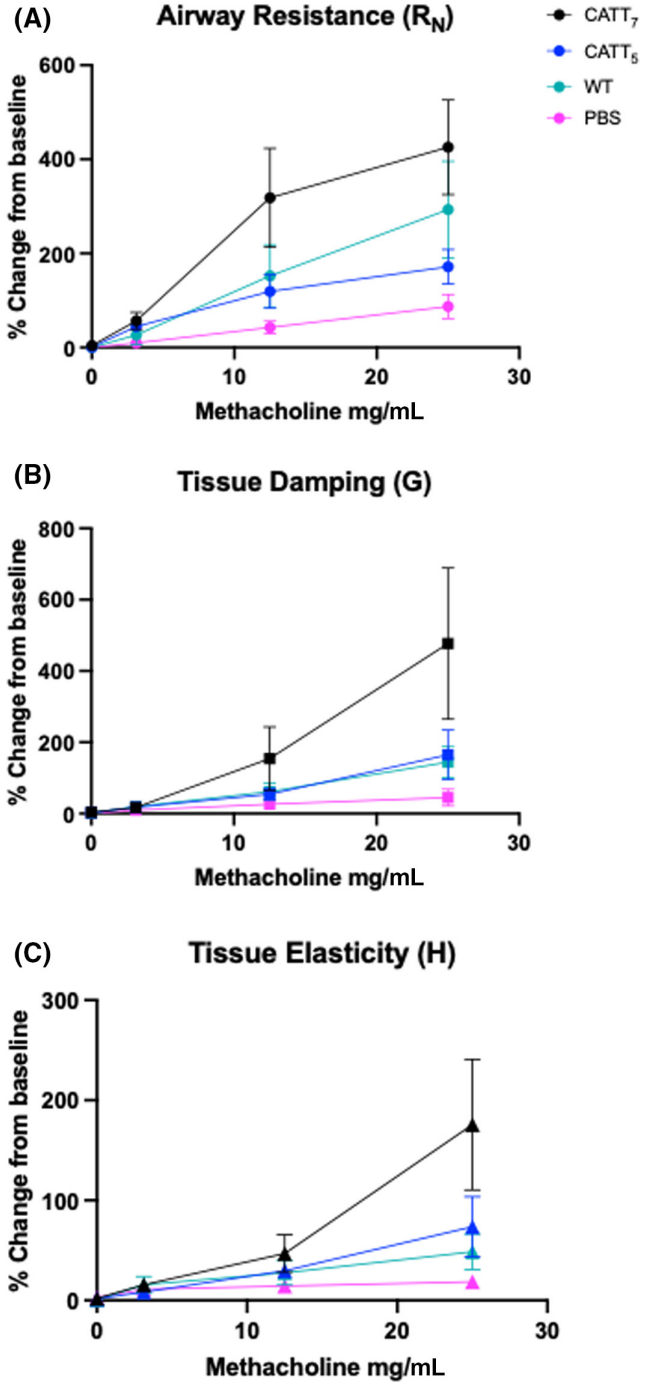

FIGURE 4 Changes in lung mechanics in response to increasing concentrations of methacholine in HDM-challenged $CATT_7$, $CATT_5$, and WT mice. Airway hyperresponsiveness determined (A) by airway resistance, (B) tissue damping, and (C) tissue elastance (R_N, G, and H respectively). Data are presented as peak response normalized to the baseline and expressed as % increase over baseline ± SEM; $N = 6$ per group.

that due to genetic differences, C57BL/6 mice have a higher resistance to airway hyperresponsiveness compared to the more sensitive BALB/c mice in acute airway inflammatory models[23,24] and this is reflected here in our

humanized MIF mice. These data show that $CATT_7$ mice challenged with HDM exhibit higher levels of airway remodeling and AHR compared to WT C57BL/6 mice.

3.5 | The MIF inhibitor SCD-19 decreases HDM-induced total cell counts and Th2 cytokines in BALF from $CATT_7$ mice

High human MIF expression has been demonstrated to play a role in driving the physiological hallmarks of allergic airway inflammation such as eosinophil infiltration (Figure 2A,B), increased Th2 cytokines (Figure 2D–F), goblet cell hyperplasia (Figure 3A,B), subepithelial collagen deposition (Figure 3C,D), and decreased lung function (Figure 4).

MIF is known to initiate its biological effects through its active site.[25] Therefore, to fully elucidate MIF's role in our model, the MIF antagonist SCD-19 was utilized to block this active site, as this alters the conformation of MIF and impairs its interaction with other molecules. Throughout the previous data, no significant difference was noted between the low MIF expressing $CATT_5$ mice and WT mice. Thus, the remainder of this study focused on comparing the high MIF expressing $CATT_7$ mice and WT mice. In addition to receiving HDM challenge, SCD-19 was administered intraperitoneally twice a week for three weeks.

Administration of SCD-19 to $CATT_7$ mice challenged with HDM significantly decreased human MIF production in BMDMs derived from $CATT_7$ mice (Supp. Figure 1). The total BALF cell count was decreased in $CATT_7$ HDM-challenged mice that received SCD-19 compared to HDM-challenged $CATT_7$ mice that received the vehicle control (Figure 5A). There was no significant difference between WT groups. BALF from SCD-19-treated $CATT_7$ mice had decreased numbers of eosinophils compared to $CATT_7$ mice that received the vehicle control (Figure 5B). There was no significant difference between the WT groups. Although not statistically significant, there is a visible trend

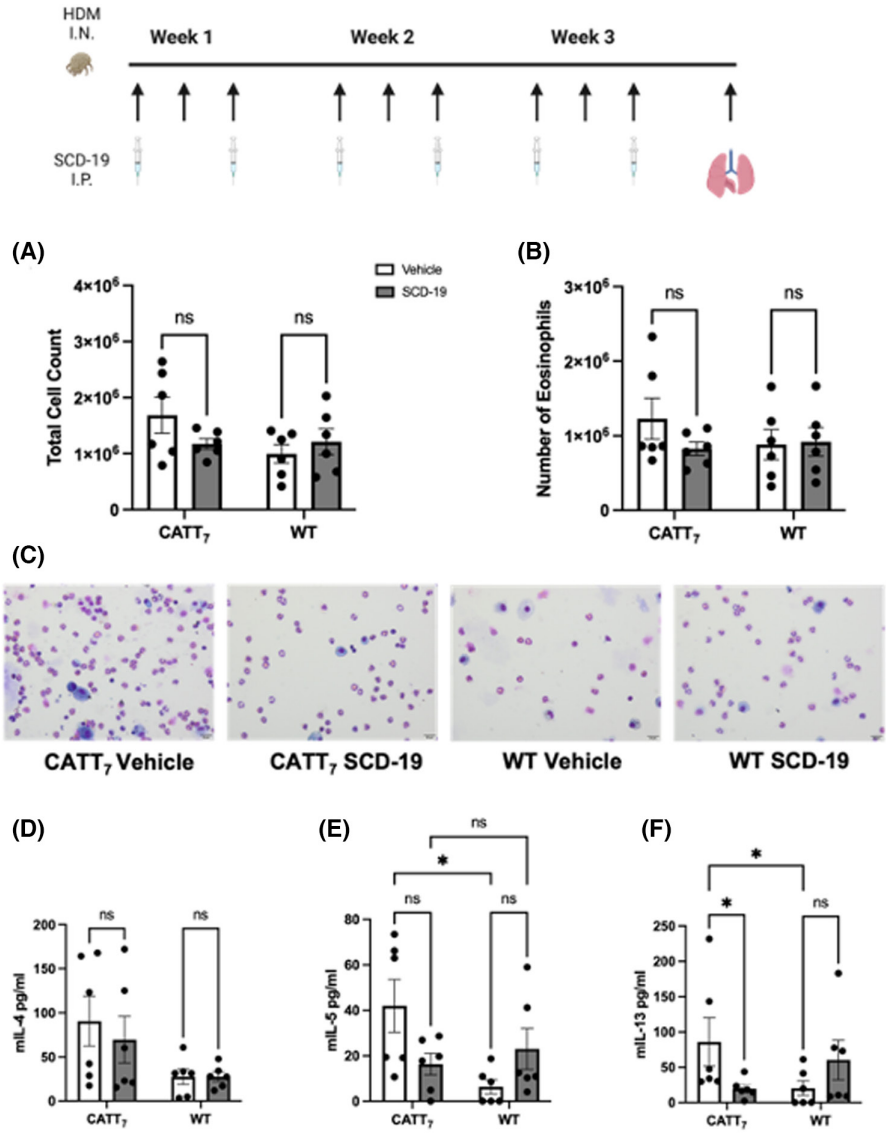

FIGURE 5 MIF inhibitor SCD-19 decreases total cell counts and Th2 cytokines in BALF from $CATT_7$ mice. Mice were challenged with 25 μg of HDM I.N. three times a week for three weeks, in addition to receiving 35 mg/kg of SCD-19 or vehicle control I.P. twice weekly for three weeks. Schematic created using Biorender.com. (A) Total cell count recovered from BAL fluid. (B) Number of Eosinophils from differential cell counts of BAL fluid from $CATT_7$ and WT mice. (C) 300 cells were counted and identified based on morphology. Cytokine levels of (D) IL-4, (E) IL-5, and (F) IL-13 in the BAL fluid determined by ELISA. Data are presented as mean ± SEM; $N = 6$ per group. *$p < .05$; **$p < .01$; ***$p < .001$; ****$p < .0001$.

of decreased total cellular infiltration in the BALF of SCD-19-treated $CATT_7$ mice compared to vehicle control mice.

No SCD-19-specific differences were observed in BALF IL-4 protein levels (Figure 5D). However, lower levels of IL-5 were detected in the BALF of SCD-19 $CATT_7$ mice compared to vehicle control $CATT_7$ mice (Figure 5E). There was no significant difference between SCD-19 and vehicle control WT groups, which was expected as we have previously noted that WT mice already have low levels of MIF production. Importantly, levels of BALF IL-13 were significantly decreased in SCD-19 $CATT_7$ mice compared to vehicle control $CATT_7$ mice (Figure 5F).

3.6 | SCD-19 significantly decreases HDM-induced lung pathology in $CATT_7$ mice

High levels of human MIF in the $CATT_7$ mice drive airway remodeling and inflammation following repeated exposure to the clinically relevant allergen HDM. Here we examined the capacity for SCD-19 to prevent this exacerbation-related pathology.

SCD-19 significantly abrogated the number of PAS-positive cells present compared to $CATT_7$ mice that received the vehicle control (Figure 6A,B). As expected, there was no significant difference between WT mice that received SCD-19 and the vehicle control (Figure 6A,B). In high human MIF expressing $CATT_7$ mice, SCD-19 significantly reduced the percentage of subepithelial collagen present after three weeks of intervention, compared to the vehicle control (Figure 6C,D). $CATT_7$ vehicle mouse lung sections had statistically significant higher levels of collagen deposition compared to WT vehicle mice. Moreover, SCD-19 had no effect in WT mice (Figure 6C,D). Lastly, lung sections were analyzed for cellular infiltration using H&E staining. High expression of human MIF amplified cellular infiltration, as $CATT_7$ mice that received SCD-19 had a significantly lower H&E score compared to those that received the vehicle control (Figure 6E,F). $CATT_7$

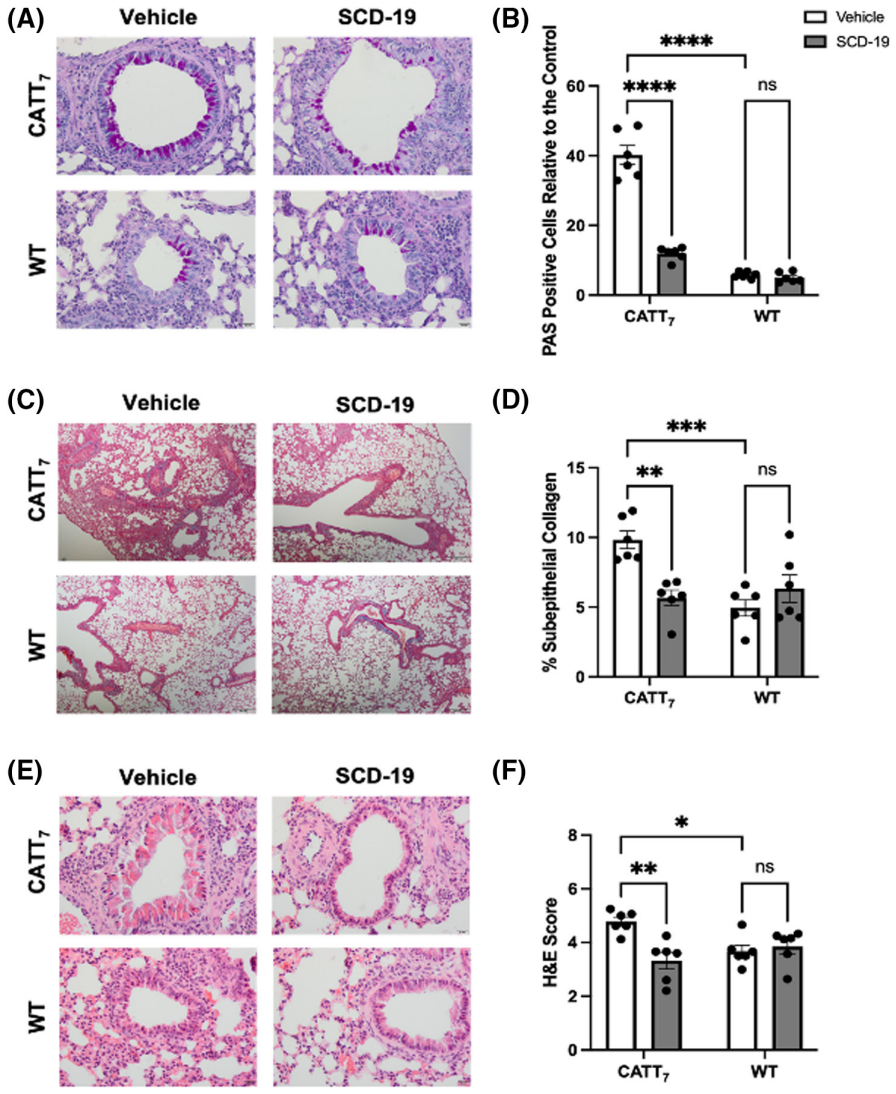

FIGURE 6 MIF antagonist SCD-19 significantly decreases HDM-induced allergic airway inflammation in $CATT_7$ mice. (A) Representative images of lung tissue stained with Periodic Acid Schiff at 20× magnification, scale bar = 20 μm. (B) Goblet cell hyperplasia was investigated through the quantitation of PAS-positive cells relative to the control. (C) Representative images of lung tissue stained with Masson's trichrome at 4× magnification, scale bar = 200 μm. (D) Quantitation of % subepithelial collagen. (E) Representative images of lung tissue stained with H&E from WT and $CATT_7$ mice challenged with HDM or PBS control and received SCD-19 or vehicle control at 20× magnification, scale bar = 20 μm. (F) Quantitation of airway inflammation in H&E-stained lung tissue. Data are presented as mean ± SEM; $N = 6$ per group. *$p < .05$; **$p < .01$; ***$p < .001$; ****$p < .0001$.

vehicle mice had significantly higher H&E scores compared to WT vehicle mice. Moreover, similarly to our previous histological findings, SCD-19 had no effect in WT mice (Figure 6E,F). In a similar manner, the MIF inhibitor; ISO-1 significantly reduced goblet cell hyperplasia, subepithelial collagen deposition and airway inflammation in CATT7 mice challenged with HDM (Supporting Information Figure S2). In WT mice, ISO-1 had no effect (Supporting Information Figure S2).

These data support our hypothesis that MIF is a key factor in driving acute airway inflammation in our house dust mite model, as blocking the biological activity of MIF reduced lung inflammation.

3.7 | SCD-19 improves lung function by decreasing airway resistance in $CATT_7$ mice in response to increasing concentrations of methacholine

We have previously shown that mice possessing the high human MIF expression allele ($CATT_7$) had increased airway resistance (Figure 4A), tissue damping (Figure 4B), and tissue elasticity (Figure 4C) after inhaling increasing concentrations of methacholine compared to mice possessing the low human MIF expression allele ($CATT_5$) and WT mice.

To further investigate our hypothesis that human MIF is driving the development of preclinical signs of allergic airway inflammation following HDM challenge in the $CATT_7$ mice, we measured the respiratory mechanics of mice that received SCD-19. In $CATT_7$ mice, SCD-19 had the ability to decrease HDM-induced inflammation at a mechanical level, by reducing the percentage increase of airway resistance (Figure 7A), tissue damping (Figure 7B), and tissue elasticity (Figure 7C) from baseline, compared to $CATT_7$ vehicle mice.

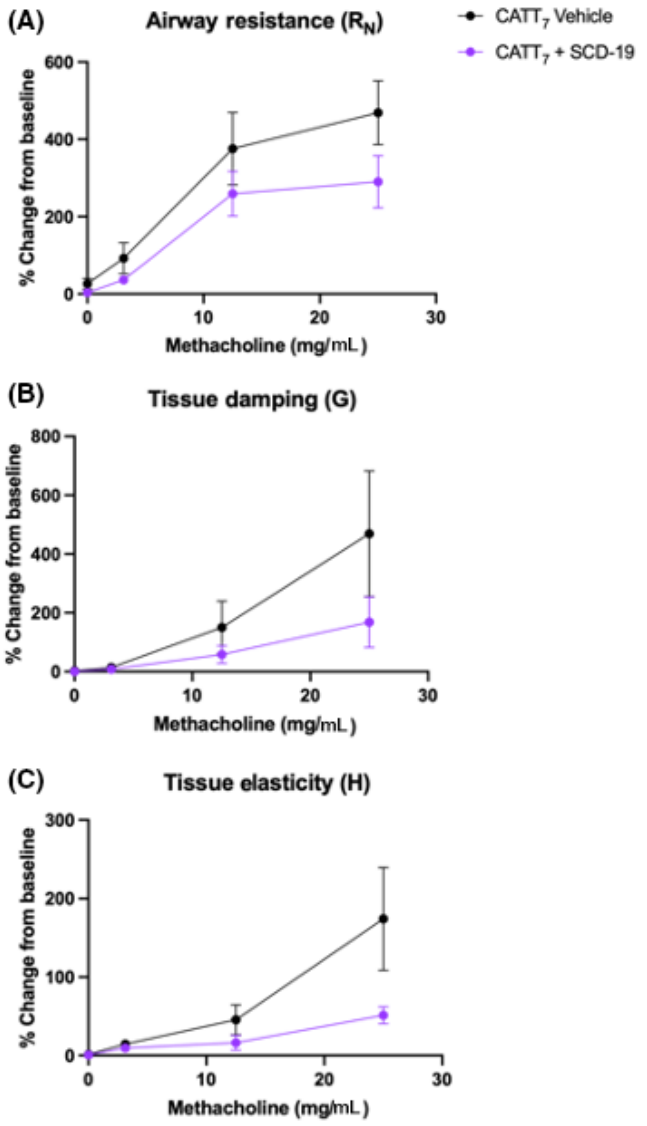

FIGURE 7 SCD-19 can decrease HDM-induced airway resistance (R_N), tissue damping (G), and tissue elasticity (H) in $CATT_7$ mice compared to vehicle control. $CATT_7$ mice were challenged with 25 μg of HDM or PBS control I.N. three times a week for three weeks, in addition to receiving 35 mg/kg of SCD-19 or vehicle control I.P. twice weekly for three weeks. 24 hr after last challenge, a tracheostomy was performed and lung function was measured using a FlexiVent® instrument (SCIREQ) in response to PBS or increasing concentrations of methacholine (3.125, 12.5, and 25 mg/mL). (A) Airway Resistance. (B) Tissue Damping. (C) Tissue Elasticity. Data are presented as peak response normalized to the baseline and expressed as % increase over baseline $N = 4–6$ per group.

4 | DISCUSSION

The biological role of macrophage migration inhibitory factor (MIF) has been previously documented in a plethora of inflammatory lung conditions,[19,26–31] including asthma.[10,13,16,32,33] The low human MIF expressing $CATT_5$ promoter polymorphism correlates with a milder manifestation of asthma symptoms.[10] We hypothesized that the $CATT_7$ promoter polymorphism which expresses high levels of human MIF could be linked to increased severity of allergic asthma. Using novel humanized MIF mice to create a physiological scale of allergic airway inflammation in response to the clinically relevant aeroallergen house dust mite, this study set out to investigate the biological role of this pro-inflammatory cytokine on key hallmarks associated with this atopic condition.

We demonstrate that intranasal challenge of HDM can drive enhanced MIF production in the lung of $CATT_7$ and $CATT_5$ mice, perhaps illustrating a positive feedback loop resulting in the exacerbations of physiological asthmatic characteristics. In a similar fashion, MIF is known to act

in an autocrine and paracrine fashion to promote downstream cytokine production.[18,21,34,35]

MIF's crucial contribution in this model of house dust mite-induced allergic airway inflammation was particularly clear at a histological level with significantly increased mucin-producing goblet cell hyperplasia and subepithelial collagen deposition in the presence of high levels of human MIF in $CATT_7$ mice. Airway remodeling occurs in uncontrolled cases of asthma, as repeated lung injury by inhaled insults and over-production of fibrotic tissue result in goblet cell hyperplasia and increased subepithelial collagen. This alteration in tissue architecture has consequences in the mechanical functioning of the lung, resulting in an increase in airway hyperresponsiveness, resistance, tissue damping, and elasticity. Our findings further clarified the physiological role of MIF in HDM-induced airway inflammation, as humanized high MIF expressing $CATT_7$ mice had increased airway resistance, tissue damping (energy dissipation into alveoli), and elastance (energy conservation in the alveoli) in response to increasing concentrations of the chemical bronchoconstrictor methacholine. This study provides new insights on the role of MIF in driving airway remodeling.

Blockade of MIF using the small molecule antagonist (S,R)3-(4-hy-droxyphenyl)-4,5-dihydro-5-isoxazole acetic acid methyl ester (ISO-1) has been shown to significantly reduce the pathology associated with OVA-induced,[36] HDM-induced[14] airway inflammation and remodeling and in a neutrophilic experimental severe asthma model.[37] The MIF small molecule inhibitor SCD-19 has been tested in a range of disease systems including lung cancer[25] and infectious disease[38] studies. SCD-19 potently inhibits MIF activity but its therapeutic efficacy had not been tested in an allergic airway inflammation model. Although previous studies have utilized anti-MIF antibodies and the small molecule inhibitor ISO-1 in mouse models of inflammatory conditions,[14,15,36,39] this is the first study to do so in humanized MIF mice expressing human relevant MIF polymorphic alleles.

In this study, SCD-19 significantly mitigated the MIF-associated increase in inflammatory histopathology, in a dose-dependent manner, reiterating the importance of this cytokine in the induction and maintenance of experimental asthma, as described previously.[36] SCD-19 decreased the total cells present in bronchoalveolar lavage in $CATT_7$ mice. SCD-19 had no effect on IL-4 production, but decreased IL-5 and significantly decreased IL-13 production in the BALF from $CATT_7$ mice compared to vehicle control. In line with our data, administration of an anti-MIF antibody in an OVA model also did not affect IL-4 levels in BALF, but anti-MIF treatment during OVA sensitization significantly decreased eosinophil infiltration in BALB/c mice.[13] Conversely in C57BL/6 mice, MIF inhibition with SCD-19 did not decrease eosinophil infiltration in the BALF of HDM-challenged $CATT_7$. Transgenic mice are routinely generated on a C57BL/6 background, which may be a limitation of this study, as Th2 atopic allergy models are usually performed in BALB/c. As a result, readouts may have a lower baseline than those performed in BALB/c mice. Similarly, levels of cellular and eosinophil infiltration may be lower than suspected in our model, due to the mice used being generated of the C57BL/6 genetic background. Furthermore, SCD-19 may not decrease eosinophil infiltration as efficiently as seen with an anti-MIF antibody in an OVA model,[13] as our Th2 response was not high enough at baseline levels to be further suppressed by SCD-19. The timing of MIF inhibitor administration is fundamental, as the use of ISO-1 in a model of severe neutrophilic asthma could only abrogate HDM-induced airway inflammation when administered both 30 min prior and 6 h after allergen challenge.[37] Taking into account the SCD-19 dosing regimen, along with the suboptimal genetic background of the mice used, this may help to explain the incomplete effects of SCD-19 in this model. As previously mentioned, collagen deposition and goblet cell hyperplasia were seen to be significantly increased at this acute timepoint, but more HDM challenges might be required to see the full effects of chronic inflammation in our model. SCD-19 blocks MIF's conformationally sensitive tautomerase active site that overlaps functionally with MIF (CD74) receptor binding. Here we show that SCD-19 extensively diminishes HDM-induced histopathology in $CATT_7$ mice, along with having a subtle anti-inflammatory impact in the BALF of these mice when administered starting at first allergen challenge. Moreover, SCD-19 abrogated the airway resistance (R_N), tissue damping (G), and tissue elasticity (H) in $CATT_7$ mice compared to the vehicle control, showing a clear association between lower levels of tissue remodeling at a histological level and overall lung function.

In terms of asthma therapies, MIF is known to counter-regulate the effects of glucocorticoids, a steroidal treatment to manage severe asthmatic symptoms. In the future, small molecular weight MIF inhibitors may not only be used as a monotherapy for asthma patients with high MIF expression 7–7 genotypes (those genetically pre-dispositioned to secrete higher levels of this pro-inflammatory cytokine), but also as part of a synergistic regimen where they could initially work to inhibit MIF function, but also to enhance or restore the efficacy of glucocorticoids in the clinic.

This study demonstrated the ability of the MIF antagonist SCD-19 to abrogate HDM-induced cellular

infiltration, goblet cell hyperplasia, and subepithelial fibrosis. Furthermore, SCD-19 decreased airway hypersensitivity, but did not affect cell populations within the BALF retrieved from these novel humanized MIF mice.

Here we demonstrate that high MIF allele expression leads to enhanced severity of allergic airway inflammation driven by the clinically relevant allergen HDM. This study is the first to use novel humanized MIF mice to investigate the role of endogenous MIF expression on house dust mite-induced allergic asthma by utilizing small molecular weight inhibitors in vivo.

To conclude, this study demonstrates the important role of MIF in further driving allergic airway inflammation and potentially airway remodeling and provides a novel, clinically relevant, and reproducible model of allergic airway remodeling. Further experiments are required however, perhaps using therapeutic as opposed to prophylactic administration of SCD-19 to determine the ability of SCD-19 to reduce airway remodeling. These data pave the way for a new therapeutic avenue for the utilization of small molecule anti-MIF strategies that are both ant-inflammatory and that can potentially reduce airway remodeling in allergic asthma. This study is of high scientific and translational relevance given the obvious superiority of small molecules over biologic approaches (e.g., antibodies) to treating asthma. The validation of the humanized MIF mouse model is an additional advance, as it will enable the utility of this model in downstream pharmaceutical development, both in asthma and other MIF-dependent diseases in the sphere of airway disease, oncology, infection, and autoimmunity.

AUTHOR CONTRIBUTIONS

Hazel Dunbar performed research, data analysis, study design, and wrote the manuscript. Ian J. Hawthorne performed research, data analysis, study design and wrote the manuscript. Hazel Dunbar and Ian J. Hawthorne should be conjoint first authors. Courteney Tunstead performed research and data analysis. Seamas C. Donnelly and Michelle E. Armstrong provided reagents, contributed to study design and data analysis. Karen English designed and supervised the study and wrote the manuscript. All authors approved the final manuscript.

ACKNOWLEDGMENTS

We would like to thank Deirdre Daly, Gillian O'Meara, and Shannon Grellan for their exceptional care of our animals used in this study. Open access funding provided by IReL.

FUNDING INFORMATION

This research was supported by an Irish Research Council Laureate Award to KE (IRCLA/2017/288).

DISCLOSURES

The authors declare no conflict of interest.

DATA AVAILABILITY STATEMENT

The data that support the findings of this study are available on request from the corresponding author.

ORCID

Hazel Dunbar https://orcid.org/0000-0003-4613-8833
Ian J. Hawthorne https://orcid.org/0000-0002-5444-2643
Courteney Tunstead https://orcid.org/0000-0001-5343-7984
Michelle E. Armstrong https://orcid.org/0000-0001-7729-755X
Seamas C. Donnelly https://orcid.org/0000-0001-7145-1843
Karen English https://orcid.org/0000-0002-7932-4256

REFERENCES

1. Dharmage SC, Perret JL, Custovic A. Epidemiology of asthma in children and adults. *Front Pediatr*. 2019;7:246.
2. Djukanovic R, Roche WR, Wilson JW, et al. Mucosal inflammation in asthma. *Am Rev Respir Dis*. 1990;142:434-457.
3. Holgate ST, Wenzel S, Postma DS, Weiss ST, Renz H, Sly PD. Asthma. *Nat Rev Dis Primers*. 2015;1:15025.
4. Robays LJ, Lanckacker EA, Moerloose KB, et al. Concomitant inhalation of cigarette smoke and aerosolized protein activates airway dendritic cells and induces allergic airway inflammation in a TLR-independent way. *J Immunol*. 2009;183:2758-2766.
5. Custovic A. To what extent is allergen exposure a risk factor for the development of allergic disease? *Clin Exp Allergy*. 2015;45:54-62.
6. Dullaers M, Schuijs MJ, Willart M, et al. House dust mite-driven asthma and allergen-specific T cells depend on B cells when the amount of inhaled allergen is limiting. *J Allergy Clin Immunol*. 2017;140:76-88.e7.
7. Gregory LG, Lloyd CM. Orchestrating house dust mite-associated allergy in the lung. *Trends Immunol*. 2011;32:402-411.
8. Robinson DS, Hamid Q, Ying S, et al. Predominant TH2-like bronchoalveolar T-lymphocyte population in atopic asthma. *N Engl J Med*. 1992;326:298-304.
9. Joseph C, Tatler AL. Pathobiology of airway remodeling in asthma: the emerging role of integrins. *J Asthma Allergy*. 2022;15:595-610.
10. Mizue Y, Ghani S, Leng L, et al. Role for macrophage migration inhibitory factor in asthma. *Proc Natl Acad Sci USA*. 2005;102:14410-14415.
11. Baugh JA, Chitnis S, Donnelly SC, et al. A functional promoter polymorphism in the macrophage migration inhibitory factor (MIF) gene associated with disease severity in rheumatoid arthritis. *Genes Immun*. 2002;3:170-176.
12. Plant BJ, Ghani S, O'Mahony MJ, et al. Sarcoidosis and MIF gene polymorphism: a case-control study in an Irish population. *Eur Respir J*. 2007;29:325-329.
13. Magalhaes ES, Mourao-Sa DS, Vieira-de-Abreu A, et al. Macrophage migration inhibitory factor is essential for allergic asthma but not for Th2 differentiation. *Eur J Immunol*. 2007;37:1097-1106.

14. Lan H, Luo L, Chen Y, Wang M, Yu Z, Gong Y. MIF signaling blocking alleviates airway inflammation and airway epithelial barrier disruption in a HDM-induced asthma model. *Cell Immunol*. 2020;347:103965.
15. Amano T, Nishihira J, Miki I. Blockade of macrophage migration inhibitory factor (MIF) prevents the antigen-induced response in a murine model of allergic airway inflammation. *Inflamm Res*. 2007;56:24-31.
16. Li R, Wang F, Wei J, et al. The role of macrophage migration inhibitory factor (MIF) in asthmatic airway remodeling. *Allergy Asthma Immunol Res*. 2021;13:88-105.
17. Bloom J, Metz C, Nalawade S, et al. Identification of Iguratimod as an inhibitor of macrophage migration inhibitory factor (MIF) with steroid-sparing potential. *J Biol Chem*. 2016;291:26502-26514.
18. Calandra T, Bucala R. Macrophage migration inhibitory factor: a counter-regulator of glucocorticoid action and critical mediator of septic shock. *J Inflamm*. 1995;47:39-51.
19. Shin JJ, Fan W, Par-Young J, et al. MIF Is a common genetic determinant of COVID-19 symptomatic infection and severity. *QJM*. 2022;116:205-212.
20. Hoegl SE, Ehrentraut H, Brodsky KS, et al. NK cells regulate CXCR2+ neutrophil recruitment during acute lung injury. *J Leukocyte Biol*. 2016;101:471-480.
21. Das R, Moss JE, Robinson E, et al. Role of macrophage migration inhibitory factor in the Th2 immune response to epicutaneous sensitization. *J Clin Immunol*. 2011;31:666-680.
22. Boucherat O, Boczkowski J, Jeannotte L, Delacourt C. Cellular and molecular mechanisms of goblet cell metaplasia in the respiratory airways. *Exp Lung Res*. 2013;39:207-216.
23. Atochina EN, Beers MF, Tomer Y, et al. Attenuated allergic airway hyperresponsiveness in C57BL/6 mice is associated with enhanced surfactant protein (SP)-D production following allergic sensitization. *Respir Res*. 2003;4:15.
24. Van Hove CL, Maes T, Cataldo DD, et al. Comparison of acute inflammatory and chronic structural asthma-like responses between C57BL/6 and BALB/c mice. *Int Arch Allergy Immunol*. 2009;149:195-207.
25. Mawhinney L, Armstrong ME, O'Reilly C, et al. Macrophage migration inhibitory factor (MIF) enzymatic activity and lung cancer. *Mol Med*. 2015;20:729-735.
26. Adamali H, Armstrong ME, McLaughlin AM, et al. Macrophage migration inhibitory factor enzymatic activity, lung inflammation, and cystic fibrosis. *Am J Respir Crit Care Med*. 2012;186:162-169.
27. Florez-Sampedro L, Soto-Gamez A, Poelarends GJ, Melgert BN. The role of MIF in chronic lung diseases: looking beyond inflammation. *Am J Physiol Lung Cell Mol Physiol*. 2020;318:L1183-L1197.
28. Florez-Sampedro L, Brandsma CA, de Vries M, et al. Genetic regulation of gene expression of MIF family members in lung tissue. *Sci Rep*. 2020;10:16980.
29. Melotti P, Mafficini A, Lebecque P, et al. Impact of MIF gene promoter polymorphism on F508del cystic fibrosis patients. *PLoS One*. 2014;9:e114274.
30. Plant BJ, Gallagher CG, Bucala R, et al. Cystic fibrosis, disease severity, and a macrophage migration inhibitory factor polymorphism. *Am J Respir Crit Care Med*. 2005;172:1412-1415.
31. Smith CA, Tyrell DJ, Kulkarni UA, et al. Macrophage migration inhibitory factor enhances influenza-associated mortality in mice. *JCI Insight*. 2019;4:e128034.
32. Kobayashi M, Nasuhara Y, Kamachi A, et al. Role of macrophage migration inhibitory factor in ovalbumin-induced airway inflammation in rats. *Eur Respir J*. 2006;27:726-734.
33. Rossi AG, Haslett C, Hirani N, et al. Human circulating eosinophils secrete macrophage migration inhibitory factor (MIF). Potential role in asthma. *J Clin Invest*. 1998;101:2869-2874.
34. Mitchell RA, Liao H, Chesney J, et al. Macrophage migration inhibitory factor (MIF) sustains macrophage proinflammatory function by inhibiting p53: regulatory role in the innate immune response. *Proc Natl Acad Sci USA*. 2002;99:345-350.
35. Roger T, David J, Glauser MP, Calandra T. MIF regulates innate immune responses through modulation of Toll-like receptor 4. *Nature*. 2001;414:920-924.
36. Chen PF, Luo YL, Wang W, et al. ISO-1, a macrophage migration inhibitory factor antagonist, inhibits airway remodeling in a murine model of chronic asthma. *Mol Med*. 2010;16:400-408.
37. Allam V, Pavlidis S, Liu G, et al. Macrophage migration inhibitory factor promotes glucocorticoid resistance of neutrophilic inflammation in a murine model of severe asthma. *Thorax*. 2022;78:661-673.
38. Tynan A, Mawhinney L, Armstrong ME, et al. Macrophage migration inhibitory factor enhances Pseudomonas aeruginosa biofilm formation, potentially contributing to cystic fibrosis pathogenesis. *FASEB J*. 2017;31:5102-5110.
39. Luo Y, Yi H, Huang X, et al. Inhibition of macrophage migration inhibitory factor (MIF) as a therapeutic target in bleomycin-induced pulmonary fibrosis rats. *Am J Physiol Lung Cell Mol Physiol*. 2021;321:L6-L16.

SUPPORTING INFORMATION

Additional supporting information can be found online in the Supporting Information section at the end of this article.

How to cite this article: Dunbar H, Hawthorne IJ, Tunstead C, Armstrong ME, Donnelly SC, English K. Blockade of MIF biological activity ameliorates house dust mite-induced allergic airway inflammation in humanized MIF mice. *The FASEB Journal*. 2023;37:e23072. doi:10.1096/fj.202300787R

Molecular Therapy
Original Article

Human macrophage migration inhibitory factor potentiates mesenchymal stromal cell efficacy in a clinically relevant model of allergic asthma

Ian J. Hawthorne,[1,2,8] Hazel Dunbar,[1,2,8] Courteney Tunstead,[1,2] Tamara Schorpp,[1,2] Daniel J. Weiss,[3] Sara Rolandsson Enes,[4] Claudia C. dos Santos,[5,6] Michelle E. Armstrong,[7] Seamas C. Donnelly,[7] and Karen English[1,2]

[1]Kathleen Lonsdale Institute for Human Health Research, Maynooth University, Maynooth, Co. Kildare, Ireland; [2]Department of Biology, Maynooth University, Maynooth, Co. Kildare, Ireland; [3]Department of Medicine, 226 Health Sciences Research Facility, Larner College of Medicine, University of Vermont, Burlington, VT 05405, USA; [4]Department of Experimental Medical Science, Faculty of Medicine, Lund University, 22100 Lund, Sweden; [5]The Keenan Research Centre for Biomedical Science of St. Michael's Hospital, 30 Bond Street, Toronto, ON, Canada; [6]Institute of Medical Sciences and Interdepartmental Division of Critical Care, Faculty of Medicine, University of Toronto, Toronto, ON, Canada; [7]Department of Medicine, Trinity College Dublin, Dublin, Ireland

Current asthma therapies focus on reducing symptoms but fail to restore existing structural damage. Mesenchymal stromal cell (MSC) administration can ameliorate airway inflammation and reverse airway remodeling. However, differences in patient disease microenvironments seem to influence MSC therapeutic effects. A polymorphic CATT tetranucleotide repeat at position 794 of the human macrophage migration inhibitory factor (hMIF) gene has been associated with increased susceptibility to and severity of asthma. We investigated the efficacy of human MSCs in high- vs. low-hMIF environments and the impact of MIF pre-licensing of MSCs using humanized MIF mice in a clinically relevant house dust mite (HDM) model of allergic asthma. MSCs significantly attenuated airway inflammation and airway remodeling in high-MIF-expressing $CATT_7$ mice but not in $CATT_5$ or wild-type littermates. Differences in efficacy were correlated with increased MSC retention in the lungs of $CATT_7$ mice. MIF licensing potentiated MSC anti-inflammatory effects at a previously ineffective dose. Mechanistically, MIF binding to CD74 expressed on MSCs leads to upregulation of cyclooxygenase 2 (COX-2) expression. Blockade of CD74 or COX-2 function in MSCs prior to administration attenuated the efficacy of MIF-licensed MSCs *in vivo*. These findings suggest that MSC administration may be more efficacious in severe asthma patients with high MIF genotypes ($CATT_{6/7/8}$).

INTRODUCTION

Allergic asthma is characterized by chronic airway inflammation and airway remodeling, which refers to the structural changes in the airways. Currently, there is a heavy reliance on inhaled corticosteroids and long-acting β2-adrenoceptor agonists in the treatment of allergic asthma. The recent introduction of novel biologics, such as benralizumab and dupilumab targeting Th2 cytokine receptors and tezepelumab targeting the alarmin thymic stromal lymphopoietin (TSLP), have been shown to significantly reduce allergic airway inflammation, leading to reduced exacerbation and improved forced expiratory volume 1 ($FEV_{1)}$ values.[1–4] However, not all patients are responders, and evidence for biologics to reverse existing airway remodeling in patients is limited so far.[5] Thus, there is scope for novel therapeutics with the capacity to attenuate inflammation and reverse remodeling to address the pitfalls in the current treatment and management of allergic asthma.

Mesenchymal stromal cells (MSCs) have immunomodulatory and antifibrotic properties and proven therapeutic effects in a range of allergic airway inflammation models and are currently under investigation in two clinical trials for asthma (ClinicalTrials.gov: NCT05147688 and NCT05035862). Administration of MSCs intratracheally or intravenously has been shown to be effective in reducing airway inflammation and airway hyperresponsiveness in ovalbumin (OVA),[6–17] house dust mite (HDM),[18–24] and *Aspergillus* hyphal extract[25,26] models. However, other studies have failed to demonstrate efficacy in experimental asthma models.[7,14,23,24,27,28] To understand the mechanisms involved and to make MSCs a viable therapeutic in the clinic, more focused translational work is needed.

Under basal conditions (for example, in healthy animals or individuals), MSC administration does not seem to alter immunological status or function (homeostasis is preserved). MSCs only become licensed to an anti-inflammatory phenotype in the presence of extrinsic factors.[29] When licensed, MSCs modulate their surrounding microenvironment.[30] Importantly, their therapeutic effect is blunted in the presence of interferon γ (IFNγ), nuclear factor κB (NF-κB), or tumor necrosis factor alpha (TNF-α) receptor blockade/inhibition.[31–33] Moreover, in

Received 5 July 2023; accepted 14 September 2023;
https://doi.org/10.1016/j.ymthe.2023.09.013.

[8]These author contributed equally

Correspondence: Karen English, PhD, Kathleen Lonsdale Institute for Human Health Research, Department of Biology, Maynooth University, Maynooth, Co. Kildare, Ireland.
E-mail: karen.english@mu.ie

the absence of appropriate signals to license anti-inflammatory functions, MSCs may even exacerbate disease.[34–36] Licensing has been shown to improve MSC therapeutic efficacy by activating MSC anti-inflammatory characteristics prior to administration. Licensing through exposure to hypoxia,[37,38] inflammatory cytokines,[39,40] and pharmacological factors[41] has been shown to improve MSC efficacy in a range of inflammatory diseases. Moreover, licensing of MSCs with serum from HDM-challenged mice[18] or with serum from acute respiratory distress syndrome (ARDS) patients[42] enhanced MSC therapeutic efficacy *in vivo* in pre-clinical lung disease models. However, there are also *in vitro* studies reporting differential and, in some cases, negative effects of patient samples (ARDS versus cystic fibrosis (CF)) on MSC survival and function.[42–44]

Macrophage migration inhibitory factor (MIF) is an important regulator of host inflammatory responses, demonstrated by its ability to promote the production of other inflammatory mediators. For example, MIF has been shown to amplify the expression of TNF, IFNγ, interleukin-1β (IL-1β), IL-2, IL-6, and IL-8 from immune cells.[45–48] This augmentation of immune signals contributes to MIF-mediated pathogenesis by acting to sustain inflammatory responses. This has been shown in a range of inflammatory diseases where the absence of MIF is associated with lower levels of pro-inflammatory cytokines, resulting in reduced pathology. For example, MIF knockout ($MIF^{-/-}$) mice display a less severe phenotype when exposed to OVA compared with control mice,[49–52] and the use of anti-MIF antibodies or a small-molecule inhibitor (ISO-1) results in reduced Th2 cytokines in models of allergic airway inflammation.[51,53–56] High levels of MIF as a result of longer CATT repeats, such as $CATT_7$, have been shown to increase severity in a range of diseases, including severe anemia,[57] pneumococcal meningitis,[58] multiple sclerosis,[59] tuberculosis,[60] and coronavirus disease 2019 (COVID-19).[61] Importantly, associations between the CATT polymorphism and asthma incidence and severity have been observed.[52] Not only do these studies show the pivotal role that MIF plays in pro-inflammatory diseases, they also affirm the importance of differences in the MIF CATT polymorphism.

Our previous work established a dominant role of MIF allelic variants in the severity of HDM-induced allergic asthma.[62] Using humanized high-expressing and low-expressing MIF mice in an HDM model of allergic airway inflammation, we demonstrated the pivotal role MIF plays in exacerbating asthma pathogenesis. High levels of human MIF resulted in a significant increase in airway inflammation as a result of elevated levels of Th2 cytokines promoting infiltration of eosinophils into the airways. Furthermore, high levels of MIF were associated with airway remodeling with significant mucus hyperplasia, subepithelial collagen deposition, and airway hyperresponsiveness generating a more severe asthma phenotype. MIF has been shown to promote MSC migration *in vitro*;[63] however, the effect of MIF on MSC immunosuppressive function or therapeutic efficacy *in vivo* is unknown. Here, we sought to investigate the relationship between MIF and MSCs *in vivo* and to define conditions for optimal MSC therapeutic efficacy. High-MIF-expressing $CATT_7$, low-MIF-expressing $CATT_5$, and wild-type (WT) mice were used as a platform to investigate the role of MIF on MSC efficacy in a clinically relevant HDM-induced mouse model of allergic airway inflammation.

RESULTS

Human bone marrow-derived MSCs (BM-MSCs) significantly reduce airway remodeling in $CATT_7$ mice challenged with HDM

First, to investigate the impact of high- and low-expressing MIF alleles on MSC treatment of allergic airway inflammation, we examined the lung histology. $CATT_7$, $CATT_5$, and the WT were randomized to HDM or mock (saline) intranasally 3 times a week for 3 weeks. Mice were then further randomized to 1×10^6 human BM-MSCs or equal-volume saline administered via tail vein injection on day 14. On day 21, lung tissue was removed, formalin fixed, and sectioned onto slides (Figure 1A). Slides were stained with periodic acid-Schiff (PAS) to highlight mucin production to assess the level of goblet cell hyperplasia. $CATT_7$ mice exhibit significantly higher levels of goblet cell hyperplasia compared with WT and $CATT_5$ mice. Administration of BM-MSCs reduced the level of goblet cell hyperplasia in all groups to almost background levels, with a significant reduction in the number of mucin-secreting cells in the airways of HDM-challenged $CATT_7$ mice (Figures 1B and 1C).

Subepithelial fibrosis was significantly increased in HDM-challenged $CATT_7$ mice compared with the lower-MIF-expressing $CATT_5$ and WT groups. BM-MSC administration reduced the level of subepithelial fibrosis to almost background levels in all groups, with significantly reduced subepithelial collagen deposition in HDM-challenged $CATT_7$ mice (Figures 1D and 1E). In $CATT_5$ and WT mice challenged with HDM, BM-MSC administration had a small but not significant therapeutic effect. BM-MSC administration significantly mitigated increased inflammatory infiltrate and H&E pathological score in $CATT_7$ mice challenged with HDM (Figure S1).

Human BM-MSCs significantly reduce airway inflammation in $CATT_7$ mice challenged with HDM

Total cell counts were significantly elevated in the bronchoalveolar lavage fluid (BALF) of $CATT_7$ mice following HDM challenge (Figure 2A). MSCs significantly reduced the number of total infiltrating cells in the BALF of $CATT_7$ mice (Figure 2A). Differential cell counts identified eosinophils as the main cells infiltrating the lung tissue following HDM challenge, and MSCs significantly decreased infiltrating eosinophils in $CATT_7$ mice but had no effect in the $CATT_5$ and WT groups (Figure 2B). IL-4 and IL-13 were significantly elevated in the BALF of $CATT_7$ mice following HDM challenge (Figures 2C and 2D). These Th2 cytokines are not significantly upregulated in $CATT_5$ or WT mice. While MSCs significantly decreased IL-4 and IL-13 in $CATT_7$ mice, MSC treatment did not reduce and, in some cases, increased Th2 cytokines in the BALF of $CATT_5$ and WT mice (Figures 2C and 2D). These data show that BM-MSCs are effective at alleviating eosinophil infiltration and reducing Th2 cytokines in a high-MIF-expressing model of allergic asthma and that MSCs require a threshold level of inflammation to mediate their therapeutic effects.

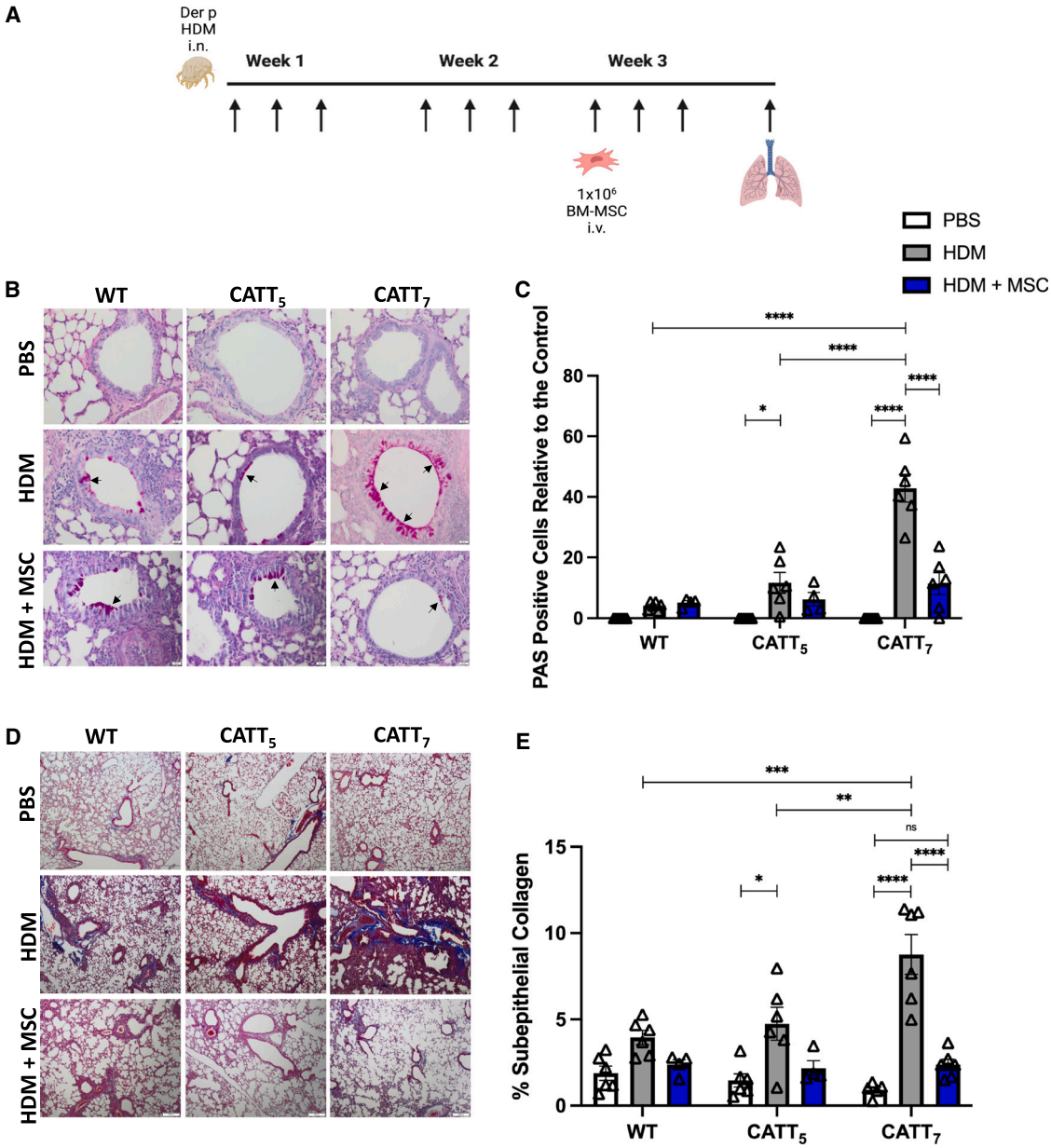

Figure 1. Human BM-MSCs significantly reduce goblet cell metaplasia and collagen deposition in $CATT_7$ mice challenged with HDM

(A) PBS and HDM groups received PBS or HDM i.n. 3 times a week for 3 consecutive weeks. 1×10^6 human BM-MSCs were administered i.v. to the HDM+MSC groups on day 14. Mice were sacrificed on day 21 (schematic created with BioRender). (B) Representative images of lung tissue from WT, $CATT_5$, and $CATT_7$ mice stained with periodic acid-Schiff (PAS) at 20× magnification; scale bar, 20 μm. Arrows show examples of mucin-containing goblet cells. (C) Goblet cell hyperplasia was investigated through the quantitation of PAS-positive cells. (D) Representative images of lung tissue stained with Masson's trichome at 4× magnification; scale bar, 200 μm.
(E) Quantitation of the percentage of subepithelial collagen. Data are presented as mean ± SEM; n = 6 per group. Human BM-MSC donors 001-177 and 003-310 were used (RoosterBio). Statistical analysis was carried out using one-way ANOVA followed by the post hoc Tukey's multiple-comparisons test: *$p < 0.05$, ***$p < 0.001$, ****$p < 0.0001$; ns, non-significant.

High levels of human MIF (hMIF) significantly enhance BM-MSC retention in an HDM model of allergic asthma

Next, we analyzed the biodistribution of MSCs following administration into HDM-challenged WT, $CATT_5$, and $CATT_7$ mice. 1×10^6 fluorescently labeled BM-MSCs were administered intravenously (i.v.) via tail vein injection on day 14. On day 15, mice were sacrificed, and the lungs were prepared for CryoViz imaging (Figures 3A–3C). Significantly higher numbers of labeled MSCs were detected in the

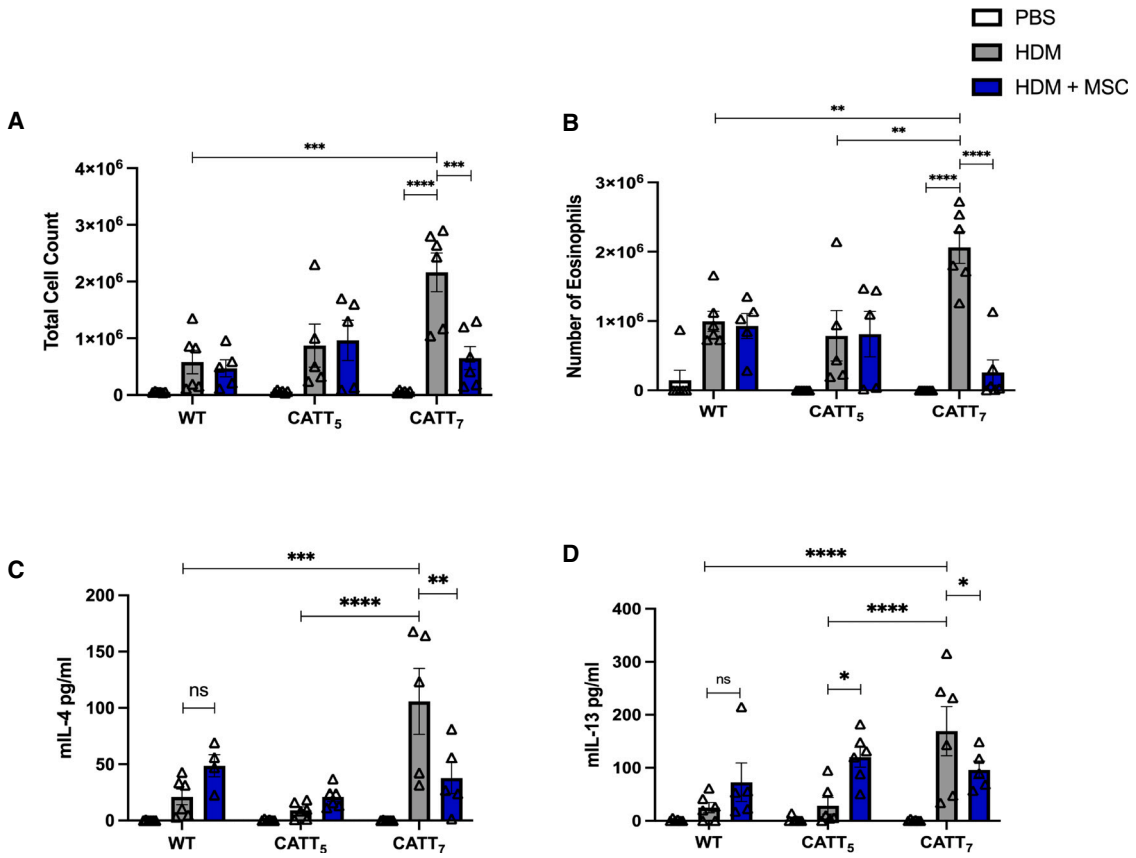

Figure 2. Human BM-MSCs significantly reduce levels of Th2 cytokines in the BALF of $CATT_7$ mice challenged with HDM

PBS and HDM groups received PBS or HDM i.n. 3 times a week for 3 consecutive weeks. 1×10^6 human BM-MSCs were administered i.v. to the HDM+MSC groups on day 14. BAL was performed 4 h post final HDM challenge on day 18. (A) Total cell count recovered from the BALF.

(B) BALF eosinophil count, determined by differential staining of cytospins. (C and D) Cytokine levels of (C) IL-4 and (D) IL-13 in the BALF, determined by ELISA. White bars, PBS; gray bars, HDM blue bars, HDM+MSC. Data are presented as mean ± SEM; n = 5–6 per group. Human BM-MSC donors 001-177 and 003-310 were used (RoosterBio). Statistical analysis was carried out using one-way ANOVA followed by the post hoc Tukey's multiple-comparisons test: *p < 0.05, **p < 0.01, ***p < 0.001, ****p < 0.0001, ns, non-significant.

lungs of high-MIF-expressing $CATT_7$ mice compared with the low-expressing $CATT_5$ or WT littermate control (Figures 3C and 3D). However, the number of clusters of labeled BM-MSCs within the lungs remained unchanged among the groups (Figure 3E). Taken together, these data suggest that prolonged MSC pulmonary retention time increases the number of MSCs retained at the site of inflammation 24 h post administration. These data suggest that high levels of MIF may provide a longer window for MSCs to carry out their therapeutic effects.

The influence of MIF on MSC expression of immunomodulatory factors and MSC cytokine licensing *in vitro*

MSCs mediate their therapeutic effects via expression or production of secreted factors *in vitro* and *in vivo*,[64] and licensing with proinflammatory cytokines such as IFNγ or TNF-α[65–69] can enhance expression of immunomodulatory mediators. Here, we characterized the effect of recombinant hMIF on the expression of indolamine 2-3-dioxygenase (IDO), cyclooxygenase 2 (COX-2), prostaglandin E synthase (PTGES), intercellular adhesion molecule-1 (ICAM-1), and hepatocyte growth factor (HGF) in untreated MSCs or MSCs licensed with IFNγ or TNF-α. Recombinant hMIF (rhMIF; 1 ng/mL) stimulation alone did not increase expression of IDO, COX-2, PTGES, ICAM-1, or HGF (Figures 4A–4E) in human BM-MSCs. Following licensing with TNF-α, MIF stimulation enhanced MSC expression of COX-2 and PTGES (Figures 4B and 4C). In IFNγ-licensed MSCs, rhMIF stimulation did not enhance MSC expression of IDO or HGF and significantly reduced ICAM-1 expression (Figures 4A, 4D, and 4E). We confirmed these findings at the protein level for IDO and COX-2 using intracellular flow cytometry (Figures 4F and 4G). Using increasing doses of rhMIF (1, 10, or 100 ng/mL), we showed that COX-2 expression is increased in a dose-dependent manner by rhMIF stimulation in TNF-α-licensed MSCs, with COX-2 expression plateauing at 10 ng/mL of rhMIF (Figure 4H). The MIF receptor CD74 is expressed by MSCs; however, rhMIF stimulation (dose range 1, 10, or 100 ng/mL) does not enhance CD74 expression (Figure 4I).

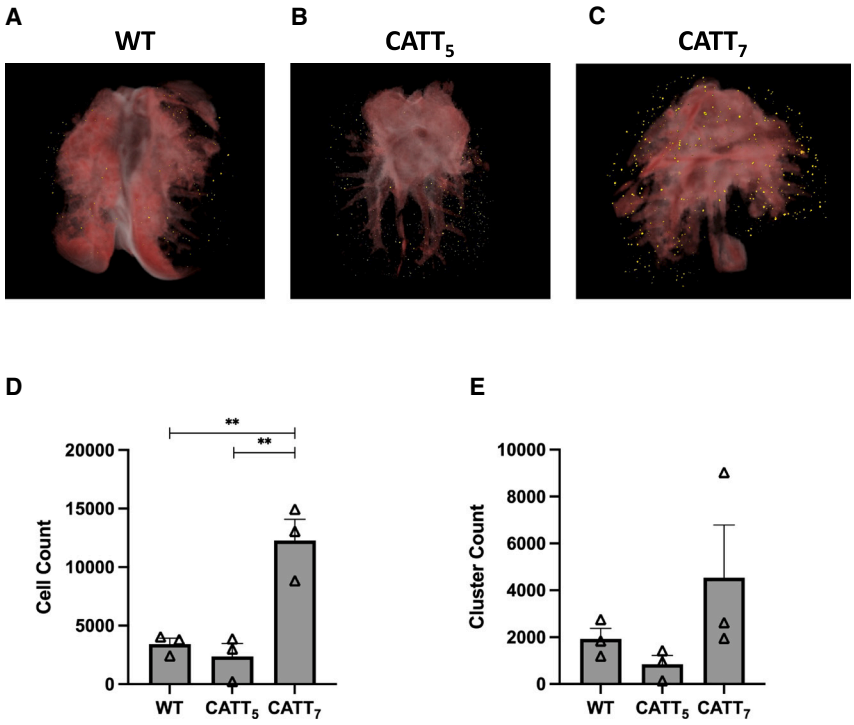

Figure 3. High levels of hMIF significantly enhance BM-MSC retention in an HDM model of allergic asthma

HDM were administered i.n. 3 times a week for 2 weeks. On day 14, 1×10^6 Qtracker 625-labeled hMSCs were administered i.v. to WT, $CATT_5$, or $CATT_7$ mice. 24 h later the lungs were harvested, embedded in OCT compound and frozen at −80. Tissue blocks were sectioned and imaged using the CryoViz (BioInvision) imaging system. (A–C) 3D images show representative lung images from (A) WT, (B) $CATT_5$, and (C) $CATT_7$ mice, with detected MSCs shown in yellow. (D and E) Total number of MSCs detected in the lungs (D) and number of clusters (E) were quantified using CryoViz quantification software. Data are presented as mean ± SEM; n = 3 per group. Human BM-MSC donor 001-177 was used (RoosterBio). Statistical analysis was carried out using one-way ANOVA followed by the post hoc Tukey's multiple-comparisons test: $^{**}p < 0.01$.

$CATT_7$ MIF licensing enhances MSC expansion and immunosuppressive function *in vitro*

To investigate the effect of endogenous MIF from $CATT_7$ mice on MSC expression of immunomodulatory factors, we generated BM-derived macrophages (BMDMs) from $CATT_7$ mice and used the conditioned medium (CM) as a source of endogenous hMIF (Figure 5A) to license MSCs. The concentration of hMIF in $CATT_7$ BMDM CM ranged from ∼3,000–4,000 pg/mL (Figure S2).

MIF may have a negative role in the regulation of IDO expression as $MIF^{-/-}$ mice produce more IDO;[70] however, MIF has an established role as an upstream positive regulator of COX-2 through activation of the mitogen-activated protein kinase (MAPK) signaling pathway.[71,72] IDO, COX-2, and PGE2 are widely reported mediators of MSC immunosuppression.[39,73] MSCs constitutively express COX-2 but not IDO. IFNγ licensing of MSCs leads to expression of IDO, while TNF-α enhances MSC COX-2 expression.[68] Here we show that $CATT_7$ MIF stimulation reduces MSC IDO production (Figures 5B and 5C); however, the percentage of COX-2 expressing MSCs was significantly increased following $CATT_7$ MIF stimulation (Figures 5D and 5E). Human MSCs express the MIF receptor CD74, and this expression is maintained and not increased following exposure to $CATT_7$ MIF CM (Figure 5F). In line with another study,[74] we show that IFNγ stimulation leads to significantly increased MSC CD74 expression and that $CATT_7$ MIF CM does not significantly alter that (Figure 5F). This aligns with our data showing that MIF does not enhance IFNγ-regulated IDO expression. Given the potentiating effect of MIF on the TNF-α-regulated gene COX-2 in MSCs, we examined the influence of $CATT_7$ MIF on MSC expression of the TNF-α-regulated genes tumor necrosis factor-inducible gene 6 (TSG-6) and prostaglandin-endoperoxide synthase 2 (PTGS2). The presence of $CATT_7$ MIF CM significantly reduced TSG-6 in TNF-α-stimulated MSCs (Figure 5G) but did not significantly alter the expression of PTGS2 (Figure 5H). MSCs licensed with high levels of hMIF from $CATT_7$ CM displayed enhanced suppression of T cell proliferation compared with the untreated MSCs; however, this was not statistically significant in the frequency of proliferating $CD3^+$ T cells (Figure 5I) or the number of proliferating $CD3^+$ T cells (Figure 5J). The presence of SCD-19 abrogated the enhanced suppression mediated by hMIF-licensed MSCs because the number of proliferating $CD3^+$ T cells was significantly increased compared with the ^{CATT7}MSC group (Figure 5J).

Previous studies have shown that MIF has the ability to support cell proliferation *in vitro*.[75–77] Increasing the number of MSCs within the inflammatory niche could prove to be important in enhancing MSC immunoregulatory effects. High levels of MIF significantly enhanced MSC expansion *in vitro* compared with the complete medium control group (Figure 5K). Blockade of MIF using SCD-19 confirmed the role of MIF in driving MSC expansion (Figure 5K). These data might help to explain the enhanced retention of MSCs in $CATT_7$ HDM-challenged mice (Figure 3), but further experiments would be required to confirm that.

Titration of BM-MSC doses in $CATT_7$ mice challenged with HDM

Next, we investigated whether MIF licensing could improve MSC efficacy in the high-MIF-expressing $CATT_7$ mice challenged with HDM. To do this, we first investigated the dose at which MSCs lose efficacy. MSCs at doses of 1×10^6, 5×10^5, 1×10^5, and 5×10^4 were administered i.v. into HDM-challenged $CATT_7$ on day 14 (Figure 6A). MSCs maintained efficacy as low as 1×10^5 cells with

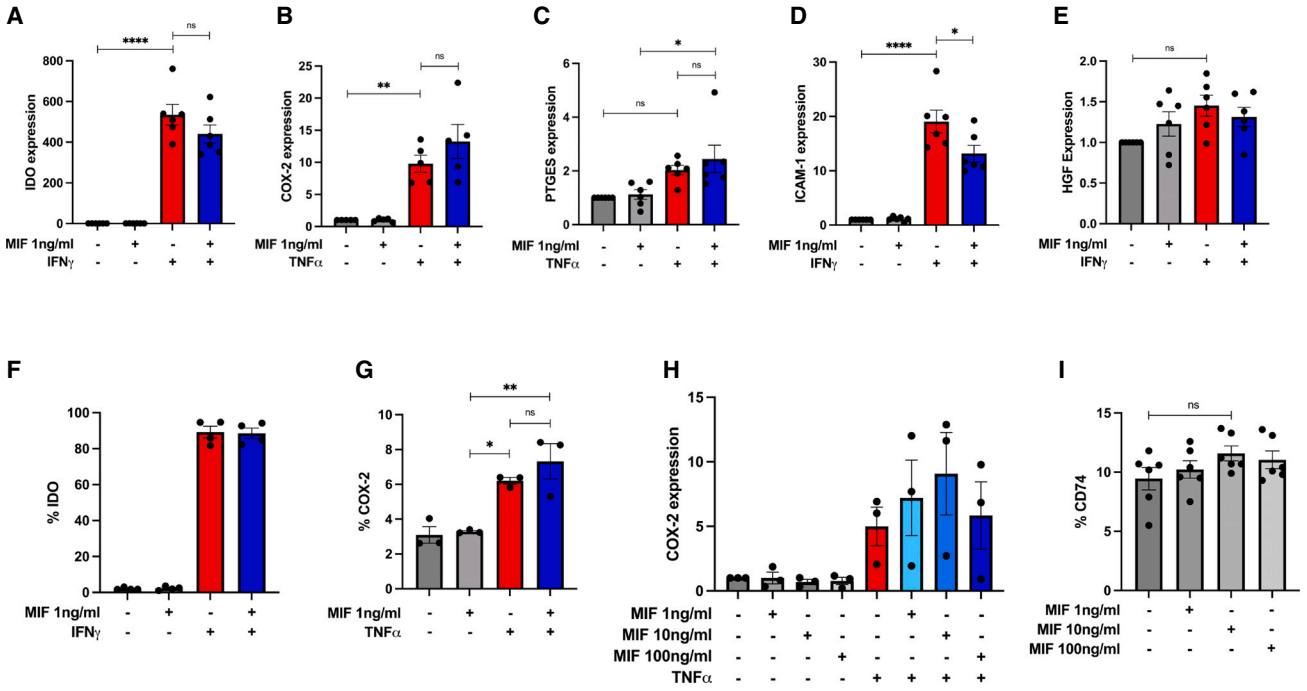

Figure 4. Influence of rhMIF licensing on MSC expression of immunomodulatory factors *in vitro*

(A–E) Gene expression of IDO, COX-2, PTGES, ICAM-1, and HGF by hBM-MSCs after stimulation with rhMIF (1 ng/mL), human TNF-α or human IFNγ for 24 h. Data are presented as mean ± SEM and are representative of 3 independent experiments. Human BM-MSC donors 001-177, 003-310, and 003-307 were used (RoosterBio). Statistical analysis was carried out using one-way ANOVA: *p < 0.05, **p < 0.01, ****p < 0.0001, ns, non-significant.

reduced immune cell infiltration (Figures 6B and 6C) and reduced Th2 cytokines IL-4 (Figure 6D) and IL-13 (Figure 6E). We observed that BM-MSCs were no longer able to carry out their immunosuppressive effects at a dose of 5×10^4. At 5×10^4, BM-MSCs were unable to reduce the number of eosinophils infiltrating the lungs (Figures 6B and 6C) or regulate Th2 cytokine production (Figures 6D and 6E).

MIF licensing restores MSC efficacy at low doses in $CATT_7$ mice

To investigate the effect of MIF licensing on MSC therapeutic efficacy, MSCs were first licensed *in vitro* by stimulation with BMDM CM from $CATT_7$ or knockout (KO) mice for 24 h 5×10^4 MSCs, MIF-licensed MSCs (^{CATT7}MSC), or MIF KO-licensed MSCs (^{KO}MSC) were administered i.v. into $CATT_7$ mice via tail vein injection on day 14 in HDM-challenged mice. On day 18, BALF was collected, cell counts were performed, and Th2 cytokines were measured (Figure 7A). Only ^{CATT7}MSC administration significantly reduced total cell counts and the number of eosinophils in $CATT_7$ mice challenged with HDM (Figures 7B and 7C). ^{CATT7}MSCs markedly reduced IL-4 and IL-13 levels compared with the control group although not significantly (Figures 7D and 7E). The control MSC group and the ^{KO}MSC group displayed similar levels of immune cell infiltration and Th2 cytokine production, suggesting that the effects observed in the ^{CATT7}MSC group are specific to MIF-licensed MSCs. These data show that MIF licensing can restore MSC immunosuppressive function at doses that would normally be ineffective.

Blocking COX-2 abrogates therapeutic efficacy of MIF licensed BM-MSCs

COX-2 is the rate-limiting enzyme involved in the synthesis of arachidonic acid to PGE2, a key mediator in the immunomodulatory effects of MSCs.[78] To assess the role of COX-2 on MIF-licensed MSCs, we inhibited COX-2 with indomethacin. MSCs were treated with indomethacin (10 μM) for 30 min. Following the 30-min pre-treatment, cells were incubated with $CATT_7$ CM for 24 h. To further validate the involvement of MIF in the improvement of MSC efficacy, MSCs were exposed to an anti-CD74 neutralizing antibody (10 μg/mL) or immunoglobulin G1 (IgG1) isotype control (10 μg/mL) for 30 min. MSCs were then incubated with $CATT_7$ CM for 24 h (Figure 8A). Analysis of the BALF cell counts showed that pre-treating MSCs with indomethacin before administration significantly reduces ^{CATT7}MSCs' ability to suppress immune cell infiltration in the BALF of $CATT_7$ mice challenged with HDM (Figures 8B and 8C). Additionally, the analysis of the Th2 cytokines in the BALF showed a marked increase in IL-4 (Figure 8D) and a significant increase in the level of IL-13 (Figure 8E) in the indomethacin group compared with the control MIF-licensed MSC group. Taken together, these results show that COX-2 is an important mediator in the enhancement of therapeutic efficacy associated with MIF licensing. Furthermore, blocking of CD74 abrogates MIF licensed BM-MSC suppression of eosinophil infiltration and type 2 cytokines in the BALF (Figure 8). These data indicate that MIF enhances MSCs' immunomodulatory capacity mainly through CD74 signaling to upregulate COX-2 production.

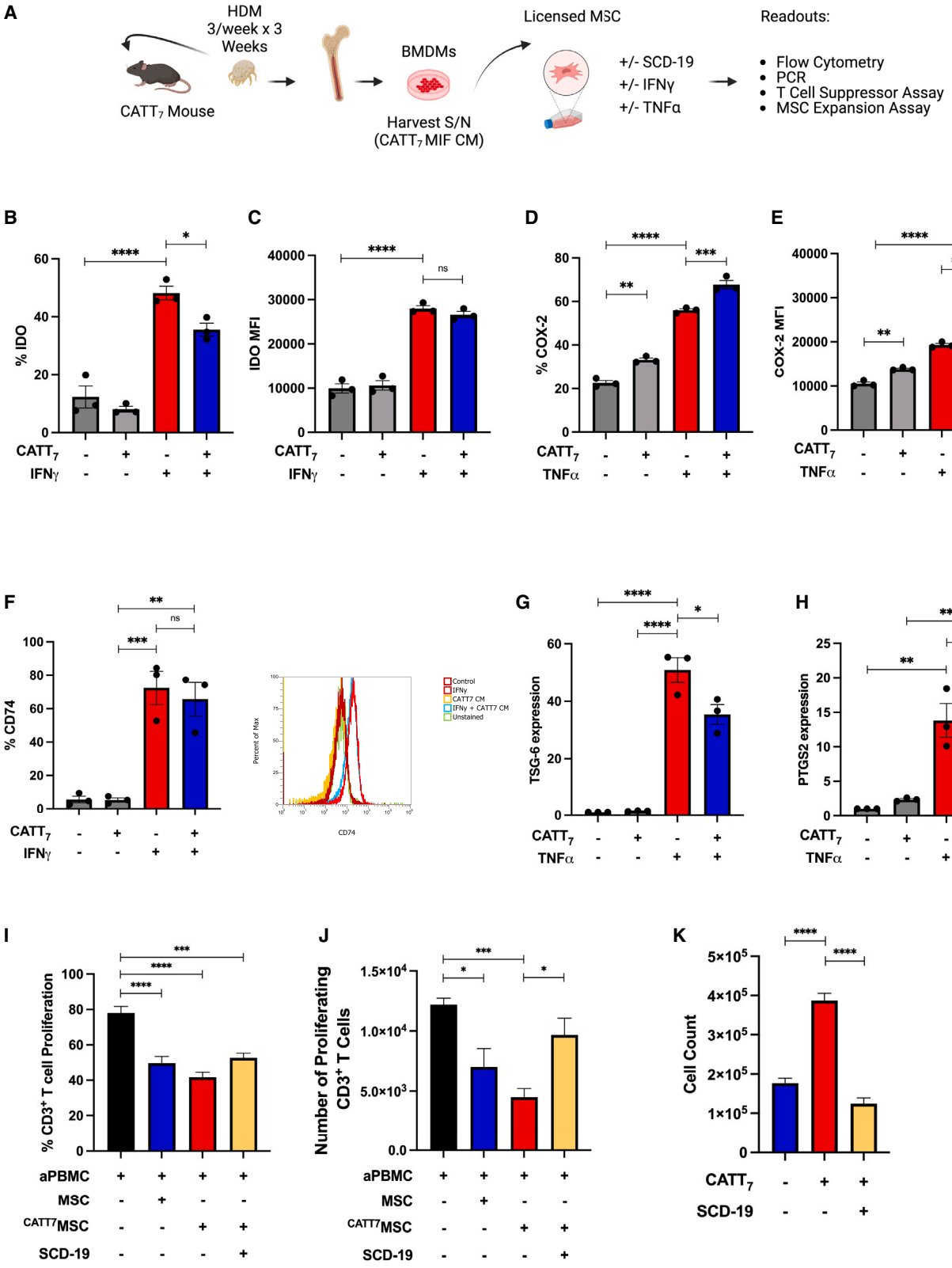

(legend on next page)

DISCUSSION

Our main results advance the field of MSC-based therapeutics for asthma by demonstrating that (1) MSC treatment is highly effective in ameliorating airway inflammation; (2) their therapeutic potential can be enhanced by MSC-MIF licensing, as demonstrated in high-MIF-expressing $CATT_7$ mice; and finally (3) the mechanism of MIF licensing is dependent on MSC-CD74 expression levels that drive COX-2 expression in MSCs. Our data align with the literature demonstrating the ability of human MSCs to ameliorate eosinophil infiltration by reducing the levels of Th2 cytokines.[8,10–12,25,79] In addition to reducing inflammation, MSCs also alleviate features of airway remodeling in the $CATT_7$ mice. Interestingly, while MSCs were effective at reducing the severity of goblet cell hyperplasia and subepithelial fibrosis in all groups, we did not observe the same changes in type 2 inflammatory markers in the BALF of WT and low-MIF-expressing $CATT_5$ mice, suggesting that high levels of MIF may be responsible for improving MSC efficacy. The reduced efficacy of MSCs in the WT and $CATT_5$ mice can likely be attributed to a lack of inflammation present, associated with a bias toward Th1 immunity in C57BL/6 mice compared with more Th2 bias in BALB/c mice, influencing the level of Th2 response in our HDM challenge model.[80] There have been several instances where researchers also observed poor responses to MSC treatment of allergic airway inflammation in C57BL/6 mice.[7,23] More recently, Castro et al.[21] report the requirement of at least 2 doses of human adipose derived (AD)-MSCs to reverse airway remodeling and alleviate inflammation in HDM-challenged C57BL/6 mice.

We show that a single human MSC dose is capable of significantly decreasing airway remodeling in $CATT_7$ mice. This suggests that high levels of MIF may facilitate activation of MSCs, improving their therapeutic efficacy and leading to reversal of airway remodeling. The literature surrounding MSCs' effect on airway remodeling is conflicting; however, the majority of the current literature demonstrates that MSCs can attenuate airway remodeling.[8,10,14,15,17,18,28] Others report a deficit in MSCs capacity to ameliorate goblet cell hyperplasia[14,19,23] or subepithelial collagen deposition.[9,28] Reasons for these discrepancies include the source of MSCs,[8,23,81] genotypic mouse model differences, severity of the mouse models, time of infusion, MSC fitness, dosing, and route of administration.[27]

Our previous studies have demonstrated that pro-inflammatory cytokine licensing of MSCs or MSC-like cells; multipotent adult progenitor cells (MAPCs) enhance their retention under inflammatory conditions and correlate with enhanced therapeutic efficacy.[39,82] We detected significantly higher numbers of MSCs in the lungs of HDM-challenged $CATT_7$ mice compared with $CATT_5$ or littermate controls 24 h following administration. It has been suggested that short-term effects of MSCs are mediated by their diverse secretome and that the longer-term effects of MSC therapy are a result of direct interaction with other cell types.[83] Increased longevity at the site of injury allows MSCs a longer period to secrete soluble factors and interact with cells in the inflammatory microenvironment. MSC retention in the $CATT_7$ HDM-challenged mice is an important observation, and future work will determine whether enhanced retention is also involved in the enhanced MSC efficacy observed.

Taken together, these data suggest that MSCs are more efficacious in the high-MIF environment of $CATT_7$ mice. By investigating the effects of different concentrations of a human cytokine on the efficacy of human MSCs in a model of allergic asthma using a clinically relevant allergen, we identified a specific disease microenvironment that supports and enhances MSC efficacy. The use of our humanized model aims to provide a more accurate depiction of how human MSCs would interact in subsets of patients compared with conventional murine models. Of course, despite exploring the effect of a human cytokine on human MSCs, there are still limitations because we are unable to fully mimic clinical severe allergic asthma, and the use of transgenic MIF mice on a C57BL/6 background meant that control WT mice do not develop a high level of type 2 inflammation. However, these results may have implications for tailoring MSC treatment in cases of severe asthma. Our results have demonstrated that MSCs are less efficacious in low-MIF environments. Patients with 5/5 haplotypes tend to have lower levels of circulating MIF[84] and therefore may not respond as well to MSC treatment. Patients with 6/6, 7/7, or 8/8 haplotypes are more likely to have high levels of circulating MIF,[52,85,86] which may lead to greater MSC activation and enhanced therapeutic efficacy.

Following the discovery that MSC administration into $CATT_7$ mice led to improved MSC efficacy, we investigated strategies to use high-MIF microenvironments to potentiate the effects of MSCs. Past work in our lab has focused on different licensing strategies of MSCs to enhance MSC efficacy. Previously, we have demonstrated how IFNγ licensing can improve MSC efficacy in a humanized model of acute graft versus host disease (GvHD) and how endogenous factors such as peroxisome proliferator-activated receptor (PPAR) δ ligands or treatments like cyclosporine A can influence this.[39,40] Other

Figure 5. $CATT_7$ MIF licensing enhances MSC expansion and immunosuppressive function *in vitro*

(A) Schematic (created using BioRender) depicting the generation of $CATT_7$ MIF CM and experimental design. (B–E) Percentage or mean fluorescence intensity (MFI) of IDO or COX-2 expression in human BM-MSCs, measured by flow cytometry after cells were stimulated with $CATT_7$ MIF CM, human TNF-α, or human IFNγ for 24 h. (F) Percentage expression and representative histogram plots of CD74 surface expression on human MSCs, measured by flow cytometry after cells were stimulated with $CATT_7$ MIF CM and human IFNγ for 24 h. (G and H) Relative gene expression of TSG-6 and PTGS2 by hBM-MSCs after cells were stimulated with endogenous hMIF ($CATT_7$ CM) and human TNF-α for 6 h. (I and J) Licensing of MSCs with supernatants generated from BMDMs from $CATT_7$ HDM-challenged mice enhances MSC suppression of (I) frequency (percent) and (J) absolute number of $CD3^+$ T cells proliferating. Blockade of MIF using SCD-19 (100 μM) in the BMDM supernatants 1 h before addition to MSCs abrogates the enhanced effect of MIF on MSC suppression of T cell proliferation.

(K) Licensing of MSCs with $CATT_7$ MIF CM enhances MSC expansion *in vitro*. Addition of the MIF inhibitor SCD-19 (100 μM) to $CATT_7$ MIF CM 1 h before MSC licensing prevents MIF-enhanced MSC expansion. Data are presented as mean ± SEM and are representative of 3 independent experiments. Human BM-MSC donors 001-177, 003-310, and 003-307 were used (RoosterBio). Statistical analysis was carried out using a one-way ANOVA or unpaired t test: $^*p < 0.05$, $^{**}p < 0.01$, $^{***}p < 0.001$, $^{****}p < 0.0001$.

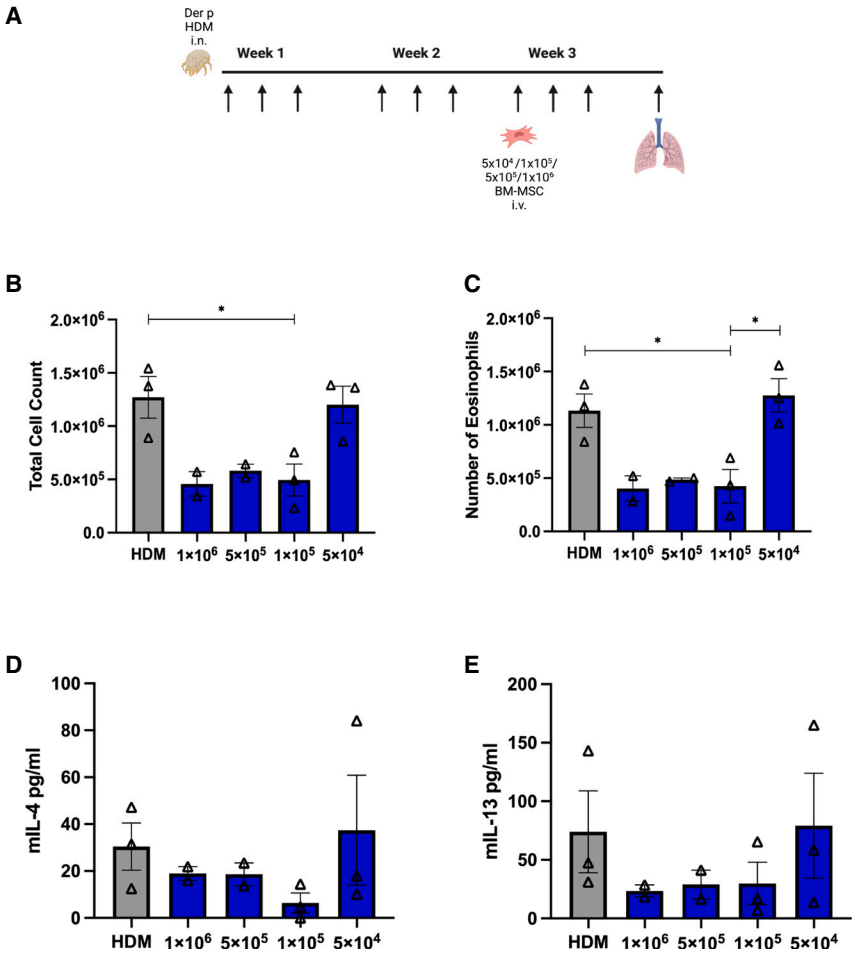

Figure 6. Titration of BM-MSC doses in CATT$_7$ mice challenged with HDM

(A) To determine the point where MSCs lose efficacy in CATT$_7$ mice, a range of doses were administered on day 14. BAL was performed 4 h post final HDM challenge on day 18 (schematic created with BioRender). (B) Total cell count recovered from the BALF.

(C) Number of eosinophils obtained from the BALF. (D and E) Cytokine levels of (D) IL-4 and (E) IL-13 in the BALF, determined by ELISA. Data are presented as mean ± SEM; n = 2–3 per group. Human BM-MSC donors 001-177 and 003-310 were used (RoosterBio). Statistical analysis was carried out using one-way ANOVA followed by the post hoc Tukey's multiple-comparisons test: *p < 0.05.

studies have shown how licensing with pharmacological agents or endogenous factors can further enhance the effects of MSC therapy in preclinical models of asthma.[18,19,87]

One of the main criticisms of preclinical research is the use of doses that far exceed what would be reasonable in the clinic. Analysis of clinical trials using i.v. injection of MSCs reveals that the minimal effective dose used ranges from 1–2 million cells/kg.[88] Studies that have investigated i.v. administration of MSCs in preclinical models of allergic asthma, administering doses that equate to 4–40 million cells/kg, with the majority at the higher end of the scale.[8,10,12,16,20–22,25,26,28,79,89–92] The efficacy observed with MIF-licensed MSCs using 5×10^4 cells per mouse results in an effective dose of 2 million cells/kg. This shows that, through MIF licensing, we are able to restore MSC efficacy at a dose akin to what is used in clinical trials.

We then sought to elucidate the mechanisms involved. Given our use of human MSCs in a mouse host, the interspecies ligand/receptor non-functionality can raise questions about how human MSCs might mediate their effects in a mouse host. We and others have shown that human MSCs can indeed mediate protective effects in mouse hosts.[8,10–12,14–17,21,24,25,33,93] Four studies have tracked human MSC biodistribution following i.v. administration in patients with chronic obstructive pulmonary disease (COPD),[94] liver cirrhosis,[95] hemophilia A,[96] or breast cancer.[97] No MSCs were detected in the blood 1 h post infusion. MSCs were distributed mainly in the lungs[95] or lungs and liver[96] 48 h post i.v. infusion, with the signal decreasing thereafter. Therefore, these studies suggest that biodistribution of human MSCs following i.v. administration in humans aligns with the studies investigating MSC biodistribution in mouse models.[98]

In terms of mechanism, MIF-mediated signal transduction is primarily initiated by binding to MIF's classical receptor, CD74.[99] We showed that blocking CD74 on the surface of MSCs ultimately abolished their immunosuppressive abilities. These findings not only reaffirmed that the licensing with CATT$_7$ CM was MIF mediated, but it also showed that these effects were dependent on binding to CD74. MIF signal transduction through CD74 binding has been shown to initiate a range of signaling pathways that induce cell proliferation, resistance to apoptosis, and the promotion of repair.[100–104] Furthermore, MIF binding to CD74 has been shown to activate cytosolic phospholipase A2 (cPLA$_2$). Moreover, cPLA$_2$ activation results in the mobilization of arachidonic acid from membrane phospholipids, which is a precursor to the synthesis of prostaglandins.[105] Interestingly, MIF can upregulate COX-2 expression, a rate-limiting step in the synthesis of prostaglandins such as PGE2;[71,72,106] however, MIF has been shown to have no effect on the expression of COX-1.[71]

The COX-2/PGE2 pathway has been extensively documented as being one of the key mediators driving MSC immunomodulation.[39,68,107,108] Our data show that MIF stimulation enhances the expression of COX-2, but not TSG-6 or PTGS2, in untreated and TNF-α-licensed MSCs. We hypothesized that the COX-2/PGE2 pathway could be involved in the restoration of MSCs'

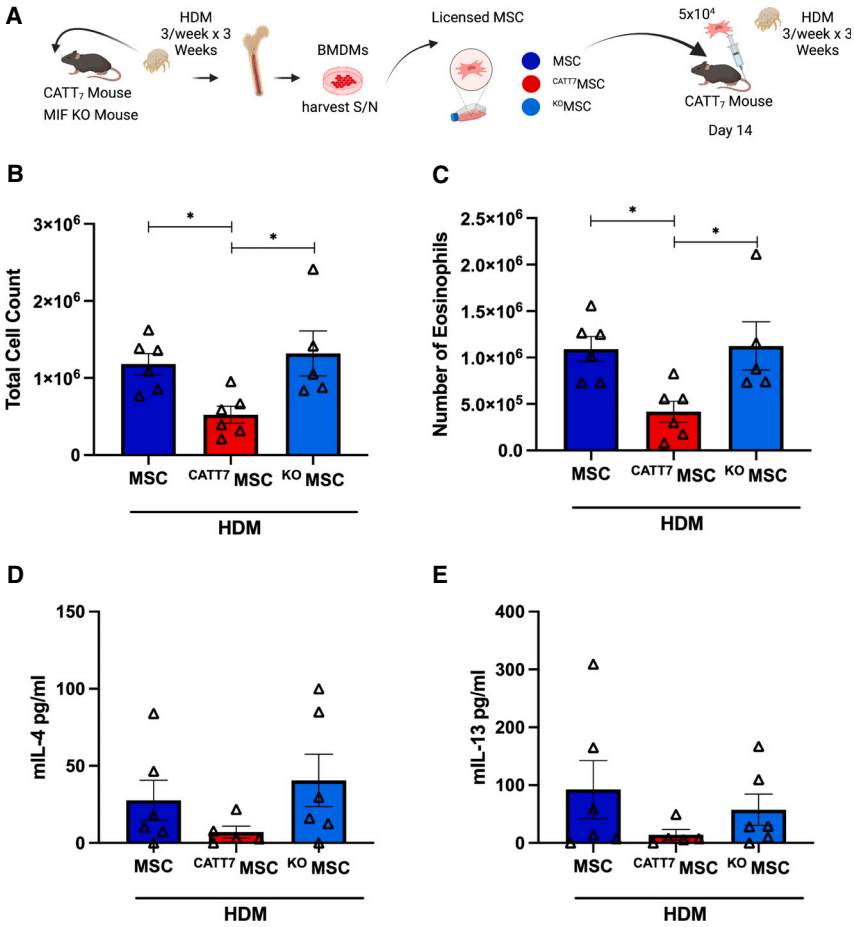

Figure 7. MIF licensing restores MSC efficacy at low doses in $CATT_7$ mice

(A) 5×10^4 MSCs were administered to HDM-challenged $CATT_7$ mice on day 14. ^{CATT7}MSCs were licensed with $CATT_7$ BMDM supernatant for 24 h prior to i.v. administration. The control group ^{KO}MSCs were generated by licensing MSCs with BMDM supernatant from MIF KO mice 24 h prior to i.v. administration. BAL was performed 4 h post final HDM challenge on day 18 (schematic created with BioRender). (B and C) Total number of cells in the BALF were determined (B), and differential cell counts were performed on the collected cells to determine the numbers of eosinophils (C). (D and E) Cytokine levels of (D) IL-4 and (E) IL-13 in the BALF determined by ELISA. Data are presented as mean ± SEM; n = 5–6 per group. Human BM-MSC donors 001-177 and 003-310 were used (RoosterBio). Statistical analysis was carried out using one-way ANOVA followed by the post hoc Tukey's multiple-comparisons test: *$p < 0.05$.

immunomodulatory capacity following $CATT_7$ licensing. To investigate, we pre-treated MSCs with indomethacin prior to licensing. Indomethacin is a potent non-selective inhibitor of COX-1 and COX-2.[109] We showed that blocking COX-2 abrogated the therapeutic efficacy of $CATT_7$ licensed MSCs. Interestingly we observed that blocking of COX-2 via indomethacin had a more pronounced effect than blocking CD74. COX-2 is constitutively expressed in human MSCs; therefore, inhibition with indomethacin also blocks basal COX-2 expression, which will contribute to the effects observed.

These data show that MIF licensing can improve MSC therapeutic efficacy through the upregulation of COX-2, which likely drives PGE2 production. Our data agree with several studies in the literature that also reveal the ability of MIF to improve MSC efficacy *in vivo*.[110–112] Zhu et al.,[110] Liu et al.,[111] and Zhang et al.[112] demonstrated the ability of MIF to improve MSC therapeutic efficacy by transducing MSCs with a lentiviral vector containing *Mif* cDNA, thus promoting MIF overexpression.[110–112] Furthermore, Zhang et al.[113] demonstrated the ability of MIF to upregulate COX-2 expression and promote PGE2 production in astrocytes. Here, we further demonstrate the effects of *ex vivo* MIF licensing on MSC therapeutic efficacy by showing that binding to CD74 and increased COX-2 expression enhances MSCs' immunomodulatory abilities.

The knowledge gained from this study can be used to further optimize MSCs as a therapy and provide a basis for future studies regarding the effects of MSCs on the immune response in high-MIF environments, such as in asthma patients exhibiting the $CATT_7$ polymorphism.

MATERIALS AND METHODS

Ethics approval

All procedures involving the use of animals or human materials were carried out by licensed personnel. Ethics approval for all work was granted by the biological research ethics committee of Maynooth University (BRESC-2018-013). Project authorization was received from the Scientific Animal Protection Unit of the Health Products Regulatory Agency (HPRA) under AE19124/P022, where the terms of the animal experiments within this project were outlined and adhered to in accordance with the Animal Research: Reporting of In Vivo Experiments (ARRIVE) criteria.

Human BM-MSC culture

BM-MSCs from three different human donors were obtained from RoosterBio (Frederick, MD, USA). MSCs were first expanded in RoosterBio proprietary expansion medium (RoosterBasal and RoosterBooster) for the first two passages according to the manufacturer's instructions. Following this, MSCs were cultured and maintained in Dulbecco's modified Eagle's medium (DMEM) low glucose (Sigma-Aldrich, Arklow, Wicklow, Ireland) supplemented with 10% (v/v) fetal bovine serum (FBS; BioSera, Cholet, France) and 1% (v/v) penicillin/streptomycin (Sigma-Aldrich). Human MSCs were seeded at 1×10^6 cells per T175 flask and cultured at 37 °c in 5% CO_2. Medium was replenished every 2–3 days, and cells were passaged when they achieved 80% confluency. All experiments were carried out between passages 2–5.

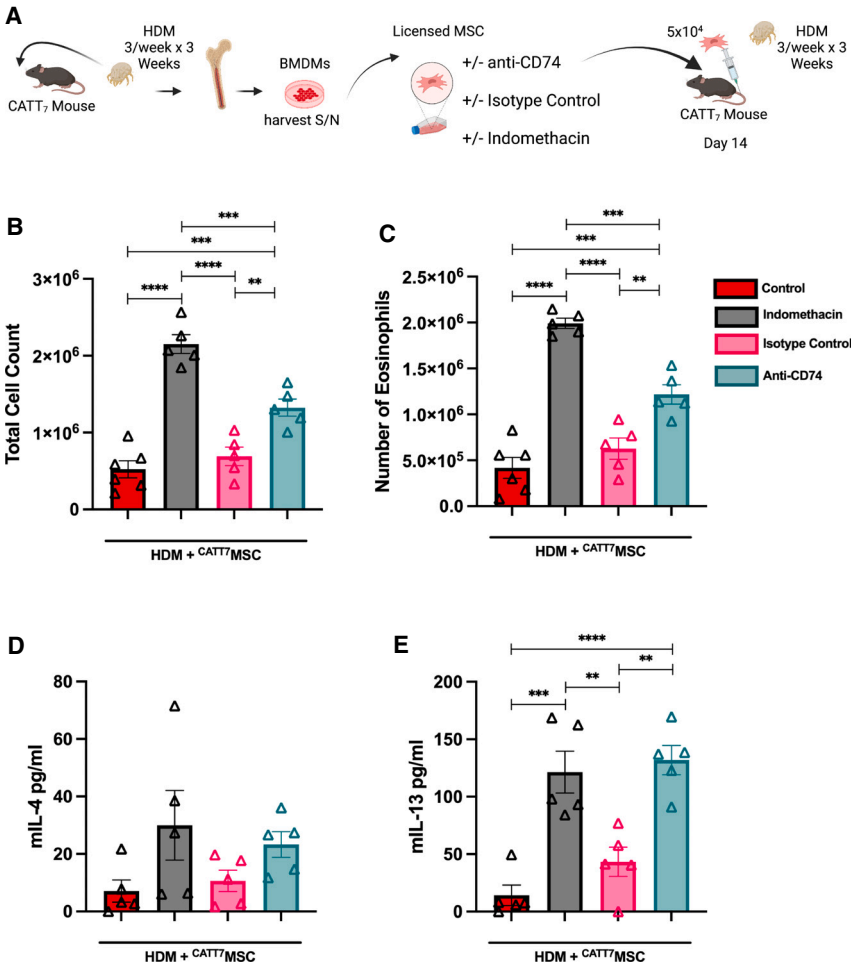

Figure 8. MIF-Licensed MSCs mediate their protective effects in HDM-induced allergic airway inflammation in a CD74- and COX-2-dependent manner in $CATT_7$ mice

(A) 5×10^4 MSCs were exposed to the COX-2 inhibitor indomethacin, an anti-CD74 neutralizing antibody, or an isotype control antibody for 24 h *in vitro*. All MSCs were licensed with $CATT_7$ BMDM supernatant for 24 h prior to i.v. administration. BAL was performed 4 h post final HDM challenge on day 18 (schematic created with BioRender). (B and C) Total number of cells in the BALF were determined (B), and differential cell counts were performed on the collected cells to determine the numbers of eosinophils (C). (D and E) Cytokine levels of (D) IL-4 and (E) IL-13 in the BALF, determined by ELISA. Data are presented as mean ± SEM; n = 5–6 per group. Human BM-MSC donors 001-177 and 003-310 were used (RoosterBio). Statistical analysis was carried out using one-way ANOVA followed by the post hoc Tukey's multiple-comparisons test: $^{**}p < 0.01$, $^{***}p < 0.001$, $^{****}p < 0.0001$.

MSC characterization

BM-MSCs from three different human donors (identified as 001-177, 003-307, and 003-310) from RoosterBio were characterized by analyzing the expression of cell surface markers. All MSCs donors were found to be negative for CD34 (fluorescein isothiocyanate [FITC]), CD45 (Allophycocyanin (APC)), and human leukocyte antigen-DR (HLA-DR) (phycoerythrin (PE)) and positive for CD73 (APC), CD90 (FITC), and CD105 (PE) (BD Pharmingen, San Diego, CA, USA) by the Attune Nxt flow cytometer (Figure S3).

Animal strains

Two C57BL/6 mouse strains expressing the human high- or low-expression MIF alleles (MIF^{CATT7} [(C57BL/6NTac-Miftm3884.1(MIF)Tac-Tg(CAG-Flpe)2Arte] and MIF^{CATT5} [C57BL/6NTac-Miftm3883.1(-MIF)Tac-Tg(CAG-Flpe)2Arte] mice) were created using vector-based recombinant replacement of murine *Mif* by Taconic Biosciences (Rensselaer, NY, USA) (Figure 1). Validation of the expression of human and not murine *MIF* mRNA was verified by qPCR, and −794 CATT-length-dependent stimulated MIF production was confirmed *in vivo*.[61] Littermate WT and $MIF^{-/-}$ (MIF KO)[114] (a kind donation from R. Bucala, Yale School of Medicine, Yale University, New Haven, CT, USA) mice were used as controls.

HDM-induced airway inflammation model and therapeutic protocol

Both male and female MIF^{CATT7}, MIF^{CATT5}, or WT mice aged 6–12 weeks were challenged with 25 μg HDM extract (*Dermatophagoides pteronyssinus*; Greer Laboratories, Lenoir, NC, USA) in 25 μL phosphate-buffered saline (PBS) intranasally (i.n.) 3 days weekly for 3 weeks under light isoflurane anesthesia. Control mice were challenged with 25 μL PBS under the same conditions. On day 14, after HDM challenge, mice received an i.v. injection of 1×10^6 MSCs in 300 μL into the tail vein.[115] For the dose curve, 1×10^6, 5×10^5, 1×10^5, and 5×10^4 were administered i.v. into HDM-challenged $CATT_7$ mice on day 14. 5×10^4 was selected as the dose at which MSCs lose efficacy.

Licensing of MSCs with endogenous hMIF

Supernatants containing endogenous hMIF were generated from BMDMs of C57BL/6 mouse strains expressing the high-expressing MIF allele ($CATT_7$). $CATT_7$ mice were challenged with HDM in 25 μL PBS i.n. 3 days weekly for 3 weeks under light isoflurane anesthesia. 4 h post final challenge, femora and tibiae were flushed with warm Roswell Park Memorial Institute (RPMI) 1640 medium GlutaMAX (Gibco, Paisley, UK) supplemented with 10% (v/v) heat-inactivated FBS (BioSera) and 1% (v/v) penicillin/streptomycin (Sigma-Aldrich). Cells were collected and seeded into T175 flasks in cRPMI supplemented with 10% L929 CM. The L929 cell line produces high amounts of macrophage colony stimulating factor (M-CSF) and other proteins stimulating macrophage differentiation.

After 96 h, supernatants were collected, sterile filtered (0.22 μM pore size), and stored at −20°C. The CM generated in this manner will be referred to as $CATT_7$ CM. Additionally, KO CM was generated from MIF KO mice as a control. Licensing MSCs was performed by removing existing medium, washing with PBS, and incubating cells with $CATT_7$ CM (^{CATT7}MSC) or MIF KO CM (^{KO}MSC) for 24 h. To account for variability of hMIF levels between $CATT_7$ mice and to ensure that WT mice did not produce hMIF, $CATT_7$, $CATT_5$, and WT supernatants were measured by hMIF ELISA (R&D Systems, MN, USA) as described previously (Figure S2).[62] 5×10^4 licensed MSCs were administered i.v. into HDM-challenged $CATT_7$ mice on day 14. Where indicated, MSCs were treated with the COX-2 inhibitor indomethacin (10 μM) for 30 min. Following pre-treatment, MSCs were licensed with $CATT_7$ CM for 24 h as described above. Moreover, mouse anti-CD74 neutralizing antibody and isotype control were added to the assay. MSCs were pre-treated with anti-CD74 neutralizing antibody (clone LN2; 10 μg/mL) or IgG1 κ isotype control (clone T8E5; 10 μg/mL) for 30 min. MSCs were then licensed with $CATT_7$ CM for 24 h before administration.

Collection of BALF

On day 18, 4 h post final challenge, mice were sacrificed for cell and cytokine analysis of the BALF. BALF was obtained through 3 gentle aspirations of PBS. After centrifugation, protease inhibitor cocktail (Roche Diagnostics, Mannheim, Germany) was added to the supernatants before Th2 cytokine analysis. Total numbers of viable BALF cells were counted using ethidium bromide/acridine orange staining on a hemocytometer and then pelleted onto microscope slides by cytocentrifugation. Slides were stained with Kwik Diff kit stain (Richard-Allan Scientific, Kalamazoo, MI, USA), and coverslips were mounted using dibutylphthalate polystyrene xylene (DPX) mounting medium (Sigma-Aldrich). Differential cells counts were derived by counting a minimum of 300 leukocytes on randomly selected fields under a light microscope at 20× magnification.

ELISA

Levels of mouse interleukin-4 (mIL-4) (BioLegend, San Diego, CA, USA) and mIL-13 (eBioscience, San Diego, CA, USA) were determined using commercial ELISA kits according to the manufacturer's instructions.

Lung histology

On day 21, mice were sacrificed for histological analysis. Lungs were removed and fixed in 10% neutral buffered formalin and paraffin embedded, and 5-μm slices were mounted onto slides for histological analysis. Lung tissue was stained with H&E, PAS, or Masson's trichrome to analyze immune cell infiltration, goblet cell hyperplasia, or subepithelial collagen deposition, respectively. H&E analysis was carried out as described previously.[116] Goblet cell hyperplasia was determined by the percentage of PAS-positive cells in airways relative to airway diameter. Subepithelial collagen deposition was calculated by analyzing the percentage of positive staining using the trainable Weka segmentation plugin on Fiji open-source software.

Cryo-imaging

1×10^6 MSCs were labeled with the Qtracker 625 labeling kit (Invitrogen, Paisley, UK) according to the manufacturer's instructions before being administered i.v. on day 14. On day 15, mice were humanely euthanized, and the lungs were embedded in mounting medium for cryotomy (O.C.T. compound, VWR Chemicals, Leuven, Switzerland), frozen in liquid nitrogen, and stored at −80°C. Lungs were sectioned into 40-μm slices and imaged with the automated CryoViz imaging system (BioInvision, Cleveland, OH, USA). Images were then processed to generate 3D images using CryoViz processing, and the number of detected cells was quantified using cell detection software (BioInvision).[39]

Analysis of gene expression

Total RNA was extracted using TRIzol (Ambion Life Sciences, Cambridgeshire, UK) according to manufacturer's instructions. RNA concentrations were measured using a spectrophotometer (Nanodrop 2000, Thermo Scientific, Wilmington, DE, USA) and equalized to 100 ng/μL before cDNA synthesis. cDNA synthesis was performed according to the manufacturer's instructions (Quantabio, MA, USA). Real-time PCR was carried out using PerfeCta SYBR Green FastMix (Quantabio). Expression of human COX-2, PTGES, IDO, ICAM-1, HGF, TSG-6, and PTGS2 (primer sequence information is available in Table S1) was quantified in relation to the housekeeper gene HPRT using the ΔCT method. The fold change in the relative gene expression was determined by calculating the $2^{-\Delta\Delta CT}$ values.

MSC expansion assay

1.4×10^5 MSCs were seeded out into T25 flasks in complete Dulbecco's Modified Eagle Medium (cDMEM) or 50:50 cDMEM and WT CM or $CATT_7$ CM for 72 h. Cells were trypsinized and stained with ethidium bromide/acridine orange and counted on a hemocytometer. The MIF inhibitor SCD-19 (100 μM) was used to determine MIF specificity. In such cases, CM was pre-incubated with SCD-19 1 h before the expansion assay.

Intracellular staining of COX-2 and IDO

MSCs were seeded at 1×10^5 cells per well in 6-well plates. MSCs were stimulated with recombinant human IFNγ at low (5 ng/mL) or high (40 ng/mL) concentration, TNF-α (5–10 ng/mL; PeproTech, London, UK), rhMIF (1 ng/mL; provided by Rick Bucala, Yale), or endogenous MIF ($CATT_7$ CM) for 24 h. Cells were prepared for intracellular staining using the Intracellular FoxP3 kit according to the manufacturer's instructions. Cells were stained with COX-2 (PE) or IDO (APC) (BD Pharmingen) for 45 min. Cells were then washed in flow cytometry staining buffer and acquired using the Attune Nxt flow cytometer.

Surface staining of CD74

MSCs were seeded at 1×10^5 cells per well in 6-well plates. MSCs were stimulated with recombinant human IFNγ (5 ng/mL, PeproTech), rhMIF (1, 10, or 100 ng/mL), or endogenous MIF ($CATT_7$ CM) for 24 h. Cells were stained with CD74 (PE, BD Pharmingen) for

45 min. Cells were then washed in flow cytometry staining buffer and acquired using the Attune Nxt flow cytometer.

T cell suppression assay

Human PBMCs were isolated from buffy packs (Irish Blood Transfusion Service) by Ficoll density gradient centrifugation. 5×10^4 carboxyfluorescein succinimidyl ester (CFSE)-labeled PBMC were co-cultured (Thermo Fisher Scientific, Eugene, OR, USA) with BM-MSCs at a 1:20 ratio (2.5×10^3 cells/well). 24 h prior to co-culture, BM-MSCs were incubated with $CATT_7$ CM or $CATT_7$ CM + SCD-19 (100 μM). After 24 h, BM-MSCs were washed with PBS before adding the PBMCs. Activation and expansion of human T cells was carried out using ImmunoCult human CD3/CD28 T cell activator antibody mix (STEMCELL Technologies, Cambridge, UK). After 4 days, PBMCs were harvested, and the frequency (percent) and number of proliferating $CD3^+$ T cells were analyzed by flow cytometry (Attune Nxt flow cytometer).

Statistical analysis

Mice were randomized. Observers assessing endpoints were blinded to group assignment. Data for individual animals and independent experiments are presented as individual symbols. All data are presented as mean ± SEM. Results of two or more groups were compared by one-way analysis of variance (ANOVA) followed by the post hoc Tukey's multiple comparison test. GraphPad Prism (GraphPad, San Diego, CA, USA) was used for all statistical analyses.

DATA AND CODE AVAILABILITY

The data that support the findings of this study are available upon request from the corresponding author.

SUPPLEMENTAL INFORMATION

Supplemental information can be found online at https://doi.org/10.1016/j.ymthe.2023.09.013.

ACKNOWLEDGMENTS

This research was supported by an Irish Research Council Laureate Award to K.E. (IRCLA/2017/288). This publication has emanated from research supported in part by a research grant from Science Foundation Ireland (SFI) under grant 12/RI/2346 (2), an infrastructure award supporting the CryoViz and SFI grant 16/RI/3399, and an infrastructure award supporting the Attune Nxt. We would like to thank Deirdre Daly, Gillian O'Meara, and Shannon Grellan for exceptional care of our animals used in this study.

AUTHOR CONTRIBUTIONS

I.J.H. performed research, data analysis, and study design and wrote the manuscript. H.D. performed research, data analysis, and study design and wrote the manuscript. C.T. and T.S. performed research and data analysis. D.J.W., S.R.E., and C.C.d.S. contributed to study design and data analysis. S.C.D. and M.E.A. provided reagents and contributed to study design and data analysis. K.E. designed and supervised the study and wrote the manuscript. All authors approved the final manuscript.

DECLARATION OF INTERESTS

The authors declare no competing interests.

REFERENCES

1. Sverrild, A., Hansen, S., Hvidtfeldt, M., Clausson, C.M., Cozzolino, O., Cerps, S., Uller, L., Backer, V., Erjefält, J., and Porsbjerg, C. (2022). The effect of tezepelumab on airway hyperresponsiveness to mannitol in asthma (UPSTREAM). Eur. Respir. J. *59*, 2101296.
2. Bleecker, E.R., FitzGerald, J.M., Chanez, P., Papi, A., Weinstein, S.F., Barker, P., Sproule, S., Gilmartin, G., Aurivillius, M., Werkström, V., et al. (2016). Efficacy and safety of benralizumab for patients with severe asthma uncontrolled with high-dosage inhaled corticosteroids and long-acting β2-agonists (SIROCCO): a randomised, multicentre, placebo-controlled phase 3 trial. Lancet Lond. Engl. *388*, 2115–2127.
3. Corren, J., Castro, M., O'Riordan, T., Hanania, N.A., Pavord, I.D., Quirce, S., Chipps, B.E., Wenzel, S.E., Thangavelu, K., Rice, M.S., et al. (2020). Dupilumab efficacy in patients with uncontrolled, moderate-to-severe allergic asthma. J. Allergy Clin. Immunol. Pract. *8*, 516–526.
4. Ortega, H.G., Yancey, S.W., Mayer, B., Gunsoy, N.B., Keene, O.N., Bleecker, E.R., Brightling, C.E., and Pavord, I.D. (2016). Severe eosinophilic asthma treated with mepolizumab stratified by baseline eosinophil thresholds: a secondary analysis of the DREAM and MENSA studies. Lancet Respir. Med. *4*, 549–556.
5. Chan, R., and Lipworth, B. (2023). Efficacy of biologic therapy on airway hyperresponsiveness in asthma. Ann. Allergy Asthma Immunol. Off Publ. Am. Coll. Allergy Asthma Immunol. 00121–00127.
6. Goodwin, M., Sueblinvong, V., Eisenhauer, P., Ziats, N.P., LeClair, L., Poynter, M.E., Steele, C., Rincon, M., and Weiss, D.J. (2011). Bone marrow-derived mesenchymal stromal cells inhibit Th2-mediated allergic airways inflammation in mice. Stem Cells *29*, 1137–1148.
7. Abreu, S.C., Antunes, M.A., de Castro, J.C., de Oliveira, M.V., Bandeira, E., Ornellas, D.S., Diaz, B.L., Morales, M.M., Xisto, D.G., and Rocco, P.R.M. (2013). Bone marrow-derived mononuclear cells vs. mesenchymal stromal cells in experimental allergic asthma. Respir. Physiol. Neurobiol. *187*, 190–198.
8. Choi, J.Y., Hur, J., Jeon, S., Jung, C.K., and Rhee, C.K. (2022). Effects of human adipose tissue- and bone marrow-derived mesenchymal stem cells on airway inflammation and remodeling in a murine model of chronic asthma. Sci. Rep. *12*, 12032.
9. Dai, R., Yu, Y., Yan, G., Hou, X., Ni, Y., and Shi, G. (2018). Intratracheal administration of adipose derived mesenchymal stem cells alleviates chronic asthma in a mouse model. BMC Pulm. Med. *18*, 131.
10. de Castro, L.L., Xisto, D.G., Kitoko, J.Z., Cruz, F.F., Olsen, P.C., Redondo, P.A.G., Ferreira, T.P.T., Weiss, D.J., Martins, M.A., Morales, M.M., and Rocco, P.R.M. (2017). Human adipose tissue mesenchymal stromal cells and their extracellular vesicles act differentially on lung mechanics and inflammation in experimental allergic asthma. Stem Cell Res. Ther. *8*, 151.
11. Hur, J., Kang, J.Y., Kim, Y.K., Lee, S.Y., Jeon, S., Kim, Y., Jung, C.K., and Rhee, C.K. (2020). Evaluation of human MSCs treatment frequency on airway inflammation in a mouse model of acute asthma. J. Korean Med. Sci. *35*, e188.
12. Mathias, L.J., Khong, S.M.L., Spyroglou, L., Payne, N.L., Siatskas, C., Thorburn, A.N., Boyd, R.L., and Heng, T.S.P. (2013). Alveolar macrophages are critical for the inhibition of allergic asthma by mesenchymal stromal cells. J. Immunol. 1950 *191*, 5914–5924.
13. Ou-Yang, H.F., Huang, Y., Hu, X.B., and Wu, C.G. (2011). Suppression of allergic airway inflammation in a mouse model of asthma by exogenous mesenchymal stem cells. Exp. Biol. Med. *236*, 1461–1467.
14. Royce, S.G., Mao, W., Lim, R., Kelly, K., and Samuel, C.S. (2019). iPSC- and mesenchymoangioblast-derived mesenchymal stem cells provide greater protection against experimental chronic allergic airways disease compared with a clinically used corticosteroid. FASEB J. Off Publ. Fed. Am. Soc. Exp. Biol. *33*, 6402–6411.
15. Royce, S.G., Rele, S., Broughton, B.R.S., Kelly, K., and Samuel, C.S. (2017). Intranasal administration of mesenchymoangioblast-derived mesenchymal stem cells abrogates airway fibrosis and airway hyperresponsiveness associated with chronic allergic airways disease. FASEB J. *31*, 4168–4178.

16. Song, X., Xie, S., Lu, K., and Wang, C. (2015). Mesenchymal stem cells alleviate experimental asthma by inducing polarization of alveolar macrophages. Inflammation *38*, 485–492.

17. Zhong, H., Fan, X.L., Fang, S.B., Lin, Y.D., Wen, W., and Fu, Q.L. (2019). Human pluripotent stem cell-derived mesenchymal stem cells prevent chronic allergic airway inflammation via TGF-β1-Smad2/Smad3 signaling pathway in mice. Mol. Immunol. *109*, 51–57.

18. Abreu, S.C., Xisto, D.G., de Oliveira, T.B., Blanco, N.G., de Castro, L.L., Kitoko, J.Z., Olsen, P.C., Lopes-Pacheco, M., Morales, M.M., Weiss, D.J., and Rocco, P.R.M. (2019). Serum from asthmatic mice potentiates the therapeutic effects of mesenchymal stromal cells in experimental allergic asthma. Stem Cells Transl. Med. *8*, 301–312.

19. Abreu, S.C., Lopes-Pacheco, M., da Silva, A.L., Xisto, D.G., de Oliveira, T.B., Kitoko, J.Z., de Castro, L.L., Amorim, N.R., Martins, V., Silva, L.H.A., et al. (2018). Eicosapentaenoic acid enhances the effects of mesenchymal stromal cell therapy in experimental allergic asthma. Front. Immunol. *9*, 1147.

20. Braza, F., Dirou, S., Forest, V., Sauzeau, V., Hassoun, D., Chesné, J., Cheminant-Muller, M.A., Sagan, C., Magnan, A., and Lemarchand, P. (2016). Mesenchymal stem cells induce suppressive macrophages through phagocytosis in a mouse model of asthma. STEM CELLS *34*, 1836–1845.

21. Castro, L.L., Kitoko, J.Z., Xisto, D.G., Olsen, P.C., Guedes, H.L.M., Morales, M.M., Lopes-Pacheco, M., Cruz, F.F., and Rocco, P.R.M. (2020). Multiple doses of adipose tissue-derived mesenchymal stromal cells induce immunosuppression in experimental asthma. Stem Cells Transl. Med. *9*, 250–260.

22. Duong, K.M., Arikkatt, J., Ullah, M.A., Lynch, J.P., Zhang, V., Atkinson, K., Sly, P.D., and Phipps, S. (2015). Immunomodulation of airway epithelium cell activation by mesenchymal stromal cells ameliorates house dust mite-induced airway inflammation in mice. Am. J. Respir. Cell Mol. Biol. *53*, 615–624.

23. Kitoko, J.Z., de Castro, L.L., Nascimento, A.P., Abreu, S.C., Cruz, F.F., Arantes, A.C., Xisto, D.G., Martins, M.A., Morales, M.M., Rocco, P.R.M., and Olsen, P.C. (2018). Therapeutic administration of bone marrow-derived mesenchymal stromal cells reduces airway inflammation without up-regulating Tregs in experimental asthma. Clin. Exp. Allergy *48*, 205–216.

24. Shin, J.W., Ryu, S., Ham, J., Jung, K., Lee, S., Chung, D.H., Kang, H.R., and Kim, H.Y. (2021). Mesenchymal stem cells suppress severe asthma by directly regulating Th2 cells and type 2 innate lymphoid cells. Mol. Cells *44*, 580–590.

25. Cruz, F.F., Borg, Z.D., Goodwin, M., Sokocevic, D., Wagner, D.E., Coffey, A., Antunes, M., Robinson, K.L., Mitsialis, S.A., Kourembanas, S., et al. (2015). Systemic administration of human bone marrow-derived mesenchymal stromal cell extracellular vesicles ameliorates aspergillus hyphal extract-induced allergic airway inflammation in immunocompetent mice. Stem Cells Transl. Med. *4*, 1302–1316.

26. Lathrop, M.J., Brooks, E.M., Bonenfant, N.R., Sokocevic, D., Borg, Z.D., Goodwin, M., Loi, R., Cruz, F., Dunaway, C.W., Steele, C., and Weiss, D.J. (2014). Mesenchymal stromal cells mediate Aspergillus hyphal extract-induced allergic airway inflammation by inhibition of the Th17 signaling pathway. Stem Cells Transl. Med. *3*, 194–205.

27. Abreu, S.C., Antunes, M.A., Xisto, D.G., Cruz, F.F., Branco, V.C., Bandeira, E., Zola Kitoko, J., de Araújo, A.F., Dellatorre-Texeira, L., Olsen, P.C., et al. (2017). Bone marrow, adipose, and lung tissue-derived murine mesenchymal stromal cells release different mediators and differentially affect airway and lung parenchyma in experimental asthma. Stem Cells Transl. Med. *6*, 1557–1567.

28. Mariñas-Pardo, L., Mirones, I., Amor-Carro, Ó., Fraga-Iriso, R., Lema-Costa, B., Cubillo, I., Rodríguez Milla, M.Á., García-Castro, J., and Ramos-Barbón, D. (2014). Mesenchymal stem cells regulate airway contractile tissue remodeling in murine experimental asthma. Allergy *69*, 730–740.

29. Dunbar, H., Weiss, D.J., Rolandsson Enes, S., Laffey, J.G., and English, K. (2021). The inflammatory lung microenvironment; a key mediator in MSC licensing. Cells *10*, 2982.

30. Liu, J., Gao, J., Liang, Z., Gao, C., Niu, Q., Wu, F., and Zhang, L. (2022). Mesenchymal stem cells and their microenvironment. Stem Cell Res. Ther. *13*, 429.

31. Sudres, M., Norol, F., Trenado, A., Grégoire, S., Charlotte, F., Levacher, B., Lataillade, J.J., Bourin, P., Holy, X., Vernant, J.P., et al. (2006). Bone marrow mesenchymal stem cells suppress lymphocyte proliferation in vitro but fail to prevent graft-versus-host disease in mice. J. Immunol. 1950 *176*, 7761–7767.

32. Dorronsoro, A., Ferrin, I., Salcedo, J.M., Jakobsson, E., Fernández-Rueda, J., Lang, V., Sepulveda, P., Fechter, K., Pennington, D., and Trigueros, C. (2014). Human mesenchymal stromal cells modulate T-cell responses through TNF-α-mediated activation of NF-κB. Eur. J. Immunol. *44*, 480–488.

33. Tobin, L.M., Healy, M.E., English, K., and Mahon, B.P. (2013). Human mesenchymal stem cells suppress donor CD4(+) T cell proliferation and reduce pathology in a humanized mouse model of acute graft-versus-host disease. Clin. Exp. Immunol. *172*, 333–348.

34. Weiss, D.J., English, K., Krasnodembskaya, A., Isaza-Correa, J.M., Hawthorne, I.J., and Mahon, B.P. (2019). The necrobiology of mesenchymal stromal cells affects therapeutic efficacy. Front. Immunol. *10*, 1228.

35. Islam, D., Huang, Y., Fanelli, V., Delsedime, L., Wu, S., Khang, J., Han, B., Grassi, A., Li, M., Xu, Y., et al. (2019). Identification and modulation of microenvironment is crucial for effective mesenchymal stromal cell therapy in acute lung injury. Am. J. Respir. Crit. Care Med. *199*, 1214–1224.

36. Ankrum, J.A., Ong, J.F., and Karp, J.M. (2014). Mesenchymal stem cells: immune evasive, not immune privileged. Nat. Biotechnol. *32*, 252–260.

37. Mathew, S.A., Chandravanshi, B., and Bhonde, R. (2017). Hypoxia primed placental mesenchymal stem cells for wound healing. Life Sci. *182*, 85–92.

38. Roemeling-van Rhijn, M., Mensah, F.K.F., Korevaar, S.S., Leijs, M.J., van Osch, G.J.V.M., Ijzermans, J.N.M., Betjes, M.G.H., Baan, C.C., Weimar, W., and Hoogduijn, M.J. (2013). Effects of hypoxia on the immunomodulatory properties of adipose tissue-derived mesenchymal stem cells. Front. Immunol. *4*, 203.

39. Carty, F., Dunbar, H., Hawthorne, I.J., Ting, A.E., Stubblefield, S.R., Van't Hof, W., and English, K. (2021). IFN-γ and PPARδ influence the efficacy and retention of multipotent adult progenitor cells in graft vs host disease. Stem Cells Transl. Med. *10*, 1561–1574.

40. Corbett, J.M., Hawthorne, I., Dunbar, H., Coulter, I., Chonghaile, M.N., Flynn, C.M., and English, K. (2021). Cyclosporine A and IFNγ licencing enhances human mesenchymal stromal cell potency in a humanised mouse model of acute graft versus host disease. Stem Cell Res. Ther. *12*, 238.

41. Silva, J.D., Lopes-Pacheco, M., de Castro, L.L., Kitoko, J.Z., Trivelin, S.A., Amorim, N.R., Capelozzi, V.L., Morales, M.M., Gutfilen, B., de Souza, S.A.L., et al. (2019). Eicosapentaenoic acid potentiates the therapeutic effects of adipose tissue-derived mesenchymal stromal cells on lung and distal organ injury in experimental sepsis. Stem Cell Res. Ther. *10*, 264.

42. Bustos, M.L., Huleihel, L., Meyer, E.M., Donnenberg, A.D., Donnenberg, V.S., Sciurba, J.D., Mroz, L., McVerry, B.J., Ellis, B.M., Kaminski, N., and Rojas, M. (2013). Activation of human mesenchymal stem cells impacts their therapeutic abilities in lung injury by increasing interleukin (IL)-10 and IL-1RN levels. Stem Cells Transl. Med. *2*, 884–895.

43. Rolandsson Enes, S., Hampton, T.H., Barua, J., McKenna, D.H., Dos Santos, C.C., Amiel, E., Ashare, A., Liu, K.D., Krasnodembskaya, A.D., English, K., et al. (2021). Healthy versus inflamed lung environments differentially affect mesenchymal stromal cells. Eur. Respir. J. *58*, 2004149.

44. Abreu, S.C., Hampton, T.H., Hoffman, E., Dearborn, J., Ashare, A., Singh Sidhu, K., Matthews, D.E., McKenna, D.H., Amiel, E., Barua, J., et al. (2020). Differential effects of the cystic fibrosis lung inflammatory environment on mesenchymal stromal cells. Am. J. Physiol-lung Cell Mol Physiol. 2020 ajplung.00218.

45. Bacher, M., Metz, C.N., Calandra, T., Mayer, K., Chesney, J., Lohoff, M., Gemsa, D., Donnelly, T., and Bucala, R. (1996). An essential regulatory role for macrophage migration inhibitory factor in T-cell activation. Proc. Natl. Acad. Sci. USA *93*, 7849–7854.

46. Calandra, T., Bernhagen, J., Metz, C.N., Spiegel, L.A., Bacher, M., Donnelly, T., Cerami, A., and Bucala, R. (1995). MIF as a glucocorticoid-induced modulator of cytokine production. Nature *377*, 68–71.

47. Calandra, T., Bernhagen, J., Mitchell, R.A., and Bucala, R. (1994). The macrophage is an important and previously unrecognized source of macrophage migration inhibitory factor. J. Exp. Med. *179*, 1895–1902.

48. Donnelly, S.C., Haslett, C., Reid, P.T., Grant, I.S., Wallace, W.A., Metz, C.N., Bruce, L.J., and Bucala, R. (1997). Regulatory role for macrophage migration inhibitory factor in acute respiratory distress syndrome. Nat. Med. *3*, 320–323.

49. Das, R., Moss, J.E., Robinson, E., Roberts, S., Levy, R., Mizue, Y., Leng, L., McDonald, C., Tigelaar, R.E., Herrick, C.A., and Bucala, R. (2011). Role of macrophage migration inhibitory factor in the Th2 immune response to epicutaneous sensitization. J. Clin. Immunol. *31*, 666–680.

50. Li, R., Wang, F., Wei, J., Lin, Y., Tang, G., Rao, L., Ma, L., Xu, Q., Wu, J., Lv, Q., et al. (2021). The role of macrophage migration inhibitory factor (MIF) in asthmatic airway remodeling. Allergy Asthma Immunol. Res. *13*, 88–105.

51. Magalhães, E.S., Mourao-Sa, D.S., Vieira-de-Abreu, A., Figueiredo, R.T., Pires, A.L., Farias-Filho, F.A., Fonseca, B.P.F., Viola, J.P.B., Metz, C., Martins, M.A., et al. (2007). Macrophage migration inhibitory factor is essential for allergic asthma but not for Th2 differentiation. Eur. J. Immunol. *37*, 1097–1106.

52. Mizue, Y., Ghani, S., Leng, L., McDonald, C., Kong, P., Baugh, J., Lane, S.J., Craft, J., Nishihira, J., Donnelly, S.C., et al. (2005). Role for macrophage migration inhibitory factor in asthma. Proc. Natl. Acad. Sci. USA *102*, 14410–14415.

53. Allam, V.S.R.R., Pavlidis, S., Liu, G., Kermani, N.Z., Simpson, J., To, J., Donnelly, S., Guo, Y.K., Hansbro, P.M., Phipps, S., et al. (2022). Macrophage migration inhibitory factor promotes glucocorticoid resistance of neutrophilic inflammation in a murine model of severe asthma. Thorax *78*, 661–673. thoraxjnl-2021-218555.

54. Amano, T., Nishihira, J., and Miki, I. (2007). Blockade of macrophage migration inhibitory factor (MIF) prevents the antigen-induced response in a murine model of allergic airway inflammation. Inflamm. Res. *56*, 24–31.

55. Kobayashi, M., Nasuhara, Y., Kamachi, A., Tanino, Y., Betsuyaku, T., Yamaguchi, E., Nishihira, J., and Nishimura, M. (2006). Role of macrophage migration inhibitory factor in ovalbumin-induced airway inflammation in rats. Eur. Respir. J. *27*, 726–734.

56. Chen, P.F., Luo, Y.l., Wang, W., Wang, J.x., Lai, W.y., Hu, S.m., Cheng, K.F., and Al-Abed, Y. (2010). ISO-1, a macrophage migration inhibitory factor antagonist, inhibits airway remodeling in a murine model of chronic asthma. Mol. Med. *16*, 400–408.

57. Awandare, G.A., Martinson, J.J., Were, T., Ouma, C., Davenport, G.C., Ong'echa, J.M., Wang, W., Leng, L., Ferrell, R.E., Bucala, R., and Perkins, D.J. (2009). Macrophage migration inhibitory factor (MIF) promoter polymorphisms and susceptibility to severe malarial anemia. J. Infect. Dis. *200*, 629–637.

58. Savva, A., Brouwer, M.C., Roger, T., Valls Serón, M., Le Roy, D., Ferwerda, B., van der Ende, A., Bochud, P.Y., van de Beek, D., and Calandra, T. (2016). Functional polymorphisms of macrophage migration inhibitory factor as predictors of morbidity and mortality of pneumococcal meningitis. Proc. Natl. Acad. Sci. *113*, 3597–3602.

59. Benedek, G., Meza-Romero, R., Jordan, K., Zhang, Y., Nguyen, H., Kent, G., Li, J., Siu, E., Frazer, J., Piecychna, M., et al. (2017). MIF and D-DT are potential disease severity modifiers in male MS subjects. Proc. Natl. Acad. Sci. USA *114*, E8421–E8429.

60. Liu, A., Bao, F., and Voravuthikunchai, S.P. (2018). CATT polymorphism in MIF gene promoter is closely related to human pulmonary tuberculosis in a southwestern China population. Int. J. Immunopathol. Pharmacol. *32*, 205873841877710.

61. Shin, J.J., Fan, W., Par-Young, J., Piecychna, M., Leng, L., Israni-Winger, K., Qing, H., Gu, J., Zhao, H., Schulz, W.L., et al. (2022). MIF is a common genetic determinant of COVID-19 symptomatic infection and severity. QJM Mon J. Assoc. Physicians, hcac234.

62. Dunbar, H., Hawthorne, I.J., Tunstead, C., Armstrong, M.E., Donnelly, S.C., and English, K. (2023). Blockade of MIF biological activity ameliorates house dust mite-induced allergic airway inflammation in humanised MIF mice. FASEB J. *37*, e23072.

63. Lourenco, S., Teixeira, V.H., Kalber, T., Jose, R.J., Floto, R.A., and Janes, S.M. (2015). Macrophage Migration Inhibitory Factor - CXCR4 is the dominant chemotactic axis in human mesenchymal stem cell recruitment to tumors. J. Immunol. 1950 *194*, 3463–3474.

64. English, K. (2013). Mechanisms of mesenchymal stromal cell immunomodulation. Immunol. Cell Biol. *91*, 19–26.

65. Chinnadurai, R., Rajan, D., Ng, S., McCullough, K., Arafat, D., Waller, E.K., Anderson, L.J., Gibson, G., and Galipeau, J. (2017). Immune dysfunctionality of replicative senescent mesenchymal stromal cells is corrected by IFNγ priming. Blood Adv. *1*, 628–643.

66. Chinnadurai, R., Copland, I.B., Garcia, M.A., Petersen, C.T., Lewis, C.N., Waller, E.K., Kirk, A.D., and Galipeau, J. (2016). Cryopreserved mesenchymal stromal cells are susceptible to T-cell mediated apoptosis which is partly rescued by IFNγ licensing. Stem Cells *34*, 2429–2442.

67. Chinnadurai, R., Bates, P.D., Kunugi, K.A., Nickel, K.P., DeWerd, L.A., Capitini, C.M., Galipeau, J., and Kimple, R.J. (2021). Dichotomic potency of IFNγ licensed allogeneic mesenchymal stromal cells in animal models of acute radiation syndrome and graft versus host disease. Front. Immunol. 12. https://www.frontiersin.org/articles/10.3389/fimmu.2021.708950.

68. English, K., Barry, F.P., Field-Corbett, C.P., and Mahon, B.P. (2007). IFN-γ and TNF-α differentially regulate immunomodulation by murine mesenchymal stem cells. Immunol. Lett. *110*, 91–100.

69. Murphy, N., Treacy, O., Lynch, K., Morcos, M., Lohan, P., Howard, L., Fahy, G., Griffin, M.D., Ryan, A.E., and Ritter, T. (2019). TNF-α/IL-1β-licensed mesenchymal stromal cells promote corneal allograft survival via myeloid cell-mediated induction of Foxp3+ regulatory T cells in the lung. FASEB J. Off Publ. Fed. Am. Soc. Exp. Biol. *33*, 9404–9421.

70. Gomes, A.O., Barbosa, B.F., Franco, P.S., Ribeiro, M., Silva, R.J., Gois, P.S.G., Almeida, K.C., Angeloni, M.B., Castro, A.S., Guirelli, P.M., et al. (2018). Macrophage migration inhibitory factor (MIF) prevents maternal death, but contributes to poor fetal outcome during congenital toxoplasmosis. Front. Microbiol. *9*, 906.

71. Carli, C., Metz, C.N., Al-Abed, Y., Naccache, P.H., and Akoum, A. (2009). Up-regulation of cyclooxygenase-2 expression and prostaglandin E2 production in human endometriotic cells by macrophage migration inhibitory factor: involvement of novel kinase signaling pathways. Endocrinology *150*, 3128–3137.

72. Mitchell, R.A., Liao, H., Chesney, J., Fingerle-Rowson, G., Baugh, J., David, J., and Bucala, R. (2002). Macrophage migration inhibitory factor (MIF) sustains macrophage proinflammatory function by inhibiting p53: regulatory role in the innate immune response. Proc. Natl. Acad. Sci. USA *99*, 345–350.

73. Li, D., Han, Y., Zhuang, Y., Fu, J., Liu, H., Shi, Q., and Ju, X. (2015). Overexpression of COX-2 but not indoleamine 2,3-dioxygenase-1 enhances the immunosuppressive ability of human umbilical cord-derived mesenchymal stem cells. Int. J. Mol. Med. *35*, 1309–1316.

74. Guan, Q., Ezzati, P., Spicer, V., Krokhin, O., Wall, D., and Wilkins, J.A. (2017). Interferon γ induced compositional changes in human bone marrow derived mesenchymal stem/stromal cells. Clin. Proteomics *14*, 26.

75. Lan, H., Wang, N., Chen, Y., Wang, X., Gong, Y., Qi, X., Luo, Y., and Yao, F. (2018). Macrophage migration inhibitory factor (MIF) promotes rat airway muscle cell proliferation and migration mediated by ERK1/2 and FAK signaling. Cell Biol. Int. *42*, 75–83.

76. Ohta, S., Misawa, A., Fukaya, R., Inoue, S., Kanemura, Y., Okano, H., Kawakami, Y., and Toda, M. (2012). Macrophage migration inhibitory factor (MIF) promotes cell survival and proliferation of neural stem/progenitor cells. J. Cell Sci. *125* (Pt 13), 3210–3220.

77. Utispan, K., and Koontongkaew, S. (2021). Macrophage migration inhibitory factor modulates proliferation, cell cycle, and apoptotic activity in head and neck cancer cell lines. J. Dent. Sci. *16*, 342–348.

78. Kulesza, A., Paczek, L., and Burdzinska, A. (2023). The Role of COX-2 and PGE2 in the Regulation of Immunomodulation and Other Functions of Mesenchymal Stromal Cells. Biomedicines *11*, 445.

79. Lin, Y.D., Fan, X.L., Zhang, H., Fang, S.B., Li, C.L., Deng, M.X., Qin, Z.L., Peng, Y.Q., Zhang, H.Y., and Fu, Q.L. (2018). The genes involved in asthma with the treatment of human embryonic stem cell-derived mesenchymal stem cells. Mol. Immunol. *95*, 47–55.

80. Fallon, P.G., and Schwartz, C. (2020). The high and lows of type 2 asthma and mouse models. J. Allergy Clin. Immunol. *145*, 496–498.

81. Hass, R., Kasper, C., Böhm, S., and Jacobs, R. (2011). Different populations and sources of human mesenchymal stem cells (MSC): A comparison of adult and neonatal tissue-derived MSC. Cell Commun. Signal. *9*, 12.

82. Carty, F., Corbett, J.M., Cunha, J.P.M.C.M., Reading, J.L., Tree, T.I.M., Ting, A.E., Stubblefield, S.R., and English, K. (2018). Multipotent adult progenitor cells suppress T Cell activation in in vivo models of homeostatic proliferation in a prostaglandin E2-dependent manner. Front. Immunol. *9*, 645.

83. de Witte, S.F.H., Merino, A.M., Franquesa, M., Strini, T., van Zoggel, J.A.A., Korevaar, S.S., Luk, F., Gargesha, M., O'Flynn, L., Roy, D., et al. (2017). Cytokine treatment optimises the immunotherapeutic effects of umbilical cord-derived MSC for treatment of inflammatory liver disease. Stem Cell Res. Ther. *8*, 140.

84. Baugh, J.A., Chitnis, S., Donnelly, S.C., Monteiro, J., Lin, X., Plant, B.J., Wolfe, F., Gregersen, P.K., and Bucala, R. (2002). A functional promoter polymorphism in the macrophage migration inhibitory factor (MIF) gene associated with disease severity in rheumatoid arthritis. Genes Immun. *3*, 170–176.

85. Renner, P., Roger, T., and Calandra, T. (2005). Macrophage migration inhibitory factor: gene polymorphisms and susceptibility to inflammatory diseases. Clin. Infect. Dis. *41*, S513–S519.

86. Plant, B.J., Gallagher, C.G., Bucala, R., Baugh, J.A., Chappell, S., Morgan, L., O'Connor, C.M., Morgan, K., and Donnelly, S.C. (2005). Cystic fibrosis, disease severity, and a macrophage migration inhibitory factor polymorphism. Am. J. Respir. Crit. Care Med. *172*, 1412–1415.

87. Kim, R.L., Bang, J.Y., Kim, J., Mo, Y., Kim, Y., Lee, C.G., Elias, J.A., Kim, H.Y., and Kang, H.R. (2022). Mesenchymal stem cells exert their anti-asthmatic effects through macrophage modulation in a murine chronic asthma model. Sci. Rep. *12*, 9811.

88. Kabat, M., Bobkov, I., Kumar, S., and Grumet, M. (2019). Trends in mesenchymal stem cell clinical trials 2004-2018: Is efficacy optimal in a narrow dose range? Stem Cells Transl. Med. *9*, 17–27.

89. Malaquias, M.a.S., Oyama, L.A., Jericó, P.C., Costa, I., Padilha, G., Nagashima, S., Lopes-Pacheco, M., Rebelatto, C.L.K., Michelotto, P.V., Xisto, D.G., et al. (2018). Effects of mesenchymal stromal cells play a role the oxidant/antioxidant balance in a murine model of asthma. Allergol. Immunopathol. *46*, 136–143.

90. Kwak, J., Choi, S.J., Oh, W., Yang, Y.S., Jeon, H.B., and Jeon, E.S. (2018). Cobalt chloride enhances the anti-inflammatory potency of human umbilical cord blood-derived mesenchymal stem cells through the ERK-HIF-1α-microRNA-146a-mediated signaling pathway. Stem Cells Int. *2018*, 4978763.

91. Hong, G.H., Kwon, H.S., Lee, K.Y., Ha, E.H., Moon, K.A., Kim, S.W., Oh, W., Kim, T.B., Moon, H.B., and Cho, Y.S. (2017). hMSCs suppress neutrophil-dominant airway inflammation in a murine model of asthma. Exp. Mol. Med. *49*, e288.

92. Cruz, F.F., Borg, Z.D., Goodwin, M., Coffey, A.L., Wagner, D.E., Rocco, P.R.M., and Weiss, D.J. (2016). CD11b+ and Sca-1+ cells exert the main beneficial effects of systemically administered bone marrow-derived mononuclear cells in a murine model of mixed Th2/Th17 allergic airway inflammation. Stem Cells Transl. Med. *5*, 488–499.

93. Zhilai, Z., Biling, M., Sujun, Q., Chao, D., Benchao, S., Shuai, H., Shun, Y., and Hui, Z. (2016). Preconditioning in lowered oxygen enhances the therapeutic potential of human umbilical mesenchymal stem cells in a rat model of spinal cord injury. Brain Res. *1642*, 426–435.

94. Armitage, J., Tan, D.B.A., Troedson, R., Young, P., Lam, K.V., Shaw, K., Sturm, M., Weiss, D.J., and Moodley, Y.P. (2018). Mesenchymal stromal cell infusion modulates systemic immunological responses in stable COPD patients: a phase I pilot study. Eur. Respir. J. *51*, 1702369.

95. Gholamrezanezhad, A., Mirpour, S., Bagheri, M., Mohamadnejad, M., Alimoghaddam, K., Abdolahzadeh, L., Saghari, M., and Malekzadeh, R. (2011). In vivo tracking of 111In-oxine labeled mesenchymal stem cells following infusion in patients with advanced cirrhosis. Nucl. Med. Biol. *38*, 961–967.

96. Sokal, E.M., Lombard, C.A., Roelants, V., Najimi, M., Varma, S., Sargiacomo, C., Ravau, J., Mazza, G., Jamar, F., Versavau, J., et al. (2017). Biodistribution of liver-derived mesenchymal stem cells after peripheral injection in a hemophilia A patient. Transplantation *101*, 1845–1851.

97. Koç, O.N., Gerson, S.L., Cooper, B.W., Dyhouse, S.M., Haynesworth, S.E., Caplan, A.I., and Lazarus, H.M. (2000). Rapid hematopoietic recovery after coinfusion of autologous-blood stem cells and culture-expanded marrow mesenchymal stem cells in advanced breast cancer patients receiving high-dose chemotherapy. J. Clin. Oncol. *18*, 307–316.

98. Sanchez-Diaz, M., Quiñones-Vico, M.I., Sanabria de la Torre, R., Montero-Vílchez, T., Sierra-Sánchez, A., Molina-Leyva, A., and Arias-Santiago, S. (2021). Biodistribution of mesenchymal stromal cells after administration in animal models and humans: a systematic review. J. Clin. Med. *10*, 2925.

99. Kang, I., and Bucala, R. (2019). The immunobiology of MIF: function, genetics and prospects for precision medicine. Nat. Rev. Rheumatol. *15*, 427–437.

100. Farr, L., Ghosh, S., and Moonah, S. (2020). Role of MIF cytokine/CD74 receptor pathway in protecting against injury and promoting repair. Front. Immunol. *11*, 1273.

101. Bucala, R., and Shachar, I. (2014). The integral role of CD74 in antigen presentation, MIF signal transduction, and B cell survival and homeostasis. Mini Rev. Med. Chem. *14*, 1132–1138.

102. Imaoka, M., Tanese, K., Masugi, Y., Hayashi, M., and Sakamoto, M. (2019). Macrophage migration inhibitory factor-CD74 interaction regulates the expression of programmed cell death ligand 1 in melanoma cells. Cancer Sci. *110*, 2273–2283.

103. Klasen, C., Ziehm, T., Huber, M., Asare, Y., Kapurniotu, A., Shachar, I., Bernhagen, J., and El Bounkari, O. (2018). LPS-mediated cell surface expression of CD74 promotes the proliferation of B cells in response to MIF. Cell. Signal. *46*, 32–42.

104. Soppert, J., Kraemer, S., Beckers, C., Averdunk, L., Möllmann, J., Denecke, B., Goetzenich, A., Marx, G., Bernhagen, J., and Stoppe, C. (2018). Soluble CD74 reroutes MIF/CXCR4/AKT-mediated survival of cardiac myofibroblasts to necroptosis. J. Am. Heart Assoc. *7*, e009384.

105. Flaster, H., Bernhagen, J., Calandra, T., and Bucala, R. (2007). The macrophage migration inhibitory factor-glucocorticoid dyad: regulation of inflammation and immunity. Mol. Endocrinol. *21*, 1267–1280.

106. Sampey, A.V., Hall, P.H., Mitchell, R.A., Metz, C.N., and Morand, E.F. (2001). Regulation of synoviocyte phospholipase A2 and cyclooxygenase 2 by macrophage migration inhibitory factor. Arthritis Rheum. *44*, 1273–1280.

107. Duffy, M.M., Pindjakova, J., Hanley, S.A., McCarthy, C., Weidhofer, G.A., Sweeney, E.M., English, K., Shaw, G., Murphy, J.M., Barry, F.P., et al. (2011). Mesenchymal stem cell inhibition of T-helper 17 cell- differentiation is triggered by cell–cell contact and mediated by prostaglandin E2 via the EP4 receptor. Eur. J. Immunol. *41*, 2840–2851.

108. Cahill, E.F., Kennelly, H., Carty, F., Mahon, B.P., and English, K. (2016). Hepatocyte growth factor is required for mesenchymal stromal cell protection against bleomycin-induced pulmonary fibrosis. Stem Cells Transl. Med. *5*, 1307–1318.

109. Sun, L., Chen, K., Jiang, Z., Chen, X., Ma, J., Ma, Q., and Duan, W. (2018). Indometacin inhibits the proliferation and activation of human pancreatic stellate cells through the downregulation of COX-2. Oncol. Rep. *39*, 2243–2251.

110. Zhu, W., Sun, L., Zhao, P., Liu, Y., Zhang, J., Zhang, Y., Hong, Y., Zhu, Y., Lu, Y., Zhao, W., et al. (2021). Macrophage migration inhibitory factor facilitates the therapeutic efficacy of mesenchymal stem cells derived exosomes in acute myocardial infarction through upregulating miR-133a-3p. J. Nanobiotechnology *19*, 61.

111. Liu, X., Li, X., Zhu, W., Zhang, Y., Hong, Y., Liang, X., Fan, B., Zhao, H., He, H., and Zhang, F. (2020). Exosomes from mesenchymal stem cells overexpressing MIF enhance myocardial repair. J. Cell. Physiol. *235*, 8010–8022.

112. Zhang, Y., Zhu, W., He, H., Fan, B., Deng, R., Hong, Y., Liang, X., Zhao, H., Li, X., and Zhang, F. (2019). Macrophage migration inhibitory factor rejuvenates aged human mesenchymal stem cells and improves myocardial repair. Aging *11*, 12641–12660.

113. Zhang, Y., Zhou, Y., Chen, S., Hu, Y., Zhu, Z., Wang, Y., Du, N., Song, T., Yang, Y., Guo, A., and Wang, Y. (2019). Macrophage migration inhibitory factor facilitates prostaglandin E2 production of astrocytes to tune inflammatory milieu following spinal cord injury. J. Neuroinflammation *16*, 85.

114. Fingerle-Rowson, G., Petrenko, O., Metz, C.N., Forsthuber, T.G., Mitchell, R., Huss, R., Moll, U., Müller, W., and Bucala, R. (2003). The p53-dependent effects of macrophage migration inhibitory factor revealed by gene targeting. Proc. Natl. Acad. Sci. USA *100*, 9354–9359.

115. Cahill, E.F., Tobin, L.M., Carty, F., Mahon, B.P., and English, K. (2015). Jagged-1 is required for the expansion of CD4+ CD25+ FoxP3+ regulatory T cells and tolerogenic dendritic cells by murine mesenchymal stromal cells. Stem Cell Res. Ther. *6*, 19.

116. Ehrentraut, H., Clambey, E.T., McNamee, E.N., Brodsky, K.S., Ehrentraut, S.F., Poth, J.M., Riegel, A.K., Westrich, J.A., Colgan, S.P., and Eltzschig, H.K. (2013). CD73+ regulatory T cells contribute to adenosine-mediated resolution of acute lung injury. FASEB J. Off Publ. Fed. Am. Soc. Exp. Biol. *27*, 2207–2219.

Cytotherapy 000 (2024) 1–7

7.6

Contents lists available at ScienceDirect

CYTOTHERAPY

journal homepage: www.isct-cytotherapy.org

International Society ISCT Cell & Gene Therapy®

Short Report

Mesenchymal stromal cells dampen trained immunity in house dust mite-primed macrophages expressing human macrophage migration inhibitory factor polymorphism

Hazel Dunbar[1,2], Ian J. Hawthorne[1,2], Courteney Tunstead[1,2], Eóin N. McNamee[1,2], Daniel J. Weiss[3], Michelle E. Armstrong[4], Seamas C. Donnelly[4], Karen English[1,2,*]

[1] *Department of Biology, Maynooth University, Maynooth, Ireland*
[2] *Kathleen Lonsdale Institute for Human Health Research, Maynooth University, Maynooth, Ireland*
[3] *Department of Medicine, Larner College of Medicine, University of Vermont, Burlington, Vermont, USA*
[4] *Department of Medicine, Trinity College Dublin and Tallaght University Hospital, Dublin, Ireland*

ARTICLE INFO

Article History:
Received 7 February 2024
Accepted 8 May 2024
Available online xxx

Key Words:
bone marrow-derived macrophages
house dust mite
innate training
macrophage migration inhibitory factor
mesenchymal stromal cells
polarization

ABSTRACT

Background: Trained immunity results in long-term immunological memory, provoking a faster and greater immune response when innate immune cells encounter a secondary, often heterologous, stimulus. We have previously shown that house dust mite (HDM)-induced innate training is amplified in mice expressing the human macrophage migration inhibitory factor (MIF) $CATT_7$ functional polymorphism.
Aim: This study investigated the ability of mesenchymal stromal cells (MSCs) to modulate MIF-driven trained immunity both *in vitro* and *in vivo*.
Methods: Compared with wild-type mice, *in vivo* HDM-primed bone marrow-derived macrophages (BMDMs) from $CATT_7$ mice expressed significantly higher levels of M1-associated genes following lipopolysaccharide stimulation *ex vivo*. Co-cultures of $CATT_7$ BMDMs with MSCs suppressed this HDM-primed effect, with tumor necrosis factor alpha (TNF-α) being significantly decreased in a cyclooxygenase 2 (COX-2)-dependent manner. Interestingly, interleukin 6 (IL-6) was suppressed by MSCs independently of COX-2. In an *in vitro* training assay, MSCs significantly abrogated the enhanced production of pro-inflammatory cytokines by HDM-trained $CATT_7$ BMDMs when co-cultured at the time of HDM stimulus on day 0, displaying their therapeutic efficacy in modulating an overzealous human MIF-dependent immune response. Utilizing an *in vivo* model of HDM-induced trained immunity, MSCs administered systemically on day 10 and day 11 suppressed this trained phenomenon by significantly reducing TNF-α and reducing IL-6 and C-C motif chemokine ligand 17 (CCL17) production.
Conclusions: This novel study elucidates how MSCs can attenuate an MIF-driven, HDM-trained response in $CATT_7$ mice in a model of allergic airway inflammation.

Introduction

The concept of innate immune memory has developed significantly over the past decade. Innate immune cells, including macrophages, can undergo a process called trained immunity, whereby various stimuli, including pathogenic agents such as β-glucan, can alter the cells to produce increased levels of pro-inflammatory cytokines in response to subsequent stimuli. This trained immunity is associated with a rest period between the initial and secondary heterologous stimulus, inducing epigenetic remodeling [1]. Although trained immunity can boost the immune system and provide non-specific protection against pathogens, it can also be maladaptive, contributing to a hyper-inflammatory state, leading to autoimmunity and chronic inflammatory disease [2].

To investigate the pathophysiology of allergic asthma, pre-clinical models involving repetitive intranasal administration of the clinically relevant aeroallergen house dust mite (HDM) are commonly used, as these models reproduce many aspects of human allergic asthma, such as eosinophil infiltration and goblet cell hyperplasia [3–6]. The capacity for HDM to induce trained immunity in mouse and human macrophages was recently identified, in which macrophages from HDM-allergic mice and HDM-allergic asthma patients displayed a significantly elevated pro-inflammatory phenotype with epigenetic changes [3,7–9].

* Correspondence: Karen English, PhD, Kathleen Lonsdale Institute for Human Health Research, Maynooth University, Maynooth, Ireland.
E-mail address: karen.english@mu.ie (K. English).

https://doi.org/10.1016/j.jcyt.2024.05.010

The pro-inflammatory cytokine macrophage migration inhibitory factor (MIF) is associated with a range of inflammatory diseases, including sepsis, autoimmune disease and severe asthma [10–12]. The MIF $CATT_7$ allele correlates with high MIF expression [4,13]. We have demonstrated exacerbated HDM-induced airway inflammation in mice expressing the human MIF $CATT_7$ allele [4,6]. Recently, using *in vitro* assays and an *in vivo* model of trained immunity, we identified a novel role for the high-expression MIF $CATT_7$ allele in significantly enhancing HDM-induced trained immunity in mouse bone marrow-derived macrophages (BMDMs) [5].

Mesenchymal stromal cells (MSCs) have demonstrated therapeutic efficacy in inflammatory diseases, such as in an HDM-induced model of allergic airway inflammation, in which we demonstrated that MSCs significantly attenuated airway inflammation, cellular infiltration and cytokine production in a cyclooxygenase 2 (COX-2)-dependent manner [6]. MSC therapeutic efficacy requires the presence of macrophages [14,15], in which complex bi-directional cross-talk between these cell populations can determine the inflammatory fate of their resident microenvironment. MSCs can modulate macrophages through active (secretion of TSG-6 and prostaglandin E2) and passive (being phagocytosed, secreting microRNA containing exosomes and mitochondrial transfer) means [16,17]. Moreover, MSCs are primarily known to polarize macrophages to an M2 (anti-inflammatory) phenotype [18–24], which in turn triggers macrophages to secrete mediators that can act to activate MSCs and further boost their immunomodulatory efficacy [16]. Conversely, there is also evidence that MSCs can polarize macrophages to an M1 phenotype [25,26]. However, to date we have not investigated the impact of MSCs on macrophages in high MIF-expressing $CATT_7$ mice challenged with HDM.

This novel research describes the immunosuppressive capacity of human MSCs to block MIF-enhanced M1 priming in macrophages from HDM-challenged mice in a COX-2 partially dependent manner. Importantly, we show for the first time that MSCs can dampen HDM-induced trained immunity *in vitro* and *in vivo*.

Methods

Ethical approval and Health Products Regulatory Authority compliance

Ethical approval for all work was granted by the ethics committee of Maynooth University (BRESC-2018-13). Project Authorization was received from the Health Products Regulatory Authority (AE19124/P022), whereby the terms of the animal experiments within this project were outlined and adhered to.

Pre-clinical model of acute allergic airway inflammation

Human MIF-expressing $CATT_7$ mice and wild-type (WT) littermate controls were challenged with 25 μg of HDM intranasally as previously described [4,6].

Generation of L929-conditioned medium (macrophage colony-stimulating factor)

L929 cells were cultured in Roswell Park Memorial Institute (RPMI) 1640 medium with GlutaMAX (Thermo Fisher Scientific, Paisley, UK) supplemented with 10% heat-inactivated fetal bovine serum (Biosera, Cholet, France) and 10% penicillin/streptomycin (Sigma-Aldrich, Arklow, Wicklow, Ireland) (referred to as cRPMI) and incubated at 37°C in 5% carbon dioxide/20% oxygen for 7 days. Supernatant was collected, centrifuged and passed through a 0.2-μm filter and aliquoted and stored at −80°C. L929-conditioned medium will be referred to as macrophage colony-stimulating factor (M-CSF) throughout the article.

In vitro *innate priming assay (BMDMs)*

After HDM challenge *in vivo*, bone marrow was isolated from $CATT_7$ and WT mice 4 h after last challenge. A total of 1.5×10^6 bone marrow cells were seeded in cRPMI supplemented with 20% M-CSF in tissue culture grade six-well plates. Medium was changed on day 3 and day 6 to remove non-adherent cells. On day 7, differentiated BMDMs were stimulated for 24 h with lipopolysaccharide (LPS) (from *Escherichia coli* O111:B4) (100 ng/mL) (Sigma-Aldrich, Arklow, Wicklow, Ireland) to drive M1 polarization or murine interleukin (IL) 4 (10 ng/mL) (R&D Systems, Abingdon, UK) to drive M2 polarization. Cells and supernatants were harvested and stored at −20°C for RNA and protein analysis.

In vitro *innate training assay (hematopoietic stem and progenitor cells)*

Naive $CATT_7$ or WT bone marrow was isolated from femurs and tibiae and centrifuged at 300 × g for 5 min. Whole bone marrow containing hematopoietic stem and progenitor cells (HSPCs) was seeded at 1.5×10^6 cells per well in six-well non-tissue culture grade plates. After stimulating with 10 μg of HDM for 24 h, HDM was washed out. Cells were cultured in 20% M-CSF-supplemented cRPMI until day 6, when medium was changed to non-supplemented cRPMI to facilitate a rest period. Differentiated macrophages were stimulated with 100 ng/mL of LPS on day 10 for 24 h. Supernatants were harvested for enzyme-linked immunosorbent assay (ELISA).

Human bone marrow-MSC co-culture

Human bone marrow-MSCs (hBM-MSCs) (RoosterBio, Frederick, MD, USA) were expanded as previously described [6]. Afterward, MSCs were cultured and maintained in low-glucose Dulbecco's Modified Eagle's Medium (Sigma-Aldrich, Arklow, Wicklow, Ireland) supplemented with 10% (v/v) fetal bovine serum and 1% (v/v) penicillin/streptomycin. For mechanistic experiments, MSCs (passage two to four) were incubated with 10 μM NS-398 (Sigma-Aldrich, Arklow, Wicklow, Ireland) or vehicle control for 24 h before being washed and seeded in 0.4-μM transwell inserts (Corning, Corning, NY, USA) and co-cultured with HSPCs from day 0 to day 6 for innate training assays or on day 7 for 24 h for priming assays.

In vivo *innate training assay*

$CATT_7$ and WT mice were challenged with 25 μg of the HDM allergen *Dermatophagoides pteronyssinus* (Greer Laboratories, Lenoir, NC, USA) on day 0, day 8, day 9, day 10 and day 11. A total of 5×10^5 hBM-MSCs were administered intravenously on day 10 and day 11. On day 18, bone marrow was isolated and BMDMs generated. Cells were stimulated with LPS (100 ng/mL) for 24 h on day 7.

Cytokine quantification by ELISA

BMDM supernatants were analyzed for murine TNF-α, IL-6 and IL-1β (BioLegend, San Diego, CA, USA) as well as C-C motif chemokine ligand 17 (CCL17) (R&D Systems, Abingdon, UK) by ELISA. The absorbance (optical density) of the samples and standards was measured at 450 nm for all ELISAs using a microplate reader (CLARIOstar Plus; BMG Labtech, Bucks, UK).

Analysis of gene expression

Total RNA was extracted using TRIzol (Thermo Fisher Scientific, Cambridgeshire, UK). RNA concentrations were equalized to 100 ng/μL. Complementary DNA synthesis was performed using a qScript

cDNA Synthesis Kit (Quantabio, Beverly, MA, USA) according to the manufacturer's instructions. Real-time polymerase chain reaction was carried out using PerfeCTa SYBR Green FastMix (Quantabio, Beverly, MA, USA). Expression was quantified in relation to the housekeeper gene *HPRT* using the ΔCT method. The fold change in the relative gene expression was determined by calculating the $2-\Delta\Delta CT$ values.

Statistical analysis

Mice were randomized to control or treatment groups by a researcher blinded to the experimental protocol and endpoints. Observers assessing endpoints were blinded to group assignment. Data for individual animals and independent experiments are presented as individual symbols. All data are presented as mean ± standard error of the mean. Results of two or more groups were compared by one-way analysis of variance followed by post-hoc Tukey multiple comparison test. Prism (GraphPad Software, San Diego, CA, USA) was used for all statistical analyses.

Results

HDM challenge in CATT$_7$ mice enhances pro-inflammatory macrophage polarization

Previously, we elucidated the inflammatory status of WT and CATT$_7$ mice exposed to HDM or phosphate-buffered saline (PBS) control, measuring cytokine levels in lung homogenates [5]. However, to capture the effects of HDM training on the bone marrow niche, we focused on BMDMs for this study. CATT$_7$ mice challenged with HDM three times a week for 3 weeks exhibited a boosted M1 phenotype, with significantly elevated expression of genes associated with classically activated M1 macrophages (Figure 1). Compared with naive BMDMs, *tnfα* expression was significantly upregulated in both WT and CATT$_7$ BMDMs challenged with HDM *in vivo* and stimulated with LPS *in vitro* (Figure 1B). Interestingly, BMDMs from HDM-CATT$_7$ mice demonstrated significantly elevated *il-6* (Figure 1C), *il-1β* (Figure 1D) and *nos2* (Figure 1E) expression compared with naive CATT$_7$ mice after a secondary

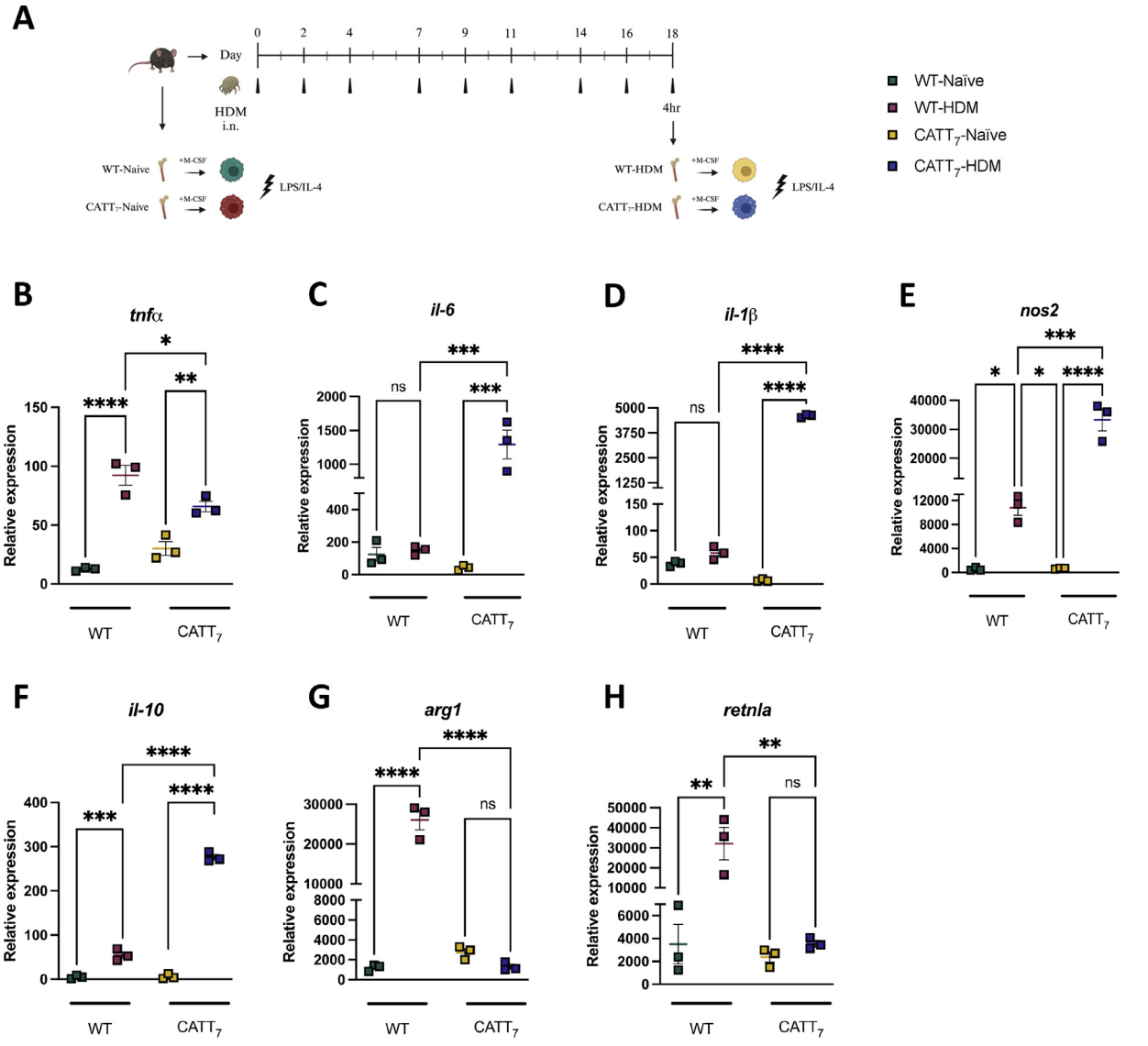

Fig. 1. HDM primes BMDMs from CATT$_7$ mice, increasing their relative M1 gene expression. (A) Model of allergic airway inflammation to investigate HDM-induced trained immunity. Bone marrow was isolated from naive or HDM-challenged WT and CATT$_7$ mice 4 h after last challenge and differentiated with M-CSF over 7 days. (B–F) M1 and (G,H) M2 macrophage marker expression in BMDMs polarized with LPS or IL-4 on day 7 for 24 h was measured by PCR. Each data point represents a single animal. Data are presented as mean ± SEM (n = 3 mice per group). ns, $P > 0.05$, $^{*}P < 0.05$, $^{**}P < 0.01$, $^{***}P < 0.001$, $^{****}P < 0.0001$. PCR, polymerase chain reaction; SEM, standard error of the mean; i.n., intranasal.

heterologous LPS stimulation. In HDM-challenged WT BMDMs, *nos2* was significantly increased but approximately 4-fold less than in HDM-CATT$_7$ BMDMs (Figure 1E). This effect for other M1 genes was not observed in BMDMs from HDM-WT mice, as no significant difference in *il-6* (Figure 1C) or *il-1β* (Figure 1D) was observed. Although not strictly associated with the M1 phenotype, *il-10* was significantly increased in HDM-challenged, LPS-stimulated WT BMDMs, albeit approximately 5-fold lower than in CATT$_7$ BMDMs (Figure 1F). By contrast, M2 polarization induced by IL-4 stimulation led to significantly increased levels of *arg1* and *retnla* in HDM-challenged WT BMDMs but not in CATT$_7$ BMDMs (Figure 1G,H).

hBM-MSCs block HDM macrophage priming effect in a COX-2 partially dependent manner

MSCs are known for their ability to calm an overzealous immune response through the secretion of paracrine immunomodulatory factors [17,27–30]. Here we investigated the ability of MSCs to block HDM priming of an M1 phenotype in BMDMs from CATT$_7$ mice (Figure 2A). Using a transwell system, hBM-MSCs co-cultured with differentiated CATT$_7$ BMDMs on day 7 significantly reduced M1 marker gene expression after LPS stimulation (Figure 2B–F). MSCs significantly decreased *tnfα* gene expression in CATT$_7$ and WT mice. By contrast, MSCs significantly decreased TNF-α protein production in CATT$_7$ mice but not in WT mice (Figure 2B). Furthermore, when co-cultured with BMDMs from CATT$_7$ mice, MSCs significantly reduced *il-6* (Figure 2C) and *il-1β* (Figure 2D) gene expression and protein production in CATT$_7$ BMDMs but not in WT BMDMs. Following this trend, MSCs significantly decreased *nos2* expression in CATT$_7$ mice; however, MSCs had no significant effect on the expression of *nos2* in BMDMs from WT mice (Figure 2E). MSCs also significantly reduced *il-10* expression in CATT$_7$ BMDMs but not in WT BMDMs (Figure 2F).

MSC co-culture with CATT$_7$ BMDMs had no significant effect on *arg1* expression after IL-4 stimulation (Figure 2G). MSCs co-cultured with HDM-WT BMDMs significantly decreased *arg1* gene expression to levels comparable to those expressed by HDM-CATT$_7$ BMDMs. Finally, as CATT$_7$ BMDMs did not exhibit increased expression of *retnla* after HDM priming, it was not surprising that no effect was seen with this gene after MSC co-culture (Figure 2H). MSC co-culture with HDM-WT BMDMs had no significant effect on *retnla* expression.

We next sought to elucidate the mechanism by which MSCs suppressed the pro-inflammatory signature in HDM-CATT$_7$ BMDMs. As cyclooxygenase is known to facilitate the immunosuppressive capabilities of MSCs [6], we investigated the role of this enzyme in MSC suppression of CATT$_7$ BMDM pro-inflammatory cytokine production (Figure 2A). COX-2 was found to have a mechanistic role in MSC-mediated suppression of TNF-α, as MSCs pre-treated with the COX-2 inhibitor NS-398 prior to co-culture with CATT$_7$ BMDMs could no longer significantly suppress TNF-α production (Figure 2I). However, other factors may play a role in the suppression of CATT$_7$ pro-inflammatory markers, as COX-2 inhibition had no effect on MSC suppression of IL-6 production by CATT$_7$ BMDMs (Figure 2J).

hBM-MSCs block HDM-induced trained immunity in macrophages from CATT$_7$ mice in vitro *and* in vivo

We used an *in vitro* HDM-induced model of trained immunity to investigate whether MSCs could also block trained immunity in HSPCs within whole bone marrow cells (Figure 3A). Bone marrow cells from CATT$_7$ mice trained with HDM *in vitro* on day 0 followed by a rest period and subsequent stimulation with LPS produced significantly increased levels of TNF-α (Figure 3B) and higher levels of IL-6 (Figure 3C) compared with cells exposed to HDM alone or LPS alone, indicative of a trained immunity phenotype. Importantly, we have previously demonstrated that human MIF expression in CATT$_7$ mice plays a key role in enhancing HDM-induced trained immunity, with evidence of epigenetic remodeling [5]. Strikingly, CATT$_7$ BMDMs derived from HSPCs that were co-cultured with MSCs on day 0 illustrated a significant reduction in TNF-α production (Figure 3B). MSC transwell co-culture also decreased the level of IL-6 protein production by trained CATT$_7$ BMDMs; however, this was not statistically significant (Figure 3C). MSCs had no significant effect on TNF-α and IL-6 production by CATT$_7$ BMDMs that received only LPS stimulation, proving the importance of having both a primary HDM stimulus on day 0 and a rest period followed by a secondary LPS stimulus in this innate immunity *in vitro* assay.

Next, we translated these findings in an *in vivo* model of HDM-induced innate immune training in humanized MIF CATT$_7$ mice. CATT$_7$ mice were HDM-challenged on day 0, day 8, day 9, day 10 and day 11. MSCs were administered intravenously on day 10 and day 11 (Figure 3D). After a rest period of 7 days, bone marrow was harvested on day 18 and BMDMs were differentiated as described. No significant differences were seen in TNF-α production between groups (Figure 3E). However, HDM-CATT$_7$ BMDMs had significantly increased levels of IL-6 production after LPS stimulation compared with PBS-CATT$_7$ BMDMs (Figure 3F). MSC administration significantly decreased levels of IL-6 production after LPS stimulation compared with those that did not receive MSC treatment. CCL17, a known marker of HDM-induced trained immunity [7], increased (although not significantly) in BMDMs from HDM-CATT$_7$ mice after LPS stimulation compared with PBS control mice (Figure 3G). Administration of MSCs decreased CCL17 production in HDM-CATT$_7$ BMDMs compared with those that did not receive MSC treatment.

Discussion

Previously, we demonstrated the immunomodulatory effects of hBM-MSCs in a model of HDM-induced airway inflammation [6]. In this study, we illustrated the ability of MSCs to modulate HDM-induced trained immunity *in vitro* and *in vivo*. hBM-MSCs co-cultured with CATT$_7$ BMDMs using transwells significantly suppressed the M1 pro-inflammatory signature after HDM priming. Furthermore, MSCs significantly reduced M2 marker *arg1* in BMDMs from WT mice. When co-cultured with CATT$_7$ BMDMs, MSCs had no significant effect on this M2 marker. COX-2 inhibition abolished the ability of MSCs to significantly suppress TNF-α production. Interestingly, MSC-COX-2 activity was not involved in MSC suppression of BMDM IL-6 production, suggesting that other unidentified soluble factors may be involved in MSC suppression of other M1-associated pro-inflammatory cytokines produced by BMDMs.

MSCs can communicate with HSPCs within the bone marrow niche not only through extracellular soluble mediators and exosomes [31,32] but also by intracellular means through organelles called migrasomes [33]. Therefore, hBM-MSCs were co-cultured with HSPCs from CATT$_7$ mice using transwell inserts to elucidate whether these immunomodulatory cells could block or suppress HDM-induced trained immunity in macrophages. Strikingly, MSCs were able to significantly reduce TNF-α and reduce IL-6 production by CATT$_7$ BMDMs trained with HDM when co-cultured with HSPCs from day 0. MSCs had no significant effect on HSPC-derived BMDMs that received only the secondary LPS stimulus. It is important to note that MSCs are present in the transwell co-culture with HSPCs trained with HDM from day 0 to day 6; however, the LPS stimulus is added on day 10 in the absence of MSCs. These data clearly illustrate the ability of MSCs to block HDM imprinting on HSPCs on day 0 and leave a lasting immunomodulatory memory, seen in HSPC-derived macrophages on day 11 [34]. Other groups have illustrated the ability of MSCs to block trained immunity in models of ischemic stroke [35] and pulmonary bacterial infection [36]; however, this study is the first to demonstrate the ability of MSCs to block this HDM-induced innate training *in vivo* in mice expressing the human MIF CATT$_7$ polymorphism.

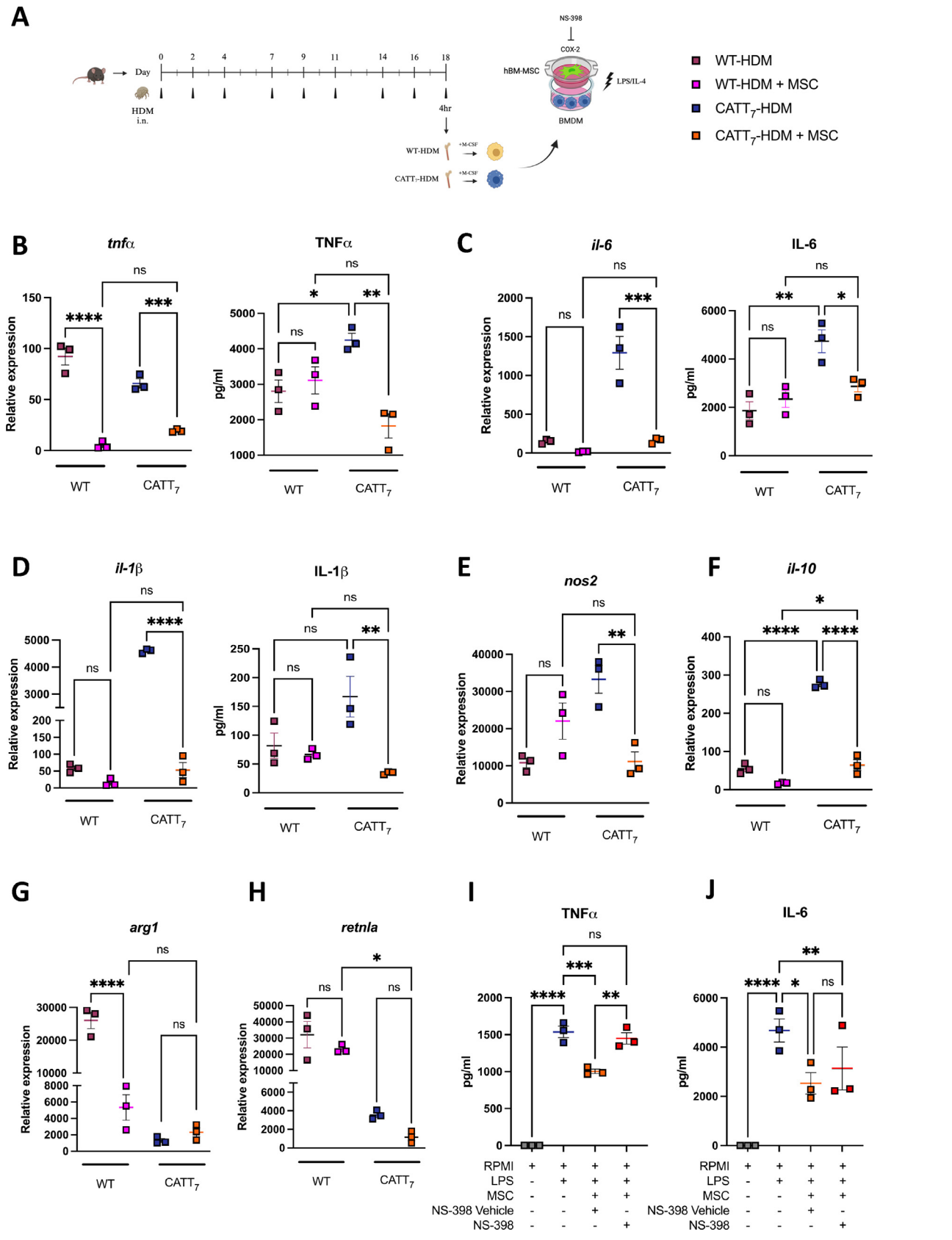

Fig. 2. hBM-MSCs block HDM-induced priming effect in $CATT_7$ mice, decreasing M1 macrophage gene expression. (A) Bone marrow cells containing HSPCs were isolated from HDM-challenged WT and $CATT_7$ mice 4 h after last challenge and differentiated with M-CSF over 7 days. On day 7, hBM-MSCs were co-cultured with BMDMs using 0.4-μM transwells at time of polarization with LPS or IL-4 for 24 h. (B–F) Gene expression and protein production of M1 macrophage markers in BMDMs measured by PCR or ELISA. (G,H) Gene expression of M2 markers *arg1* and *retnla*. (I,J) To investigate the role of COX-2 in the ability of MSCs to suppress trained immunity in $CATT_7$ BMDMs, MSCs were pre-exposed to the COX-2 inhibitor NS-398 or vehicle control for 24 h prior to co-culture with BMDMs in transwells. TNF-α and IL-6 protein production in supernatants from $CATT_7$ BMDMs co-cultured with MSCs ± NS-398 or vehicle control was measured by ELISA. Each data point represents a single animal. Data are presented as mean ± SEM (n = 3 mice per group). ns, $P > 0.05$, $^{*}P < 0.05$, $^{**}P < 0.01$, $^{***}P < 0.001$, $^{****}P < 0.0001$. PCR, polymerase chain reaction; SEM, standard error of the mean; i.n., intranasal.

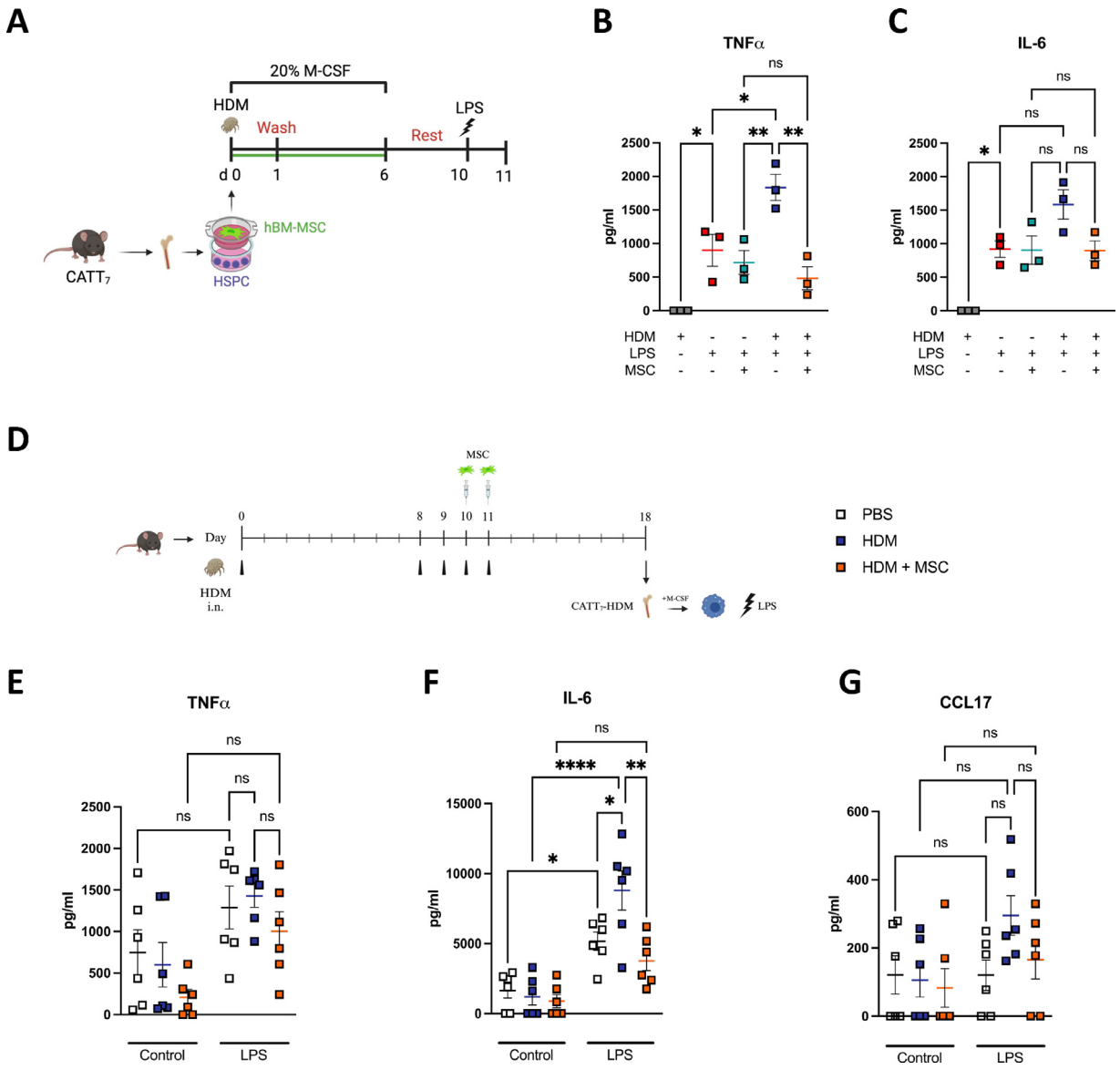

Fig. 3. hBM-MSCs block HDM-induced innate immune training effect in HSPCs from $CATT_7$ mice *in vitro* and *in vivo*. (A) Experimental protocol for *in vitro* trained immunity assay. Bone marrow containing HSPCs was isolated on day 0 and co-cultured with MSCs in transwells during training window with HDM (24 h). HDM stimulus was washed out on day 1. On day 6, MSC transwells were removed from co-culture and differentiated BMDMs entered a rest period. BMDMs received a second stimulus of LPS on day 10 for 24 h, in which cells and supernatants were harvested for gene expression and protein analysis. (B) TNF-α and (C) IL-6 protein production in differentiated BMDM supernatants was analyzed by ELISA. Each data point represents pooled triplicate samples per animal. (D) *In vivo* model of HDM-induced innate training in which mice received HDM challenge (i.n.) on day 0, day 8, day 9, day 10 and day 11. MSCs were administered intravenously on day 10 and day 11. After a rest period of 7 days, bone marrow was isolated and BMDMs were differentiated over 7 days with M-CSF before receiving a second stimulus of LPS on day 7 for 24 h. (E) TNF-α, (F) IL-6 and (G) CCL17 protein production in differentiated BMDM supernatants stimulated with LPS for 24 h was analyzed by ELISA. Each data point represents a single animal. Data are presented as mean ± SEM (n = 3–6 mice per group). ns, $P > 0.05$, $^{*}P < 0.05$, $^{**}P < 0.01$, $^{****}P < 0.0001$. d, day; SEM, standard error of the mean; i.n., intranasal.

The potential ability of MSCs to inhibit epigenetic modifications in response to HDM training within $CATT_7$ HSPCs has clinical implications. By disrupting the epigenetic reprogramming of immune cells, MSCs can exert immunomodulatory effects and reduce amplified inflammatory responses associated with a trained immune system. These findings strengthen the argument that MSC-based therapies could be beneficial for individuals with conditions characterized by these aberrant immune responses, such as asthma, specifically in the context of our HDM-induced model of allergic airway inflammation, with 50–85% of asthmatics allergic to HDM [3,9,37–39]. These data further demonstrate the universal therapeutic efficacy of MSCs at different time points of disease progression, in which they can not only calm an established immune response [6] but also prophylactically prevent HDM-induced epigenetic rewiring, thus modulating the immune response against future infection or immunological insults.

Declaration of Competing Interest

The authors have no commercial, proprietary or financial interest in the products or companies described in this article.

Funding

This study was supported by an Irish Research Council Laureate Award (KE; IRCLA/2017/288). This study was supported in part by a COVID HEA research grant from Maynooth University and a research grant from Science Foundation Ireland (grant no. 12/RI/2346).

Author Contributions

Conception and design of the study: HD, IJH, ENM, DJW, SCD, MEA and KE. Acquisition of data: HD, IJH and CT. Analysis and interpretation of data: HD, IJH, DJW, SCD and MEA. Drafting or revising the manuscript: HD and KE. All authors have approved the final article

Data Availability Statement

The data that support the findings of this study are available on request from the corresponding author.

References

[1] Divangahi M, Aaby P, Khader SA, Barreiro LB, Bekkering S, Chavakis T, et al. Trained immunity, tolerance, priming and differentiation: distinct immunological processes. Nature Immunology 2021;22(1):2–6.

[2] Netea MG, Domínguez-Andrés J, Barreiro LB, Chavakis T, Divangahi M, Fuchs E, et al. Defining trained immunity and its role in health and disease. Nature Reviews Immunology 2020;20(6):375–88.

[3] Woo LN, Guo WY, Wang X, Young A, Salehi S, Hin A, et al. A 4-Week Model of House Dust Mite (HDM) Induced Allergic Airways Inflammation with Airway Remodeling. Scientific Reports 2018;8(1):1–11.

[4] Dunbar H, Hawthorne IJ, Tunstead C, Armstrong ME, Donnelly SC, English K. Blockade of MIF biological activity ameliorates house dust mite-induced allergic airway inflammation in humanized MIF mice. The FASEB Journal 2023;37(8):e23072.

[5] Dunbar H, Hawthorne IJ, McNamee EN, Armstrong ME, Donnelly SC, English K. The human MIF polymorphism $CATT_7$ enhances pro-inflammatory macrophage polarization in a clinically relevant model of allergic airway inflammation. FASEB J 2024;38(6):e23576.

[6] Hawthorne IJ, Dunbar H, Tunstead C, Schorpp T, Weiss DJ, Enes SR, et al. Human macrophage migration inhibitory factor potentiates mesenchymal stromal cell efficacy in a clinically relevant model of allergic asthma. Molecular Therapy 2023;31(11):3243–58.

[7] Lechner A, Henkel FDR, Hartung F, Bohnacker S, Alessandrini F, Gubernatorova EO, et al. Macrophages acquire a TNF-dependent inflammatory memory in allergic asthma. Journal of Allergy and Clinical Immunology 2022;149(6):2078–90.

[8] Park SY, Kang MJ, Jin N, Lee SY, Lee YY, Jo S, et al. House dust mite-induced Akt-ERK1/2-C/EBP beta pathway triggers CCL20-mediated inflammation and epithelial-mesenchymal transition for airway remodeling. The FASEB Journal 2022;36(9):e22452.

[9] Caraballo L. Exploring the relationship between house dust mites and asthma. Expert Rev Clin Immunol 2024: 1–4.

[10] Bernhagen J, Calandra T, Mitchell RA, Martin SB, Tracey KJ, Voelter W, et al. MIF Is a Pituitary-Derived Cytokine That Potentiates Lethal Endotoxaemia. Nature 1993;365(6448):756–9.

[11] Bernhagen J, Calandra T, Bucala R. The emerging role of MIF in septic shock and infection. Biotherapy 1994;8(2):123–7.

[12] Mizue Y, Ghani S, Leng L, McDonald C, Kong P, Baugh J, et al. Role for macrophage migration inhibitory factor in asthma. Proceedings of the National Academy of Sciences of the United States of America 2005;102(40):14410–5.

[13] Shin JJ, Fan W, Par-Young J, Piecychna M, Leng L, Israni-Winger K, et al. MIF is a common genetic determinant of COVID-19 symptomatic infection and severity. QJM: An International Journal of Medicine 2023;116(3):205–12.

[14] Galipeau J. Macrophages at the Nexus of Mesenchymal Stromal Cell Potency: The Emerging Role of Chemokine Cooperativity. Stem Cells 2021;39(9):1145–54.

[15] Mathias LJ, Khong SM, Spyroglou L, Payne NL, Siatskas C, Thorburn AN, et al. Alveolar macrophages are critical for the inhibition of allergic asthma by mesenchymal stromal cells. J Immun (Baltimore, Md 1950) 2013;191(12):5914–24.

[16] Carty F, Mahon BP, English K. The influence of macrophages on mesenchymal stromal cell therapy: passive or aggressive agents? Clin Exp Immunol 2017;188(1):1–11.

[17] Dunbar H, Weiss DJ, Rolandsson Enes S, Laffey JG, English K. The Inflammatory Lung Microenvironment; a Key Mediator in MSC Licensing. Cells 2021;10(11):2982.

[18] Biswas S, Mandal G, Roy Chowdhury S, Purohit S, Payne KK, Anadon C, et al. Exosomes Produced by Mesenchymal Stem Cells Drive Differentiation of Myeloid Cells into Immunosuppressive M2-Polarized Macrophages in Breast Cancer. The Journal of Immunology 2019;203(12):3447–60.

[19] Braza F, Dirou S, Forest V, Sauzeau V, Hassoun D, Chesné J, et al. Mesenchymal Stem Cells Induce Suppressive Macrophages Through Phagocytosis in a Mouse Model of Asthma. Stem Cells. 2016;34(7):1836–45.

[20] François M, Romieu-Mourez R, Li M, Galipeau J. Human MSC Suppression Correlates With Cytokine Induction of Indoleamine 2,3-dioxygenase and Bystander M2 Macrophage Differentiation. Mol Ther 2012;20(1):187–95.

[21] Kim J, Hematti P. Mesenchymal stem cell-educated macrophages: A novel type of alternatively activated macrophages. Experimental Hematology 2009;37(12):1445–53.

[22] Selleri S, Bifsha P, Civini S, Pacelli C, Dieng MM, Lemieux W, et al. Human mesenchymal stromal cell-secreted lactate induces M2-macrophage differentiation by metabolic reprogramming. Oncotarget 2016;7(21):30193–210.

[23] Xie Z, Hao H, Tong C, Cheng Y, Liu J, Pang Y, et al. Human umbilical cord-derived mesenchymal stem cells elicit macrophages into an anti-inflammatory phenotype to alleviate insulin resistance in type 2 diabetic rats. Stem Cells 2016;34(3):627–39.

[24] Yuan Y, Yuan L, Li L, Liu F, Liu J, Chen Y, et al. Mitochondrial Transfer from Mesenchymal Stem Cells to Macrophages Restricts Inflammation and Alleviates Kidney Injury in Diabetic Nephropathy Mice via PGC-1α Activation. Stem Cells. 2021;39(7):913–28.

[25] Dameshghi S, Zavaran-Hosseini A, Soudi S, Shirazi FJ, Nojehdehi S, Hashemi SM. Mesenchymal stem cells alter macrophage immune responses to Leishmania major infection in both susceptible and resistance mice. Immunology Letters 2016;170:15–26.

[26] Rabani R, Volchuk A, Jerkic M, Ormesher L, Garces-Ramirez L, Canton J, et al. Mesenchymal stem cells enhance NOX2-dependent reactive oxygen species production and bacterial killing in macrophages during sepsis. European Respiratory Journal 2018;51(4):1702021.

[27] Cahill EF, Kennelly H, Carty F, Mahon BP, English K. Hepatocyte Growth Factor Is Required for Mesenchymal Stromal Cell Protection Against Bleomycin-Induced Pulmonary Fibrosis. Stem Cells Transl Med 2016;5(10):1307–18.

[28] English K. Mechanisms of mesenchymal stromal cell immunomodulation. Immunol Cell Biol 2013;91(1):19–26.

[29] Kennelly H, Mahon BP, English K. Human mesenchymal stromal cells exert HGF dependent cytoprotective effects in a human relevant pre-clinical model of COPD. Sci Rep 2016;6:38207.

[30] Xia J, Minamino S, Kuwabara K, Arai S. Stem cell secretome as a new booster for regenerative medicine. BioScience Trends 2019;13(4):299–307.

[31] Fichtel P, von Bonin M, Kuhnert R, Möbus K, Bornhäuser M, Wobus M. Mesenchymal Stromal Cell-Derived Extracellular Vesicles Modulate Hematopoietic Stem and Progenitor Cell Viability and the Expression of Cell Cycle Regulators in an Age-dependent Manner. Frontiers in Bioengineering and Biotechnology 2022;10:892661.

[32] Yin K, Wang S, Zhao RC. Exosomes from mesenchymal stem/stromal cells: a new therapeutic paradigm. Biomarker Research 2019;7(1):8.

[33] Deniz IA, Karbanová J, Wobus M, Bornhäuser M, Wimberger P, Kuhlmann JD, et al. Mesenchymal stromal cell-associated migrasomes: a new source of chemoattractant for cells of hematopoietic origin. Cell Communication and Signaling 2023;21(1):36.

[34] Ng Kelvin S, Kuncewicz Thomas M, Karp Jeffrey M. Beyond Hit-and-Run: Stem Cells Leave a Lasting Memory. Cell Metabolism. 2015;22(4):541–3.

[35] Feng Y-W, Wu C, Liang F-Y, Lin T, Li W-Q, Jing Y-H, et al. hUCMSCs Mitigate LPS-Induced Trained Immunity in Ischemic Stroke. Front Immunol 2020;11:1746.

[36] Ng J, Marneth AE, Griffith A, Younger D, Ghanta S, Jiao A, et al. Mesenchymal Stromal Cells Facilitate Neutrophil-Trained Immunity by Reprogramming Hematopoietic Stem Cells. J Innate Immun 2023;15(1):765–81.

[37] Acevedo N, Zakzuk J, Caraballo L. House Dust Mite Allergy Under Changing Environments. Allergy, Asthma & Immunology Research 2019;11(4):450.

[38] Gregory LG, Lloyd CM. Orchestrating house dust mite-associated allergy in the lung. Trends in Immunology 2011;32(9):402–11.

[39] Nelson RP, DiNicolo R, Fernández-Caldas E, Seleznick MJ, Lockey RF, Good RA. Allergen-specific IgE levels and mite allergen exposure in children with acute asthma first seen in an emergency department and in nonasthmatic control subjects. Journal of Allergy and Clinical Immunology 1996;98(2):258–63.

Cytotherapy 000 (2024) 1–12

Contents lists available at ScienceDirect

CYTOTHERAPY

journal homepage: www.isct-cytotherapy.org

Full-Length Article

Mesenchymal stromal cells can block palmitate training of macrophages via cyclooxygenase-2 and interleukin-1 receptor antagonist

Laura M. Bitterlich[1,2], Courteney Tunstead[1,2], Andrew E. Hogan[1,2], James A. Ankrum[3,4], Karen English[1,2,*]

[1] Kathleen Lonsdale Institute for Human Health Research, Maynooth University, Maynooth, Ireland
[2] Department of Biology, Maynooth University, Maynooth, Ireland
[3] University of Iowa Fraternal Order of Eagles Diabetes Research Center, University of Iowa, Iowa City, Iowa, USA
[4] Roy J. Carver Department of Biomedical Engineering, University of Iowa, Iowa City, Iowa, USA

ARTICLE INFO

Article History:
Received 26 June 2024
Accepted 21 October 2024
Available online xxx

Key Words:
innate training
macrophages
mesenchymal stromal cells
obesity
palmitate

ABSTRACT

Innate training of macrophages can be beneficial for the clearance of pathogens. However, for certain chronic conditions, innate training can have detrimental effects due to an excessive production of pro-inflammatory cytokines. Obesity is a condition that is associated with a range of increased pro-inflammatory training stimuli including the free fatty acid palmitate. Mesenchymal stromal cells (MSCs) are powerful immunomodulators and known to suppress inflammatory macrophages via a range of soluble factors. We show that palmitate training of murine bone-marrow-derived macrophages and human monocyte-derived macrophages (MDMs) results in an increased production of TNFα and IL-6 upon stimulation with lipopolysaccharide and is associated with epigenetic remodeling. Palmitate training led to metabolic changes, however, MSCs did not alter the metabolic profile of human MDMs. Using a transwell system, we demonstrated that human bone marrow MSCs block palmitate training in both murine and human macrophages suggesting the involvement of secreted factors. MSC disruption of the training process occurs through more than one pathway. Suppression of palmitate-enhanced TNFα production is associated with cyclooxygenase-2 activity in MSCs, while secretion of interleukin-1 receptor antagonist by MSCs is required to suppress palmitate-enhanced IL-6 production in MDMs.

Introduction

Since the discovery that the bacille Calmette-Guérin (BCG) vaccine can induce memory in macrophages, innate immune training has received ever-increasing attention [1,2]. Various pro-inflammatory training stimuli have been investigated including β-glucan, zymosan and chitin, which are ligands for dectin-1 [3–8]. In the context of BCG-induced trained immunity, innate immune cells are better equipped to clear infections [9]. However, trained immunity can also lead to detrimental effects associated with overzealous innate immune responses in chronic disease. Training with β-glucan can increase disease severity in experimental autoimmune encephalomyelitis, a mouse model of multiple sclerosis [10], rheumatoid arthritis (RA) [11,12] and systemic lupus erythematosus (SLE) [13]. Additionally, it has been hypothesized that the aberrant production of pro-inflammatory cytokines in SLE may also serve as a training stimulus itself and result in ever-increasing disease severity [14]. This hypothesis is supported by the fact that SLE is associated with high levels of the same pro-inflammatory cytokines observed in innate training: TNFα, IL-6 and IL-1β [15–17]. Furthermore, macrophages derived from SLE patients exhibit a metabolic switch toward glycolysis [18] and distinctive epigenetic modifications consistent with innate training [19,20].

In the context of chronic inflammatory conditions, the chronic pro-inflammatory environment concomitant with obesity has been

Abbreviations: 2-DG, 2-deoxy-D-glucose; BCG, bacille Calmette-Guérin; BMDM, bone marrow-derived macrophage; BSA, bovine serum albumin; COX-2, cyclooxygenase-2; cRPMI, complete RPMI; DPBS, Dulbecco's phosphate-buffered saline; ELISA, enzyme-linked immunosorbent assay; EP, E-type prostanoid receptor; FAO, fatty acid oxidation; FBS, fetal bovine serum; HDM, house dust mite; hIL-6, human IL-6; HSPCs, hematopoietic stem progenitor cells; hTNFα, human TNFα; IL-1RA, interleukin-1 receptor antagonist; LPS, lipopolysaccharide; M-CSF, macrophage colony-stimulating factor; MDM, monocyte-derived macrophage; MSC, mesenchymal stromal cell; MTA, methylthioadenosine; mTNFα, mouse TNFα; NLRP3, NLR family pyrin domain containing 3; oxLDL, oxidized cholesterol; OXPHOS, oxidative phosphorylation; Palmitate, palmitate-BSA; PBMCs, peripheral blood mononuclear cells; PGE2, prostaglandin E2; RA, rheumatoid arthritis; SLE, systemic lupus erythematosus

* Correspondence: Karen English, Kathleen Lonsdale Institute for Human Health Research, Maynooth University; Department of Biology, Maynooth University, Co. Kildare, Kilcock Road, Maynooth W23C2N1, Ireland.
E-mail address: karen.english@mu.ie (K. English).

https://doi.org/10.1016/j.jcyt.2024.10.011

associated with trained immunity. Oxidized cholesterol (oxLDL) is elevated in patients with obesity, has been associated with innate training [21–24], and oxLDL-trained macrophages have been linked to exacerbated atherosclerosis [25,26]. Saturated free fatty acids are also highly elevated in obesity and have been linked to innate training [27,28]. Interestingly, Western diet, characterized by a high percentage of saturated fat, led myeloid progenitor cells to be reprogrammed to a more pro-inflammatory state on an epigenetic level, which persisted even when the mice were switched back to a standard diet [22]. In a different study, mice fed a diet high in the saturated free fatty acid, palmitate, exhibited a hyper-inflammatory lipopolysaccharide (LPS) response and increased endotoxemia severity and mortality [27]. The pro-inflammatory effects of a high-fat diet were shown to persist in a mouse model even after weight loss, indicating that they are indeed connected to innate training and not simply inflammatory priming of the immune cells [28].

Mesenchymal stromal cells (MSCs) are powerful modulators of the immune response, especially of macrophages. MSCs have been shown to decrease macrophage secretion of TNFα, IL-6 and IL-1β in response to LPS via both cell contact-dependent and independent mechanisms, and promote macrophage-driven tissue repair [29–32]. In a mouse model where intraperitoneal LPS administration was followed 1 month later by the induction of ischemic stroke, human umbilical cord MSCs were able to reduce the training effect of LPS in microglia that led to a worse stroke outcome [33]. Dunbar et al. [34] show that MSCs can block trained immunity induced by house dust mite (HDM), both *in vitro* and *in vivo* in a mouse model of allergic asthma.

Based on this existing knowledge, we used both murine and human samples to determine if palmitate effects epigenetic changes in hematopoietic stem progenitor cells (HSPCs) and monocytes that persist throughout their differentiation into macrophages. Human bone marrow MSCs were tested for their ability to suppress palmitate training of macrophages *in vitro*, and their effects on the metabolic phenotype of the mature macrophages were measured. Finally, we elucidated two pathways involved in the suppression of innate training by human bone marrow MSCs.

Materials and Methods

Ethics approval

Ethical approval for use of mouse bone marrow cells and human work was granted by the biological research ethics committee of Maynooth University (BRESC-2022-2482563).

Human MSC culture

Human bone marrow-derived MSCs (three different donors) were purchased from RoosterBio (Frederick, MD, USA). Initially, MSCs were expanded in RoosterBio expansion medium (RoosterBasal and RoosterBooster) for passages 1 and 2 according to the manufacturer's instructions. After, MSCs were cultured and maintained up to passage 6 in low glucose Dulbecco's modified Eagle medium (Sigma-Aldrich, Wicklow, Ireland) supplemented with 10% (v/v) fetal bovine serum (FBS; Thermo Fisher Scientific, Dublin, Ireland) and 1% (v/v) penicillin/streptomycin (Sigma-Aldrich, Wicklow, Ireland). MSCs were seeded at 1×10^6 cells per T175 flask and cultured at 37°C in 5% CO_2. Medium was replenished every 2–3 days and cells were passaged at 80% confluency.

Isolation and culture of murine bone marrow-derived macrophages (BMDMs)

Male and female wildtype C57BL/6 mice were humanely euthanized via cervical dislocation. Bone marrow was isolated from femur and tibia, centrifuged at 300 g for 5 min, and red blood cells were lysed using 1X RBC lysis buffer (eBioscience/Thermo Fisher Scientific, Dublin, Ireland). Cells were centrifuged at 300 g for 5 min before seeding at a density of 4.95×10^5 cells per well in tissue culture 24 well plates. Cells were cultured for 6 days in RPMI 1640 (RPMI; BioSciences, Dublin, Ireland) supplemented with 10% (v/v) heat-inactivated FBS (Thermo Fisher Scientific, Dublin, Ireland), 1% (v/v/) penicillin/streptomycin (Sigma-Aldrich, Wicklow, Ireland) (complete RPMI [cRPMI]), and 20% L929 conditioned medium as source of macrophage colony-stimulating factor (M-CSF). On day 5, cells were detached by gentle scraping with the tip of a Pasteur pipette, collected and centrifuged at 300 g for 5 min. BMDMs were then seeded into 96 well flat bottom plates at a density of 2×10^4 cells per well for further analysis.

Isolation and culture of human monocyte-derived macrophages (MDMs)

Human peripheral blood mononuclear cells (PBMCs) were isolated from buffy coats received from the Irish Blood Transfusion Service (Saint James' Hospital, Dublin, Ireland). PBMCs were seeded at a density of 2×10^6 cells/well in tissue culture 24-well plates or 10×10^6 cells/well in 6 well plates and allowed to adhere for 60 min. Cells were washed with Dulbecco's Phosphate-Buffered Saline (DPBS; Merck, Cork, Ireland) to remove any nonadherent cells and medium was replaced. Cells were cultured in 500 μL cRPMI, supplemented with 5% human male AB plasma (Merck, Cork, Ireland) for 6 days, to differentiate monocytes into MDMs. On day 5, cells were detached by first washing them with DPBS, then adding 300 μL per well of lidocaine detachment buffer (0.5% bovine serum albumin (BSA; Merck) and 5 mg/mL lidocaine HCL (Fluorochem, Cork, Ireland) for 20–30 min at 37°C. Cells were gently collected in a centrifugation tube. An amount of 400 μL DPBS was added to wells, remaining cells were gently dislodged with the tip of a Pasteur pipette, collected in the same tube, and centrifuged at 300 g for 5 min. MDMs were then seeded into 96 well flat bottom plates at a density of 1×10^4 cells per well for further analysis.

MDM training

PBMCs were isolated from buffy coats from 4 different donors and seeded in TC-coated 6 well plates at 10×10^6 cells/well in serum-free RPMI and monocytes were allowed to adhere for 60 min. Nonadherent cells were washed off with warm PBS and medium was replaced with 1 mL abRPMI (RPMI + 10% heat inactivated FBS + 1% P/S + 5% human AB serum). For training, medium was supplemented with 0.3 mM palmitate-BSA. 2×10^5 MSCs from 3 donors were seeded in transwells and pretreated with 10 μM NS-398 for 24 h, thoroughly washed with PBS, and then added to monocyte wells during training period. For interleukin-1 receptor antagonist (IL-1Ra) neutralization experiments, 10 μg/mL human IL-1ra/IL-1F3 antibody or an equal concentration of antigoat IgG control were utilized. After 24 h of training, supernatants were collected for cytokine array and monocytes were washed three times with warm PBS. An amount of 700 μL abRPMI were added. After 24 h, wells were topped up with another 300 μL abRPMI. Monocytes were differentiated into macrophages. On day 6, cells were stimulated with 100 ng/mL LPS for 24 h.

Cytokine array

A Proteome Profiler Human Cytokine Array Kit was purchased from R&D Systems and supernatants from untrained monocytes, palmitate-trained monocytes, palmitate + MSC-trained monocytes, and MSCs exposed to palmitate were analyzed following the manufacturer's instructions. An amount of 1 mL supernatant was used for each sample and all four samples were processed, imaged and analyzed in parallel. Analysis was performed using ImageJ.

BMDM training

Mouse bone marrow containing HSPCs were isolated and seeded as described above. To study epigenetic modifications, 1 mM of the methyltransferase inhibitor methylthioadenosine (MTA; Sigma) or DMSO as a vehicle control were added 30 min prior to any stimulus, including the L-929 conditioned medium (M-CSF) for differentiation. Without removing the MTA cells were treated with either a medium control (cRPMI + 20% M-CSF), 0.3 mM palmitate-BSA (palmitate; Cayman Chemicals, MI, USA) or 0.3 mM palmitate-BSA and 4×10^4 MSCs in a transwell for 24 h. The transwell and medium were then removed and the well thoroughly washed with PBS. The murine HPSCs needed to undergo multiple centrifugation steps to ensure a proper washout of the palmitate and were then seeded back into their wells. The cells then underwent a rest and differentiation period until day 5, at which point they were detached, counted and seeded into 96 well flat bottom plates at a density of 2×10^4 (BMDMs) cells per well and allowed to adhere overnight. On day 6, the medium was replaced with fresh medium containing 100 ng/mL LPS for 24 h. Finally, supernatants were collected for analysis by enzyme-linked immunosorbent assay (ELISA).

Flow cytometry

MDM surface phenotype was analyzed after the 24 h LPS stimulation using the Attune Nxt flow cytometer. Gating was performed on live (live/dead stain, near-IR fluorescent reactive dye, Invitrogen), $CD14^+$ (PE) cells using antibodies for CD206 (Pacific Blue), HLA-DR (FITC), CD11b (PE-Cy7), CD86 (APC) and CD163 (PerCP). Data were analyzed using floreada.io.

Metabolic phenotyping

To determine metabolic dependence of cytokine production in response to LPS, human MDMs were trained with 0.3 mM palmitate with or without MSCs in a 0.4 μm transwell as described before. After training, cells of each treatment group were split into a vehicle control and an inhibitor treatment, and then treated with either a metabolic inhibitor or its corresponding vehicle control (Supplementary Table 1) for 1 h, followed by a 24 h stimulation with 100 ng/mL LPS in continuing presence of the inhibitors.

Enzyme-linked immunosorbent assay (ELISA)

Levels of mouse TNFα (mTNFα), mouse IL-6, human TNFα (hTNFα) and human IL-6 (hIL-6) (all BioLegend, CA, USA) in cell culture supernatant were determined using ELISA kits following the manufacturer's instructions. Samples were diluted as necessary to be within standard range. Analysis was carried out in corning 96-well half-area plates (Thermo Fisher Scientific, Dublin, Ireland).

Analysis of gene expression

Total RNA was extracted from naïve, or palmitate-exposed human bone marrow MSCs using TRIzol (Ambion Life Sciences, Cambridgeshire, UK) following the manufacturer's instructions. RNA concentrations were measured via spectrophotometry (Nanodrop 2000, Thermo Fisher Scientific, DE, USA). For cDNA synthesis, 500 ng RNA were used following the manufacturer's instructions (Quantabio, MA, USA). Real-time PCR was carried out using PerfeCta SYBR Green FastMix (Quantabio, MA, USA). Prostaglandin-endoperoxide synthase 2 (*PTGS2*) and *IL1RN* (primer sequence information is available in Supplementary Table 2) was qualified in relation to the housekeeping gene hypoxanthine-guanine phosphoribosyltransferase (*HPRT*), using the ΔCT method. The fold change in gene expression relative to the control was determined via calculating the $2^{-\Delta\Delta CT}$ values.

RNA-Seq data analysis

A publicly available RNA sequencing dataset (GEO: GSM4748241) of human CD14+ monocytes, that had been exposed to 200 mM palmitate for a period of 30 min, 2, 4, or 12 h was utilized to investigate the downstream signaling cascade in the cells in response to palmitate. Processed datasets were downloaded, genes (2 h) in the hypothesized pathway were identified using their Entrez ID and fragments per kilobase of transcript per million mapped reads (FPKM) of the differentially expressed genes were plotted. A heat map was further generated using Flourish software, to highlight the Log 2 Fold Changes (Log2FC) between genes in the IL-1 signaling pathway, and other targets of interest from the cytokine array. Data is a representation of 3 PBMC donors.

Statistical analysis

An ordinary One-Way ANOVA with Tukey's multiple comparisons test was performed to test for statistical significance between multiple experimental groups, and an unpaired *t*-test with Welch's correction was performed to test for statistical significance between two experimental groups. GraphPad Prism version 10.1.0 was used for statistical computations and graphing.

Results

Methyltransferases play a crucial role in palmitate training of macrophages

Innate training has been associated with epigenetic modifications [1,35,36], including DNA and histone methylation [37,38] by methyltransferases. To investigate if methylation plays a role in palmitate training of macrophages, bone marrow cells containing HSPCs were isolated from the femurs and tibias of healthy mice and exposed to the methyltransferase inhibitor MTA for 30 min prior to the addition of the training stimuli palmitate (0.3 mM) for 24 h (Figure 1A). Both untrained and trained BMDMs did not produce any detectable amounts of mTNFα (Figure 1B) or IL-6 (Figure 1C) at baseline. In response to LPS, mTNFα and mouse IL-6 expression by trained BMDMs significantly exceeded that of the untrained controls, but inhibition of methyltransferase activity in the MTA group reduced cytokine production back to baseline, while the DMSO vehicle control had no effect.

Studies investigating the training effects of palmitate on macrophages have so far only been carried out in animal models [27,28,39,40]. Thus, we sought to investigate if palmitate can train human monocyte-derived macrophages (MDMs). palmitate-trained human MDMs produced significantly increased levels of hTNFα (Figure 1D) and hIL-6 (Figure 1E) compared to the untrained cells, with MTA suppressing this training effect. To confirm that MDMs were undergoing a rest period and did not continue to express pro-inflammatory cytokines, supernatants were taken each time medium was changed (24 h, 5 days, 6 days) and analyzed for hTNFα and hIL-6 (Supplementary Figure 1). Both quickly returned to undetectable levels, with IL-6 levels remaining elevated on day 5 due to the medium not being changed between 24 h and 5 days.

Human bone marrow MSCs can suppress palmitate training of macrophages

MSCs are known for their immunosuppressive characteristics, including suppression of macrophage function [30,41–43], but there is little research on their effects on innate immune cell training [33,44]. Based on a recent paper showing that MSCs can suppress training by HDM [34], our hypothesis was that MSCs are also able to block the palmitate training of BMDMs if present during the training

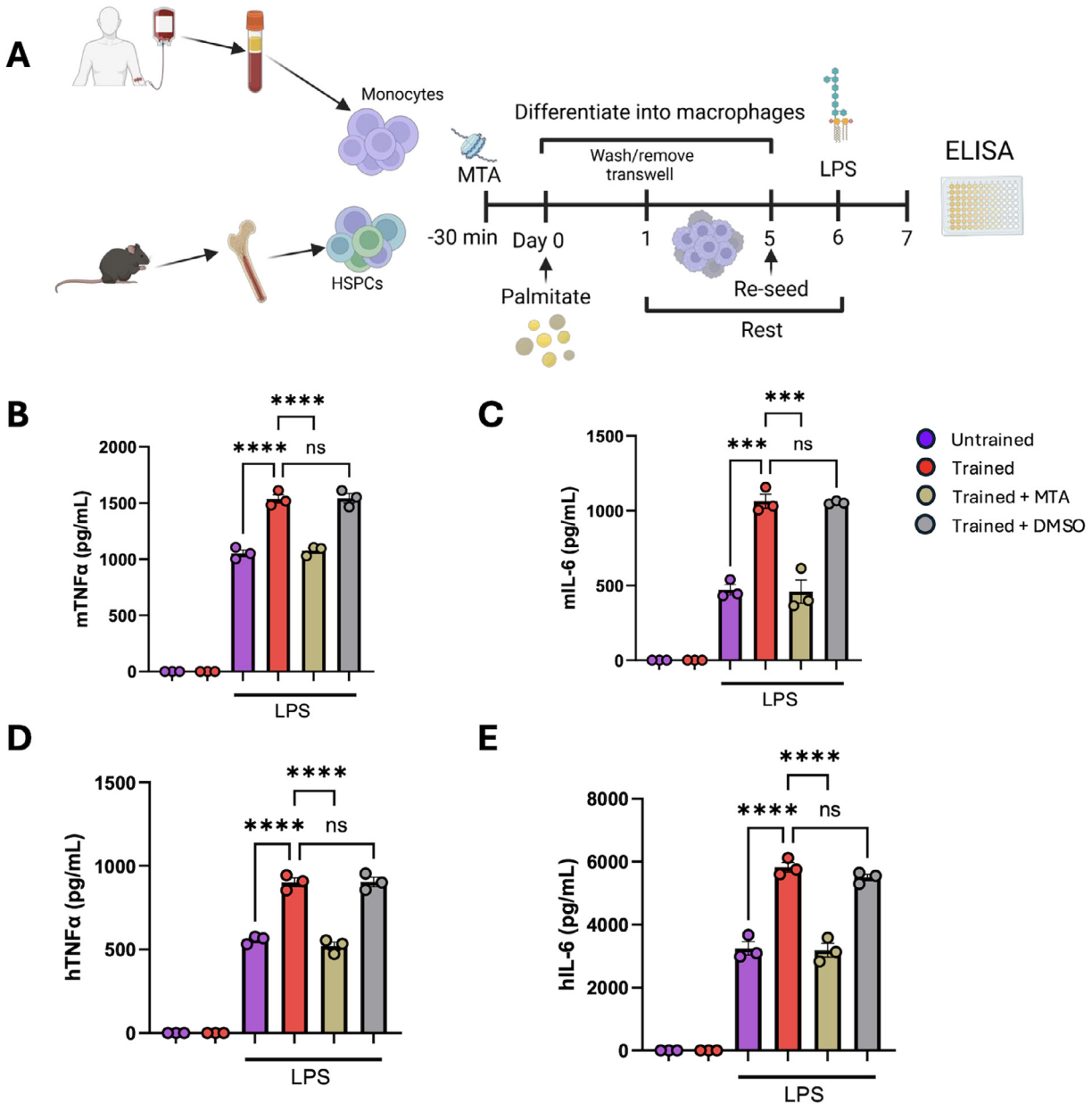

Fig. 1. Methyltransferases are required for palmitate training of macrophages (A) Experimental design: training assays were performed starting with whole bone marrow containing hematopoietic stem progenitor cells (HSPCs) isolated from the femurs and tibias of C57BL/6 mice and human monocytes derived from peripheral blood mononuclear cells (PBMCs) isolated from buffy coats. Mouse bone marrow cells or human monocytes were treated with 1 mM methylthioadenosine (MTA) 30 min before 0.3 mM palmitate were added. After 24 h, cells were thoroughly washed with DPBS and differentiated from HSPCs into bone marrow-derived macrophages (BMDMs) or from monocytes into monocyte-derived macrophages (MDMs). This differentiation period also served as a rest period from the training stimulus. On day 5, BMDMs and MDMs were re-seeded and allowed to adhere overnight, before they were stimulated with 100 ng/mL LPS for 24 h and the supernatants analyzed via ELISA. Concentrations of mouse (B) TNFα (C) IL-6, and human (D) TNFα and (E) IL-6 were measured. $n = 3$ (3 mice/3 PBMC donors). Data are presented as mean ± SEM. $^{***}P < 0.001$, $^{****}P < 0.0001$. Statistical test: Ordinary one-way ANOVA with Tukey's multiple comparisons test.

period. MSCs were seeded in a transwell and removed after the 24-h training period with the wash step (Figure 2A). Our data demonstrates that the training effect for both TNFα and IL-6 in BMDMs (Figure 2B,C) and human MDMs (Figure 2D,E) was blocked by transwell co-culture with MSCs during the training period, indicated by a reduction of the cytokine concentrations back to the levels of the untrained control.

IL-1RA is produced by MSCs in coculture with palmitate-stimulated human monocytes.

We performed a preliminary human cytokine proteome profiler array to determine what secreted factors are released by MSCs in response to being cocultured in the presence of monocytes stimulated with palmitate for 24 h. We compared the cytokine proteome profile of supernatants from monocytes, monocytes + palmitate, monocytes + palmitate + MSCs and MSCs + palmitate. This was used as a screening approach with an $n = 1$ to identify potential mediators produced by MSCs that might be responsible for the MSC suppression of cytokine production in Figure 2. With acknowledgment of the limitation of this $n = 1$ screening approach, a number of potential candidates were identified including IL-1RA, IL-16, IL-8, ICAM-1, CXCL10 and IL-6 as levels of these cytokines were higher in the monocyte + palmitate + MSC group when compared to the monocytes + palmitate group or to the MSC + palmitate group. The proteome array also demonstrated that palmitate led to increases in production of IL1α, IL1β, TNFα, CXCL1, MIP1α/MIP1β and CCL5 in monocytes (Figure 3).

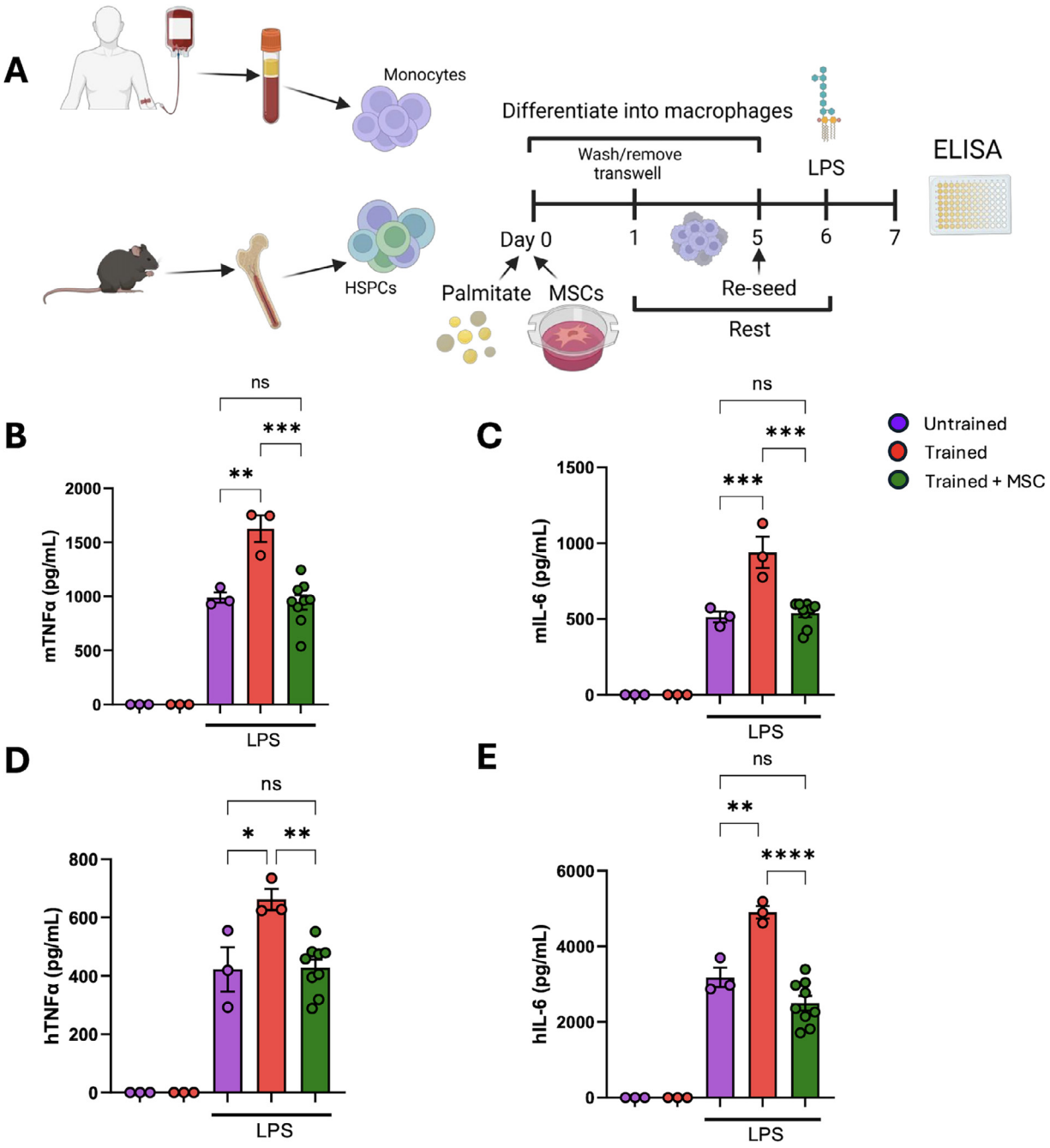

Fig. 2. MSCs block palmitate training of macrophages. (A) Experimental design: training assays were performed starting with whole bone marrow containing hematopoietic stem progenitor cells (HSPCs) isolated from the femurs and tibias of C57BL/6 mice and human monocytes derived from peripheral blood mononuclear cells (PBMCs) isolated from buffy coats. Mouse bone marrow cells or human monocytes were exposed to 0.3 mM palmitate and human bone marrow MSCs in a transwell. After 24 h, the transwell was removed, cells were thoroughly washed with DPBS and differentiated from HSPCs into bone marrow-derived macrophages (BMDMs) or from monocytes into monocyte-derived macrophages (MDMs). This differentiation period also served as a rest period from the training stimulus. On day 5, BMDMs and MDMs were re-seeded and allowed to adhere overnight, before they were stimulated with 100 ng/mL LPS for 24 h and the supernatants analyzed via ELISA. Concentrations of (B) mouse TNFα, (C) mouse IL-6, (D) human TNFα and (E) human IL-6 were measured. $n = 3–9$ (3 mice/PBMC donors, 3 MSC donors). Data are presented as mean ± SEM. $^{*}P < 0.05$, $^{**}P < 0.01$, $^{***}P < 0.001$, $^{****}P < 0.0001$. Statistical test: Ordinary one-way ANOVA with Tukey's multiple comparisons test.

Palmitate training drives an M2 MDM phenotype which is not altered by MSCs

In addition to enhancing proinflammatory cytokine production, training of MDMs with various stimuli can lead to changes in phenotype [45]. Studies have shown that palmitate exposure drives an M2 phenotype with increased CD206 expression and decreased HLA-DR expression [46,47]. In our study, untrained human MDMs stimulated with LPS expressed significantly increased levels of M1 markers CD86 and HLA-DR while the frequency of cells expressing the M2 marker CD163 significantly decreased and the mean fluorescence intensity (MFI) of the M2-associated marker CD11b significantly decreased (Supplementary Figure 2). Palmitate training in MDMs led to a phenotypic switch from M1–M2 following stimulation with LPS with significantly increased CD206+ frequency and MFI and significantly decreased expression of CD86 and HLA-DR MFI. Presence of MSCs in a transwell co-culture during palmitate training did not alter the phenotype of MDMs following LPS stimulation (Supplementary Figure 2). This is aligned with studies investigating trained immunity that show elevated expression of

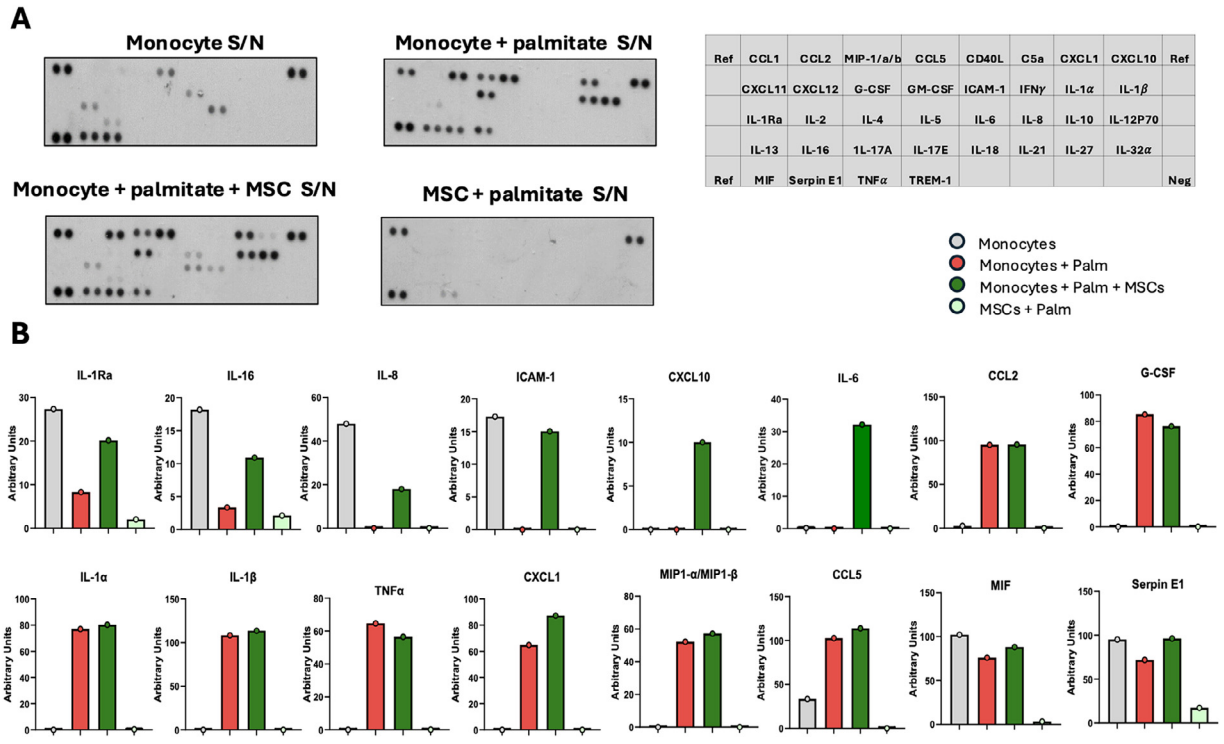

Fig. 3. IL1RA is produced by MSCs in coculture with palmitate-stimulated human monocytes. Human peripheral blood monocytes were isolated, trained with 0.3 mM palmitate with or without the presence of MSCs in a transwell. After 24 h, supernatants were collected from the four groups (monocytes; monocytes + palmitate; monocytes + palmitate + MSC; MSC + palmitate) and probed using a human cytokine proteome profiler array. (A) Image of blot of cytokine array. All four samples were imaged at the same time to avoid different exposure times. Exposure time was 10 min ($n = 1$ per group). A total of 36 different cytokines were probed as outlined in the key (top right). (B) The arbitrary units for each cytokine detected (IL-1Ra, IL-16, IL-8, ICAM-1, CXCL10, IL-6, CCL2, G-CSF, IL-1α, IL-1β, TNFα, CXCL1, MIP1a/MIP1B, CCL5, MIF and Serpin E1) were plotted comparing each of the four groups.

CD206 following training in the context of BCG and exercise-induced trained immunity [48,49]. At the same time others studies confirm our findings that palmitate exposure/training leads to elevated production of pro-inflammatory cytokines including TNF-α, IL-1β, IL-6 and IL-8 [50,51]. Therefore, it seems in the case of palmitate-induced trained immunity the elevated production of pro-inflammatory cytokines and the macrophage phenotype may be distinctly or differentially regulated.

RNA-Seq identification of pro-inflammatory signaling pathway involved in palmitate-trained monocyte activation of MSCs

The preliminary proteome profiler array suggested that monocytes produce elevated levels of IL-1α, IL-1β, TNF-α, CXCL1, MIP1a/MIP1b, CCL2, CCL5 and G-CSF (Figure 3). We confirmed these findings using a publicly available RNA-sequencing dataset on palmitate-stimulated monocyte-derived macrophages showing significant induction/elevation of CXCL1, IL-6, IL-1β, IL-1α, IL-8 and TNFα (Figure 4). Moreover, the RNA-Seq data set revealed significantly elevated levels of IL-8, TLR2 and NLR family pyrin domain containing 3 (NLRP3) (Figure 4). Published studies have shown that palmitate can induce heterodimerization of TLR2 with TLR1 in human blood monocytes. This heterodimerization leads to downstream signaling culminating in pro-IL-1β cleavage by caspase-1 and subsequent secretion of mature IL-1β [52]. Palmitate has also been shown to stimulate NLRP3 inflammasome activation [53]. Release of IL-1β has been shown to induce IL-6 production [54] and TNFα [55].

MSCs do not cause a metabolic switch in trained MDMs

Innate training with a pro-inflammatory stimulus is known to affect the metabolic phenotype of macrophages, usually switching to a more glycolytic phenotype [23,56,57]. Differentially, Lundahl et al. [56] describes how training with an anti-inflammatory stimulus can lead to a switch to oxidative phosphorylation (OXPHOS) and a higher reliance on glutamine metabolism for the expression of TNFα and IL-6. Training with palmitate has been shown to increase macrophage metabolism, with both maximal extracellular acidification rate and oxygen consumption rate being elevated [28]. In different contexts, MSCs have been shown to be able to shift the metabolism of LPS-activated macrophages toward OXPHOS via secretion of prostaglandin E2 (PGE2) [58] or lactate [59] and decrease glycolytic activity via extracellular vesicles [60]. Using metabolic inhibitors, we characterized the metabolic pathways involved in cytokine production in palmitate-trained human MDMs and investigated if MSCs alter metabolism in these trained MDMs.

Inhibition of glucose metabolism using 2-deoxy-D-glucose (Figure 5A) significantly reduced hTNFα and hIL-6 production in untrained, trained and trained with MSCs MDMs pointing toward a high dependence on glucose for the production of pro-inflammatory cytokines. Blockade of mitochondrial respiration using oligomycin (Figure 5B) resulted in an upward trend in production of hTNFα in all groups. Given that blockade of mitochondrial respiration via oligomycin blocks OXPHOS and promotes glycolysis, this data suggests that the increased usage of the glycolytic pathway promoted increased expression of hTNFα (Figure 5B). In contrast, hIL-6 expression seemed more linked to OXPHOS and dropped when mitochondrial respiration was inhibited (Figure 5B). Inhibition of fatty acid oxidation (FAO) using etomoxir did not have an effect on hTNFα expression (Figure 5C). Once again, hIL-6 expression was negatively affected by etomoxir across all groups. Finally, inhibition of glutamine metabolism using CB839 affected hTNFα expression only in the untrained control (Figure 5D) but not in the trained and trained with MSCs group. For hIL-6 expression, inhibiting glutamine metabolism again decreased the cytokine in all three groups (Figure 5D). Although MSCs are able to suppress palmitate training in MDMs,

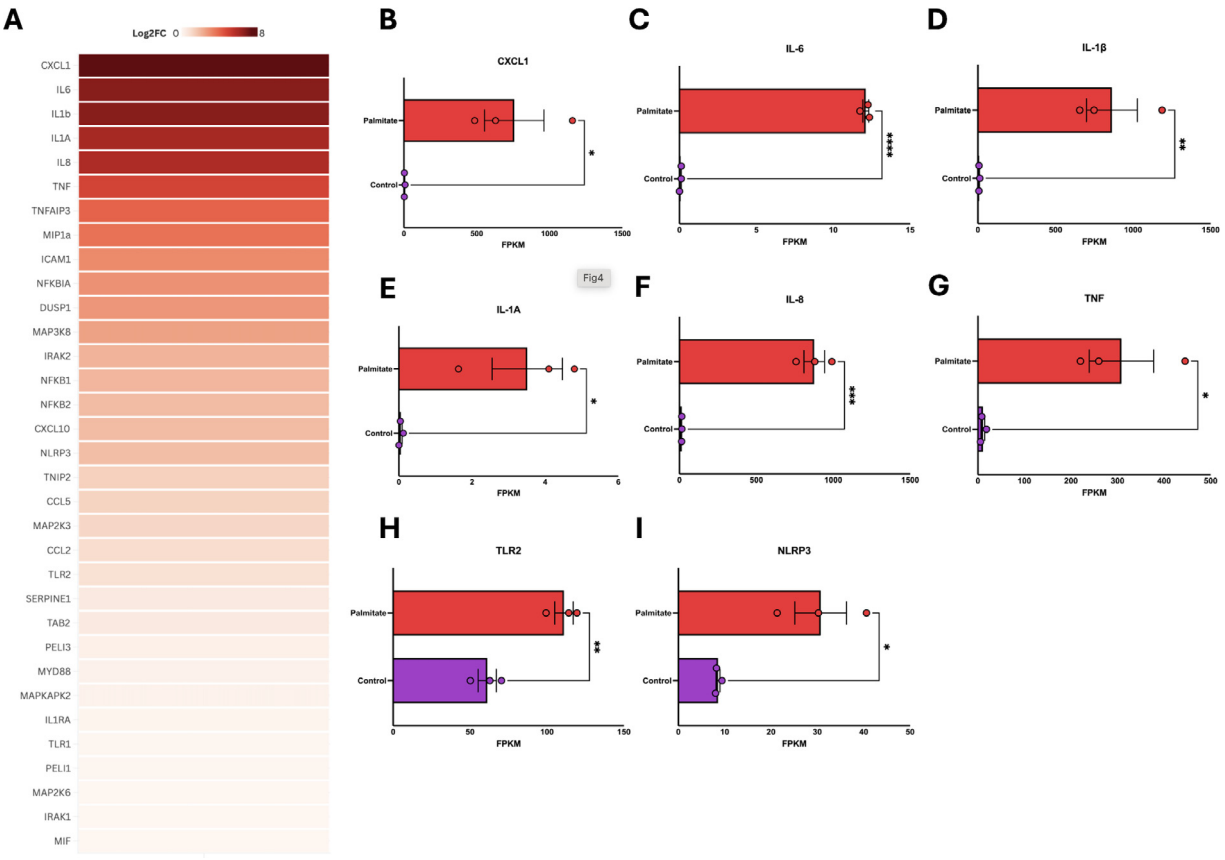

Fig. 4. RNA-Seq identification of pro-inflammatory signaling pathways upregulated in palmitate-trained monocytes. A publicly available RNA sequencing dataset (GEO: GSM4748241) of human CD14+ monocytes, that had been exposed to 200 mM palmitate for a period of 2 h was utilized to investigate the downstream signaling cascade in the cells in response to palmitate. Human monocytes derived from 3 independent PBMC donors were exposed to palmitate and sent for sequencing. The (A) Log2FC of components of the IL-1 signaling cascade were observed and plotted in heat-map format using Flourish. The FPKM from genes of interest, (B) *cxcl1*, (C) *il-6* (D) *il-1β*, (E) *il-1a*, (F) *il-8*, (G) *tnf*, (H) *tlr2* and (I) *nlrp3* were also plotted, for each individual PBMC donor. Data is presented as mean ± SEM; $n = 3$ per group; $^{*}P < 0.05$, $^{**}P < 0.01$, $^{***}P < 0.001$, $^{****}P < 0.0001$.

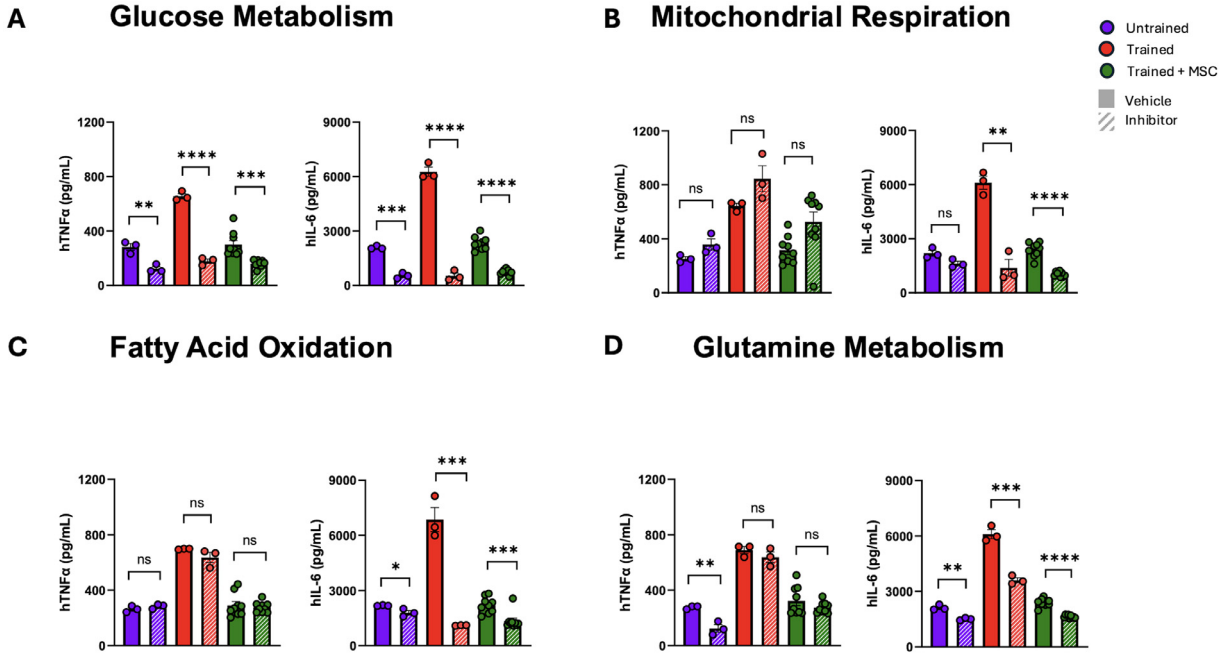

Fig. 5. The presence of MSCs during palmitate training does not affect macrophage metabolic phenotype. Human peripheral blood monocytes were isolated, trained with 0.3 mM palmitate with or without the presence of MSCs in a transwell, and differentiated into macrophages. After counting and re-seeding, MDMs were then stimulated with 100 ng/mL LPS in presence of either 5 mM 2-DG (A), 1 μM oligomycin (B), 3 μM etomoxir (C) or 10 μM CB839 (D) or the corresponding vehicle control for 24 h. Human TNFα and human IL-6 - were measured via ELISA and quantified relative to the vehicle control. $n = 3–9$ (3 PBMC donors, 3 MSC donors). Data are presented as mean ± SEM. $^{**}P < 0.01$, $^{***}P < 0.001$, $^{****}P < 0.0001$. Statistical test: Unpaired *t*-test with Welch's correction (carried out between vehicle and inhibitor of same treatment group).

their presence during training did not alter the metabolic profile of trained MDMs.

MSCs block palmitate training of MDMs via cyclooxygenase-2 (COX-2) and IL-1RA

When it comes to the suppression of macrophage-produced TNFα and IL-6 in response to LPS stimulation by MSCs, PGE2, produced via the COX-2 pathway, is frequently identified as the primary mediator [43,58,61,62]. The signaling behind the COX-2 pathway leading to blockade of TNFα or other pro-inflammatory mediators by MSCs has been extensively documented by us and others. We have previously shown that upregulation of COX-2 leads to PGE2 production by MSCs [43]. MSC-derived PGE2 binds to monocytes via EP2/EP4 receptors [63] which can activate adenylate cyclase and increase cAMP followed by enhancement of C/EBP-β and inhibition of M1 macrophages [64]. Here, we show that palmitate leads to significantly increased levels of PTGS2 the gene that codes for COX-2 (Figure 6A).

Additionally, inflammasomes and IL-1β signaling have been implicated as being of importance in innate training [4,22,65]. The cytokine proteome profile array identified elevated levels of IL-1RA produced by MSCs + monocytes + palmitate when compared to monocytes + palmitate or MSC + palmitate (Figure 3). MSC-derived IL-1RA has been shown to promote M2 macrophage polarization *in vitro* [66] and to mediate MSC protective effects in a lung injury model [67]. TNFα dose-dependently increases MSC production of IL-1RA [68]. Indeed our findings from the proteome profiler array support the published evidence that palmitate induces the production of IL-1β and TNFα in monocytes and MSCs produce higher levels of IL-1RA when co-cultured with monocytes exposed to palmitate. Palmitate significantly increases IL-1RN gene expression in MSCs (Figure 6B). Using the COX-2 inhibitor NS-398 pretreatment of MSCs or an IL-1Ra neutralizing antibody during the training period, we investigated the role of these factors in MSC blockade of the elevated proinflammatory cytokines TNFα and IL-6 associated with palmitate induce trained immunity. Interestingly, while inhibiting COX-2 activity in MSCs restored the palmitate training response for hTNFα in MDMs, it had no tangible effect on MSC suppression of the training effect on hIL-6 expression (Figure 6C). Similarly, addition of the IL-1RA neutralizing antibody did not affect MSC suppression of the training effect on hTNFα expression, while hIL-6 was restored back to the elevated levels of the trained response (Figure 6D). This indicates that the training takes place via more than one signaling pathway, and MSCs interfere with these pathways by multiple means.

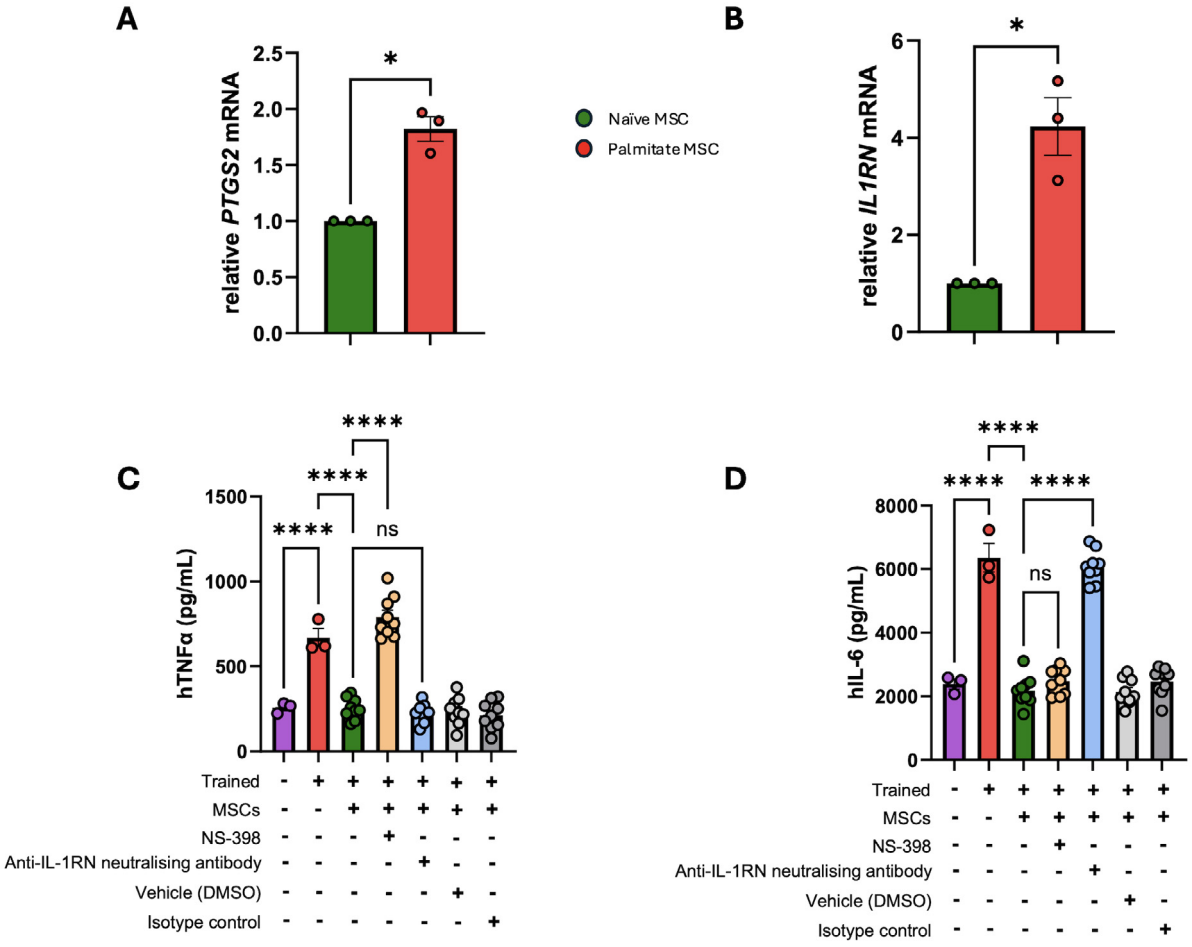

Fig. 6. MSCs block palmitate training via COX-2 and IL-1Ra. Human bone marrow MSCs were exposed to 0.3 mM palmitate for 24 h. Relative *PTGS2* (A) and *IL-1RN* (B) mRNA expression were measured via qPCR. $n = 3$ (3 MSC donors). Human MDMs were trained with 0.3 mM palmitate, with or without the presence of MSCs in a transwell. To suppress COX-2 activity, MSCs were pretreated with 10 μM NS-398 for 24 h before training. To neutralize MSC-derived IL-1Ra, 10 ng/mL anti-IL-1RA neutralizing antibody was added during the training period. On day 6 after training, MDMs were stimulated with 100 ng/mL LPS for 24 h. Human TNFα (C) and IL-6 (D) were measured. $n = 3–9$ (3 PBMC donors, 3 MSC donors). Data are presented as mean ± SEM. $^{*}P < 0.05$, $^{****}P < 0.0001$. Statistical test: Unpaired *t*-test with Welch's correction (A and B) and ordinary one-way ANOVA with Tukey's multiple comparisons test (C and D).

Discussion

Obesity is known to cause a chronic state of inflammation [69–73] and innate immune cells can retain an elevated pro-inflammatory phenotype even after weight loss, which is consistent with innate training [28,74]. OxLDL, which is typically elevated in patients with obesity [75,76], has been investigated and confirmed as a pro-inflammatory innate training stimulus in obesity. Innate training by oxLDL is associated with lasting epigenetic and metabolic changes in macrophages, specifically with an increase in glycolytic activity via mTOR and HIF-1α signaling [3,21,24]. Palmitate, a pro-inflammatory saturated free fatty acid that is also elevated in obesity and known to cause detrimental health effects [50,77–82] has so far only received very little attention regarding its ability to promote innate training. Differential findings show that palmitate can drive a pro-inflammatory [27] or immunoparalysed [40] phenotype. In our hands, both murine and human macrophages responded to 0.3 mM palmitate as a training stimulus with an increased pro-inflammatory response after re-stimulation with 100 ng/mL LPS. This is in line with the results published by Seufert et al. [27], where the authors used a concentration of 0.5 mM palmitate. Our data showed that palmitate-trained monocyte-derived macrophages display an M2 phenotype following LPS re-stimulation with increased CD206+ expression. This aligns with the published studies investigating the influence of palmitate on macrophage phenotype [46,47]. Moreover, innate immune training studies have also demonstrated a switch to a CD206 + macrophage phenotype [48,49]. Although proinflammatory cytokine production usually correlates with an M1 phenotype, there are published studies supporting our data whereby palmitate stimulation leads to significantly increased levels of pro-inflammatory cytokines [50,51] and an M2 macrophage phenotype [46,47]. While the presence of MSCs blocked the palmitate-induced elevated pro-inflammatory cytokine release in trained macrophages, MSCs did not alter the palmitate-induced M2 phenotype switch in LPS re-stimulated cells.

General nutrition and specifically cellular exposure to palmitate are known to affect DNA methylation [83–86]. The observation that inhibiting DNA and histone methylation via MTA prevents macrophage training by palmitate aligns with studies of other training stimuli, including the BCG vaccine [35] and LPS [87,88]. Our study is the first that links palmitate training to methyltransferase activity in human macrophages.

While trained immunity in macrophages has initially caught attention as a beneficial mechanism that helps clear infections [1,9], further studies have shown that trained macrophages can also have pathogenic effects that need to be addressed [10–13]. MSCs can suppress an acute inflammatory macrophage response [30,41,61] thus we hypothesized that MSCs may be capable of suppressing palmitate-mediated training through soluble factors. For our model, we first demonstrated that MSCs are able to suppress palmitate training in murine BMDMs, and then replicated the experiment in human MDMs, demonstrating a cross-species mechanism of action that is nevertheless relevant in the context of human cells.

Previously, it has been shown that pro-inflammatory innate training, including palmitate training, shifts cells toward a more glycolytic phenotype [2,28,89,90]. Meanwhile, anti-inflammatory training, for example with a combination of IL-13 and IL-4, can switch macrophages toward a more OXPHOS-heavy metabolic phenotype [56]. As our experiments demonstrated that MSCs had a suppressive effect on the pro-inflammatory training, we assumed that they had an anti-inflammatory influence on the macrophages and might thus cause a metabolic switch opposing the palmitate training. However, this was not the case. For all four metabolic pathways that were inhibited, glucose metabolism, mitochondrial respiration, FAO and glutamine metabolism, palmitate-trained macrophages and macrophages that were palmitate-trained in the presence of MSCs demonstrated the same trends when exposed to the respective inhibitors. TNFα expression heavily relied on glucose metabolism and trended upward when mitochondrial respiration was inhibited, suggesting a strong reliance on glycolysis. Meanwhile, FAO and glutamine metabolism played no significant role in the expression of this cytokine. IL-6, on the other hand, was significantly reduced in response to each of the metabolic inhibitors, indicating that the macrophages are not exclusively relying on glycolysis.

Given that MSCs did not affect the metabolic phenotype of trained macrophages, their suppressive activity must be exerted through different means, and through a secreted factor given that MSCs were separated from MDMs via a transwell. Based on the use of human MSCs in our experiments, species nonspecific metabolites were the most likely candidates. A cytokine proteome profile screen identified a number of potential factors including IL-1RA that might be involved in the MSC blockade of trained immunity. The COX-2/PGE2 pathway has been described as crucial for macrophage suppression [30,41,61,91] and has been described as a pathway via which MSCs suppress training of murine macrophages by HDM [34]. We confirmed that inhibition of COX-2 activity in the MSCs restored the increased TNFα response of the palmitate training, but not the IL-6 response. Suppression of TNFα expression via PGE2 happens primarily via signaling through the E-type prostanoid receptor (EP) 2 and EP4. PGE2 binds to EP2/EP4, leading to an increase in intracellular cyclic adenosine monophosphate, and eventual suppression of NFκB [92–97]. A second major player in innate immune training is the NLRP3 inflammasome, specifically the IL-1 signaling associated with it [3,65,98]. Palmitate and a high-fat diet, in general, are known activators of NLRP3 [22,99–101], and could thus be activating this particular training pathway. It is known that MSCs can express IL-1RA [102–104] and while cross-species reactivity between human and mouse is imperfect, human IL-1RA has been shown to be functional in rabbit articular chondrocytes [105], a murine myocardial ischemia-reperfusion model [106], and to be able to bind to both bovine and murine fibroblasts [107]. Although preliminary data (with an $n = 1$) the proteome profile array combined with this evidence provided sufficient basis to suspect MSC-derived IL-1RA as a potential cause for the inhibition of palmitate-mediated training. Indeed, addition of a human IL-1RA neutralizing antibody during the training period, but not of the isotype control, restored the training effect on IL-6 expression. As a result, we were able to demonstrate that there are two pathways involved in palmitate training of macrophages, which MSCs block through different secreted factors.

The ability of human bone marrow MSCs to suppress innate training through COX-2 expression has recently been described in a mouse model of HDM-induced allergic asthma [34], and human umbilical cord MSCs have been shown to be able to suppress the effects of LPS training in microglia 2 weeks after the training stimulus [33]. Other studies investigating MSCs in the context of neutrophil training have shown that MSCs can affect the HSPCs in the bone marrow which, in the case of neutrophils, is directly associated with altered myeloid proliferation [44,108]. These findings are particularly important given that our initial experiments involve blocking the training of murine HSPCs, as they demonstrate that human MSCs and MSC-secreted factors are able to affect the murine bone marrow niche. However, further experiments are needed to verify these changes for our model.

In summary, as a factor that is highly elevated in patients with obesity, palmitate poses a risk as a pro-inflammatory stimulus, altering macrophages on an epigenetic level. MSCs are able to block the changes in cytokine expression, via the expression of COX-2 and secretion of IL-1RA. Further research is required to determine if MSCs can successfully reverse palmitate training after it has already occurred, instead of blocking it during the process. This new knowledge may provide insights on the potential application of MSCs in chronic conditions where trained immunity may have detrimental

effects, to prevent repeated training of innate immune cells and consistent worsening of disease.

Declaration of competing interest

The authors declare that they have no competing interests.

Funding

This publication has emanated from research supported by the John & Pat Hume doctoral awards of Maynooth University, the Maynooth University Department of Biology Contingency Research Fund and in part by a research grant from Science Foundation Ireland (SFI) under Grant Number 16/RI/3399.

Author Contributions

LMB: Conception and design, generation of data, data analysis and interpretation, manuscript writing. CT: Data analysis and interpretation. AEH: Conception and design, data interpretation and manuscript writing. JAA: Manuscript writing. KE: Conception and design, manuscript writing, final approval of manuscript.

Data Availability

The datasets used and/or analyzed during the current study are available from the corresponding author on reasonable request.

Acknowledgments

We would like to acknowledge the Irish Blood Transfusion Service for providing access to anonymized blood components for our research. Any nondata illustrations were created with BioRender.

Supplementary materials

Supplementary material associated with this article can be found in the online version at doi:10.1016/j.jcyt.2024.10.011.

References

[1] Kaufmann E, Sanz J, Dunn JL, Khan N, Mendonça L, Pacis A, et al. BCG educates hematopoietic stem cells to generate protective innate immunity against tuberculosis. Cell 2018;172:176–90.e19 https://doi.org/10.1016/j.cell.2017.12.031.
[2] Arts RJW, Carvalho A, La Rocca C, Palma C, Rodrigues F. Silvestre R, et al. Immunometabolic pathways in BCG-induced trained immunity. Cell Rep 2016;17:2562–71. https://doi.org/10.1016/j.celrep.2016.11.011.
[3] Stothers CL, Burelbach KR, Owen AM, Patil NK, McBride MA. Bohannon JK , et al. Beta-glucan induces distinct and protective innate immune memory in differentiated macrophages. J Immunol 2021;207:2785–98. https://doi.org/10.4049/jimmunol.2100107.
[4] Moorlag SJCFM, Khan N, Novakovic B, Kaufmann E, Jansen T, van Crevel R, et al. β-glucan induces protective trained immunity against mycobacterium tuberculosis infection: a key role for IL-1. Cell Rep 2020;31:107634. https://doi.org/10.1016/j.celrep.2020.107634.
[5] Cheng QJ, Farrell K, Fenn J, Ma Z, Makanani SK, Siemsen J, et al. Dectin-1 ligands produce distinct training phenotypes in human monocytes through differential activation of signaling networks. Sci Rep 2024;14:1454. https://doi.org/10.1038/s41598-024-51620-8.
[6] Rizzetto L, Ifrim DC, Moretti S, Tocci N, Cheng SH. Quintin J, et al. Fungal chitin induces trained immunity in human monocytes during cross-talk of the host with saccharomyces cerevisiae. J Biol Chem 2016;291:7961–72. https://doi.org/10.1074/jbc.M115.699645.
[7] Cunningham KT, Finlay CM, Mills KHG. Helminth imprinting of hematopoietic stem cells sustains anti-inflammatory trained innate immunity that attenuates autoimmune disease. J Immunol 2021;206:1618–30. https://doi.org/10.4049/jimmunol.2001225.
[8] Zakeri A, Everts B, Williams AR, Nejsum P. Antigens from the parasitic nematode Trichuris suis induce metabolic reprogramming and trained immunity to constrain inflammatory responses in macrophages. Cytokine 2022;156:155919. https://doi.org/10.1016/j.cyto.2022.155919.
[9] Arts RJW, Moorlag SJCFM, Novakovic B, Wang SY, Oosting M, Kumar V, et al. BCG vaccination protects against experimental viral infection in humans through the induction of cytokines associated with trained immunity. Cell Host & Microbe 2018;23:89–100.e5. https://doi.org/10.1016/j.chom.2017.12.010.
[10] Sato F, Nakamura Y, Katsuki A, Khadka S, Ahmad I, Omura S, et al. Curdlan, a microbial β-glucan, has contrasting effects on autoimmune and viral models of multiple sclerosis. Front Cell Infect Microbiol 2022;12:805302. https://doi.org/10.3389/fcimb.2022.805302.
[11] Hida S, Nagi-Miura N, Adachi Y, Ohno N. β-glucan derived from zymosan acts as an adjuvant for collagen-induced arthritis. Microbiol Immunol 2006;50:453–61. https://doi.org/10.1111/j.1348-0421.2006.tb03814.x.
[12] Hida S, Miura NN, Adachi Y, Ohno N. Effect of *Candida albicans* cell wall glucan as adjuvant for induction of autoimmune arthritis in mice. J Autoimmun 2005;25:93–101. https://doi.org/10.1016/j.jaut.2005.06.002.
[13] Fagone P, Mangano K, Mammana S, Quattrocchi C, Magro G, Coco M, et al. Acceleration of SLE-like syndrome development in NZBxNZW F1 mice by beta-glucan. Lupus 2014;23:407–11. https://doi.org/10.1177/0961203314522333.
[14] Ochando J, Mulder WJM, Madsen JC, Netea MG, Duivenvoorden R. Trained immunity—basic concepts and contributions to immunopathology. Nat Rev Nephrol 2023;19:23–37. https://doi.org/10.1038/s41581-022-00633-5.
[15] Davas EM, Tsirogianni A, Kappou I, Karamitsos D, Economidoi I. Dantis PC Serum IL-6, TNFalpha, p55 srTNFalpha, p75srTNFalpha, srIL-2alpha levels and disease activity in systemic lupus erythematosus. Clin Rheumatol 1999;18:17–22. https://doi.org/10.1007/s100670050045.
[16] McCarthy EM, Smith S, Lee RZ, Cunnane G, Doran M, Donnelly S, et al. The association of cytokines with disease activity and damage scores in systemic lupus erythematosus patients. Rheumatology 2014;53:1586–94. https://doi.org/10.1093/rheumatology/ket428.
[17] Sabry A, Sheashaa H, El-Husseini A, Mahmoud K, Eldahshan K, George S, et al. Proinflammatory cytokines (TNF-alpha and IL-6) in Egyptian patients with SLE: its correlation with disease activity. Cytokine 2006;35:148–53. https://doi.org/10.1016/j.cyto.2006.07.023.
[18] Jing C, Castro-Dopico T, Richoz N, Tuong ZK, Ferdinand JR. Lok LSC, et al. Macrophage metabolic reprogramming presents a therapeutic target in lupus nephritis. Proc Natl Acad Sci USA 2020;117:15160–71. https://doi.org/10.1073/pnas.2000943117.
[19] Sullivan KE, Suriano A, Dietzmann K, Lin J, Goldman D, Petri MA. The TNFα locus is altered in monocytes from patients with systemic lupus erythematosus. Clin Immunol 2007;123:74–81. https://doi.org/10.1016/j.clim.2006.12.008.
[20] Leung YT, Shi L, Maurer K, Song L, Zhang Z, Petri M, et al. Interferon regulatory factor 1 and histone H4 acetylation in systemic lupus erythematosus. Epigenetics 2015;10:191–9. https://doi.org/10.1080/15592294.2015.1009764.
[21] Sohrabi Y, Lagache SMM, Schnack L, Godfrey R, Kahles F, Bruemmer D, et al. mTOR-dependent oxidative stress regulates oxLDL-induced trained innate immunity in human monocytes. Front Immunol 2019;9:3155. https://doi.org/10.3389/fimmu.2018.03155.
[22] Christ A, Günther P, Lauterbach MAR, Duewell P, Biswas D, Pelka K, et al. Western diet triggers NLRP3-dependent innate immune reprogramming. Cell 2018;172:162–75.e14. https://doi.org/10.1016/j.cell.2017.12.013.
[23] Bekkering S, Blok BA, Joosten LAB, Riksen NP, van Crevel R, Netea MG. In vitro experimental model of trained innate immunity in human primary monocytes. Clin Vaccine Immunol 2016;23:926–33. https://doi.org/10.1128/CVI.00349-16.
[24] Keating ST, Groh L, Thiem K, Bekkering S, Li Y, Matzaraki V, et al. Rewiring of glucose metabolism defines trained immunity induced by oxidized low-density lipoprotein. J Mol Med 2020;98:819–31. https://doi.org/10.1007/s00109-020-01915-w.
[25] Groh LA, Verel DE, van der Heijden CDCC, Matzaraki V, Moorlag SJCFM, de Bree LC, et al. Immune modulatory effects of progesterone on oxLDL-induced trained immunity in monocytes. J Leukoc Biol 2022;112:279–88. https://doi.org/10.1002/JLB.3AB1220-846R.
[26] Bekkering S, van den Munckhof I, Nielen T, Lamfers E, Dinarello C, Rutten J, et al. Innate immune cell activation and epigenetic remodeling in symptomatic and asymptomatic atherosclerosis in humans in vivo. Atherosclerosis 2016;254:228–36. https://doi.org/10.1016/j.atherosclerosis.2016.10.019.
[27] Seufert AL, Hickman JW, Traxler SK, Peterson RM, Waugh TA, Lashley SJ, et al. Enriched dietary saturated fatty acids induce trained immunity via ceramide production that enhances severity of endotoxemia and clearance of infection. eLife 2022;11:e76744 https://doi.org/10.7554/eLife.76744.
[28] Caslin HL, Cottam MA, Piñon JM, Boney LY, Hasty AH Weight cycling induces innate immune memory in adipose tissue macrophages. Front Immunol 2023;13:984859. https://doi.org/10.3389/fimmu.2022.984859.
[29] Galipeau J, Sensebe L. Mesenchymal stromal cells: clinical challenges and therapeutic opportunities. Cell Stem Cell 2018;22:824–33. https://doi.org/10.1016/j.stem.2018.05.004.
[30] Galleu A, Riffo-Vasquez Y, Trento C, Lomas C, Dolcetti L, Cheung TS, et al. Apoptosis in mesenchymal stromal cells induces in vivo recipient-mediated immunomodulation. Sci Transl Med 2017;9:eaam7828. https://doi.org/10.1126/scitranslmed.aam7828.
[31] Cheung TS, Giacomini C, Cereda M, Avivar-Valderas A, Capece D, Bertolino GM, et al. Apoptosis in mesenchymal stromal cells activates an immunosuppressive secretome predicting clinical response in Crohn's disease. Mol Ther 2023;31:3531–44. https://doi.org/10.1016/j.ymthe.2023.10.004.
[32] English K. Mechanisms of mesenchymal stromal cell immunomodulation. Immunol Cell Biol 2012;91:19–26. https://doi.org/10.1038/icb.2012.56.
[33] Feng Y, Wu C, Liang F, Lin T, Li WQ, Jing YH, et al. hUCMSCs mitigate LPS-induced trained immunity in ischemic stroke. Front Immunol 2020;11:1746. https://doi.org/10.3389/fimmu.2020.01746.

[34] Dunbar H, Hawthorne IJ, Tunstead C, McNamee EN, Weiss DJ, Armstrong ME, et al. Mesenchymal stromal cells dampen trained immunity in house dust mite-primed macrophages expressing human macrophage migration inhibitory factor polymorphism. Cytotherapy 2024;26(10):1245–51. https://doi.org/10.1016/j.jcyt.2024.05.010.
[35] Kleinnijenhuis J, Quintin J, Preijers F, Joosten LAB, Ifrim DC, Saeed S, et al. Bacille Calmette-Guérin induces NOD2-dependent nonspecific protection from reinfection via epigenetic reprogramming of monocytes. Proc Natl Acad Sci USA 2012;109:17537–42. https://doi.org/10.1073/pnas.1202870109.
[36] Netea MG. Training innate immunity: the changing concept of immunological memory in innate host defence. Eur J Clin Invest 2013;43:881–4. https://doi.org/10.1111/eci.12132.
[37] Moore LD, Le T, Fan G. DNA methylation and its basic function. Neuropsychopharmacology 2013;38:23–38. https://doi.org/10.1038/npp.2012.112.
[38] Greer EL, Shi Y. Histone methylation: a dynamic mark in health, disease and inheritance. Nat Rev Genet 2012;13:343–57. https://doi.org/10.1038/nrg3173.
[39] Tracy LM, Bergqvist F, Ivanova EV, Jacobsen KT, Iverfeldt K. Exposure to the saturated free fatty acid palmitate alters BV-2 microglia inflammatory response. J Mol Neurosci 2013;51:805–12. https://doi.org/10.1007/s12031-013-0068-7.
[40] Howe A-M, Burke S, O'Reilly ME, McGillicuddy FC, Costello DA. Palmitic acid and oleic acid differently modulate TLR2-mediated inflammatory responses in microglia and macrophages. Mol Neurobiol 2022;59:2348–62. https://doi.org/10.1007/s12035-022-02756-z.
[41] Cheung TS, Galleu A, von Bonin M, Bornhauser M, Dazzi F. Apoptotic mesenchymal stromal cells induce prostaglandin E2 in monocytes: implications for the monitoring of mesenchymal stromal cell activity. Haematologica 2019;104:e438–41. https://doi.org/10.3324/haematol.2018.214767.
[42] Tobin LM, Healy ME, English K, Mahon BP. Human mesenchymal stem cells suppress donor CD4(+) T cell proliferation and reduce pathology in a humanized mouse model of acute graft-versus-host disease. Clin Exp Immunol 2013;172:333–48. https://doi.org/10.1111/cei.12056.
[43] English K, Barry FP, Field-Corbett CP, Mahon BP. IFN-γ and TNF-α differentially regulate immunomodulation by murine mesenchymal stem cells. Immunol Lett 2007;110:91–100. https://doi.org/10.1016/j.imlet.2007.04.001.
[44] Ng J, Marneth AE, Griffith A, Younger D, Ghanta S, Jiao A, et al. Mesenchymal stromal cells facilitate neutrophil-trained immunity by reprogramming hematopoietic stem cells. J Innate Immun 2023;15:765–81. https://doi.org/10.1159/000533732.
[45] Murphy DM, Cox DJ, Connolly SA, Breen EP, Brugman AAI, Phelan JJ, et al. Trained immunity is induced in humans after immunization with an adenoviral vector COVID-19 vaccine. J Clin Invest 2023;133:e162581. https://doi.org/10.1172/JCI162581.
[46] Xiu F, Diao L, Qi P, Catapano M, Jeschke MG. Palmitate differentially regulates the polarization of differentiating and differentiated macrophages. Immunology 2016;147:82–96. https://doi.org/10.1111/imm.12543.
[47] Albakri MM, Huang SC-C, Tashkandi HN, Sieg SF. Fatty acids secreted from head and neck cancer induce M2-like macrophages. J Leukoc Biol 2022;112:617–28. https://doi.org/10.1002/JLB.1A0521-251R.
[48] Jeljeli M, Chêne C, Chouzenoux S, Thomas M, Segain B, Doridot L, et al. LPSlow-macrophages alleviate the outcome of graft-versus-host disease without aggravating lymphoma growth in mice. Front Immunol 2021;12:670776. https://doi.org/10.3389/fimmu.2021.670776.
[49] Murugathasan M, Jafari A, Amandeep A, Hassan SA, Chihata M. Abdul-Sater AA Moderate exercise induces trained immunity in macrophages. Am J Physiol-Cell Physiol 2023;325:C429–42. https://doi.org/10.1152/ajpcell.00130.2023.
[50] Riera-Borrull M, Cuevas VD, Alonso B, Vega MA, Joven J, Izquierdo E, et al. Palmitate conditions macrophages for enhanced responses toward inflammatory stimuli via JNK activation. J Immunol 2017;199:3858–69. https://doi.org/10.4049/jimmunol.1700845.
[51] Muir LA, Cho KW, Geletka LM, Baker NA, Flesher CG, Ehlers AP, et al. Human CD206+ macrophages associate with diabetes and adipose tissue lymphoid clusters. JCI Insight 2022;7:e146563 https://doi.org/10.1172/jci.insight.146563.
[52] Snodgrass RG, Huang S, Choi I-W, Rutledge JC, Hwang DH. Inflammasome-mediated secretion of IL-1β in human monocytes through TLR2 activation; modulation by dietary fatty acids. J Immunol 2013;191:4337–47. https://doi.org/10.4049/jimmunol.1300298.
[53] Shirasuna K, Karasawa T, Takahashi M. Role of the NLRP3 inflammasome in preeclampsia. Front Endocrinol (Lausanne) 2020;11:80. https://doi.org/10.3389/fendo.2020.00080.
[54] Cahill CM, Rogers JT. Interleukin (IL) 1beta induction of IL-6 is mediated by a novel phosphatidylinositol 3-kinase-dependent AKT/IkappaB kinase alpha pathway targeting activator protein-1. J Biol Chem 2008;283:25900–12. https://doi.org/10.1074/jbc.M707692200.
[55] Ledesma E, Martínez I, Córdova Y, Rodríguez-Sosa M, Monroy A, Mora L, et al. Interleukin-1 beta (IL-1beta) induces tumor necrosis factor alpha (TNF-alpha) expression on mouse myeloid multipotent cell line 32D cl3 and inhibits their proliferation. Cytokine 2004;26:66–72. https://doi.org/10.1016/j.cyto.2003.12.009.
[56] Lundahl ML, Mitermite M, Ryan DG, Case S, Williams NC, Yang M, et al. Macrophage innate training induced by IL-4 and IL-13 activation enhances OXPHOS driven anti-mycobacterial responses. eLife 2022;11:e74690. https://doi.org/10.7554/eLife.74690.
[57] Netea MG, Domínguez-Andrés J, Barreiro LB, Chavakis T, Divangahi M, Fuchs E, et al. Defining trained immunity and its role in health and disease. Nat Rev Immunol 2020;20:375–88. https://doi.org/10.1038/s41577-020-0285-6.
[58] Vasandan AB, Jahnavi S, Shashank C, Prasad P, Kumar A, Prasanna SJ. Human Mesenchymal stem cells program macrophage plasticity by altering their metabolic status via a PGE2-dependent mechanism. Sci Rep 2016;6:38308. https://doi.org/10.1038/srep38308.
[59] Selleri S, Bifsha P, Civini S, Pacelli C, Dieng MM, Lemieux W, et al. Human mesenchymal stromal cell-secreted lactate induces M2-macrophage differentiation by metabolic reprogramming. Oncotarget 2016;7:30193–210. https://doi.org/10.18632/oncotarget.8623.
[60] Pei L, Li R, Wang X, Xu D, Gong F, Chen W, et al. MSCs-derived extracellular vesicles alleviate sepsis-associated liver dysfunction by inhibiting macrophage glycolysis-mediated inflammatory response. Int Immunopharmacol 2024;128:111575. https://doi.org/10.1016/j.intimp.2024.111575.
[61] Braza F, Dirou S, Forest V, Sauzeau V, Hassoun D, Chesné J, et al. Mesenchymal stem cells induce suppressive macrophages through phagocytosis in a mouse model of asthma. Stem Cells 2016;34:1836–45. https://doi.org/10.1002/stem.2344.
[62] Maggini J, Mirkin G, Bognanni I, Holmberg J, Piazzón IM, Nepomnaschy I, et al. Mouse bone marrow-derived mesenchymal stromal cells turn activated macrophages into a regulatory-like profile. PLoS One 2010;5:e9252. https://doi.org/10.1371/journal.pone.0009252.
[63] Duffy MM, Pindjakova J, Hanley SA, McCarthy C, Weidhofer GA, Sweeney EM, et al. Mesenchymal stem cell inhibition of T-helper 17 cell-differentiation is triggered by cell-cell contact and mediated by prostaglandin E2 via the EP4 receptor. Eur J Immunol 2011;41:2840–51. https://doi.org/10.1002/eji.201141499.
[64] Luque-Campos N, Bustamante-Barrientos FA, Pradenas C, García C, Araya MJ, Bohaud C, et al. The macrophage response is driven by mesenchymal stem cell-mediated metabolic reprogramming. Front Immunol 2021;12:624746. https://doi.org/10.3389/fimmu.2021.624746.
[65] Lee G, Ahn H, Lee E, Lee G-S. The role of NLRP3 inflammasomes in trained immunity. FBL 2023;28:210. https://doi.org/10.31083/j.fbl2809210.
[66] Luz-Crawford P, Djouad F, Toupet K, Bony C, Franquesa M, Hoogduijn MJ, et al. Mesenchymal stem cell-derived interleukin 1 receptor antagonist promotes macrophage polarization and inhibits B cell differentiation. Stem Cells 2016;34:483–92. https://doi.org/10.1002/stem.2254.
[67] Ortiz LA, DuTreil M, Fattman C, Pandey AC, Torres G, Go K, et al. Interleukin 1 receptor antagonist mediates the antiinflammatory and antifibrotic effect of mesenchymal stem cells during lung injury. Proc Natl Acad Sci USA 2007;104:11002–7. https://doi.org/10.1073/pnas.0704421104.
[68] Gabner S, Ertl R, Velde K, Rennder M, Jenner F, Egerbacher M, et al. Cytokine-induced interleukin-1 receptor antagonist protein expression in genetically engineered equine mesenchymal stem cells for osteoarthritis treatment. J Gene Med 2018;20:e3021. https://doi.org/10.1002/jgm.3021.
[69] Hotamisligil GS, Shargill NS, Spiegelman BM. Adipose expression of tumor necrosis factor-alpha: direct role in obesity-linked insulin resistance. Science 1993;259:87–91. https://doi.org/10.1126/science.7678183.
[70] Hotamisligil GS, Arner P, Caro JF, Atkinson RL, Spiegelman BM. Increased adipose tissue expression of tumor necrosis factor-alpha in human obesity and insulin resistance. J Clin Invest 1995;95:2409–15. https://doi.org/10.1172/JCI117936.
[71] Schmidt FM, Weschenfelder J, Sander C, Minkwitz J, Thormann J, Chittka T, et al. Inflammatory cytokines in general and central obesity and modulating effects of physical activity. PLoS One 2015;10:e0121971. https://doi.org/10.1371/journal.pone.0121971.
[72] Saltiel AR, Olefsky JM. Inflammatory mechanisms linking obesity and metabolic disease. J Clin Invest 2017;127:1–4. https://doi.org/10.1172/JCI92035.
[73] Michelet X, Dyck L, Hogan A, Loftus RM, Duquette D, Wei K, et al. Metabolic reprogramming of natural killer cells in obesity limits antitumor responses. Nat Immunol 2018;19:1330–40. https://doi.org/10.1038/s41590-018-0251-7.
[74] Hata M, Andriessen EMMA, Hata M, Diaz-Marin R, Fournier F, Crespo-Garcia S, et al. Past history of obesity triggers persistent epigenetic changes in innate immunity and exacerbates neuroinflammation. Science 2023;379:45–62. https://doi.org/10.1126/science.abj8894.
[75] Siklova M, Koc M, Rossmeislová L, Kraml P. Serum oxLDL-β2GPI complex reflects metabolic syndrome and inflammation in adipose tissue in obese. Int J Obes (Lond) 2018;42:405–11. https://doi.org/10.1038/ijo.2017.260.
[76] Njajou OT, Kanaya AM, Holvoet P, Connelly S, Strotmeyer ES, Harris TB, et al. Association between oxidized LDL, obesity and type 2 diabetes in a population-based cohort, the health, aging and body composition study. Diabetes Metab Res Rev 2009;25:733–9. https://doi.org/10.1002/dmrr.1011.
[77] Zezina E, Snodgrass RG, Schreiber Y, Zukunft S, Schürmann C, Heringdorf ZDM, et al. Mitochondrial fragmentation in human macrophages attenuates palmitate-induced inflammatory responses. Biochim Biophys Acta Mol Cell Biol Lipids 2018;1863:433–46. https://doi.org/10.1016/j.bbalip.2018.01.009.
[78] Kochumon S, Wilson A, Chandy B, Shenouda S, Tuomilehto J, Sindhu S, et al. Palmitate activates CCL4 expression in human monocytic cells via TLR4/MyD88 dependent activation of NF-κB/MAPK/PI3K signaling systems. Cell Physiol Biochem 2018;46:953–64. https://doi.org/10.1159/000488824.
[79] Melo HM, Seixas da Silva G, Sant'Ana MR, Teixeira CVL, Clarke JR, Miya Coreixas VS, et al. Palmitate is increased in the cerebrospinal fluid of humans with obesity and induces memory impairment in mice via pro-inflammatory TNF-α. Cell Rep 2020;30:2180−94.e8. https://doi.org/10.1016/j.celrep.2020.01.072.
[80] Macchioni L, Petricciuolo M, Davidescu M, Fettucciari K, Scarpelli P, Vitale R, et al. Palmitate lipotoxicity in enteric glial cells: lipid remodeling and mitochondrial ROS are responsible for cyt c release outside mitochondria. Biochim Biophys Acta Mol Cell Biol Lipids 2018;1863:895–908. https://doi.org/10.1016/j.bbalip.2018.04.021.

[81] Mauro C, Smith J, Cucchi D, Coe D, Fu H, Bonacina F, et al. Obesity-induced metabolic stress leads to biased effector memory CD4(+) T cell differentiation via PI3K p110delta-Akt-mediated signals. Cell Metab 2017;25:593–609. https://doi.org/10.1016/j.cmet.2017.01.008.
[82] Zhou H, Urso C, Jadeja V. Saturated fatty acids in obesity-associated inflammation. J Inflamm Res 2020;13:1–14. https://doi.org/10.2147/JIR.S229691.
[83] Hall E, Volkov P, Dayeh T, Bacos K, Rönn T, Nitert MD, et al. Effects of palmitate on genome-wide mRNA expression and DNA methylation patterns in human pancreatic islets. BMC Med 2014;12:103. https://doi.org/10.1186/1741-7015-12-103.
[84] Abdul QA, Yu BP, Chung HY, Jung HA, Choi JS. Epigenetic modifications of gene expression by lifestyle and environment. Arch Pharm Res 2017;40:1219–37. https://doi.org/10.1007/s12272-017-0973-3.
[85] Boyle KE, Patinkin ZW, Shapiro ALB, Bader C, Vanderlinden L, Kechris K, et al. Maternal obesity alters fatty acid oxidation, AMPK activity, and associated DNA methylation in mesenchymal stem cells from human infants. Mol Metab 2017;6:1503–16. https://doi.org/10.1016/j.molmet.2017.08.012.
[86] Davis FM, denDekker A, Joshi AD, Wolf SJ, Audu C, Melvin WJ, et al. Palmitate-TLR4 signaling regulates the histone demethylase, JMJD3, in macrophages and impairs diabetic wound healing. Eur J Immunol 2020;50:1929–40. https://doi.org/10.1002/eji.202048651.
[87] Cao L, Zhu T, Lang X, Jia S, Yang Y, Zhu C, et al. Inhibiting DNA methylation improves survival in severe sepsis by regulating NF-κB pathway. Front Immunol 2020;11:1360.
[88] Weisheit CK, Klüners A, Wild L, Casalter A, Heilmann-Heimbach S, Sivalingam S, et al. Sustained immunoparalysis in endotoxin-tolerized monocytic cells. Mediators Inflamm 2020;2020:8294342. https://doi.org/10.1155/2020/8294342.
[89] Cheng S-C, Quintin J, Cramer RA, Shepardson KM, Saeed S, Kumar V, et al. mTOR- and HIF-1α-mediated aerobic glycolysis as metabolic basis for trained immunity. Science 2014;345:1250684. https://doi.org/10.1126/science.1250684.
[90] Arts RJW, Novakovic B, ter Horst R, Carvalho A, Bekkering S, Lachmandas E, et al. Glutaminolysis and fumarate accumulation integrate immunometabolic and epigenetic programs in trained immunity. Cell Metab 2016;24:807–19. https://doi.org/10.1016/j.cmet.2016.10.008.
[91] Yang Z, Concannon J, Ng KS, Seyb K, Mortensen LJ, Ranganath S, et al. Tetrandrine identified in a small molecule screen to activate mesenchymal stem cells for enhanced immunomodulation. Sci Rep 2016;6:30263. https://doi.org/10.1038/srep30263.
[92] Cavalli G, Tengesdal IW, Gresnigt M, Nemkov T, Arts RJW, Domínguez-Andrés J, et al. The anti-inflammatory cytokine interleukin-37 is an inhibitor of trained immunity. Cell Rep 2021;35:108955. https://doi.org/10.1016/j.celrep.2021.108955.
[93] Saleh LS, Vanderheyden C, Frederickson A, Bryant SJ. Prostaglandin E2 and its receptor EP2 modulate macrophage activation and fusion in vitro. ACS Biomater Sci Eng 2020;6:2668–81. https://doi.org/10.1021/acsbiomaterials.9b01180.
[94] Aronoff DM, Canetti C, Peters-Golden M. Prostaglandin E2 inhibits alveolar macrophage phagocytosis through an E-prostanoid 2 receptor-mediated increase in intracellular cyclic AMP12. J Immunol 2004;173:559–65. https://doi.org/10.4049/jimmunol.173.1.559.
[95] Julia Xu X, Reichner JS, Mastrofrancesco B, Henry WL, Albina JE. Prostaglandin E2 suppresses LPS-stimulated IFNβ production. J Immunol 2008;180:2125−2131.
[96] Ratcliffe MJ, Walding A, Shelton PA, Flaherty A. Dougall IG Activation of E-prostanoid4 and E-prostanoid2 receptors inhibits TNF-α release from human alveolar macrophages. Eur Respir J 2007;29:986–94. https://doi.org/10.1183/09031936.00131606.
[97] Gill SK, Yao Y, Kay LJ, Bewley MA, Marriott HM. Peachell PT The anti-inflammatory effects of PGE2 on human lung macrophages are mediated by the EP4 receptor. Br J Pharmacol 2016;173:3099–109. https://doi.org/10.1111/bph.13565.
[98] Feng Y, Lin L, Wu T, Feng Y, Liang F, Li G, et al. Cortical microinfarcts potentiate recurrent ischemic injury through NLRP3-dependent trained immunity. Cell Death Dis 2024;15:36. https://doi.org/10.1038/s41419-023-06414-7.
[99] Korbecki J, Bajdak-Rusinek K. The effect of palmitic acid on inflammatory response in macrophages: an overview of molecular mechanisms. Inflamm Res 2019;68:915–32. https://doi.org/10.1007/s00011-019-01273-5.
[100] Vandanmagsar B, Youm Y-H, Ravussin A, Galgani JE, Stadler K, Mynatt RL, et al. The NLRP3 inflammasome instigates obesity-induced inflammation and insulin resistance. Nat Med 2011;17:179–88. https://doi.org/10.1038/nm.2279.
[101] Scheiblich H, Schlütter A, Golenbock DT, Latz E, Martinez-Martinez P. Heneka MT Activation of the NLRP3 inflammasome in microglia: the role of ceramide. J Neurochem 2017;143:534–50. https://doi.org/10.1111/jnc.14225.
[102] Bustos ML, Huleihel L, Meyer EM, Donnenberg AD, Donnenberg VS, Sciurba JD, et al. Activation of human mesenchymal stem cells impacts their therapeutic abilities in lung injury by increasing interleukin (IL)-10 and IL-1RN levels. STEM CELLS Transl Med 2013;2:884–95. https://doi.org/10.5966/sctm.2013-0033.
[103] Lee K, Park N, Jung H, Rim YE, Nam Y, Lee J, et al. Mesenchymal stem cells ameliorate experimental arthritis via expression of interleukin-1 receptor antagonist. PLoS One 2018;13:e0193086. https://doi.org/10.1371/journal.pone.0193086.
[104] Zheng Y, Dong X, Wang X, Wang J, Chen S, He Y, et al. Exosomes derived from adipose tissue-derived mesenchymal stromal cells prevent medication-related osteonecrosis of the jaw through IL-1RA. Int J Mol Sci 2023;24:8694. https://doi.org/10.3390/ijms24108694.
[105] Arend WP, Welgus HG, Thompson RC, Eisenberg SP. Biological properties of recombinant human monocyte-derived interleukin 1 receptor antagonist. J Clin Invest 1990;85:1694–7. https://doi.org/10.1172/JCI114622.
[106] Toldo S, Schatz AM, Mezzaroma E, Chawla R, Stallard TW, Stallard WC, et al. Recombinant human interleukin-1 receptor antagonist provides cardioprotection during myocardial ischemia reperfusion in the mouse. Cardiovasc Drugs Ther 2012;26:273–6. https://doi.org/10.1007/s10557-012-6389-x.
[107] Lederer JA, Czuprynski CJ. Species-specific binding of IL-1, but not the IL-1 receptor antagonist, by fibroblasts. Cytokine 1994;6:154–61. https://doi.org/10.1016/1043-4666(94)90037-X.
[108] Ng J, Guo F, Marneth AE, Ghanta S, Kwon MY, Keegan J, et al. Augmenting emergency granulopoiesis with CpG conditioned mesenchymal stromal cells in murine neutropenic sepsis. Blood Adv 2020;4:4965–79. https://doi.org/10.1182/bloodadvances.2020002556.

WILEY-VCH

European Journal of Immunology
Basic • Clinical • Translational

RESEARCH ARTICLE OPEN ACCESS

Allergy and Inflammation

The VEGF-Mediated Cytoprotective Ability of MIF-Licensed Mesenchymal Stromal Cells in House Dust Mite-Induced Epithelial Damage

Hazel Dunbar[1,2] | Ian J. Hawthorne[1,2] | Courteney Tunstead[1,2] | Molly Dunlop[1,2] | Evelina Volkova[1,2] | Daniel J. Weiss[3] | Claudia C. dos Santos[4,5] | Michelle E. Armstrong[6] | Seamas C. Donnelly[6] | Karen English[1,2]

[1]Kathleen Lonsdale Institute for Human Health Research, Maynooth University, Maynooth, Co. Kildare, Ireland | [2]Department of Biology, Maynooth University, Maynooth, Co. Kildare, Ireland | [3]Department of Medicine, 226 Health Sciences Research Facility, Larner College of Medicine, University of Vermont, Burlington, Vermont, USA | [4]The Keenan Research Centre for Biomedical Science of St. Michael's Hospital, Toronto, Ontario, Canada | [5]Institute of Medical Sciences and Interdepartmental Division of Critical Care, Faculty of Medicine, University of Toronto, Toronto, Ontario, Canada | [6]Department of Medicine, Trinity College Dublin and Tallaght Hospital, Dublin, Ireland

Correspondence: Karen English (karen.english@mu.ie)

Received: 18 April 2024 | **Revised:** 16 October 2024 | **Accepted:** 23 October 2024

Funding: Irish Research Council IRCLA/2017/288, Science Foundation Ireland 12/RI/2346, Higher Education Authority HEA COVID grant to Maynooth University

Keywords: airway epithelial | house dust mite | macrophage migration inhibitory factor | mesenchymal stromal cells | vascular endothelial growth factor

ABSTRACT

Enhancing mesenchymal stromal cell (MSC) therapeutic efficacy through licensing with proinflammatory cytokines is now well established. We have previously shown that macrophage migration inhibitory factor (MIF)-licensed MSCs exerted significantly enhanced therapeutic efficacy in reducing inflammation in house dust mite (HDM)-driven allergic asthma. Soluble mediators released into the MSC secretome boast cytoprotective properties equal to those associated with the cell itself. In asthma, epithelial barrier damage caused by the inhalation of allergens like HDM drives goblet cell hyperplasia. Vascular endothelial growth factor (VEGF) plays a pivotal role in the repair and maintenance of airway epithelial integrity. Human bone marrow-derived MSCs expressed the MIF receptors CD74, CXCR2, and CXCR4. Endogenous MIF from high MIF expressing $CATT_7$ bone marrow-derived macrophages increased MSC production of VEGF through the MIF CXCR4 chemokine receptor, where preincubation with CXCR4 inhibitor mitigated this effect. $CATT_7$-MIF licensed MSC conditioned media containing increased levels of VEGF significantly enhanced bronchial epithelial wound healing via migration and proliferation in vitro. Blocking VEGFR2 or the use of mitomycin C abrogated this effect. Furthermore, $CATT_7$-MIF MSC CM significantly decreased goblet cell hyperplasia after the HDM challenge in vivo. This was confirmed to be VEGF-dependent, as the use of anti-human VEGF neutralising antibody abrogated this effect. Overall, this study highlights that MIF-licenced MSCs show enhanced production of VEGF, which has the capacity to repair the lung epithelium.

1 | Introduction

Mesenchymal stromal cells (MSCs) are renowned for their cytoprotective abilities elicited through secreted factors including miRNA [1], mitochondrial DNA [2–4], lipids (prostaglandin E2), extracellular vesicles (EV) [5–7], metabolites (kynurenine) and cytokines (TNF and IL-6) [8–10]. Furthermore, newly emerging data outlines the importance of MSC-derived apoptotic bodies in their therapeutic efficacy, making the secretome their main mechanism of action [11–15]. MSCs are known to elicit their

anti-apoptotic and pro-regenerative effects through the production of vascular endothelial growth factor (VEGF) [16–18] and have been shown to enhance B cell survival in a VEGF-dependent manner [19].

In preclinical models of lung disease, conditioned media from MSCs (MSC CM) has proven to be as potent as the cellular counterpart [5, 20–23]. After lipopolysaccharide (LPS)-induced injury, bone marrow-derived MSC CM mitigated neutrophil influx and alternatively activated wound healing associated M2 alveolar macrophages, dampening lung injury in an IGF-1 dependent manner [24]. Similarly, murine MSC CM rescued lung fibroblasts from a cigarette-smoked-induced lung injury, illustrating the positive role of MSC-secreted factors in facilitating epithelial regeneration [22, 23, 25]. More recent studies also follow this narrative, demonstrating the potent effects of MSC CM in preclinical lung disease [26–29].

Extensive literature illustrates the benefits of licensing MSCs prior to administration [30–37], which can be carried out by modifying the environment in which these cells grow through exogenous stimulation, genetic manipulation, or even the addition of chemical agents. The asthmatic lung can act as a suitable environment for the activation of MSCs in vivo, as it contains a multitude of pro-inflammatory cytokines including macrophage migration inhibitory factor (MIF) [34]. MIF has not only been found at elevated levels in the bronchoalveolar lavage fluid of asthma patients [38] but its level of expression has been linked to disease severity [39]. Low expression of MIF is associated with a low number of repeats of the tetranucleotide repeat polymorphism 'CATT' located within the promoter region of the MIF gene [40]. Using novel humanised MIF mice expressing the 7-repeat allele termed $CATT_7$, we have shown that high expression of human MIF drives airway inflammation following the house dust mite (HDM) challenge [41]. Our group has also demonstrated the ability of $CATT_7$-MIF licensing to enhance MSCs immunomodulatory effects in vivo [42].

Epithelial cells lining the airways play a key role in defence mechanisms against external pathogens and thus, disease [43]. In asthmatics, repetitive mechanical exacerbations due to inhaled agents or non-specific stimuli can result in physical or biological injury of the airways and/or abnormal cycles of wound healing [44–46], where epithelial cell apoptosis and damage can drive further airway remodelling [47, 48]. MSCs have illustrated efficacy in resolving damage inflicted by these repeated exacerbations by repairing endothelial barrier integrity [49] and increasing wound healing [50].

This study sets out to investigate the capacity for MIF-licensing to enhance the in vitro and in vivo cytoprotective functions of the MSC secretome and to identify the mechanisms involved using a clinically relevant HDM-induced allergic airway model.

2 | Materials and Methods

2.1 | Ethical Approval and HPRA Compliance

All procedures involving the use of animals were carried out by licensed personnel. Ethical approval for all work was granted by the ethics committee of Maynooth University (BRESC-2018-13). Project authorisation was received from the HPRA (AE19124/P022), whereby animal experiments were carried out in accordance with the Animal Research: Reporting of In Vivo Experiments (ARRIVE) criteria.

2.2 | Cell Culture

Human bone marrow-derived mesenchymal stromal cells (hBM-MSCs) (RoosterBio Frederick, MD, USA) were expanded for two passages according to the manufacturer's instructions. Following this, MSCs were cultured and maintained in DMEM low glucose (Sigma-Aldrich, Arklow, Wicklow, Ireland) supplemented with 10% (v/v) fetal bovine serum (BioSera, Cholet, France) and 1% (v/v) penicillin/streptomycin (Sigma-Aldrich, Arklow, Wicklow, Ireland). Human alveolar epithelial cells (A549) and human normal bronchial epithelial cells (BEAS-2B) were cultured in complete low glucose DMEM (Sigma-Aldrich, Arklow, Wicklow, Ireland). All cells were incubated at 37°C/5% CO_2/20% O_2.

2.3 | Generation of L929 Conditioned Media (M-CSF)

L929 cells were thawed, seeded in complete RPMI-1640 medium GlutaMAX (Gibco, Paisley, UK), and incubated at 37°C/5% CO_2/20% O_2 for 7 days. The supernatant was collected, centrifuged, and filtered (0.2 μm), and conditioned media containing M-CSF was aliquoted and stored at −80°C. L929 conditioned media will be referred to as M-CSF throughout the text.

2.4 | Surface Staining of MIF Receptors

MSCs were seeded at 1×10^5 cells per well in six-well plates. MSCs were stimulated with rhMIF (1, 10, or 100 ng/mL), or endogenous MIF ($CATT_7$ CM) for 24 h. Cells were stained with CD74 (PE, BD Pharmingen, Berkshire, UK), CXCR2 (CD182) (PerCP-eFluor 710, eBioscience, San Diego, CA, USA), or CXCR4 (CD184) (APC, eBioscience, San Diego, CA, USA) for 45 min. Cells were then washed in flow cytometry staining buffer and acquired using the Attune Nxt flow cytometer.

2.5 | Animal Strains

A C57BL/6 mouse strain expressing the human high-expression $CATT_7$ MIF allele (M*IF*$CATT_7$ [(C57BL/6NTac-Miftm3884.1(MIF)Tac-Tg(CAG-Flpe)2Arte] mice) was created using vector-based recombinant replacement of murine MIF by Taconic Biosciences (Rensselaer, NY, USA). The entire mouse MIF promoter has been deleted and replaced by inserting the human MIF promoter region. Validation of human but not murine MIF mRNA expression was verified by qPCR, and −794 CATT-length dependent stimulated MIF production was confirmed in vivo [51]. Littermate wildtype (WT) and MIF−/− (MIF knockout) mice (R. Bucala, Yale School of Medicine, Yale University, New Haven, CT, USA) were used as controls. All mice were housed according to the HPRA SAP (Ireland) guidelines.

2.6 | Model of HDM-Induced Allergic Airway Inflammation

$CATT_7$ transgenic humanised MIF mice were intranasally (I.N.) challenged with 25 μg of *Dermatophagoides pteronyssinus* (endotoxin content of 9937.5 EU/vial) (Greer Laboratories Inc, Lenoir, NC, USA) on days 0, 2, 4, 7, 9, 11, 14, 16, and 18.

2.7 | Histological Analysis

On day 21 of the HDM model, lungs were harvested. Tissue was fixed in 10% (v/v) neutral buffered formalin (Sigma-Aldrich) for 24 h, processed, and embedded in paraffin wax (Shandon Pathcentre, Runcorn, UK). For periodic acid Schiff (PAS) (Abcam, Cambridge, UK) staining, tissue sections (5 μm) were stained, air dried, and a coverslip mounted with DPX mounting media (Sigma-Aldrich, Wicklow, Ireland). 20× images were taken using an Olympus BX51 light microscope. Images were scored by counting the number of PAS-positive mucin-producing goblet cells, relative to the diameter of the airway in a blinded manner.

2.8 | Generation of CATT7 MIF Conditioned Media

Mice were humanely euthanised using the cervical dislocation technique on day 18, 4 h after the last HDM challenge. Bone marrow was isolated from the femur and tibia and centrifuged at 300*g* for 5 min and red blood cells were lysed (eBioscience, San Diego, CA, USA). Cells were seeded in two T175 flasks per mouse. Cells were grown for 72 h in complete RPMI-1640 medium GlutaMAX (Gibco) supplemented with 20% L929 conditioned media. Supernatants were collected, centrifuged, and filter sterilised to remove cell debris. Aliquots were stored at −20°C. Aliquots were not freeze-thawed. To account for the variability of human MIF levels between $CATT_7$ mice and to verify that WT mice did not produce human MIF, supernatants were measured by human MIF ELISA (R&D) [41].

2.9 | Generation of MSC Conditioned Media

hBM-MSCs were cultured as described. Documented concentrations of rhMIF (1, 100, or 400 ng/mL) [52, 53] or conditioned media generated by bone marrow-derived macrophages (BMDMs) from $CATT_7$, WT, or MIF−/− mice were added with fresh cDMEM at a 1:1 ratio for 24 h. Cells were washed with warm PBS and replaced with serum-free media. After 48 h, supernatants were collected and centrifuged to remove cell debris. Aliquots were stored at −20°C.

2.10 | Generation of MIF Inhibited SCD-19 Conditioned Media

SCD-19 (3-(2-methylphenyl)-1H-isochromen-1-one) (Specs.net, the Netherlands) was reconstituted in 70% ethanol and diluted in PBS to a working concentration of 100 μM. SCD-19 was added to BMDM-derived $CATT_7$ and WT supernatant for 1 h in a shaking incubator at 37°C before the supernatants were added at a 1:1 ratio into flasks containing human BM-MSCs.

2.11 | Wound Healing Assay

The underside of a six-well plate (Sarstedt, Nümbrecht, Germany) was scratched with three horizontal lines using a scalpel and a ruler to allow for accurate analysis. A549 or BEAS-2B cells were seeded out at a density of 1 × 105/mL/well. When cells are 60–80% confluent, a single perpendicular vertical scratch was made with a sterile p200 tip. Wells were washed with warm PBS to remove cell debris. cDMEM and MIF-MSC conditioned media were added in a 1:1 ratio. On day 0, baseline measurements (100% open) were taken using Optika imaging software and a Nikon imaging microscope. Plates were incubated at 37°C/5% CO2/20% O2 for 48 h, or until one scratch had sufficiently closed. Cells were fixed with 10% neutral buffered formalin for 8 min, air dried, and stained with crystal violet (Sigma) for 4 min. ImageJ software was used to measure the percentage of wound closure of each image (Figure S1), relative to the 100% baseline measurements taken on day 0 (Table S1).

2.12 | Use of VEGFR2 Inhibitor SU-5416

To investigate if VEGF was facilitating MSCs' ability to enhance wound closure in A549 and BEAS-2B epithelial cells, a VEGFR2 inhibitor SU-5416 (Tocris) was used. 10 μM of SU-5416 or a DMSO vehicle control was added to A549 or BEAS-2B cells for 4 h before the scratch was created and conditioned media was added.

2.13 | Use of Cell Cycle Inhibitor Mitomycin C

BEAS-2B cells were exposed to 10 μg/mL Mitomycin C (MMC), for 2 h, before being washed off with PBS. Cells were then scratched and a conditioned medium was added.

2.14 | Preparation of $CATT_7$ MSC CM for In Vivo Administration

MSC CM and $CATT_7$ CM were generated as previously described. To concentrate the levels of human VEGF present, Amicon Ultra-0.5 Centrifugal Filter Units (Sigma-Aldrich) with a molecular weight cut-off of 50 kDa were used as per the manufacturer's instructions. An anti-human VEGF neutralising antibody (Bevacizumab Biosimilar) or human IgG1 isotype control was added to the concentrated conditioned media. 30 μL of conditioned media was administered intranasally on day 14 of the HDM model.

2.15 | VEGF Elisa

MIF-licensed MSC supernatants were collected and centrifuged at 300*g* for 5 min to remove debris, before being stored at −20°C. ELISAs were carried out according to the manufacturer's instructions (R&D Systems).

2.16 | Gene Expression Analysis

At the 48 h timepoint, the cells were also harvested for gene expression studies of genes that indicate proliferation: *pcna* and *mib1/ki67* (detailed in Table S2). Total RNA was extracted using TRIzol (Ambion Life Sciences) according to the manufacturer's instructions. cDNA synthesis was performed using the manufacturer's instructions (Quantobio cDNA synthesis kit). Real-time-polymerase chain reaction (RT-PCR) was carried out using PerfeCta SYBR Green FastMix (Quantbio). Expression was quantified in relation to the housekeeper gene HPRT using the ΔCT method. The fold change in the relative gene expression was determined by calculating the $2^{-\Delta\Delta CT}$ values.

2.17 | Statistical Analysis

Mice were randomised. Observers assessing end-points were blinded to group assignments. Data for individual animals and independent experiments are presented as individual symbols. All data are presented as mean ± SEM. Results of two or more groups were compared by one-way or two-way analysis of variance (ANOVA) followed by the post hoc Tukey's multiple comparison test. GraphPad Prism (GraphPad Software Inc., San Diego, CA, USA) was used for all statistical analyses.

3 | Results

3.1 | Human BM-MSCs Constitutively Express Canonical and Non-Canonical MIF Receptors

To explore the interaction between MIF and MSCs, we sought to determine whether MSCs express the classical (CD74) and non-classical MIF receptors (CXCR2 and CXCR4) by flow cytometric analysis (Figure 1A). MSCs constitutively expressed MIF receptors CD74, CXCR2, and CXCR4, with CXCR4 most highly expressed (Figure 1). Interestingly, there was large inter-donor variability in CXCR4 expression and this aligns with other studies [54].

Next, we investigated if MIF binding influences receptor expression. Recombinant human MIF (rhMIF) did not affect the MSC expression levels of MIF receptors CD74 (Figure 1B), CXCR2 (Figure 1C), or CXCR4 (Figure 1D). We also utilised endogenous MIF from our humanised $CATT_7$ MIF mice as an alternative method of licensing MSCs (Figure 2A), a process which we have previously shown significantly enhances MSC therapeutic efficacy [42]. As expected, $CATT_7$ mice that express the high MIF expression allele produce significantly higher levels of human MIF compared with WT controls (Figure 2B). Similar to the observations with rhMIF (Figure 1B–D), exposure to high levels of endogenous MIF from $CATT_7$ CM across several timepoints (1, 6, and 24 h) had no effect on the percentage of CD74 (Figure 1E), CXCR2 (Figure 1F), and CXCR4 (Figure 1G) expression on the cell surface of MSCs. Thus, these data indicate that MSCs have the ability to interact with human MIF, through both the classical CD74 receptor, but also non-classical chemokine CXCR2 and CXCR4 receptors.

3.2 | Recombinant and Endogenous MIF Stimulates MSC Secretion of VEGF

Activation of MSCs boosts their cytoprotective effects through the production of soluble mediators [55, 56]. MSCs were licensed with different concentrations of rhMIF (1, 100, or 400 ng/mL) or with BMDM supernatants from HDM-challenged human MIF-expressing $CATT_7$ mice, $MIF^{-/-}$ and WT mice (Figure 2A). As MIF is known to be stored in intracellular pools, being secreted only after stimulation [57–60], high MIF-expressing $CATT_7$ mice, $MIF^{-/-}$ mice, and WT mice were exposed to a model of house dust mite-induced acute allergic airway inflammation prior to generating BMDM supernatants. The supernatants from BMDMs isolated from WT, $MIF^{-/-}$, and $CATT_7$ mice were measured by human MIF ELISA, where only $CATT_7$ BMDM supernatant contained high levels of human MIF, thus serving as a source of endogenous MIF (Figure 2B).

VEGF, an important soluble factor secreted by MSCs [16, 19, 61], is a trophic factor known to play a role in wound healing [62]. After licensing MSCs with rhMIF, human VEGF (hVEGF) levels in rhMIF-MSC CM supernatants were measured by ELISA (Figure 2C). MSCs stimulated with all concentrations of rhMIF exhibited significantly elevated levels of hVEGF in a dose-dependent manner. MSCs licensed with 100 and 400 ng/mL rhMIF secreted the highest hVEGF protein levels, with no statistical difference between the two concentrations (Figure 2C). Thus, 100 ng/mL of rhMIF was used to license MSCs for the remainder of the study.

Alternatively, after licensing MSCs with $CATT_7$-derived human MIF, WT-derived murine MIF, or no MIF ($MIF^{-/-}$), VEGF protein levels in the endogenous MIF-MSC CM were measured by ELISA (Figure 2D). $MIF^{-/-}$ and murine MIF-expressing WT mice did not significantly increase VEGF production by MSCs compared with cDMEM control (Figure 2D). Conversely, MSCs licensed with $CATT_7$ supernatants containing human MIF displayed significantly elevated VEGF protein levels in the associated conditioned media, compared with those licensed with $MIF^{-/-}$ or WT supernatants. This shows that human, but not murine MIF, drives enhanced VEGF production by human MSCs (Figure 2D).

3.3 | MIF Signaling Through CXCR4, but Not CXCR2 or CD74, Leads to Enhanced VEGF Production in MSCs

MIF licensing significantly increased MSC production of VEGF (Figure 2). As previously discussed, MIF signals through canonical (CD74) and non-canonical receptors (CXCR2 and CXCR4), are all constitutively expressed on the surface of MSCs (Figure 1). Thus, to further validate the involvement of MIF in the licensing of MSC cytoprotective ability, MSCs were exposed to an anti-CD74 neutralising antibody (10 mg/mL) or immunoglobulin G1 (IgG1) isotype control (10 mg/mL) for 30 min before being incubated with $CATT_7$ CM for 24 h. Similarly, a CXCR2 chemokine receptor inhibitor (Reparixin; 40 μM) or a CXCR4 chemokine receptor inhibitor (AMD3100) (50 μg/mL) were used to determine if MIF's non-canonical receptors were responsible for the MIF-MSC interaction, resulting in enhanced VEGF production into the MSC secretome.

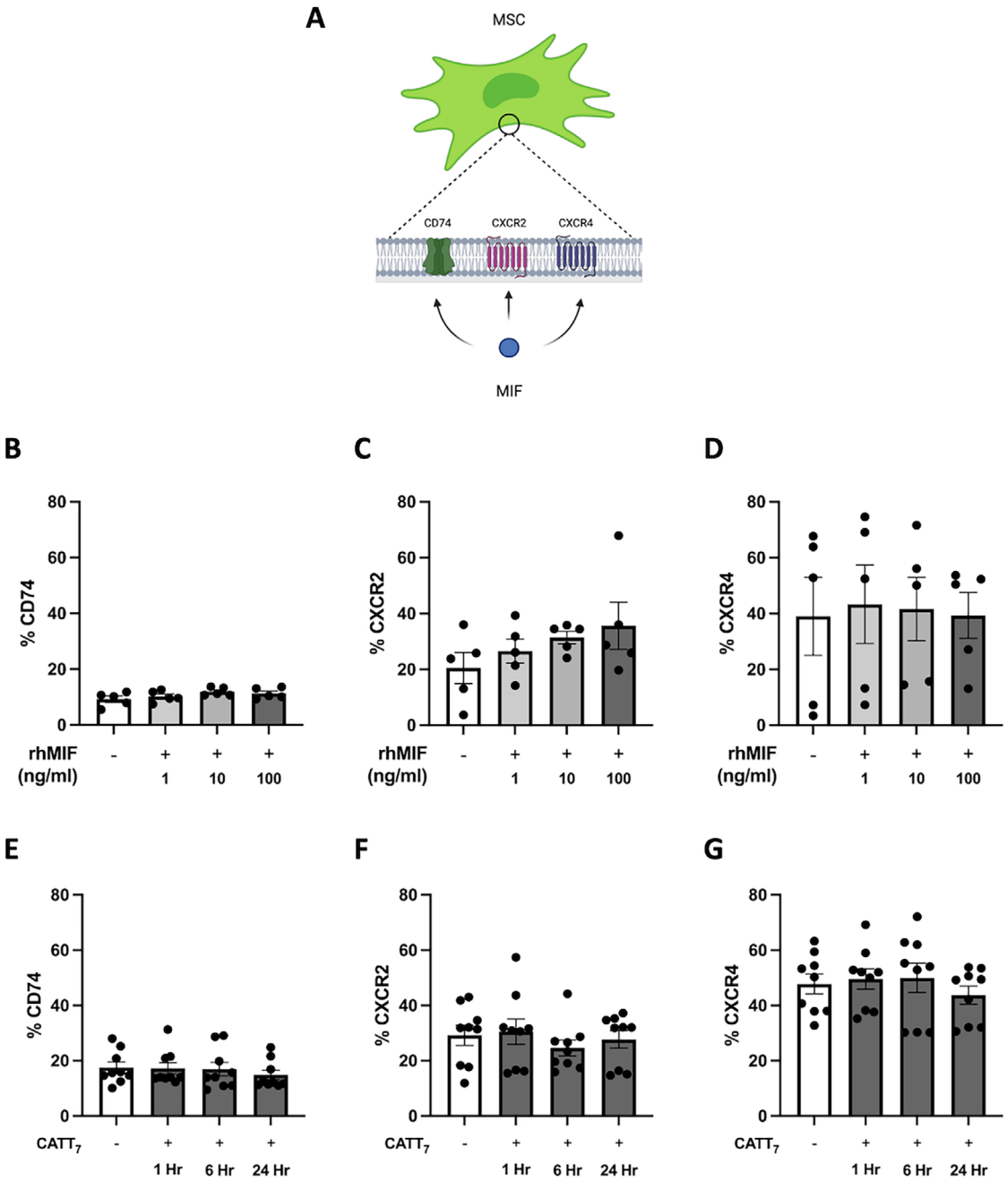

FIGURE 1 | Human BM-MSCs constitutively express canonical and non-canonical MIF receptors. A, Human BM-MSCs expressing MIF receptors CD74, CXCR2, and CXCR4 on their cell surface. MSCs were treated with different concentrations of rhMIF (1, 10, and 100 ng/mL) for 6 h, and percentage of (B) CD74, (C) CXCR2, (D) CXCR4 expression were measured by flow cytometry. Additionally, MSCs were treated with endogenous hMIF generated from BMDMs from $CATT_7$ HDM challenged mice ($CATT_7$ CM) where the percentage of (E) CD74, (F) CXCR2, (G) CXCR4 expression was assessed after endogenous hMIF stimulation at 6, 12, and 24 h timepoints. Data are presented as mean ± SEM and represent three independent experiments; no statistically significant differences were found by one-way ANOVA.

$CATT_7$-MSC CM had significantly increased levels of VEGF production compared with MSCs that were not licensed (Figure 3A). Interestingly, MSCs that were pre-treated with the CXCR4 chemokine receptor inhibitor AMD3100 but not vehicle control prior to $CATT_7$ CM licensing had significantly less VEGF production compared with MSCs that were licensing with $CATT_7$ CM alone (Figure 3A), demonstrating that MIF licensing of MSCs was dependent on the CXCR4 receptor. No significant difference was noted between reparixin pre-treated $CATT_7$-MSC CM and vehicle control $CATT_7$-MSC CM groups, indicating that MIF-MSC signalling is independent of CXCR2 (Figure 3B). Lastly, MSCs pretreated with the CD74 neutralizing antibody prior to $CATT_7$-CM licensing did not have significantly different levels of VEGF compared with MSCs licensed with $CATT_7$-CM (Figure 3C). Similarly, the addition of an IgG1 isotype control prior to MSCs being licensed with $CATT_7$-CM had no significant effect on MSC production of VEGF, concluding that MIF also does not signal through the CD74 receptor on the surface of

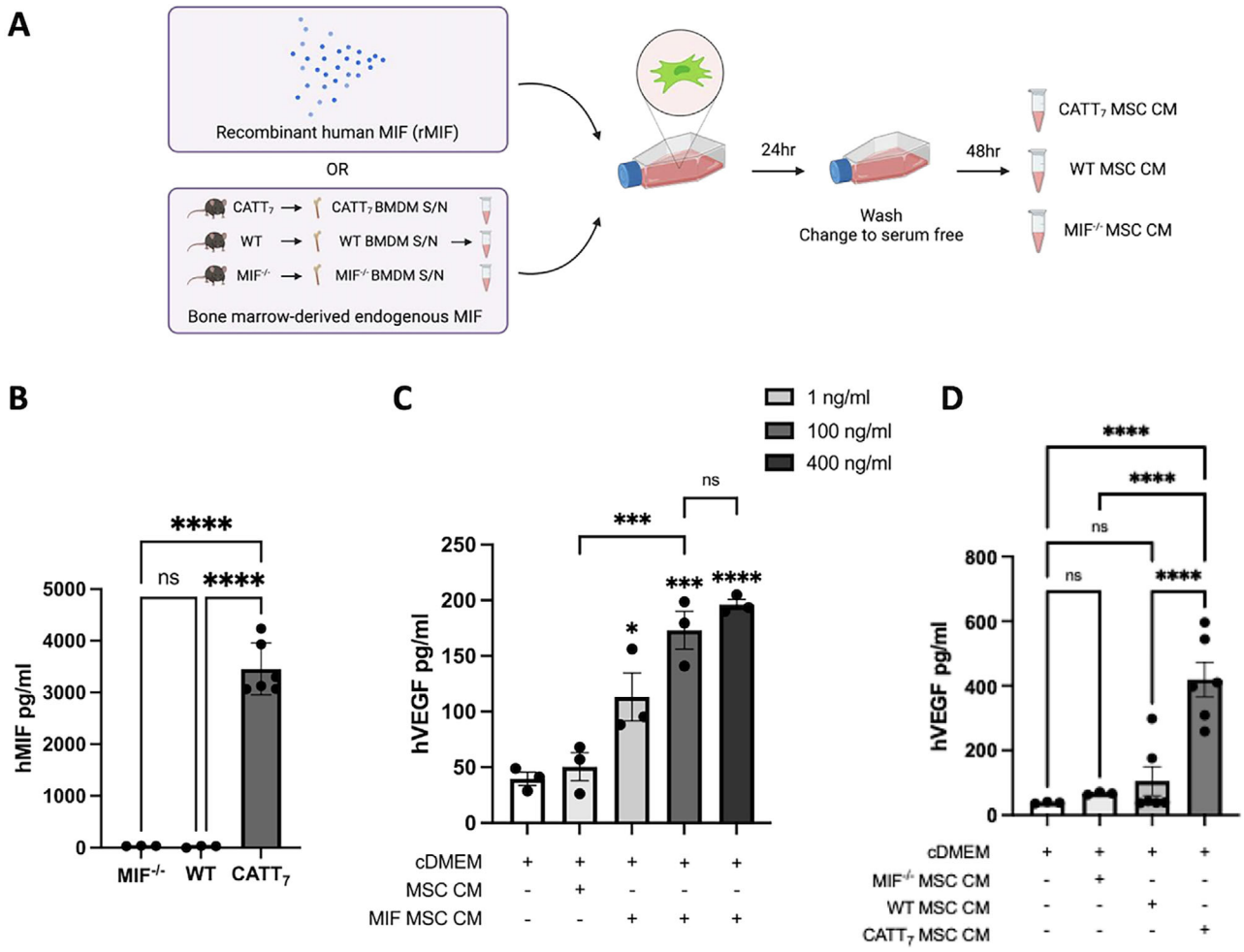

FIGURE 2 | Recombinant or endogenous MIF stimulates MSC secretion of VEGF. A, Schematic depicting the generation of MIF MSC conditioned media using recombinant human MIF or endogenous human MIF generated from BMDMs of $CATT_7$ transgenic mice that were challenged with HDM for 3 weeks. HDM-challenged WT and MIF knockout ($MIF^{-/-}$) mice that do not express human MIF were used as controls. B, Levels of hMIF detected in the BMDMs of $MIF^{-/-}$, WT, and $CATT_7$ mice challenged with 25 μg of HDM for 3 weeks. ($n = 3$–6 mice). (C) Human VEGF protein levels in MSC conditioned media supernatants, measured by ELISA, after licensing with different concentrations of recombinant human MIF (1, 100, and 400 ng/mL). (D) Human VEGF protein levels in MIF MSC conditioned media supernatants, using bone marrow-derived supernatants from high MIF expressing $CATT_7$ mice, $MIF^{-/-}$ mice, or WT mice ($n = 3$–6). Data are presented as mean ± SEM and represent three independent experiments. Statistical significance was determined by one-way ANOVA; ns = non-significant; $^*p < 0.05$, $^{***}p < 0.001$, $^{****}p < 0.0001$.

MSCs (Figure 3C). Thus, these data conclude that MIF signaling through CXCR4, but not CXCR2 or CD74 leads to enhanced VEGF production in MSCs.

3.4 | Endogenous $CATT_7$-MIF MSC Conditioned Media Drives Bronchial Epithelial Wound Closure in a VEGF-Dependent Manner

In the asthmatic lung, repeated exacerbations can inflict injury on the membrane epithelium of the lung. Furthermore, the role of VEGF in wound healing is established in a variety of different conditions [62–64], such as type 1 diabetes [65] and pulmonary fibrosis [66]. We have shown that the increased levels of VEGF observed in CM from rhMIF-licensed MSCs (Figure 2C) and endogenous $CATT_7$-MSC CM (Figure 2D) drive airway epithelial cell wound closure in human alveolar basal epithelial cells; A549s (Figure S2B,C). Using the more physiologically relevant normal human bronchial epithelial cell line (BEAS-2B), we show that $CATT_7$-MSC CM significantly increased the percentage of wound closure compared with WT-MSC CM and cDMEM groups (Figure 4A) (Table S1). To validate the role of VEGF in bronchial epithelial wound closure, a potent and specific VEGFR2 inhibitor, SU-5416 was used to block the VEGF receptor on the surface of epithelial cells prior to the addition of $CATT_7$-MSC CM (Figure 4A). Blocking VEGFR2 on BEAS-2B cells attenuated the significant enhancement of wound closure mediated by $CATT_7$-MSC CM, but not WT-MSC CM (Figure 4A,B), illustrating the importance of human $CATT_7$ MIF licensing in MSC-derived VEGF production and BEAS-2B wound closure, and that murine MIF does not drive wound closure in a VEGF-dependent manner. Similarly, the application of SU-5416 to A549s demonstrated the important role of MIF licensing on MSC's cytoprotective abilities (Figure S2B,C). BEAS-2B cells pretreated with the vehicle control prior to the addition of $CATT_7$-MIF MSC CM maintained a significant increase in percentage wound closure mediated by

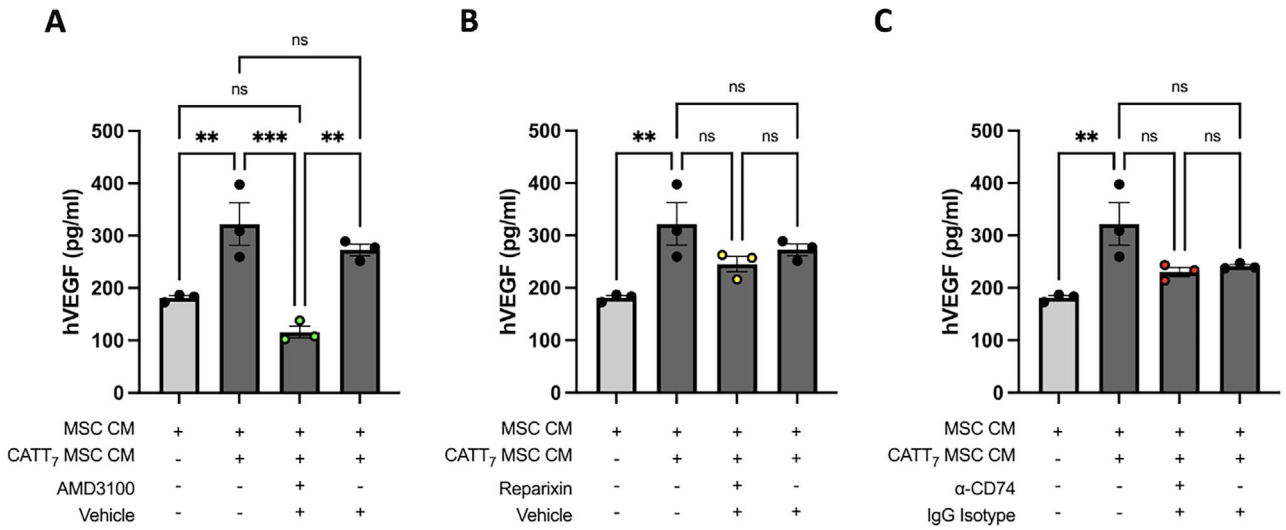

FIGURE 3 | MIF signaling through CXCR4, but not CXCR2 or CD74 leads to enhanced VEGF production in MSCs. MIF MSC conditioned media was generated by licensing MSCs with endogenous human MIF secreted by BMDMs of HDM-challenged $CATT_7$ transgenic mice. To investigate the MIF receptor involved in enhanced VEGF production by MSCs, inhibitors of (A) CXCR4 (AMD3100), (B) CXCR2 (reparixin), or (C) a CD74 neutralizing antibody were used. Prior to endogenous MIF licensing, MSCs were exposed to inhibitors, vehicle control (DMSO), or IgG Isotype control for 30 min. After 24 h, media was removed and cells were washed with PBS before being replaced with serum-free media for 48 h. VEGF production was measured by human VEGF ELISA. Data are presented as mean ± SEM and represent three independent experiments. Statistical significance was determined by one-way ANOVA; ns = non-significant; $^{*}p < 0.05$, $^{**}p < 0.01$, $^{***}p < 0.001$, $^{****}p < 0.0001$.

$CATT_7$-MIF MSC CM. The use of a VEGFR2 inhibitor had no off-target, non-specific effects on the general growth of these cells, as cDMEM wells treated with SU-5416 had no significant difference in percentage wound closure compared with cDMEM alone (Figure 4A). The increase in wound closure associated with CM from $CATT_7$-MIF licensed MSCs is illustrated in Figure 4B. Furthermore, when the VEGFR2 was blocked using SU-5416 but not vehicle control, the inhibition of wound closure was clear (Figure 4B).

To prove that conditioned media from another cell type could not facilitate enhanced wound closure in alveolar epithelial cells, or that a positive VEGF feedback loop in A549 conditioned media was encouraging self-renewal of these cells, conditioned media from A549 cells was used as a negative control. A549 conditioned media did not significantly increase the percentage of wound closure in A549 epithelial cells (Figure S2B,C).

We have elucidated that human, but not murine, MIF drives VEGF production from MSCs (Figure 4F) and thus facilitates a significant increase in wound closure (Figure 4A,B). We performed experiments to determine the effect of SU-5416 on the proliferation of BEAS-2B cells. In wound closure experiments, the addition of SU-5416 had no significant effect on BEAS-2B cells cultured in cDMEM (Figure 4C); however, SU-5416 significantly reduced wound closure mediated by $CATT_7$ MSC-CM (Figure 4C). We also used mitomycin C, a cell cycle antagonist to inhibit cell proliferation. We show that the addition of mitomycin C significantly reduced wound closure mediated by $CATT_7$ MSC-CM (Figure 4C). We also examined the expression of two genes associated with proliferation; *pcna* and *ki67*. $CATT_7$ MSC-CM significantly increased the expression of *pcna* and *ki67* in BEAS-2B cells (Figure 4D,E). While SU-5416 had no significant effect on BEAS-2B cells exposed to $CATT_7$ MSC-CM, the addition of mitomycin C significantly decreased the expression of *pcna* and *ki67* (Figure 4D,E). Together, these findings support a role for both migration and proliferation in the enhancement of wound closure mediated by $CATT_7$ MSC-CM.

To fully elucidate this MIF-associated effect on MSC CM increase in wound closure, an MIF inhibitor SCD-19 was used to block MIF's biological activity prior to MSC licensing. When endogenous $CATT_7$ MIF supernatants were incubated with 100 μM of SCD-19 for 1 h prior to MSC licensing, MIF inhibition significantly decreased MSC-mediated VEGF production compared with cDMEM controls (Figure 4F). Importantly, SCD-19 did not affect WT-derived MIF supernatants, as no significant difference in VEGF production was noted.

SCD-19, but not vehicle control, effectively decreased the capacity for $CATT_7$-MSC CM to enhance wound closure in bronchial epithelial cells (Figure 4G,H). These data conclude that high levels of human MIF from $CATT_7$ BMDM-derived supernatants can license MSCs to produce increased levels of VEGF (Figures 2D and 4F), with increased efficacy than those licensed with recombinant MIF (Figure 2C). Following this narrative, conditioned media generated from endogenous human MIF-licensed MSCs can significantly increase wound closure in BEAS-2B cells in a VEGF-dependent manner (Figure 4A,B), illustrating MIF's specific role through utilising a potent MIF antagonist SCD-19 (Figure 4G,H).

3.5 | VEGF Produced by MIF-Licensed MSCs Reduces HDM-Induced Goblet Cell Hyperplasia

VEGF, specifically through VEGFR2 (KDR) signalling, has previously been shown to protect against goblet cell metaplasia

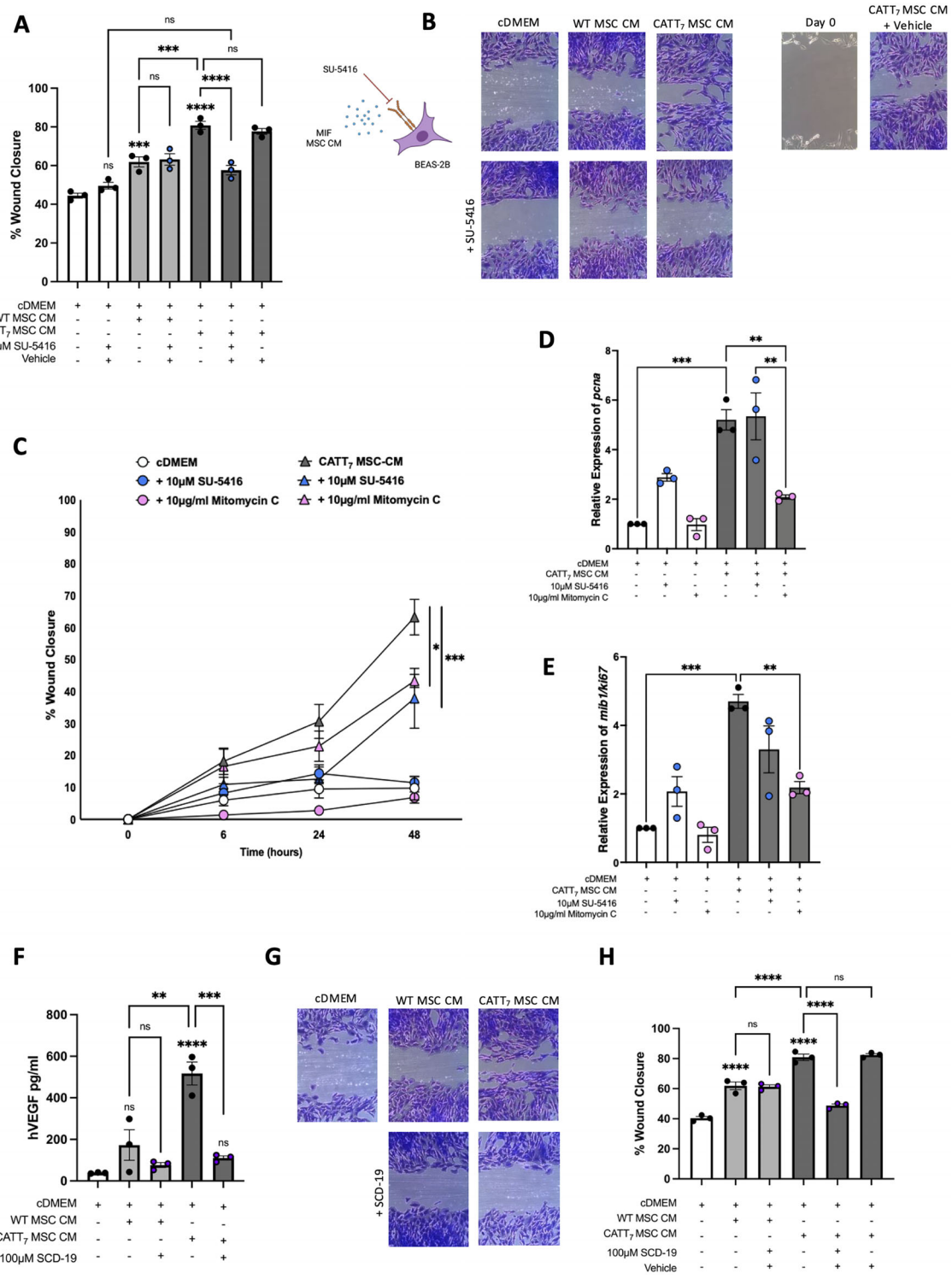

FIGURE 4 | Endogenous $CATT_7$-MIF MSC conditioned media drives bronchial epithelial wound closure in a VEGF-dependent manner. Using a human bronchial epithelial cell line (BEAS-2B), a scratch assay was carried out to investigate the impact of MIF MSC CM in bronchial cell wound closure. A, B, A VEGFR2 inhibitor SU-5416 (10 μM) or vehicle control (DMSO) was added to BEAS-2B for 4 h prior to the addition of WT or $CATT_7$ MIF MSC CM. C, The cell cycle inhibitor mitomycin C (10 μg/mL) was added to BEAS-2B for 2 h before being washed off with PBS prior to the addition of cDMEM or $CATT_7$ MIF MSC CM. Wound healing was quantified at 6, 24, and 48 h and cells were harvested for gene expression analysis of (D) *pcna* and (E) *ki67* at 48 h. F–H, To block MIF activity, a MIF inhibitor SCD-19 (100 μM) or vehicle control (DMSO) was added to WT and $CATT_7$ BMDM supernatants for 1 h before being added to BEAS-2B cells. After 48 h, or until the first scratch had closed, media was removed and cells were fixed with 10% neutral buffered formalin and stained with crystal violet before being imaged using Optika imaging software on a Nikon imaging microscope. Percentage wound closure relative to day 0 baseline was calculated using Image J software. Data are presented as mean ± SEM and represent three independent experiments. Statistical significance was determined by one-way ANOVA in (A, D–F, H) and two-way ANOVA in (C); ns = non-significant; $^*p < 0.05$, $^{**}p < 0.01$, $^{***}p < 0.001$, $^{****}p < 0.0001$.

during processes of goblet cell renewal [67]. Thus, we set out to investigate the therapeutic capacity of VEGF present in $CATT_7$-MIF MSC CM in an HDM model of allergic airway inflammation. To elucidate the specific role of MSC-derived VEGF in vivo, an anti-human VEGF neutralising antibody or IgG isotype control was used (Figure 5A).

After MSC CM and $CATT_7$-MIF MSC CM were generated as previously described (Figure 2A), supernatants were concentrated using ultracentrifugal filters with a molecular cut-off of 50 kDa (VEGF molecular weight: 45 kDa) to allow for intranasal administration on day 14 of the HDM model (Figure 5A). To neutralise MSC-derived VEGF present in conditioned media, a bevacizumab biosimilar anti-VEGF monoclonal antibody or IgG isotype control was added to the supernatant at 8 ng/mL prior to I.N. administration on day 14.

To ensure the efficacy of the VEGF neutralising antibody, VEGF protein in the MSC CM was measured using a human VEGF ELISA. As expected, $CATT_7$ MSC CM contained significantly elevated levels of VEGF compared with that present in conditioned media from unlicensed MSCs (Figure 5B). $CATT_7$ MSC CM + α-VEGF had a significantly decreased concentration of VEGF present, compared with both $CATT_7$ MSC CM, and $CATT_7$ MSC CM + IgG isotype control (Figure 5B).

To investigate the therapeutic role of $CATT_7$ MSC CM in a model of HDM-induced allergic asthma, lungs were harvested on day 21 and processed for histological analysis, tissue sections were stained with PAS to visualise and measure levels of airway goblet cell hyperplasia. $CATT_7$ MSC CM, but not MSC CM significantly reduced HDM-induced goblet cell hyperplasia (Figure 5C,D), reiterating the importance of human MIF in licensing MSC's cytoprotective efficacy. However, administration of $CATT_7$ MSC CM treated with α-VEGF neutralising antibody, but not an IgG control antibody could no longer significantly decrease the number of PAS-positive cells in HDM-challenged mice, demonstrating the role of VEGF in epithelial protection against goblet cell hyperplasia. This study demonstrates that MIF-licensing significantly increases VEGF production by MSCs which is responsible for the enhanced cytoprotective effects of $CATT_7$-licensed MSC CM in airway epithelial cells in vitro and in a clinically relevant pre-clinical model of HDM-induced allergic airway inflammation.

4 | Discussion

This study set out to investigate the cytoprotective mechanisms associated with the MIF-licensed MSC secretome in the context of epithelial injury in vitro and in vivo. Human BM-MSCs express the canonical (CD74) and non-canonical (CXCR2 and CXCR4) MIF receptors allowing MSCs to respond to MIF present in the microenvironment. Previously, we have demonstrated that MIF can promote the expansion and immunosuppressive function of human BM-MSCs in vitro and significantly increase the retention of human BM-MSCs in vivo in an HDM model of allergic asthma [42]. MIF signals through different receptors depending on the function. We have previously shown that CD74 is required for MIF-licensed MSC immunomodulation and to significantly increase the retention of human BM-MSCs in vivo in an HDM model of allergic asthma [42]. Differentially, CXCR4 has been shown to mediate MSC chemotaxis to MIF [68]. Here we show that MIF-licensing significantly enhances MSC secretion of VEGF in a CXCR4-dependent manner. In addition to rhMIF, endogenous human MIF produced by $CATT_7$ BMDMs also had the capacity to license MSCs leading to significantly increased MSC-derived VEGF secretion. Importantly, the use of WT BMDM CM to license MSCs did not have the same effect. This novel finding indicates that human, but not murine, MIF boosts the production of MSC-derived VEGF. This supports the idea that the communication between exogenously administered MSCs and macrophages plays an important role in dictating MSC therapeutic effects.

MIF has previously been shown to upregulate VEGF production in the conditioned media of synovial fluid mononuclear cells [69] and endometrial stromal cells [70] promoting new blood vessel formation. Functionally, $CATT_7$-MIF licensed MSC CM exerted superior wound healing capacity in normal bronchial epithelial cells (BEAS-2Bs) compared with naive MSC CM or WT-licensed MSC CM. MSC CM has been previously shown to promote wound healing in airway epithelial cells via growth factors including HGF and KGF [23, 71].

Our group and others have highlighted the importance of licensing MSCs to enhance their therapeutic efficacy [42, 72, 73], however, less is understood about the influence of licensing approaches on MSC cytoprotective functions. Licensing approaches using IFNγ and hypoxia [74], or IFNγ and TNFα [75] have previously been used to enhance the cytoprotective/wound healing properties of MSC CM. VEGF production from MSCs has been shown to be increased by licensing MSCs with hypoxia [76–80], fibroblast growth factor-2 [81], TGF-α [82], IL-1β [83], and LPS [84]. However, we are the first to demonstrate enhanced VEGF production from MSCs licensed with human MIF, a clinically relevant proinflammatory cytokine in a range of inflammatory diseases including asthma.

Blockade of MIF using the small molecule inhibitor, demonstrated the specificity of MIF in licensing MSCs to produce significantly increased levels of VEGF. This provides a novel mechanistic insight into how MIF can license MSCs and enhance their cytoprotective function, specifically their ability to provide protection against a dysregulated airway epithelial barrier and thus, also prevent the development of airway goblet cell hyperplasia after allergen challenge in vivo. The limitation of our study is that although we show a role for MSC-CM-derived VEGF, we have not identified the mechanism of how this MSC-CM-derived VEGF contributes to the repair of HDM-induced epithelial damage in mice. Moreover, our findings of effects mediated by human VEGF on mouse epithelial cells in vivo add further complexity. However, human VEGF has been shown to act on mouse epithelial cells both in vitro and in vivo [85, 86].

VEGF has historically played a central role in epithelial repair and the maintenance of epithelial barrier integrity, where VEGF-deficient mice had increased levels of bronchial and alveolar apoptosis [87]. VEGF enhanced wound healing, survival, and proliferation of airway epithelial cells [88, 89]. Furthermore, VEGF overexpression reduced bleomycin-induced cell death in a model of idiopathic pulmonary fibrosis [66]. Interestingly, VEGF-A and

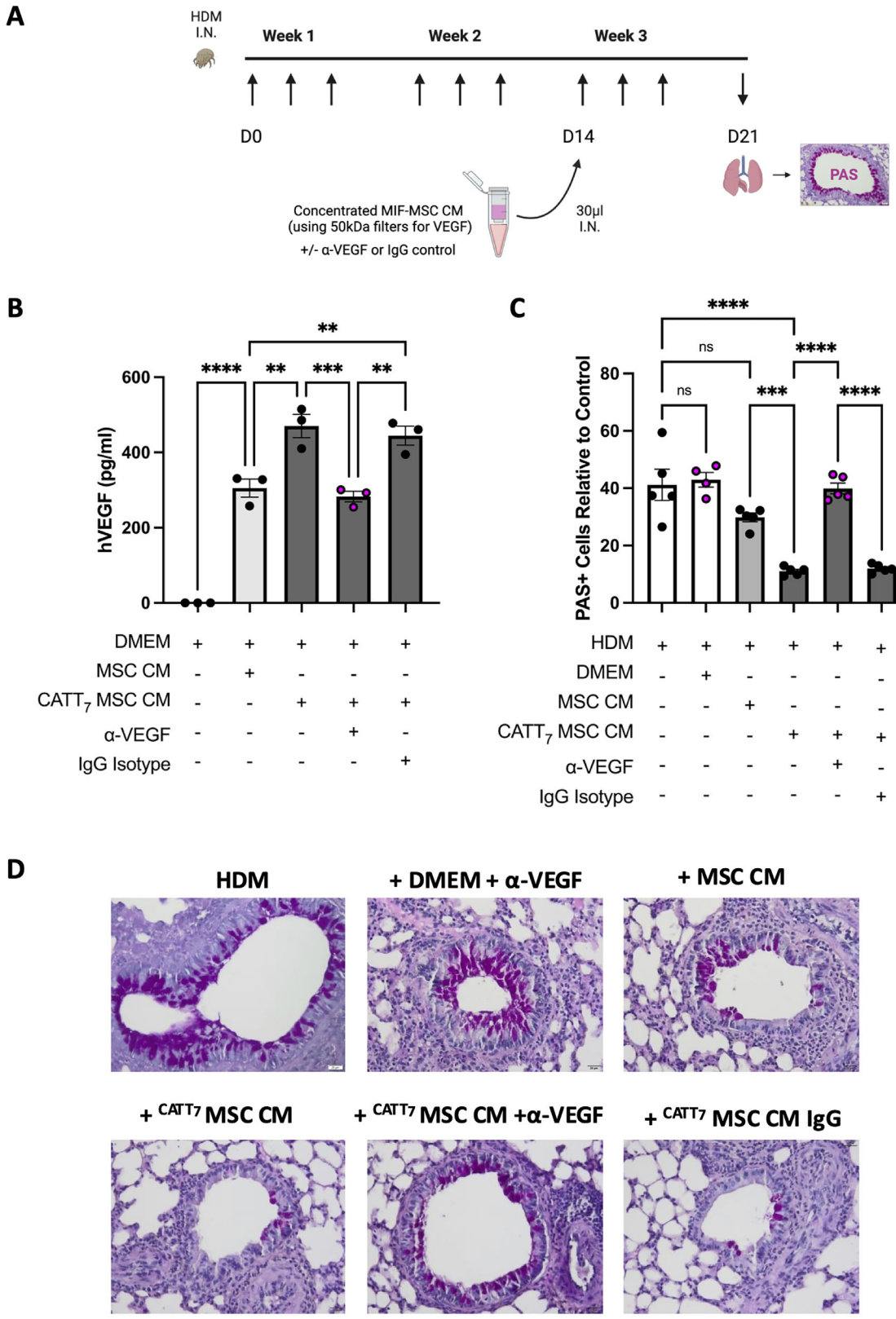

FIGURE 5 | VEGF produced by MIF-licensed MSCs reduces HDM-induced goblet cell hyperplasia. A, $CATT_7$ mice were challenged with 25 µg of HDM intranasally I.N. three times a week for 3 weeks. MIF MSC CM containing VEGF was concentrated using 50 kDa Amicon filters. A, VEGF-neutralizing antibody (8 ng/mL) or IgG isotype control was added before intranasal administration on day 14. B, VEGF levels were measured by VEGF ELISA. C, D, Lungs were harvested on day 21 for histological analysis by staining goblet cells with periodic acid Schiff (PAS). Slides were imaged and the number of PAS-positive cells (magenta) relative to the control were quantified using ImageJ software. $N = 4–5$ mice per group. Data are presented as mean ± SEM. Statistical significance was determined by one-way ANOVA; ns = non-significant, $^{**}p < 0.01$, $^{***}p < 0.001$, $^{****}p < 0.0001$.

its receptor VEGFR2 have been shown to have a protective role in the defence against mucous cell metaplasia, commonly documented in asthma and cystic fibrosis [67]. In asthma, if VEGF-A levels are decreased, the transcription factor Sox9 is upregulated, driving the club to goblet cell differentiation, exacerbating disease [67]. These studies, along with the data presented throughout this manuscript depict the protective role of VEGF in the repair and regulation of the airway epithelial barrier, decreasing goblet cell hyperplasia after the HDM challenge in vivo.

In the lung, there has been evidence of MSC-derived VEGF having a protective role in acute lung injury [90, 91]; however, the effect of MSC-secreted VEGF in allergic asthma is unknown. Thus, this manuscript is the first to demonstrate the impact of MSC-VEGF on epithelial cells in vitro, and in vivo in a clinically relevant model of HDM-induced acute allergic asthma.

Author Contributions

Hazel Dunbar performed research, analysed the data, designed the study, and wrote the manuscript. Ian J. Hawthorne performed research, analysed the data, and designed the study. Courteney Tunstead performed research and analysed the data. Molly Dunlop and Evelina Volkova performed research. Daniel J. Weiss and Claudia C. dos Santos contributed to the study design and data analysis. Seamas C. Donnelly and Michelle E. Armstrong provided reagents and contributed to the study design and data analysis. Karen English designed and supervised the study and wrote the manuscript. All authors approved the final manuscript.

Acknowledgements

This research was supported by an Irish Research Council Laureate Award to KE (IRCLA/2017/288). This publication has emanated from research supported in part by a COVID HEA research grant from Maynooth University, a research grant from Science Foundation Ireland (SFI) under grant 12/RI/2346, an infrastructure award supporting the Attune Nxt.

Open access funding provided by IReL.

Conflicts of Interest

The authors declare no conflicts of interest.

Data Availability Statement

The data that support the findings of this study are available from the corresponding author upon reasonable request.

Peer review

The peer review history for this article is available at https://publons.com/publon/10.1002/eji.202451205.

References

1. C. L. Li, Z. B. Xu, X. L. Fan, et al., "MicroRNA-21 Mediates the Protective Effects of Mesenchymal Stem Cells Derived From iPSCs to Human Bronchial Epithelial Cell Injury Under Hypoxia," *Cell Transplantation* 27, no. 3 (2018): 571–583.

2. T. Ahmad, S. Mukherjee, B. Pattnaik, et al., "Miro1 regulates Intercellular Mitochondrial Transport & Enhances Mesenchymal Stem Cell Rescue Efficacy," *Embo Journal* 33, no. 9 (2014): 994–1010.

3. T. J. Morrison, M. V. Jackson, E. K. Cunningham, et al., "Mesenchymal Stromal Cells Modulate Macrophages in Clinically Relevant Lung Injury Models by Extracellular Vesicle Mitochondrial Transfer," *American Journal of Respiratory and Critical Care Medicine* 196, no. 10 (2017): 1275–1286.

4. Y. Yao, X. L. Fan, D. Jiang, et al., "Connexin 43-Mediated Mitochondrial Transfer of iPSC-MSCs Alleviates Asthma Inflammation," *Stem Cell Reports* 11, no. 5 (2018): 1120–1135.

5. F. F. Cruz, Z. D. Borg, M. Goodwin, et al., "Systemic Administration of Human Bone Marrow-Derived Mesenchymal Stromal Cell Extracellular Vesicles Ameliorates Aspergillus Hyphal Extract-Induced Allergic Airway Inflammation in Immunocompetent Mice," *Stem Cells Translational Medicine* 4, no. 11 (2015): 1302–1316.

6. K. S. Park, E. Bandeira, G. V. Shelke, C. Lässer, and J. Lötvall, "Enhancement of Therapeutic Potential of Mesenchymal Stem Cell-Derived Extracellular Vesicles," *Stem Cell Research & Therapy* 10 (2019): 288.

7. C. C. Dos Santos, M. Lopes-Pacheco, K. English, S. Rolandsson Enes, A. Krasnodembskaya, and P. R. M. Rocco, "The MSC-EV-microRNAome: A Perspective on Therapeutic Mechanisms of Action in Sepsis and ARDS," *Cells* 13, no. 2 (2024): 122.

8. K. English, "Mechanisms of Mesenchymal Stromal Cell Immunomodulation," *Immunology and Cell Biology* 91, no. 1 (2013): 19–26.

9. I. Szabłowska-Gadomska, S. Rudziński, and M. Dymowska, "Secretome of Mesenchymal Stromal Cells as a Possible Innovative Therapeutic Tool in Facial Nerve Injury Treatment," *BioMed Research International* 2023 (2023): 8427200.

10. J. Xia, S. Minamino, K. Kuwabara, and S. Arai, "Stem Cell Secretome as a New Booster for Regenerative Medicine," *BioScience Trends* 13, no. 4 (2019): 299–307.

11. J. Liu, X. Qiu, Y. Lv, et al., "Apoptotic Bodies Derived From Mesenchymal Stem Cells Promote Cutaneous Wound Healing via Regulating the Functions of Macrophages," *Stem Cell Research & Therapy* 11, no. 1 (2020): 507.

12. G. Műzes and F. Sipos, "Mesenchymal Stem Cell-Derived Secretome: A Potential Therapeutic Option for Autoimmune and Immune-Mediated Inflammatory Diseases," *Cells* 11, no. 15 (2022): 2300.

13. S. H. M. Pang, J. D'Rozario, S. Mendonca, et al., "Mesenchymal Stromal Cell Apoptosis Is Required for Their Therapeutic Function," *Nature Communications* 12, no. 1 (2021): 6495.

14. D. J. Weiss, K. English, A. Krasnodembskaya, J. M. Isaza-Correa, I. J. Hawthorne, and B. P. Mahon, "The Necrobiology of Mesenchymal Stromal Cells Affects Therapeutic Efficacy," *Frontiers in Immunology* 10 (2019): 1228.

15. K. English, "Apoptotic MSCs, COX2/PGE2 and Clinical Efficacy in Crohn Fistula," *Molecular Therapy* 31, no. 12 (2023): 3364–3366.

16. Q. Ge, H. Zhang, J. Hou, et al., "VEGF Secreted by Mesenchymal Stem Cells Mediates the Differentiation of Endothelial Progenitor Cells Into Endothelial Cells via Paracrine Mechanisms," *Molecular Medicine Reports* 17, no. 1 (2018): 1667–1675.

17. Y. Han, J. Yang, J. Fang, et al., "The Secretion Profile of Mesenchymal Stem Cells and Potential Applications in Treating human Diseases," *Signal Transduction and Targeted Therapy* 7, no. 1 (2022): 1–19.

18. I. Kozhukharova, N. Minkevich, L. Alekseenko, A. Domnina, and O. Lyublinskaya, "Paracrine and Autocrine Effects of VEGF Are Enhanced in Human eMSC Spheroids," *International Journal of Molecular Sciences* 23, no. 22 (2022): 14324.

19. M. E. Healy, R. Bergin, B. P. Mahon, and K. English, "Mesenchymal Stromal Cells Protect Against Caspase 3-mediated Apoptosis of CD19(+) Peripheral B Cells Through Contact-dependent Upregulation of VEGF," *Stem Cells and Development* 24, no. 20 (2015): 2391–2402.

20. E. F. Cahill, L. M. Tobin, F. Carty, B. P. Mahon, and K. English, "Jagged-1 Is Required for the Expansion of CD4+ CD25+ FoxP3+ Regulatory T Cells and Tolerogenic Dendritic Cells by Murine Mesenchymal Stromal Cells," *Stem Cell Research & Therapy* 6, no. 1 (2015): 19.

21. K. English, J. M. Ryan, L. Tobin, M. J. Murphy, F. P. Barry, and B. P. Mahon, "Cell Contact, Prostaglandin E(2) and Transforming Growth Factor Beta 1 Play Non-redundant Roles in human Mesenchymal Stem Cell Induction of CD4+CD25(High) Forkhead Box P3+ Regulatory T Cells," *Clinical and Experimental Immunology* 156, no. 1 (2009): 149–160.

22. H. Kennelly, B. P. Mahon, and K. English, "Human Mesenchymal Stromal Cells Exert HGF Dependent Cytoprotective Effects in a Human Relevant Pre-clinical Model of COPD," *Scientific Reports* 6 (2016): 38207.

23. E. F. Cahill, H. Kennelly, F. Carty, B. P. Mahon, and K. English, "Hepatocyte Growth Factor Is Required for Mesenchymal Stromal Cell Protection Against Bleomycin-Induced Pulmonary Fibrosis," *Stem Cells Translational Medicine* 5, no. 10 (2016): 1307–1318.

24. L. Ionescu, R. N. Byrne, T. van Haaften, et al., "Stem Cell Conditioned Medium Improves Acute Lung Injury in Mice: In Vivo Evidence for Stem Cell Paracrine Action," *American Journal of Physiology Lung Cellular and Molecular Physiology* 303, no. 11 (2012): L967–977.

25. S. Y. Kim, J. H. Lee, H. J. Kim, et al., "Mesenchymal Stem Cell-conditioned media Recovers Lung Fibroblasts From Cigarette Smoke-induced Damage," *American Journal of Physiology Lung Cellular and Molecular Physiology* 302, no. 9 (2012): L891–908.

26. D. Kruk, M. Wisman, J. A. Noordhoek, et al., "Paracrine Regulation of Alveolar Epithelial Damage and Repair Responses by Human Lung-Resident Mesenchymal Stromal Cells," *Cells* 10, no. 11 (2021): 2860.

27. A. Moreira, R. Naqvi, K. Hall, et al., "Effects of Mesenchymal Stromal Cell-conditioned media on Measures of Lung Structure and Function: A Systematic Review and Meta-analysis of Preclinical Studies," *Stem Cell Research & Therapy* 11, no. 1 (2020): 399.

28. V. Y. F. Su, C. S. Lin, S. C. Hung, and K. Y. Yang, "Mesenchymal Stem Cell-Conditioned Medium Induces Neutrophil Apoptosis Associated With Inhibition of the NF-κB Pathway in Endotoxin-Induced Acute Lung Injury," *International Journal of Molecular Sciences* 20, no. 9 (2019): 2208.

29. Z. Zhou, Y. Hua, Y. Ding, et al., "Conditioned Medium of Bone Marrow Mesenchymal Stem Cells Involved in Acute Lung Injury by Regulating Epithelial Sodium Channels via miR-34c," *Frontiers in Bioengineering and Biotechnology* 9 (2021): 640116.

30. L. Boland, A. J. Burand, A. J. Brown, D. Boyt, V. A. Lira, and J. A. Ankrum, "IFN-γ and TNF-α Pre-licensing Protects Mesenchymal Stromal Cells From the Pro-inflammatory Effects of Palmitate," *Molecular Therapy* 26, no. 3 (2018): 860–873.

31. D. T. Boyt, L. K. Boland, A. J. Burand, A. J. Brown, and J. A. Ankrum, "Dose and Duration of Interferon γ Pre-licensing Interact With Donor Characteristics to Influence the Expression and Function of Indoleamine-2,3-dioxygenase in Mesenchymal Stromal Cells," *Journal of the Royal Society, Interface* 17, no. 167 (2020): 20190815.

32. C. AÉS, S. MRR, T. Alencar-Silva, J. L. Carvalho, and F. Saldanha-Araujo, "Mesenchymal Stem Cells Immunomodulation: The Road to IFN-γ Licensing and the Path Ahead," *Cytokine & Growth Factor Reviews* 47 (2019): 32–42.

33. H. Y. Cheng, M. R. Anggelia, C. H. Lin, and C. F. Lin, "Preconditioned Mesenchymal Stromal Cells to Improve Allotransplantation Outcome," *Cells* 10, no. 9 (2021): 2325.

34. H. Dunbar, D. J. Weiss, S. Rolandsson Enes, J. G. Laffey, and K. English, "The Inflammatory Lung Microenvironment; a Key Mediator in MSC Licensing," *Cells* 10, no. 11 (2021): 2982.

35. M. Á. de Pedro, M. Gómez-Serrano, F. Marinaro, et al., "IFN-Gamma and TNF-Alpha as a Priming Strategy to Enhance the Immunomodulatory Capacity of Secretomes From Menstrual Blood-Derived Stromal Cells," *International Journal of Molecular Sciences* 22, no. 22 (2021): 12177.

36. A. Hackel, S. Vollmer, K. Bruderek, S. Lang, and S. Brandau, "Immunological Priming of Mesenchymal Stromal/Stem Cells and Their Extracellular Vesicles Augments Their Therapeutic Benefits in Experimental Graft-versus-host Disease via Engagement of PD-1 Ligands," *Frontiers in Immunology* 14 (2023): 1078551.

37. C. Noronha N de, A. Mizukami, C. Caliári-Oliveira, et al., "Priming Approaches to Improve the Efficacy of Mesenchymal Stromal Cell-based Therapies," *Stem Cell Research & Therapy* 10, no. 1 (2019): 131.

38. Y. Mizue, S. Ghani, L. Leng, et al., "Role for Macrophage Migration Inhibitory Factor in Asthma," *PNAS* 102, no. 40 (2005): 14410–14415.

39. B. J. Plant, C. G. Gallagher, R. Bucala, et al., "Cystic Fibrosis, Disease Severity, and a Macrophage Migration Inhibitory Factor Polymorphism," *American Journal of Respiratory and Critical Care Medicine* 172, no. 11 (2005): 1412–1415.

40. J. A. Baugh, S. Chitnis, S. C. Donnelly, et al., "A Functional Promoter Polymorphism in the Macrophage Migration Inhibitory Factor (MIF) Gene Associated With Disease Severity in Rheumatoid Arthritis," *Genes and Immunity* 3, no. 3 (2002): 170–176.

41. H. Dunbar, I. J. Hawthorne, C. Tunstead, M. E. Armstrong, S. C. Donnelly, and K. English, "Blockade of MIF Biological Activity Ameliorates House Dust Mite-induced Allergic Airway Inflammation in Humanized MIF Mice," *Faseb Journal* 37, no. 8 (2023): e23072.

42. I. J. Hawthorne, H. Dunbar, C. Tunstead, et al., "Human Macrophage Migration Inhibitory Factor Potentiates Mesenchymal Stromal Cell Efficacy in a Clinically Relevant Model of Allergic Asthma," *Molecular Therapy* 31, no. 11 (2023): 3243–3258.

43. N. K. Altorki, G. J. Markowitz, D. Gao, et al., "The Lung Microenvironment: An Important Regulator of Tumour Growth and Metastasis," *Nature Reviews Cancer* 19, no. 1 (2019): 9–31.

44. A. Hsieh, N. Assadinia, and T. L. Hackett, "Airway Remodeling Heterogeneity in Asthma and Its Relationship to Disease Outcomes," *Frontiers in Physiology* 14 (2023): 1113100.

45. A. L. Tatler, "Asthmatic Airway Remodeling: Long Overlooked but Too Important to Ignore," *Annals of Translational Medicine* 11, no. 2 (2023): 29.

46. G. Varricchi, S. Ferri, J. Pepys, R. Poto, G. Spadaro, E. Nappi, et al., "Biologics and Airway Remodeling in Severe Asthma," *Allergy* 77, no. 12 (2022): 3538–3552.

47. X. Ke, D. C. Do, C. Li, et al., "Ras Homolog family Member A/Rho-associated Protein Kinase 1 Signaling Modulates Lineage Commitment of Mesenchymal Stem Cells in Asthmatic Patients Through Lymphoid Enhancer-binding Factor 1," *Journal of Allergy and Clinical Immunology* 143, no. 4 (2019): 1560–1574.

48. X. Yu, L. Yu, B. Guo, R. Chen, and C. Qiu, "A Narrative Review of Research Advances in Mesenchymal Stem Cell Therapy for Asthma," *Annals of Translational Medicine* 8, no. 21 (2020): 1461.

49. S. Pati, A. Y. Khakoo, J. Zhao, et al., "Human Mesenchymal Stem Cells Inhibit Vascular Permeability by Modulating Vascular Endothelial Cadherin/β-Catenin Signaling," *Stem Cells and Development* 20, no. 1 (2011): 89–101.

50. B. R. Zhou, Y. Xu, S. L. Guo, et al., "The Effect of Conditioned media of Adipose-derived Stem Cells on Wound Healing After Ablative Fractional Carbon Dioxide Laser Resurfacing," *BioMed Research International* 2013 (2013): 519126.

51. J. J. Shin, W. Fan, J. Par-Young, et al., "MIF Is a Common Genetic Determinant of COVID-19 Symptomatic Infection and Severity," *Qjm* 116, no. 3 (2023): 205–212.

52. L. Mawhinney, M. E. Armstrong, C. O' Reilly, et al., "Macrophage Migration Inhibitory Factor (MIF) Enzymatic Activity and Lung Cancer," *Molecular Medicine* 20, no. 1 (2015): 729–735.

53. A. Tynan, L. Mawhinney, M. E. Armstrong, et al., "Macrophage Migration Inhibitory Factor Enhances Pseudomonas aeruginosa Biofilm Formation, Potentially Contributing to Cystic Fibrosis Pathogenesis," *Faseb Journal* 31, no. 11 (2017): 5102–5110.

54. A. Trivedi, M. Lin, B. Miyazawa, et al., "Inter- and Intra-donor Variability in Bone Marrow–derived Mesenchymal Stromal Cells: Implications for Clinical Applications," *Cytotherapy* 26, no. 9 (2024): 1062–1075.

55. K. Lynch, O. Treacy, X. Chen, et al., "TGF-β1-Licensed Murine MSCs Show Superior Therapeutic Efficacy in Modulating Corneal Allograft Immune Rejection in Vivo," *Molecular Therapy* 28, no. 9 (2020): 2023–2043.

56. C. Tunstead, E. Volkova, H. Dunbar, et al., "The ARDS Microenvironment Enhances MSC-induced Repair via VEGF in Experimental Acute Lung Inflammation," *Molecular Therapy [Internet]*, https://www.sciencedirect.com/science/article/pii/S1525001624005252.

57. M. Bacher, C. N. Metz, T. Calandra, et al., "An Essential Regulatory Role for Macrophage Migration Inhibitory Factor in T-cell Activation," *PNAS* 93, no. 15 (1996): 7849–7854.

58. J. Bernhagen, R. A. Mitchell, T. Calandra, W. Voelter, A. Cerami, and R. Bucala, "Purification, Bioactivity, and Secondary Structure Analysis of Mouse and human Macrophage Migration Inhibitory Factor (MIF)," *Biochemistry* 33, no. 47 (1994): 14144–14155.

59. T. Calandra, J. Bernhagen, R. A. Mitchell, and R. Bucala, "The Macrophage Is an Important and Previously Unrecognized Source of Macrophage Migration Inhibitory Factor," *Journal of Experimental Medicine* 179, no. 6 (1994): 1895–1902.

60. T. Calandra and T. Roger, "Macrophage Migration Inhibitory Factor: A Regulator of Innate Immunity," *Nature Reviews Immunology* 3, no. 10 (2003): 791–800.

61. I. Arutyunyan, T. Fatkhudinov, E. Kananykhina, et al., "Role of VEGF-A in Angiogenesis Promoted by Umbilical Cord-derived Mesenchymal Stromal/Stem Cells: In Vitro Study," *Stem Cell Research & Therapy* 7 (2016): 46.

62. K. E. Johnson and T. A. Wilgus, "Vascular Endothelial Growth Factor and Angiogenesis in the Regulation of Cutaneous Wound Repair," *Adv Wound Care (New Rochelle)* 3, no. 10 (2014): 647–661.

63. L. A. DiPietro, "Angiogenesis and Wound Repair: When Enough Is Enough," *J Leukoc Biol* 100, no. 5 (2016): 979–984.

64. F. Shams, H. Moravvej, S. Hosseinzadeh, et al., "Overexpression of VEGF in Dermal Fibroblast Cells Accelerates the Angiogenesis and Wound Healing Function: In Vitro and in Vivo Studies," *Scientific Reports* 12, no. 1 (2022): 18529.

65. M. J. V. White, P. S. Briquez, D. A. V. White, and J. A. V.-A. Hubbell, "PDGF-BB and HB-EGF Engineered for Promiscuous Super Affinity to the Extracellular Matrix Improve Wound Healing in a Model of Type 1 Diabetes," *Npj Regen Med* 6, no. 1 (2021): 1–12.

66. L. A. Murray, D. M. Habiel, M. Hohmann, et al., "Antifibrotic Role of Vascular Endothelial Growth Factor in Pulmonary Fibrosis," *JCI Insight* 2, no. 16: e92192.

67. M. Jiang, Y. Fang, Y. Li, et al., "VEGF Receptor 2 (KDR) Protects Airways From Mucus Metaplasia Through a Sox9-dependent Pathway," *Developmental Cell* 56, no. 11 (2021): 1646–1660.

68. S. Lourenco, V. H. Teixeira, T. Kalber, R. J. Jose, R. A. Floto, and S. M. Janes, "Macrophage Migration Inhibitory Factor-CXCR4 Is the Dominant Chemotactic Axis in human Mesenchymal Stem Cell Recruitment to Tumors," *Journal of Immunology* 194, no. 7 (2015): 3463–3474.

69. H. R. Kim, M. K. Park, M. L. Cho, C. H. Yoon, S. H. Lee, S. H. Park, L. Leng, R. Bucala, I. Kang, J. Choe, and H. Y. Kim, "Macrophage migration inhibitory factor upregulates angiogenic factors and correlates with clinical measures in rheumatoid arthritis" *J Rheumatol.* 34 no. 5: (2007): 927–936.

70. V. Veillat, C. Carli, C. N. Metz, Y. Al-Abed, P. H. Naccache, and A. Akoum, "Macrophage Migration Inhibitory Factor Elicits an Angiogenic Phenotype in human Ectopic Endometrial Cells and Triggers the Production of Major Angiogenic Factors via CD44, CD74, and MAPK Signaling Pathways," *Journal of Clinical Endocrinology and Metabolism* 95, no. 12 (2010): E403–412.

71. G. F. Curley, M. Hayes, B. Ansari, et al., "Mesenchymal Stem Cells Enhance Recovery and Repair Following Ventilator-induced Lung Injury in the Rat," *Thorax* 67, no. 6 (2012): 496–501.

72. F. Carty, H. Dunbar, I. J. Hawthorne, et al., "IFN-γ and PPARδ Influence the Efficacy and Retention of Multipotent Adult Progenitor Cells in Graft vs Host Disease," *Stem Cells Translational Medicine* 10, no. 11 (2021): 1561–1574.

73. J. M. Corbett, I. Hawthorne, H. Dunbar, et al., "Cyclosporine A and IFNγ Licencing Enhances human Mesenchymal Stromal Cell Potency in a Humanised Mouse Model of Acute Graft versus Host Disease," *Stem Cell Research & Therapy* 12, no. 1 (2021): 238.

74. S. Wang, F. Umrath, W. Cen, A. J. Salgado, S. Reinert, and D. Alexander, "Pre-Conditioning With IFN-γ and Hypoxia Enhances the Angiogenic Potential of iPSC-Derived MSC Secretome," *Cells* 11, no. 6 (2022): 988.

75. C. Liu, Y. Xu, Y. Lu, et al., "Mesenchymal Stromal Cells Pretreated With Proinflammatory Cytokines Enhance Skin Wound Healing via IL-6-dependent M2 Polarization," *Stem Cell Research & Therapy* 13, no. 1 (2022): 414.

76. F. A. Fierro, A. J. O'Neal, J. R. Beegle, et al., "Hypoxic Pre-conditioning Increases the Infiltration of Endothelial Cells Into Scaffolds for Dermal Regeneration Pre-seeded With Mesenchymal Stem Cells," *Frontiers in Cell and Developmental Biology* 3 (2015): 68.

77. N. Ishiuchi, A. Nakashima, S. Doi, et al., "Hypoxia-preconditioned Mesenchymal Stem Cells Prevent Renal Fibrosis and Inflammation in Ischemia-reperfusion Rats," *Stem Cell Research & Therapy* 11, no. 1 (2020): 130.

78. C. A. Lagonda, F. B. Tjahjadi, D. Fauza, and Y. Kusnadi, "Hypoxia Increases Vegf Secretion in Multiple Sources of Mesenchymal Stem Cell," *Cytotherapy* 20, no. 5 (2018): S44–5.

79. A. M. Bader, K. Klose, K. Bieback, et al., "Hypoxic Preconditioning Increases Survival and Pro-Angiogenic Capacity of Human Cord Blood Mesenchymal Stromal Cells in Vitro," *PLoS ONE* 10, no. 9 (2015): e0138477.

80. V. Razban, A. S. Lotfi, M. Soleimani, H. Ahmadi, M. Massumi, S. Khajeh, et al., "HIF-1α Overexpression Induces Angiogenesis in Mesenchymal Stem Cells," *BioResearch Open Access* 1, no. 4 (2012): 174–183.

81. C. Gorin, G. Y. Rochefort, R. Bascetin, et al., "Priming Dental Pulp Stem Cells With Fibroblast Growth Factor-2 Increases Angiogenesis of Implanted Tissue-Engineered Constructs Through Hepatocyte Growth Factor and Vascular Endothelial Growth Factor Secretion," *Stem Cells Translational Medicine* 5, no. 3 (2016): 392–404.

82. Y. Wang, P. R. Crisostomo, M. Wang, T. A. Markel, N. M. Novotny, and D. R. Meldrum, "TGF-alpha Increases human Mesenchymal Stem Cell-secreted VEGF by MEK- and PI3-K- but Not JNK- or ERK-Dependent Mechanisms," *American Journal of Physiology Regulatory, Integrative and Comparative Physiology* 295, no. 4 (2008): R1115–1123.

83. D. W. Koch, A. K. Berglund, K. M. Messenger, J. M. Gilbertie, I. M. Ellis, and L. V. Schnabel, "Interleukin-1β in Tendon Injury Enhances Reparative Gene and Protein Expression in Mesenchymal Stem Cells," *Front Vet Sci* 9 (2022): 963759.

84. Y. Yao, F. Zhang, L. Wang, et al., "Lipopolysaccharide Preconditioning Enhances the Efficacy of Mesenchymal Stem Cells Transplantation in a Rat Model of Acute Myocardial Infarction," *Journal of Biomedical Science* 16, no. 1 (2009): 74.

85. E. Kokki, T. Karttunen, V. Olsson, K. Kinnunen, and S. Ylä-Herttuala, "Human Vascular Endothelial Growth Factor A165 Expression Induces the Mouse Model of Neovascular Age-Related Macular Degeneration," *Genes (Basel)* 9, no. 9 (2018): 438.

86. E. Mujagic, R. Gianni-Barrera, M. Trani, A. Patel, L. Gürke, M. Heberer, et al., "Induction of Aberrant Vascular Growth, but Not of Normal Angiogenesis, by Cell-based Expression of Different Doses of human and Mouse VEGF Is Species-dependent," *Hum Gene Ther Methods* 24, no. 1 (2013): 28–37.

87. K. Tang, H. B. Rossiter, P. D. Wagner, and E. C. Breen, "Lung-targeted VEGF Inactivation Leads to an Emphysema Phenotype in Mice," *J Appl Physiol (1985)* 97, no. 4 (2004): 1559–1566. discussion 1549.

88. M. Mura, B. Han, C. F. Andrade, et al., "The Early Responses of VEGF and Its Receptors During Acute Lung Injury: Implication of VEGF in Alveolar Epithelial Cell Survival," *Critical Care (London, England)* 10, no. 5 (2006): R130.

89. A. Ohwada, Y. Yoshioka, K. Iwabuchi, I. Nagaoka, T. Dambara, and Y. Fukuchi, "VEGF Regulates the Proliferation of Acid-Exposed Alveolar Lining Epithelial Cells," *Thorax* 58, no. 4 (2003): 328–332.

90. S. Y. Ahn, W. S. Park, Y. E. Kim, et al., "Vascular Endothelial Growth Factor Mediates the Therapeutic Efficacy of Mesenchymal Stem Cell-derived Extracellular Vesicles Against Neonatal Hyperoxic Lung Injury," *Experimental & Molecular Medicine* 50, no. 4 (2018): 1–12.

91. Q. Chen, J. Lin, Z. Deng, and W. Qian, "Exosomes Derived From Human Umbilical Cord Mesenchymal Stem Cells Protect Against Papain-induced Emphysema by Preventing Apoptosis Through Activating VEGF-VEGFR2-Mediated AKT and MEK/ERK Pathways in Rats," *Regenerative Therapy* 21 (2022): 216–224.

Supporting Information

Additional supporting information can be found online in the Supporting Information section.